ISSN 0711-6659

# canadian acoustics
# acoustique canadienne

Journal of the Canadian Acoustical Association - Journal de l'Association Canadienne d'Acoustique

SEPTEMBER 2011
Volume 39 -- Number 3

SEPTEMBRE 2011
Volume 39 -- Numéro 3



# PROCEEDINGS

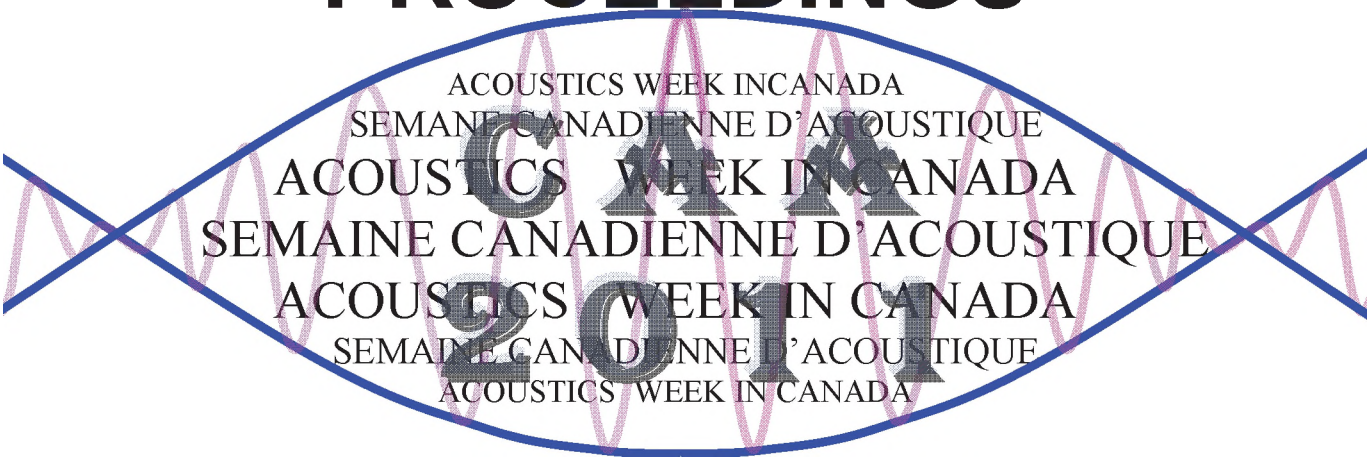


# COMPTES RENDUS

# canadian acoustics

# acoustique canadienne

**THE CANADIAN ACOUSTICAL ASSOCIATION**
**P.O. BOX 1351, STATION "F"**
**TORONTO, ONTARIO M4Y 2V9**

**L'ASSOCIATION CANADIENNE D'ACOUSTIQUE**
**C.P. 1351, SUCCURSALE "F"**
**TORONTO, ONTARIO M4Y 2V9**

CANADIAN ACOUSTICS publishes refereed articles and news items on all aspects of acoustics and vibration. Articles reporting new research or applications, as well as review or tutorial papers and shorter technical notes are welcomed, in English or in French. Submissions should be sent directly to the Editor-in-Chief. Complete instructions to authors concerning the required camera-ready copy are presented at the end of this issue.

ACOUSTIQUE CANADIENNE publie des articles arbitrés et des informations sur tous les domaines de l'acoustique et des vibrations. On invite les auteurs à soumettre des manuscrits, rédigés en français ou en anglais, concernant des travaux inédits, des états de question ou des notes techniques. Les soumissions doivent être envoyées au rédacteur en chef. Les instructions pour la présentation des textes sont exposées à la fin de cette publication.

CANADIAN ACOUSTICS is published four times a year - in March, June, September and December. The deadline for submission of material is the first day of the month preceeding the issue month. Copyright on articles is held by the author(s), who should be contacted regarding reproduction. Annual subscription: $35 (student); $80 (individual, institution); $350 (sustaining - see back cover). Back issues (when available) may be obtained from the CAA Secretary - price $20 including postage. Advertisement prices: $350 (full page- $1200 for four issues); $200 (half page - $700 for four issues); $150 (quarter page - $500 for four issues). Contact the Associate Editor (advertising) to place advertisements. Canadian Publication Mail Product Sales Agreement No. 0557188.

ACOUSTIQUE CANADIENNE est publiée quatre fois par année - en mars, juin, septembre et décembre. La date de tombée pour la soumission de matériel est fixée au premier jour du mois précédant la publication d'un numéro donné. Les droits d'auteur d'un article appartiennent à (aux) auteur(s). Toute demande de reproduction doit leur être acheminée. Abonnement annuel: $35 (étudiant); $80 (individuel, société); $350 (soutien - voir la couverture arrière). D'anciens numéros (non-épuisés) peuvent être obtenus du Secrétaire de l'ACA - prix: $20 (affranchissement inclus). Prix d'annonces publicitaires: $350 (page pleine - $1200 pour quatre publications); $200 (demi page - $700 pour quatre publications); $150 (quart de page - $500 pour quatre publications). Contacter le rédacteur associé (publicité) afin de placer des annonces. Société canadienne des postes - Envois de publications canadiennes - Numéro de convention 0557188.

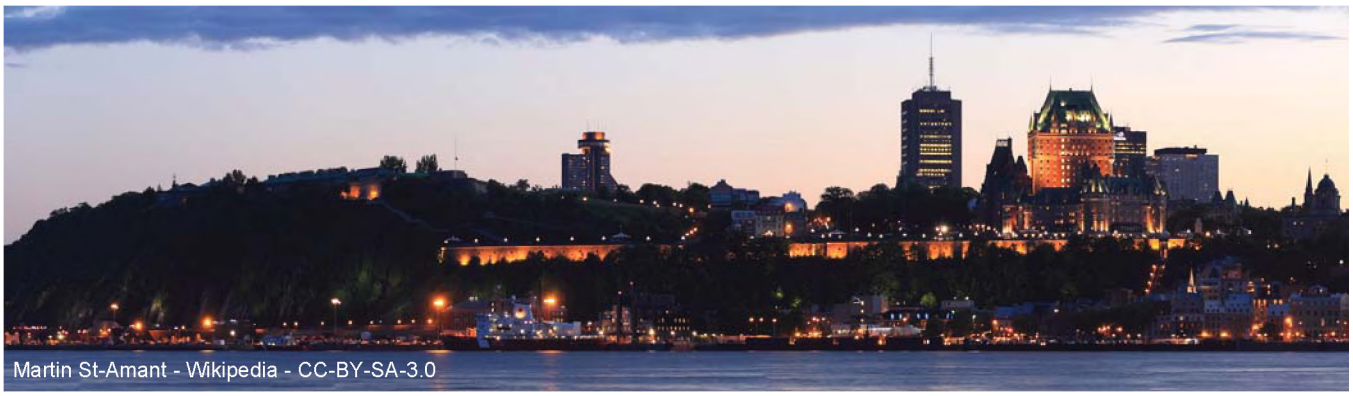


# ACOUSTICS WEEK IN CANADA
# SEMAINE CANADIENNE D'ACOUSTIQUE

## Hôtel Château Laurier Québec
## Quebec City, 12-14 October 2011
## Ville de Québec, 12 au 14 octobre 2011

### Organizing Committee / Comité organisateur

| | |
|---|---|
| Conference Chair / Président : | *Christian Giguère* |
| Technical Chairs / Directeurs scientifiques : | *Jérémie Voix* |
| | *Hugues Nélisse* |
| Exhibition / Exposition : | *André L'Espérance* |
| Logistics / Logistique : | *François Bergeron* |
| | *Jean-Philippe Migneron* |
| Website / Site internet : | *Nicolas Ellaham* |



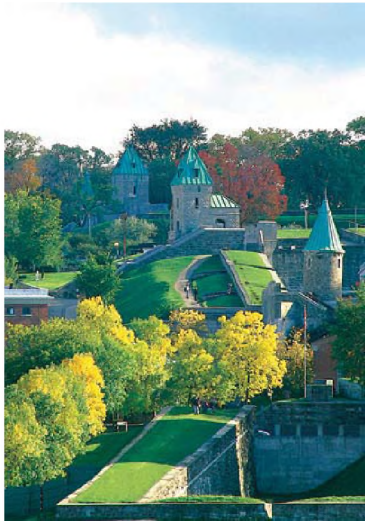

(Photos: Yves Tessier Tessima, La Maison Simons, Brigitte Ostiguy)

# Sponsors / Commanditaires:









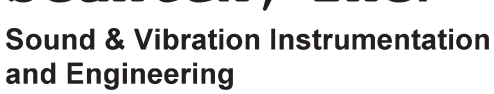




# Exhibitors / Exposants:













(as of 15 August / en date du 15 août)

## EDITORIAL/ ÉDITORIAL

Welcome to the proceedings issue of Acoustics Week in Canada 2011. I hope it will provide a lasting account of our annual conference to be held in Quebec City, October 12-14. It is my pleasure to invite you to this beautiful city in a conference venue, Hôtel Château Laurier Québec, very near the old city walls and literally on the Plains of Abraham overlooking the St. Lawrence River. As it happens, it will be the 50th annual meeting of our organization. You will not want to be anywhere else than in Quebec City to celebrate this milestone with your acoustical friends!

We have assembled a most complete technical and social program for our presenters and delegates. Over 120 contributed talks organized into fifteen topic areas will be delivered. New this year, a session on Education is being organized covering initiatives and challenges in teaching acoustics to our diverse populations of students in mechanical engineering, architecture, audiology and music. A session on Case Studies in Acoustics is also being organized which we hope could become a permanent fixture at our meetings. The plenary talks at the start of each day will highlight regional expertise on cochlear implants (in French), sound and artistic creativity (in English), and acoustic imaging methods (in English). On Wednesday, a Welcome Reception is being offered on the highest observation gallery in Quebec City, concurrently with the meeting of the Acoustical Standards Committee. Thursday will include the Exhibition of acoustical equipment and products as usual as well as the Annual Banquet and Awards Ceremony. On Friday, prizes for the three best student presentations at the congress will be presented.

On behalf of the organizing committee, we hope that all our efforts in the past few months will bring you to Quebec City to be part of this exciting acoustical event.

Christian Giguère
Conference Chair

Bienvenue au numéro des actes du congrès de la Semaine canadienne d'acoustique édition 2011. Il reflètera bien, je l'espère, les activités entourant notre congrès annuel qui se tiendra à Québec du 12 au 14 octobre. C'est donc avec plaisir que je vous invite à participer à ce congrès à l'Hôtel Château Laurier Québec tout près du Vieux-Québec, aux abords des Plaines d'Abraham et surplombant le fleuve Saint-Laurent. De surcroit, cette année marque la 50ième rencontre annuelle de notre organisation. Vous ne pourrez vous imaginer être ailleurs qu'à Québec pour célébrer cette étape importante avec vos collègues acousticiens!

Nous avons préparé un programme scientifique et social des plus complet pour nos présentateurs et délégués. Plus de 120 communications orales regroupées en quinze champs d'intérêt seront présentées. Une nouveauté cette année, une session portant sur l'enseignement est au programme et couvrira différentes initiatives pédagogiques et les défis de l'enseignement de l'acoustique à nos diverses populations d'étudiants en génie mécanique, architecture, audiologie et musique. Une session ciblant des études de cas en acoustique est également organisée. Une telle session, nous l'espérons, pourrait devenir un thème permanent lors de nos congrès. Les conférences plénières, au début de chaque journée, illustreront l'expertise régionale en implants cochléaires (en français), création sonore (en anglais) et méthodes d'imagerie acoustique (en anglais). Le mercredi, une réception de bienvenue sera offerte à la galerie d'observation la plus élevée à Québec au haut du complexe G en parallèle avec la réunion du Comité des normes acoustiques. La journée du jeudi comprendra comme à l'habitude l'exposition technique d'équipement et produits en acoustique ainsi que le banquet annuel et la remise des prix. Le vendredi, les prix pour les trois meilleures présentations étudiantes seront décernés.

Au nom du comité organisateur, nous espérons que tous les efforts des derniers mois vous amèneront à Québec pour participer à cet événement qui promet d'être des plus intéressant.

Christian Giguère
Président du congrès

# Table of Contents/Tables des matières

Human Vibration Analyzer Type 4447

# ENSURING GOOD VIBRATION

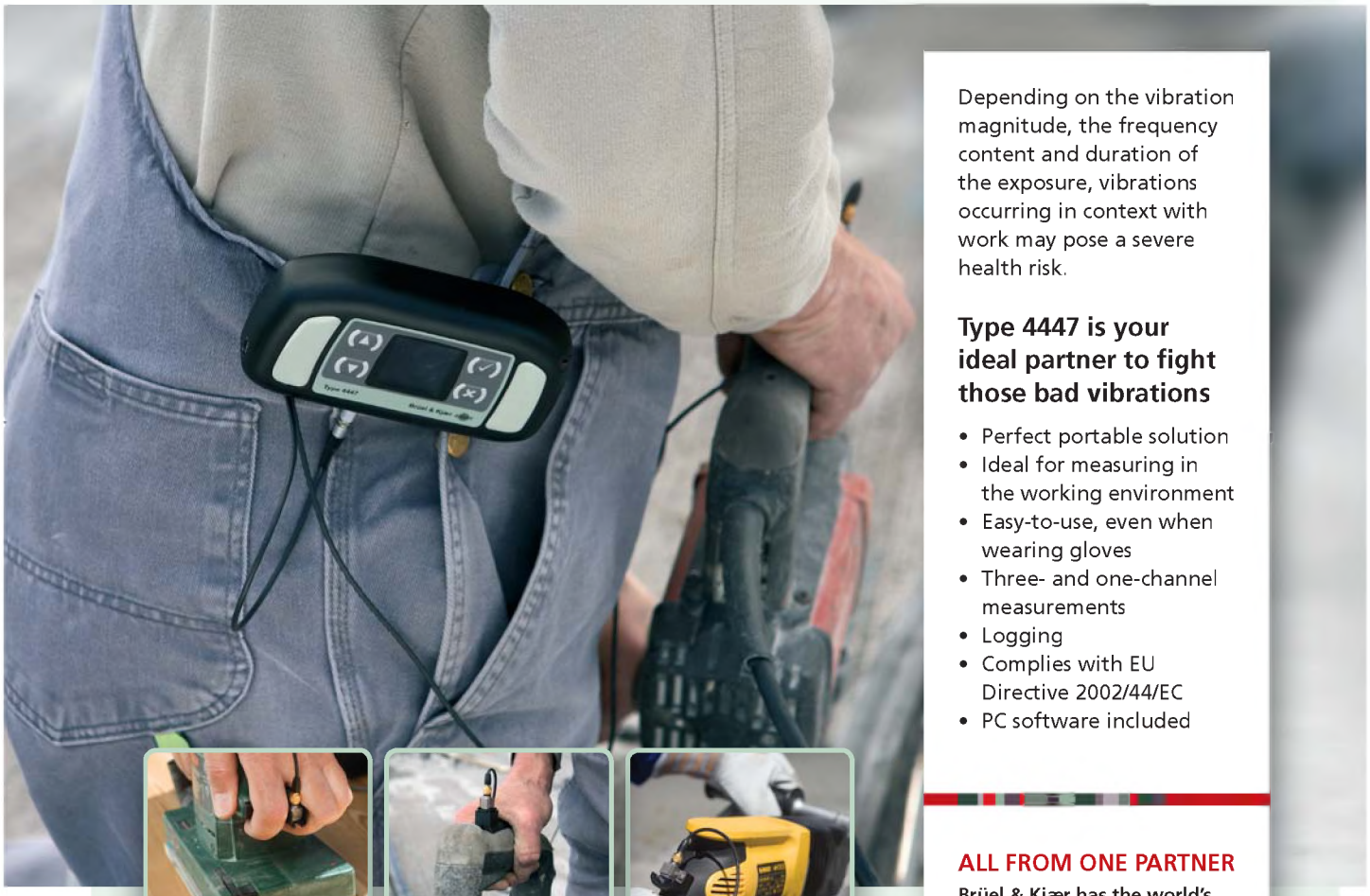







Depending on the vibration magnitude, the frequency content and duration of the exposure, vibrations occurring in context with work may pose a severe health risk.

## Type 4447 is your ideal partner to fight those bad vibrations

- Perfect portable solution
- Ideal for measuring in the working environment
- Easy-to-use, even when wearing gloves
- Three- and one-channel measurements
- Logging
- Complies with EU Directive 2002/44/EC
- PC software included

## ALL FROM ONE PARTNER

**Brüel & Kjær has the world's most comprehensive range of sound and vibration test and measurement systems**

**www.bksv.com/Type4447**

BH 1007 - 11

Brüel & Kjær North America Inc. · 2815 A Colonnades Court · Norcross, GA · 30071-1588
Telephone: 770 209 6907 · Fax: 770 448 3246 · www.bkhome.com · bkinfo@bksv.com

HEADQUARTERS: Brüel & Kjær Sound & Vibration Measurement A/S · DK-2850 Nærum · Denmark
Telephone: +45 7741 2000 · Fax: +45 4580 1405 · www.bksv.com · info@bksv.com

Local representatives and service organisations worldwide

Brüel & Kjær

*creating sustainable value*

| DAY ONE | WEDNESDAY 12 October 2011<br>Registration Open at 8:00, Foyer Des Plaines | | |
|---|---|---|---|
| 8:50–9:00 | Welcome | | |
| 9:00–10:00 | Plenary: Isabelle MILLETTE & Maurice BHÉRER (Room: Des Plaines BC)<br>*L'implant cochléaire au Québec en 2011* | | |
| 10:00–10:20 | COFFEE BREAK | | |
| | ROOM: Du Jardin | ROOM: Des Plaines B | ROOM: Des Plaines C |
| 10:20–12:20 | *AEROACOUSTICS* | *BUILDING & ARCHITECTURAL ACOUSTICS I* | *SPEECH COMMUNICATION I* |
| 12:20–1:20 | LUNCH (Des Plaines A) | | |
| 1:20–3:20 | *AEROACOUSTICS / ACOUSTICAL MATERIAL* | *BUILDING & ARCHITECTURAL ACOUSTICS II* | *HEARING SCIENCES I* |
| 3:20–3:40 | COFFEE BREAK | | |
| 3:40–5:00 | *ACOUSTICAL MATERIAL* | *STANDARDS & REGULATIONS* | *HEARING SCIENCES II* |
| 5:00–10:00 | Acoustical Standards Committee Meeting (All welcome, ROOM: George V) | | |
| 6:30-8:00 | WELCOME RECEPTION<br>(Observatoire de la Capitale, Édifice Marie-Guyart Complexe G, 31st Floor) | | |

| DAY TWO | THURSDAY 13 October 2011<br>EXHIBITION: 9:40–5:20 (Room Des Plaines A) | | |
|---|---|---|---|
| 8:35–9:40 | Plenary: Jocelyn ROBERT (Room: Des Plaines BC)<br>*Art, Sound, Paradigms* | | |
| 9:40–10:20 | COFFEE BREAK | | |
| | ROOM: Du Jardin | ROOM: Des Plaines B | ROOM: Des Plaines C |
| 10:20–12:00 | *HEARING PROTECTION* | *NOISE CONTROL* | *SPEECH COMMUNICATION II* |
| 12:00–1:00 | LUNCH (Abraham Martin) | | |
| 1:00–3:00 | *HEARING PROTECTION / MUSICAL ACOUSTICS* | *CASE STUDIES* | *SPEECH COMMUNICATION III* |
| 3:00–3:40 | COFFEE BREAK | | |
| 3:40–5:20 | *MUSICAL ACOUSTICS* | *ENVIRONMENTAL NOISE* | *SPEECH COMMUNICATION IV* |
| 5:30–6:30 | CAA ANNUAL GENERAL MEETING (ROOM: Du Jardin) | | |
| 6:30–9:30 | AWC 2011 BANQUET & AWARDS (Des Plaines A, Cash Bar open at 6:30) | | |

| DAY THREE | FRIDAY 14 October 2011 | | |
|---|---|---|---|
| 8:35–9:40 | Plenary: Alain BERRY (Room: Des Plaines BC)<br>*A few acoustic imaging methods based on microphone antennas* | | |
| 9:40–10:00 | COFFEE BREAK | | |
| | ROOM: Du Jardin | ROOM: Des Plaines B | ROOM: Des Plaines C |
| 10:00–12:00 | *VIBRATION / EDUCATION* | *BIOACOUSTICS / UNDERWATER ACOUSTICS* | *SPEECH COMMUNICATION V* |
| 12:00–1:20 | LUNCH & STUDENT PRESENTATION AWARDS (Des Plaines A) | | |
| 1:20–2:40 | *EDUCATION* | *UNDERWATER ACOUSTICS* | *SPEECH COMMUNICATION VI* |
| 2:40 | FAREWELL | | |

| JOUR 1 | MERCREDI 12 octobre 2011<br>Kiosque d'inscription ouvert à partir de 8:00, Foyer Des Plaines | | |
|---|---|---|---|
| 8:50–9:00 | Mot de bienvenue | | |
| 9:00–10:00 | Plénière: Isabelle MILLETTE & Maurice BHÉRER (Salle Des Plaines BC)<br>*L'implant cochléaire au Québec en 2011* | | |
| 10:00–10:20 | PAUSE-CAFÉ | | |
| | Salle Du Jardin | Salle Des Plaines B | Salle Des Plaines C |
| 10:20–12:20 | *AÉROACOUSTIQUE* | *ACOUSTIQUE ARCHITECTURALE ET DU BÂTIMENT I* | *COMMUNICATION PAROLE I* |
| 12:20–13:20 | LUNCH (Des Plaines A) | | |
| 13:20–15:20 | *AÉROACOUSTIQUE / MATÉRIAUX ACOUSTIQUES* | *ACOUSTIQUE ARCHITECTURALE ET DU BÂTIMENT II* | *SCIENCES DE L'AUDITION I* |
| 15:20–15:40 | PAUSE-CAFÉ | | |
| 15:40–17:00 | *MATÉRIAUX ACOUSTIQUES* | *NORMALISATION & RÉGLEMENTATION* | *SCIENCES DE L'AUDITION II* |
| 17:00–22:00 | Comité de normalisation en acoustique (Ouvert à tous, Salle George V) | | |
| 18:30-20:00 | RÉCEPTION DE BIENVENUE<br>(Observatoire de la Capitale, Édifice Marie-Guyart Complexe G, 31e étage) | | |

| JOUR 2 | JEUDI 13 octobre 2011<br>EXPOSITION TECHNIQUE: 9:40–17:30 (salle Des Plaines A) | | |
|---|---|---|---|
| 8:35–9:40 | Plénière: Jocelyn ROBERT (Salle Des Plaines BC)<br>*Art, Sound, Paradigms* | | |
| 9:40–10:20 | PAUSE-CAFÉ | | |
| | Salle Du Jardin | Salle Des Plaines B | Salle Des Plaines C |
| 10:20–12:00 | *PROTECTION AUDITIVE I* | *CONTRÔLE DU BRUIT* | *COMMUNICATION PAROLE II* |
| 12:00–13:00 | LUNCH (Abraham Martin) | | |
| 13:00–15:00 | *PROTECTION AUDITIVE II / ACOUSTIQUE MUSICALE* | *ÉTUDES DE CAS EN ACOUSTIQUE* | *COMMUNICATION PAROLE III* |
| 15:00–15:40 | PAUSE-CAFÉ | | |
| 15:40–17:20 | *ACOUSTIQUE MUSICALE* | *BRUIT ENVIRONNEMENTAL* | *COMMUNICATION PAROLE IV* |
| 17:30–18:30 | ASSEMBLÉE GÉNÉRALE ANNUELLE DE L'ACA (Salle Du Jardin) | | |
| 18:30–22:00 | BANQUET ET REMISE DES PRIX 2011 (Des Plaines A, Bar payant à partir de 18:30) | | |

| JOUR 3 | VENDREDI 14 octobre 2011 | | |
|---|---|---|---|
| 8:35–9:40 | Plénière: Alain BERRY (Salle Des Plaines BC)<br>*A few acoustic imaging methods based on microphone antennas* | | |
| 9:40–10:00 | PAUSE-CAFÉ | | |
| | Salle Du Jardin | Salle Des Plaines B | Salle Des Plaines C |
| 10:00–12:00 | *VIBRATIONS / ENSEIGNEMENT* | *BIOACOUSTIQUE / ACOUSTIQUE SOUS-MARINE* | *COMMUNICATION PAROLE VI* |
| 12:00–13:20 | LUNCH & PRIX POUR MEILLEURES COMMUNICATIONS ÉTUDIANTES (Des Plaines A) | | |
| 13:20–14:40 | *ENSEIGNEMENT* | *ACOUSTIQUE SOUS-MARINE* | *COMMUNICATION PAROLE VI* |
| 14:40 | Clôture du congrès | | |

# SOUND PACKAGE FOR A MAGNESIUM ALLOY DASH PANEL

**Aljosa Rakic, Raymond Panneton, and Noureddine Atalla**
Dept. of Mechanical Engineering, Université de Sherbrooke, 2500 boul. Université, Québec, Canada, J1K 3R1

## 1. INTRODUCTION

New government regulations require automotive industries to reduce greenhouse gas emissions. It can be realised by increasing the energy efficiency of the automobile powertrain or by reducing the total weight of the vehicle.

The automobile companies such as Ford and Volkswagen decided to use magnesium alloy (AZ31B) to replace some steel parts of the car. The magnesium alloy has several advantages over steel. It is more malleable, more ductile, lighter, and it has a higher stiffness weight ratio. However, its low mass gives a poor sound transmission loss performance compared to steel. Thus, it is necessary to develop a new sound package for magnesium alloy.

The methodology described in this paper is to optimize a new acoustic treatment of a 2-mm thick magnesium alloy dash panel. In addition, a constraint is imposed on the mass per unit area of the dash panel with its treatment. The results of the new acoustic treatment are compared with a reference sound package.

## 2. METHODS

### 2.1 Reference sound package

Figure 1 shows the sound package typically used on the automobile dash panel [SY, 2010]. It is a multilayer of insulating and absorbing materials of various thicknesses. The mass per unit area of this treatment with a 0.9-mm thick steel dash panel is 10.15 kg/m$^2$.

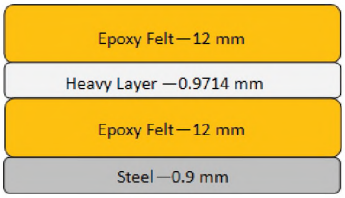


**Figure 1. Typical sound package for the steel dash panel**

Applying this same treatment on a magnesium alloy dash panel of 2 mm thickness, the noise reduction (NR) performance is lower than the one with steel as shown in Figure 2. The *NR* is the acoustical pressure reduction inside the car cabin due to the dash panel and sound package. The *NR* mathematical expression will be given later in this paper.

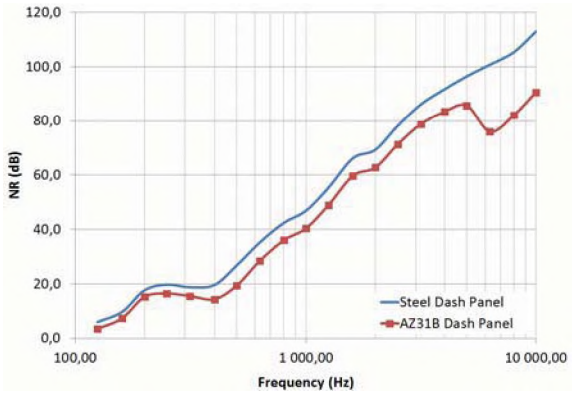


**Figure 2. *NR* comparison between the reference sound package installed on a steel dash panel and on a magnesium alloy dash panel.**

### 2.2 Methodology

A 3D model of a car has been designed in the statistical energy analysis (SEA) software VA ONE to calculate the average sound absorption of the car cabin. This model takes into account the sound absorption of seats, roof, floor and doors. The average absorption has been used to calculate the *NR* of the dash panel for optimization process [ATALA, 2011]. It is given by:

$$NR = TL - 10\log_{10}\frac{A_S}{A_C\tilde{\alpha}} \qquad \text{(Eq. 1)}$$

where $TL$ is the transmission loss of the dash panel and sound package, $\tilde{\alpha}$ is the average absorption of cabin car, $A_c$ is the cabin car surface area and $A_s$ is the dash panel surface area.

An optimization program was developed in the Matlab environment. The genetic algorithm presented by [KINCAID *and al.*, 2002] is used as an optimization process. Acoustic indicators of the dash panel were calculated with the transfer matrix module of the NOVA software. The cost function to maximize is :

$$C.F. = \sum_{i}^{N}\left[NR^i_{NEW} - NR^i_{REF}\right] \qquad \text{(Eq. 2)}$$

where $NR^i_{NEW}$ is the *NR* for the new sound package installed on magnesium alloy dash panel at the *i*th frequency and $NR^i_{REF}$ is the *NR* of the corresponding reference sound package with steel dash panel. Optimization frequency

range goes from 125 Hz to 10,000 Hz. In addition, new acoustic treatments concepts are classified by their performances corresponding to the differences between the NR.

## 3. RESULTS

Three concepts emerged after optimization and are shown in Figure 3.

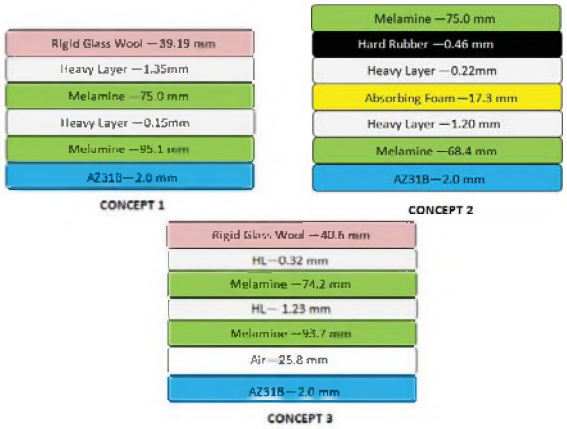


**Figure 3. Three concepts emerged after optimization**

The first concept is composed of absorbers and insulators materials. A similar structure was used for the second concept. Only a small damping material layer (hard rubber) was added to improve the transmission loss at low frequencies. The optimization was performed on 33 different materials considering the following criteria: the type of materials, the thickness of each layer, the positioning of the each material in the multilayer. An optimization constraint of 8.5 kg/m$^2$ has been imposed on the maximum surface density.

In concept 3, an air plenum was added to the multilayer. The air plenum is a separator between two layers and can improve transmission loss of the multilayer. The same optimization process than the one used for concept 1 was used for concept 3. However, an additional constraint was added to ensure that the multilayer cannot end by the air plenum.

## 4. DISCUSSION AND CONCLUSIONS

Figure 4 shows the noise reduction of each concept compared to the reference treatment.

Table 1 presents, for each considered concept, the surface density and their average gain in dB of *NR* with frequency compared to the reference dash panel.

For frequencies above 250 Hz, concept 1 shows a very good improvement in the *NR* (between 4 dB and 48 dB). For frequencies below 250 Hz, the transmission loss of the reference treatment is very important due to its mass, giving

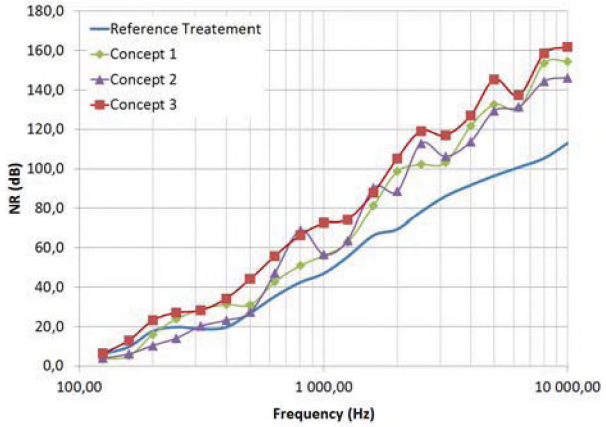


**Figure 4. *NR* of each concept compared to standard treatment**

**Table 1. Average gain in dB of NR**

| Concept | Surface density | Gain |
|---|---|---|
| 1 | 8.26 kg/m$^2$ | 16.2 dB |
| 2 | 8.47 kg/m$^2$ | 15.0 dB |
| 3 | 8.40 kg/m$^2$ | 25.0 dB |

it an advantage over concept 1. However, the average gain of concept 1 over the reference treatment is 16.2 dB for the whole optimization frequency range.

The results for concept 2 are close to those obtained for concept 1. The addition of the damping material was not sufficient to improve the *NR* at low frequencies (125 Hz to 250 Hz).

Finally, concept 3 shows the best *NR* over the whole frequency range. However, the main disadvantage of concept 3 is the difficulty to maintain an air layer in its fabrication. It is possible by installing rigid supports but this will add some extra mass. Also, the total thickness of this concept is too large for real car application. The next step of the optimization process is to impose the maximum thickness constraint and to fabricate prototypes of the three concepts to validate these results.

## REFERENCES


ALLARD, J-F., ATALLA, N. (2009). *Propagation of sound in porous media: modeling sound absorbing materials,* Second edition, John Wiley.

ATALLA, N. (2011). *Méthode numérique pour les interactions fluide structure,* Course note, University of Sherbooke.

KINCAID, K.R., GRIFFITH, M.M., SYKES, R., SOBIESKI, J. (2002). *Bell-Curve Genetic Algorithm for mixed Continuous and Discrete Optimization Problems,* AIAA Paper 2002-1731.

SY, D., (2010). *Modélisation et optimisation des performances acoustiques d'un tablier d'automobile en alliage de magnésium,* Master Thesis, Université de Sherbrooke.


## ACKNOWLEDGEMENTS


The authors would like to thank AUTO 21 for the financial support of this project.

# THREE-MICROPHONE TWO-CAVITY METHOD FOR MEASURING SOUND TRANSMISSION LOSS IN A MODIFIED IMPEDANCE TUBE

**Yacoubou SALISSOU Raymond PANNETON and Olivier DOUTRES**
GAUS, Department of mechanical engineering, Université de Sherbrooke, Québec, Canada, J1K 2R1
Yacoubou.Salissou@USherbrooke.ca, Raymond.Panneton@USherbrooke.ca, Olivier.Doutres@USherbrooke.ca

## 1. INTRODUCTION

The normal incidence sound transmission loss (*nSTL*) is an important indicator to assess the sound insulation property of acoustic materials. A literature review of the main methods used to measure the *nSTL* using a plane wave tubes is given elsewhere by the authors[1]. Today, the two most recognized methods are the four-microphone two-load (4M2L)[2] and one-load (4M1L) methods[3]. While the 4M2L method is a general method, the 4M1L method is limited to materials being geometrically symmetric and invokes the reciprocity principle[4].

In an attempt to reduce the number of microphones, a method based on two upstream microphones only was proposed[5]. However, when tested experimentally, the method has singularities that are not yet resolved[6]. For symmetrical materials, this difficulty was circumvented by adding a third microphone on the hard termination cap backing the sample[7,8]. The resulting three-microphone method was proved to be efficient for characterizing the dynamic properties. In parallel to the present work, Rodriguez *et al.*[9] presented a generalization of the latter three-microphone method (the 3M-TMTC method). However, their approach is restricted to samples with flat and symmetrical surfaces as the third microphone is in direct contact with the sample. The present paper describes a general three-microphone two-load (3M2L) method which generalizes the three-microphone methods. It may be seen as a particular case of the 4M2L method when the surface impedances of the two loads are known.

## 2. THEORY

A schematic view of the modified impedance tube used in the proposed 3M2L method is shown in Figure 1. The apparatus consists of a finite length rigid walled impedance tube with circularly shaped and uniform inner cross-section. The tube features a loudspeaker (source) at one end and a movable piston (rigid end) at the other end. The loudspeaker is used to generate a plane wave field in the impedance tube. There are two microphones flush mounted upstream the test sample and one microphone flush mounted on the rigid end. Two different air cavities of thickness $D_i$ ($i=1,2$) are inserted between the sample and the rigid end. Assuming a unit amplitude incident plane wave with time dependence of the form $exp(j\omega t)$, the acoustic pressures p(x) and velocities u(x) upstream and downstream the test sample are respectively given by

$$\left.\begin{aligned} p(x) &= e^{-jk_0x} + R_i e^{jk_0x} \\ u(x) &= \left(e^{-jk_0x} - R_i e^{jk_0x}\right)/Z_0 \end{aligned}\right\} \text{ for } x \le 0$$
$$\left.\begin{aligned} p(x) &= 2A_i e^{-jk_0L_i}\cos\left(k_0(x-L_i)\right) \\ u(x) &= \left[-j2A_i e^{-jk_0L_i}\sin\left(k_0(x-L_i)\right)/Z_0\right] \end{aligned}\right\} \text{ for } x \ge d \quad (1)$$

where subscript $i$ refers to a value obtained with an air cavity of thickness $D_i$, $L_i=d+D_i$, $d$ is the thickness of the sample, $Z_0=\rho_0 c_0$ is the characteristic acoustic impedance of ambient air with $\rho_0$ and $c_0$ the density of air and the speed of sound wave in air respectively, $k_0$ is the wave number in air, $R_i$ is the complex sound reflection coefficient at the surface of the sample (i.e. at x = 0), $2A_i$ is the maximum pressure amplitude of the standing wave downstream the sample, and $j^2 = -1$. The geometrical variables are defined in Figure 1. The reflection coefficient $R_i$ is obtained from,

$$R_i = \left(H_{12}(D_i) - e^{jk_0s}\right)e^{2jk_0L}\Big/\left(e^{-jk_0s} - H_{12}(D_i)\right), \quad (2)$$

$H_{12}(D_i)$ is the transfer function between microphones 1 and 2 (i.e., p(μ1) /p(μ2)) with an air cavity of thickness $D_i$, s is the spacing between microphones 1 and 2 and L is the distance between microphone 2 and the front surface of the sample. Using Eq.(1), the transfer function $H_{31}$ between microphones 3 and 1 (i.e., p(μ3) /p(μ1)) is written as

$$H_{31}(D_i) = 2A_i e^{-jk_0L_i}\Big/\left(e^{jk_0(L+s)} + R_i e^{-jk_0(L+s)}\right), \quad (3)$$

which yields the following expression for $A_i$

$$2A_i e^{-jk_0L_i} = H_{31}(D_i)\left(e^{jk_0(L+s)} + R_i e^{-jk_0(L+s)}\right). \quad (4)$$

Using the transfer matrix relation, the acoustic pressure and velocity at $x = 0$ and $x = d$ can be linked as,

$$\begin{Bmatrix} 1+R_i \\ (1-R_i)/Z_0 \end{Bmatrix} = \begin{bmatrix} T_{11} & T_{12} \\ T_{21} & T_{22} \end{bmatrix} \begin{Bmatrix} \cos(k_0D_i) \\ j\sin(k_0D_i)/Z_0 \end{Bmatrix} 2A_i e^{-jk_0L_i}. \quad (5)$$

Now, if two measurements are successively done with cavities of thickness $D_1$ and $D_2$, Eq.(5) yields four linear relations and four unknowns. The four unknowns are the transfer matrix coefficients. Solving the system of linear equations yields the transfer matrix coefficients and the transmission coefficient of the test sample is deduced from,

$$\tau = 2e^{jk_0 d} \Big/ \left( T_{11} + T_{12}/Z_0 + Z_0 T_{21} + T_{22} \right) . \quad (6)$$

$$nSTL = -10 \log_{10} |\tau|^2 \quad (7)$$

As one can note, only two measurements and three microphones are required for measuring *nSTL*. The procedure is not limited to symmetrical samples and does not invoke the reciprocity principle[4].

## 3. EXPERIMENTAL TESTS AND RESULTS

Three microphones ($\mu_1$, $\mu_2$, $\mu_3$) and four channels ($ch_1$, $ch_2$, $ch_3$, $ch_4$) are used for measuring the required four transfer functions ($H_{12}(D_1)$, $H_{13}(D_1)$, $H_{12}(D_2)$, $H_{13}(D_2)$). Each microphone $\mu_i$ is connected to channel $ch_i$ to form measurement line $\mu_i ch_i$, and $ch_4$ is the output source signal. For correcting the measured transfer functions for amplitude and phase mismatches between the three measurement lines, the sensor-switching technique as described in ASTM E2611-09 is used. Here line $\mu_1 ch_1$ is the reference line. Consequently the calibration is successively made between $\mu_1 ch_1$ and $\mu_2 ch_2$ and between $\mu_1 ch_1$ and $\mu_3 ch_3$ using microphone positions 1 and 2.

As a first validation the 3M2L, an air layer (with $d = 80$ mm) seeing as a symmetrical sample is tested. The air layer is placed at the sample position shown in Figure 1. From Figure 2, one can note that if the transfer functions are not corrected, poor results are obtained compared to the theoretical results. From Figure 3 one can see that the three methods (3M2L, 4M2L and 3M-TMTC) compare very well. However, the 3M-TMTC shows a singularity at 2157 Hz, due to the tested resonant air layer which shows a zero particle velocity at $x = 0$ when $f = c_0/2d$ (here, $c_0 = 345$ Hz, and $d = 80$ mm).

Next, a 20-mm thick step discontinuity (see Figure 4) seeing as a non-symmetrical sample is tested and compared to the standard 4M2L method and 3M-TMTC method. One can note that similar results are obtained between the 3M2L and 4M2L methods, however 4M2L is noisier compare to 3M2L. The 3M2L results are also noisier compared to those of the air layer, due to the fact that the step discontinuity is quite reflective. In this case, microphones 1 and 2 may coincide with pressure nodes and microphone 3 may have a poor signal-to-noise ratio. The problem may be larger in 4M2L since microphone 3 is always at a maximum pressure in the 3M2L; which is not the case for the 4M2L. The 3M-TMTC results are not so good. This is due to the fact that the sample is backed on the rigid termination. In this case, microphone 3 is in the near field.


## ACKNOWLEDGEMENTS

N.S.E.R.C., REGAL, and ALCAN supported this work.


## REFERENCES


[1]Salissou and Panneton, J. Acoust. Soc. Am., 125(4), 2083 (2009)
[2]Lung and Dodge, J. Acoust. Soc. Am., 73, 867 (1983)
[3]Song and Bolton, J. Acoust. Soc. Am., 107(3), 1131 (2000)
[4]Allard et al., Wave Motion 17(4), 329 (1993)
[5]Panneton R., J. Acoust. Soc. Am., 125(3), 1490 (2009)
[6]Panneton R., Internoise Noise proceedings, 218, 4277 (2009)
[7]Salissou and Panneton, J. Acoust. Soc. Am., 128(5), 2868 (2010)
[8]Doutres et al., Appl. Acoust. 71(6), 506 (2010)
[9]Rodriguez et al., J. Acoust. Soc. Am., 192(5), 3056 (2011)


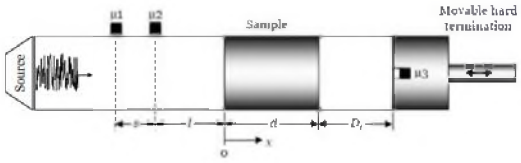


**Figure 1:** Experimental setup of the 3M2L

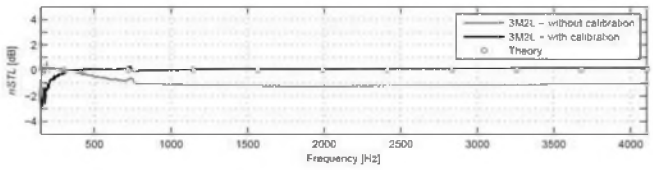


**Figure 2:** nSTL of a symmetrical sample (80-mm air layer). Comparison between the theory and the proposed 3M2L method with and without sensor-switching calibration

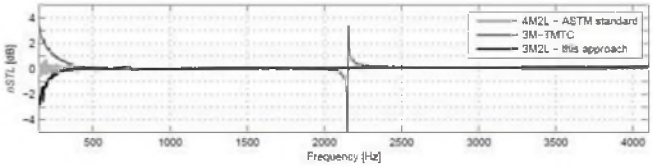


**Figure 3:** nSTL of a symmetrical sample (*80-mm* air layer). Comparisons between the proposed 3M2L method, the standard 4M2L method, and the 3M-TMTC method

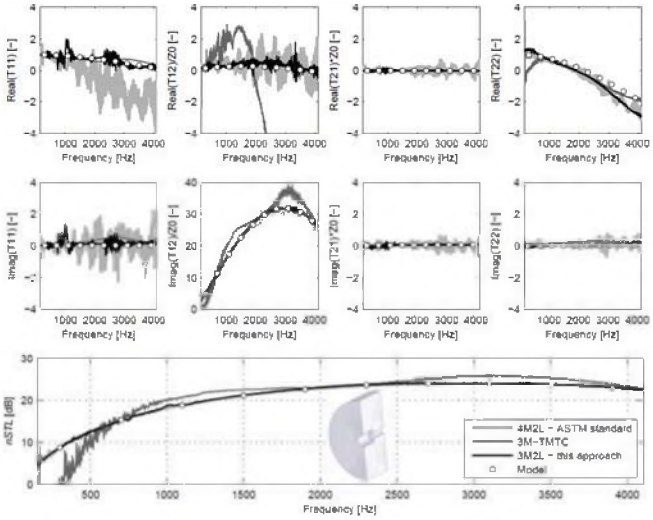


**Figure 4:** Transfer matrix coefficients and nSTL of an asymmetrical sample (step discontinuity). Comparisons between the proposed 3M2L method, the standard 4M2L method, and the 3M-TMTC method.

# ACOUSTIC MODEL FOR SHODDY-BASED FIBRE ABSORBERS

**John Manning and Raymond Panneton**
GAUS, Dept. of Mech. Engineering, Université de Sherbrooke, 2500 Boul. de l'Université, Quebec, Canada, J1K 2R1
John.Peter.Manning@USherbrooke.ca, Raymond.Panneton@USherbrooke.ca

## 1. INTRODUCTION

As the world becomes more mechanized and increasing populations push people closer together, the need for sustainable noise reduction and control methods become ever more important to maintain individual comfort and quality of life. Post-industrial and post-consumer recycled fibres, otherwise known as 'shoddies' have been used in the manufacture of fibrous noise absorbers for many years. Shoddies as a raw material have historically been a low cost, lower quality alternative but have recently garnered more attention as a sustainable alternative since they are sourced from diverted waste streams and are fully recyclable. The acoustic behaviour of shoddies is not well understood when compared to more ubiquitous porous materials such as fiberglass and certain polymeric foams. Designers must therefore rely on predictive models that are either highly complex or simpler models developed for different materials. Complex models such as the model developed by Biot[1] require several material properties that may be difficult to measure. Simpler models include those developed by Delaney and Bazley[2] for fiberglass and Garai and Pompoli[3] for PET fibres but to the author's knowledge no model exists for shoddy fibres.

This project seeks to investigate the acoustic behaviour of sound absorbers composed primarily of shoddy fibres and to create a simple predictive acoustic model based on the materials bulk density only. The model is semi-empirical, semi-phenomenological based on the equivalent fluid hypothesis.

## 2. METHOD

The sample set for this study consisted of three shoddy-based fibrous materials manufactured by three different techniques: thermal bonding, resin bonding and mechanical bonding. For each material, three constructions (unique combination of bulk density and thickness) were tested. Materials were tested directly for airflow resistivity and porosity. Static thermal permeability, viscous characteristic length and thermal characteristic length were determined using the indirect methods of Panneton-Olny[4,5]. Characteristic impedance, complex wavenumber and absorption were measured using an impedance tube for frequencies from 300 - 4000Hz. Empirical formulas were then derived that linked each parameter to the material's bulk density. In addition, estimates of the distribution of fibre diameter within each of the three materials were made based on a microscope analysis.

Several popular equivalent fluid models were chosen and populated with one or more of the parameters measured above depending on the complexity of the model. These models include: the model of Delaney and Bazley, two models proposed by Miki[6], the model of Johnson[7] in conjunction with the model of Champoux-Allard[8], and the model of Johnson in conjunction with the model of Lafarge[9]. Each model was evaluated based on its ability to effectively predict the materials characteristic impedance and normal incidence absorption and the most accurate model selected.

## 3. RESULTS

Estimates on the average fibre diameter for each material are as follows: mechanically bonded - 19.4μm, thermally bonded - 23.8μm, resin bonded - 19.7μm.

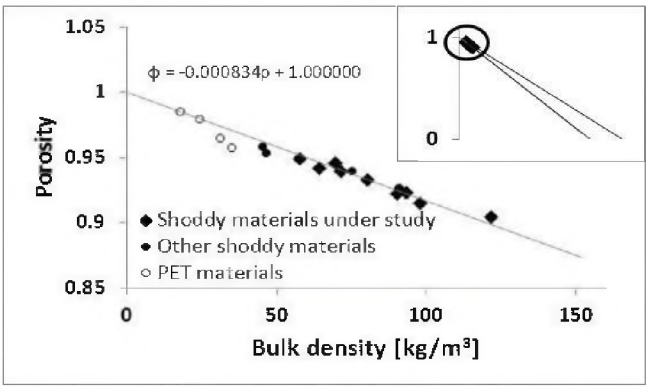


**Figure 1. Porosity as a function of bulk density.**

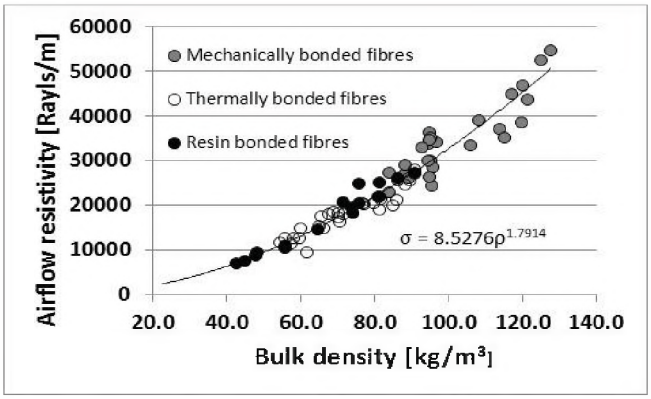


**Figure 2. Airflow resistivity as a function of bulk density.**

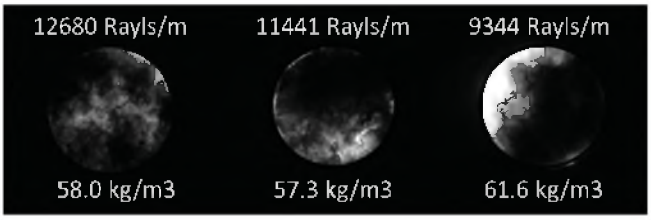


**Figure 3. Effect of web inhomogeneity on flow resistivity.**

**Table 1. Expressions linking model parameters to bulk density**

| | |
|---|---|
| Porosity ($\phi$) | $1-\phi = 0.000834\rho$ |
| Flow resistivity ($\sigma$) | $\sigma = 8.527\rho^{1.7914}$ [Rayls/m] |
| Tortuosity ($\alpha_\infty$) | $\alpha_\infty = 1$ |
| Viscous char. length ($\Lambda$)<br>Thermal char. length ($\Lambda'$)<br>[mech. bonded = mb]<br>[thermally bonded = tb]<br>[resin bonded = rb] | $\Lambda_{mb} = 28.1$, $\Lambda'_{mb} = 3.415\rho^{-1.928}$ x$10^5$<br>$\Lambda_{tb} = -0.746\rho+104.9$<br>$\Lambda'_{tb} = -0.755\rho+156.0$ [μm]<br>$\Lambda_{rb} = -0.874\rho+115.6$<br>$\Lambda'_{rb} = -1.416\rho+182.3$ |
| Static therm. perm. ($k_0'$) | $k_0' = 44.55\rho^{-1.269}$ [x$10^{-8}$ m$^2$] |

## 4. DISCUSSION AND CONCLUSIONS

Figure 2 shows the porosity to bulk density relationship with porosity defined as $\phi = 1$ - [solid volume/total volume]. For highly porous samples the differences in measured porosity is negligible between similar materials as illustrated in the top right inset chart of figure 2. As most shoddy-absorbers are manufactured with a high porosity, a single expression linking porosity to bulk density was chosen to describe the behaviour of all three material types.

Shoddy fibre absorbers are inherently more variable than homogeneous fibre materials. Poor textile recycling, dense fibre packing, poor fibre blending and adhesives cause localized differences in the web bulk density as shown in figure 3. Unfortunately these inhomogeneities occur on a scale at or near the sample size for measuring flow resistivity and acoustic parameters by standard means. This leads to scatter in the sample measurements. On average, the flow resistivity can be predicted well but individual results may vary widely. The effect can be mitigated by using a larger test sample, however, these tests are more expensive and labour intensive. The second pronounced effect is a microscopic one. Raw shoddy contains a haphazard mix of different fibre types and sizes and characterizing the microstructure for use in predictive models is difficult. Each material will possess a distinct flow resistivity - bulk density relationship that is dependent on fibre diameter. However, due to the uncertainty in the measurement of the average fibre diameter, the scatter in the resistivity vs. density data and in the interest of simplicity, a single power law expression has been chosen to reflect the dependence of airflow resistivity on bulk density for all three material types. The estimates of average fibre diameter may be used with a modified Bies-Hansen formulation[10] to derive individual flow-resistivity to density formulas for each material but the improvement is doubtful considering the variation in individual tests. Average fibre diameters are suggested to provide a reference for validity of the model in terms of fibre size and to enable comparisons with other models where fibre diameter is considered.

Table 1 summarizes the individual parameter's dependence on bulk density. Tortuosity is assumed to be unity as highly-porous fibrous materials regularly display a tortuosity very near to 1. The model exchanges a minor loss in precision for this simplification. Charts of the characteristic lengths and static thermal permeability have been omitted for brevity. The behaviour of the characteristic lengths is such that individual expressions relating the characteristic lengths to bulk density for each material type are chosen in favour of general expressions. The behaviour of thermally bonded and resin bonded materials are similar and adhere remarkably well to the 2:1, $\Lambda'$:$\Lambda$ ratio predicted by the theoretical expression for the characteristic lengths of highly porous fibre materials[11]. The behaviour of the mechanically bonded material begins to differ at high bulk densities, but it should be noted that at these densities, the mechanically bonded samples are approaching porosities for which highly porous assumptions are no longer valid. The method chosen for determining the characteristic lengths relies on acoustic measurements to determine the dynamic density and dynamic bulk modulus. The results of these tests can be affected by the web inhomogeneity problem. By comparing the characteristic lengths, acoustic results, flow resistivity tests and bulk density data, erratic samples were filtered out and were not considered in the derivation of the characteristic length - bulk density relations.

After populating each selected model with the relations outlined in table 1, the most accurate model at predicting acoustic indicators was the model of Johnson-Lafarge. It is suggested that this model be used to predict the acoustic behaviour of shoddy-based sound absorbers. The test samples are a good representation of the range of densities and thicknesses of the material that are commercially produced and the model is considered valid within this range.

## REFERENCES

[1]Biot, J. Acoust. Soc. Am., 28, 168 (1956).
[2]M.E. Delany and E.N. Bazley, Applied Acoustics, 3, 105 (1970)
[3]M. Garai and F. Pompoli, Applied Acoustics, 66, 1383 (2005)
[4]R. Panneton and X. Olny, J. Acoust. Soc. Am., 119, 2027 (2006)
[5]R. Panneton and X. Olny, J. Acoust. Soc. Am., 123, 814 (2008)
[6]Y. Miki, J. Acoust. Soc. Japan, 11, 19 (1990)
[7]D.L. Johnson et al, J. Fluid Mech. 176, 379 (1987)
[8]Y. Champoux and J.F. Allard, J. Appl. Phys. 20, 1975 (1991)
[9]D. Lafarge et al. J. Acoust. Soc. Am., 102, 1995 (1997)
[10]D.. Bies and C.H. Hansen, Applied Acoustics, 13, 357 (1980)
[11]J.F. Allard, Propagation of sound in porous media, Elsevier, NY (1993).

# TRANSMISSION LOSS OF A SOUND INSULATING PANEL MADE FROM CHARGED RECYCLABLE THERMOPLASTIC

**Jean-Philippe REGNARD, Raymond PANNETON, Saïd ELKOUN, and Rémy ODDO**
Department of Mechanical Engineering, University of Sherbrooke, Québec, Canada, J1K 2R1

## 1. INTRODUCTION

Nowadays, the design and fabrication of acoustic materials must integrate environmental regulations and sustainable development policies. Therefore it is not surprising that the use of recycled and/or recyclable materials is regarded as an effective way to comply with those rules [1-2]. Among available materials, thermoplastic polymers seem to be potential candidates for sound barrier applications due to their recyclability.

In the literature, many works deal with recycled thermoplastic-based sound absorbing materials but, in contrast, few works are really devoted to sound insulation materials [3].

This paper aimed at investigating the sound insulation property of composites made of recyclable thermoplastic charged with heavy particles. Then, their simulated transmission loss, in the frequency range of 10 to 10 kHz, is compared to those of commercial materials.

### 1.1 Theoretical Background

Figure 1 presents the theoretical evolution of transmission loss (TL) of an infinite panel as a function of frequency excited by an oblique incidence acoustic wave. Generally, the curve is characterized by the presence of three regions: (1) a mass-controlled region, (2) a critical frequency region, and (3) a stiffness-controlled region. The drop in the TL curve is limited by the structural damping of the panel. The frequency at which TL drops is termed critical frequency ($f_c$). It corresponds to the frequency where the natural bending wave speed of the panel equals the trace speed of the excitation acoustic wave.

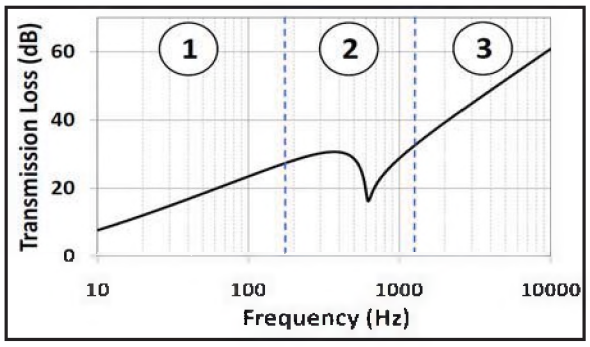


**Figure 1. Transmission loss of an infinite panel vs. frequency**

The critical frequency is given by:

$$f_c = \frac{c_0^2}{2\pi \sin^2\theta}\sqrt{\frac{\rho 12(1-\nu^2)}{Eh^2}}$$

where $\rho$ is the density of the material, $h$ the thickness of the wall, $E$ is Young modulus of the material, $\omega$ the angular frequency, $\theta$ the incidence angle of the acoustic wave, $\nu$ is the Poisson ratio, and $c_0$ the sound speed in air.

It is important to mention that $f_c$ is mainly dependent on Young modulus and shifted toward higher frequency as $E$ decreases. In addition and for better acoustic performances, it is preferable that $f_c$ is out of the frequency range of interest (*i.e.* > 10kHz). In other words, for large panels, TL vs. frequency of an optimal acoustic panel should exhibit only region 1, where TL is essentially governed by mass law. This latter is density-dependent primarily and increases with density. Accordingly, lowering $E$ and increasing $\rho$ or, in other words, decreasing ($E/\rho$) ratio is a good manner to enhance noise insulating properties of a given material. Consequently, in this work ($E/\rho$) ratio was taken as the criterion to evaluate the sound insulation perforrnance of various composites.

## 2. MATERIALS AND EXPERIMENTAL PROCEDURE

### 2.1 Materials

Polyethylene (PE) is the most used thermoplastic polymer worldwide. Behind this generic name lies several types of PE, where linear low density polyethylene (LLDPE) is the most common one. It is characterized by a Young modulus and density of 700 MPa and 930 kg/m$^3$, respectively. In this work, the LLDPE Sclair FP-120A, purchased from Nova Chemicials, was used.

It is important to point out that the density of LLDPE is lower than those of the conventional materials used in construction (*e.g.* 2200 kg/m$^3$ for concrete). Consequently, it's necessary to increase LLDPE density by, for instance, adding heavier particles.

Metal particles are often used to improve the electrical properties of materials; however Young modulus increases too [4]. Nonetheless, it has been shown that the use of large spherical particles can limit this increase [5]. Consequently to increase significantly the density of LLDPE, 3.175 mm radius metal beads were added to LLDPE matrix.

### 2.2 Sample preparation

LLDPE/metal beads composites having a volume fraction $\phi$ of 0, 12.5 and 23%, respectively, were elaborated by compression melt molding at 250°C using a hydraulic press. All samples were held at 250°C for 15 minutes and then air cooled to room temperature. Three samples were made for 0 and 12.5% concentrations while 2 were elaborated for the 23% composition.

During samples fabrication, a particular attention was paid to samples preparation in order to have a random beads distribution and an average distance between beads lower than the lower wavelength $\lambda$ corresponding to the highest frequency in frequency range of interest (i.e. 10 kHz or $\lambda \approx$ 3.4 mm).

### 2.3 Characterization

To analyze acoustic property of elaborated composites ($E/\rho$) ratio is required. Therefore, tensile mechanical tests, following ASTM E 756-04 standard, were carried out to determine Young modulus of all composites. Subsequently, and in order to reduce composites rigidity, samples microstructure was modified by subjected all composites to a special procedure. Then, Young modulus was again re-evaluated. Buoyancy method was used to assess the composites density.

## 3. RESULTS

Table 1 depicts ($E/\rho$) ratios for unmodified and modified composites. As can be seen ($E/\rho$) ratio decreases as $\phi$ increases and, as expected, the induced micro-structural modification decreases more significantly the ratio.

**Table 1. $(E/\rho)$ for unmodified and modified composites**

| $\phi$ (%) | $(E/\rho)_{\text{unmodified composite}}$ | $(E/\rho)_{\text{modified composite}}$ |
|---|---|---|
| 10.9 | $0.67_1$ | $0.51_9$ |
| 12.4 | $0.62_6$ | $0.41_8$ |
| 13.8 | $0.61_8$ | $0.43_2$ |
| 23.2 | $0.50_7$ | $0.32_6$ |
| 23.4 | $0.53_4$ | $0.31_8$ |

Simulated TL for infinite panels was obtained, by means of NOVA vibro-acoustic software. Figure 4 shows the simulated TL of the 23% LLDPE/beads composite and the TL of 4 mm thickness conventional materials such as concrete, glass and gypsum.

As it can clearly be seen, the composite with $\phi$=23% appears to be better than conventional materials. Indeed, the TL vs. frequency curve of this composite shows either higher or equal TL than gypsum, concrete or glass but, in contrast, the coincidence frequency, $f_c$, is no longer present.

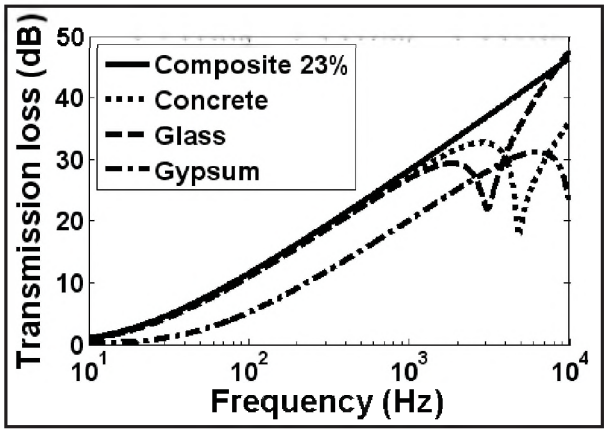


**Figure. 3. Transmission loss vs. frequency of an LLDPE/beads composite and conventional materials**

## 4. CONCLUSION

In this work, it was shown that the sound insulation properties of a material made of recyclable thermoplastic can be assessed by the rigidity to density ratio, ($E/\rho$) and, enhanced by reducing this ratio. Consequently, this ratio was used to evaluate the acoustic performances of composites, elaborated by compression melt molding and consisting of linear low density polyethylene, a thermoplastic polymer, and metal beads. Furthermore, all composites were subjected to a particular procedure to induce micro-structural changes in order to lower more ($E/\rho$) ratio. Finally it was clearly demonstrated that modified composites exhibits no coincidence frequency in the frequency range of interest, and have higher or similar transmission loss as compared to conventional materials such as concrete, glass or gypsum.

## REFERENCES

[1] Saadeghvaziri, M. A., MacBain, K. (1998). Sound barrier applications of recycled plastics. Transportation Research Record, n° 1626, p. 85-92.

[2] Asdrubali, F. (2006). Survey on the acoustical properties of new sustainable materials for noise control. Acta Acustica United With Acustica, vol. 92, p. S89.

[3] Choi, J.-W., Hwang, Y. (2010). Preparation and sound insulation properties of thermoplastic elastomer composites with CaCO3 filler, Korean Journal of Materials Research, Japan, volume 20, issue 9, p. 467 – 471.

[4] Nurazreena, Hussain, L.B., Ismail, H., Mariatti, M. (2006). Metal filled high density polyethylene composites – Electrical and tensile properties. Journal of Thermoplastic Composite Materials, Vol. 19, Issue 4, p. 413 – 425.

[5] Shao-Yun, F. et al (2008). Effects of particle size, particle/matrix interface adhesion and particle loading on mechanical properties of particulate–polymer composites. Composites Part B: engineering, Vol. 39, Issue 6, p. 933 – 961.

# ASSESSMENT OF ACOUSTIC PROPERTIES OF DIFFERENT RECYCLED POLYMER-BASED MATERIALS FOR ROAD WORK SOUND BARRIER WALLS APPLICATION

**Julien Biboud, Raymond Panneton, Saïd Elkoun, and Rémy Oddo**
Department of Mechanical Engineering, GAUS, Université de Sherbrooke, Sherbrooke, Qc, Canada, J1K 2R1

## 1. INTRODUCTION

Due to their high sound absorption efficiency, rock and glass wools are largely used as sound absorber materials and particularly for the design of sound barrier panels. However, their fabrication is highly energy-consuming. Indeed, rock and glass used in the wool fabrication process required high temperatures (i.e. above 1,000°C), which are much higher than any polymer processing temperatures. In addition, centrifuges and burners, two energy-consuming equipments, are also required for fiber forming process [1]. Besides, the process is not over yet as wool has no mechanical strength. Accordingly, a thermoset resin, such as phenolic resin, is sprayed over fibers where it polymerizes and cross-links. Generally, the amount of resin used varies between 1 to 5% and 4 to 14% for rock and glass wools respectively [2]. It is important to highlight that cross-linking process is irreversible. Thus, if environmental concerns and sustainable development policies must be taking into account, the use of rock or glass wool as sound absorbent materials may be no longer adequate.

The objective of this paper is to investigate on environmentally-friendly alternatives for rock and glass wools in sound barrier walls applications. To achieve this goal, various recycled fibers-based materials were characterized and compared to evaluate their sound absorption potential. Eventually, best materials will be incorporated in an experimental on-scale sound barrier wall and tested.

## 2. MATERIALS AND EXPERIMENTS

### 2.1. Materials

To meet the objective of the study, the criteria to select materials are twofold. Indeed, chosen materials *i)* must be recycled and *ii)* exhibit acoustical performance. To satisfy both criteria and knowing that porosity is one of the key parameters for sound absorption efficiency, materials selection could be among recycled fiber-polymers category.

Table 1 depicts selected materials. For sake of simplicity selected materials were termed A, B, C and D respectively. The various entries of the table indicate the polymer fibers type, origin, and supplier's name.

**Table 1. Description of selected materials**

| Material designation | Type of polymer fibers | origin | Supplier |
|---|---|---|---|
| A | Polyester | Post-industrial | Leigh textile (Montreal, Qc, Canada) |
| B | Blend | Residential carpet waste | |
| C | Cotton | Post -consum-mation clothes | |
| D | Cotton | recycled cotton-based insulation | Jasztex (Montreal, Qc, Canada) |

### 2.2. Experiments

Around road-work construction sites, the most disturbing frequencies are between 500 and 2,000 Hz. Therefore, the materials should be acoustically efficient within this frequency range, and all measurements should be carried out, at least, on this frequency range.

Sound absorption coefficients were assessed in laboratory on small specimens and in-situ on an on-scale sound barrier wall.

Laboratory measurements

Absorption coefficient was measured by means of an impedance tube following the standard method ASTM E 1050-98. All tests were performed on 44.45 mm diameter samples with a thickness of 50 mm for materials A, B and C and 67 mm for material D. Under this configuration, the validity frequency range of measurements lies between 150 to 4,000Hz.

In-situ measurements

To obtain material absorption property and insertion loss, an experimental sound barrier wall was built (figure 1). This wall is characterized by three 4x4 m sections composed of 6 removable panels made of galvanized steel perforated on one side and filled with sound absorber.

**Figure 1. Experimental on-scale sound barrier wall**

Physical properties measurements

Generally to simulate the sound absorption coefficient *versus* frequency of selected materials using a model such asthe Johnson–Champoux-Allard (JCA) model [3], the knowledge of porosity ($\phi$), density ($\rho$), airflow resistivity ($\sigma$), tortuosity ($\alpha_\infty$), viscous ($\Lambda$) and thermal characteristic lengths ($\Lambda$') is needed. Thus, porosity and density were determined using a pressure mass method described by the Salissous and Panneton [4] while the other parameters were measured following the method described by Attala and Panneton [5]. Table 2 presents the obtained parameters for the 4 selected materials (i.e. A, B, C and D).

**Table 2. Measured physical properties of selected materials**

| Materials | $\rho$ *(kg/m$^3$)* | $\Phi$ *(%)* | $\sigma$ *(Ns/m$^4$)* | $\alpha_\infty$ *(-)* | $\Lambda$ *(μm)* | $\Lambda$' *(μm)* |
|---|---|---|---|---|---|---|
| **A** | 85 | 99 | 18,428 | 1 | 87.6 | 721.6 |
| **B** | 100 | 84 | 20,277 | 1 | 72.3 | 466 |
| **C** | 45 | 95 | 18,184 | 1 | 58.8 | 875 |
| **D** | 26.5 | 95 | 3,730 | 1 | 164 | 490 |

## 3. RESULTS

Figure 2 shows the absorption coefficient as a function of frequency for the 4 selected materials. For sake of comparison, simulated absorption curves of rock and glass wools were also included. As can be seen, materials A, B and C have similar absorption coefficients over the whole range of frequency. More interestingly, those 3 materials seem to be better than rock or glass wool as they exhibit higher absorption coefficients. Only material D appears to be less efficient in spite of its larger thickness. This result can be ascribed to a lack of compaction as it has the lowest density among the 4 selected materials. Consequently one can, reasonably, expect that, if compactness of this material is increased, sound absorption coefficient of this material would be, at least, comparable to that of material C which is cotton-based material.

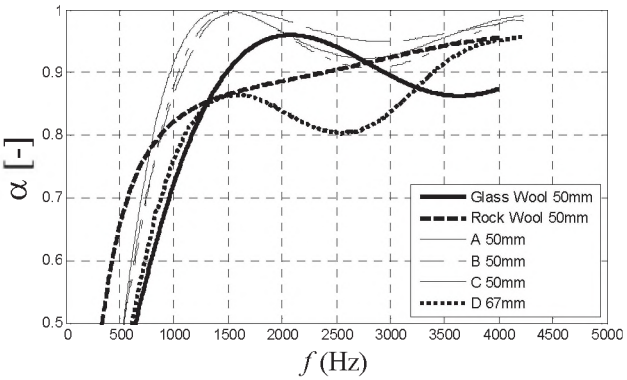


**Figure 2. Comparison of measured absorption coefficients of selected materials and simulated absorptions of rock and glass wools.**

Following these results, some selected materials will be tested on the experimental on-scale sound barrier wall. The acoustic characterization and modeling are presently underway and the results will be presented at the conference.

## 4. CONCLUDING REMARKS

In this paper sound absorption efficiency of 4 selected recycled polymer-based materials were investigated. It was shown that, in terms of sound absorption, the selected recycled fiber-polymers seem to be equal or better than rock or glass wool. Due to this encouraging result, acoustic characterization of the recycled material on an experimental on-scale sound barrier wall and modeling are presently in progress.

## REFERENCES

[1] Lehamann J.-C. (2010), Formulation du verre et produits verriers, Techniques de l'ingénieur, J 2 296, p.13.

[2] Chevalier M. (1991), Phénoplastes ou phénols-formols, Technique de l'ingénieur, A 3 435, p.19.

[3] Allard J.F. and Champoux Y. (1992), New empirical equations for sound propagation in rigid frame fibrous materials, J. Acoust. Soc. Am. 91(6), 3346-3353.

[4] Salissous, Y. and Panneton, R. (2007). Pressure/mass method to measure open porosity of porous solids. J. Appl. Phys. 101, 124913.1-124913.7.

[5] Atalla, Y. and Panneton, R. (2005). Inverse acoustical characterization of open cell porous media using impedance tube measurements. Canadian Acoustics, volume 33, numéro 1, p. 11-24.

## ACKNOWLEDGEMENTS

The authors would like to thank the Ministère des Transports du Québec (MTQ) for financial support and Leigh Textile and Jasztex for providing materials.

# SWITCHGRASS-BASED NOISE ABSORBING MATERIAL: CHARACTERIZATION AND MODELING

**K. Verdière[1], R. Panneton[1], S. Elkoun[1], J. M. Lavoie[2] and R. Oddo[1]**
[1] Department of Mechanical Engineering, GAUS, Université de Sherbrooke, Sherbrooke, Qc, Canada, J1K 2R1
[2] Department of Chemical Engineering, Université de Sherbrooke, Sherbrooke, Qc, Canada, J1K 2R1

## 1. INTRODUCTION

For decades, noise reduction on road construction sites has been a major issue for transportation agencies worldwide. Noise pollution is a real health concern in our modern society and frequent or permanent exposure to noise can cause irreversible health damage such as permanent hearing loss. One effective way to decrease noise in construction sites is to build sound-absorbing barrier walls. However, and in addition to have appropriate acoustic properties, the design and fabrication of such walls must comply with environmental regulations and sustainable development policies. Consequently, developing sound or absorbent barrier materials made of plant or plant residues can be regarded as an effective way to take environmental concerns into account. In this work, the potential of using *Panicum virgatum* (switchgrass), a tallgrass plant largely available in North America, as an acoustic absorbent was investigated. Thus, in this paper, the sound absorption coefficient of switchgrass-based material was assessed and modeled.

## 2. MATERIAL, SAMPLES PREPARATION AND TECHNIQUES

### 2.1. Material

Switchgrass is a tall grass plant largely present in North America and especially in Canada. It grows from rhizomes and is characterized by stems that can reach, like bamboo or sugarcane, up to 2 meters high. Moreover, its roots can be as deep as 2 meters. This plant belongs to the perennial plants family, meaning that after a 2 year growth period it can live up to 10 years. Switchgrass is actually investigated for energy production (including fuel pellets or bioethanol), soil conservation and erosion and, to a lesser extent, as feedstock for bioplastics production.

### 2.2. Sample preparation

In order to characterize and model the plant absorption performances, switchgrass stems were cut at various lengths (ranging from 5 to 40 mm) and were randomly stacked (figures 1a and 1b). Porosity and density measurements were performed on disc-shaped specimens (100 mm diameter by 90 mm thick).

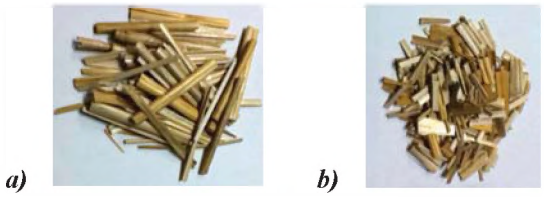


**Figure 1. Randomly stacked switchgrass with stems length of: a) 40 mm and b) 10 mm**

### 2.3. Techniques

The porosity and density were determined using a pressure mass method that was previously reported in literature [1]. It is important to mention that during the measurement, samples were not compressed, the only pressure to which they were subjected being their own weight. For all prepared specimens, absorption coefficient was obtained according to the ASTM E 1050-98 method whilst the absorption tests were obtained following testing made on a 100 mm diameter impedance tube (Brüel & Kjær Type 4206) using 90 mm thick samples. Besides, all the measurements were performed in the frequency range of 200 to 2,000 Hz which corresponds, somewhat well, to the frequency range of noise in construction sites.

## 3. RESULTS AND MODELLING

### 3.1. Effect of stems length on the sound absorption coefficient

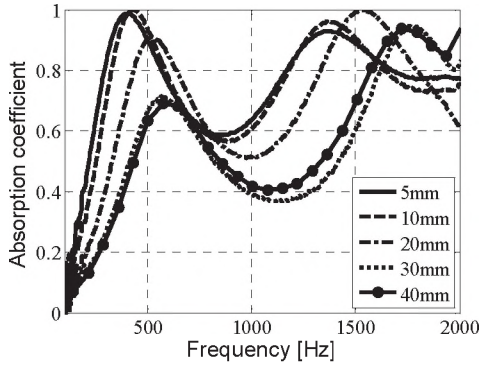


**Figure 2. Sound absorption coefficient vs. frequency of randomly stacked switchgrass with various stem lengths.**

Figure 2 depicts absorption coefficient as a function of frequency for randomly stacked switchgrass with stem lengths varying from 5 to 40 mm. As can be seen, absorption coefficient increases and the maxima shifted toward lower frequency as stem length decreases.

### 3.2. Modelling

#### 3.2.1. Johnson Champoux Alard's model (JCA)

In order to simulate the sound absorption coefficient *versus* frequency of the randomly stacked switchgrass stems, the Johnson Champoux Alard model (JCA) was used [2]. The JCA model requires 5 parameters in order to calculate the sound absorption: porosity, airflow resistivity, tortuosity, viscous and thermal characteristic lengths. These parameters were determined experimentally.

**Table 1. Parameters of Johnson Champoux Alard's model**

| Stem length (mm) | Porosity | Resistivity ($N.m^{-4}.s$) | Lv (µm) | Lth (µm) | Tortuosity |
|---|---|---|---|---|---|
| **5** | $0.77_5$ | 3660 | 123.7 | 480.6 | $2.3_9$ |
| **10** | $0.78_6$ | 1359 | 153.2 | 688.5 | $2.5_0$ |
| **20** | $0.81_4$ | 150 | 258.6 | 905.1 | $2.3_2$ |
| **40** | $0.84_6$ | 1 | 441.5 | 1293.5 | $2.1_0$ |

#### 3.2.2. Kim *et al.* 's model

To simulate the sound absorption of porous concrete, Kim *et al.* have proposed a model based on the theory of spheres packing [3]. This model takes into account geometrical parameters of spheres, the porosity and the space between two adjacent layers of spheres (compactness). In our case, this approach can be applied as far as one can approximate the shape of switchgrass stems by a sphere. This assumption is verified as far as width and length of stems are in the same order of magnitude. Thus, for this study, such a model can reasonably be applied to short stem lengths such as 5 mm.

**Table 2. Parameters of Kim *et al.* 's model**

| Porosity | Radius of aggregates (mm) | Diameter of apertures (mm) | Shape of aggregates | Thickness (mm) |
|---|---|---|---|---|
| $0,77_5$ | 1 | 0.5 | Packed lattice (k=1) | 90 |

#### 3.2.3. Comparison

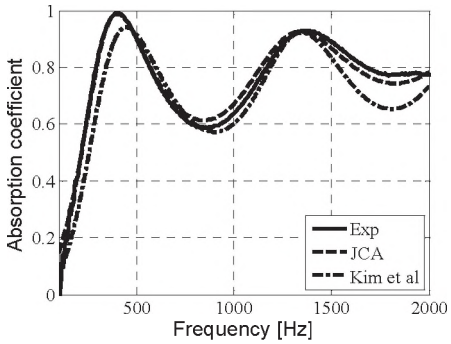


**Figure 3. Comparison between sound absorption obtained using JCA and Kim et al. models and experimental data**

Figure 3 compares the sound absorption obtained with the JCA and Kim *et al.* models to experimental data for the 5 mm length stems randomly stacked switchgrass. As can be seen, both models show similarities with the empirical values; however the JCA model seems to be better as it matches the measured absorption coefficient over the whole range of frequency.

#### 3.2.4. Robustness of models

To validate parameters of both models and consequently to test their robustness, all parameters were kept constant and a simulation was performed on a 100 mm diameter and 44 mm thick sample. Then, the sample was elaborated and its absorption coefficient was assessed and compared to simulated values (figure 4). As can be seen, the simulated and evaluated absorption coefficients match which allows validation of the modeled parameters. Again in that case, the JCA model seems to be better than Kim *et al.* 's model.

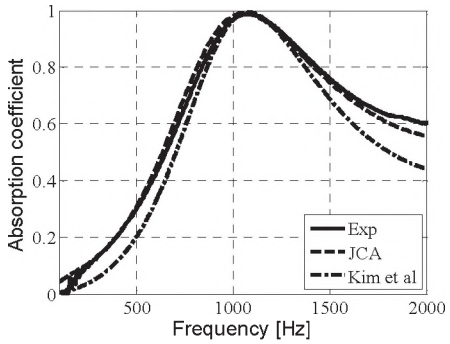


**Figure 4. Validation of JCA and Kim's parameters models**

## 4. CONCLUSION

In this paper, the potential of using switchgrass as noise absorbent material was investigated. Thus, samples of randomly stacked switchgrass stems of various lengths were elaborated and characterized. Two models were used to simulate the sound absorption coefficient and compared to experimental data. The Johnson Champoux Alard model was shown to be the most reliable model which allows the assumption that it can be used to find the optimal thickness for the design of switchgrass-based sound absorbing panels.

## REFERENCES

[1] Salissous, Y. And Panneton, R. (2007). Pressure/mass method to measure open porosity of porous solids. J. Appl. Phys. **101**, 124913.1-124913.7

[2] Allard, J. F., Atalla, N. (2009). Propagation of sound in porous media: modeling sound absorbing materials (2nd ed.), Elsevier Applied Science, New York.

[3] Kim, H. K. et Lee, H. K. (2010). Acoustic absorption modeling of porous concrete considering the gradation and shape of aggregates and void ratio. J. Sound and Vib. **329** (7), 866-879.

## ACKNOWLEDGEMENTS

The authors would like to thank the Ministère des Transports du Québec (MTQ) for its financial support.

# UTILISATION DE TECHNIQUES DE REPRODUCTION DE CHAMPS SONORES POUR LA SYNTHÈSE DE CHAMPS SPATIALEMENT CORRÉLÉS

**Olivier ROBIN[1], Rokhiya DIA[1], Alain BERRY[1] et Stéphane MOREAU[1]**
[1]GAUS, Université de Sherbrooke, 2500, Bd de l'Université, Sherbrooke, QC, J1H1K3, CANADA

## 1. INTRODUCTION

De nombreuses structures peuvent être soumises à des fluctuations de pression pariétale, souvent conséquences de leur vitesse de déplacement dans un fluide (fuselage d'avion, coque de sous-marin) et pouvant contribuer au rayonnement acoustique de la structure (bruit intérieur). Ces fluctuations sont aléatoires, de structure complexe et comportent une composante acoustique et une composante fonction de la vitesse de convection.

Quel que soit le champ aléatoire considéré, sa reproduction expérimentale et donc le test vibroacoustique de pièces mécaniques reste une tâche ardue. Celle d'un Champ Acoustique Diffus (CAD) en chambres couplées montre souvent des imperfections. La synthèse d'une Couche Limite Turbulente (CLT) parfaitement développée demande des mises en œuvre complexes et coûteuses en souffleries, qui comportent souvent des environnements acoustiques et vibratoires difficiles à maîtriser. La distinction des composantes acoustiques et convectives est également une problématique encore largement explorée, que ce soit en termes d'instrumentation ou de traitement des données de mesure [Arguillat, 2010]. La reproduction sur une surface d'une CLT dans des conditions maîtrisées a été envisagée à l'aide d'un réseau de haut-parleurs en champ proche [Bravo, 2011], ou d'une antenne synthétique [Aucejo, 2010].

Nous proposons ici deux méthodes pour la reproduction de la partie acoustique de ces champs aléatoires. Les Densités Interspectrales de Puissance (DIP) les décrivant sont utilisées pour simuler la synthèse de champs sur un plan grâce à un réseau plan de monopôles. On suppose que les champs d'intérêt peuvent être décrits par une superposition d'ondes planes. Les résultats sont analysés dans le domaine fréquence - nombre d'onde.

## 2. MÉTHODES DE REPRODUCTION DE CHAMPS

### 2.1 Wave Field Synthesis

La « Wave Field Synthesis » (WFS) est une méthode de reproduction spatiale de champs sonores qui utilise un ensemble de haut-parleurs. Cette technique est basée sur le principe de Huygens qui a comme idée de remplacer par des sources secondaires un front d'onde rayonné par une source primaire [Berkhout, 1993]. L'approche théorique consiste à utiliser l'intégrale de Kirchhoff-Helmholtz afin de définir un champ de pression sur une surface ② où les sources de reproduction sont placées à partir d'un champ de pression cible sur une surface parallèle ① (voir figure 1). Le champ de vitesse des sources est ensuite déduit grâce à l'équation d'Euler, ce qui permet finalement de déterminer le champ de pression reconstruit avec l'intégrale de Rayleigh.

### 2.2 Holographie acoustique

L'holographie acoustique est une technique très répandue pour la prédiction de la pression acoustique ou de la vitesse particulaire par l'intermédiaire d'une mesure de ces mêmes quantités sur une surface [Williams, 1999]. Elle est plus rarement envisagée comme une technique de reproduction, pour par exemple imposer des vitesses particulaires dans un plan afin de synthétiser un champ de pression dans un autre plan. Les relations de l'holographie sont ici utilisées pour propager un champ de pression à synthétiser sur une surface de reproduction ① vers un réseau plan de sources ②, et pour définir les vitesses particulaires à imposer à ces mêmes sources (voir figure 1).

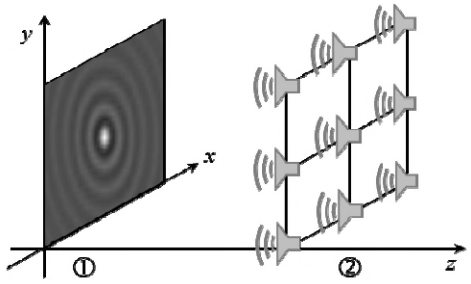


**Figure 1. Schéma de principe des deux méthodes; la DIP spatiale à reproduire, sur le plan 1, est celle d'un CAD**

## 3. CHAMPS SPATIALEMENT CORRÉLÉS

Le CAD théorique correspond à une superposition aléatoire d'ondes planes se propageant à la célérité des ondes acoustiques $c_0$ (nombre d'onde $k_0=\omega/c_0$), et réparties de façon isotrope en espace (champ défini à une fréquence donnée). L'expression analytique de sa DIP spatiale et en nombre d'onde peut être trouvée dans [Arguillat, 2010].

La CLT peut être également théoriquement décrite par une superposition d'ondes planes décorrélées. Par contre, son spectre en nombre d'onde n'est pas limité au seul cercle acoustique de rayon $k_0$, est fortement anisotrope et dicté par la vitesse de convection $U_c$. Elle définit le maximum de l'énergie d'une CLT (le pic convectif) situé en un nombre d'onde $k=k_c$ $(=\omega/U_c)$ selon la direction de l'écoulement, ici $k_x$ (le spectre selon $k_y$, direction transverse à l'écoulement, est symétrique autour de 0). Le modèle de Corcos [Corcos, 1963] est utilisé ici, dont l'expression de la DIP spatiale et en nombre d'onde sont données dans [Aucejo, 2010].

## 4. RÉSULTATS

Toutes les simulations sont effectuées pour une fréquence de 1000 Hz (λ=0,34m). Deux surfaces planes espacées de λ/2 sont considérées. Leurs dimensions sont égales ([-3λ;3λ]), et la discrétisation du plan de sources est de λ/2. La DIP de pression $S_{pp}$ générée sur le plan de reproduction, par l'imposition de la DIP de vitesse au réseau de sources, est calculée à l'aide de l'intégrale de Rayleigh. Les figures 2 et 3 illustrent des résultats de simulation obtenus pour un CAD et une CLT (seule la direction $k_x$ est considérée ici). La propagation est supposée se dérouler dans des conditions de champ libre.

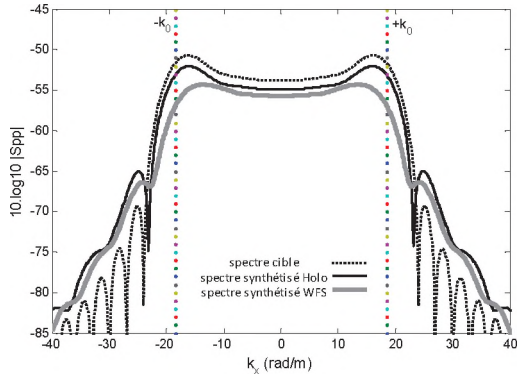


**Figure 2. Reproduction d'un CAD – Comparaisons entre spectre à reproduire et spectre reproduit**

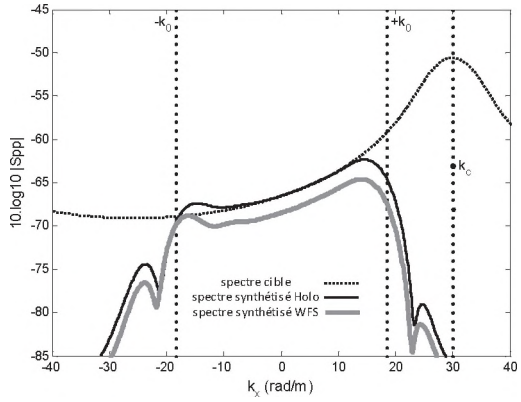


**Figure 3. Reproduction d'une CLT subsonique (basée sur un modèle de Corcos – $U_c$=210 m/s)**

Que ce soit pour un CAD ou une CLT subsonique, l'allure de la partie acoustique en nombre d'onde est correctement reproduite. Le cas d'une CLT supersonique a également été exploré, et fournit de bons résultats. Un point important à souligner est la reproduction des phénomènes 'souhaités' : pour le CAD, un phénomène isotrope, sans direction de propagation privilégiée; pour la CLT, un phénomène effectivement propagatif dans la direction de l'écoulement est synthétisé.

L'erreur de reproduction en amplitude est définie comme la moyenne quadratique de l'écart en valeur absolue entre spectre à reproduire et spectre reproduit (normalisée par la valeur absolue du spectre cible). Elle est calculée dans le domaine des nombres d'onde acoustiques ($k \leq |k_0|$). Pour la reproduction d'un CAD, l'erreur de reproduction pour la WFS (holographie) est de 28,6 % (11,8 %). Dans le cas de la CLT, l'erreur de reproduction est de 30 % (10,1 %).

## 5. DISCUSSION ET CONCLUSION

Les résultats de simulation obtenus montrent que la reproduction dans le domaine acoustique d'un CAD ou d'une CLT fournit de bons résultats. L'allure des spectres en nombre d'onde est correctement reconstruite, et les erreurs en amplitude sont globalement comprises entre 10 et 30 % pour le cas considéré. L'holographie acoustique fournit ici des résultats sensiblement meilleurs que la WFS. Mais comparativement, l'approche WFS peut être étendue facilement à des géométries plus complexes, et demande également moins de traitements des signaux (opérations dans le domaine spatial uniquement, aucune transformée de Fourier). Nous estimons donc que les deux approches présentent un intérêt pour cette reproduction.

Un des points qui peut paraître restrictif est la limitation au domaine acoustique. Néanmoins, cela convient naturellement pour un CAD, et pourrait permettre d'éviter d'utilisation de chambre réverbérante par l'utilisation de réseau de sources face à des panneaux à tester. De plus, la possibilité de reproduire la partie acoustique dans des conditions maitrisées permet de comparer la réponse de structures sous excitation isotrope et anisotrope, ce qui est déjà un point d'importance. D'autre part, on peut envisager de mieux analyser les contributions respectives des composantes acoustiques et convectives dans le cas d'une CLT.

## RÉFÉRENCES


Arguillat, B., Ricot, D., Bailly, C., Robert, G. (**2010**). "Measured wavenumber: Frequency spectrum associated with acoustic and aerodynamic wall pressure fluctuations," J. Acoust. Soc. Am. **128(4)**, 1647-1655.

Aucejo, M., Maxit, L., Guyader, J.-L. (**2010**). "Utilisation d'une antenne synthétique pour simuler l'effet d'une couche limite turbulente," in *Proceedings 10ème Congrès Français d'Acoustique* (Lyon, 12-16 avril 2010).

Berkhout A. J., De Vries D., Vogel P., (**1993**). "Acoustic control by wave field synthesis," J. Acoust. Soc. Am. **93**(5), 2764-2778.

Bravo, T., Maury, C., (**2011**). "A synthesis approach for reproducing the response of aircraft panels to a turbulent boundary layer excitation," J. Acoust. Soc. Am. **129**(1), 143-153.

Corcos, G.M. (**1963**). "Resolution of pressure in turbulence," J. Acoust. Soc. Am. **35**(2), 192-199.

Williams, E.G. (**1999**). *Fourier Acoustics : Sound Radiation and Nearfield Acoustic Holography* (Academic Press).


## REMERCIEMENTS


Les auteurs remercient le CRSNG et Bombardier Aéronautique, au travers de la chaire d'acoustique appliquée à l'aviation.

# SOURCE LOCALIZATION OF AIRCRAFT ENGINES WITH CIRCULAR MICROPHONE ARRAYS

**Iman Khatami[1] and Alain Berry[2]**

[1]Dept. of Mechanical Engineering, Université de Sherbrooke, 2500 Boulv. de l'université, Sherbrooke, Québec, Canada, J1K2R1, Iman.Khatami@usherbrooke.ca

[2] Dept. of Mechanical Engineering, Université de Sherbrooke, 2500 Boulv. de l'université, Sherbrooke, Québec, Canada, J1K2R1, Alain.Berry@usherbrooke.ca

## 1. INTRODUCTION

Turbo-engines are an important of exterior noise of jet aircraft. Many researchers have attempted to develop methods to identify and locate the various noise sources of aero-engines (fan, compressor, turbine, combustion, jet exhaust). Among the acoustical localization techniques, the beamforming method [1] and Inverse method [2] are very common. In a recent past, hybrid methods using subspace analysis and beamforming have been particularly developed, such as the MUSIC [3] and ESPRIT [4] methods. The aim is to split relevantly signal and noise components into identified subspaces to attenuate the measurement noise. Sarradj [5] proposed a different subspace-based beamforming method focused on signal subspace and leading to a computationally efficient estimation of the source strength and location. The general idea of these approaches is to improve the performance of beamforming by estimating the assigned distribution of sources through the solution of an inverse problem. Recently inverse problems in acoustic imaging have been devoted to the selection of the optimal regularization parameter [6] which is a key aspect of inverse problems.

The goal of this research is the discrimination of inlet and exhaust sources in aircraft engines using far field microphone arrays. The proposed acoustic source identification method in this study is based on a combination of inverse modeling and conventional beamforming. It was initially investigated at university of Sherbrooke for sound field extrapolation in small, closed environments based on sound field measurement with a microphone array. The method has proven to provide source localization in free-field, diffuse field and modal situations with a better spatial resolution than conventional beamforming and inverse methods.

## 2. METHODS

This section discusses inverse problems in general as well as Tikhonov regularization theory and presents the beamforming regularization approach proposed in this research.

### 2.1 Inverse Method

We assume here that the acoustic sources are represented by a set of $L$ point sources and also there are $M$ microphones to measure the magnitude of the sound sources. The sampled direct radiation problem is written in matrix form

$$\mathbf{p} = \mathbf{G}\mathbf{q} \tag{1}$$

Where $\mathbf{p}$ is a $M \times 1$ vector of complex sound pressure values at the microphone locations, $\mathbf{G}$ is a $M \times L$ vector matrix of free-field Green's functions between the $L$ point sources and $M$ sound pressure measurement points, $\mathbf{q}$ is a $L \times 1$ vector of unknown complex source strengths. In the inverse method, the minimization of the 2-norm of the error between the reconstructed sound pressure $\mathbf{p}$ assuming a set of $L$ point sources and the measured sound pressure $\hat{\mathbf{p}}$ is calculated. The problem is then to find the optimal $\mathbf{q}$ for the minimization problem

$$\boldsymbol{q}_{opt} = arg\ min\{|\hat{\mathbf{p}} - \mathbf{G}\mathbf{q}|^2\} \tag{2}$$

Most of the time the inverse problem is ill-conditioned, implying that the solution $\boldsymbol{q}_{opt}$ is very sensitive to measurement noise and model uncertainty. To prevent this problem, Tikhonov regularization method is used [6],

$$\boldsymbol{q}_{opt} = arg\ min\{|\hat{\mathbf{p}} - \mathbf{G}\mathbf{q}|^2 + \lambda^2|\mathbf{L}\mathbf{q}|^2\} \tag{3}$$

where λ is the regularization parameter and $\mathbf{L}$ is the discrete smoothing norm used to shape the regularization. The solution of this minimization problem is

$$\boldsymbol{q}_{opt} = \frac{\boldsymbol{G}^H\mathbf{p}}{\boldsymbol{G}^H\mathbf{G} + \lambda\boldsymbol{L}^H\mathbf{L}} \tag{4}$$

### 2.2 Beamforming Regularization (Hybrid)

The main idea behind the proposed hybrid approach is to find a "best" smoothing norm $\mathbf{L}$ in our problem. This can be done by observing that part of the solution given by eq 4 involves a beamforming delay-and-sum operation. In this case the beamforming delay-and-sum operation is given by

$$\boldsymbol{q}_{BF} = \boldsymbol{G}^H\hat{\mathbf{p}} \tag{5}$$

which is equal to the numerator of eq 4. The beamformer output is defined by

$$\boldsymbol{q}_{BF}{}^H\boldsymbol{q}_{BF} = \hat{\mathbf{p}}^{\mathrm{H}}\boldsymbol{G}\boldsymbol{G}^H\hat{\mathbf{p}} \tag{6}$$

An application of the general Tikhonov regularization [6] problem eq.4 is therefore to use the special case where the regularization matrix **L** is related to the beamforming output,

$$\boldsymbol{L} = [diag(|\boldsymbol{G}^{\boldsymbol{H}}\hat{\mathbf{p}}|/\|\boldsymbol{G}^{\boldsymbol{H}}\hat{\mathbf{p}}\|_{\infty})]^{-1} \quad (7)$$

So the minimization problem thus becomes

$$\boldsymbol{q}_{\boldsymbol{opt}} = arg\ min\{|\hat{\mathbf{p}} - \mathbf{Gq}|^2 + \lambda^2|[diag(|\boldsymbol{G}^{\boldsymbol{H}}\hat{\mathbf{p}}|/\|\boldsymbol{G}^{\boldsymbol{H}}\hat{\mathbf{p}}\|_{\infty})]^{-1}\mathbf{q}|\} \quad (8)$$

### 2.3 Experiments

A laboratory test set-up was designed to validate the source identification approach. A small-scale replica of a free field static engine test was installed in a hemi-anechoïc chamber. The engine was experimentally modelled by two open cylindrical waveguides fitted with a loudspeaker at their ends (placed back-to-back to simulate inlet and exhaust noise) to measure the sound pressure field of the sources, a semi-circular configuration of microphones was set up around the small-scale engine.

## 3. RESULTS

Experiments were repeated for different inputs of the loudspeakers (tonal, band-limited white noise and combination of tonal and band-limited white noise). The experimental data were then post-processed using the various source identification approaches (Beamforming, inverse and Hybrid) to validate the best method. Figure 1 shows the output of the three methods for two broadband sources simulating the inlet and outlet of a small-scale engine. 60 microphones were set-up on two rings around the small-scale engine at an average radius of approximately 2m and axi-symmetry of the sound field was assumed. The Figure 1 shows that the Hybrid method can identify the location of the source in inlet and outlet of the engine.

## 4. DISCUSSION AND CONCLUSIONS

The results of experimental data show that the Hybrid method is an effective technique for discrimination of inlet and exhaust noise in aero-engines. Also, the results show that spatial source resolution in Hybrid method is better than with the beamforming method and inverse method.

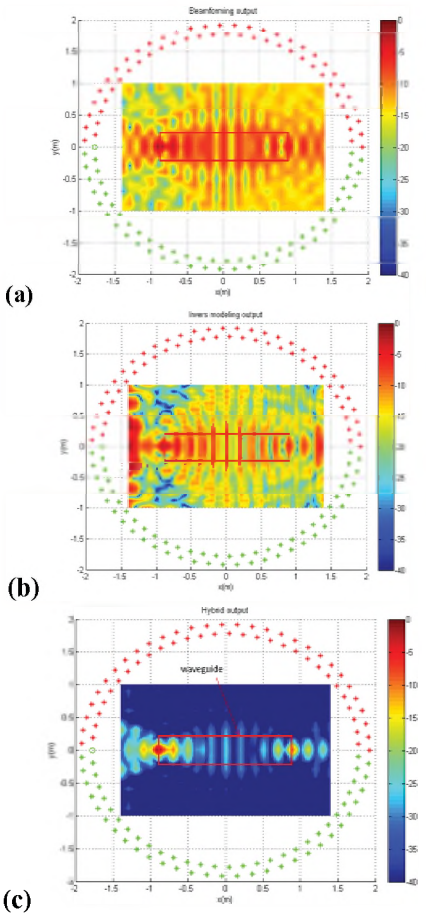


**Figure 1. Output of Beamforming(a), Inverse(b) and Hybrid method (c) for two broadband sources that the left source is 6db stronger that the right source, frequency=1Khz, 60 microphones**

## REFERENCES

[1] Ulf Michel, Deutsches Zentrum, für Luft, "History of acoustic Beamfomring", Berlin Beamforming Conference (BeBeC), 2006.

[2] P. A. Nelson and S. H. Yoon, Estimation of acoustic source strength by inverse methods: Part 1, condition of the inverse problem, journal of sound and vibration (2000)233(4), 643-668.

[3] R.O. Schmidt, Multiple emitter location and signal parameter estimation. IEEE Transactions on Antennas and Propagation, AP-34, 276–280. March, 1986.

[4] R. Roy, A. Paulraj, T. Kailath, ESPRIT: a subspace rotation approach to estimation of parameters of cisoids in noise, IEEE Transactions on Acoustics, Speech and Signal Processing 34 (1986) 1340–1342.

[5] E. Sarradj, A fast signal subspace approach for the determination of absolute levels from phased microphone array measurements, Journal of Sound and Vibration, 329 (2008) 1553–1569.

[6] S.H. Yoon, P.A. Nelson, Estimation of acoustics source strength by inverse method: Part II, experimental investigation of methods for choosing regularization parameters, Journal of Sound and Vibration 233 (2000) 669–705.

## ACKNOWLEDGEMENT

The authors wish to thank NSERC and Pratt & Whitney Canada for their financial support.

# DIRECT NUMERICAL SIMULATION OF SELF-NOISE OF AN INSTALLED CONTROL-DIFFUSION AIRFOIL

**Sanjosé, M.[1], Moreau, S.[1]**

[1]Dept. of Mechanical Engineering, University of Sherbrooke, 2500 blvd de l'université., QC, CANADA, J1K1T1

## 1. INTRODUCTION

Recent improvements have led to a strong reduction of tonal noise in rotating machines. Broadband noise contribution is therefore becoming more and more important. One of the main broadband noise source is the sound produced at the blade trailing edges. Even in undisturbed incoming flows, the boundary layer development on any lifting surface generates pressure fluctuations and vorticity distortions that diffract at the trailing edge and produce acoustic waves.

Many numerical studies have tried to analyze the flow around airfoils to isolate the trailing-edge (TE) noise mechanisms. In the present study the compressible flow around a controlled diffusion (CD) airfoil is investigated in a full anechoic open-jet facility. The chord based Reynolds number of the configuration is $1.5 \times 10^5$ and the Mach number is 0.05, characteristic of low speed fan systems. This configuration has become an excellent test case for trailing-edge noise as extensive aerodynamic and acoustic data have already been obtained both experimentally and numerically [1-4]. In the present study, the trailing edge noise sources of the CD airfoil and their propagation in the anechoic wind tunnel are simulated in a single step for the first time, using the Lattice Boltzmann Method (LBM) implemented in the PowerFlow solver 4.3a.

## 2. NUMERICAL METHODOLOGY

The LBM solves the time and space evolution of a discrete particle distribution function on a lattice grid. The method is naturally transient and compressible, and has been successfully applied to aeroacoustics problems at similar Reynolds number [5,6].

As shown in [3], the open-jet facility has a major effect on the flow around the airfoil. Therefore the jet shear layers are also simulated in the present computational domain. Moreover the high Reynolds number of the flow based on the airfoil chord length and the turbulent transition on the airfoil surface that is triggered by a thin laminar recirculation bubble at the leading-edge, require a very fine mesh achieving DNS resolution in the vicinity of the airfoil. Cell sizes are 15µm on the profile surface achieving a dimensionless wall distance $y^+$ of 1 on the airfoil. The mesh has 640 million cubic elements or voxels. The simulation has been initialized by a 2D field which has been duplicated in the span-wise direction. The computation has been run on 512 processors Intel Xeon X5560 @ 2.80GHz for 255 hrs to simulate 15 through-flow times, statistics are aquired on the last 10 through-flow times. Further details of the numerical methodology are provided in [7].

## 3. RESULTS

### 3.1. Flow field around the airfoil

An instantaneous velocity field around the airfoil in the region achieving DNS resolution is shown in Fig. 1. At the leading edge a laminar recirculation bubble appears. Close to the reattachment point a turbulent boundary layer develops. When the curvature changes, the adverse pressure gradient leads to an increase of the boundary layer thickness. At the trailing edge, the laminar boundary layer coming from the pressure side destabilizes into a small vortex-shedding. This Von Karman street then interacts with the fully turbulent vortical structures coming from the suction side turbulent boundary layer.


**Figure 2. Instantaneous velocity field.**

### 3.2. Mean flow analysis

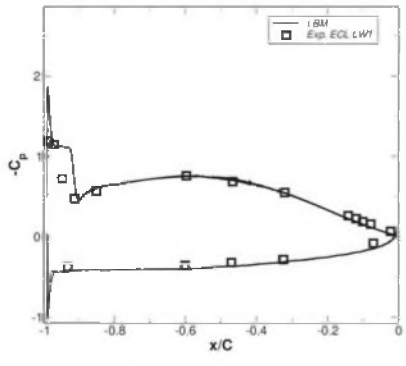


**Figure 2. Mean pressure coefficient along airfoil**

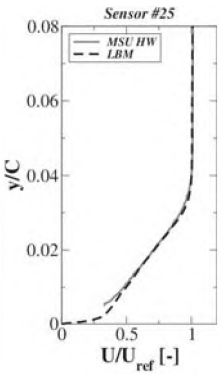


**Figure 3. Mean boundary layer profile before the trailing-edge**

The mean pressure coefficient along the airfoil is in excellent agreement with the experiments as shown in Fig. 2. Compared to previous incompressible LES results [4], this LBM simulation, due to the finer resolution at the surface, provides a closer agreement with experiment, especially the favorable pressure gradient after the reattachment point is well captured. The boundary layer

evolution along the suction side is also well predicted especially at the last location near the trailing as shown in Fig. 3. This is a key point to precisely predict the trailing-edge noise mechanism.

### 3.3. Unsteady flow analysis

The instantaneous contours of dilatation , provided in Fig. 4, show the acoustic waves propagation around the airfoil. The main acoustic source is the TE, which radiates as a dipole source. The non compacity of the source can be seen by the cardioid radiation pattern in the anechoic room (more radiation toward the leading edge). The waves reflect on the corners of the nozzle lips. As in the NACA12 study of [8] a secondary source, at higher frequency (closer wave fringes) appears on the suction side, near the leading edge, close to the reattachment point of the recirculation bubble.

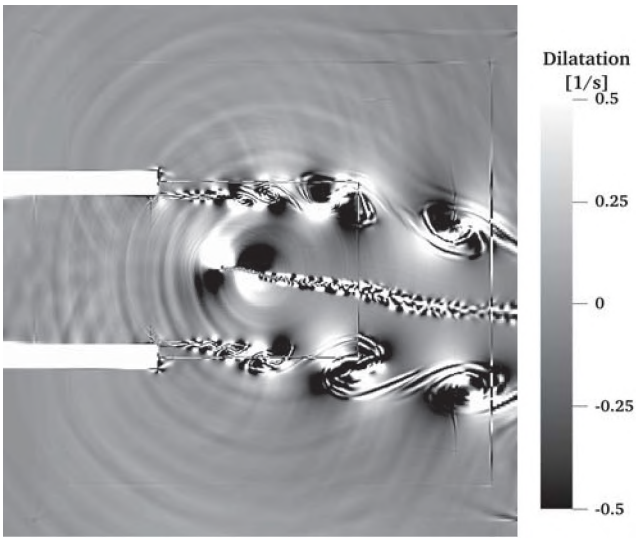


**Figure 4. Instantaneous dilatation field in the anechoic chamber.**

The wall pressure spectral density near the trailing-edge of the profile provides an excellent agreement with experimental data [8]. A better frequency roll-off is even predicted than in previous incompressible LES.

The acoustic radiation at 90° with respect to the main flow direction is compared to experimental measurements recorded at 2m from the profile in Fig.5. The simulation captures the correct levels above 200 Hz. The noise decay at high frequency is not seen in the measurements as the background noise in the anechoic room is reached.

## 4. CONCLUSIONS

Both trailing-edge noise and fully resolved turbulent flow have been numerically investigated with a Lattice Boltzmann Method on the installed Controlled-Diffusion airfoil at a high Reynolds number based on the chord length of $1.5 \times 10^5$ including the wind tunnel environment. The present study focuses on the configuration at 8° angle of attack, and is compared to experimental data.

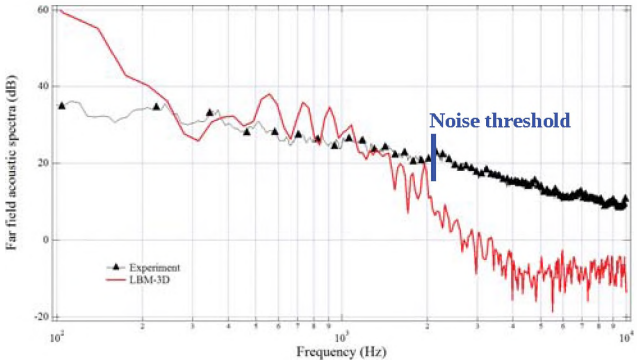


**Figure 5. Sound pressure levels at 90° and 2m from the airfoil.**

The laminar recirculation bubble at the leading-edge of the CD profile has been successfully captured by simulating the full jet width of the mock-up and using a DNS resolution in the vicinity of the profile. This laminar recirculation triggers a turbulent transition of the boundary layer on the suction side. Turbulent structures are scattered at the trailing-edge as non-compact sources of the self noise mechanism. Mean pressure loading on the airfoil and mean boundary layer profiles are in good agreement with experiments. The noise propagation is directly simulated by the LBM in the full computational domain, thanks to a fine discretisation.

## REFERENCES

[1] Moreau, S., Neal, D., and Foss, J. **(2006)**. "Hot-Wire Measurements Around a Controlled Diffusion Airfoil in an Open-Jet Anechoic Wind Tunnel," J. Fluid Eng., **128(**4), 699–706.

[2] Roger, M. and Moreau, S. **(2004)**. "Broadband Self Noise from loaded fan blades," AIAA J., **42**(3), 536–544.

[3] Moreau, S., Henner, M., Iaccarino, G., Wang, M., and Roger, M. **(2003)**. "Analysis of flow conditions in free-jet experiments for studying airfoil self-noise," AIAA J., **41(**10), 1895–1905.

[4] Wang, M., Moreau, S., Iaccarino, G., and Roger, M., **(2009)**. "LES prediction of wall-pressure fluctuations and noise of a low-speed airfoil," Int. J. Aeroacoustics, **8**(3), 177–197.

[5] Brès, G., Pérot, F., and Freed, D. **(2009)**. "Properties of the Lattice-Boltzmann method for acoustics," in *15th AIAA/CEAS Aeroacoustics Conf.*, 2009-**3395**, **(**Miami, FL).

[6] Brès, G., **(2011)**. "Flow and noise predictions for Tandem Cylinders in a realistic wind-tunnel configuration," in *17th AIAA/CEAS Aeroacoustics Conf.*, 2011-**2824**, **(**Portland, OR).

[7] Sanjosé, M., Moreau, S., Kim, M-S., Pérot, F., **(2011)**. "Direct self-noise simulation of the installed Controlled Diffusion airfoil," in *17th AIAA/CEAS Aeroacoustics Conf.*, 2011-**2716**, **(**Portland, OR).

[8] Jones, L., Sandberg, R., and Sandham, N., **(2010)**. "Stability and receptivity characteristics of a laminar separation bubble on an aerofoil," J. Fluid Mech., **648**,. 257–296.

## ACKNOWLEDGEMENTS

The authors want to acknowledge the RQCHP analysts for the help they provided in preparing the 3D case, and the Exa corporation for providing licenses and technical support. They also want to thank CLUMEQ, RQCHP and Compute Canada consortiums that have provided the computational resources.

# AEROACOUSTIC PREDICTION OF AN AUTOMOTIVE COOLING FAN

**Stéphan Magne[1], Stéphane Moreau[1], Alain Berry[1] and Marlène Sanjose[1]**
[1]GAUS, Dept. of Mechanics, Université de Sherbrooke, Québec, Canada, J1K 2R1, Stephan.Magne@USherbrooke.ca

## 1. INTRODUCTION

The acoustic noise from low-speed cooling fans can be divided into two contributions: tonal noise and broadband noise. The latter is associated with the turbulence in the flow whereas the former is generated by the periodic components of the blade loads. Both have significant impact on the overall acoustic radiation, but for the human hearing, the tonal noise is a major annoyance and is, consequently, a prior challenge for manufacturers.

By installing a periodical circular obstruction at the inlet of a fan, Gérard *et al.* [1] have shown that the induced flow distortion is able to reduce the tonal noise. Although both analytical and experimental approaches have been carried out on this method, the aeroacoustic mechanisms have not yet been fully understood. As a first step to achieve a direct aerodynamic simulation of the interaction between a rotor and an obstruction, the aeroacoustic prediction of a single rotor in a typical fan test configuration is first studied.

## 2. AERODYNAMIC SIMULATION

### 2.1 Numerical configuration

The fan considered here is a typical automotive cooling fan on which both experimental and numerical data exist [2-4]. It is a 9-blade axial fan containing an L-shaped rotating ring and a short hub. Both the flow rate and the rotational speed are chosen to match the nominal point of this machine, respectively 2500 $m^3/h$ and 2500 rpm. The 380 mm outer diameter implies typical Mach number up to 0.15 at the blade tip (low subsonic), with a Reynolds number based on the chord of about $1.5\times10^5$ at midspan (transient turbulent regime). In this configuration, the rotor is flushed mounted on a plenum wall, as it is in a typical fan performance test bench.

In order to reduce the computational cost, only one blade passage is meshed and a uniform blade distribution is therefore assumed. Two multi-block structured meshes are generated using *Gridgen* for a total of 5.2 million nodes. Both have the same fine grid distribution, which was shown to yield proper wall resolution with *CFX*. Despite the same number of nodes, the "thin" mesh is more refined in the blade tip region, where the $y^+$ criterion is kept under 8 on the blade surfaces.

The resolution of the unsteady 3D compressible Reynolds Averaged Navier-Stokes equations is performed by the code *Turb'Flow* dedicated to turbomachinery and developed at Ecole Centrale de Lyon. The discretization of the equations is performed by a 2nd order spatial centered scheme of Jameson and a Runge-Kutta temporal scheme with 5 steps. The flow rate is imposed at the inlet of the domain on a spherical plenum, feeding the rotor uniformly. Downstream, a porous domain is set to ensure a positive axial flow at the outlet, where the pressure is imposed with a radial equilibrium. The initial aerodynamic field is generated analytically with a uniform field and a steady RANS simulation is carried out in order to reduce the convergence duration. Once the aerodynamic field is established, a constant global time step is set to achieve the unsteady simulation. To preserve the stability of the schemes the time step is set to $8.9\times10^{-8}$ s for the "thin" mesh and $5.3\times10^{-8}$ s for the "coarse" mesh. The convergence is checked by monitoring the pressure and the flow rate on different surfaces along the simulation domain.

### 2.2 Aerodynamic results

The validation of the overall fan performance is achieved by comparing the static pressure rise across the rotor with the previous simulations and experimental data, shown as a bandwidth that accounts for the moulding and prototyping variability. On this short computational domain, the total pressure rise is taken between two planes close to the rotor. In Figure 1, the present result shows a very good agreement with existing experimental and numerical data.

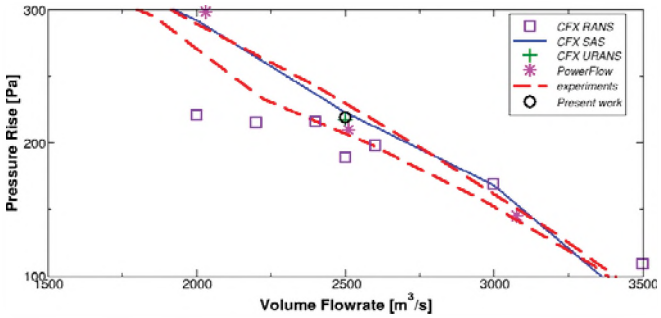


**Figure 1: Fan performance.**

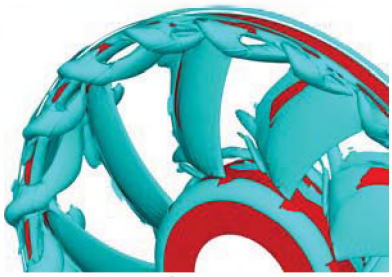

**Figure 2: Iso-surface of the *Q*-factor on the rotor (all the other surfaces being hidden), "thin" mesh.**

As observed previously [5], the dominant flow unsteadiness can be observed at the rotor tip. In Figure 2, the nature of the flow is very well highlighted by the *Q*-factor (a vortex identification technique). As a matter of fact, the pressure rise across the fan creates a flow recirculation in the tip clearance. This recirculation interacts with the rotor leading-edge and generates an unsteady blade load. In the present configuration, two tip vortices can be seen for each blade

passage, rotating at about 500 rpm. A speed reduction is thus observed in the tip clearance between the downstream and the upstream flow. Besides, this speed difference implies that each blade impacts a vortex structure at the frequency $f = N_{vortices} \times \Omega_{relative} = 600$ Hz.

## 3. ACOUSTIC PREDICTION

### 3.1 Acoustic solver

The acoustic radiation is computed by a Ffowcs-Williams and Hawkings analogy based on the near field fluctuations provided by the aerodynamic simulation. The code *Foxwhawk*, developed by Casalino [6], is used for this purpose. Taking advantage of the forward-time formulation of the FW-H equation, this code allows a concurrent flow/noise simulation. The transient pressure on the blade surfaces is imported and *Foxwhawk* generates automatically the complete rotor configuration before the acoustic integrations, taking into account the phase delay between each blade. Considering the Mach numbers at the blade tip, only the thickness noise and the loading noise are computed and the effects of the quadrupole noise are neglected.

The acoustic pressure fluctuations are computed at 26 microphones equally distributed on a sphere, each being 1 m away from the rotor centre. Considering the blade passage frequency at 375 Hz, this distance can be considered as the far field.

### 3.2 Acoustic results

Only 3 blade passage periods were recorded for the purpose of this paper. Although this short duration cannot yet yield well resolved tones, it shows the correct trend. The sound pressure level at each microphone shows a dipole-like directivity with a maximum on the rotor axis. Moreover, the integration of the acoustic intensity over the sphere leads to an excellent prediction of the total emitted acoustic power: 82 and 83 dB for the "coarse" and the "thin" meshes respectively, compared to 82±2 dB measured in a reverberant wind tunnel.

The power spectral density of the acoustic pressure at two microphones is presented in Figures 3 and 4, one microphone being on the rotor axis and the other in the rotor plane. The results for both meshes confirm the predicted tone at the frequency of the impact between the tip recirculation structure and the blades (600 Hz). However, several harmonics now appear in the "thin" mesh spectrum up to 3 kHz, which suggests a better resolution of the flow structures near the blade tip. Besides, the two tip vortices per blade passage are more dissimilar for the "coarse" mesh, yielding a more powerful peak at 300Hz. All these tones are also present in the experimental measurements [4].

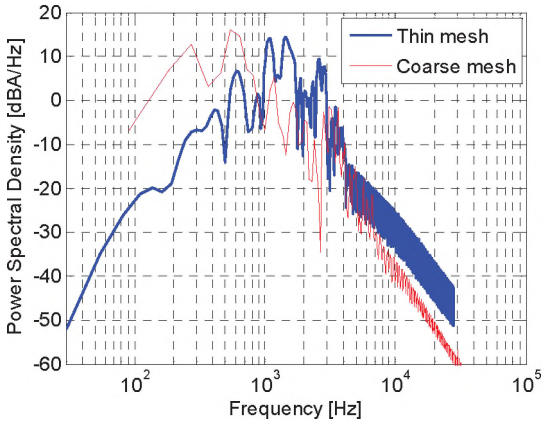


**Figure 3: Microphone at 1 m on the rotor axis.**

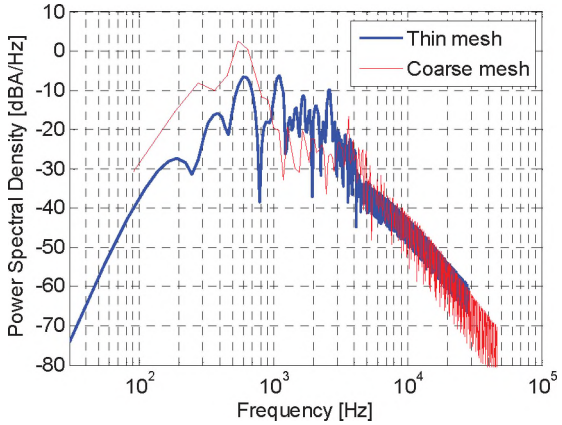


**Figure 4: Microphone at 1 m in the rotor plane.**

## 4. CONCLUSION

Aerodynamic simulation of an automotive fan has been successfully achieved. This computation has highlighted the dominant flow structures that are the dominant sources of unsteadiness on the rotor surfaces and therefore the major sources of noise. As a second step, acoustic prediction has been performed using an acoustic analogy based on the static pressure fluctuation on the blades. A very good agreement is found with the experimental measurements both on the tonal content and the acoustic power emitted.

Future work will include a longer recording period which will lead to a more accurate acoustic prediction. Finally, an obstruction will be placed upstream the fan and aeroacoustic mechanisms will be studied in further details.

## REFERENCES


**[1]** Gérard A., Berry A., Masson P., Gervais Y. (2009). Modelling of tonal noise control from subsonic axial fans using flow control obstructions. *Journal of Sound and Vibration*, 321(1-2), 26-44.

**[2]** Foss J., Neal D., Henner M., & Moreau S. (2001). *Evaluating CFD Models of Axial Fans by Comparisons with Phase-Averaged Experimental Data*. In Vehicle Thermal Management Systems.

**[3]** Moreau S., Sanjose M., Magne S., & Henner M. (2011). *Unsteady Turbulent Simulations of Low-Speed Axial Fans*. In 46th Symposium of Applied Aerodynamics (3AF).

**[4]** Pérot F., Kim M., Moreau S., Henner M., & Neal D. (2010). *Direct Aeroacoustics Prediction of a Low Speed Axial Fan*. In 16th AIAA/CEAS Aeroacoustics Conference.

**[5]** Moreau S., Henner M., & Neal D. (2005). *3D Rotor-Stator Interaction in Automotive Engine Cooling Fan Systems*. In European Turbomachine Conference.

**[6]** Casalino D. (2003). An advanced time approach for acoustic analogy predictions. *Journal of Sound and Vibration*, 261(4).

# EVALUATION OF JET NOISE PREDICTION CAPABILITIES OF STOCHASTIC AND STATISTICAL MODELS

**Bécotte, L. C., Fosso-Pouangué. A., Moreau, S. and Atalla, N.**
GAUS, Faculté de Génie, Université de Sherbrooke, Sherbrooke, Quebec, Canada

## 1. INTRODUCTION

With the progressive reduction of the maximal noise level acceptable for aircraft, the ability to predict the noise at a design stage is now required by the aeronautic industry. At take-off conditions, jet noise remains the main noise source and is considered here. The present study consists in developing and evaluating a quick methodology for the prediction of jet noise based on Reynolds-Averaged Navier-Stokes (RANS) simulations. Since these mean simulations only give the averaged solution and that the turbulence noise is produced by the velocity fluctuations, a model is required to compute acoustic data. Two statistical models, the Mani, Gliebe, Balsa and Khavaran (MGBK) [1] and Self [2] models are compared with a stochastic model, the Stochastic Noise Generation and Radiation (SNGR) [3].

## 2. TEST CASES & RANS SIMULATIONS

### 2.1 Experimental data base

Two 2 inch nozzles have been used in the present study: the Acoustic Reference Nozzle 2" (ARN2) and the Simple Metal Chevron 000 (SMC000) nozzle. For the operating conditions, multiple set-points of Tanna's test matrix [4] have been used. For the calibration of the models, two jet velocities ($M_j$=0.5 and 0.9) and two temperatures ($T_j/T_\infty$=1 and 1.76) are considered.

### 2.2 RANS simulations

The RANS simulations were performed using the standard $k$-$\varepsilon$ model of Fluent 6.3.26. A typical result of turbulent kinetic energy ($k$) is shown in figure 1 for a high-speed subsonic cold jet and the SMC000 nozzle. Various jet properties were validated using experimental data [5], including the axial velocity and the turbulent kinetic energy ($K$) on the jet centerline as shown in figure 2 for the lower Mach number case on the same nozzle.

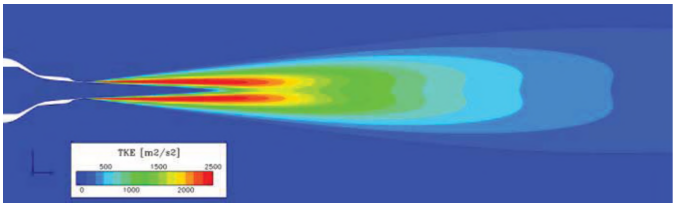


**Figure 1. RANS turbulent kinetic energy contours (SMC000 nozzle, $M_j$=0.9 jet).**

## 3. JET NOISE METHODS

Two methods have been selected to evaluate their capabilities in jet noise prediction, one stochastic, the SNGR method [3], and one statistical, the MGBK method [1] or a simplified model proposed by Self [2].

### 3.1 SNGR

The SNGR method is based on Kraichnan's turbulence model and expresses the turbulent velocity as a summation of Fourier modes for each turbulent scale. The von Karman spectrum is used to get the turbulent velocity of each scale and random functions following probabilistic laws determine the direction and phase. The summation of all turbulence scales at each point of the domain produces the turbulent velocity field for one time step. By repeating the process with a new random generation, the turbulent velocity time signal is given by Eq. (1), where $u_n$ is the velocity amplitude, $k_n$ the wave number, $\psi_n$ the phase and $\sigma_n$ the direction of the turbulence scale $n$ [3]:

$$u'(\vec{x},t) = 2\sum_{n=1}^{N} u_n \cos(\vec{k}_n \cdot \vec{x} + \psi_n)\vec{\sigma}_n \qquad (1)$$

The various SNGR models are characterized by different time and space correlation introduced into Karweit's baseline model. Béchara's model [3] has been selected here, which uses a frequency domain Gaussian filter $f_0 = c/K$, $\left|\tilde{H}(f)\right| = \exp\left[{(f-f_0)^2}/{af_0^2}\right]$ to regenerate the temporal correlation. The final step of the SNGR method is the propagation of the sources. Lighthill's acoustic analogy has been used to yield the far-field acoustic pressure.

### 3.2 MGBK

The MGB method originally developed by Mani et al. [1] was further developed by Khavaran to become the MGBK model, which consists in modeling the two point correlation tensor and propagate the noise to the far field using RANS data. Eq. (2) shows the averaged square acoustic pressure as a function of $\psi_{self}$, the self noise intensity of the source propagated to the observer, and $a_{ij}$, the quadrupôle-directivity tensor.

$$\overline{p'^2}(R,\theta,\omega) = \int_v \Psi_{self}\left(a_{11} + 2a_{22} + 4a_{12} + 2a_{23}\right) d\vec{r} \qquad (2)$$

In this study, Frendi's formulation [6] was used to determine the empirical constants required in Eq. (2).

## 4. RESULTS

### 4.1 SNGR Aerodynamics Results

For the SNGR methods, both the one point spectral analysis and the r.m.s. statistics of the velocity field were verified. From the one point spectral analysis, a constant $a$=25 was determined for Béchara's filter. Figure 2 (right) shows the turbulent kinetic energy of the SNGR models and is compared with the RANS results and experimental data [5]. Béchara's filter greatly reduces the turbulent kinetic energy levels and over-corrects Karweit's model. An additional correction was therefore developed to force the turbulent kinetic energy of the SNGR velocity signal to be at the same level than the RANS data and therefore to preserve turbulent kinetic energy.

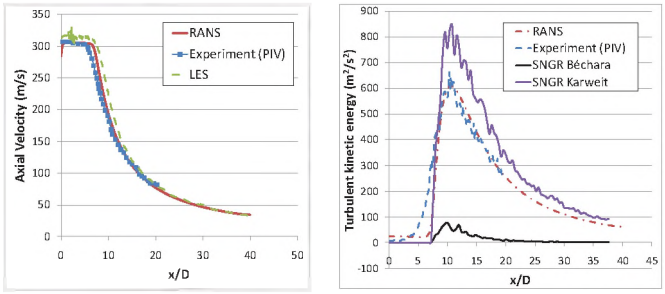


**Figure 2. Axial velocity profile (left), Turbulent Kinetic energy (right) along the axis (SMC000, $M_j$=0.5, $T_j/T_\infty$=1)**

### 4.2 Acoustic results

Figure 3 compares the Sound Pressure Level (SPL) in 1/3 octave for several set-points predicted by both MGBK and Self methods, with SHJAR experimental acoustic data [7].

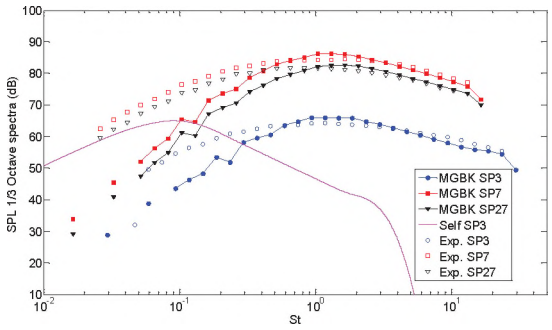


**Figure 3. Sound Pressure Level 1/3 octave spectra, (SMC000 nozzle, $M_j$=0.9, $T_j/T_\infty$=1 and 1.76)**

For all cases, the MGBK results follow the experimental data with a difference less than 3dB for Strouhal numbers larger than 0.7. Below this limit, the SPL is under estimated by MGBK. The low frequency divergence is actually a known weakness of MGBK model because the geometric parameters are disregarded, which can significantly influence the low frequency part of the spectrum. Self's simplified model is found to predict the peak radiation at much lower frequency and to have a much quicker roll-off at higher frequencies.

Béchara's SNGR model presently yields too large levels, which is traced to the derivation of the Lighthill tensor in the acoustical analogy. In the future, some regularization of the flow field will be required to obtain reliable derivatives.

## 5. DISCUSSION AND CONCLUSIONS

Two different methods based on RANS flow fields have been implemented and tested to predict jet noise. For the MGBK method, the results are in good agreement with the experimental data around 90° for all jet conditions tested, and for Strouhal numbers beyond 0.7. Yet, a more elaborate form of the directivity that includes shielding coefficients is required to predict noise over a wider range of angles. Self's simplified model was not found to yield the proper peak efficiency and correct roll-off at high frequencies. For the SNGR method, since the aerodynamic properties of the turbulent field have been validated and corrected to conserve energy, the noise over-prediction seen in the use of the Lighthill analogy is traced to the lack of differentiability of the stochastic field that will require some future regularization.

## REFERENCES


[1] Mani, R., Stringas, E. J., Wang, J. C. F., Balsa, T. F., Gliebe, P. R., Kantola, R. A. (**1977**), "High Velocity Jet Noise Source Location and Reduction," Task 2, *FAA report*. FAA-RD-76-79-II, Cincinnati, Ohio.

[2] Self, R.H. (**2004**), "Jet noise prediction using the Lighthill acoustic analogy," *J. Sound Vib.*, **275**, pp. 757-768.

[3] Béchara, W., Bailly, C., Lafon, P., et Candel, S. (**1994**), "Stochastic Approach to Noise Modeling for Free Turbulent Flows," *AIAA J*, **32** (3), pp. 462.

[4] Tanna, H. K., Dean, P. D., Burrin, R. H.(**1976**), "The Generation & radiation of supersonic jet noise - Turbulent mixing noise data," *FAA report*, TR-76-65-VOL-3.

[5] Engblom W., Georgiadis N., Khavaran, A. (**2005**), "Investigation of Variable-Diffusion Turbulence Model Correction for Round Jets," *11th AIAA/CEAS Aeroacoustics Conference*, AIAA 2005-3085.

[6] Frendi, A., Nesman, T., Wang, T.-S (**2001**), "Computational and experimental study of the linear aerospike engine noise," *AIAA J*, **39** (8), pp.1485-1492.

[7] Brown, C., Bridges J., (**2006**), "Small Hot Jet Acoustic Rig Validation," *NASA Report*, TM-2006-214234, Cleveland, Ohio.


## ACKNOWLEDGEMENTS


The authors wish to thank the support of NSERC and Pratt & Whitney Canada through the Industrial Chair in Acoustics.

# UNCERTAINTY QUANTIFICATION FOR THE TRAILING-EDGE NOISE OF A CONTROLLED-DIFFUSION AIRFOIL

**Christophe, J.[1], Moreau, S.[2], and Schram, C.[1]**

[1]Dept. of Environmental and Applied Fluid Dynamics, von Karman Institute for Fluid Dynamics, 72 chaussée de Waterloo, Rhodes-St-Genèse, Belgium, 1640, julien.christophe@vki.ac.be

[2]Dépt de Génie Mécanique, Université de Sherbrooke, 2500 Boul. de l'Université, Sherbrooke QC, Canada, J1K2R1

## 1. INTRODUCTION

In modern rotating machines, due to the significant effort put on reducing annoying discrete tones, the broadband noise is an important contribution to the overall noise level, as in fans, turboengines or wind turbines. A key source of broadband noise is the trailing-edge noise, caused by the scattering of boundary-layer pressure fluctuations into acoustic waves at the trailing-edge of any lifting surface. Numerical methods to evaluate this noise are more often using steady RANS computations for computational cost reasons, requiring modelling and introducing then uncertainties. The present study aims at assessing uncertainties associated with the prediction of trailing-edge noise, through an uncertainty quantification (UQ) framework, using RANS computations or conventional LES computations, in order to determine their respective robustness and accuracy.

## 2. METHODOLOGY FOR UQ

The approach to uncertainty quantification (UQ) of airfoil trailing-edge noise is illustrated in Figure 1. The considered case is a Controlled-Diffusion airfoil of chord $C$ placed in the large anechoic wind tunnel in Ecole Centrale de Lyon (LWT), and held by two horizontal side plates. The angle of attack (aoa) is 8° and the airfoil upstream velocity $U_0$ is 16 m/s, which corresponds to a Reynolds number based on the airfoil chord $Re_C$=1.6 x $10^5$.

As in previous studies (Moreau *et al.* 2006), a RANS computation of the complete experimental setup of the large anechoic wind tunnel in Ecole Centrale de Lyon (LWT), including the nozzle and part of the anechoic chamber has been done that captures the strong jet-airfoil interaction and its impact on airfoil loading. The boundary conditions are extracted ($U$ and $V$ profiles) for a smaller domain embedded in the jet potential core. This final result is obtained by two different procedures, both producing a wall frequency pressure spectrum $\Phi_{pp}$ used in Amiet's theory (Amiet 1976) to predict the far-field sound spectrum $S_{pp}$.

In the first approach, an unsteady LES on the restricted domain with the above extracted velocity profiles, directly yields the trailing edge wall pressure spectrum. The second approach, less expensive but requiring more modeling, uses steady RANS computations on a two-dimensional slice of the restricted domain, with the same boundary condition profiles as for the LES. From this RANS computation, the primitive variables ($U_1$, $U_2$, $k$ and $\omega$ or $\varepsilon$ depending on the RANS turbulence model) are extracted through a boundary layer profile at the trailing-edge of the airfoil. Those

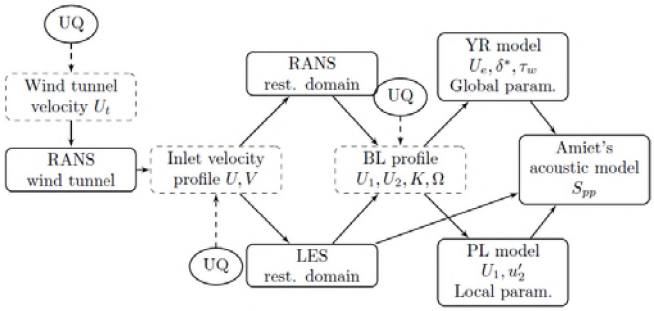


**Figure 1. Uncertainty quantification methodology.**

variables are then used in the two wall-pressure models investigated in the present study. On the one hand, Rozenberg et al. 2010 proposed a model (YR) only based on global boundary layer parameters from the boundary layer profile, mainly the external velocity $U_e$, a boundary layer thickness $\delta$ and the wall shear stress $\tau_w$. On the other hand, the model of Panton & Linebarger 1974 uses local parameters i.e. the streamwise velocity profile $U_1$ and the crosswise velocity fluctuation profile $u'_2$.

RANS computations are obtained with the solver Ansys Fluent 12, using the Shear-Stress-Transport (SST) $k$-$\omega$ turbulence model. The computational grid is a two-dimensional cut perpendicular to the airfoil span of the structured mesh used by Wang *et al.* 2004. The LES are performed by the CDP code of Stanford University using the dynamic subgrid-scale model. The mesh CDP-B is taken from Moreau *et al.* 2006 and has 1.5 million cells. The same inflow/outflow conditions are used in the RANS and LES computations and periodic boundary conditions are applied in the spanwise direction for the 3D LES domain.

The uncertainty is introduced at the inlet boundary of the restricted computational domain. The physical variations in the experimental flow measurements are taken into account by selecting a 2.5% error bound on the streamwise velocity $U$ and a 10% error bound on the crosswise velocity $V$ around the deterministic numerical solution. A set of 9 velocity inlet profiles are determined using a Clenshaw-Curtis quadrature and the corresponding RANS and LES computations are run. Both components $U$ and $V$ are assumed random variables with uniform distribution within their interval of variation. The stochastic collocation method is used to estimate the uncertainties.

## 3. RESULTS

The flow around the airfoil is illustrated in Figure 2 by iso-surfaces of $Q$ for the LES. As in previous studies

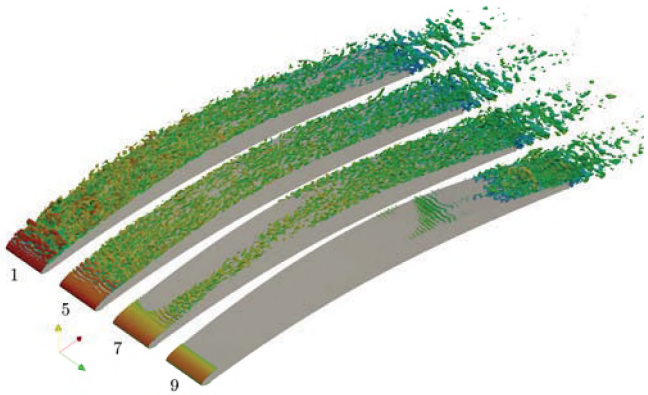


**Figure 2. Isosurfaces of the Q factor ($QC^2/C_0^2$ = 2000) coloured by velocity magnitude for inflow conditions corresponding to LES computations # 1,5,7,9.**

(Wang *et al.* 2004, Moreau *et al.* 2006), in LES #1 and #5 (reference), small instabilities form close to the reattachment point of the laminar recirculation bubble. The flow tends to re-laminarise toward the mid-chord due to the favorable pressure gradient. When this gradient becomes adverse, the turbulent boundary layer thickens again and larger turbulent structures appear near the trailing-edge. In LES #7, the acceleration around the leading-edge still yields a weak flow separation at the leading-edge, which is not strong enough to trigger transition over the whole span. Turbulence only develops over a narrow band and only the adverse pressure gradient after mid-chord triggers the full transition and turbulence development. In LES #9, the acceleration around the leading-edge is no longer strong enough to trigger a flow separation at the leading-edge and no transition occurs before mid-chord. Flow separation occurs beyond mid-chord that triggers the transition close to the trailing edge. This observation is a significant departure from RANS computations where the second recirculation zone beyond mid-chord never occurs for low aoa. This difference is related to the used RANS modelisation that is considering fully turbulent flows and therefore cannot correctly take into account the laminar and transition regions whereas LES calculations do.

From the RANS computations, boundary-layer profiles are extracted near the trailing-edge and the two reconstruction methods are applied to obtain the trailing-edge wall-pressure spectra. From the LES computations, the trailing-edge spectrum is directly computed from the wall-pressure fluctuations. The wall-pressure spectra are then used in Amiet's theory to compute the radiated far-field sound. The corresponding results together with experimental measurements are shown in Figure 3, in terms of mean and 100% uncertainty bars. A good agreement with experiments is found for both methods using RANS information. Larger uncertainty bars are found at high frequencies using the YR model due to the large uncertainties involved in wall shear-stress determination, on which the model is based at high frequencies. The PL model, not based on the wall shear-stress variable, shows less variation at low frequencies but

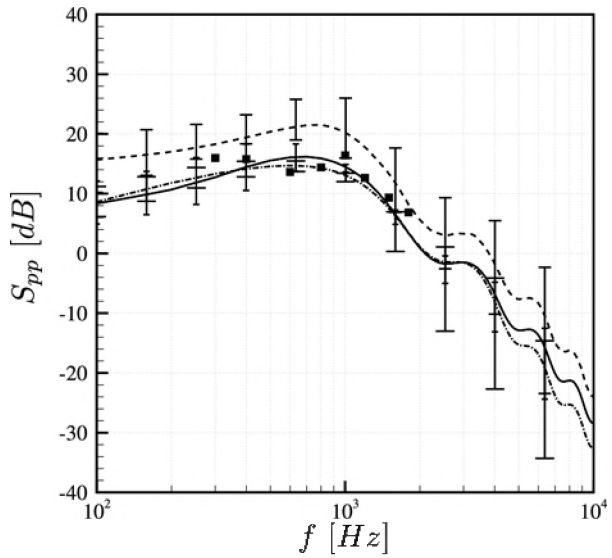


**Figure 3. Means and uncertainty bars of far-field acoustic spectra in the mid-span plane above the airfoil (θ = 90_) at R = 2 m from the trailing edge. (dash-dot and large uncertainty bars) YR model, (plain and small uncertainty bars) PL model, (dash and medium uncertainty bar) LES. (Square) Experiments.**

larger uncertainties at low frequencies caused by the low statistical convergence of the Monte-Carlo integration technique used to integrate the boundary-layer profiles. Finally, due to a different flow behaviour in LES #7 to 9, the LES results are shifted to higher levels by about 8 dB. Consequently, the LES uncertainty bars are also found larger than those of the RANS computations.

## REFERENCES

Amiet, R.K. (1976), "Noise due to Turbulent Flow past a Trailing Edge", J. of Sound and Vib., 47(3), 387-393.

Moreau, S., Neal, D., Khalighi, Y., Wang, M. and Iaccarino, G. (2006) "Validation of Unstructured-Mesh LES of the Trailing-Edge Flow and Noise of a Controlled-Diffusion Airfoil." In *Proceedings of the Summer Program 2006*. Centre for Turbulence Research, Stanford Univ./NASA Ames.

Rozenberg, Y., Moreau, S., Henner, M. and Morris, S. C. (2010) "Fan Trailing-Edge Noise Prediction Using RANS Simulations." In *16th AIAA/CEAS Aeroacoustics Conference*. AIAA-2010-3720.

Panton, R. L. and Linebarger, J. H. (1974) "Wall Pressure Spectra Calculations for Equilibrium Boundary Layers." J. Fluid Mech., 65(2), 261-287.

Wang, M., Moreau, S., Iaccarino, G. and Roger, M. (2004) "LES Prediction of Pressure Fluctuations on a Low Speed Airfoil." In *Annual Research Briefs*. Centre for Turbulence Research, Stanford Univ./NASA Ames.

## ACKNOWLEDGEMENTS

The authors would like to thank Stanford University for providing the necessary computational resources. The participation of the first author to the conference is supported through the FP7-ECOQUEST project (Grant Agreement no 233541).

# JET NOISE PREDICTION USING A FULLY UNSTRUCTURED LARGE EDDY SIMULATION SOLVER

**Arnaud Fosso Pouangué[1], Marlène Sanjosé[1] and Stéphane Moreau[1]**
[1]GAUS, Faculté de Génie, Université de Sherbrooke, Sherbrooke, Quebec, Canada (Arnaud.Fosso@USherbrooke.ca)

## 1. INTRODUCTION

Jet noise has been subject of intensive research for sixty years, since it is the major contribution to aircraft noise at take off. Recent work to reduce jet noise sound emission investigates various noise reduction devices such as dual stream nozzles, chevrons, microjets injection, and lobed mixers. Most advanced state-of-art tools are based on high-order, low-dispersive and low-dissipative schemes designed for structured hexahedral grids. However, numerical methods based on fully unstructured grids are known to be better adapted to deal with complex geometries as those found in noise reduction devices. In a previous work [1], a comparison of this methodology with a high-order structured dedicated solver on jet configurations without nozzle has been performed. This comparison demonstrated the promising capabilities of a fully unstructured methodology. The present work deals with simple jet configurations including a nozzle geometry. This is a necessary step towards the simulation of geometrically complex jet noise reduction devices.

## 2. JET CONFIGURATION

The jet configuration considered is a cold 0.9 Mach jet. The nozzle considered is the SMC000 nozzle as shown in Figure 1. The diameter of the nozzle is $D$=5.08cm.

**Figure 1. SMC nozzle: 0.9 jet Q-criterion isosurface.**

## 3. NUMERICAL PROCEDURE

The grid is fully unstructured using only tetrahedral elements. Maximum cell sizes in the acoustic source area, namely the mixing layer and the transition region (up to $20D$ from the nozzle exit), allow capturing frequencies at least up to a Strouhal number (Str) of 1.5. A finer meshing is done in the nozzle boundary layer in order to allow a natural transition to turbulence of the mixing layer at the nozzle exit. In that zone, waves are resolved up to Str=5. The grid contains 7 million points and 43 million cells.

All inlet and outlet boundary conditions are defined using non-reflecting Navier-Stokes boundary conditions [2]. At the nozzle inlet, total pressure and temperature are prescribed while a very small co-flow is prescribed at the inlet outside the nozzle. At the oulet, only a far-field pressure is prescribed.

The computations are initialized using mean flow fields provided by a RANS simulation [3] using the k-ε model. The numerical scheme used is a two-step Taylor-Galerkin scheme 3rd order in time and space. The WALE subgrid scale model [4] is used. The CFL is fixed to 0.7.

Acoustic sources data are collected on surfaces at about 1.5D from the jet in order to avoid dispersion and dissipation effects and limit the grid size. Acoustic prediction is then performed using the permeable surface formulation of the Ffowcs-Williams and Hawkings analogy implemented in the MCAAP code [5].

## 4. RESULTS

### 4.1 Turbulent flow statistics

The computations have been run for about $300D/U$. This is enough to converge statistics data. The results (named SMC in figures) are compared to results obtained experimentally [6]. They are also compared to numerical results obtained by the simulations of Bogey and Bailly [7], performed with low-dispersive and low-dissipative schemes on a structured grid of comparable size without the nozzle geometry (named Bogey et al.). Numerical results obtained in a previous work [1] on a fully unstructured grid of comparable size but without nozzle geometry (named W/O Nozzle) are also presented. The two simulations without nozzle use a vortex ring excitation to mimic the effect of the nozzle. The "W/O Nozzle" results have been shifted by $5D$ to account for a delayed transition to turbulence.

Figure 2 shows the evolution of the centerline mean axial velocity. The velocity decay is in a very good agreement with experiments. Only the SMC computations predict the correct potential core length without forcing.

Figure 3 presents the evolution of axial turbulent intensities both along the jet centerline and lip line. Once again, results named "W/O Nozzle" have been shifted. Along the centerline, the turbulent intensity peaks and the levels in the transition region are in good agreement with experiments [6] and Bogey and Bailly computations [7]. The axial turbulent intensity along the lip line increases rapidly, showing that the jet mixing layer is already turbulent at the nozzle exit even if no excitation have been introduced in the SMC computations. The peak is reached at about $2D$ is higher than in experiments [8]. It might be due to vortex

pairing. However, this peak is lower than the peak obtained by Bogey and Bailly. This peak could also be due to instabilities in the vicinity of the lips. It does not appear in "W/O Nozzle" results as no vortex pairing has been detected. The mixing layer development should be investigated further. Overall, the turbulent flow results are very satisfactory.

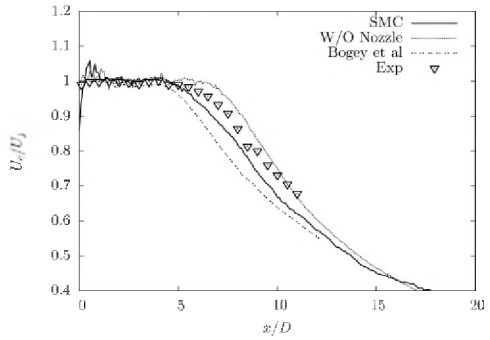


**Figure 2. Mean centerline velocity decay.**

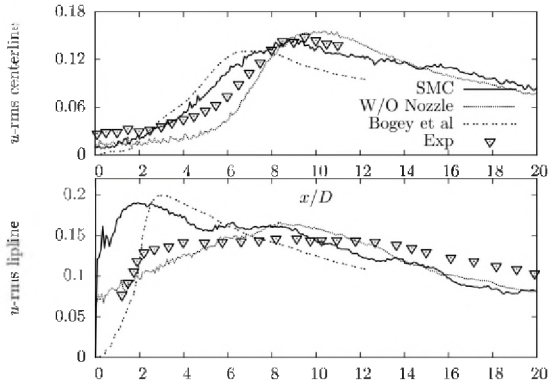


**Figure 3. Axial turbulence intensities. Top: centerline. Bottom: lipline.**

### 4.2 Acoustic results

Acoustic source data have been recorded during only $40D/U$ with a time step of $0.008D/U$. Therefore, low frequencies are not completely resolved but high frequencies are only limited by the mesh size cutoff. The acoustic data computed at 30° and 90° from the jet axis, 100D from the origin are shown on Figure 4. The agreement with experimental data [9] is very good. A dominant mode around a Strouhal number of 1.5 could be observed at 90°. It is probably due to vortex pairing occurring around $x=2D$ in the mixing layer.

## 5. DISCUSSION AND CONCLUSIONS

In the present study, the possibility to study jet noise using Large Eddy Simulation methodology on a fully unstructured tetrahedral mesh has been investigated. Both aerodynamic (the turbulent structure) and aeroacoustic results obtained on cold jets with and without nozzle geometry show good agreement with experiments. It is worth noting that, at this point of the survey, with the nozzle geometry, no excitation method is needed to obtain a turbulent mixing layer at the nozzle exit. Further investigations will look at the vortex pairing still present in the simulation. They will also asses the dependence of the flow field on the mes and the inlet conditions. The coherence of jet noise sources will be checked.

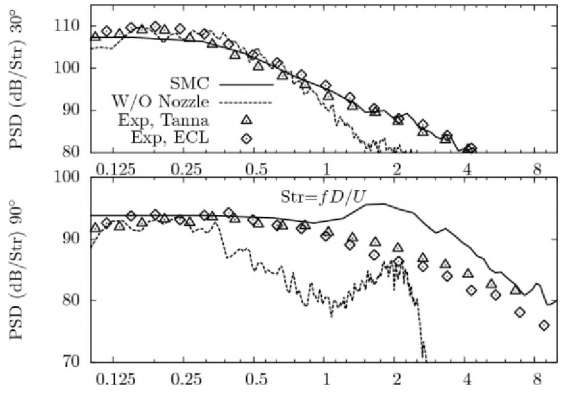


**Figure 4. Spectra of acoustic pressure at 100D.**

## REFERENCES


[1] Sanjose, M., Moreau, S., Najafi-Yazdi, A. and Fosso P., A. (**2011**). "A Comparison between Galerkin and Compact Schemes for Jet Noise Prediction," 17th AIAA/CEAS Aeroacoustics Conference, AIAA 2011-2833.

[2] Poinsot, T. and Lele, S., (**1992**)."Boundary Conditions for Direct Simulations of Compressible Viscous Flows," Journal of Computational Physics, 101(1), 104-129.

[3] Bécotte, L., Fosso-P., A., Moreau, S. and Attala, N., (**2011**). "Evaluation of Jet Noise Prediction Capabilities of stochastic and Statistical models", Acoustic Week in Canada, Quebec, 2011.

[4] Nicoud, F. and Ducros, F., (**1999**), "Subgrid-scale stress modelling based on the square of the velocity gradient", Flow, Turbulence and Combustion, 62(3), 183-200.

[5] Najafi-Yazdi, A., Brès, G. and Mongeau, L.,(**2011**). "An acoustic analogy formulation for moving sources in uniformly moving media", Proceedings of The Royal Society A, 467(2125), 144-165.

[6] Power, O., Kerhervé, F., Fitzpatrick, J. and Jordan, P., (**2004**). "Measurements of Turbulent Statistics in High Subsonic Jets", 10th AIAA/CEAS Aeroacoustics Conference, AIAA 2004-3021.

[7] Bogey, C. and Bailly, C., (**2006**)."Computation of a high reynolds number jet and its radiated noise using large eddy simulation based on explicit filtering", Computers and Fluids, 35, 1344–1358.

[8] Bridges, and Wernet, M. (**2010**). "Establishing Consensus Turbulence Statistics for Hot Subsonic Jets", 16th AIAA/CEAS Aeroacoustics Conference, AIAA 2010-3751.

[9] Bogey, C., Barré, S., Fleury, V., Bailly, C. and Juvé, D., (**2007**). "Experimental study of the spectral properties of near-field and far-field jet noise", International Journal of Aeroacoustics, 6(2), 73-92.


## ACKNOWLEDGEMENTS


The authors want to thank A. Najafi-Yazdi for providing MCAAP and CERFACS for providing AVBP for academic purpose. The authors gratefully acknowledge P. Jordan, Y. Gervais, C. Bogey and C. Bailly for providing us experimental data.

# EFFECTS OF HIGH-INTENSITY FOCUSED ULTRASOUND WITH DIFFERENT ACOUSTIC DOSES ON NEURAL TISSUES *IN VITRO*

**Mosa Alhamami*, Steven Tran, and Jahan Tavakkoli**
Advanced Biomedical Ultrasound Imaging and Therapy Laboratory, Department of Physics, Ryerson University, 350 Victoria St., Toronto, Ontario, Canada, M5B 2K3
*E-mail: mosa.alhamami@gmail.com

## 1. INTRODUCTION

Replacing invasive surgical procedures with non-invasive, bloodless interventions can lead to significant advancements in the field of medicine. Therefore, development of non-invasive therapies is of utmost importance. By applying the physical principles of acoustics, high-intensity focused ultrasound (HIFU) has been introduced as a promising therapeutic modality due its capability to induce thermal and mechanical effects in deep-seated tissues of interest selectively and non-invasively.

Ultrasound-induced nerve conduction block has been investigated *in vitro* and *in vivo* [1-4]. Foley et al. (2004) created permanent nerve block and suppression of nerve function by thermally coagulating rabbit sciatic nerves *in vivo* using a 3.2-MHz HIFU transducer with a focal acoustic intensity of 1480 to 1850 W/cm$^2$ and 36 ± 14 (mean± SD) seconds of sonication [4]. Using a 3.5-MHz ultrasound transducer, the effects of unfocused, continuous wave ultrasound on *in vitro* frog sciatic nerves at three different acoustic power levels (1, 2 and 3 W) was studies for a sonication time of 5 minutes [1]. Ultrasound exposure at acoustic power of 1 W resulted in nerve stimulation by increasing the compound action potential (CAP) amplitude by 8%. A progressive decrease in the nerve CAP amplitude was observed for 2 and 3 W ultrasound exposures [1].

Although the aforementioned studies have investigated the effects of focused and unfocused ultrasound with different acoustic power levels or intensities on nerve conduction *in vivo* and *in vitro*, little is known about the combined effects of acoustic intensity and sonication time on nerve conduction. The product of the acoustic intensity and sonication time yields a treatment parameter that was termed acoustic dose [5]. The goal of this study is to investigate the dose-dependent biologic effects of HIFU on lobster's ventral nerve cord *in vitro*.

## 2. MATERIALS AND METHODS

A spherically concaved HIFU transducer with resonance frequency of 2.2 MHz was utilized. The aperture diameter of the transducer is 5.0 cm and its radius of curvature is 7.5 cm. Thus, the f-number of this transducer is 1.5. The HIFU transducer was brought in close proximity to the target tissue. Depending on the acoustic dose level, two tissue targeting methods were utilized in this study.

### 2.1 Low- and medium-level acoustic doses

For low-and medium-level acoustic doses treatments, a ventral nerve cord was excised from a marine lobster (*Homarus Americanus*) and placed on a nerve chamber to measure its CAP before and after exposure to HIFU using an electrophysiology system (BIOPAC Systems, Inc., Goleta, CA) connected to a computer. Droplets of Ringer's solution (462 mM NaCl, 16 mM KCl, 26 mM $CaCl_2$, 8 mM $MgCl_2$, 10 mM tris, 10 mM maleic acid, and 11 mM glucose) were provided to the neural tissue to supply vital nutrients and ions.

Because the HIFU transducer is strongly focused, both low and medium-level acoustic doses were achieved by placing the neural tissue in the pre-focal region of the HIFU transducer. Using a linear acoustic and temperature simulation (LATS), the spatial-peak temporal-average intensity ($I_{SPTA}$) was determined [6]. In the low-level acoustic dose treatment, the $I_{SPTA}$ was around 3.3 W/cm$^2$ and the sonication time was 10 seconds (i.e. acoustic dose of 32.5 J/cm$^2$). In the medium-level acoustic dose treatment, the $I_{SPTA}$ was around 13.3 W/cm$^2$ and the sonication time was 10 seconds (i.e. acoustic dose of 132.6 J/cm$^2$).

### 2.2 High-level acoustic dose

For treatments with high levels of acoustic dose, the lobster's ventral nerve cord was sandwiched between the nerve chamber and an *in vitro* chicken breast tissue, a scenario that resembles *in vivo* experiments. A SONIX RP® clinical ultrasound imaging system (Ultrasonix Medical Corp., Richmond, BC, Canada) was utilized to monitor treatment in real time pre-, during and post-exposure to HIFU therapy via its EC4-9/10 R endocavity imaging probe (Ultrasonix Medical Corp., Richmond, BC, Canada). The imaging probe was aligned with the therapeutic HIFU transducer such that the focal zone of the therapeutic transducer appears on the screen of the ultrasound imager, thereby guiding the acoustic therapy to the target (i.e. the neural tissue). Similar to the previous treatments, Ringer's solution was supplied to the neural tissue. The sonication time for high-level acoustic dose therapy was 5 seconds and the $I_{SPTA}$, as determined by LATS, was around 5500 W/cm$^2$ (i.e. acoustic dose of 27500 J/cm$^2$).

## 3. RESULTS

Results of the HIFU exposures to neural tissues at the three difference acoustic dose levels are shown in figure 1 and summarized in table 1.

At low-level acoustic dose, the nerve CAP amplitude increased by 18.0% after a 10-second HIFU exposure of around 3.3 W/cm$^2$. At medium-level acoustic dose, the nerve CAP amplitude decreased by 5.4% following a 10-second HIFU exposure of around 13.3 W/cm$^2$. A greater suppression in the nerve CAP amplitude was achieved at high-level acoustic dose. A 5-second HIFU exposure of around 5500 W/cm$^2$ resulted in a 57.8% decrease in the nerve CAP amplitude. Moreover, gross examination of the chicken breast and neural tissues subjected to the high-level acoustic dose reveals a discoloration and coagulative necrosis in a localized volume where both tissues meet.

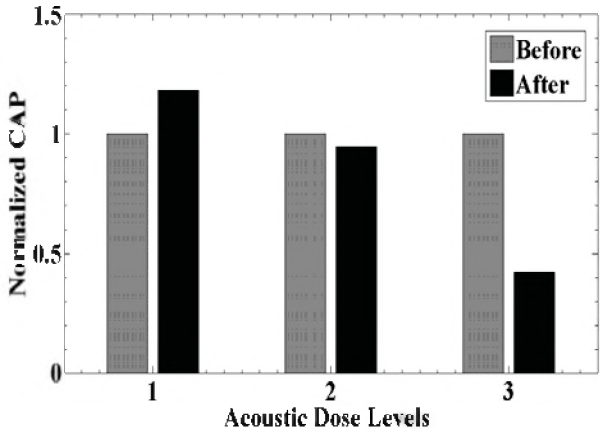


**Figure 1. A comparison of the normalized nerve CAP amplitudes before and after HIFU treatments at the three different acoustic dose levels (1: low-level acoustic dose; 2: medium-level acoustic dose; 3: high-level acoustic dose).**

**Table 1. Summary of the results**

| | Low-level acoustic dose | Medium-level acoustic dose | High-level acoustic dose |
|---|---|---|---|
| Relative effect of HIFU on CAP amplitude | Increase by 18.0% | Decrease by 5.4% | Decrease by 57.8% |

## 4. DISCUSSION AND CONCLUSIONS

Decrease in the nerve CAP amplitude after HIFU treatment at high and medium acoustic dose levels demonstrates the ability of HIFU to induce nerve conduction block primarily due to its thermal mechanism, which is more pronounced at high acoustic dose levels. The thermal effect of HIFU therapy has been previously shown to be responsible for conduction block of frog sciatic nerve *in vitro* [3]. The ultrasound-induced reduction of the CAP amplitude has been attributed to the ability of ultrasound's thermal effect to partially disable the axonal ion channels of the nerve, reducing the number of ions ($Na^+$ and $K^+$) passing through the axonal membranes and thus decreasing the nerve CAP amplitude [1]. On the other hand, increase in the nerve CAP amplitude after HIFU treatment at low-level acoustic dose demonstrates the ability of HIFU to stimulate neural tissues primarily due to its mechanical mechanism (non-thermal effect). By producing a change in their membrane potential, the mechanical force of HIFU therapy has been proposed to be responsible for stimulating neural structures [7]. Ultrasound-induced nerve stimulation, as evidenced by an increase in the nerve CAP amplitude, has recently been attributed to the opening of the axonal ion channels with the mechanical stimulation of ultrasound, allowing more ions to pass through the axonal membranes and thereby augmenting the nerve CAP amplitude [1].

Results of this study demonstrate the great advantage of HIFU as a non-invasive and localized acoustic therapy with promising applications in neurology, neurosurgery, and anesthesiology and pain management [8].

## REFERENCES

[1] Tsui, P., Wang, S. & Huang, C. (2005). In vitro effect of ultrasound with different energies on the conduction properties of neural tissue. *Ultrasonics, 43,* 560-565.

[2] Young, R. & Henneman, E. (1961). Reversible block of nerve conduction by ultrasound. *Archives of Neurology, 4,* 95-101.

[3] Colucci, V., Strichartz, G., Jolesz, F., Vykhodtseva, N., Hynynen, K. (2009). Focused ultrasound effects on nerve action potential in vitro. *Ultrasound in Medicine and Biology, 35(10),* 1737-1747.

[4] Foley, J.L., Little, J.W., Starr F.L. III, Frantz C., Vaezy S. (2004). Image-guided HIFU neurolysis of peripheral nerves to treat spasticity and pain. *Ultrasound in Medicine Biology, 30,* 1199–1207.

[5] Foley, J. L., Vaezy, S., & Crum, L. A. (2007). Applications of high-intensity focused ultrasound in medicine: Spotlight on neurological applications. *Applied Acoustics, 68(3),* 245-259.

[6] Butt, F. & Tavakkoli, J. (2011). *Linear Acoustic and Temperature Simulation (LATS).* User Manual, Ryerson University, Toronto, ON, Canada.

[7] Gavrilov, L. R., Tsirulnikov, E. M., Davies, I.A. (1996). Application of focused ultrasound for the stimulation of neural structures. *Ultrasound in Medicine and Biology, 22,*179–192.

[8] Alhamami, M. (2011). *Development and Testing of an Image-Guided HIFU System for Neurological Applications.* Undergraduate Thesis, Ryerson University, Toronto, ON, Canada

## ACKNOWLEDGEMENTS

The authors would like to thank Arthur Worthington for his technical assistance. This work was supported by the Ontario Research Fund-Research Excellence program (ORF-RE) and the Natural Science & Engineering Research Council of Canada-Undergraduate Student Research Award (NSERC-USRA).

# HIGH INTENSITY FOCUSED ULTRASOUND AND MICROBUBBLE INDUCED TISSUE ABLATION: EFFECT OF TREATMENT EXPOSURE ON THERMAL LESION VOLUME AND TEMPERATURE

**Sonal Bhadane, Jahan Tavakkoli, and Raffi Karshafian**
Dept. of Physics, Ryerson University, 350 Victoria Street, Toronto, Ontario, Canada, M5B 2K3

## 1. INTRODUCTION

High intensity focused ultrasound (HIFU) with microbubbles has demonstrated the enhancement of the therapeutic efficacy of HIFU [1, 2]. Acoustically stimulated microbubbles that consist of the perflurocarbon gas enclosed in lipid shell enhance the bioeffects induced through cavitation (mechanical effect) and thermal mechanisms [3, 4, 5]. Holt and Roy have experimentally demonstrated that ultrasonically induced cavitation bubbles locally enhance tissue heating in HIFU treatment [6]. The ultrasonic intensity for inducing cavitational bioeffects can be reduced by orders of magnitude with administration of such an agent externally. This is especially important for the treatment of deep-seated tumors, where the ultrasonic power high enough for the treatment is difficult to deliver. Current limitations are creating and controlling the cavitation microbubbles. This issue can be resolved, if the ultrasonic absorption of tissues can be significantly increased in a well-controlled manner with administration of microbubble agents externally.

The current study investigates the effects of ultrasound treatment parameters and microbubble concentration on the HIFU lesion volume and temperature.

## 2. METHODS

Figure 1 shows the HIFU system that consists of a therapeutic ultrasound unit and an imaging ultrasound unit. A therapeutic transducer made of a high-power PZT4 crystal (Boston Piezo-optics Inc., Boston, MA) with a diameter of 50 mm and a focal length of 75 mm was used. The imaging was done using the EC9-5/10 Endovaginal microconvex transducer (Ultrasonix Inc., Richmond, BC) that was aligned with the HIFU transducer. Artenga® microbubbles (MBs) (Artenga Inc, Ottawa, CA) with the mean bubble diameter of 2 μm and concentration of $10^9$ microbubbles/ml were injected into the *ex vivo* chicken breast tissue. The *ex vivo* chicken breast tissue was treated with US (HIFU alone) and USMB (HIFU and microbubbles). Lesions were created using HIFU exposure of intensities ranging from approximately 600 to 2500 W/cm$^2$ for 5 seconds exposure duration. The lesion volume and peak temperature were measured at varying intensities (600 to 2500 W/cm$^{2)}$ and varying microbubble concentrations (0%, 10%, 25%, 50%, 75% and 100%). K-type thermocouple was used to measure the peak temperature. The lesion volume was approximated to be an ellipsoid. Volume of ellipsoid was used to calculate the lesion volumes.

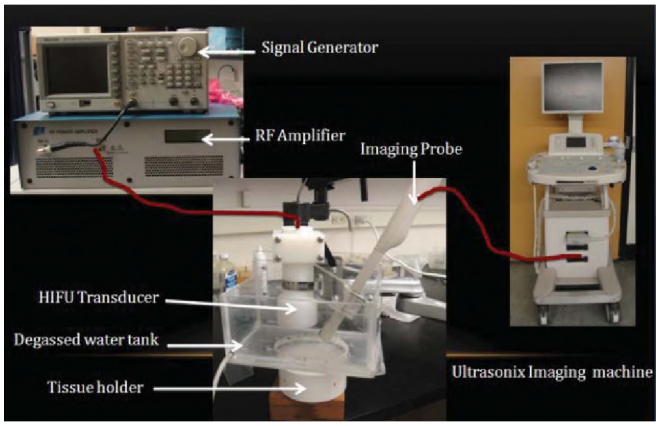


**Figure 1. Experimental setup**

## 3. RESULTS

The lesion volume and peak temperature for various intensities in absence and presence of microbubbles are shown in figures 2 and 3 respectively. The lesion volumes for both the groups (US and USMB) at intensities greater then 1200 W/cm$^2$ are stastically signifiant. There is no significant difference between the lesion volumes at intensities below 1200 W/cm$^2$. The peak temperature for the USMB treatment compared to the US treatment alone is stastically significant ($p<0.05$) (Figure 3).

Figure 4 shows the graph for lesion voume as a function of peak temperature. The lesion volume for US and USMB treatments increase constantly as same rate as the peak temperature rises to approximately 70 °C. However lesion volume increase more rapidly for the USMB treatment over 70 °C.

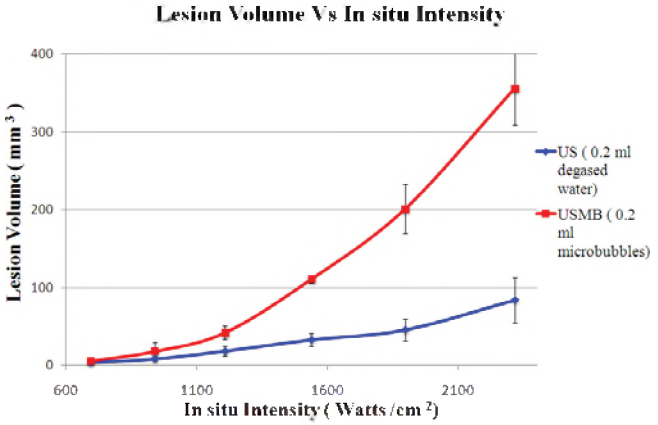


**Figure 2. Lesion volume vs. *in situ* intensity at constant microbubble concentration (100% MBs)**

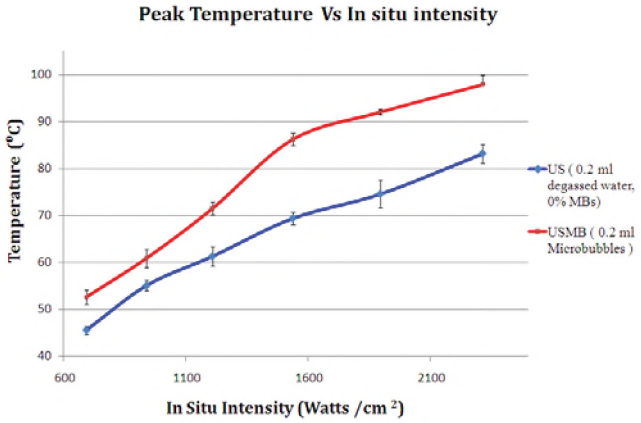


**Figure 3. Peak Temperature vs. *in situ* intensity at constant microbubble concentration (100% MBs)**

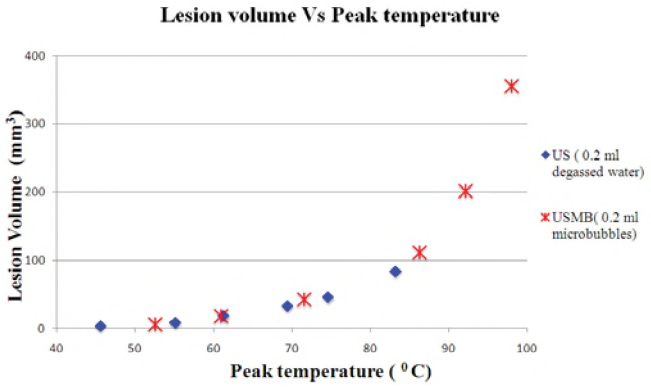


**Figure 4. Lesion volume vs. Peak temperature**

## 4. DISCUSSION AND CONCLUSIONS

In the active group, larger tissue volume was coagulated in the presence of MBs, despite equal exposure time. This shows that the MBs enhance the tissue ablation induced by HIFU. HIFU causes localized tissue temperature rise because ultrasound energy is converted to heat. As for the mechanisms by which the MBs in the ultrasound field cause enhanced heating, two factors are considered to be important: heating by oscillation or explosion of microbubble contrast agents exposed to HIFU, and cavitation bubbles generated by the HIFU exposure.

It was noted that the lesion volume for the US and USMB treatment was same for until upto 70 °C. This indicates that the thermal mechanism was the only prominent mechinism of the tissue damage. However, the lesion volume for the USMB treatment rose at higher rate then the US treatment. This indicates that the mechanisms other then thermal damage also play role in the tissue damage. Therotically these results can be explained by thermal damping, viscous damping and acoustical damping (explained eleswhere) [6].

In conclusion, enhancements in HIFU tissue ablation efficacy are achievable using controlled microbubble induced tissue ablation. Furture work includes measuring lesion volume and Peak temperature at various microbubble concentration to determine the appropriate treatment combination.

## REFERENCES

1. He W, Wang W, Zhou P, Wang YX, Zhou P, Li RZ, Wang JS, Ahuja AT. (2010). Enhanced Ablation of High Intensity Focused Ultrasound with Microbubbles: An Experimental Study on Rabbit Hepatic VX2 Tumors. Cardiovasc Intervent Radiol. [Epub ahead of print].

2. Yu T, Fan X, Xiong S, Hu K, Wang Z. (2006). Microbubbles assist goat liver ablation by high intensity focused ultrasound. Eur Radiol. 16(7): 1557-63.

3.Hynynen K. (1991). "The threshold for thermally significant cavitation in dog's thigh muscle in vivo". Ultrasound Med Biol.17(2):157-69.

4.Sokka SD, King R, Hynynen K. (2003) MRI-guided gas bubble enhanced ultrasound heating in in vivo rabbit thigh. Phys Med Biol.48(2):223-41.

5.Umemura S, Kawabata K, Sasaki K. (2005). "In vivo acceleration of ultrasonic tissue heating by microbubble agent". IEEE Trans Ultrason Ferroelectr Freq Control.52 (10): 1690-8

6. Holt RG, Roy RA. (2001) Measurements of bubble-enhanced heating from focused, MHz-frequency ultrasound in a tissue-mimicking material. Ultrasound Med Biol.27 (10): 1399-412.

## ACKNOWLEDGEMENTS

This work was partially funded by grants from NSERC and Ryerson start-up research funds. We would also like to thank Mosa Alhamami and Arthur Worthington from the Dept. of Physics, Ryerson University, for their technical supports to this work.

# ULTRASONIC CHARACTERISTICS FOR GEL FORMATION IN THE CALIFORNIA MASTITIS TEST

**Chien-Hsing Chen[1], Chih-Hsin Hung [2], Yu –Yao Lee [1], Xin-Lun Chen[1]**
[1] Dept. of Information Technology, Meiho University, Neipu, Pingtung, Taiwan, jameschen@meiho.edu.tw
[2] Institute of Biotechnology and Chemical Engineering, I-Shou University, Kaohsiung city, Taiwan, chhung@isu.edu.tw

## 1. INTRODUCTION

Mastitis is one of the most serious and costly diseases affecting dairy cow production (Heringstad et al., 2000). Measurement of the somatic cell count (SCC) in raw milk is widely accepted as the most useful indirect indicator of mastitis and milk quality. SCC actually only can be counted in laboratories. To achieve a faster, but less accurate result, some farmers use a simple, inexpensive, cow-side test, known as the California Mastitis Test (CMT) (Schalm et al., 1957), to provide a qualitative estimate of SCC in the foremilk of individual cows or quarters. CMT is an indirect method to detect infected quarters on the farm based upon the reaction of special detergents with DNA of somatic cells and increasing the viscosity of the mixture which is proportional to the SCC, and an evaluation of the degree of gel formation is done by gently rotating CMT paddle. However, the interpretation can be subjective, and this might result in false positives and negatives.

CMT was mechanized by a ball viscosimeter (Tolle et al., 1976). Fast analysis devices, or systems, would be highly desirable as they would allow an on-line response to the changes in media components. However, most on-line systems currently used have a low accuracy. The rheology of the gel formed in the CMT was investigated by using both capillary and rotational viscometry (Verbeek et al., 2008) and found that the gel is non-Newtonian, but the initial phase of viscosity increase was not due to shear dependence, but rather due to the gelation reaction. It can therefore be deduced that the rheology of the gel is complicated not only by it being non-Newtonian, but also by the strong dependence on test conditions. These make designing a successful sensor much more challenging.

On this background, ultrasound is becoming an alternative technique for the on-line monitoring of mastitis based on CMT. Most important features of ultrasonic systems are robustness, non-invasiveness, precision, low cost, rapidity and easy automation. Furthermore, ultrasound can be used to analyze opaque materials, offering an alternative to electromagnetic waves based devices. Recently, on-line ultrasonic techniques have been used for monitoring alcoholic fermentations (Becker et al. 2001; Resa et al. 2004), dairy fermentations (Elvira et al. 2002), dough fermentations (Elmehdi et al. 2003) and Escherichia coli growth (Reddy et al. 2001; Sierra et al. 2010).

Understanding the ultrasonic properties of the CMT gel is important in the design and operation of the automated CMT. The purpose of this paper is to investigate ultrasonic characteristic of the CMT gel formation and to determine whether a reliable and inexpensive automated on-line SCC detector based on CMT might be developed. Therefore, in this work, measurements of ultrasonic velocity and attenuation in the CMT gel have been carried out and used to understand ultrasonic velocity and attenuation changes.

## 2. APPARATUS AND METHOD

An ultrasonic waveform (4 cycles) acquired is shown in fig. 1. The first pulse wave, peak 1a, was the input wave and the second pulse wave, peak 2a, was the output wave. Then the next incoming wave is the input wave obtained by the first pulse wave in fig. 1. From the waveform signal data, the ultrasonic velocity (c, m/s) and attenuation (α, neper/m) of the CMT gel were calculated as follows (Ay et al., 1994):

$$c=8d/t_r \quad (1)$$

$$\alpha=[1/(2d)]\ln\Delta V \quad (2)$$

where $t_r=\frac{1}{2}[(t_{5a}-t_{1a})+(t_{5b}-t_{1b})]$, d= distance traversed by the ultrasonic pulse (m), and

$$\Delta V=\frac{1}{8}\left[\frac{V_{1b}}{V_{2b}}+\frac{V_{2b}}{V_{3b}}+\frac{V_{3b}}{V_{4b}}+\frac{V_{4b}}{V_{5b}}+\frac{V_{1a}}{V_{2a}}+\frac{V_{2a}}{V_{3a}}+\frac{V_{3a}}{V_{4a}}+\frac{V_{4a}}{V_{5a}}\right]$$

where $V_{1a}$, $V_{1b}$, etc. are signal amplitudes (V) and $t_{1a}$, $t_{1b}$, etc. are the time (s) corresponding to different peaks in fig. 1.

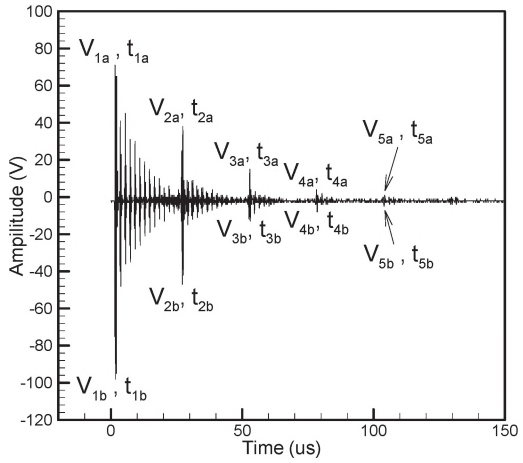


**Figure 1. Waveform of ultrasonic pulse travelled through the sample**

An ultrasonic pulse echo experimental set up was used. The system was comprised of one 1-MHz central frequency ultrasonic longitudinal wave transducers (Model P/N V314, Panametrics), an ultrasonic pulser-receiver (Model 5072PR, Panametrics), a digital storage oscilloscope (Model 2430, Tektronix) and, via a general purpose interface bus (GPIB), stored in a computer equipped with analysis software to obtain the time of flight, which is the time taken by the ultrasonic pulse to travel through the sample.

The transducer was mounted in the one side of the circular cross section of a cylinder sample tank submerged in water bath at 30±0.1℃ in order to minimize the influence

of the temperature on the measurements. The traversing distance between the transducer and the reflective surface of the cylinder was 1.9 cm. Raw milk (6ml) was combined 1:1 with an anionic surfactant (SDS: sodium dodecylsulphate, 0.1g/ml, in distilled water). All experiments were replicated three times. The ultrasonic signals were collected continuously after CMT reagent addition for 10 seconds.

## 3. RESULTS

The ultrasonic velocity and attenuation in CMT milk gel were measured at SCC=72.5($10^3$/ml), 30℃ and f=1MHz as shown in fig. 2 to fig. 3, separately. Dashed lines are linear fitting of the experimental data. These preliminary results indicated that ultrasonic velocity and attenuation increased with time duration in CMT milk, which is sensitive to the degree of mixing during gelation.

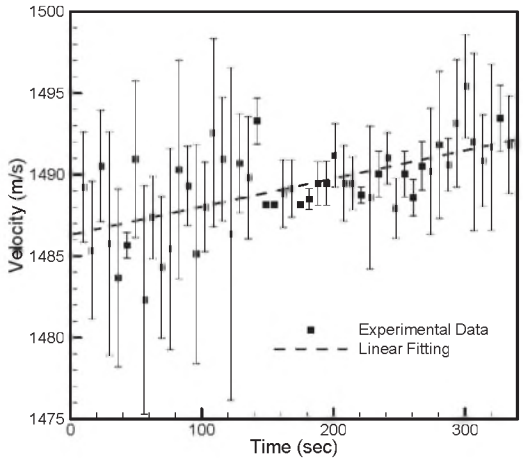


**Figure 2. Ultrasonic velocity in CMT milk, at SCC=72.5 ($10^3$/ml), T = 30°C and f = 1 MHz.**

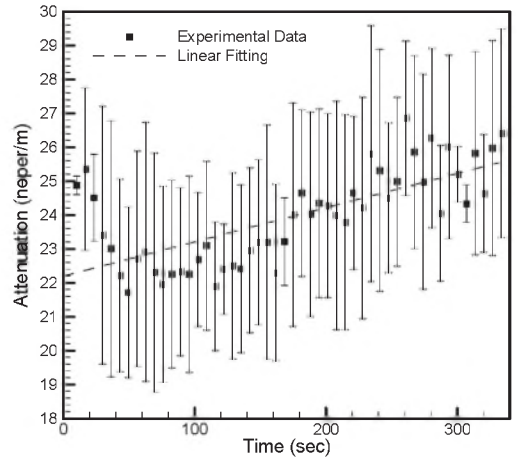


**Figure 3. Ultrasonic attenuation in CMT milk, at SCC=72.5 ($10^3$/ml), T = 30°C and f = 1 MHz.**

## 4. DISCUSSION AND CONCLUSIONS

Due to the more DNA dissolved out of cells depended on the degree of mixing during gelation, the gel viscosity increases with the mixing duration, which induces the increase in the velocity. Results also demonstrate that attenuation increases with mixing duration, probably due to the friction of ultrasound propagated in gelation obviously affected by the gel viscosity, which may tend some ultrasonic energy to be adsorbed and tuned into heat.

However, attenuation is decreased in the initial state and then increased after about 50 seconds. The main reason is that CMT gel is non-homogeneous mixing, which is caused sediment phenomenon by gravity effect without any shear application at the beginning of measurement. Then, mixing effect is continued to increase gel viscosity during gel reaction, which induces the increase in attenuation. CMT relies on the fact that the viscosity of the non-Newtonian gel formed during the test is proportional to the SCC concentration. In this study pulse-echo ultrasonic technique is used to preliminary investigate the ultrasonic characteristics in CMT gelation. However, there is a need for further identifying for SCC concentrations relative to accuracy of CMT rank using ultrasonic technology in the future.

## REFERENCES


Becker, T., Mitzscherling, M., & Delgado, A. (**2001**), "Ultrasonic velocity - a non-invasive method for the determination of density during beer fermentation," Eng. in Life Sciences, **1**(2), 61-67.

Ay Chyung, Sundaram Gunasekaran (**2003**), "Numerical method for determining ultrasonic wave diffusivity through coagulating milk gel system," J. Food Engineering, **58**, 103-110.

Elmehdi, H. M., Page, J. H., & Scanlon, M. G. (**2003**), "Monitoring dough fermentation using acoustic waves," Transaction of IChemE, **81**(Part C), 217-223.

Elvira, L., Resa, P., & Espinosa, F. (**2002**), "Montero de ultrasonic propagation and thermal changes during milk gelation processes," Proceedings of Forum Acusticum, Sevilla.

Heringstad, B., Klemetsdal, G., Ruane, J., (**2000**), "Selection for mastitis resistance in dairy cattle-a review with focus on the situation in the Nordic countries," Livest. Prod. Sci. **64**, 95-106.

Schalm OW, Noorlander D. (**1957**), "Experiments and observations leading to development of the California mastitis test," J. American Veterinary Medical Association **130**, 199-204.

Reddy BR, Babu YH, Reddy DL (**2001**), "Ultrasonic measurements in Escherichia coli at various growth stages," Mater Lett. **49**(1), 47-50

Resa, P., Elvira, L., & Montero de Espinosa, F. (**2004**), "Concentration control in alcoholic fermentation processes from ultrasonic velocity measurements," Food Research International, **37**, 587-594.

Sierra C, Elvira L, García JL, Resa P, Galán B. (**2010**), "Monitoring Escherichia coli growth in M63 media by ultrasonic noninvasive methods and correlation with spectrophotometric and HPLC techniques," Appl Microbiol Biotechnol. **85**(3), 813-821.

Verbeek CJ, Xia SS, Whyte D. (**2008**), "Rheology of the gel formed in the California Mastitis Test," J Dairy Res. **75**(4), 385-91.


## ACKNOWLEDGEMENTS


This study represents part of the results obtained under Contract No. NSC 99-2221-E-276 -002 sponsored by the National Science Council of Taiwan.

# THE USE OF ELASTIC INTERLAYERS FOR IMPROVING SOUND INSULATION IN ATTACHED DWELLINGS: FIELD STUDY RESULTS FROM TIMBER FRAME, MASONRY, AND STEEL FRAME APARTMENTS IN THE UK.

**Roderick Mackenzie[1] and R. Sean Smith[1]**

[1]Building Performance Centre, Institute for Sustainable Construction, Edinburgh Napier University, 42 Colinton Road, Edinburgh, United Kingdom, EH10 5BT, ro.mackenzie@napier.ac.uk

## 1. INTRODUCTION

The benefit of using elastic interlayers for addressing flanking transmission at critical T-junctions has often been investigated over previous decades and continues today. Yet their use was never viable commercially for a mass housing market application, given standard UK wall and floor designs could meet the building regulation requirements, whilst still being the dominant pathway for acoustic transmission. When more stringent regulations were introduced, wall and floor flanking pathways began to dominate on-site performances, limiting potential improvements.

This paper outlines the development and field testing of two mass-market elastic interlayers, for walls and for floors. Both products have repeatedly turned what were adequately performance partitions into the highest performing mass-market walls and floors in the UK, and have acted as a robust safety net to prevent floors and walls that were compromised by poor workmanship from failing Building regulations. Each product has been shortlisted for the 'Housing Product of the Year' in 2009 and 2010.

## 2. BACKGROUND

### 2.1 Regulation changes

During the last ten years, sound insulation performance targets for residential partitions have steadily increased. In England and Wales, Approved Document Part E (ADE) of the Building Regulations 2003 (amended 2004) changed the calculation criteria for airborne measurement from the previous $D_{nTw}$ criteria to $D_{nTw} + C_{tr}$, with minimum airborne levels set at 45 dB (43 dB for refurbishments). It was also stipulated that all new-build housing should have 10% of each site undergo pre-completion acoustic field testing (PCT) to ISO-140 Parts 4 and 7. However, home builders do not have to conduct PCT if they build to standardized 'Robust Detail' wall and floor designs. These have been proven to repeatably and reproducibly meet a minimum target of 48 dB, with a mean result of 50 dB from all 30 application tests, 5 dB above ADE 2003. Further the sustainability document 'the Code for Sustainable Homes' (CSH) introduced in 2006, required further increases in performance levels. To achieve the maximum 4 credits under the CSH, a minimum level of 53 dB must be achieved (for impact, 54 dB $L'_{nTw}$). Although it was introduced initially for new-build social (public) housing, it may become mandatory for all new-build private housing during the next decade.

### 2.2. Flanking transmission

Consistent achievement of these higher levels is difficult for current wall and floor constructions without the use of either independent linings, or thicker walls/floors than are currently standard constructions. Additionally, with higher partition insulation, flanking noise begins to influence or even become a dominant factor in controlling the achievable level of sound insulation. Previous studies have shown that elastic interlayers placed at wall-floor junctions reduce bending wave flanking transmission, albeit with varying results across the frequency range due to the wave type attenuated (Craik *et al.*, 1995, Crispina *et al.*, 2008). Ruff and Fischer showed that when bitumen-based membranes are used as isolation under lightweight gypsum walls, the wall achieved greater $R_w$ levels than other elastic interlayers (Ruff *et al.*, 2009).

## 2. DESIGNING ELASTIC INTERLAYERS

Flanking noise accounts for 12 of the 13 basic transmission pathways between attached dwellings, taking place via structural junctions, cavities, or unintentional workmanship errors. Designing elastic interlayers for use in mass-market housing requires the products to meet certain criteria. Isolation solutions developed must firstly be effective, enabling improvements over current partition designs. However, they must be less expensive to the client than alternatives (such as independent wall linings) and readily compatible with current partition designs. Additionally, to maintain current build methods for apartments, any elastic interlayers must be thin, relatively incompressible, and not promote slippage. Finally, they should be sufficiently robust as to ensure correct installation.

## 3. WALL INTERLAYERS: BRIDGESTOP

Prior to 2008, it has not been possible to build lightweight cavity blockwork walls between attached dwellings off raft foundations, due to acoustic transmission flanking across the continual concrete raft. However 70% of all new builds in England & Wales are built using traditional blockwork construction, despite many new builds being built on brownfield sites which may require such raft foundations or gas barriers. As an alternative timber frame or solid walls were often built, which limit the attainable

acoustic performance and build options. Additionally, in attached houses that have continuous vertical cavities up three or more stories, a noticeable drop in wall acoustic performance can be observed from the 2nd floor to ground floor of up to 6 dB ($D_{nT,w}$ +$C_{tr}$), attributable to mortar collection on wall ties. Thus a combined effect of transmission through the raft and the mortar bridging can reduce the walls performance by up to 8 dB ($D_{nT,w}$ +$C_{tr}$).

To try and address these issues, a research project was carried out via a joint venture between Icopal Ltd. and the Building Performance Centre (BPC) at Edinburgh Napier University. Early on in the design process, it became apparent that a 3mm bitumen-aluminium composite interlayer alone satisfied the above criteria for mass-market housing. The Icopal Bridgestop system (Figure 1) acts both as an isolator at lower frequencies and as an acoustic dampener for high frequencies. By placing the continuous isolator under each leaf (simplifying installation), there is a doubled isolation effect between wall leaf and support and wall leaf to wall leaf. The issue of mortar droppings forming a bridging pathway between leafs at the base of the cavity is also addressed by a 10 mm recycled foam quilt fixed at the base of the cavity to isolate any mortar accumulation.

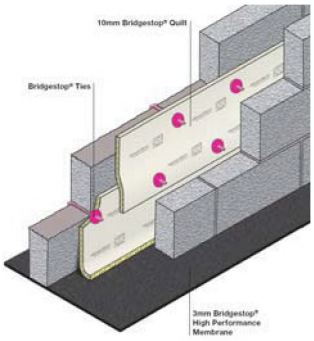


**Figure 1 The Bridgestop system**

Figure 2 shows the airborne sound insulation results from identical masonry cavity blockwork walls built with Bridgestop (57 dB) and without (49 dB) on a set of row housing in England.

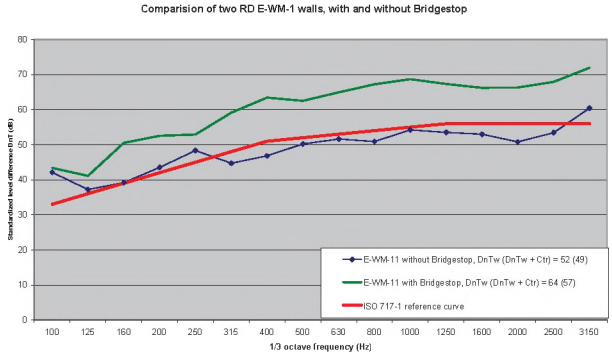


**Figure 2 100mm cavity block walls with and without Bridgestop**

Early field testing showed that the use of Bridgestop improved airborne sound insulation by an average of ~ 8 dB ($D_{nTw}$ + $C_{tr}$) for cavity walls.

After 30 further results, Bridgestop was awarded its own Robust Detail, and became the first wall type to consistently meet the maximum performance targets of the CSH. It also allowed, for the first time since the publication of ADE, the building of cavity blockwork walls of raft foundations, resulting in a groundworks saving to the contractor of ~19%. However, the issue of flanking transmission between partition floors still remained.

## 4. FLOOR INTERLAYERS: WALL CAP

The Wall Cap membrane used similar Bridgestop technology to isolate the critical acoustic junction between each load-bearing wall head and the separate floor structure. This reduces eight of the twelve acoustic flanking pathways. For the heat-retaining benefits of effectively edge-sealing the cavity from heated air convection, the Wall Cap 400 is fixed to both leaves across the cavity wall and over non-party wall heads.

It has been now been site tested on masonry and steel frame constructions, and laboratory testing for timber frame. For masonry, two clear benefits have been seen. Firstly, direct benefits to airborne and impact sound insulation can be seen on identical-construction plots (150 mm pre-cast concrete slab, 150 mm metal frame ceiling, 40 mm screed), four with Wall Cap and without three without Wall Cap. The plots without Wall Cap got a mean result of 49 dB ($D_{nTw}$ + $C_{tr}$) and 53 $L'_{nTw}$. The plots with Wall Cap got a mean result of 54 dB ($D_{nTw}$ + $C_{tr}$) and 49 $L'_{nTw}$. Secondly, In several separate apartments where the screed had clearly breeched through the underscreed to the walls, an event which would normally see a floor failing impact tests, the floors still passed the building regulations of ADE 2003. For Steel Frame, on the eight tests conducted so far on steel-concrete composite RD E-FS-1 floors, which would typically get a mean result < 53 dB ($D_{nTw}$ + $C_{tr}$), mean airborne results were 58 dB, and mean impact results 45 dB ($L'_{nTw}$). Its use in steel frame to date has achieved Candidate Robust Details Stage A status. Timber frame sites are still being sought.

## REFERENCES

Craik, R.J.M, Osipov, A.G., "Structural isolation of walls using elastic interlayers," 1995, Applied Acoustics 46, pp. 233-249

Crispina, C., Ingelaerea B., and Vermeir G., "Innovative building systems to improve the acoustical quality in lightweight masonry constructions: Application of resilient joints at junctions - PART 1: analysis of the experimental results, " 2008, Paper presented at Euronoise 2008, Paris, 29 June – 4 July

Ruff A., Fischer H.M., "Direct sound insulation of lightweight solid walls," 2009, Paper presented at EuroNoise 2009, Edinburgh, October 26-28, Sound Insulation in Buildings session.

## ACKNOWLEDGEMENTS

Development of the Wall Cap system supported by Scottish Enterprise Proof of Concept fund.

# EXAMINING AIRBORNE SOUND TRANSMISSION LOSS IN VARIOUS WALL CONSTRUCTIONS

**Wilson Byrick**[1]
[1] Pliteq Inc., 1370 Don Mills Rd., Toronto, Ontario, M3B 3N7, wbyrick@pliteq.com

## 1. INTRODUCTION

Wood stud walls show poor sound isolation properties unless treated with additional mass or decoupling techniques. In this paper the performance of various common wall constructions are compared. This study is intended as a guide to better design and construct wall assemblies that meet and exceed minimum code for multi-family dwellings.

### 1.1. Wall Types

There are 5 wall types tested in this study. They are single stud, staggered stud, double stud, single stud with resilient channel and single stud with GenieClip™ sound isolation clips.

Single Stud Wall

In all constructions tested the following materials were used; nom 2x4 wood studs spaced 406mm O.C., R-13 un-faced fibreglass batts 89mm thick and 15.9mm Type X gypsum board was screwed to the studs or framing members with 25mm drywall screws spaced 203mm O.C. around the perimeter and 305mm O.C. in the field.

Staggered Stud Wall

The perimeter frame was 2x6 wood with a single head and sill plate. Nom 2x4 wood studs were staggered at 203mm O.C. R13 insulation was installed in the stud space.

Double Stud Wall

Two frames were constructed consisting of 2x4 wood studs spaced 406mm O.C. There was a 25mm gap between the two frames. R13 insulation was installed in both stud spaces.

### 1.2. Non-Structural Framing and Gypsum Board Layers

Two types of framing were used in an attempt to decouple the gypsum board from the structural studs. The first was a 12.5mm Dietrich single leg RC deluxe resilient channels with dog bone slots. These were attached to the studs and oriented horizontally with the resilient leg above the screw leg and spaced 610mm O.C.

The GenieClip™ type RST was also used and attached to the studs at a vertical spacing of 610mm O.C. and a horizontal spacing of 1.22m O.C. 22.2mm, 25 Gauge drywall furring channels were installed into the GenieClips.

All five assembly types were tested with 1 and 2 layers of gypsum board on both sides.

## 2. METHODS

All constructions were assembled and tested in accordance to ASTM E90-09, and ASTM E2235-04. The test chamber source and receiving room volumes are 204 and 148.4 cubic meters respectively. Western Electro-Acoustic Laboratory is accredited by the United States Department of Commerce, National Institute of Standards and Technology under the National Voluntary Accreditation Program (NVLAP) Lab code 100256-0 for this test procedure.

## 3. RESULTS

The data is shown below. Where 1,1 is denoted this indicates that the test had 1 layer of 15.9mm Type X gypsum wallboard on both the source and receiving side of the wall. 2,2 denotes a double layer on either side.

In figures 1 and 2 the legend is as follows: Double Stud – Black, GenieClip – Red, Deluxe RC – Orange, Staggered stud – Blue, Direct attach – Green. The bars at the bottom show the deficiency from the STC contour, providing an idea of where the curve and overall rating was controlled.

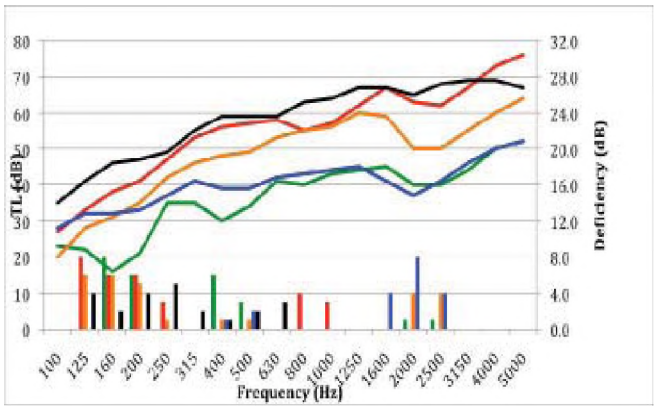


**Figure 1. ASTM E90 Test Results for Single Layer (1,1) Wall Constructions**

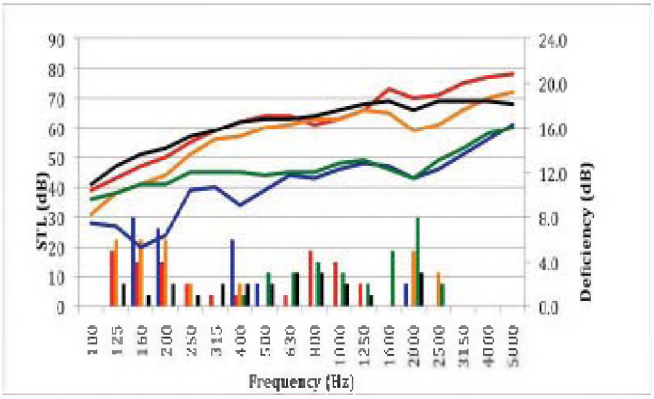


**Figure 2. ASTM E90 Test Results for Double Layer (2,2) Wall Constructions**

**Table 1. STC Test Results for All Constructions**

| Wall Type | STC – 1,1 | STC – 2,2 |
|---|---|---|
| Single Stud | 37 | 41 |
| RC Channel | 50 | 60 |
| GenieClip | 57 | 64 |
| Staggered Stud | 41 | 47 |
| Double Stud | 61 | 65 |

## 4. DISCUSSION AND CONCLUSIONS

The double stud construction yielded the highest transmission loss results at low frequencies and the highest overall STC. The decoupled wall is much more effective than simply adding mass. Doubling the drywall only produced a 4dB increase, while creating a decoupled second row of studs and top and bottom plates produced an increase of 24dB. The low frequency performance of the double stud wall was 3-4dB better than any other partition in this test series.

The staggered stud walls performed very poorly overall with large deficiencies from 500Hz and up. High frequency vibration easily by-passed any attempt to decouple the opposite drywall layers via the common top and bottom plates. At the critical resonant frequency of 2000Hz, (for 5/8" drywall) the staggered wall produced the same TL as a single stud wall, providing zero improvement.

Although the drywall layers were attached to separate and staggered stud rows, the common plates allowed most vibration to by pass this attempt to decouple the wall. The increase in performance on single and double layer systems was only 4 and 6 dB respectively. Even a staggered stud wall with double layers of drywall on both sides did not achieve minimum code for multi-family construction.

When it is not feasible to build a double stud wall, decoupling can be simulated by using resilient metal framing materials. The "z" shaped deluxe resilient channel produced a 13dB improvement. By using the GenieClip the overall STC was increased by 20dB. The rubber isolation material molded to the GenieClip resulted in a 7dB improvement over resilient channel. The isolation clip wall was also better than RC-channel at low frequency by 2-3dB from 63 Hz and up. Above 1600Hz in a double layer system, the GenieClip wall actually outperformed all others including the double stud.

It is important to note that the resilient channel was installed with the resilient leg up, which allows gravity and the weight of the drywall to pull the channel away from the structure. Also screws were carefully placed as not to be driven through the channel to the structural studs. Both of these installation errors result in resilient channel commonly being "short-circuited". Resilient channel failure is a common observation by Acoustical Engineers. Short circuited resilient channel results in up to a 10 STC point reduction. The GenieClip system cannot be short-circuited provided 2.5" screws are not used to secure gypsum board.

## REFERENCES

Long, Marshall. (2006). *Architectural Acoustics* (Elsevier Inc., Burlington, MA)

Harris, Cyril M. (1998). *Acoustical Measurements and Noise Control* (Acoustical Society of America, Woodbury, NY)

LoVerde, J., & Dong, W. (2009). *Quantitative comparisons of resilient channel designs and installation methods.*

## ACKNOWLEDGEMENTS

Thank you to the staff at WEAL acoustical laboratories including Gary Mange and John LoVerde and to my colleagues at Pliteq Inc. including Ian Keiper and Paul Downey.

# ASTM METRICS FOR RATING SPEECH PRIVACY OF CLOSED ROOMS AND OPEN PLAN SPACES

**Bradford N. Gover and John S. Bradley**
National Research Council Institute for Research in Construction, Ottawa, ON K1A 0R6, Canada
brad.gover@nrc-cnrc.gc.ca

## 1. INTRODUCTION

ASTM International currently publishes two measurement standards for assessing speech privacy in building spaces. ASTM E2638 "Standard Test Method for Objective Measurement of the Speech Privacy Provided by a Closed Room" [1] is applicable only to enclosed spaces, and includes the definition of a measure called Speech Privacy Class (SPC). ASTM E1130 "Standard Test Method for Objective Measurement of Speech Privacy in Open Plan Spaces Using Articulation Index" [2] is applicable only to open plan spaces, and uses the Articulation Index (AI) as a privacy measure. This paper discusses the relationship between the two metrics, and their suitability for use in any type of space, including spaces not fitting the definition of either open or closed.

## 2. ASTM E2638

The E2638 method provides a rating of the average performance of a closed room – without any assumptions as to talker location – to each of a number of listener positions outside the room, close to the room boundaries. The level of a spatially uniform, broadband noise sound field is taken as the "source" level, and the corresponding levels at listener positions are taken as the "receive" levels. The level difference between the two is the measure of sound insulation that is part of the method.

For each receiving point, the level difference *LD(avg)* is added to the background noise $L_b(avg)$ to yield the Speech Privacy Class SPC = *LD(avg)* + $L_b(avg)$. Here "*(avg)*" means the 1/3-octave band values are arithmetically averaged from 160 to 5000 Hz.

## 3. ASTM E1130

The E1130 method provides a rating of the speech privacy between a specific source position and orientation and receiver position, in an open plan space. A calibrated loudspeaker with a specified directionality is required, and the reference "source" level is determined in a free field. The receive level is determined in the open plan space under consideration, and the difference between the two is the relevant measure of sound insulation. From this so-called "level reduction", and the measured background noise level, the AI is calculated, for a specified speech spectrum. AI by definition ranges from 0 (no intelligibility) to 1 (total intelligibility). E1130 also includes the definition of a metric called Privacy Index, which is simply a re-normalization: PI = (1 – AI) x 100%.

## 4. SPC AND PI

Regardless of how 1/3-octave band values of sound insulation and background noise are measured, both metrics (SPC and PI) can subsequently be calculated. Figure 1 shows the relationship for 100 simulated cases involving a wide range (in terms of spectral shape) of "level difference" or "level reduction", and of background noise.

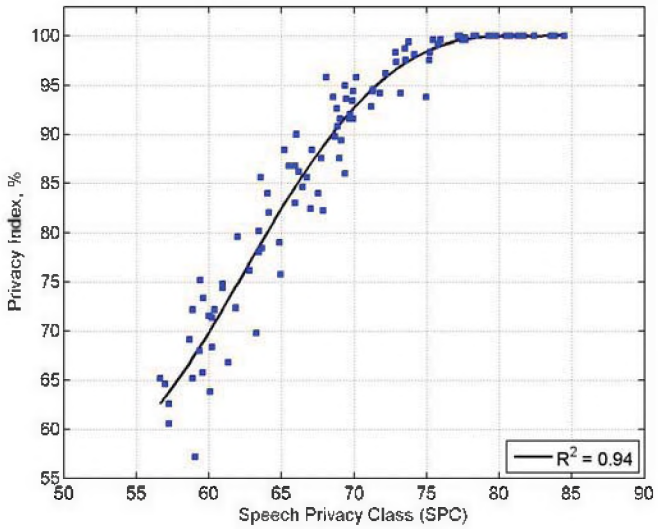


**Figure 1. Relationship between Privacy Index, PI (per ASTM E1130) and Speech Privacy Class, SPC (per ASTM E2638). The $R^2$ of the 4th-order polynomial fit is 0.94.**

Notice first that the correlation between SPC and PI is high ($R^2$ = 0.94). Also notice that, because PI is by definition limited to a maximum value of 100%, but SPC is not limited, a wide range of physical conditions are represented in the region PI > 95%. The sound insulation or noise can vary by ~12 dB, and yet PI varies by only a few percent.

E2638 includes a table of categories that identifies the frequency with which speech sounds would be audible or intelligible for various SPC values. These categories are given in Table 1 along with the corresponding SPC value, and, from the curve fit in Fig. 1, the corresponding equivalent PI value. E1130 includes definitions of "normal" and "confidential" speech privacy; the corresponding PI values are given in Table 2, along with the equivalent SPC values (from Fig. 1).

Based on the relationship of Fig. 1, the "Minimal Speech Privacy" category (SPC 70) is very nearly equivalent to "Confidential Speech Privacy" (PI = 95%). These results agree with those in Fig.5 of Ref. [3], using the specified voice spectrum to determine SPC.

**Table 1: Categories of speech privacy defined in ASTM E2638 with corresponding SPC and equivalent PI values.**

| E2638 Categories | SPC | Equivalent PI, % |
|---|---|---|
| Minimal speech privacy | 70 | 93 |
| Standard speech privacy | 75 | 98 |
| Standard speech security | 80 | 100 |
| High speech security | 85 | 100 |
| Very high speech security | 90 | 100 |

**Table 2: Categories of speech privacy defined in ASTM E1130 with corresponding PI and equivalent SPC values.**

| E1130 Categories | PI,% | Equivalent SPC |
|---|---|---|
| Normal speech privacy | 80 | 64 |
| Confidential speech privacy | 95 | 71 |

## 5. SPEECH INTELLIGIBILITY AND PRIVACY THRESHOLDS

Figure 2 shows the relationship between speech intelligibility scores and SPC (top) and PI (bottom), for a listening test described in Ref. [4]. The high correlation for both metrics implies both are useful for rating intelligibility over a wide range (from 100% to 0%).

Figure 3 shows the relationship between the percentage of listeners correctly identifying: at least one word from test sentences (labeled "Intelligibility"); and, the presence of speech sounds (labeled "Audibility"), also from experiments described in Ref. [4]. The correlations are high in all cases, but are somewhat higher for SPC (top) than for PI (bottom).

Notice that due to the truncation of PI (to a maximum value of 100%), the ability to distinguish among cases of moderate to high privacy is poor. All conditions higher than SPC 75 correspond to conditions for which PI > 98%. In this range, the audibility ranged from 100% (all listeners heard speech sounds) to 0% (no listeners heard speech sounds), and intelligibility ranged from about 15% to 0%.

Note that the relationships in Figs. 2 and 3 between intelligibility and thresholds and the two metrics should not be considered unique: varying the speech level, for a given SPC or PI, would result in different subjective scores. Only because the same source speech level was used for all tests in Figs. 2 and 3, are comparisons possible.

## 6. DISCUSSION

The two current ASTM metrics for rating speech privacy of building spaces are highly correlated, and both seem well suited for use in conditions where speech is intelligible, such as in open plan spaces. Of the two, SPC is best suited for use in conditions of high privacy, where speech is not intelligible. SPC also offers practicality in that a difference in, for example, 5 dB of sound insulation will correspond to a difference of 5 in SPC, whereas the corresponding difference in PI depends on the absolute value, and could be 0–2% for conditions of high privacy.

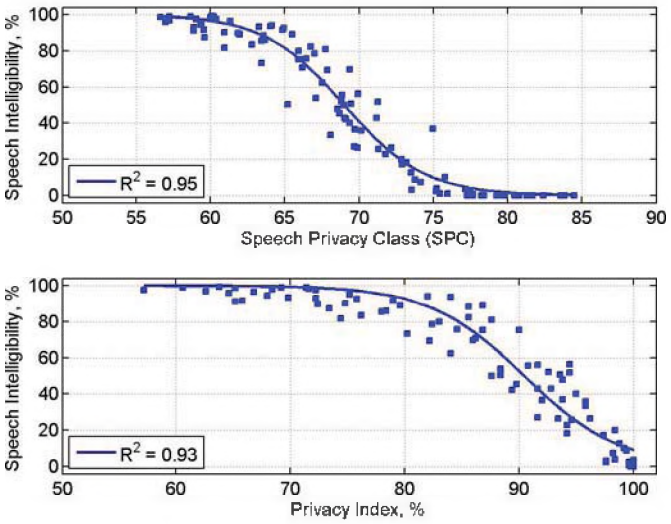


**Figure 2. Speech intelligibility (% words understood) vs SPC (top) and PI (bottom). The $R^2$ of the Boltzmann curve fit is shown on each.**

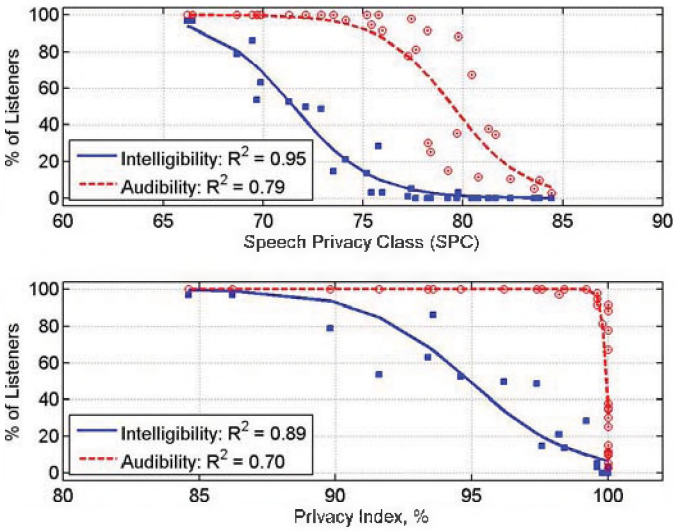


**Figure 3. Fraction of listening test participants (in %) correctly identifying at least one word (Intelligibility – squares) and identifying the presence of speech sounds (Audibility – circles) vs SPC (top) and PI (bottom). The $R^2$ of the Boltzmann curve fits are shown on each plot.**

## REFERENCES


[1] ASTM E2638-10 ASTM Intl., West Conshohocken, PA.

[2] ASTM E1130-08 ASTM Intl., West Conshohocken, PA.

[3] J.S. Bradley, "Comparisons of Speech Privacy Measures," Proceedings of INTER-NOISE 2009 (Ottawa).

[4] B.N. Gover and J.S. Bradley, "Measures for assessing architectural speech security (privacy) of closed offices and meeting rooms," *J. Acoust. Soc. Am.* **116**, 3480–3490 (2004).


## ACKNOWLEDGEMENTS


Parts of this work jointly funded by the Royal Canadian Mounted Police (RCMP) and Public Works and Government Services Canada (PWGSC).

# SOUND TRANSMISSION LOSS IMPROVEMENT BY A VISCOELASTIC MATERIAL USED IN A CONSTRAINED LAYER DAMPING SYSTEM

**Ivan Sabourin, Stefan Schoenwald, Jan-Gerrit Richter and Berndt Zeitler**
National Research Council Canada, 1200 Montreal Road, Ottawa, ON, K1A 0R6, Canada, Ivan.Sabourin@nrc-cnrc.gc.ca

## 1. INTRODUCTION

At NRC-IRC, a double leaf wall assembly has been tested with and without a constrained layer damper (CLD) to determine the improvement on the sound transmission loss (TL). In parallel, a Statistical Energy Analysis (SEA) model was derived to estimate the effect of the loss factor on the airborne TL. The theoretical and measured improvements will be compared in this paper.

The total loss factors (η) estimated from measurements [1] for the undamped and damped leaves of the wall assemblies were used as input data in the derived SEA model to estimate the relationship between total loss factor of the leaves and transmission loss. The SEA model could also be applied to other processes that change the total loss factor of the separating leafs.

A constrained layer damper is a viscoelastic material that is embedded between two parallel plates. The vibration energy in the first leaf creates shear strain in the viscoelastic material which dissipates kinetic energy into heat. A CLD is an effective way to maximize transmission loss through a partition by increasing its damping.

## 2. SETUP

The wall specimens described below were installed in the reverberant wall sound transmission facility of IRC and the airborne TL measurements were measured according to ASTM E90.

**Specimen description (3.6 m x 2.4 m)**

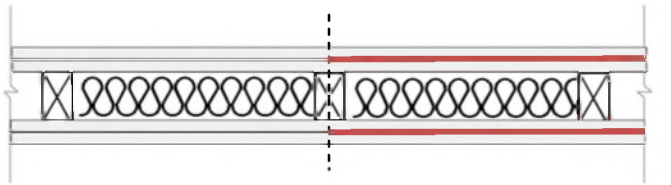


**Figure 2 – Wall assemblies viewed from above**

-2 x 4 wood studs spaced 610 mm o.c.
-2 layers of 16 mm (5/8 in.) gypsum board on each side
-Gypsum board screw spacing: *Base layer*: 41 mm screws spaced 610 mm o.c. along the edge and in the field
*Face layer*: 50 mm screws spaced 305 mm o.c. along the edge and in the field
-90 mm glass fibre insulation batts in cavity

The CLD wall assembly contains viscoelastic material embedded between the two gypsum panels on each side.

### 2.1 SEA model

SEA is a method for estimating the acoustic power flow through a system [2]. The method subdivides the system into smaller elements, the so-called subsystems (plates, beams, rooms, cavities), that support a group of resonant modes and have a sufficient modal density and modal overlap. Thus, in subsystems only resonant energy is considered that is stored by the modes and is governed by the damping. Further, coupling loss factors describe the power flow between coupled subsystems (e.g. between the room and the leaf of the wall) whereas total loss factors describe the sum of all energy losses within the subsystems. In case of the leaf of the wall the total loss factor includes internal losses due to vibration damping in the gypsum board and CLD as well as coupling losses due to radiation of sound into the room and into the cavity and vibration transmission through the frame to other subsystems.
For airborne sound transmission, a simplified SEA model system of two rooms separated by a simple double leaf wall is shown in Figure 1. The model includes only transmission paths with the leaves as resonant subsystems and hence sound transmission in the model depends on the total loss factor of the leaves. The model is only a first order approximation since non-resonant sound transmission through the leaves below the coincidence frequency that is not affected by the total loss factor of the leaves is assumed to be small and neglected.

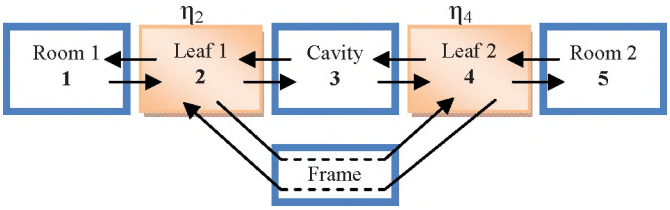


**Figure 1 – Simplified SEA model of two rooms separated by a double leaf wall**

The change in transmission loss (ΔTL) for the resonant transmission between the undamped and damped system can be calculated using the following equation:

$$\Delta TL = TL_{1-5,dampped} - TL_{1-5,undampped}$$

Using the simple SEA model and assuming the only difference in the system between the two cases is the damping of leaves 2 and 4, the change in transmission loss

can be expressed in terms of the total loss factors of the leaves:

$$\Delta TL = 10\log\left(\frac{\eta_{2,damped}\cdot\eta_{4,damped}}{\eta_{2,undamped}\cdot\eta_{4,undamped}}\right)$$

### 2.2 Measurement of the damping loss factors

The measurement of the loss factors on the wall specimens with and without the viscoelastic material was done as part of a parallel paper by J.G. Richter [1]. The reverberation method was used to measure the total loss factors on one side of the installed wall. The TL improvement was calculated for each 1/3 octave band by using the loss factors as input data in equation 1.

## 3. RESULTS AND DISCUSSION

Figure 2 contains the airborne TL curves for both wall assemblies with and without a CLD system.

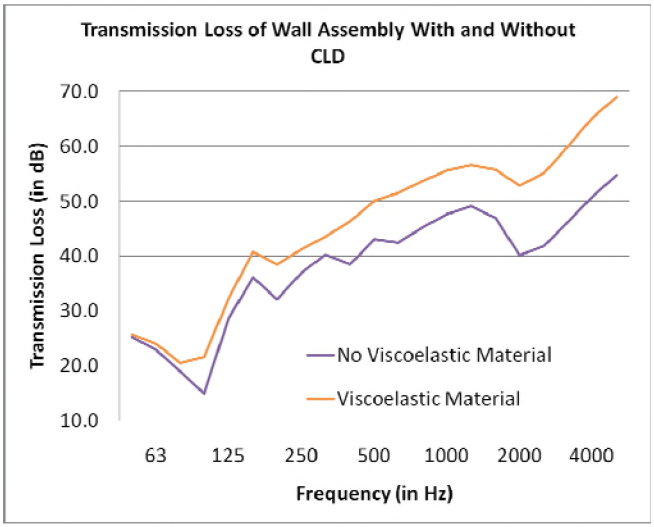


**Figure 2 – Measured transmission loss with and without constraint layer damper (CLD).**

The addition of a viscoelastic material between the leaves improves the TL significantly by more than 10 dB in the mid- and high frequency range increasing the STC rating by 8 points from 44 to 52. The critical frequency, 2000 Hz, is the same for both wall assemblies, which indicates that the stiffness properties of the leaves are not affected by the viscoelastic damping compound.

Figure 3 shows the difference in TL with and without the CLD (Figure 2) and the estimated ΔTL calculated from the SEA equation 1.

Although the curves crisscross each other, there is very good agreement between the measured and estimated ΔTL. Below the coincidence frequency the agreement is better than above, although it was expected that the estimate might be compromised by non-resonantly transmitted sound that is not considered in this simple SEA model.

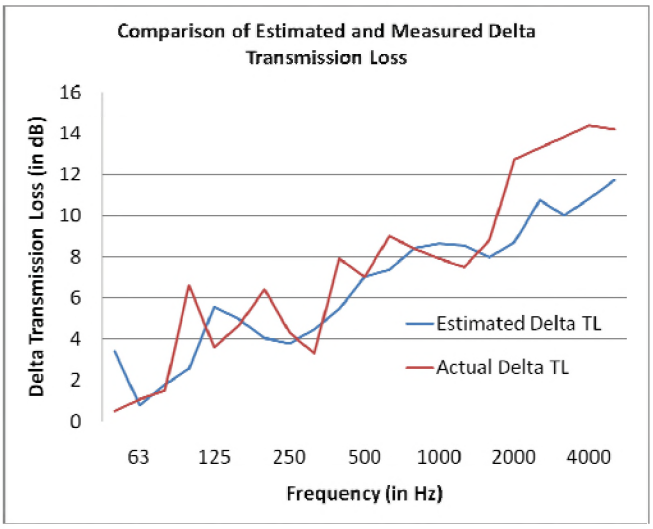


**Figure 3 – Comparison of estimated and measured change in transmission loss.**

Thus, the results support the assumption that most sound is transmitted resonantly by the frame and the cavity. The divergence above coincidence frequency can be attributed to uncertainties in the measured total loss factors, e.g. small decay range or back-coupling of radiated sound from the room.

## 4. CONCLUSION

The SEA model seems to be good enough to calculate the change of transmission loss due to added damping for a double leaf assembly and constraint layer damping is an effective way to increase the transmission loss. Knowing the relation between the damping loss factor of the leaf and the transmission loss of the partition is essential in designing better leaves and materials needed for higher performing assemblies. This paper presented a link between the material properties of the leaf and the improvement of the transmission loss.

Further work could include verification of the method with other viscoelastic materials used in a CLD application.

## REFERENCES

[1] Ritcher, Jan-Gerrit (**2011**) ,*Comparison of Different Methods to Calculate Structural Damping*, 2011 CAA Conference Proceedings

[2] Craik, Robert JM (**1996**), *Sound Transmission through Buildings using Statistical Energy Analysis*, Gower Publishing Ltd.

## ACKNOWLEDGEMENTS

The author wishes to acknowledge the work done by Jan-Gerrit Richter in calculating the total loss factors used as input for this paper.

# COMPARISON OF DIFFERENT METHODS TO MEASURE STRUCTURAL DAMPING

**Jan-Gerrit Richter, Berndt Zeitler, Ivan Sabourin and Stefan Schoenwald**
National Research Council Canada, 1200 Montreal Road, Ottawa, ON, K1A 0R6, Canada.
Jan-Gerrit.Richter@nrc-cnrc.gc.ca

## 1. INTRODUCTION

Structural damping indicates the energy loss in materials and systems respectively. Hereby, different loss mechanisms must be distinguished: namely internal losses or material damping due to conversion of kinetic energy into heat and coupling losses due to transmission of energy to adjoining systems, e.g. by structural transmission at connection points or even sound radiation from a structure into a room. Having the ability to reliably measure the damping loss factor should enhance the capability of predicting the transmission loss in wall or floor assemblies.

In the following, three different methods to obtain the damping loss factor are discussed and compared.

All methods are presented on a (2.41 m x 1.22 m x 0.012 m) Plexiglas plate to verify the methods and are further used to compare the loss factors of two wood framed walls – one with an applied constraint layer damper (CLD) and one without, both described in detail in a parallel paper [1].

## 2. METHODS

### 2.1 Reverberation Time Method

The first method, called Reverberation Time Method, uses as its name suggests the structural reverberation time, T, (time in which the energy of the system decays by 60 dB) to calculate the total loss factor $\eta$ of the system.

The dependency of the loss factor on the reverberation time is $\eta \approx \frac{2.2}{f \cdot T}$ with f being the frequency.

The reverberation time was obtained by exciting the specimen with a small force hammer at three positions using three repeats and measuring the acceleration at eight points distributed over the specimen. Schroeder Plots [2] of the responses were calculated using the Schroeder backwards integration as noted in Equation (1) and evaluated according to ISO 3382 to obtain the single reverberation times at each third octave band. The overall third octave band reverberation times are the average of all single measurements.

$$d(t) = \int_t^\infty f(x)^2 \, dx \qquad (1)$$

### 2.2 Power Injection Method

The second method, called the Power Injection Method [3], uses the relation between the power injected into a system, $P_{in}$, and the resulting space averaged vibration power, $P_v$, to obtain the total loss factor of the system

$$\eta = \frac{P_{in}}{P_v}, \text{ with}$$

$$P_{in} = \frac{1}{\omega} Im\{G_{FA}\} \text{ and } P_v = \omega \, m \, v^2,$$

where $G_{FA}$is the cross spectrum density of the force and acceleration at the drive point. This model assumes steady state excitation and a diffuse field in the system achieved through high modal density.

In the experiment the specimen is excited by a Wilcoxon F3 shaker using white noise while measuring the velocity at the same eight points as for the first method averaged for 30 seconds. The drive point force and acceleration were measured using an impedance head that was integrated into the shaker.

### 2.3 Drawaway Method

For the third method, the Drawaway Method, the decay of a propagating bending wave is evaluated to estimate the loss factor on the plate $\eta_p$ (not the total loss factor of the system). A very simplistic approach is used assuming a circular bending wave front around a point source on an isotropic infinite plate in the far field. This means reflections from the edges and near field terms are neglected leading to a wave power decay proportional to

$$P_p \sim v^2 \sim \left(\frac{1}{\sqrt{x}} e^{-k' \frac{\eta_p}{4} x}\right)^2$$

with v as the velocity on the plate, r distance from excitation point, and $k'$ as the real part of the wavenumber. The loss factor can be estimated by measuring the unknowns ($v^2$ and k'), rearranging the logarithm of Equation (2), and performing a linear regression to obtain the slope dependent on $\eta_p$.

$$\ln(v^2) + \ln(x) \sim -k' \frac{\eta_p}{2} x$$

Because of the neglected reflected wave, this loss factor is expected to underestimate the loss factor.

A method to obtain the real part of the wavenumber from drawaway measurements is described in detail in a paper by Nightingale et al. [4]. The velocity was measured while exiting the specimen with a shaker at 24 points, 5cm apart, on a straight line.

## 3. RESULTS

Comparing the methods on a Plexiglas plate shows that the results from the Reverberation Time and the Power

Injection method are reasonably similar. The Drawaway method only gives sensible results above 3000 Hz (see Figure 1)

The low agreement of the drawaway method is explained by the multiple simplifications made by the model. Even in the midrange frequency bands, reflections make detecting a clear decay impossible. At low frequencies the near field additionally distort the vibration pattern especially closer to the excitation point.

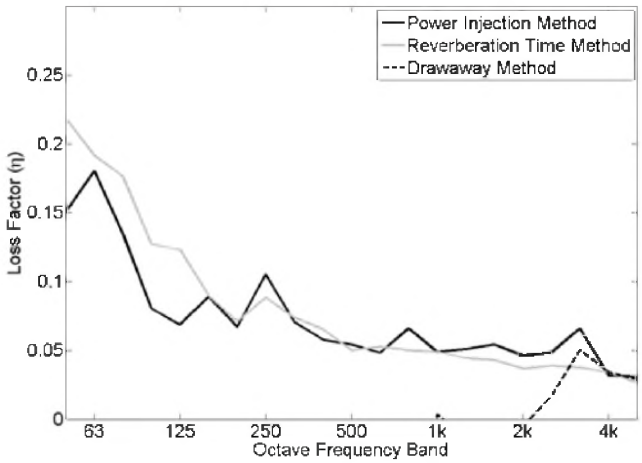


**Figure 1. Three Methods on a Plexiglas plate**

Because of the similarity between the power injection and the reverberation method, only the reverberation method is evaluated on the wall assemblies.

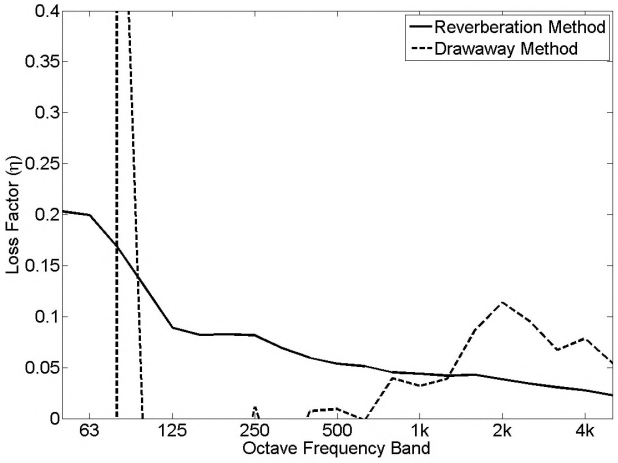


**Figure 2. Loss factor before adhesive is applied**

Figures 2 and 3 show the results of the measurements on the wall assembly before and after applying the viscoelastic material. It can be observed, that with the higher damping provided by the material, the drawaway method gives a more reasonable result in a larger frequency range, however by a factor of approximately 2 larger than with other methods. An additional error might stem from the inhomogeneous stiffening from fastening the plates to the studs.

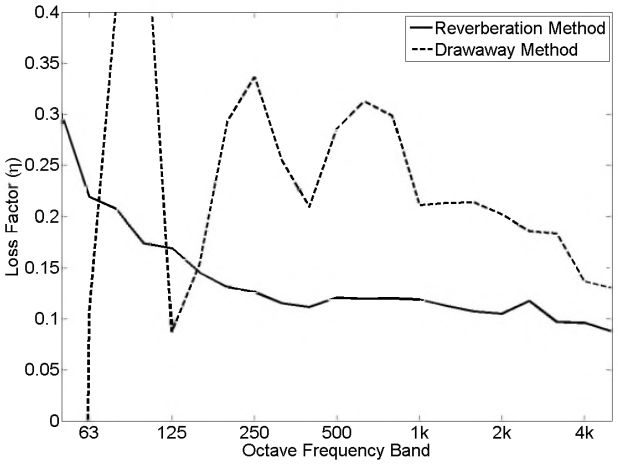


**Figure 3. Loss factor after adhesive is applied**

## 4. DISCUSSION AND CONCLUSIONS

The Reverberation Time Method is a good way to measure the total loss factor of a specimen. Although it is the most time consuming method, both in measuring and in the analysis, the results seem to be the most consistent. The power injected method gives similarly good results but will have limitations on smaller samples as the field will not be as diffuse.

The assumptions made for the drawaway method turned out to be too general. Further refinement is needed to include reflections, the near field and a none-circular expansion of the wave.

The effect of the improved damping on the airborne transmission loss according to ASTM E90 is described in a follow up paper by I. Sabourin. [3]

## REFERENCES


[1] Sabourin, I. et.al (2011). *Sound transmission loss improvement by a viscoelastic material used in a constrained layer damping system* (CAA Conference Proceedings)

[2] Schroeder, M.R. (1979). *Integrated-impulse method for measuring sound decay without using impulses* (Journal of the Acoustical Society of America Volume 66, Issue 2).

[3] Schoenwald, S. (2006). *Flanking Sound Transmission through Lightweight Framed Double Leaf Walls* (Eindhoven University Press, Eindhoven)

[4] Nightingale, T.R.T. et. al (2006). *Bending wavenumber and associated damping* (Proceedings of International Congress on Sound and Vibration, Vienna, Austria)

# ACOUSTIC SIMULATIONS OF WORSHIP SPACES

**Ramani Ramakhrishnan[1] and Romain Dumoulin[2]**
[1]Department of Architectural Science, Ryerson University, Toronto, ON, rramakri@ryerson.ca
[2]3126 Blvd. Rosemont, Montreal, Quebec, dumoulin.acoustics@gmail.com

## 1. INTRODUCTION

Acoustic simulations of religious facilities need to focus on specific acoustic parameters, due to the different aural expectations of the congregations. In mosques, the main acoustic objective is speech intelligibility; whereas in churches and synagogues, the contrasting demand between adapted reverberance for music and clarity for intelligible speech is the main issue of the acoustical design. The nature of contemporary houses of worship is to serve more than one purpose. And hence due consideration for acoustical prediction should be taken alongside the development of sound system use. Galindo et.al. used simulation software to evaluate the acoustics of European churches[1].

In this investigation, acoustical simulations were applied to provide recommendations to the proposed design of the sanctuary of a United Church in Toronto. Since the existing sanctuary is seen to provide an acceptable and satisfactory sound environment, an evaluation of the acoustic performances of the existing sanctuary was carried out with measurements of the reverberation time. Simulations were conducted using CATT Acoustic software[2]. The calibration of the model was undertaken by comparing the results of the simulation and the measured data. Two main acoustical descriptors were used for the evaluations of the new sanctuary: Reverberation Time, RT and Speech Transmission Index, STI. Standard guidelines used for reverberation times were also applied in this investigation[3].

Different scenarios as to the placement of the speakers as well as to the acoustical materials used inside the sanctuary were evaluated with CATT Acoustic. Results of the above investigations are presented below.

### 1.1. Existing Sanctuary

The sanctuary, shown in Figure 1, has an overall volume of about 1850 m$^3$ and a floor surface of 255 m$^2$. The ceiling is vaulted with a highest point reaching 9.7 m in the nave and 6.3 m in the chancel. The floor is carpeted, the furnishings are finished plaster for the walls and the ceiling and a number of large stained glass windows. The seating is wooden pews with cushions. The measurements of the reverberation time of empty room show that the values across the frequency band are 1.6 seconds or less and the measured results are shown in Figure 2.

### 1.2. New Sanctuary

The proposed sanctuary, shown in Figure 3, will be a multipurpose space. The stage for the activities could vary depending on the program. For ease of analysis, two scenarios, chancel stage and the area along the west wall, are assumed for acoustic calculations. With an overall volume of 1390 m$^3$, the hall has a rectangular shape with a squared floor surface of 223 m$^2$ and a 6.2 m high ceiling. It will be able to accommodate up to 200 people in portable wooden chairs. The current building surfaces are painted concrete for the floor, drywall construction for the ceiling and walls with wooden doors and one window.

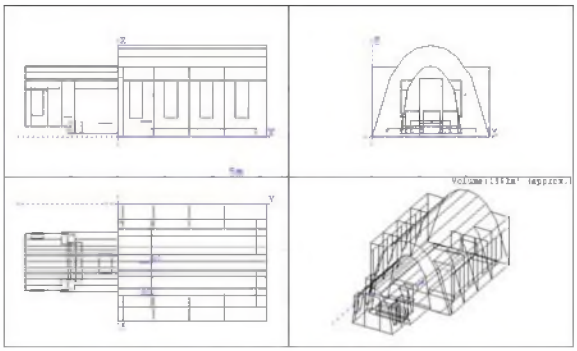

**Figure 1. Details of the Existing Sanctuary.**

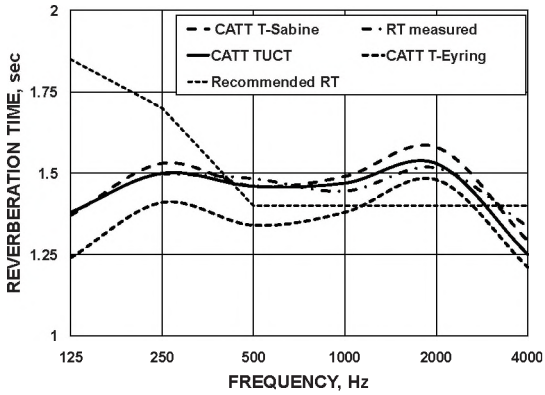


**Figure 2. Reverberation Time in the Existing Sanctuary.**

## 2. RESULTS AND DISCUSSION

### 2.1 Calibration Process

The process consists in an adjustment of the absorption and scatterings coefficients in order to match the simulated Reverberation time results to the measurements. The most adapted Scattering and absorption coefficients are chosen in the literature data for each existing material[4, 5, 6]. The CATT-ACOUSTIC Sabine and Eyring reverberation time predictions have been used in the calibration process but a

TUCT (The Universal Cone Tracer) module algorithm prediction have been launched at the end of the process to predict more accurately the simulation results.

Absorption coefficients values of "Unoccupied moderately upholstered chairs" at 1000, 2000 and 4000 Hz have been decreased to match with the characteristics of the empty wooden pews with thin cushion above a parquet floor[5]. The "Plasterboard ceiling on battens with large air-space above" absorption coefficient has been used for some parts of the ceiling and walls in order to take in consideration the absorption in low frequencies of ceiling mounted method[6]. Differences between measurements and simulated results at the 4 kHz values can be explained to be due to the importance of air absorption in this range of frequencies and the use CATT-Acoustic's pre-defined data.

### 2.2 Acoustical Simulations of the Proposed Sanctuary

CAD drawings and the interior surface materials of the proposed sanctuary, shown in Figure 3, were applied in the simulations by CATT-Acoustics. Appropriate absorption and scattering coefficient were assigned and reverberation time and STI simulations were carried out. Different scenarios were examined with the following audience parameters: empty, 100 people and 200 people. The main observation was that $RT_{60}$ values of the sanctuary are high, especially with wooden chairs, for both speech and music. Speech and music will sound muddled and discoloured. It is clear, therefore, that the $RT_{60}$ values must be reduced across the frequency bands. Different scenarios, such as reasonably upholstered chairs and adding absorbing panels, were attempted to reduce the $RT_{60}$ values.

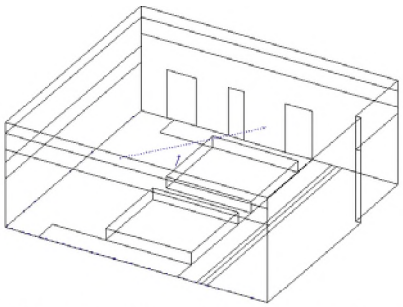

**Figure 3. Interior View of the Proposed Sanctuary.**

The acoustic panels were added along the long wall (East) in two different segments. The results of the simulation are shown in Figure 4.

Speech Transmission Index results were evaluated with a simple Yamaha speaker system with known characteristics. We assumed the speaker in the centre and the audience is distributed around the sanctuary. A slight global STI improvement due to the absorption has been noticed, as well as STI "fair" conditions. Improved STI in the range of fair to good are achieved with the use of two cluster of left-right speakers.

## 3. CONCLUSIONS

The proposed renovations of a United Church in Toronto were investigated as to their acoustic characteristics. Differences between the measured and the calculated data were found to be acceptable and hence validating the acoustical simulation method The bass absorption of the wall and ceiling plaster mounted technique, the absorption of carpeted floor and the diffusion due to the architectural details made the acoustics of the existing sanctuary more than satisfactory. Those acoustic characteristics have not been considered in the design of the new sanctuary. The lack of these aspects prevented the members of the church committee to have specific acoustics requirements and the architects to consider an acoustic design. The current simulations results were therefore provided the needed modifications of the sanctuary design.

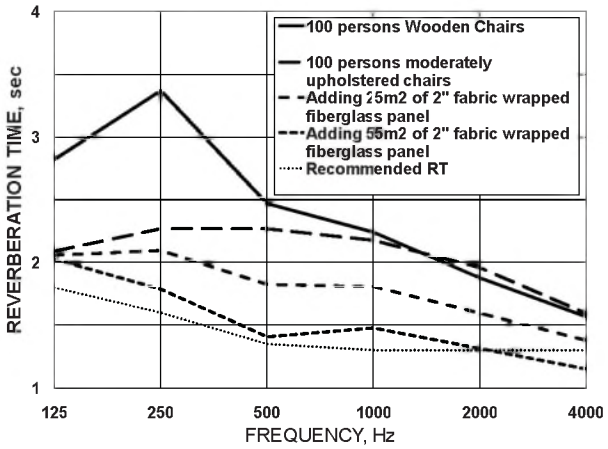


**Figure 4. Reverberation Time in the Proposed Sanctuary.**

The link between the acoustic corrections and the descriptors values can be studied and predicted even without measurements and calibration process. The main limitations of simulations that must be noted are: the lack of absorption and scattering coefficient data; and the bass frequencies prediction limitations caused by the range of prediction frequencies that are four times above Schröeder's frequency.

The main conclusion is that acoustical simulations with room acoustic software like CATT-ACOUSTICS are an effective tool to study and predict the acoustics of house of worship, where accurate prediction of reverberation times, STI evaluations and sound system studies can be performed.

## 4. REFERENCES


1. Miguel Galindo, Teófilo Zamarreño, and Sara Girón, "Acoustic simulations of Mudejar-Gothic churches," J. Acoust. Soc. Am., Vol. 126, No. 3, pp. 1207–1218 (2009).
2. CATT Acoustics. V8.0g (build 2.02) CATT (1998-2007).
3. Doelle L. L. *Environmental Acoustics,* MacGraw-Hill book company, (1972).
4. T. J. Cox and P. D'Antonio *Acoustic Absorbers and Diffusers. Theory, Design and Application,* Spon Press, London, (2004).
5. Kutruff, H, *Room Acoustics*, Elsevier Applied Science. Elsevier Science Publishers, Essex, 4th edition, (2000).
6. Vorländer *Auralization, Fundamentals of Acoustics, Modelling, Simulation, Algorithms and Acoustic Virtual Reality,* Springer-Verlag, Berlin, (2008).

# Evaluation of a New Speech Privacy Quick Test for Enclosed Rooms

**John S. Bradley and Bradford N. Gover**
National Research Council Institute for Research in Construction, Ottawa, ON K1A 0R6, Canada
John.Bradley@nrc-cnrc.gc.ca

## 1. INTRODUCTION

The speech privacy provided by an enclosed room can be assessed in terms of the Speech Privacy Class (SPC) as described in ASTM E2638 [1]. SPC is the sum of the measured ambient noise level, ($L_n$) at the position of a potential eavesdropper and the measured level difference (LD) from a room average level in an adjacent room.

$$SPC = LD(avg) + L_n(avg) \quad (1)$$

LD(avg) and $L_n$(avg) are arithmetic averages of decibel values over the 1/3-octave bands from 160 to 5000 Hz.

The E2638 procedure can identify weak points in the room sound insulation and can give an accurate rating of the overall speech privacy provided by the room. In some cases a simpler and quicker test, that could evaluate particular problems, would be more helpful. This paper reports on the development of a speech privacy Quick Test (QT) intended to provide a more focused and efficient evaluation of the speech privacy provided by parts of enclosed rooms.

Whereas the E2638 method requires multiple source and receiver positions in the source room, the QT uses a single loudspeaker position 1 m from the room boundary in the source room. As illustrated in Fig. 1, the receiver is located 0.25 m from the room boundary outside the room and opposite the sound source. This test configuration resulted from extensive tests to develop a procedure that would provide results in close agreement with the E2638 procedure [2].

## 2. MEASUREMENTS

The attenuations of 3 test walls were measured in terms of level differences (LD(f)) using the QT procedure. These were compared with LD(f) values from the full E2638 test [1] and also with standard transmission loss (TL(f)) test results. The comparisons were repeated for the 9 combinations of 3 test walls (STC 49, 46 and 32) and 3 room absorption conditions, intended to represent a wide range of constructions and room acoustics conditions. Results were repeated using both an omni-directional source (dodecahedron) and a directional source (23 cm diameter driver in non-vented enclosure). Several approaches to measuring the source levels for the QT were considered and direct measurement at a distance of 1 m in each source room was most successful [2].

## 3. HIGHLIGHTS OF RESULTS

Fig. 2 shows an example of comparisons of LD(f) and TL(f ) values for one of the 9 test conditions. The wall was

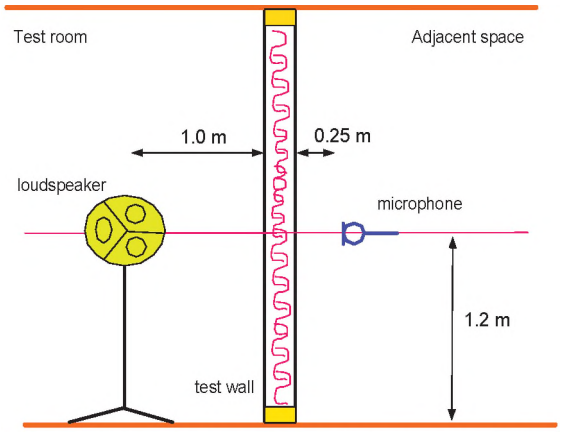


**Figure 1. Source and receiver positions for Quick Test.**

a steel stud and gypsum board construction with a measured rating of STC 49. The absorption condition corresponded to mid-frequency reverberation times of about 0.8 s in the test room and about 0.6 s in the receiving space. For this absorption condition, the E2638 test results for both the omni-directional source (OMNI) and the directional source (DIREC) gave very similar LD(f) values and these LD(f) values were quite similar to the TL(f) values up to the coincidence dip frequency (2500 Hz). For less absorptive room conditions, the TL(f) values were higher in value than the LD(f) values from the E2638 test results up to 2500 Hz.

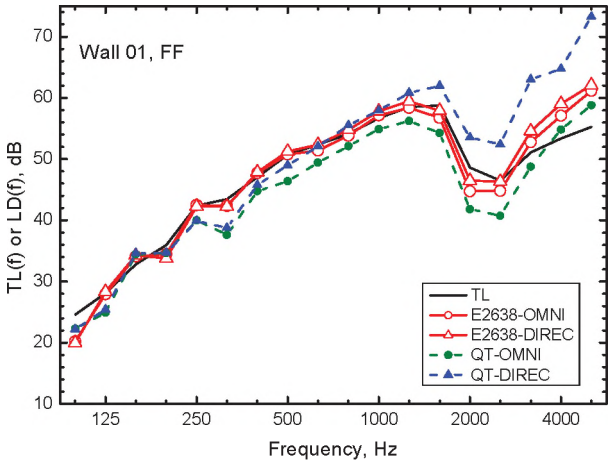


**Figure 2. Comparison of QT and E2638 test LD(f) values with TL(f) values for STC 49 rated Wall01.**

The LD(f) values from the QT procedure diverged from the other results with the differences increasing with increasing frequency. When using the OMNI source, the QT results varied in a manner approximately parallel to the E2638 results. However when the DIREC source was used, the QT results gave much larger LD(f) values at higher frequencies

than the other tests. These source-type related differences were also present for the other room absorption conditions.

When the results of two different tests vary in a somewhat parallel manner over frequency, we can more easily adjust values of one test to give approximately the same values as the other test. This was done in terms of the respective LD(avg) and TL(avg) values. Fig. 3 shows how the differences between the E2638 and QT LD(avg) values vary with room absorption. From the lowest to highest absorption conditions, the LD(avg) differences vary by a little less than 2 dB. One can use Fig. 3 to improve estimates of E2638 LD(f) values from QT LD(f) values.

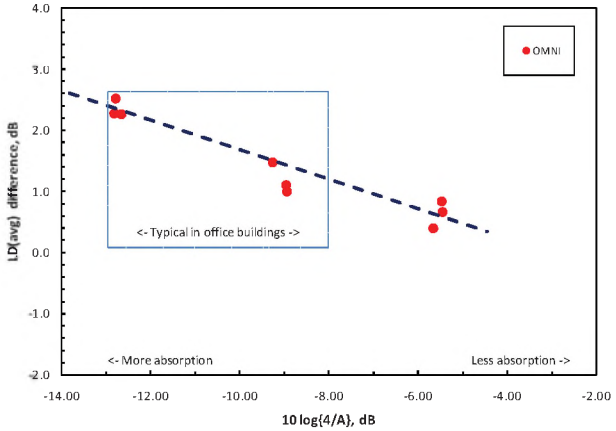


**Figure 3. E2638 test minus QT LD(avg) values versus room absorption for OMNI source results.**

Similarly, LD(avg) values from the QT were related to TL(avg) from standard sound transmission loss tests. These differences are shown in Fig. 4 for OMNI source measurements and can be used to estimate TL(avg) values from QT measurements. There is little scatter about the best fit line and the range of mean differences between these two quantities is again less than 2 dB over a wide range of room absorptions.

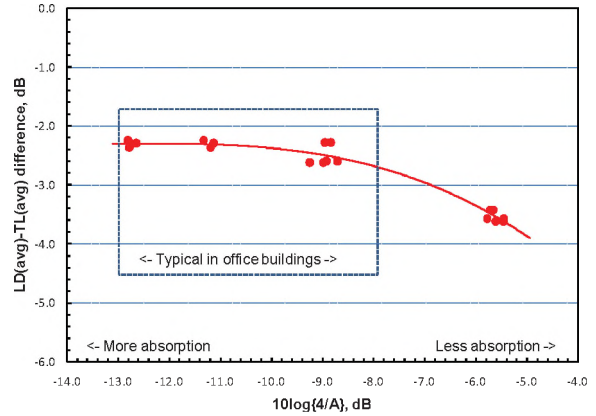


**Figure 4. LD(avg) from QT minus TL(avg) differences versus room absorption for OMNI source results.**

Fig. 5 shows two examples of applying the differences of frequency averaged values to adjust LD(f) values over a broad range of frequencies. In Fig. 5 LD(f) values from QT results, adjusted according to variations with room absorption (from Fig. 3), are compared with the measured LD(f) values from the E2638 test. Comparisons are included for both the Wall02 and Wall03 constructions and show very good agreement between the E2638 measurements and the adjusted QT results. That is, the QT procedure can be used to obtain LD(f) values that agree well with the E2638 test results at particular locations. However, this good agreement was only possible when using the OMNI source. Measurements using the DIREC source led to differences between the two methods that varied significantly over frequency. Because these variations over frequency are expected to be different for different directional sources, the QT procedure is most successful when using an OMNI source.

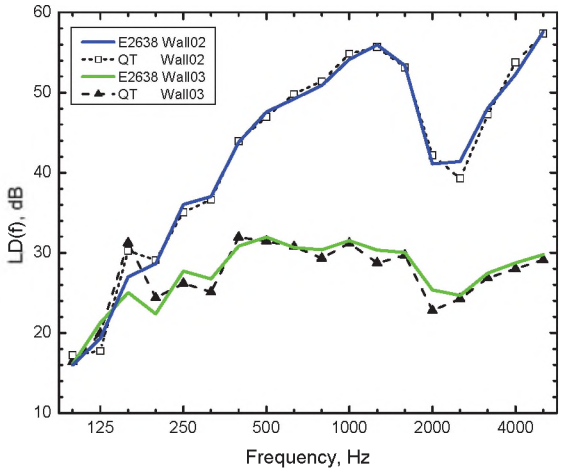


**Figure 5. Comparison of measured LD(f) values for Wall02 (STC 46) and Wall03 (STC 32) using the E2638 test results with those from adjusted QT LD(f) measurements.**

## 4. CONCLUSIONS

A new QT procedure was developed by making extensive comparisons with E2638 test results [2]. It includes using an omni-directional source, separate measurements of the source output levels, and the setup shown in Fig. 1. The QT can provide measured LD(f) values that agree well with those of the ASTM E2638 procedure.

## REFERENCES

[1] ASTM E2638-10, "Standard test method for objective measurement of the speech privacy provided by a closed room," ASTM International, West Conshohocken, PA (2010).

[2] Bradley, J.S. and Gover, B.N., "Development of a Speech Security Quick Test and Software", NRC-IRC Research Report, RR-313, (March 2011).

## ACKNOWLEDGEMENTS

This project jointly funded by Public Works and Government Services Canada (PWGSC), the Royal Canadian Mounted Police (RCMP), and the National Research Council Canada (NRC).

# NOISE REDUCTION OF A STANDARD CURTAIN WALL CONSIDERING OPENING FOR NATURAL VENTILATION

**Jean-Philippe Migneron[1] and André Potvin[1]**
[1]Groupe de recherche en ambiances physiques (GRAP), École d'architecture, Université Laval,
1, côte de la Fabrique, Québec (Qc), Canada G1R 3V6, jean-philippe.migneron.1@ulaval.ca

## 1. INTRODUCTION

The growing interest in natural or hybrid ventilation systems makes a challenge for good integration of openings in building façades. In a noisy environment, there is an important limitation for the use of direct openings with common building envelopes. As a part of a research project dedicated to this problem, it is possible to evaluate the impact of a curtain wall before testing several double-skin configurations. Experimental measurements made in laboratory conditions lead to the estimation of usual noise reduction and sound transmission class. Moreover, the airflow capacity can be assessed as a function of the aperture. Analyzing those parameters together should give useful information for the design of passive ventilation with a significant airflow when acoustical performance is an important issue.

### 1.1. Global research project

The actual study is a part of an on going project managed by the *Groupe de recherche en ambiances physiques* (GRAP) at the school of architecture of Université Laval in Quebec City. As explained, there is an interest to get air exchange through building façades without letting noise to penetrate inside. Those parameters are directly linked to the comfort of occupants by perception of physical ambiences, as for thermal environment, air quality, lighting, and sound. Acoustical treatment of building openings is complex, as many construction elements and phenomena must be considered. De Salis et al. [1] have made a remarkable review of most possibilities in relation with natural ventilation.

On the other hand, actual practice in architectural conception and design shows a need for better description of dynamic performances that involve various variables. Consequently, this long-term research points towards achieving a comparative analysis of different constructions regarding acoustics and the use of natural ventilation. After previous reports about windows [2] or a prototype for hidden silencer, this paper focuses on curtain wall. It should be followed by further try-out with multiple configurations of double skin envelopes.

### 1.2. Curtain wall sample

The proposed sample of insulated curtain wall is based on standard construction that includes an aluminium structure and windows. Chosen assembly consists in a self-standing frame divided in nine windows, three of them being operable. As it is generally the case, the overall thickness of sealed units is 25 mm (1 inch), having two glasses of 6 mm and a gap of 12 mm. Figure 1 details dimensions of the sample built in the laboratory, which represents a total transmission area of 12.7 m$^2$.

## 2. EXPERIMENTS

### 2.1. Testing facility and sample installation

Both reverberating chambers of the acoustical laboratory of Université Laval were used to achieve all data acquisitions. The first room of 200 m$^3$ is separated from the second of 60 m$^3$ by an opening of 7.9 m$^2$ (2.63 x 3.00 m). However, it must be noticed that the curtain wall was installed to fulfill dimensions of the smaller room. To be able to move the curtain wall in the future, the main structure was put into a 2x8 in. wood frame. Junctions with laboratory walls were carefully caulked with acoustical sealant, and neoprene compression joints were added to all sides.

### 2.2. Testing method

For noise insulation tests, an omni-directional loudspeaker was used in the source chamber. Measurements were made with a pink noise generator, in accordance with ASTM E90 [3]. Acquisitions of sound pressure levels and reverberation times were recorded on a real time acoustic analyzer. Those values were processed afterward to calculate transmission loss and sound transmission class index, following ASTM E413 [4].

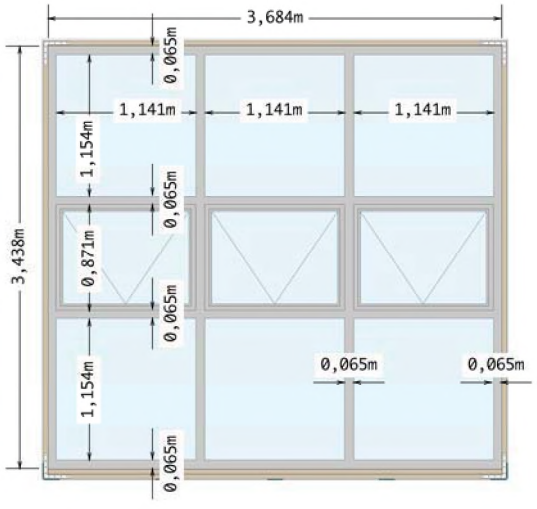


**Figure 1. Dimensions of tested curtain wall.**

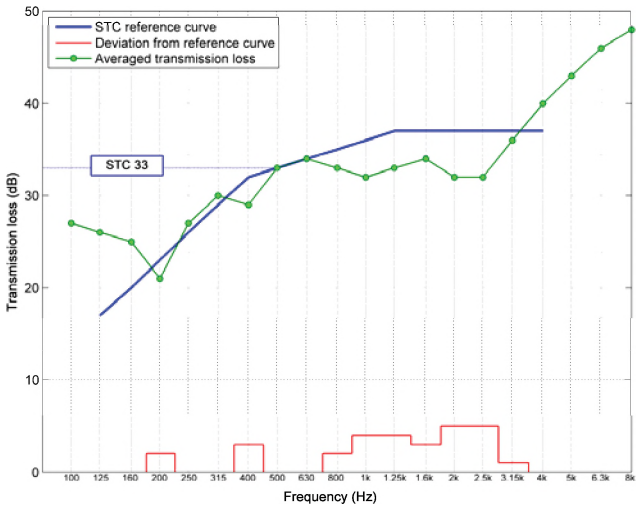


**Figure 2. STC calculation for tested curtain wall with 6/12/6 mm sealed units and closed windows.**

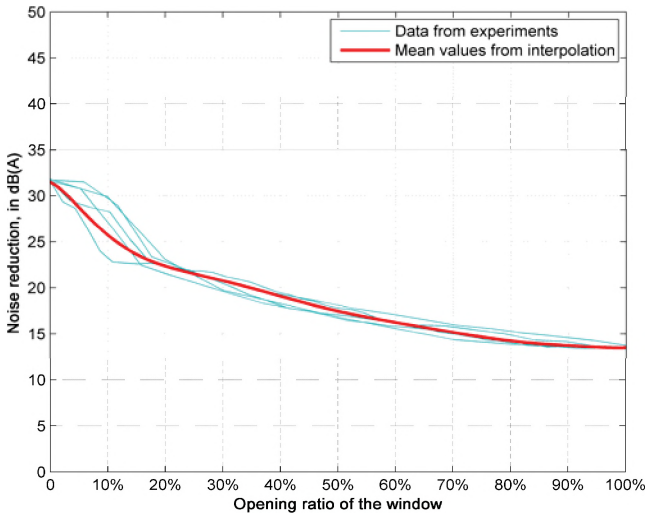


**Figure 3. Noise reduction for the curtain wall depending on the opening ratio of one operable window.**

## 3. RESULTS

### 3.1. Sound insulation of closed and half-opened wall

Firstly, evaluation of the sound insulation procured by the façade sample has been tested with all windows closed. Sound pressure levels were noted and averaged in both rooms to get the noise reduction. Reverberation time measurements made in the receiving room then allowed the calculation of normalized insulation values, which has lead to a global sound transmission class of 33. Graph of fig. 2 shows the spectrum of observed transmission loss and determination of STC. That result follows expected performance for that kind of windows.

Even if the sample is equipped with three operable windows, experiments were accomplished by opening the middle unit only. As joining both rooms with the aperture can modify sound absorption, discussed results concern only direct noise reduction. Using A-weighting for sound pressure levels, this analysis might reflect occupant's perception. Figure 3 gives the averaged interpolation of noise reduction as a function of the opening ratio, 100% being maximum position of this particular model of window. Observations reveal that sound insulation drop of around 7 dB(A) when we start to half-open the aperture. Then, the decrease is fairly constant down to a noise reduction of 13 dB(A).

### 3.2. Airflow observations

The first test made about ventilation was to check maximal free running capacities. That consists in measuring airflow with a small deferential pressure through the façade. With a constant difference of 3 Pa, it seems possible to supply an airflow over 200 litres per second with an opening ratio higher than 10%. It means that a half-opened window with a light wind could improve the air exchange rate and still offers 20 to 25 dB(A) of noise reduction.

## 4. CONCLUSIONS

The present research project aims to verify the relationship between acoustic insulation and airflow capacities for building façades. This particular study reports first results related to performances of a common curtain wall. In addition to known benefits, curtains walls can help to protect rooms from outside noise. When all windows are closed, the sound transmission class depends mostly on the glass thickness, with values generally over 30. If openings are used for natural ventilation, those tests show noise reduction in the range of 13 to 32 dB(A).

The next step will be to consider double skin assemblies as solutions to provide a good fresh air inlet with a lower annoyance caused by noise transmission.

## REFERENCES

[1] De Salis, M. H. F., Oldham, D. J. et al., (**2002**) "Noise control strategies for naturally ventilated buildings." *Building and Environment* **37**(5), 471 484.

[2] Migneron, J.-P. (**2009**) "Noise reduction of a double sliding window in relation with opening configuration," InterNoise Proceedings **218**, 4058-4065.

[3] ASTM Standard E90 (**2009**) "Standard Test Method for Laboratory Measurement of Airborne Sound Transmission Loss of Building Partitions and Elements," ASTM International, West Conshohocken, PA, DOI: 10.1520/E0090-09, www.astm.org.

[4] ASTM Standard E413 (**2010**) "Classification for Rating Sound Insulation," ASTM International, West Conshohocken, PA, DOI: 10.1520/E0413-10, www.astm.org.

## ACKNOWLEDGEMENTS

This research would have not been feasible without the contribution of A. & D. Prévost inc. and Les Miroirs St-Antoine inc. concerning the sample of curtain wall and windows. Authors also acknowledge the help of M. Leroux (GRAP) during installation and tests, along with J-G. Migneron for his support.

# ACOUSTICAL CHALLENGES FOR ACHIEVING ENHANCED ACOUSTICAL PERFORMANCE WITHIN SCHOOLS REQUIRED BY LEED®

**Zohreh Razavi**
Acoustical Consultant, Stantec Consulting Ltd., zohreh.razavi@stantec.com

## ABSTRACT

Based on the ANSI 12.6-2002(R2009) standards, a core learning space is defined as a location within building where students assemble for educational purposes such as: classrooms, conference rooms, libraries and music rooms. Spaces where good communication is important but informal learning is the primary function are called ancillary learning spaces which include gymnasiums, cafeterias and corridors.

The LEED® minimum acoustical performance – IEQ Prerequisite 3 - is to achieve a maximum background noise level of 45 dBA from HVAC systems within classrooms and core leaning spaces, and for core learning spaces smaller than 566 $m^3$, confirm that 100% of the ceiling or equivalent surface areas are covered with acoustical material achieving NRC of 0.70 or higher. For space larger than 566 m3, the reverberation time should be 1.5 seconds or shorter.

The LEED® Enhanced Acoustical Performance - IEQ Credit 9 – is building shell, classroom partitions and other core learning spaces partitions should meet the STC requirements of ANSI S12.6-2002 standard, except windows, which must meet an STC rating of at least 35. Background noise level from HVAC in classrooms and other core learning spaces shouldn't exceed 40 dBA.

The main acoustical challenges within schools where achieving enhanced acoustical performance are required by LEED® would be large windows and doors with unknown acoustical performances. A few challenges within schools will be discussed in this paper.

## 1. INTRODUCTION

The Leadership in Environmental and Energy Design (LEED®) is an internationally recognized green building certification system. Acoustics for schools was added to this rating system by the US Green Building Committee (USGBC) in 2007 and revised in 2009 [2]. In 2007, achieving a maximum background noise level in classrooms and other primary learning space of 40 dBA and 35 dBA would be approved for 1 and 2 points, respectively. In 2009, the maximum approved points for LEED® for schools is allowed to be 1 point which can be earned by meeting enhanced acoustical performance requirements. To achieve the requirement, the building shell, classroom partitions and other core learning space partitions should be designed to meet the STC requirements of ANSI Standard S12.60-2002, except windows, which must meet an STC rating of at least 35.

## 2. LEED® FOR SCHOOLS - USGBC

LEED® for schools addresses design and construction activities for both new school buildings and major renovations of existing school buildings approved under Indoor Environmental Quality –IEQ with USGBC. To earn one point with USGBC LEED® for schools, the IEQ prerequisite 3 – Minimum Acoustical Performance requirement and IEQ Credit 9 – Enhanced Acoustical Performance requirement should be met.

### 2.1 IEQ Prerequisite 3 - Minimum Acoustical Performance

The minimum acoustical performance to qualify for LEED® certification registration is to provide the required performances included in IEQ Prerequisite 3: Minimum Acoustical Performance which is as follows:

- Achieving a maximum background noise level of 45 dBA from HVAC systems in classrooms and other core learning spaces. And,
- For all classrooms and core leaning spaces smaller than 566 $m^3$ confirm 100% of all ceiling areas (excluding lights, diffusers and grills) are finished with a material that has a Noise Reduction Coefficient (NRC) of 0.70 or higher. The alternative would be that the total areas of acoustical wall panels, ceiling finishes, and other sound-absorbent finishes equal or exceed the total ceiling area of the room (excluding lights, diffusers and grills).
- For all classrooms and core leaning spaces larger than 566 $m^3$ confirm through calculations described in ANSI Standard S12.60-2002 that they are designed to have a reverberation time of 1.5 seconds or less.

### 2.2 IEQ Credit 9 - Enhanced Acoustical Performance

IEQ Credit 9 – Enhanced Acoustical Performance is to design the building shell, classroom partitions and other core learning space partitions to meet the Sound Transmission Class (STC) requirement of ANSI Standard S12.60-2002, except windows, which must meet an STC rating of at least 35.

## 3. ANSI STANDARD S12.60-2002

Based on ANSI standard S12.6-2002, a core learning space is defined as a location within a building where students assemble for educational purposes such as classrooms. Spaces where good communication is important but informal learning is the primary function

other than formal instruction are called ancillary learning spaces such as gymnasia. In LEED® for schools only acoustical performance within core learning spaces, as per ANSI S12.6-2002 standard, is considered.

### 3.1 STC Rating Requirements

An STC rating for every wall, floor, and ceiling assembly in a core learning space should comply with the tabulated levels in Table 1, as part of the ANSI S12.6-2002 standard.

**Table 1 - The required STC rating for demising walls between classroom and various adjacencies**

| Adjacent Space Type | Minimum STC Rating |
|---|---|
| Other Classrooms, Speech clinics, Healthcare rooms | 50 |
| Outdoors | 50 |
| Bathrooms/Washrooms | 53 |
| Corridor, Staircase, Office or Conference room | 45 |
| Offices, Conference/Meeting Rooms | 45 |
| Music Rooms | 60 |
| Mechanical Equipment Rooms | 60 |
| Cafeteria, Gymnasium, Indoor Swimming Pool | 60 |

## 4. LEED® FOR SCHOOLS - CaGBC

The Canadian rating systems are an adaptation of the US Green Building Council's (USGBC) LEED® System, tailored specifically for Canadian climates, construction practices and regulations. The ANSI S12.60 Standards have not been adopted in Canada. To this author's knowledge, no provincial building standards regarding classroom acoustics currently exist. However, meeting with the required performances included in USGBC would provide Innovation in Design (ID) credit under the Canadian Green Building Committee (CaGBC) LEED® Rating System.

## 5. PRACTICAL LIMITATIONS OF LEED® FOR SCHOOLS

The required acoustical performance on the doors and windows for STC rated partitions for core learning spaces are listed below:

- The STC rating of windows in all STC rated partitions should be 35;
- Doors into classrooms or other core learning spaces would be laboratory STC 30 rated or more;
- The STC rating for interior entry doors into, or between, music rooms shall be not less than STC 40.

The industry limitations that make designers decide not to pursue the LEED® for schools credit are listed below:

- A typical window assembly that achieves STC 35 is 25mm standard insulating glass (e.g. 6 mm glass – 12.7 mm air space – 6 mm glass) which is expensive for school projects;
- No information on the custom made window assemblies are available;
- No information on the STC rated doors are available from suppliers and/or manufacturer;
- To maintain the STC ratings for the doors, they should be sealed and inspected regularly which is costly and not practical for schools.

## 6. CONCLUSIONS

Over the last decade in which the LEED® rating system has been used and applied to projects, the rating system has not included acoustical credits. LEED® for schools was the first of the rating systems to adopt direct points related to acoustics. LEED® for schools – IEQ prerequisite 3 and Credit 9 address acceptable levels of reverberation time, background noise level and STC requirements for demising partitions between classrooms and their adjacencies. STC rated windows and doors are required to obtain the LEED® for schools point and unfortunately performance information is not readily available by these product manufacturers. Revisions of these requirements by evaluating the environmental noise impact and required speech privacy between classrooms and their adjacencies should be considered.

## 7. COST EFFECTIVE CONSIDERATION

The following cost saving considerations in developing the LEED® requirements would have lead in designing and building more schools with Enhanced Acoustical Performance.

- Evaluation of the environmental noise impact to determine the STC rating of the demising walls between classrooms and outdoor;
- Determining the required STC ratings of the windows within STC rated partitions with regards to its application (e.g. operable or not);
- Determining the required STC ratings of the doors depending on the required speech privacy between classrooms and their adjacencies (e.g. corridors)

## REFERENCES


[1] ANSI S12.6-2002, Acoustical Performance Criteria, Design Requirements, and Guidelines for Schools, (Approved June 26, 2002).

[2] LEED Reference Guide for Green Building Design and Construction; For the Design, U.S. Green Building Council, 2009 Edition.

# INSTRUMENTATION FOR MEASUREMENTS IN BUILDING ACOUSTICS

**Peter Hanes[1] and Bradford N. Gover [2]**

[1]Institute for National Measurement Standards, National Research Council of Canada, 1200 Montreal Road, Ontario, Canada, K1A 0R6, peter.hanes@nrc-cnrc.gc.ca

[2] Institute for Research in Construction, National Research Council of Canada, 1200 Montreal Road, Ontario, Canada, K1A 0R6, bradford.gover@nrc-cnrc.gc.ca

## 1. INTRODUCTION

The basic measurements in building acoustics are measurements of sound levels. The measured sound levels can be broadband or band-limited, frequency-weighted, and time-averaged or time-weighted. The measurements can take place in free-field, diffuse-field, or some other acoustic conditions. The sound levels can be steady or decaying. The measured quantities are usually used to determine quantities such as transmission loss or reverberation time.

One of the many factors involved in making good building acoustics measurements is the performance of the instruments that are used. Measurement systems can take many different configurations, from a simple single-channel hand-held stand-alone instrument to a complex multi-channel distributed system.

While many manufacturers provide comprehensive documentation of the performance of their products and refer to publicly-available test results, others may provide only limited and unverified information. It is rare for manufacturers to state how their products will perform when integrated with products from other manufacturers. The user needs to know whether unverified performance claims are sufficient to give confidence in the results of measurements, or whether the performance of the measurement systems should be tested.

Measurement practitioners should be able to call upon a comprehensive but practicable reference for both the specification and testing of the performance of the instruments. At present, all ASTM E33 (Building and Environmental Acoustics) measurement standards include a brief statement of requirements for microphones, but the statements are inconsistent and do not give requirements for the whole measurement system.

There is a draft ASTM Standard Specification that will attempt to address these issues[1]. The Specification is intended to be cited by ASTM measurement standards. This paper suggests how the goals can be achieved within such a Specification document, based on well-established standards for acoustical measurement instruments.

## 2. EXISTING SPECIFICATIONS

Comprehensive and agreed specifications and test methods for the various components of measurement systems already exist in international standards.

### 2.1 IEC 61672 – sound level meters

IEC 61672 is the international standard for sound level meters. The standard covers any measurement system that transduces sound pressure and displays sound level, and is not required to be a hand-held instrument. (This paper uses 'measurement system' because this term may be more familiar when referring to the diverse configurations of sound level meters that are in use.) IEC 61672 allows instruments to be defined in terms of their free-field or random-incidence response.

The performance specifications are given in the first part of the standard: IEC 61672-1[2]. For a measurement system to conform to IEC 61672, all the following conditions must apply:

a) the manufacturer has designed the measurement system to conform to the specifications for the various performance characteristics that are given in IEC 61672-1,

b) evidence is publicly available that examples of the model of measurement system have successfully passed the rigorous pattern evaluation (type-testing) that is specified in IEC 61672-2[3],

c) the individual example of the measurement system has successfully passed the simple periodic test specified in IEC 61672-3[4].

The periodic tests use an acoustical signal source (such as a multi-frequency sound calibrator or an electrostatic actuator) and an electrical signal source to test the response of the instrument to specified input signals. The periodic tests were designed to cover only the most essential characteristics and those where experience has shown that many instruments exhibit problems.

The manufacturer of a sophisticated modular measurement system could claim conformance to the specifications of IEC 61672-1 for some configurations (for example, using particular microphone models) but not for other configurations. The former configurations could meet the three conditions listed above, but the latter configurations would not meet the first two of the three conditions, however good the individual components.

IEC 61672-1 was recommended for use in Canada by the Canadian Standards Association in CSA Z107.10 in 2006[5]. Note that the ANSI S1.4-1983 and ANSI S1.43-1997

standards for sound level meters contain outdated specifications and impracticable test methods and are thus effectively obsolete[6,7].

### 2.2 IEC 61260 – band-pass filters

IEC 61260 is the international standard for fractional-octave band-pass filter sets[8]. The requirements of ANSI/ASA S1.11-2004 are almost identical to those of the international standard[9]. Both documents give specifications and test methods.

## 3. PRACTICAL IMPLEMENTATION

Measurement systems can be divided into two categories: a) those that *as a system* have been designed to conform to the requirements of IEC 61672, and b) those that have not been designed to conform to the requirements of IEC 61672, perhaps because they are not intended for professional use or they pre-date IEC 61672 or they have been assembled by the user from various available components.

### 3.1 Systems designed to conform to standards

Requirements for this category are straightforward - a measurement system for which conformance to standardized specifications (such as IEC 61672-1 and IEC 61260) is claimed should be tested using the relevant methods (IEC 61672-3 and IEC 61260).

### 3.2 Systems *not* designed to conform to standards

A measurement system that was not designed to conform to the specifications can still be tested using the relevant methods of IEC 61672-3 if the owner specifies the basic set-up information for the measurement system. The owner can specify the configuration of the system that is to be tested; for example, it may not be practicable to include in the configuration to be tested long signal cables that have little influence on the performance of the system.

The tests need only be performed for the characteristics that are necessary for the measurement of non-impulsive sound levels for building acoustics:

- response to a suitable calibrated sound calibrator
- self-generated noise
- frequency weightings
- level linearity on the reference level range
- level linearity when changing the level range
- overload indication

The owner of the measurement system might be required to look at the nominal frequency response chart for the model of microphone that is used, or to state the starting point for the tests of level linearity (preferably at the nominal level of the associated sound calibrator), or to state the limits of the ranges of sound levels that the system is expected to measure. This approach has already been tried for some sound level meters that were manufactured before the publication of IEC 61672 and was found to be practicable[10].

An instrumentation standard for building acoustics should therefore include some instructions or guidance on supplying the necessary set-up information to the test laboratory. The testing can be performed by the owner of the measurement system if they have access to the acoustical and electrical signal sources described in 2.1 above.

## 4. CONCLUSIONS

The need for agreed test methods for instrumentation for building acoustics can be addressed by reference to existing specification standards for acoustical instruments. Even for complex measurement systems that are not designed to conform to particular specification standards, it is possible to perform consistent tests of performance if the basic set-up information is specified by the user. The approach has been shown to be practicable and is recommended for adoption by standards organizations.

## REFERENCES


1. ASTM WK 11165 "Standard Specification for Systems to Measure Sound Levels in Buildings" (Draft under development) (ASTM International).
2. IEC 61672-1 (2002) *Electroacoustics – Sound level meters – Part 1: Specifications* (International Electrotechnical Commission).
3. IEC 61672-2 (2003) *Electroacoustics – Sound level meters – Part 2: Pattern evaluation tests* (International Electrotechnical Commission).
4. IEC 61672-3 (2006) *Electroacoustics – Sound level meters – Part 3: Periodic tests* (International Electrotechnical Commission)
5. CSA Z107.10-06 (2006) *Guide for the use of acoustical Standards in Canada* (Canadian Standards Association).
6. ANSI S1.4-1983 (R2006) *American National Standard Specification for sound level meters* (Acoustical Society of America).
7. ANSI S1.43-1997 (R2007) *American National Standard Specifications for integrating averaging sound level meters* (Acoustical Society of America).
8. IEC 61260 (1995) *Electroacoustics - Octave-band and fractional-octave-band filters* (International Electrotechnical Commission).
9. ANSI/ASA S1.11-2004 (R2009) *American National Standard Specification for octave-band and fractional-octave-band analog and digital filters* (Acoustical Society of America).
10. Hanes, P. (**2007**). "Measurement of the performance of sound level meters using IEC 61672-3:2006", Canadian Acoustics, **35**(3), 144-145.


## ACKNOWLEDGEMENTS


The authors gratefully acknowledge discussions with Robert A. Hallman and Rich Peppin regarding the requirements for instrumentation for building acoustics.

# VIBRATION AND LOW-FREQUENCY IMPACT SOUND GENERATED BY NORMAL HUMAN WALKING IN LIGHTWEIGHT WOOD-JOISTED FLOOR-CEILING ASSEMBLIES

**Lin Hu[1] and Jean-Philippe Migneron[2]**
[1]Department of Building Systems, FPInnovations, Quebec, Canada, Lin.Hu@fpinnovations.ca
[2]École d'architecture, Université Laval, Québec, Canada, jean-philippe.migneron.1@ulaval.ca

## 1. INTRODUCTION

Human walking generates vibrations and impact sound in lightweight wood-joisted floor-ceiling assemblies. Design methods have been developed to successfully control the perceptible vibrations and construction solutions or materials help to reduce high frequency impact sound transmission, but not low-frequency footstep noise. This paper presents two cases of unsatisfactory low-frequency footstep noise transmission in wood-framed floor-ceiling assemblies and discusses about limited remedies available.

### 1.1. Context of the study

Conventional North American floor systems in wood-framed multi-family buildings are usually built with a multi-layer topping, a wood-joisted floor and a decoupled ceiling. Footsteps made when somebody walks on the floor can excite all assemblies to vibration, which then generates impact sounds. If those assemblies lack of sufficient stiffness or solid supports, then the excessive vibrations make the occupants uncomfortable. Great efforts have been made to develop design methods to control perceptible vibrations; these have proven to be successful. However, a number of complaints over low-frequency footstep impact sound transmission were received. Occupants in condominiums described the "character" of that particular noise using terms such as "thuds", "thumps", "booming", and "drum effects". The sound resembles a pure tone sound at the fundamental natural frequencies of wood floor-ceiling assemblies (about 15-25 Hz). The measured sound pressure levels (SPL) of the impact sound using an ISO tapping machine revealed that peak SPL occurred around those frequencies. It should be noted that there is no agreement among acousticians on a suitable method to quantify low-frequency sound. Finding a remedy proved to be very challenging. The practical solution is to add a topping, but the mass of that subfloor layer is limited by the building load carrying capacity, and the thickness is limited by the room height. Furthermore, installation of a topping in an occupied building brings other constraints.

## 2 CASE OF LUMBER-JOISTS ASSEMBLY

This first study case concerns annoying low-frequency footstep sound transmission through a lumber joisted floor-ceiling assembly with a concrete topping. As previously reported by Wakefield [1], it shows that the concrete topping of 90 kg/m$^2$ did not ensure satisfactory low-frequency impact sound insulation. Even with an important attempted to retrofit the problem, occupants were still unsatisfied of thumping noises induced by the footsteps.

## 3 CASE OF I-JOISTS ASSEMBLY

### 3.1 Actual floor-ceiling assembly

The actual floor-ceiling assembly studied in the reference condominium consisted of four components: 1) a 19-mm thick hardwood finishing of 18 kg/m$^2$; 2) a 13-mm thick OSB topping of 8 kg/m$^2$ on a 6-mm thick foam impact isolation barrier; 3) a base floor system made of 300-mm deep wood I-joists spaced at 400 mm o.c. and a 16-mm thick OSB subfloor; 4) a ceiling decoupled by resilient channels spaced at 400 mm o.c and using two layers of type X gypsum board, 16-mm thick. Batt insulation 140-mm thick filled the ceiling cavity. The floor spans varied from 3.35 m to 4.88 m, depending on the type of room.

### 3.2 Tested toppings for the subfloor

Due to the limitation of the room height, the thickness of the topping was restricted to around 50 mm. This was another challenge in developing an effective remedy. Based on our experience and on previous studies, the following four topping candidates for testing were proposed : 1) standard 19-mm thick finished hardwood nailed over 19-mm thick plywood sleepers of 152 mm in width, each spaced at 152 mm. This solid assembly was mounted as a floating floor over 19-mm thick textile felt, without any glue or other attachment; 2) 16-mm OSB on 38 mm by 38 mm wood sleepers at 406-mm spacing, with the cavity filled with sand, and floating on 19-mm thick textile felt; 3) 45-mm thick raft composed of three layers of OSB and 2-mm thick insulation layers between the OSB layers, and floating on 19-mm thick textile felt; 4) 45-mm thick LVL over a 2-mm thick insulation layer.

### 3.3 Measurements

Direct noise levels in the receiving room were measured using a tapping machine located in the room above, according to ASTM E1007 method. In order to observe the transmission of the sound through the floor-ceiling assembly at lower frequencies, the spectrum range was extended between 0.8 Hz and 20 kHz. These measurements were useful in describing the footstep percieved sounds. Then, ASTM E989 method was used to normalize data and determine an approximate value for the impact sound insulation in terms of FIIC.

## 4 RESULTS WITH TOPPINGS

The measured FIIC of the original floor-ceiling assembly was 41. Table 1 summarizes the impact noise reductions from measured SPL and the increase of FIIC

after adding the 1.2 m by 1.2 m topping patches to the original noisy floor-ceiling assembly. Regarding those results, among the four toppings, topping No. 1 and 2 were more effective with respectively impact noise decrease of 12.1 dB(A) and 12.5 dB(A). That represents a direct improvement, which was greatly appreciated by occupants.

Figure 1 shows the spectra of measured sound levels with extended frequency components down to 10 Hz in the receiving room, before and after adding toppings over actual floor of the source room. Results obtained with toppings No. 1 and 2 represent two good solutions to the footstep noise transmission problem, while No. 3 and 4 are less efficient. Topping No.1, with sleepers and felt, gives a transmitted level of 56.4 dB(A), while topping No. 2, with the addition of sand, reduces the average value to 56.0 dB(A). As noticed with the actual floor, impact sound insulation is poor at lower frequencies, i.e. below 200 Hz.

By comparing the effectiveness of topping No. 4 and 1, we found that even if topping No. 4 was heavier, topping No. 1 was much more effective. Considering that topping No. 1 was floating on the 19-mm thick textile felt, but that topping No. 4 was floating on the 2-mm thick insulation layer, we can conclude that the thickness and resilience of the insulation material have a significant effect on the performance of toppings.

**Table 1. Changes in SPL and FIIC due to addition of the topping patches.**

| Topping No. | Added mass | Measured impact SPL | FIIC increase |
|---|---|---|---|
| 1 | 18 kg/m$^2$ | -12.1 dB(A) | +7 |
| 2 | 67 kg/m$^2$ | -12.5 dB(A) | +8 |
| 3 | 23 kg/m$^2$ | -10.4 dB(A) | +4 |
| 4 | 21 kg/m$^2$ | -2.9 dB(A) | +2 |

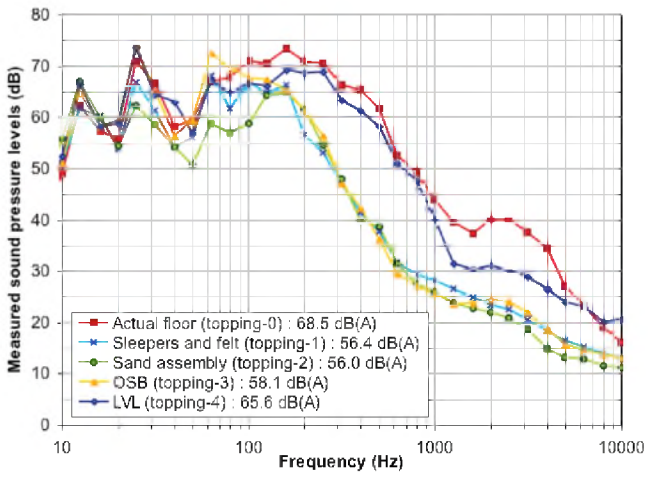


**Figure 1. Spectra of impact sound transmission through the wood I-joisted floor-ceiling assembly with and without the additional wood topping patches.**

The effect of the topping mass on the impact sound insulation was clearly shown by comparison of third octave spectra measured in the receiving room. Being aware that topping No. 2 was much heavier than topping No. 1 (67 kg/m$^2$ vs. 18 kg/m$^2$), we were not surprised to find that topping No. 2 was more effective in terms of reducing the impact sound transmission for components below 100 Hz, except for the component at the fundamental natural frequency of the floor-ceiling assembly. At this time, we do not have any explanation for this exception. However, it is often considered that the SPL measurements are not reliable at low frequencies. A review of the methods to measure SPL in that range is under way.

In a nutshell, the test results demonstrated that the proper combination of mass and sound insulation materials in toppings may provide solutions to the problem of annoying low-frequency impact sound transmission.

## 5 CONCLUSIONS

Footstep sound transmission through wood floor-ceiling assembly is a complicate problem, and needs a collective research effort. To thoroughly address the issue of poor low-frequency sound insulation with current lightweight wood floor-ceiling assemblies, we developed our research plan to:

1) Get a better understanding of physics involved in footstep low-frequency impact sound transmission through wood-joisted floor-ceiling assemblies;
2) Develop a testing method and standard for quantitative determination, and correlate it to the human perception;
3) Predict the quantitative values using the properties of the floor-ceiling assemblies;
4) Build a database of insulation material properties including density, damping, surface and compression stiffness, porosity, sound absorption coefficient, flow resistance, and price.

## REFERENCES

[1] Wakefield, C. W. (**1999**). "Control of low-frequency footstep sound & vibration transmission through a wood-framed, concrete-topped floor," J. Canadian Acoust. Ass. **27** (3), 116-117.

[2] Blazier, W. E. and DuPrée, R. B. (**1994**). "Investigation of low-frequency footfall noise in wood frame multi-family building construction," J. Acoust. Soc. Am. **96** (3), 1521-1532.

[3] Hu, L. J. (**2005**). "Acoustic performance of wood-frame buildings," Final Report No.3 for Canadian Forestry Service, Forintek Canada Corp. Sainte-Foy.

[4] ASTM E1007-04e1 (**2004**) "Standard Test Method for Field Measurement of Tapping Machine Impact Sound Transmission Through Floor-Ceiling Assemblies and Associated Support Structures," ASTM International, West Conshohocken, PA.

## ACKNOWLEDGEMENTS

FPInnovations would like to thank Natural Resources Canada (Canadian Forest Service) for the financial support of this work, and Acoustec Inc. for technical assistance.

# MEASUREMENT OF SUDDEN UNEXPLAINED HIGH-LEVEL NOISE EVENTS WITHIN RESIDENTIAL DWELLINGS

**Roderick Mackenzie[1] and R. Sean Smith[1]**
[1]Building Performance Centre, Institute for Sustainable Construction, Edinburgh Napier University, 42 Colinton Road, Edinburgh, United Kingdom, EH10 5BT, ro.mackenzie@napier.ac.uk

## 1. INTRODUCTION

In 2009 the Building Performance Centre (BPC) was asked by members of the house-building industry to investigate sudden, high-level "noise events" in different types of new build dwellings. The objective of the investigation was to record, quantify and if possible identify the source location of the noise events within the dwelling building fabric. Five sites where occupants had reported the "noise incidents" were visited at locations across the UK. At each property the occupants were interviewed, and multiple measurements were undertaken involving vibration and airborne sound levels. Diverse methods were used to induce the "noise events" and real time recordings were also carried out.

The results of the measurements conducted indicate that the source of the "noise events" is located in the gypsum board ceilings of each property. It appears there is a relationship between the stiffness of the plasterboards and a tension/compression action imposed on them by rapid changes in temperature, sudden pressure change or very slight dynamic movement, causing a "noise event" to occur.

This paper is derived from a more detailed commercial-in-confidence report by the BPC, and companies and site names involved have been withheld (BPC report S/5218/10, 2010).

## 2. SITE INVESTIGATIONS

### 2.1. Sites

Five sites were examined during the investigation (Sites A to E) consisting of apartments, detached and semi-detached homes with floor/ceiling components including attic trusses, roof trusses, metal web joists and engineered I-joists and the use of block work perimeter walls or timber frame walls.

### 2.2. Interviews

Each site occupier was interviewed for their experiences of the "noise events" including frequency of occurrence, locations of occurrence and a description of the noise itself. The noise had been described by different occupants as "*very loud*," "*a sudden noise,*" "*crack type noise,*" "*similar to a rifle shot or whiplash*," and "*like a gun shot*." It was often a sudden noise event involving one or more distinct incidents occurring within several seconds. From discussions with some of the occupants, house builders and material manufacturers a common theme was emerging.

The noise event was reported as being associated with being sourced somewhere in the ceiling zone areas across a variety of room types (living rooms, kitchens, bathrooms, etc.). It was also more frequent during colder seasons and occurred "*naturally*" after a period of time following the home's heating system being activated. However, non-seasonally it was also associated with an isolated *"natural"* temperature changes within the affected room, such as when cooking in a kitchen or shower activation in a bathroom. Further, very similar "noise events" could be induced when internal or external doors were opened quickly or potentially by someone walking on the floor above.

Anecdotally, the occupier of Site A noted that they had heard similar noises within the ceiling of the apartment below Site A, which had a single layer of plasterboard mounted on a metal frame ceiling fixed to a precast concrete floor.

### 2.3. Measurement methods

A Brüel and Kjær (B & K) Type 2250 sound level meter recorded the LAeq, LAmin, and LAmax airborne sound pressure levels and audio wav.file recordings within the room. Vibration levels were measured using uni-axial B & K Type 5308-B accelerometers fixed at different points across ceiling gypsum boards and in Site A on attic trusses. A PULSE™ 3703-B 9-channel platform with FFT and ⅓-octave analysis engines was used and enabled real-time observation of the signal content.

A total series of 36 experiments were undertaken at the five dwelling sites based on inducing the noise event by; *"Natural" occurrence* triggered by switching on the dwelling heating system and waiting for the events to occur whilst running continuous recordings; *Induced events (1)* via internal or external doors being opened very quickly in some cases after the dwelling had been pre-heated; *Induced events (2)* by walking on the upper floor level above the room; *Induced events (3)* manually pushing the ceiling system gently upwards. Hammer-tap source excitation measurements were also conducted on exposed attic trusses and plasterboard ceilings in Site A. Physical ceiling deflection measurements were also conducted on certain sites.

## 3. RESULTS

During investigative visits, some sites exhibited "naturally" occurring "noise events," either following the internal heating being turned on (~90 mins later, Site A), cooker being turned on in the Kitchen (~20 mins later, Site D), or the activation of a shower in a bathroom (~ 10 mins later, Site E). These incidents would suggest a relationship with relatively rapid temperature and/or pressure increase and the "noise event" occurrence. An example of the "noise event" from Site E is show in Figure 1, showing the change from the background noise level within a 30 second recording.

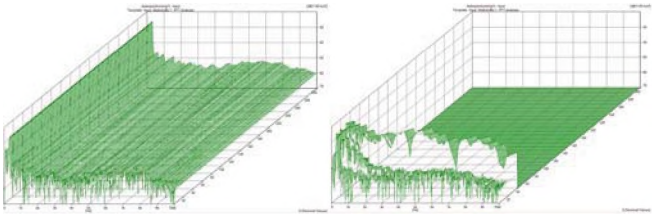

**Figure 1. Waterfall FFT display of accelerometer signal from bathroom at Site E showing the background signal (left) and a "noise event" approximately 13 minutes later (right).**

At sites A, B, C and D, it was possible to induce "noise events" through the rapid opening of internal and external doors. A clear "noise event" was found to emanate from near the centre of the room, where the measured deflection of the ceiling was 0.05mm. This suggests that it may only require only a low level, but sudden pressure change within the room to trigger the "noise incident". This also suggests that the "noise incident" can occur without any additional direct "live" loading on the floor system.

It was observed that "noise events" would often occur in split-second clusters of typically 2 or 3 events, as can be seen in Figure 2. Figure 2 also shows the FFT signal level increases from background levels caused by the first "noise event" of Figure 2.

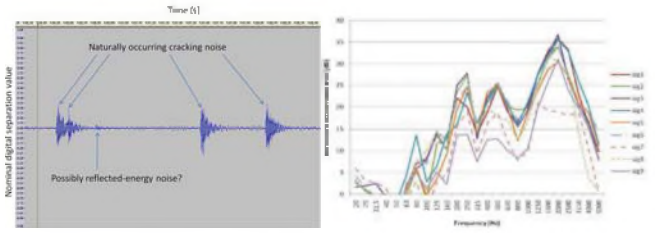


**Figure 2. Four "noise events" within 1.5 seconds, induced after heating the living room of Site A for *c.*90 mins. Time trace (left) and ⅓-octave signal responses of the first event minus background (right).**

At Sites B, C and D it was possible to induce "noise events" by slowly shifting a person's weight across floor above. At all sites a similar sounding "noise event" could be induced by manually pushing up on the ceiling boards. The ambient internal noise level within the dwelling was between 25 to 30dB. The $LA_{max}$ level of the sudden "noise event," generated by temperature change to the dwelling was 65 dB. In the case of Site B the door opening test also caused the highest "noise incident" events.

## 4. DISCUSSION

Naturally, a sudden, unexpected increase of 35dB to 40dB in noise level causes a startle reaction by occupants and can affect behaviour and quality of life.

Based on additional results derived from the manual excitation (by acoustic hammer) of the truss and ceiling board, it was possible to see that when the impact source is located on the ceiling board as opposed to the truss, the truss and ceiling board signals are very similar, often tightly packed in both shape and form. Signal 5 and 9 were the furthest ceiling board measurements by distance from the tapping source. When truss excitation occurs the difference between Signals 5, 9 (gypsum board) and 7, 8 (truss) is over 30 dB at high frequencies. When ceiling board excitation occurs, this difference (spread) is reduced to 15 dB. Most of the signal response curves in Figure 2 are tightly packed and follows a very similar pattern of vibration amplitude increases above background levels.

If the "noise incident" source is within the gypsum ceiling board then:

- In-plane waves would be formed, which would carry along the board with some minor dissipation at board edges, but be very similar in its shape and measured values across the ceiling due to less impedance from the truss junctions.
- Flexural waves would also be formed and would be expected to peak at or near the critical frequency of the gypsum board, approx 2000Hz to 3150Hz for standard gypsum board thickness 15mm to 12.5mm.

Both of these facets can be seen in Figure 2.

The diverse range of core structure elements suggested that they were not the source of "noise events". However, the common theme which does run across all the sites is the gypsum board ceilings. Overall the test data suggests that the primary source and carrying mechanism for the "noise event" is through the gypsum board ceiling.

It is suggested that further future analysis is undertaken investigating standard plasterboard types and changes to manufactured material properties which have occurred in recent years. Replacing the standard ceiling boards with high density boards and mounting these via resilient ceiling bars has eliminated the noise sources on the study sites.

## REFERENCES

Smith, R.S., (2010), *Multi-site investigation into sudden noise*, BPC Commercial Report S/5218/10, Edinburgh Napier University.

# COMPARING THE POTENTIAL OF ACOUSTIC PARAMETERS FOR THE ASSESSMENT OF THE STRENGTH OF TIMBER

**Roderick Mackenzie[1], Charles A. Fairfield[1] and R. Sean Smith[1]**
[1]Institute for Sustainable Construction, Edinburgh Napier University, 42 Colinton Road, Edinburgh, UK, EH10 5BT

## 1. INTRODUCTION

Approximately 80% of Scotland's softwood is Sitka spruce (*Picea sitchensis*) of variable quality. The ability to improve post-felling segregation coupled with early identification of low stiffness standing timber are two key issues in Scottish forestry. There is also a need for non-destructive testing (NDT) methods which evaluate the quality of existing timber structures, particularly those identifying degradation or rot. Several NDT methods for timber quality investigation are available depending upon scale. These include: visual classification, static bending machines, resistance drilling, ring counting and density assessment, X-ray tomography, microwave and near infra-red scanning. Acoustic techniques are however, cheap and portable.

The authors conducted a three year study into the relationship between acoustic NDT techniques and the mechanical properties of wood. Low frequency (LF) and ultrasonic time of flight (TOF) velocity harmonic resonant frequencies $f_0$, and damping ratio $\zeta$ were examined with regard to their influence on dynamic modulus of elasticity $E_d$, their dependence on static modulus of elasticity $E_s$, modulus of rupture $E_r$, and knot area ratio (KAR) among other parameters. In addition to recommendations on the improved use of acoustic NDT, this provided the first large-scale derivation of reference values for $E_s$ and other acoustic properties for 35 year old Sitka spruce logs and beams in Scotland (Mackenzie, 2009).

## 2. BACKGROUND

Many commercial devices measuring acoustic and ultrasonic velocities cover macro-, meso-, and micro-scale specimens. Questions remain: at what scale are the acoustic methods used applicable, what type of waveform deviation is used for detection and grading, and what are the specimens' material properties that can mislead the user? Using $v_c = \sqrt{\frac{E_d}{\rho}}$ the derived dynamic modulus $E_d$ is typically an over-estimate due to the high strain rate. Nevertheless it remains well correlated ($R^2 > 0.99$) to $E_s$ for small, clear, defect-free specimens (Andrews, 2000). Using the assumed correlation ($R^2 \approx 0.7$) between $E_s$ and $E_r$ from traditional machine grading; acoustic estimates of strength classifications become possible (Green *et al.*, 2006). Given the natural overestimation in $E_d$ (5% to 30% depending on species, specimen size and test method), strength classifications should only be assigned after measuring this overestimate. Previously, there were no relevant data for Scottish Sitka Spruce, or reference velocities for either wet or dry C16 (general grade) or C24 (structural grade) timber.

The strength is only part-influenced by stiffness and knot content: more importantly, knot location can account for up to 50% of the variability in strength (Johansson & Kliger, 2000). A method quantifying and locating knot content may produce a better $E_d$:$E_r$ correlation. Also, if (Ouis, 2005) was correct in the assertion that reverberation time acts as an indicator of rot, then $\zeta$ may also correlate with condition.

## 3. METHODS

The three test phases used Brüel & Kjær's PULSE™ 3703-B 4-channel analyser (with Fourier transform module), glue-coupled Type 5308-B uniaxial accelerometers and a PUNDIT™ 54 kHz ultrasonic tester.

### 3.1. Phase 1: acoustic method assessment

Acoustic NDT parameters were evaluated during tests on 33 controlled-homogeneity beam specimens cut from 12-layer laminated veneer panels and three solid wood beams. They were tested to determine $f$ and $\zeta$ (Q-factor method used for best repeatability) at the first eight harmonic frequencies. The LF and ultrasonic TOF velocities were also measured. Holes were then drilled (6 mm dia.) through the beams and filled with dowels to simulate knots. These holes were then re-drilled (in steps to 32 mm dia.) and larger dowels inserted. After acoustic testing, the beams were mechanically strength graded to determine $E_s$.

### 3.2. Phase 2: log testing

150 logs cut from 36 felled trees were tested by both PUNDIT™ (measuring $v_c$) and PULSE systems (for $f_0$ to $f_4$, LF TOF, and $\zeta_0$ to $\zeta_4$), the latter using the set-up in Figure 1.

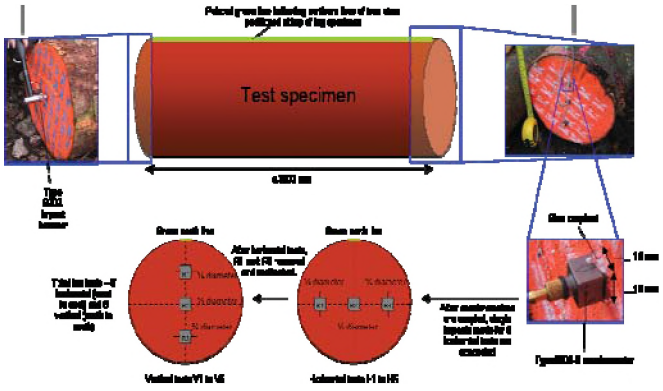


**Figure 1 Phase 2 test set-up**

### 3.3 Phase 3: beam testing

650 battens were cut from the logs and tested in the laboratory using the same method as the log tests. The beams were then mechanically strength graded to determine $E_s$: KAR and grain angle were visually assessed.

## 4. RESULTS AND DISCUSSION

### 4.1. Phase 1: acoustic method assessment

Those beams without simulated knots had the highest $v_c$, hence the highest $E_d$ and $E_s$. The usual overestimate nevertheless left good correlation between moduli ($R^2 > 0.8$) with clear wood showing the best correlation ($R^2 = 0.85$). The position of the inserted dowels (simulating knots) affected $E_d$. For a simulated mid-span knot (the anti-nodal position for the fundamental frequency), the first and third harmonic frequencies (hence $E_d$) reduced significantly (see Figure 2). The second harmonic, unaffected as its nodal point lay at this location, remained unchanged despite increasing knot size. The opposite was true for knots at ¼- and ¾- span. The damping ratio increased from 0.4% to over 0.9% as the simulated KAR increased. Resonant peak bifurcation arose with increasing KAR.

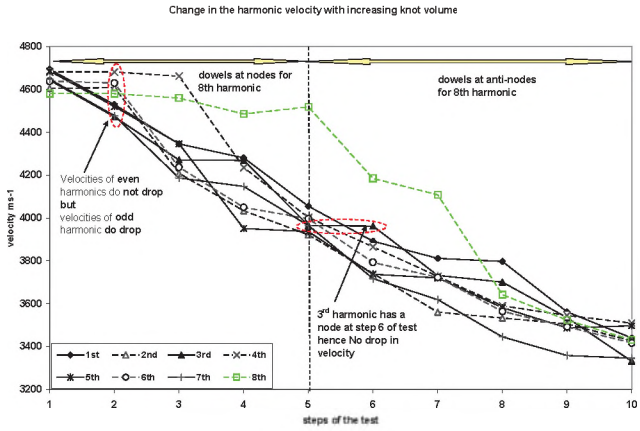


**Figure 2 Influence of 25 mm knots: Beam 33**

The number of 25 mm simulated knots was progressively increased along the beam while avoiding drilling at the anti-nodal positions of the eigth harmonic. The eigth harmonic underwent little change until holes were drilled at its anti-nodal points because harmonic frequencies are derived, not from a measurement of the whole specimen, but from discrete points along it. The fundamental frequency's waveform was weighted to the mid-span stiffness. Subsequent ($\eta^{th}$) harmonics were weighted to parts of the specimen at every 1/η fraction of the span. It should also be noted that after 32 mm dia. dowel insertion, the mean RF velocity decreased by 25%, but the LF TOF velocity by only 9%. Higher longitudinal resonance frequency harmonics gave more representative $E_s$ and $E_r$ estimates. However in larger, wet specimens there was a trade-off between accuracy and ability to detect higher harmonics.

### 4.2. Phase 2: log testing

Resonance tests on 150 Sitka spruce logs saw a 22% overestimate between their RF $E_d$ and the average $E_s$ from 645 beams later cut therefrom. Low $E_d$:$E_s$ correlations were found, the best of which lay in the second harmonic ($R^2$ = 0.31). Adjusting for the usual overestimate (*c.* 35% here) correct average log stiffness classification was achieved. This did not work with TOF-derived values: a mean of 23 GPa, a 182% overestimate, was found. For fresh Sitka spruce logs, second harmonic velocities of 3500 $ms^{-1}$ and 4115 $ms^{-1}$ were proposed as representing average thresholds for grades C16 and C24 respectively. Saw-milling practice may cause deviations from these reference velocities.

### 4.3. Phase 3: beam testing

In tests on dry beams, all acoustic methods for $E_d$ had good correlations and excellent inter-test repeatability; the first harmonic had the highest correlation to $E_s$ ($R^2$ = 0.71), whilst PUNDIT™ had lowest ($R^2$ = 0.61). The overestimate was *c.* 4.5%, except in the first harmonic with 6.3%. The third harmonic was the closest ($E_d$ to $E_s$ overestimate of 4.3%), though a reduced number of samples due to higher signal:noise ratios meant that the second harmonic was potentially more appropriate ($R^2$ = 0.69). For dry beams, reference velocities for Sitka Spruce were 4040 $ms^{-1}$ and 5070 $ms^{-1}$ for grades C16 and C24 respectively.

No significant correlation was seen between Q-factor $\zeta$ and any mechanical property (particularly KAR) of either logs or beams. No improvement in correlation to $E_s$ or $E_r$ was seen when $\zeta$ was combined with RF, LF or TOF $E_d$ data.

## REFERENCES


Andrews, M. (2002). *Which acoustic speed?* Proc. 13th Int. Symp. NDT of Wood, Berkeley, California, USA.

Green D.W., Gorman T.E., Evans J.W. & Murphy J.F. (2006), *Mechanical grading of round timber beams.* Proc. Am. Soc. Civ. Engnrs, J. Mat. Civ. Engng, **18**(1) 1-10.

Johansson M. & Kliger R. (2000) *Variability in strength and stiffness of structural Norway spruce timber - influence of raw material parameters.* Proc. WCTE 2000, Whistler, Canada.

Mackenzie R.K.T. (2009) *The non-destructive evaluation of Sitka spruce mechanical properties using acoustic methods.* PhD Thesis, Edinburgh Napier University, Edinburgh, UK.

Ouis D. (2005) *Frequency dependence of strength and damping properties of wood and their influence by structural defects and rot.* Proc. 14th Int. Symp. NDT Wood, Hannover, Germany.


## ACKNOWLEDGEMENT


This research was funded by a Scottish Funding Council Strategic Research Development Grant. The help of Forest Research's NRS staff is also gratefully acknowledged.

# INDUSTRIAL BUILDING ABSORPTION COEFFICIENT – POWER PLANT CASE STUDY

**Galen Wong[1] and Ji Cao[2]**
[1]ATCO Structures and Logistics, 100 – 170 Laurier Ave West, Ottawa, Ontario K1P 5V5, galen.wong@atcosl.com
[2]ATCO Structures and Logistics, 1243 McKnight Blvd NE, Calgary T2E 5T1, jason.cao@atcosl.com

## 1. INTRODUCTION

Building interior noise levels have been a growing concern for many industrial projects as it directly relates to worker occupational noise exposure levels. Generally, a continuous noise exposure level of 85 dBA over an 8-hour work shift is the provincial or territorial regulatory limit in Canada (CCOHS, 2011), and many companies are now working to meet that limit in their new projects. This evaluation of the interior noise levels during the project planning stage can help to identify potential noise exposure levels for future staff, and noise mitigation can be integrated into the plant design, thus avoiding more expensive future retrofit and replacement costs in trying to meet the noise exposure limits retroactively.

In the acoustical measurement and modeling of existing building interior noise levels, large differences were found between the model and measurement results. It was found that the absorption coefficient specifications for the building interior surfaces did not match those of the lab-tested specifications for those materials.

## 2. INDUSTRIAL BUILDINGS

Typical industrial buildings are constructed with a solid metal inner liner for the walls and roof, and a concrete floor, which are all acoustically reflective surfaces. With several noise sources in the room (also consisting of metal surfaces), a highly acoustically reverberant field exists. For a simple steady-state point noise source, the sound pressure level, $L_p$, in the room can be calculated via the room equation which is based on Sabine/Eyring diffuse field theories, $L_p = L_w + 10\log[(Q/4\pi r^2) + (4/R)]$ (Beranek, 1988), where $L_w$ is the source sound power level, Q is the directivity of the source, r is the distance from the source to the receptor, and R is the room constant, $R = S\alpha/(1-\alpha)$, where S is the surface area of the room and all interior objects and $\alpha$ is the area averaged absorption coefficient of the room. While the room equation allows calculation of the $L_p$ in a simple room, for more complex geometry rooms with many obstructions, complex sound sources, and absorptive surfaces which are not evenly distributed throughout the room, a computer model of the building can help to more accurately determine the noise levels within the building.

## 3. STUDY AREA

The power plant consists of six diesel engine gensets in the building. Four engines are normally in operation, with two engines as backup units. The gensets were housed in a metal building consisting of a 4" insulated wall with a solid corrugated inner liner. The roof interior panel also consisted of solid corrugated inner liner and the floor was concrete. The building dimensions were 49 m L x 35 m W x 20 m H peak, with the eave height at 18 m. In the building the six gensets were situated parallel to each other, along the centre length of the room, with six large heat recovery unit tanks situated at the exhaust end. A maintenance shop, control room and electrical room lined one length of the building, with a mezzanine floor above, containing six make-up air units. Figure 1 shows the building layout as modeled.

Significant noise sources associated with the equipment in the room included the engine air inlets and engine casing breakout. Other less significant noise sources included the engine exhaust piping and heat exchangers, the make-up air units, glycol and water pumps and other ancillary equipment in the room.

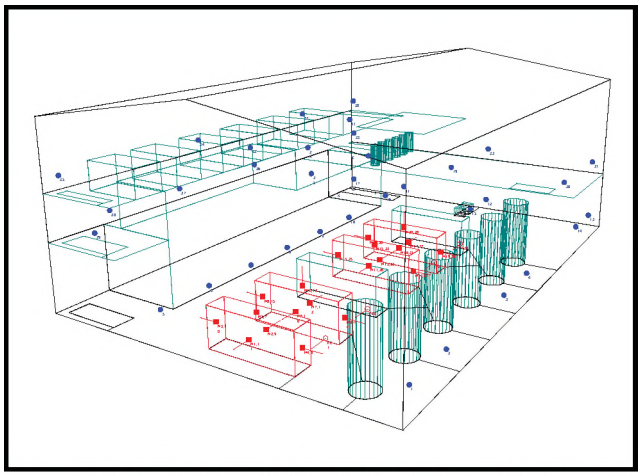

**Figure 1. Odeon 3D Model of the Power Plant**

## 4. ACOUSTIC MODEL

Odeon 10 Industrial, a ray-tracing program for room acoustical modeling, was used in this study of a power plant building. The model employs a combination of image-source, ray-tracing and ray radiosity methods to calculate the sound levels in a room (Christensen, 2009). Reflections are taken into account based on the room and obstacle geometry and the scattering and absorption coefficients. Source noise levels are input either as line, point or area sources.

Nearfield $L_p$ measurements of four of the diesel gensets were taken at the plant for the purposes of determining their $L_w$ (as per ISO 3744) for input to the model, with appropriate corrections made for the reverberant noise in the

room. Thirty-five $L_p$ measurements throughout the facility were taken to be used in verifying the model results.

## 5. RESULTS

$L_p$ throughout the building ranged from 96 dBA far from the gensets, to 105 dBA at 1m from the genset engine casing. The average sound pressure level in the open areas of the building was 100 dBA.

The initial Odeon model was completed with the input of lab-tested absorption coefficients for the room materials (Bies, 2003). These absorption coefficients are listed in Table 1 below.

**Table 1. Initial Surface Absorption Coefficients**

| Surface | Octave Band Centre Frequency [Hz] | | | | | | | |
|---|---|---|---|---|---|---|---|---|
| | 63 | 125 | 250 | 500 | 1k | 2k | 4k | 8k |
| Concrete Floor | 0.01 | 0.01 | 0.01 | 0.02 | 0.02 | 0.02 | 0.05 | 0.05 |
| Equipment, Building Walls | 0.10 | 0.13 | 0.09 | 0.08 | 0.09 | 0.11 | 0.11 | 0.10 |

With the above absorption coefficients, the model predicted significantly higher sound pressure levels within the building - up to 12 dB higher than the measured levels in several octave bands. The average difference per octave band is given in Table 2 below in the row "Initial α".

**Table 2. Differences between Model Results and Measurement Data**

| Average Difference in $L_p$, Model Prediction minus Measurement [dB] | Octave Band Centre Frequency [Hz] | | | | | | | |
|---|---|---|---|---|---|---|---|---|
| | 63 | 125 | 250 | 500 | 1k | 2k | 4k | 8k |
| Initial α | 12 | 11 | 12 | 12 | 12 | 12 | 11 | 7 |
| Limited α | 11 | 9 | 10 | 10 | 10 | 10 | 10 | 7 |
| Adjusted α | 0.3 | 0.6 | 0.2 | 0.0 | 0.2 | 0.2 | 0.1 | 0.1 |

Odeon recommends limiting the absorption coefficient to between 0.1 and 0.9 (Christensen, 2003) to avoid excessive reflection and absorption in the calculation. Applying these limits to the model, the average difference between the model predicted results and the measured levels are about 10 dB, a slight improvement over the initial model results. The differences with these absorption coefficients per octave band are given in Table 2 under the row "Limited α".

Further adjustments to the absorption coefficient of the room and equipment surfaces were made to determine the appropriate values in order to bring the model results closer to the measured levels. The average difference between the model and measurement have been reduced to less than 1 dB, as shown in Table 2 under the row, "Adjusted α". The adjusted surface absorption coefficients are listed in Table 3 below.

**Table 3. Adjusted Surface Absorption Coefficients**

| Surface | Octave Band Centre Frequency [Hz] | | | | | | | |
|---|---|---|---|---|---|---|---|---|
| | 63 | 125 | 250 | 500 | 1k | 2k | 4k | 8k |
| All Interior Reflective Surfaces | 0.55 | 0.55 | 0.50 | 0.48 | 0.48 | 0.52 | 0.58 | 0.50 |

## 6. DISCUSSION AND CONCLUSIONS

The modeling results generated by the Odeon software show that the room surface absorption coefficients must be specified much higher than the actual lab-tested levels in order for the model to correlate with the measured sound levels in the building. Surface absorption coefficients in other models of similar facilities with hard surfaces may also need to be adjusted in order to more accurately model the space and determine noise levels.

While simple, moderately absorptive rooms may model well in Odeon, some obstacles and low-absorption rooms may cause problems due to their high reflectivity and very diffuse fields. An expected diffuse sound field created in the model may not be created in actual industrial buildings. Absorption or other noise decay factors may be involved. In such cases, adjustments to lab-tested absorption coefficients may need to be performed in order to more accurately model the room.

In validating the model, more appropriate absorption coefficients have been found to accurately predict the sound pressure levels in the room. Noise mitigation treatment in the form of increased absorption to reduce the reflected noise may not be predicted accurately in the model and care must be taken in order to not underestimate the amount of absorption necessary. Local noise barriers situated around the noisy equipment may be more effective in reducing overall noise levels if the direct and first-order reflected noise are the dominant noise sources.

## REFERENCES


Beranek, L.L. (Ed.), (1988) *Noise and Vibration Control*, Revised Edition, Institute of Noise Control Engineering.

Bies, D.A., Hansen, C.H (2003) *Engineering Noise Control*, Third Edition, Spon Press.

CCOHS Canadian Centre for Occupational Health and Safety (2011) *Noise: Occupational Exposure Limits in Canada.* Retrieved from http://www.ccohs.ca/oshanswers/phys_agents/exposure_can.html

Christensen, C.L. *Odeon Room Acoustic Program Manual Version 10 Industrial, Auditorium and Combined Editions* 2009

ISO 3744:2010 Acoustics -- *Determination of sound power levels and sound energy levels of noise sources using sound pressure -- Engineering methods for an essentially free field over a reflecting plane*

# SONORISATION DES GRANDS ÉDIFICES – APPLICATION AU MÉTRO DE MONTRÉAL

**Joris Brun-Berthet**
Acoustique et Vibration, Dessau, 1080 côte du Beaver Hall, bureau 300, Montréal (Québec) H2Z 1S8
joris.brun-berthet@dessau.com

## 1 INTRODUCTION

Parmi les différents systèmes de communications, la sonorisation est un moyen très efficace pour s'adresser à un nombre important de personne. Les édifices publics sont en général munis d'un système de sonorisation permettant de diffuser des messages d'information. Pour la plupart des bâtiments, la conception d'un système de sonorisation ne représente pas un réel défi du point de vue acoustique. En effet, des environnements tels que les hôpitaux, universités et autres institutions sont essentiellement constitués d'un ensemble de petit locaux et de couloirs. La présence de plafonds suspendus et le faible volume des locaux permettent d'obtenir une réverbération adéquate. Ces lieux sont donc propices à la diffusion de messages vocaux.

Lorsqu'un système de sonorisation est requis dans de grands édifices, la réalisation du système est alors beaucoup plus problématique. La réverbération est directement proportionnelle au rapport du volume sur la surface absorbante équivalente (Loi de Sabine). Pour de grands édifices, souvent conçus avec des matériaux durables et majoritairement rigides, le volume des locaux est important et la surface absorbante équivalente est faible. La réverbération rend alors ces locaux hostiles à l'utilisation d'un système de sonorisation, d'autant plus que la diffusion de messages vocaux requière une réverbération faible pour obtenir une intelligibilité acceptable. Les recommandations pour la réverbération données dans la littérature ne sont généralement pas atteintes dans les espaces publics à grands volumes tels que gymnases, ateliers, gares, stations de métro, lieu de culte et autres espaces publics dont le volume excède souvent 10 000 $m^3$.

La présence d'un acousticien lors de la conception d'un système de sonorisation et idéalement lors de la conception du bâtiment destiné à recevoir le système est requise pour l'atteinte de performances acceptables. Malheureusement, les performances sur la sonorisation des édifices publics ne sont que très rarement décris en termes de critères objectifs.

Dans le cadre de la rénovation des stations du métro de Montréal, nous avons eu l'opportunité de concevoir, faire installer et valider la performance d'un système de sonorisation.

## 2 PRINCIPE DE CONCEPTION

### 2.1 Architecture des locaux

Pour la conception du système de sonorisation, il faut avant tout s'attarder sur les performances acoustiques des locaux en question. Lorsque les locaux sont composés principalement de béton, céramique ou autres matériaux du genre ayant un coefficient d'absorption de quelques pourcents, un traitement acoustique sur seulement 5% de la surface peut réduire le temps de réverbération d'au moins 50%.

### 2.2 Effet du public

Le public représente à la fois une surface importante d'absorption et une source de bruit à prendre en compte. La conception du système sans public est souvent conservatrice et permet d'obtenir des résultats satisfaisant en situation réelle.

### 2.3 Choix des équipements de diffusion

La sonorisation d'un édifice peut se faire soit : avec de nombreux haut-parleurs installés proche du public afin de réduire au maximum la distance entre la source et le récepteur, soit avec des haut-parleurs ayant une directivité importante et contrôlée afin d'orienter le son uniquement sur le public. La première solution a l'avantage d'utiliser des haut-parleurs standards, facilement interchangeables, mais requière une infrastructure importante en conduit et câblage qui rend l'intégration architecturale plus difficile. La deuxième solution repose sur l'utilisation de haut-parleurs spécifiques en fonction de l'architecture. Le coût en équipement est alors plus important, mais cette solution permet une meilleure intégration architecturale. Le choix de la méthode dépend alors des besoins du client et des contraintes du projet.

## 3 APPLICATION AU MÉTRO DE MONTRÉAL

Dans le cadre du remplacement du système de sonorisation du métro de Montréal, le logiciel EASE de la compagnie ADA (Acoustic Design Ahmert) a été utilisé comme outil de simulation 3D (figure 1). Il a servi à estimer la performance acoustique selon le critère STI en fonction du choix et du positionnement des haut-parleurs.

Une station est composée de plusieurs volumes, au minimum : des quais, une mezzanine, des corridors et un édicule. Habituellement, les quais représentent le volume le plus réverbérant d'une station. Celui-ci peut être couplé ou non avec les autres volumes de la station en fonction de la réverbération de ceux-ci.

Les principaux critères définis avec le client sont :

- Une intelligibilité égale à 0,45 STI dans l'ensemble des aires couvertes par le système;
- Une intelligibilité minimale de 0,30 STI dans les endroits les plus problématiques;
- Une uniformité et une standardisation des équipements pour l'ensemble des stations du métro.

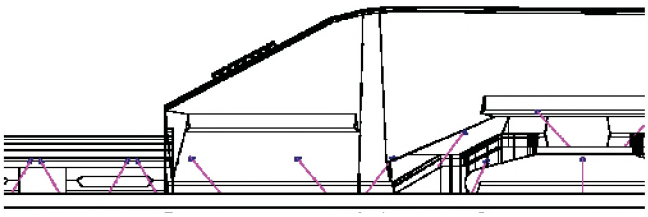

**Figure 1 Exemple de modèle de station avec positionnement et orientation des haut-parleurs**

La conception a donc été faite à partir de haut-parleurs standards localisés proche du public et répartis uniformément dans l'ensemble des aires à couvrir.

# 4 RÉSULTATS

Les résultats montrés ci-dessous représentent l'intelligibilité obtenue sur les quais des stations pour un échantillon représentatif de 10 stations. Celles-ci ont été regroupées en trois types différents. Premièrement, les stations de type 1, plus facile, où la performance obtenue est acceptable et uniforme. Deuxièmement, les stations de type 2, représentant plus de 80% des stations, où quelques difficultés ont été rencontrées. Troisièmement, les stations de type 3, plus difficiles, où la performance des zones problématiques est légèrement inférieure à la performance voulue. Les temps de réverbération moyens définis entre 500 Hz et 2 kHz, pour les trois types de station, sont montrés dans la figure 2.

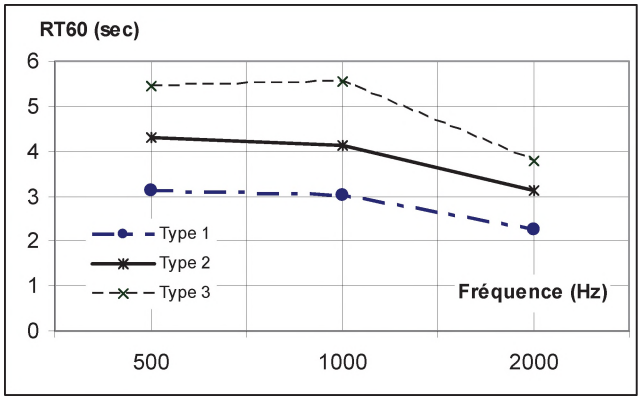


**Figure 2 Temps de réverbération en fonction du type de locaux**

## 4.1 Validation de la performance

Les résultats présentés dans le tableau 1 montrent la performance théorique estimée avec le logiciel EASE comparée à la performance mesurée.

**Tableau 1 Intelligibilité obtenue théoriquement (modèle EASE) et mesurée sur site en STI**

| Type de station | STI théorique | STI théorique minimal | STI mesuré | STI mesuré minimal |
|---|---|---|---|---|
| Type 1 | 0.47 | 0.39 | 0.48 | 0.47 |
| Type 2 | 0.48 | 0.37 | 0.55 | 0.37 |
| Type 3 | 0.45 | 0.33 | 0.48 | 0.26 |

Dans les stations de type 1 la performance réelle est toujours supérieure ou égale à la performance estimée. Les mesures montrent un STI uniforme sans aucune zone problématique. Pour les stations de type 2 la performance réelle est aussi supérieure ou égale à la performance estimée, cependant des zones problématiques ont été rencontrées. Pour les stations de type 3, la performance réelle correspond à la performance estimée, excepté dans les zones problématiques où elles s'en approchent.

## 4.2 Couplage présent

Lors de l'analyse des stations il a aussi été constaté que le couplage entre les différents volumes des stations pouvait avoir un impact important sur l'intelligibilité. Pour l'une des stations choisies, les temps de réverbération de la mezzanine sont aussi importants que ceux des quais, et à cause de contraintes architecturales, la sonorisation à la mezzanine est faite avec des haut-parleurs plus éloignés du public que sur les quais, et donc ajustés plus fort. L'effet obtenu est une intelligibilité supérieure à 0,45 STI sur les quais lorsqu'aucun message n'est diffusé sur la mezzanine, et de l'ordre de 0,43 STI lorsqu'un message est diffusé simultanément sur les quais et la mezzanine. Un délai de 20ms a donc été ajouté sur les haut-parleurs des quais pour réduire la perte d'intelligibilité sur les quais causée par l'audio provenant de la mezzanine. Théoriquement l'intelligibilité est passée de 0,43 STI à 0,47 STI. Des tests réels ont été faits après l'installation du système. Lors des mesures sur le site, l'écart de performance était encore plus marqué et l'intelligibilité est passée de 0,39 STI à 0,49 STI. Le même écart a été rencontré dans les zones problématiques.

# 5 CONCLUSION

Le travail présenté illustre une réalisation complète de sonorisation des grands édifices publics. La modélisation a permis de prédire avec précision la performance finale du système et à mettre en évidence les effets de couplage pour des locaux de volumes et de temps de réverbération comparables.

# STUDY OF THE COMPLIANCE OF A SOUND INTENSITY MAPPING DEVICE LOCATED IN SPACE BY COMPUTER VISION WITH CONVENTIONAL CERTIFIED METHODS FOR MEASURING SOUND POWER

**Jean Michel Attendu[1], Hugues Nelisse[2], Louis-Alexis Boudreault[1], and Michel Pearson[1]**
[1]Soft dB inc, Québec, P.Q, Canada, G1S 3G3, www.softdb.com
[2] Institut de Recherche Robert Sauvé en Santé et Sécurité du Travail (*IRSST*), Montréal, P.Q., Canada H3A 3C2

## 1. INTRODUCTION

A new real-time sound intensity mapping device, the *I-Track*, proposes a mean of measuring sound power that is based on sound intensity probe sweeps over planar surfaces coupled to a machine vision algorithm that associates each sound intensity measurement with coordinates in a common spatial reference. The innovation of this method relies, in particular, in the use of Fresnel ellipses and Delaunay triangulation in the process of averaging and interpolating the intensity data over the entire scanned area, which can subsequently be integrated to obtain the sound power. The main advantage of the *I-Track* device over conventional sound intensity measurement system is that the implemented spatial-based procedure allows obtaining contour maps of intensity without performing tedious point-by-point measurements by simply scanning over the area without following prescribed patterns as long as the whole area is entirely covered [1].

The conformity of the sound power data obtained with this method has never been the object of a formal investigation. Thus, it is the goal of this study to quantify the compliance of the results obtained with this technique with those obtained with standard certified methods. A first comparison was made by measuring sound intensity at discrete points, as described in the *ISO 9614-1* [2], using a calibrated source. Another comparison was made by performing sound intensity scanning as prescribed in the *ISO 9614-2* [3]. Finally, the results were also compared to the sound power data provided by the manufacturer of the calibrated source, such data being obtained using a standard microphone measurements method described in the *ISO 3745* [4].

## 2. METHODS

The measurements were undertaken in a semi-anechoic chamber. A calibrated source, the *Acculab RSS-400, was used as a noise source*. A rectangular virtual volume of 110 cm by 120 cm by 120 cm was defined symmetrically around the source in order to determine the measuring areas. The noise source is around 30 cm of height and approximately 25 cm wide. Since the noise source was placed on the ground, a reflective surface, 5 faces of the virtual volume were used for the intensity measurements. All the measurements (*I-Track* & standard procedures) were performed with the same microphones.

The measurements at discrete points were performed in accordance with the *ISO 9614-1* directives. Because of the radial symmetry of the source, only the top and one of the side faces were considered. For each of these surfaces, a 6 by 6 grid (36 evenly distributed measurement points) was used. For each of the 36 points, the duration of the measurement was approximately 20 seconds, which is considered enough for the data to stabilize over time and is consistent with the standard.

Sound intensity measurements by the scanning procedure were executed in accordance with the *ISO 9614-2*. Measurements using this method were performed for the top surface and all side surfaces. The sweeping speed always remained under 0.5 m/s and the scanning was uniform over the whole surface as prescribed by the standard.

As an alternative to the standard measurements, the *I-Track* device was used to generate sound intensity mapping, also in accordance with the *ISO 9614-2*. As mentioned previously, the *I-Track* device contains a localization apparatus that records the position of the intensity probe through a computer vision algorithm. As it was the case for the standard point-by-point measurement procedure, only the top and one of the side surfaces were considered.

## 3. RESULTS

Figure 1 presents the overall sound intensities (from 100 to 10k Hz) obtained using the standard point-by-point measurement procedure described above.

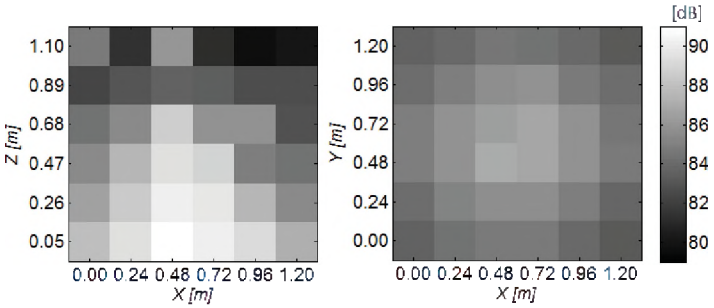


(a) Side Surface (b) Top Surface

**Figure 1 - Sound intensities obtained for the "measurement at discrete points" method (ISO 9614-1)**

A 3D representation of the experimental setup, along with an interpolation of these results is shown in figure 2. The cylindrical object exposed in figure 2 represents the source.

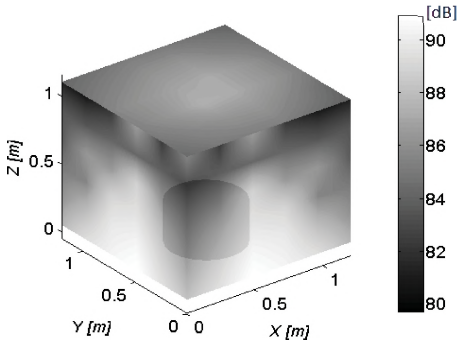


**Figure 2 – 3D Representation of the interpolated global sound intensities for the "discrete points" method (ISO 9614-1)**

Figure 3 presents the sound power obtained using the three different measurement procedures. Additionally, the source manufacturer's data was also added as a reference. As indicated by the manufacturer, this data was obtained using the hemi-anechoic calibration method described in the *ISO 3745* [4].

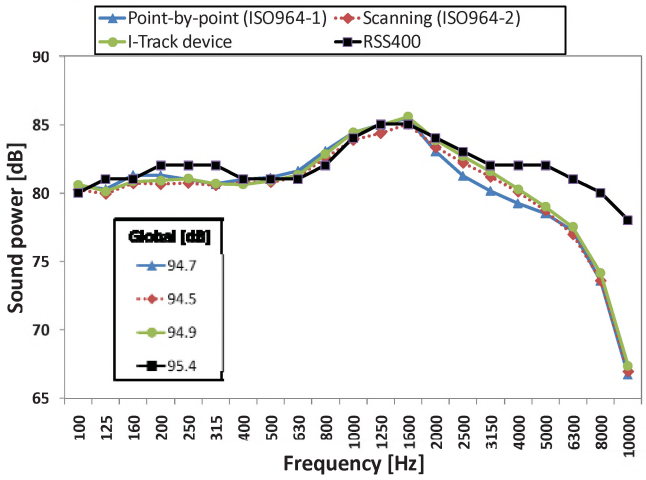


**Figure 3 – Comparison of the sound power obtained with the ISO methods and the I-Track device. RSS-400 calibrated source data are given as a reference**

Finally, figure 4 shows the overall sound intensity obtained with the *I-Track* sound mapping device. It is observed that the intensity distribution is similar to what was obtained with the measurements at discrete points.

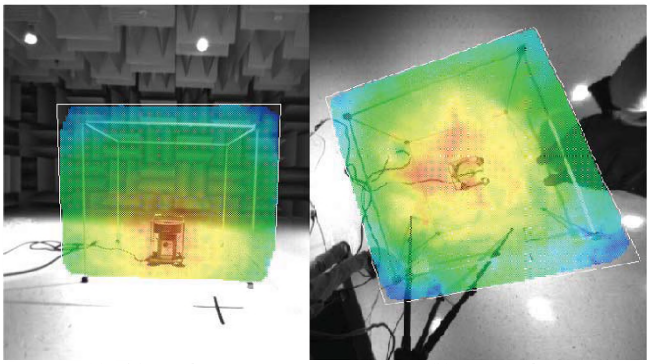

(a) Side Surface (b) Top Surface

**Figure 4 – Global sound intensity calculated using the *I-Track* sound mapping device**

## 4. DISCUSSION & CONCLUSION

As it is shown in figure 3, fairly good agreement was obtained between the three methods used in this study. Indeed, the differences in sound power levels for the various third octave bands remain under 1 dB and are under 0.5 dB for the overall sound power. These differences are within the uncertainty range of the devices used. It can thus be concluded that data obtained with the *I-Track* device is in good accordance with the ISO standard. The interpolation technique based of Fresnel ellipses and Delaunay triangulation seem to give more than adequate results over the spectrum of interest.

Notable differences were observed between the measurements data and the reference curve of the source for sound power values over 3.15 kHz. It is still unclear why there is such divergence and this issue is under investigation.

In conclusion, it has been shown that the sound intensity calculated from the *I-Track* sound mapping device complies with other intensity measurement methods, the *ISO 9614-1* and *ISO 9614-2*, over the studied frequency range. The difference is under 1 dB and within the range of uncertainties. Total sound power values as well as intensity contour maps were shown to be well captured by the I-Track device.

## REFERENCES

[1] Pearson, M., Boudreault, L.-A., L'Espérance, A., Sgard, F. (2010), Sound intensity mapping with manual swiping technique, Conference of the Canadian Acoustic Association, Victoria 2010.

[2] ISO 9614-1 (1995) Determination of sound power levels of noise sources using sound intensity. Part 1: Measurement at discrete points (International Organization for Standardization, Geneva)

[3] ISO 13091-2 (1996) Determination of sound power levels of noise sources using sound intensity. Part 2: Measurement by scanning (International Organization for Standardization, Geneva)

[4] ISO 3745 (2003) Determination of sound power levels of noise sources using sound pressure - Precision methods for anechoic and hemi-anechoic rooms. (International Organization for Standardization, Geneva)

# NOISE CONTROL OF VARIABLE SPEED DRIVE FANS: A CASE STUDY

**Adrienne Fowlie Larocque[1] and Hugh Williamson[2]**
[1]National Research Council, NRC-ASPM, 1200 Montreal Road, Building M19, Ottawa, ON, Canada, K1A0R6
[2]Hugh Williamson Associates Inc, PO Box 74056, RPO Beechwood, Ottawa, Ontario, K1M 2H9, Canada
Email: hughwilliamson@hwacoustics.ca

## 1. INTRODUCTION

Variable Speed Drive (VSD) motors allow building exhaust systems to operate more efficiently and, in principle, should lead to less noise due to a general reduction in fan speeds. Therefore, the National Research Council replaced old rooftop fans at one of its facilities, with fans selected for low-noise characteristics and equipped with VSD electric motors (Figure 1). However, as was found on this occasion, VSD can cause high frequency noise to be radiated by the electrical motor drive. This case study documents the effectiveness of the three measures to control this high frequency noise in inverter controller-type VSD electric motors: (1) insertion of acoustic lining into the electric motor enclosure; (2) modifications to the VSD electronic control parameters; and (3) vibration isolation of the electric motor.

## 2. METHODS

The three noise control measures were implemented for each fan as follows.

1. A one-inch acoustically absorbing lining was fitted inside the electric motor enclosure.
2. Control parameters within the VSD electronic controller were varied as follows: (a) switching frequency was set at 4, 8 or 12 kHz, and (b) the noise smoothing feature (dynamically varying the switching frequency over a small range) was turned on or off.
3. The electric motor was mounted on a new base plate, which was vibration-isolated from the support framework with a neoprene vibration isolation pad.

Noise measurements were made on the roof of the building, at a distance of 5 m, with all three fans operating simultaneously and under identical controller conditions. Two Bruel and Kjaer Type 2250 sound level meters were used; one was set to measure narrow band noise spectra and the other was set to measure 1/3-octave noise spectra.

## 3. RESULTS AND DISCUSSION

None of the noise control measures dramatically affected the overall noise level of the fans. Rather, treatments differed in how they affected the 4 kHz peak that was caused by the VSD controller (Figure 2).

The fitting of the acoustic absorptive lining was early in the investigation and not well documented. Anecdotal evidence comparing noise from the fans with lined enclosures to those with unlined enclosures, suggests that the differences were small and insignificant.

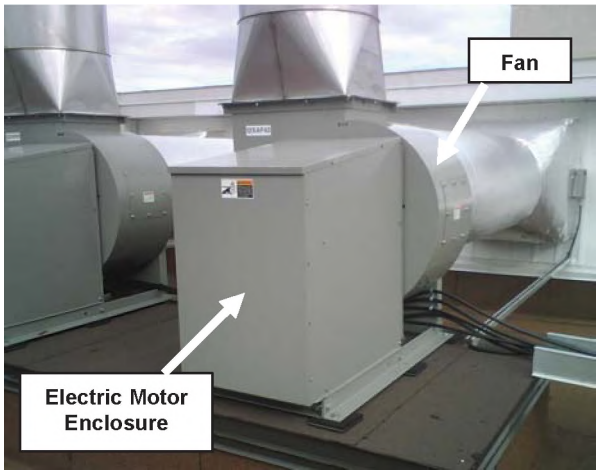


**Figure 1: Roof-top exhaust**

As shown in Table 1, changing the VSD electronic controller switching frequency (4, 8 or 12 kHz), was also found to have little effect on the sounds pressure level at 4 kHz octave band.

**Table 1: Effect of Varying Switching Frequency on A-weighted Sound Pressure Level in the 4000 Hz 1/3-octave band (no vibration isolation, noise smoothing off)**

| VSD Inverter Controller Switching Frequency | Motor Speed | |
|---|---|---|
| | 1500 rpm | 1800 rpm |
| 4 kHz | 56.9 | 60.8 |
| 8 kHz | 54.6 | 60.0 |
| 12 kHz | 56.0 | 59.0 |

However, Table 2 shows that vibration isolation resulted in significant noise reductions at the 4 kHz band. This effect was enhanced by operating the fans with the noise smoothing feature on.

**Table 2: Effect of Vibration Isolation and Noise Smoothing on A-weighted Sound Pressure Level in the 4000 Hz 1/3-octave band (Averaged over 4, 8, and 12 kHz. Basic VSD refers to operations with noise smoothing off).**

| Noise Control Measures | Motor Speed | |
|---|---|---|
| | 1500 rpm | 1800 rpm |
| Basic VSD | 55.8 | 59.9 |
| VSD with noise smoothing | 55.8 | 57.6 |
| Basic VSD with vibration isolation | 49.1 | 49.7 |
| VSD with noise smoothing and vibration isolation | 43.4 | 44.3 |

Figures 2 and 3 show that noise smoothing in the inverter controllers distinctly reduced noise in the 4 kHz band.

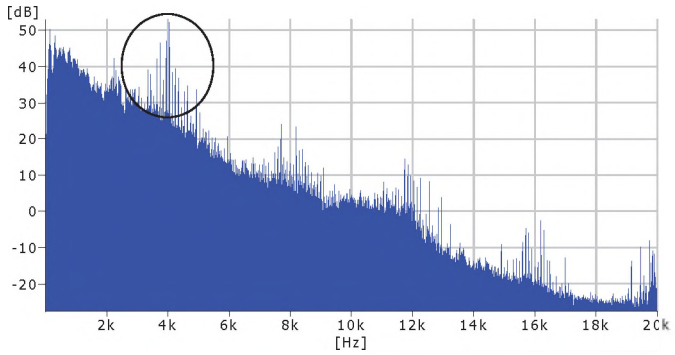


**Figure 2: A-weighted Narrow Band Noise Spectrum, Smoothing Off. Note distinct peaks near 4 kHz.**

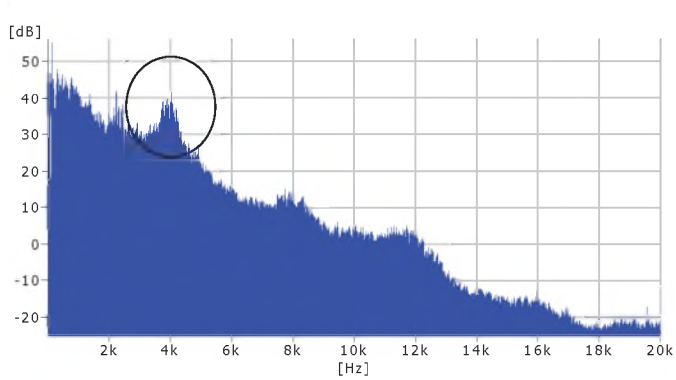


**Figure 3: A-weighted Narrow Band Noise Spectrum, Smoothing On. Note broad peaks near 4 kHz**

A characteristic of this type of VSD controller is that noise is generated when high frequency components in the electrical power to the motor cause electromagnetic resonances in the stator of the electric motor. These electromagnetic resonances induce vibrations in the stator and motor structure which produce noise. In this particular case, the noise profile generated from the VSD fans had a series of peaks in the noise spectrum at approximately 4 kHz and its higher harmonics (Figure 2). To the human ear, the sound is a high-pitched whine, and can annoy some receptors (On a piano, this frequency corresponds approximately to a high C, four octaves above middle C.).

The high frequency whine was detected when the fans were first installed. The fan enclosures were lined with a 1" thick acoustically absorbing lining, but this was ineffective. In principle, when a noise source is in a vented enclosure, and the enclosure is lined with an acoustically absorbing material, the amount of noise exiting via the enclosure vents should be reduced. However in this case, the motor was rigidly connected to the frame, transferring the vibrations to the enclosure walls. The lining was ineffective because the noise was being radiated by the whole of the enclosure walls and frame. Subsequently treating the motor with vibration isolation significantly reduced the whine noise.

Contrary to the results of previous studies (Gieras *et al.*, 2006), changing the switching frequency of the VSD controller did not significantly affect the noise profile (Table 1). Regardless of the treatment, increasing the motor speed from 1500 rpm to 1800 rpm increased the noise peak(s) in the vicinity of 4 kHz.

However, our results were consistent with observations by Gieras *et al.*, (2006), who noted that noise smoothing reduces the tonal quality of the high frequency noise from the motor. With noise smoothing off, the distinctive high-pitched whine is audible and can be very annoying to human receptors. This corresponds to the multiple peaks in the narrow band spectrum in the vicinity of 4 kHz (Figure 2). When noise smoothing is on, the whine was significantly reduced (Figure 3). This reduction of the whine noise was essentially the same regardless of the motor speed or the switching frequency.

Furthermore, when the noise smoothing and vibration isolation treatments were combined, the whine noise was very significantly reduced. As seen in Table 2, the sound pressure level (SPL) measured in the 4 kHz 1/3 Octave band was reduced by up to 13 dBA. The noise, and its associated adverse effect on human receptors, virtually disappeared.

## 4. CONCLUSIONS

Inverter controller-type VSD electric motors can cause a distinct high-pitched whine noise. In this study, the noise corresponded to peaks in the narrow band sound spectrum in the vicinity of 4 kHz.

When both noise smoothing and vibration isolation were applied, the whine noise virtually disappeared. For the three fans studied, the application of noise smoothing in combination with vibration isolation was the most effective noise control measures for the high pitched whine associated with VSD motors.

## REFERENCES

Gieras, J.R., Wang, C., Lai, J.C. (2006). *Noise in Polyphase Electric Motors* (Taylor & Francis).

## ACKNOWLEDGEMENTS

The authors gratefully acknowledge the assistance of Michael Kennedy, Facilities Maintenance Zone 3, NRC-ASPM for his assistance in completing this project.

# CURSUS DE FORMATION EN ACOUSTIQUE DE L'UNIVERSITÉ DE SHERBROOKE

**R. Panneton**
Département de génie mécanique, Université de Sherbrooke, Sherbrooke, Qc, Canada, J1K 2R1

## 1. INTRODUCTION

Par le biais du Groupe d'acoustique de l'Université de Sherbrooke (GAUS), le Département de génie mécanique de l'Université de Sherbrooke est reconnu pour ses recherches fondamentales et appliquées dans les domaines de l'acoustique, l'aéroacoustique et des vibrations. Sept professeurs, affiliés au GAUS, permettent de former des ingénieurs hautement qualifiés de 1er, 2e et 3e cycles dans des domaines liés à l'acoustique. Au premier cycle, on parle principalement de la formation de stagiaires en recherche dans les laboratoires du GAUS. Au 3e cycle, on parle du doctorat en génie mécanique menant au grade de *Philosophiæ Doctor* (Ph. D.). Au 2e cycle, on parle de la maîtrise en génie mécanique menant au grade de *Maître ès sciences appliquées* (M. Sc. A.). Pour ce dernier, l'étudiant peut choisir entre deux cheminements: celui de type recherche et celui de type cours.

Dans ce résumé, seulement les 2 cursus de formation de 2e cycle en acoustique sont présentés. Ces deux cursus permettent : (1) de former des spécialistes autonomes et compétents afin qu'ils puissent exercer une pratique professionnelle de haut niveau technique dans un des domaines liés à l'acoustique; (2) de développer des aptitudes à la recherche en génie; (3) de préparer les étudiants à des études de 3e cycle.

## 2. MAÎTRISE DE TYPE RECHERCHE

Le cheminement de type recherche compte 45 crédits, dont 30 crédits obligatoires (voir Tableau 1). De ces 30 crédits, 26 crédits s'articulent autour d'un projet de recherche en acoustique se terminant par un mémoire. Le projet est proposé par un professeur du GAUS et est généralement associé à une problématique industrielle. Il se développe en 4 étapes : 1) L'étape 1 (GMC 726) vise à rédiger durant le premier trimestre un plan de formation et d'établir les objectifs et le déroulement du projet de recherche. Elle permet aussi d'identifier les membres du comité d'encadrement. L'étape 2 (GMC 727) est la définition du projet de recherche proprement dite. Elle doit être déposée et évaluée par le comité d'encadrement à la fin du deuxième trimestre. L'étape 3 (GMC 729) est un rapport d'activités rendant compte des travaux réalisés à la fin du troisième trimestre. Le rapport est évalué par le comité d'encadrement. Finalement, l'étape 4 (SCA 730) se termine par l'évaluation et le dépôt du mémoire. De plus, le mémoire doit être présenté devant un auditoire afin de compléter les requis de l'activité GMC 728.

**Table 1. Maîtrise en génie mécanique (45 crédits). Cheminement de type RECHERCHE. Spécialisation en ACOUSTIQUE.**

| | |
|---|---|
| **ACTIVITÉS OBLIGATOIRES (30 crédits)** | |
| GMC 726 | Introduction au projet de recherche (1 cr.) |
| GMC 727 | Définition du projet de recherche (4 cr.) |
| GMC 728 | Séminaires de recherche (1 cr.) |
| SCA 701 | Méthodologie de recherche et communication (3 cr.) |
| SCA 702 | Plan de formation en maîtrise (0 cr.) |
| SCA 715 | Sécurité dans les laboratoires de recherche (0 cr.) |
| SCA 729 | Rapport d'avancement en recherche (3 cr.) |
| SCA 730 | Activités de recherche et mémoire (18 cr.) |
| **ACTIVITÉS À OPTIONS (0 à 6 crédits)** | |
| Ensemble des activités de second cycle (avec approbation) | |
| **ACTIVITÉS EN ACOUSTIQUE (9 à 15 crédits)** | |
| **Voir liste d'activités du Tableau 3 (avec approbation)** | |

**Table 2. Maîtrise en génie mécanique (45 crédits). Cheminement de type COURS. Spécialisation en ACOUSTIQUE.**

| | |
|---|---|
| **ACTIVITÉS OBLIGATOIRES (9 crédits)** | |
| GMC 807 | Définition du projet d'essai (1 cr.) |
| GMC 808 | Essai (8 cr.) |
| SCA 702 | Plan de formation en maîtrise (0 cr.) |
| SCA 716 | Sécurité dans les laboratoires (0 cr.) |
| **ACTIVITÉS À OPTIONS (9 à 24 crédits)** | |
| Ensemble des activités de second cycle (avec approbation) | |
| **PROJET DE DÉVELOPPEMENT EN ACOUSTIQUE (3 ou 6 crédits)** | |
| **GMC 805** | Projet de développement en génie mécanique I (3 cr.) |
| **GMC 806** | Projet de développement en génie mécanique II (6 cr.) |
| **ACTIVITÉS EN ACOUSTIQUE (9 à 21 crédits)** | |
| **Voir liste d'activités du Tableau 3 (avec approbation)** | |

**Table 3. Maîtrise en génie mécanique. BLOC de spécialisation en ACOUSTIQUE.**

| | |
|---|---|
| **ACTIVITÉS EN ACOUSTIQUE** | |
| GMC 720 | Acoustique fondamentale (3 cr.) |
| GMC 721 | Rayonnement acoustique des structures (3 cr.) |
| GMC 722 | Méthodes numériques en interaction fluide-structure (3 cr.) |
| GMC 723 | Contrôle actif de bruit et vibrations (3 cr.) |
| GMC 729 | Aéroacoustique (3 cr.) |
| GMC 712 | Traitement et analyse fréquentielle des données exp. (3 cr.) |

Outre ces 30 crédits obligatoires, les étudiants se spécialisant en acoustique s'inscrivent à au moins 3 des 6 activités du bloc de spécialisation en acoustique (voir Tableau 3. En général, c'est à l'étape 1 que l'étudiant fait le choix des activités avec l'approbation de son directeur de recherche.

Les activités du bloc de spécialisation en acoustique couvrent différentes méthodes d'analyse : analytiques (720/721/723/729); numériques en éléments finis (FEM) et en éléments finis de frontière (BEM) (720/722/729); énergétiques comme la *statistical energy analysis* (SEA) (722); expérimentales (720/721/723/712); contrôle actif de bruit et de vibrations (723). Plus de détails sur ces activités seront donnés lors de la conférence.

## 3. MAÎTRISE DE TYPE COURS

Le cheminement de type cours compte aussi 45 crédits, dont seulement 9 crédits obligatoires (voir Tableau 2). Le premier crédit est dédié une mini définition du projet d'essai (GMC 807), tandis que les 8 autres crédits sont liés directement à l'essai. Dans le cadre d'une spécialisation en acoustique, l'étudiant s'inscrit généralement à un projet de développement (805/806) de 3 ou 6 crédits qui est proposé et encadré par un professeur du GAUS (le superviseur). Ce projet et l'essai sont intégrés dans un même rapport qui sera évalué par le superviseur et un autre professeur. Le projet d'essai comptera donc pour 11 ou 14 crédits.

Outre ces activités obligatoires et le projet de développement, les étudiants se spécialisant en acoustique doivent, tout comme les étudiants inscrits à la maîtrise de type recherche, s'inscrire à au moins 3 des 6 activités du bloc de spécialisation en acoustique (voir Tableau 3).

Dans ce cheminement de type cours, les étudiants peuvent aussi s'inscrire à plusieurs autres cours de spécialisation en génie. Notamment, plusieurs étudiants optent pour le bloc de gestion de projet en ingénierie, totalisant jusqu'à 12 crédits (i.e., 4 cours).

## 4. DISCUSSIONS

Malgré la diversité des cours en acoustique et une formation par compétences au 1er cycle bien connue au Canada, on constate que nos 2 cursus de maîtrise en acoustique utilisent une formule d'enseignement plutôt classique.

Le Département de génie mécanique travaille présentement à la mise à jour de ses programmes de maîtrise. En acoustique, de concert avec les professeurs du GAUS, le Département proposera des modifications majeures de sa spécialisation en acoustique et des cours associés. À court terme, un microprogramme de deuxième cycle en acoustique serait créé.

# UNE EXPÉRIENCE D'ENSEIGNEMENT DE L'ACOUSTIQUE INDUSTRIELLE INTÉGRANT PÉDAGOGIE DE LA COOPÉRATION, PROJET DE SESSION ET LABORATOIRE INFORMATIQUE

**Frédéric Laville**
Département de génie mécanique, École de technologie supérieure,
1100 Notre-Dame Ouest, Montréal, Québec, Canada, H7N 4T2, frederic.laville@etsmtl.ca

## 1. INTRODUCTION

Les étudiants au baccalauréat en génie mécanique de l'École de technologie supérieure peuvent suivre un cours optionnel en acoustique industrielle. Depuis sa création, en 1994, trois approches non conventionnelles ont été utilisées conjointement dans ce cours et sont présentées successivement dans cet article :

1. Pédagogie de la coopération
2. Projet de session en équipe de réduction du bruit sur un petit appareil
3. Séances de travaux pratiques et examens en laboratoire informatique.

## 2. PÉDAGOGIE DE LA COOPÉRATION

La pédagogie de la coopération ou apprentissage coopératif en petits groupes est une méthode pédagogique où l'apprentissage de l'étudiant est basé sur ses interactions avec d'autres étudiants au sein de petits groupes auxquels diverses tâches de natures et durées variées sont données dans toutes les périodes en classe (cours, exercices dirigés, travaux pratiques, laboratoires, etc.). C'est une méthode qui a un fort potentiel d'amélioration de l'apprentissage, elle est bien documentée (les références les plus populaires sur le sujet sont les ouvrages des frères Johnson, [1] par exemple) et des formations sont offertes. Ce qui est présenté dans cet article est la mise en œuvre pratique de cette méthode dans le cadre d'un cours d'acoustique industrielle (une fois passées les premières difficultés de l'introduction d'une méthode non traditionnelle), ainsi que ses avantages et inconvénients constatés.

### 2.1 Mise en œuvre pratique

Formation des équipes.

L'approche retenue est de former des équipes pour la session. Idéalement, ce serait de former des équipes hétérogènes mais, pour faciliter la mise en œuvre avec des étudiants en fin de parcours académique et avec des habitudes d'apprentissage bien établies, le choix des coéquipiers est laissé libre avec une seule contrainte introduite récemment avec de plus grands cours-groupes : trouver des équipiers avec une plage de disponibilité commune pour les laboratoires-projet supervisés en dehors des horaires planifiés. Les équipes sont formées dès le premier cours. Le nombre est limité à 4 étudiants max (pour simplifier la gestion des travaux en équipe) et 3 étudiants minimum (pour assurer un minimum de variété dans les interactions au sein de l'équipe)

Organisation de l'espace

Un espace qui favorise le travail en équipe est important : idéalement des tables rondes seraient requises mais, pour que les salles de cours puissent aussi accueillir un enseignement traditionnel, un compromis est l'utilisation de tables de deux étudiants qui peuvent être mises face à face ou côte à côte pour travailler à quatre. Un étiquetage avec un numéro d'équipe sert à la localisation des équipes pour les étudiants et pour l'enseignant.

Quelques principes de fonctionnement

Dans cette pédagogie, l'équipe a un double but : mener à bien la tâche commune et s'assurer de l'apprentissage de tous ses membres.

Les questions sont posées au sein de l'équipe et en dernier recours à l'enseignant. Ceci est justifié par le principe que l'étudiant qui n'a pas compris le concept présenté par l'enseignant bénéficiera d'une autre explication que celle de l'enseignant et que l'étudiant qui a compris va améliorer sa compréhension en expliquant à un autre.

Choix des activités

C'est la partie qui peut nécessiter le plus de préparation car le succès de l'approche dépend beaucoup de la pertinence des activités, leur intérêt et leur variété (nature et durée). Cependant, un bon point de départ est d'entrecouper une présentation magistrale classique par de nombreux exercices d'application de longueurs et natures variables et basés sur des données différentes et complémentaires entre chaque équipe. Exemple : chaque équipe a une bouteille d'eau vidée à une hauteur différente avant calcul et mesure de la fréquence du résonateur de Helmholtz.

Évaluation

Pour favoriser la collaboration et l'entraide dans l'apprentissage au lieu de la compétition, il est important d'utiliser une évaluation critériée et non pas normative et d'en informer les étudiants.

### 2.2 Avantages et inconvénients

L'avantage principal est la plus grande implication des étudiants dans leur apprentissage. Des différences dans les niveaux de participation ont été ressenties par l'enseignant entre une séance de cours contenant un temps assez long d'exposé magistral (les étudiants hésitaient à sortir leur calculatrice pour un exercice tant ils étaient dans le mode écoute et non action) et une séance de cours contenant beaucoup d'activités en équipe (implication importante des étudiants : ils ne pensaient plus à s'arrêter à l'heure de la pause tant ils étaient impliqués dans leur activité).

Un avantage pour l'enseignant est qu'il a une très bonne idée en temps réel de la capacité des étudiants à comprendre et mettre en œuvre ce qui leur est présenté et il peut intervenir rapidement si une notion n'est pas assimilée.

Un inconvénient est qu'à priori moins de matière est couverte et il faut donc bien centrer le cours sur les apprentissages fondamentaux.

## 3. PROJET DE SESSION

L'objectif donné aux étudiants est de démontrer la faisabilité de réduire le bruit d'un appareil par des modifications qui conduiront à un prototype plus silencieux. Le prototype sert à démontrer la faisabilité de la réduction de bruit et pourra donc être réalisé avec des matériaux/montages faciles à utiliser tout en sachant que l'appareil commercial pourrait être réalisé avec des matériaux/montages adaptés à la production en grande série. La fonctionnalité de l'appareil doit être conservée (durée de fonctionnement et performances mécaniques, par exemple 80 % du débit d'air pour un sèche-cheveux)

Les grandes étapes du projet sont (1) la définition d'un objectif de réduction du bruit, (2) le diagnostic des sources de bruit et des chemins de transmission par des méthodes variées (analyse fréquentielle, modification de l'appareil, montages spéciaux, variation des conditions de fonctionnement, encoffrement partiel, etc) et (3) la conception et l'essai de solutions potentielles pour aboutir à la réalisation de la solution finale et la vérification de son efficacité.

Le projet est réparti sur 5 séances de laboratoire de deux heures aux deux semaines. Il fait l'objet de deux rapports de laboratoire évalués indépendamment du rapport final : un premier rapport de mesure de puissance acoustique normalisée selon ISO 3744 et un deuxième rapport incluant un diagnostic fréquentiel avec planification des essais de diagnostic. Il se termine par une présentation orale avec démonstration des performances lors du dernier cours et d'un rapport final remis en fin de session.

La photo de la figure 1 a été prise lors de la présentation des projets, on voit un étudiant qui opère le prototype silencieux d'appareil de son équipe (un sèche-cheveux) pour la mesure acoustique affichée sur l'écran en bandes d'octave. L'organisation de la salle de classe est typique de celle de tous les cours de la session : les étudiants sont rassemblés en équipe de 4 (ou 3) sur deux tables côte à côte.

L'avantage de ce type de projet est certainement d'atteindre les objectifs supérieurs d'apprentissage dans la taxonomie de Bloom, soit le niveau 4 *analyse* (diagnostic des sources de bruit), le niveau 5 *synthèse* (conception et réalisation de solutions) et le niveau 6 *évaluation* (analyse critique des solutions).

Les exigences sont celles associées au travail en équipe. Comme en cours les équipes sont déjà formées, le projet ne nécessite pas de nouvelle formation d'équipes, il s'intègre donc très naturellement dans la pédagogie de la coopération. Comme il s'agit d'un travail à plus long terme que ce qui est fait en cours, il est demandé aux étudiants de faire un suivi plus formel du fonctionnement de l'équipe. Un des moyens utilisés dans le cadre de ce cours est de demander de remplir plusieurs fois dans la session un questionnaire incluant une réflexion sur ce qui a bien été et ce qui serait à améliorer et les contributions respectives de chacun des membres de l'équipe. Ce questionnaire constitue aussi un mécanisme qui permet de pondérer les notes des étudiants en fonction de leurs contributions.

**Figure 1. Présentation des projets de session – mesure acoustique du prototype d'appareil silencieux avec affichage à l'écran des valeurs par bandes d'octave**

## 4. TRAVAUX PRATIQUES ET EXAMENS EN LABORATOIRE INFORMATIQUE

Une autre caractéristique de ce cours est l'utilisation assez intensive d'un outil informatique pour le calcul des phénomènes acoustiques qui doit être fait en un grand nombre de points fréquentiels. L'environnement MATLAB™ conçu pour le calcul matriciel est utilisé parce que bien adapté mais aussi parce que c'est l'environnement de calcul utilisé dans d'autres cours en génie mécanique à l'ÉTS. Pour encourager la maîtrise et l'utilisation de cet outil, les mesures suivantes ont été prises :

- Tous les calculs utilisent le même outil sauf dans les cours car cet outil n'est pas disponible et une calculatrice symbolique est utilisée.
- Les travaux pratiques de deux heures aux deux semaines se font en laboratoire informatique.
- Les examens (de mi-session et final) se font en laboratoire informatique.

## 5. CONCLUSIONS

Les deux premières approches ont chacune leur mérite propre (l'apprentissage par petits groupes induit une participation active des étudiants et le projet de session leur permet d'atteindre les plus hauts objectifs d'apprentissage) et leur utilisation conjointe a le mérite d'assurer la continuité du travail en équipe dans l'ensemble des activités de formation. La troisième approche (utilisation intensive de l'outil informatique) a le mérite de permettre la résolution de problèmes plus avancés et plus proches de la réalité industrielle. Cependant la maîtrise de cet outil informatique pourrait être augmentée avec son utilisation en cours (quand chaque étudiant disposera d'un ordinateur portable), c'est la prochaine étape.

## REFERENCES

David and Roger Johnson and Karl Smith (2006, 8th Edition). *Active Learning: Cooperation in the College Classroom*

# EVALUATION OF ROAD TRANSPORTATION NOISE MODELLING ALGORITHMS AND SOFTWARE PACKAGES

**Kevin Carr[1], Scott Penton[1], and Marcus Li[1]**
[1]Novus Environmental, 150 Research Lane Suite 105, Ontario, Canada, N1G 4T2
kevinc@novusenv.com, scottp@novusenv.com, marcusl@novusenv.com

## 1. INTRODUCTION

In a joint project sponsored by the Ontario Ministry of Transportation, the Ontario Ministry of the Environment, and GO Metrolinx, transportation noise modelling algorithms and software packages have been assessed. The goal is to determine the best computerised noise prediction models for road, rail, and light-rail transit sources, to replace ORNAMENT, STEAM, STAMSON, and STAMINA within the province of Ontario. This evaluation was based on a quantitative and qualitative evaluation of a number of factors. This paper focuses on the road noise model evaluation.

The analysis examined both software packages (for cost, usability and performance) and the prediction algorithms.

## 2. ALGORITHM EVALUATION

Acoustical algorithms were evaluated, with the goal of providing recommendations regarding transportation noise modelling in Ontario. Transportation noise modelling algorithms included in this evaluation were chosen to correspond with current practices within Ontario, as well as to explore options commonly utilised within the United States and Europe.

Transportation noise modelling algorithms explored in this study include FHWA TNM, FHWA-RD-77-108 (STAMINA), NMPB-96, ORNAMENT, RLS-90, and VBUS. Criteria used to rank algorithms include Noise Emission, Noise Propagation, Consistency with Ontario Guidelines and Practices, and Versatility and Technical Performance.

Traffic noise emissions are generally calculated accounting for traffic mix, speed, pavement type, and road gradient. In addition to these factors, TNM and NMPB-96 also consider engine noise variations due to acceleration. RLS-90, NMPB-96, and VBUS do not consider heavy and medium vehicles separately as do FHWA TNM, FHWA-RD-77-108, and ORNAMENT. From a traffic noise emission standpoint, the TNM algorithm was ranked 1st, as it uses up-to-date noise emission data, and considers the full scope of vehicle types used in Ontario.

Noise propagation calculation was ranked based on consistency with current Ontario practices, customisability, meteorology, and the effects of ground absorption. Again, the FHWA TNM algorithm was found to provide to best combination of these factors.

It should be noted that a large variation in distance attenuation factors was observed between different algorithms under controlled settings. Variation of calculated propagation values increases with distance. Figure 1 shows an example of the dispersion observed in propagation attenuation factors between models. This variation highlights the importance of adopting a standardised model to be used across the province.

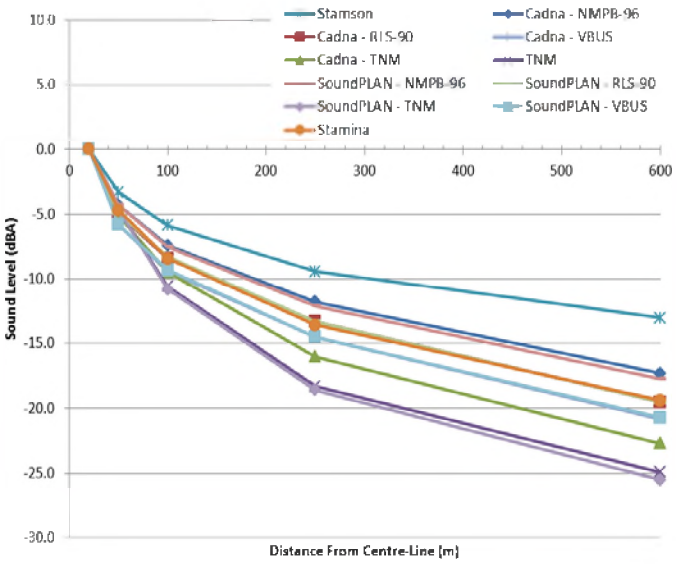


**Figure 1. 1st Storey, No Barrier, Reflective Ground**

In order to rank noise modelling algorithms, it is important to consider compatibility with current practices. Both required and extraneous input possibilities were considered. TNM is the modern algorithm most similar to STAMINA an STAMSON in terms of inputs, and has with the least amount of extraneous inputs likely to cause errors or in consistencies in the results provided by different modellers/ analysts. Therefore, FHWA TNM was ranked 1st for this category.

Technical performance was evaluated by considering the speed of the calculation as well as the potential to propagate errors. Each algorithm had deficiencies and virtues. Notably, the FHWA TNM algorithm calculates a complicated propagation algorithm for 1/3 octave band emissions separately for each vehicle type and throttle setting. As a result, FHWA TNM is significantly slower than the other algorithms. There was no algorithm with clearly better technical performance, so FHWA-RD-77-108, RLS-90, and VBUS were ranked as a tie for 1st.

**Ranking of Algorithms**

Overall, the most preferable algorithm is the FHWA TNM algorithm. This algorithm is implemented in the three top ranked software packages. The TNM algorithm is more robust and technically more advanced than most other road traffic algorithms. In addition to outranking the other algorithms in terms of technical capability the TNM algorithm is also more applicable within North America, where heavy vehicles are not only larger, but also more common.

## 3. SOFTWARE EVALUATION

The primary goal of the software evaluation study was to investigate the performance of readily-available software packages. Software packages explored in this study include STAMSON 5.1, STAMINA 2.0, TMN 2.5, Cadna/A, and SoundPLAN.

Software packages were evaluated in order to assess a number of key performance indicators. Assessed performance indicators include Cost and Market Penetration, Usability, Output, and Acoustical Performance.

Although Cadna/A and SoundPLAN are expensive and similarly priced, Cadna/A is prevalent in Ontario amongst consultants (it is mainly used for industrial noise). Although TNM 2.5 is relatively inexpensive, it is currently not used extensively within Ontario. Similarly, STAMINA is less commonly used than STAMSON, although both software packages are free. In terms of cost and market penetration, STAMSON and Cadna/A have ranked 1st and 2nd, respectively.

Considering factors such as ease of use, hardware restrictions, export and import options, and customisability, the advanced software packages Cadna/A and SoundPLAN were found to be most usable. TNM 2.5 includes features that are not available in STAMINA and STAMSON; however, the graphic user input system in the current version of TNM is very limited compared to Cadna/A and SoundPLAN.

Key output formats evaluated include the ability to provide point of reception impacts, ranked impacts, partial impacts (impacts for individual contributors), noise contours (lines of equal noise level). Tied with a rank of 1st, Cadna/A and SoundPLAN implement all of the above output formats. TNM 2.5 is not able to output partial levels without separating modelling runs. All output types are possible in both STAMINA and STAMSON, although data manipulation is necessary. STAMINA and STAMSON cannot easily produce noise contour plots.

Acoustical performance was evaluated by considering consistency between different implementations of the same algorithm, as well as speed of calculation. Only small deviations were observed for separate implementations of RLS-90 and VBUS. Implementations of NMPB-96 had slightly more variation, but there was not a clearly superior implementation. As a result, all software packages were ranked neutrally in terms of acoustical performance of all algorithms, with the exception of TNM.

Some significant variations in FHWA TNM results were observed between different software packages. The Cadna/A implementation is missing a number of key modelling parameters – namely flow resistivity (as opposed to ground absorption), grade adjustment, and import/export options. Both Cadna/A and SoundPLAN correct a number of known glitches within TNM 2.5. However, both packages include an option to include these errors for conformity with TNM 2.5. Unfortunately, neither software package is endorsed by the FHWA, and as a result, each program includes a disclaimer, and notes not being fully implemented. As a result, despite obvious errors, and long calculation times, TNM 2.5 was ranked preferable in terms of acoustical performance.

**Ranking of Software**

Cadna/A and SoundPLAN achieved 1st and 2nd rank, respectively, with TNM 2.5 ranking 3rd. Based on the unofficial nature of the Cadna/A and SoundPLAN implementations of the TNM algorithms, TNM 2.5 was ranked most preferable in terms of TNM implementation.

## 4. INTERIM RESULTS

Our work to date points towards recommending the use of the current TNM 2.5 algorithm and software package for use in evaluating road noise impacts. The official FHWA TNM software package is relatively inexpensive. The algorithm includes up-to-date noise emission factors, consistent with North American traffic types.

Other more advanced software packages such as Cadna/A and SoundPLAN offer better user interfaces and additional analysis features. However, there are inconsistencies in the results from TNM 2.5, Cadna/A, and SoundPLAN, which are still being investigated.

Should TNM 3.0 be released and endorsed by the FHWA, as is expected in the near future, it will offer many improvements over TNM 2.5 in terms of usability.

## ACKNOWLEDGEMENTS

Novus Environmental would like to thank the Ministry of Transportation, the Ministry of the Environment, and GO Metrolinx for granting us the opportunity to work on such an interesting and important project.

# ADDRESSING LOW FREQUENCY SOUND AND INFRASOUND FROM WIND TURBINES

**Brian Howe[1], Nick McCabe[2], and Ian Bonsma[3]**
[1]HGC Engineering, 2000 Argentia Road, Plaza One, Suite 203, Mississauga, ON, L5N 1P7, bhowe@hgcengineering.com
[2]HGC Engineering, nmccabe@hgcengineering.com [3]HGC Engineering, ibonsma@hgcengineering.com

## 1. INTRODUCTION

Wind power increasingly forms part of the renewable energy strategy in Ontario, but it is not without opposition from some individuals and groups. One of the key issues is sound, and there is a debate concerning the health impact of low frequency sound and infrasound from wind turbines.

Of significance in this debate was an appeal to the Environmental Review Tribunal (ERT) of the Ministry of the Environment's (MOE) approval of a wind farm near Chatham. Although the ERT concluded that the appellants had not shown that the wind farm will cause serious harm to human health, and dismissed the appeals, they did note in their decision that "the research in this area is at quite an early stage and that our collective understanding of the impacts of wind turbines on human health will likely progress as further research and analysis is undertaken".

HGC Engineering was retained by the MOE to appear at the hearing and to provide a literature review of materials related to low frequency noise and infrasound associated with large, modern, upwind wind turbine generators. Research focused on journal articles, and technical papers and reports presented at conferences, as well as guidelines or regulations from other jurisdictions. The aim of the study was to provide recommendations and guidance to the MOE, as the approving body under the Renewable Energy Act, on how best to address low frequency sound and infrasound from wind turbines. This paper summarises the key findings and presents the recommendations from that study.

## 2. SUMMARY OF FINDINGS

Modern wind turbines produce broadband noise, with the dominant sound source related to turbulence at the trailing edge of the blades. In relation to human perception of the sound, the dominant frequency range is not the low frequency or infrasonic ranges, but low frequency sound will routinely be an audible component of the acoustic impact. The degree of audibility depends on the wind conditions, the degree of masking from other noises and the distance from the wind turbines. In instances where audible acoustic tones are present, typically related to mechanical or gearbox noise, the frequency of these tones can be within the low frequency range.

In the infrasonic range, at frequencies less than about 20 Hz, there is strong evidence that the sound pressure levels produced by modern upwind turbines will be well below (on the order of 20 dB below) the average threshold of human hearing, at the setback distances typical in Ontario.

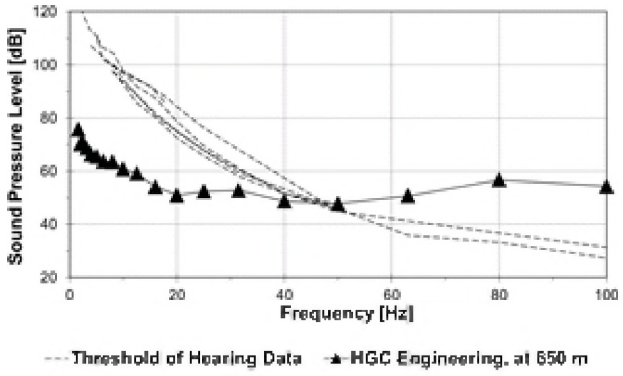


**Sample Sound Levels at Low and Infrasonic Frequencies**

Although some authors have raised concerns, most literature dealing with the subject indicates that infrasonic noise below the threshold of hearing will have no effect on health. It should be acknowledged that this does not conclusively eliminate the possibility that under exceptional circumstances – rare atmospheric conditions or some alternate turbine designs – infrasound levels could be heard. There are also large variations in individual sensitivities to infrasound.

Publications by medical professionals indicate that, at the typical setback distances in Ontario, the overall magnitude of the sound pressure levels produced by wind turbine generators does not represent a direct health risk. This includes noise at low and infrasound frequencies.

The audible sound from wind turbines at the closest typical receptor distances in Ontario is nonetheless expected to result in a non-trivial percentage of persons being highly annoyed. As with sounds from many sources, research has shown that annoyance associated with wind turbines can be expected to contribute to stress related health impacts in some persons. The relationship between the sound level and the prevalence of annoyance is complicated, and is often influenced by other non-acoustic factors. This situation does not relate exclusively to the low frequency component of the audible noise impact of wind turbines. In many instances, the amplitude modulation of the broadband sound is noted as the most prevalent audible characteristic.

Indoors, low frequency components of the sound can become emphasized by room and structural characteristics. Complaints of low frequency noise described in the literature are commonly related to indoor noise.

The measurement of infrasonic sound pressure levels is more difficult than the measurement of sound levels in the

audible range. Sophisticated instrumentation, transducers, and analysis are required to extend the range down to a very low frequency, on the order of 1 Hz. In addition, the wind itself can strongly excite the microphone, leading to acoustic signals at frequencies in the infrasonic range. Conducting infrasound measurements using an in-ground system, such as that developed by NASA, or conducting measurements within residences can reduce this influence.

Issues related to low frequency noise and infrasound can be caused by noise from many different industrial and transportation related sources. Some countries, such as Denmark and Sweden, have developed comprehensive regulatory guidelines which address generic low frequency noise and infrasound assessment. Other countries have guidelines specifically addressing audible sound from wind turbines, but do not specifically address low frequency noise and infrasound. For instance, the recent New Zealand guideline addresses tonality, but does not provide cautionary low frequency limits due to the "paucity of evidence" of related health impacts.

There is audible sound in the low frequency range associated with the sound of wind turbines. Nonetheless, because the outdoor sound level impact is not chiefly a low frequency issue, the use of overall A-weighted criteria is still appropriate for the assessment of overall sound impact. The concept of penalizing the acoustic impact if the sound from the wind turbines is tonal – often a low frequency problem – is also appropriate. Currently, the MOE uses a 5 dB penalty, and the identification of a tone is a subjective judgment; other jurisdictions use a quantitative approach.

The MOE has not published measurement procedures or criteria for addressing indoor noise intrusions or infrasound due to wind turbines or other industrial sources of sound. There are only a few jurisdictions which have guidance, instrumentation specifications, or measurement procedures that could be used to appropriately address infrasound.

## 3. RECOMMENDATIONS

1. A review of the current technical literature and international assessment standards concerning low frequency noise and infrasound does not indicate that there is a need for the MOE to change the fundamental approach used in Ontario for the assessment of wind turbine noise. It is recommended that outdoor A-weighted sound levels at sensitive receptors continue to be used to evaluate the compliance of sound from wind turbines. Additionally, penalties for audibly distinctive characteristics of the sound should continue to be used by the MOE. In particular, sound with strong mechanical tones which often occur within the low frequency range should be penalized.

2. There is some disagreement and uncertainty in the literature of some of the subjects discussed in this review, and research efforts are ongoing. It is recommended that the MOE continue to monitor technical developments in this area and keep informed of regulatory policies that may be introduced in other jurisdictions. Should the MOE develop guidelines in respect of low frequency noise and infrasound, these guidelines should retain a degree of flexibility in order to adapt to changes or improvements offered by international research in the future.

3. Since it is evident that complaints related to low frequency noise from wind turbines often arise from the characteristics of the sound impact indoors, and since the indoor low frequency sound levels and frequency spectra can differ markedly from those outdoors, it is recommended that the MOE consider adopting or developing a protocol to provide guidance for addressing such complaints. Given the significant variation in sound impact from house to house as a function of room layout and sound transmission characteristics, this protocol cannot replace the current compliance guidelines, but would prove helpful in assessing unique situations.

4. Infrasound from wind turbines is not expected to be heard by humans or pose an issue for human health, and as such, routine measurement of infrasonic sound pressure levels from operating wind farms is not warranted to the same degree that the measurement and monitoring of overall A-weighted sound pressure levels are. Nonetheless, there are aspects of infrasound from wind turbines that are not unanimously accepted by all technical and medical practitioners and there remains a degree of public apprehension associated with infrasound. It is therefore recommended that the MOE consider adopting or endorsing measurement procedures described in the literature that could be used to quantify the infrasonic levels in specific situations.

## REFERENCES

Erickson v. Director, Ministry of the Environment, Ontario Environmental Review Tribunal Decision, Case Nos 10-121/10-122, (2011).

HGC Engineering, "Low Frequency Noise and Infrasound Associated with Wind Turbine Generator Systems: A Literature Review", Ontario Ministry of the Environment, (2010).

## ACKNOWLEDGEMENTS

Input from the Ontario Ministry of the Environment, and in particular Vic Schroter and John Kowalewski, is acknowledged with thanks.

# LEARNING FROM EVIDENCE OF SOUND EXPERIENCED FROM WIND TURBINES

**William K.G. Palmer**[1]
[1] TRI-LEA-EM, RR 5, 76 Sideroad 33-34 Saugeen, Paisley, ON, Canada, N0G 2N0, trileaem@bmts.com

## 1. INTRODUCTION

Wind turbine sound regulations are generally based on A-weighted sound levels, reducing the effect of frequencies outside 500-11,000 Hz by more than 3dB. Wind turbine sound predominates at lower frequencies where human audibility and physiological response still exists. Regulatory limits are not intended to pose annoyance, yet placement of wind turbines near homes is reported to cause significant annoyance, sleep deprivation, and adverse effects.

Large industrial wind turbines produce a unique sound signature, cyclical in both amplitude and frequency, from a source that varies in a cyclical pattern of position and distance relative to listening points, since the principal sound source arises from turbulence following the trailing edge of the outer quarter of the blades, an annular ring 75 to 100 metres in diameter, a noticeable variation in relation to the 500 to 3000 metres from turbines to impacted receptors.

This paper relates factors identified previously by others to facts determined by recording and analyzing the differences in samples of sound over a full year at sites in a wind power development of 110 Vestas V82 turbines in Ontario's Bruce County, located acceptably to provincial regulators for spacing from wind turbines, and at control sites in the same environment at greater distances from the turbines.

## 2. METHODS

This paper will identify key findings related to the subject of sound of wind turbines identified by others at the Fourth International Meeting on Wind Turbine Noise held in Rome, in April 2011, and the 161st Meeting of the American Acoustical Society, in Seattle, in May 2011. Then, this paper will outline how the research conducted in this study relates to the issues raised by others.

### 2.1 Key Findings from Recent Conferences

No rigorous epidemiological study has been conducted by any jurisdiction, which would be necessary to show a direct relationship between the sound produced by wind turbines and health effects, as was done to show the suspected but unproven link between smoking and health.

The need for research to show direct clinical evidence was identified by Greg Tocci[1], as the requirement for policy makers to move sound from annoyance, to a health effect. Tocci commented that this had resulted in a 30-year period of "benign neglect" of sound in the US, although he noted work in progress in Europe sponsored by the WHO with regard to "The burden of disease from environmental noise" at conferences in 2005, '07, and '11, chaired by Rohku Kim.

Papers presented have shown wind turbines do produce a distinctive sound[2,3]. Sound levels similar to those experienced by people living at approved setbacks from wind turbines has been shown to produce direct and adverse impacts on blood pressure (systolic and diastolic), on heart rate, and on respiration rate[4]. The link between wind turbine sound and sleep disruption was noted by researchers[5,6,7].

Further, the evidence from qualified sleep researchers[5,8,9] shows "annoyance" of sleep disruption from any cause can result in delayed sleep onset, recalled awakening (for periods of >30 seconds), and perhaps most importantly, in repetitive non-recalled arousals (for periods of < 30 seconds). These, sleep researchers state, can have adverse impacts of fatigue, decreased performance, increased accident rates, cardio-vascular impacts, and diabetes.

Salt presented[10] a physiological link between the response of the ear to low frequency sound unrelated to audibility. Specifically, the response of the outer hair cells of the ear, and the response of the fluid in the inner ear to infrasound may be enhanced, and Salt stated it is premature to dismiss the influence of wind turbine noise on the ear. Literature identifies the link between the response of the fluid in the inner ear and motion sickness and disruption to balance.

A number of presenters discussed the psychoacoustic linkage between the "soundscape" and annoyance. George Luz presented a tutorial[11] identifying that noise sensitivity (about 1 in 5 people) does not decrease over time, while it may increase. Luz concluded with a statement about airport siting, "it may be premature to infer that decision makers at the studied airport *planned to cause harm to minority groups. Less invidiously,* decision makers might try to please important constituents (such as the median voter), without thinking through the possibility that decisions to help median voters may cause harm to others." The applicability to wind turbine siting was chilling.

A number of papers showed the consequence of not having a basis for noise standards when developing public policy. The conflict between potential community benefit (such as jobs) was often traded by municipal governments[11,12,13] against occasional "annoyance", and there was great diversity between what was acceptable in one community versus another. This clearly identified that a government policy that gives total control of the siting of wind turbines to individual municipalities is inadequate to protect citizens.

Many speakers identified the necessity to listen to the noise sources to identify special characteristics they possess, not just to record level as the "quality" impacts annoyance. The conferences identified a number of ways in which the sound

from wind turbines is unique, and how the particular characteristic of the sound makes wind turbines more annoying. Richarz[14], presented on audible low-frequency wind turbine sound. He noted that auto-correlation of measured wind turbine sounds exhibits distinct, periodic "low frequency" pulses that when propagation effects are accounted for, result in an audible swoosh. McCabe[15] reported he had identified elevated levels of amplitude modulation with a diurnal pattern, more noticeable at night, which might be why wind turbines are more annoying than other sources. di Napoli[16] reported on very strong amplitude modulation from monitored turbines and that it is not possible to conclude that amplitude modulation decreases with distance, as do simple assessments. Lundmark[17] reported that it was not possible to compare wind turbine sound to beach noise or waterfalls, and explained why turbine sounds were disruptive, rather than calming.

### 2.2 The Method of the Current Research

Digitized sound samples were recorded at 6 nearby sites in the environment of a wind power development during all seasons of the year. The method is explained in detail and detailed results are presented in the reference[18].

## 3. RESULTS

This study showed that receptors at setbacks approved by Ontario regulators for wind turbines experienced sound levels 20 dB higher at all octaves up to 1000 Hz compared to a site in the same environment 5000 metres from the wind turbines any time the turbines were operating, even at very low power. The study also identified frequency and amplitude changes in the sound from wind turbines, which make them even more noticeable; much like the wee-woo of emergency vehicle sirens makes them noticeable. The work also showed that actual sound readings taken by the acoustical consultant of the proponent of a wind farm in response to a complaint identified that sound levels exceeded the predicted value fully half of the time at midnight, were 3dB or higher above the predicted value at least 25% of the time at midnight, and were correlated to turbine power, not ambient wind speed.

## 4. DISCUSSION AND CONCLUSIONS

While "direct health effects" from the sound from wind turbines has not been shown by epidemiological study, clear links to adverse health effects from increases in sound level, roughness, etc. are shown, increasing blood pressure (systolic and diastolic), heart rate and respiratory rate.

The link between sound with special characteristics (e.g. cyclical amplitude and frequency modulation) and annoyance is known. The link between annoyance and sleep disturbance is known. The link between sleep disturbance and adverse health effects is well established. While some 1 in 5 people are more "noise sensitive" than others, no evidence suggests "attitude training" will erase this. The consequence of setting regulations without adequate basis, or using local regulation without protective guidance is clear. Evidence shows the low frequency dominance of wind turbine sound, and it's human perception.

This paper has shown evidence that sound level at receptor locations approved in Ontario is some 20 dB higher at all octaves up to 1000 Hz compared to sites in the same environment distant from wind turbines. The increase in sound is shown to be due to the wind turbines, not ambient wind. Cyclical amplitude and frequency shift of the sound is shown to be related to the wind turbines.

Thus, the link between the sound from wind turbines, to annoyance, hence sleep disturbance, and hence to adverse health effects is established, but yet no epidemiological studies have been conducted to prove the direct health effect. Still, to ignore concerns identified and to continue to site wind turbines by current regulations would seem to be imprudent, if not negligent.

## REFERENCES


Papers presented at *2011 Wind Turbine Noise Conference*, Rome available at http://www.windturbinenoise2011.org/ (wtn 2011)

Papers presented ay the Acoustical Society of America 161st Meeting in Seattle are identified on the ASA website: http://acousticalsociety.org/meetings/past_meeting_program/seattle/seattle_program (asa 161)

1. Tocci, G, Sykes, D. *Harmonizing national and worldwide acoustical guidelines for healthcare* asa 161
2. Bowdler, D. *Why Wind Turbine Noise Annoys* wtn 2011
3. Hunt, M, *Assessment of Wind Turbine Noise Using NZ Standard NZS6808:2010* wtn 2011
4. Hsu T.Y, Ryherd E, Ackerman J, and Persson-Waye K , *Psychoacoustic measurements and their relationship to patient physiology in an intensive care unit* asa 161
5. Hanning C, Nissenbaum M, *Selection of outcome measures in assessing sleep disturbance from wind turbine noise* wtn 2011
6. van den Berg F. *An overview of residential health effects in relation to wind turbine noise* wtn 2011
7. Shepherd, D, *Wind turbine noise and health-related quality of life of nearby residents: a cross sectional study in NZ* wtn 2011
8. Solet, J.M. *In defense of sleep* asa 161
9. Solet, J.M. et al, *Validating Acoustic Guidelines for HC Facilities: The Sound Sleep Study*, 2010 (Center for Health Design)
10. Salt. A. *Responses of the Inner Ear to Infrasound* wtn 2011
11. Schomer, P. *A community noise law for wind turbines* asa 161
12. Park, I *Environmental noise study and follow-up measurements at the White River Amphitheatre in Auburn, WA* asa 161
13. Pettijohn S.D. *Locating a new outdoor performance venue amidst public concern and the resulting sound level impacts at the remote amphitheater site* asa 161
14. Richarz, W *Audible low frequency wind turbine sound* asa 161
15. McCabe, N, *Detection and Quantification of Amplitude Modulation in Wind Turbine Noise* wtn 2011
16. di Napoli, C, *Long Distance Amplitude Modulation* wtn 2011
17. Lundmark, G, *Measurement of Swish Noise A New Method wtn*
18. Palmer, W. *Collecting data on wind turbine sound to identify causes of identified concerns* asa 161, available for download at http://asadl.org/poma/resource/1/pmarcw/v12/i1/p040003_s1?bypassSSO=1 ( or enter http://asadl.org/search Palmer wind turbine)

# IMPLEMENTATION OF REMOTE NOISE AND VIBRATION MONITORING SYSTEM AT THE PANYNJ WORLD TRADE CENTER

**Sharon Paul Carpenter[1], Dayna Sherwood[1], and Joseph Leung[2]**
[1]Paul Carpenter Associates, Inc., 248 Columbia Turnpike, Bldg 3 Suite 115, Florham Park, NJ, U.S.A. 07932
[2] ButterJAM LLC, 303 East 33rd Street, Suite 4P, New York, NY, U.S.A. 10016

## 1. INTRODUCTION

Rebuilding the Port Authority of New York & New Jersey (PANYNJ) World Trade Center (WTC) site is a complex endeavor involving a multitude of contractors and agencies. The Federal Transit Administration (FTA) established site-wide Environmental Performance Commitments (EPCs) for several environmental disciplines including noise and vibration. On behalf of the PANYNJ, Paul Carpenter Associates, Inc. (PCA) initiated, deployed and currently maintains a state-of-the-art remote noise and vibration monitoring system. The monitoring system includes four (4) noise and five (5) vibration monitors placed along the perimeter of the WTC site in Lower Manhattan. ButterJAM established a web interface which queries noise and vibration monitoring databases within the off-site server. The data is automatically sent to an innovative compliance website which displays appropriate data and allows access by authorized users. The system provides e-mail alerts, warning of any noise or vibration limit exceedance or equipment malfunction. In addition, the system automatically generates reports and directly e-mails reports to authorized personnel.

This paper introduces the noise and vibration monitoring system, generally describes the operation and features of the system and accompanying website and discusses challenges as well as lessons learned while commencing this large-scale data portal.

## 2. MONITORING SYSTEM

PCA performed research to identify remote noise and vibration monitoring equipment that met the compliance reporting needs for the WTC site. The following sections describe the monitoring system chosen by PCA on behalf of the PANYNJ.

### 2.1. Noise Monitoring

PCA chose the Bruel & Kjaer 3639 Noise Monitoring Terminal (NMT) for remote noise monitoring at the WTC site. Each NMT includes a Bruel & Kjaer Type 2250 hand-held analyzer/sound level meter, a Bruel & Kjaer 4952 outdoor microphone, Bruel & Kjaer 7843 Environmental Noise Management Software, a First Power FP12170 12-V back-up battery, a Sierra Wireless Raven X V4221-V wireless modem and a digital multi-band directional antenna 489-DB. The sound level meter, wireless modem and back-up battery are stored within a cabinet. Each NMT requires AC power and adequate cellular signal strength. The rear mounting bracket allows for installation on street light poles within the perimeter of the WTC. Currently, NMTs are located along the north, east, south, and southwest quadrants of the site.

### 2.1. Vibration Monitoring

PCA chose the Instantel Series IV Advanced Vibration Monitor for remote vibration monitoring at the WTC site. The system includes the vibration monitor, a triaxial geophone and battery-power supplies as well as a serial 3G modem to allow cellular data transmission. The system also includes the Blastware Compliance Module software, which enables transfer of the data to an off-site server. The vibration monitors are located within five historic structures of significance near the perimeter of the site.

## 3. WEB INTERFACE

The noise and vibration monitoring system documents source levels and remotely transmits data in real-time to a project-specific server, via cellular technology. The off-site server is located within the PCA office. ButterJAM developed a web-based content management system which allows for quick deployment of data using modular building blocks and customizable configuration schemas. The web interface queries specific data stored on the PCA server from within the Bruel & Kjaer and Instantel databases. Customized reporting modules were written to provide easy-to-read formatted PDFs which are generated automatically as well as on-demand based upon real-time data and calculations. Security modules were added to enforce complete access control and user restrictions. Data modules were written to provide specific processing and data intake routines to interpret data generated by the WTC on-site noise and vibration monitoring system. Within each created module, routines were added to sense and detect any conditions that warrant alerts or special processing. Additional modules enhance the usability and functions requested to analyze and interpret the data more efficiently. The end result is a website that is virtually automated in data intake, processing, display and reporting.

## 4. COMPLIANCE WEBSITE

ButterJam created an innovative compliance website utilizing the noise and vibration data queried from the Bruel & Kjaer and Instantel systems, respectively. The website serves as a user-friendly platform for authorized PCA and PANYNJ personnel to quickly identify real-time noise and vibration data. In addition, the website catalogues and

archives all previous data. By traversing the calendar module on the website, users can view previous data sets instantly.

In order to present noise data in a user-friendly format, data from each NMT is separated by individual noise web pages. A time history graph detailing 1-min $L_{eq}$ noise level data documented during the current 24-hour period is rendered in real-time. The graph includes a static line depicting noise compliance levels by time of day. In addition, hourly $L_{eq}$ noise data is included within a 24-hour table.

Each noise web page includes uploaded audio files recorded by the system based on pre-set trigger levels. The user may download or listen to the audio files directly from the website. Providing these audio files on the website enables PCA and PANYNJ officials the opportunity to identify specific construction activities that may have caused noise exceedances or complaints.

The compliance website also provides several unique features including a post-processing tool for noting noise data documented during inappropriate weather conditions. Authorized users may also enter notations and observations on the website as well. This feature is especially useful to track noise sources unrelated to the WTC site in the event of noise exceedances or complaints. Lastly, each noise web page includes compliance noise data within a table highlighting the current and previous four (4) periods, which converts to the color red in the event an exceedance is documented.

Each vibration web page includes a time history graph, which plots maximum peak vector sum (PVS) levels based on the current 24-hour period. In addition, the time history graph includes a static line depicting the vibration compliance level. The maximum PVS levels for each hour are listed within a 24-hour vibration table.

In order to provide the PANYNJ with timely daily summary reports, the system automatically generates the report at a specific time each day. Daily reports are automatically emailed to select individuals and made available on the website. In addition, monthly reports are automatically generated and catalogued on the website.

## 5. ALERTS

The system was established to provide three (3) types of automated alerts. Alerts are sent by the system and received by authorized individuals simultaneously via e-mail with pre-defined messages. In the event one of the noise or vibration monitors fails to submit data, an alert is automatically sent to PCA staff for troubleshooting. The second type of alert is sent to PCA staff and selected PANYNJ individuals indicating a noise or vibration level exceedance. Lastly, the third type of alert generated in the morning by the system is a courtesy indicating the number of audio files recorded and uploaded to the compliance website during the overnight period.

## 6. CHALLENGES / LESSONS LEARNED

PCA faces several logistical issues with maintaining operation of the remote noise and vibration system. Our challenges and lessons learned are listed below.

Strong cellular signal - Most vibration monitors were placed within basements or sub-basements where cellular signals are weak. PCA installed stronger antennas however periods of weak signal occasionally persist. In the event the signal is too weak to conduct the automated data transfer, PCA manually pushes data once signal strength recovers.

Continuous, uninterrupted power - AC power is supplied to all NMTs. Several NMTs receive site power from the WTC electrical grid. In the past, power had been accidentally interrupted, and units failed to report data. To ensure continuous AC power, site electricians provide the NMTs with secured, dedicated power.

Calibration Downtime - Each noise and vibration monitor requires yearly laboratory calibration. Under the first year of operation, PANYNJ requested PCA remove all vibration units during a period when no heavy blasting was expected. However, the PANYNJ requested complete noise coverage during calibration. Therefore, a spare NMT was installed to replace each unit when individually sent in for calibration. All units were calibrated and re-installed at the site within a two week period. The calibration process is logistically challenging and requires several months lead time.

Software Upgrades – The noise and vibration monitoring software systems were found to possess programming bugs. PCA communicated issues with the software manufacturers to resolve software glitches. Both manufacturers are currently developing fixes to improve operating systems.

## 7. CONCLUSIONS

The remote monitoring system and supportive web-based system developed by PCA and ButterJAM provide a technically advanced form of reporting and client interaction. The automatic reporting and alert system allows pre-selected parties to receive reports and alerts simultaneously. This form of posting exemplifies this era and offers an immediate, accurate and inventive method of project delivery.

## ACKNOWLEDGEMENTS

PCA would like to recognize Mr. Daniel Webber, Materials Engineer at the PANYNJ, who demonstrated incredible patience and trust in our vision.

# ATTITUDES AND BELIEFS CONCERNING HEARING PROTECTORS AND NOISE EXPOSURE

**Annelies Bockstael[1], Lieve De Bruyne[2], Bart Vinck[2], and Dick Botteldooren[1]**
[1]Acoustics Research Group, Ghent University, Sint-Pietersnieuwstraat 41, 9000 Gent, Belgium,
annelies.bockstael@intec.ugent.be
[2]Department of Oto-rhino-laryngology and logopaedic-audiologic sciences, Ghent University, De Pintelaan 185, 9000 Gent, Belgium

## 1. INTRODUCTION

Ongoing research aims at identifying the variables that influence or even determine the actual use of personal protectors at the work floor (Arezes, 2006). In this regard, risk perception, perceived self-efficacy and normative influences have been cited as critical issues. The current study investigates influential factors from a practical hearing-conservation point of view trying to answer the question what should be focused on to promote effective implementation of personal hearing protectors at the work floor? The parameters under study are related to three major categories (1) knowledge about the risk of noise exposure in general and possible harmfulness of exposure levels at the work floor, (2) attitudes, beliefs and feelings with respect to personal hearing protectors and (3) perceived safety climate. Within and across these groups, a certain hierarchy will be established and the mutual relationship between independent variables will be assessed.

## 2. MATERIALS AND METHODS

A written questionnaire has been distributed among the work force of four different Belgian companies engaged in in various industrial activities. The majority of the questions are a Dutch translation of the Noise at Work Questionnaire drawn up by Purdy et al. (2002) and are to be answered on a 5-point Likert-scale. The whole survey has been thoroughly analysed beforehand to establish a valid, comprehensible and consistent tool, suitable for the study at hand.

Within the participating companies, the use of hearing protection is either obligatory or – in few cases – at least recommended by the European Directive 2003/10/EC and the applicable Belgian legislation. Noise measurements by the researchers themselves confirm exposure levels of at least 80 dB(A) and mostly higher than 87 dB(A).

After excluding incorrectly completed questionnaires, 106 usable versions could be retained. All participants appear to be male and are on average 38.8 years old (standard deviation 11.1) with 12.1 year of working experience (standard deviation 10.4) in the company.

The use of hearing protectors is assessed by comparing the self-reported daily noise exposure (in hours) with the reported daily use of hearing protectors (in hours). These numbers are converted to a dichotomous variable, i.e. continuous use of protectors while exposed to noise or not. This means that people reporting wearing protectors only part of the time, are also considered as non-users, an approach justified by the finding that even temporal removal of a hearing protector largely compromises its actual attenuation (Arezes, 2006).

Based on this outcome, logistic regression is carried out to assess the probability that people will use their hearing protectors consistently while exposed to noise. The attitudes and beliefs addressed through the survey are selected as candidate independent variables. Conclusions on a variable's contribution to the model are based on the statistical significance of their coefficients ($\alpha$=0.05) and changes in model deviance and AIC (Akaike information criterion) – measures of a model's goodness-of-fit – when this variable is added.

## 3. RESULTS

Although all participants work in companies where hearing conservation measures are obligatory (or in the odd case advised), only half of them (55.7%) report consistently wearing hearing protectors while exposed to noise. In contrast, most people are aware of the relationship between excessive noise exposure and hearing loss (90.6%). This discrepancy has been reported worldwide (Ologe, 2005). Now the obvious question is why people do not translate their general knowledge into preventive actions and what can be done to improve the situation.

A first issue here seems applying general 'rules' to one's personal situation. Despite the fact that all participants work in noisy places, 26% of them claim not to be exposed to harmful sound. Although low, this percentage is satisfying since it is quite low compared to what Arezes found in 2006, possibly due to cultural differences or general increase in awareness of noise-induced hearing loss over time. Nevertheless it also shows that one-fourth of the employees potentially underestimates their noise exposure, which is all the worse because the probability of consistent hearing protection use increases with increasing risk perception, both in this study (p=0.04) and previous work (Arezes, 2006).

Acknowledging the risk of noise exposure is one thing, people should probably also be convinced about their protectors' benefits before they will actually wear them. In this regard, Quick (2008) has found that a general positive attitude towards hearing protection largely determines the intention to use them. In this study, the group of participants opining that hearing protectors prevent hearing loss is not

overwhelming (65%), but then again this item appears to be less relevant for consistent use ($p>0.05$). A possible explanation for the difference with Quick's work is that the latter has investigated the relationship between attitude and intention to wear hearing protectors, whereas the current analysis has reported behaviour as the outcome variable.

Another aspect with respect to hearing protectors is perceived self-efficacy. Narrowing down this concept to reported knowledge shows that in this study 85% feels confident about how to use hearing protectors correctly, but this statement is not statistically related to actual consistent use ($p>0.05$). However, if self-efficacy is interpreted in a broader sense of perceived behavioural control, i.e. balancing pros and cons of hearing protectors against each other to decide on final use, this parameter is shown to influence clearly consistent use (Arezes, 2006; Quick, 2008). Rather than general beliefs about hearing protectors (cf. supra), concrete everyday experiences are clearly important, namely comfort ($p<0.001$), ease to use ($p<0.01$), communication with colleagues ($p<0.01$) and perception of warning signals ($0.1>p>0.05$).

Finally, as always, human behaviour has an important social component, which also plays its role in hearing protection. For instance, in Quick's research (2008), subjective norm is the only parameter that influences both the intention to wear protectors and directly the final behaviour, additionally Arezes (2008) names perceived safety climate as an important predictor. In this study, subjective norm related to consistent hearing protection use appears limited to the workplace ($0.1>p>0.05$) and the behaviour of co-workers ($p<0.05$), meaning that other employees like clerks or family members have no significant influence on reported behaviour ($p>0.05$). In accordance to Arezes (2006), reported control at the workplace also ($p<0.01$) positively influences the actual use of protectors. By contrast, individual guidance has no clear influence.

The analyses described above have allowed identifying the most influential parameters, but since hearing conservation programs cannot handle everything at the same time, building a hierarchy might help to establish priorities. Statistical modelling reveals that for the current dataset reported wearing most strongly depends on practical, down-to-earth considerations like (in order of statistical significance) comfort, control and ease to use.

The importance of control as an exponent of the perceived safety climate is expected from Quick (2008). However, Arezes (2006) argues that although control does help to improve the use of hearing protectors, it does not lead to increased risk perception and hence the desired behaviour is only established when people know themselves to be supervised, which is in the long run not a sustainable approach. Our study indeed confirms that more control or individual guidance do not seem to increase risk perception.

By contrast, these results do not suggest that individual guidance is pointless in terms of hearing conservation because it appears to influence the reported comfort. For the participants who report no individual guidance, almost half of them (46%) find their protectors more or less uncomfortable. Conversely, this number drops down to 17% in the group where individual guidance is given, those trends are in accordance with work done by Tsukada (2008). Moreover, control as such seems not capable to realise the positive effects of an individualized approach since feelings of discomfort are reported independently of this variable.

## 4. DISCUSSION AND CONCLUSION

The study presented in this paper suggests that reported use of hearing protectors depends more on practical constraints then general beliefs and attitudes. This contests by no means the importance of concepts like risk perception, rather it suggests that principles are relatively easily put aside by practical considerations. Control appears an influential factor, but relying on this parameter only is an unsustainable approach. Control mechanisms are only one link in the network of hearing conservation, though definitely a vital one. The importance of comfort and ease of use is already well-known and confirmed by the current study. Apparently people behave quite pragmatically when respecting general (health) rules causes discomfort. In this regard, individual guidance in selection and use of suitable hearing protection might be a real boon.

## REFERENCES


Arezes, P.M., Miguel, A. S. (2006). "Does risk recognition affect workers' hearing protection utilisation rate?" International Journal of Industrial Ergonomics 36, 1037-1043.

Arezes, P.M., Miguel, A. S. (2008). "Risk perception and safety behaviour: A study in an occupational environment," Safety Science 46, 900-907.

Ologe, F. E., Akande, T.M., Olaijde, T. G. (2005). "Noise exposure, awareness, attitudes and the use of hearing protection in a steel rolling mill in Nigeria," Occupational Medicine 55, 487-489.

Purdy, S.C., Williams, W. (2002). "Development of the Noise at Work Questionnaire to assess perceptions of noise in the workplace," Journal of Occupational Health Safety – Australia and New Zealand 18, 77-83.

Quick, B. L., Stephenson, M.T., Witte, K., Vaught, C., Booth-Butterfiel, S., Patel, D. (2008). "An examination of antecedents to coal miners' hearing protection behaviours: A test of the theory of planned behaviour," Journal of Safety Research 39, 329-338.

Tsukada, T., Sakakibara, H. (2008). "A trail of individual education for hearing protection with an instrument that measures the noise attenuation effect of wearing earplugs," Industrial Health 46, 393-396.


## ACKNOWLEDGEMENTS


Annelies Bockstael is a postdoctoral fellow of the Research Foundation-Flanders; the support of this organization is gratefully acknowledged.

# DEVELOPMENT OF A 3D FINITE ELEMENT MODEL OF THE HUMAN EXTERNAL EAR FOR SIMULATION OF THE AUDITORY OCCLUSION EFFECT

**Martin K. Brummund[1], Yvan Petit[1], Franck Sgard[1,2], and Frédéric Laville[1]**

[1]Dept. of Mechanical Engineering, École de technologie supérieure, 1100 Rue Notre Dame O., Montréal, Québec, Canada, H3C1K3, martin.brummund.1@ens.etsmtl.ca

[2]Service de la recherche, IRSST, 505 Boulevard de Maisonneuve O., Montréal, Québec, Canada, H3A3C2

## 1. INTRODUCTION

Approximately 120 million workers worldwide are at risk of developing professional hearing loss (WHO, 2001). Hearing protection devices, such as earplugs (EP), are a frequently used short term solution to protect workers from hazardous noise. Wearing EPs, however, causes distortion of the wearer's voice and amplification of physiological noises; also referred to as the occlusion effect (OE). The OE, as well as other auditory and physical limitations, reduces the comfort of an EP. Consequently, workers often only wear EPs for short periods of time (Berger, 2000; Lusk et al., 1998; Morata et al., 2001). This leaves them prone to hearing loss. Numerical models present a valuable means to improve the outlined shortcomings because they can aid to better assess and design hearing protectors. The present study describes the development of a novel coupled linear elasto-acoustic 3D finite element model of the human external ear. This genuine model is employed to simulate the auditory OE. In the following, preliminary research findings are presented.

## 2. METHODS

Simulation of the OE was carried out in three steps. First, the geometry of the human external ear was reconstructed. Secondly, a model of an earplug was coupled to the open ear model. Lastly, the sound pressure levels (*SPL*) at the tympanic membrane of the open and occluded ears were subtracted to determine the OE.

### 2.1 Model geometry

To ensure high model authenticity, 100 transverse-axial anatomical images of a female cadaver head (age = 59 years) were used for 3D reconstruction. All images were obtained via the Visible Human Project® database (NLM, MD, USA). 3D reconstruction of the ear canal as well as the bony, cartilaginous and skin tissues was carried out in slicOmatic 4.3 (TomoVision, QC, Canada). The obtained voxel model (voxel height = 0,33mm, length = 0,33mm, depth = 0,33mm) was imported into CATIA V5 (DS, France) for further processing.

### 2.2 Material properties

The biomaterial properties of the bony and cartilaginous tissues were approximated using literature findings. The skin tissue of the ear canal entrance and walls was modeled using soft rubber.

### 2.3 Boundary conditions

To account for the interaction with neighbouring tissues, as well as the environment, several boundary conditions were included in the model. The unoccluded ear canal entrance was expressed through a frequency dependent impedance of a flat disc. The skin tissue around the ear canal entrance was free in its movements. Circumferential (perpendicular to ear canal entrance) and medial (parallel to ear canal entrance) tissue boundaries were modeled using roller constraints. Finally, the eardrum impedance was expressed through a two-piston model (Shaw, 1977; Shaw & Stinson, 1981).

### 2.4 Model excitation

A surface distributed force of magnitude $1\text{Nm}^{-2}$ was introduced normal to the circumferential boundaries of the bony tissue. This method was chosen to simulate a bone conducted excitation which is required to trigger an OE upon EP insertion.

### 2.5 EP model

It was assumed that the insertion of an EP would only deform the EP and that the ear canal would keep its original shape. Following this initial hypothesis, the model of a moulded silicone earplug of known material properties was inserted into the model. First, the insertion depth of the EP was set to 7mm to simulate a shallow insertion. Secondly, the EP model was inserted 22mm into the ear canal to model a deep insertion scenario.

### 2.6 Model resolution

All model domains were imported into COMSOL 4.0 (COMSOL, Inc., Sweden) for 3D finite element analysis. Each domain was meshed individually (according to the four elements per wavelength criterion ($\lambda/4$)) using tetrahedral elements. Sound pressure levels (*SPL*) of the open and occluded ear models were calculated as follows:

$$SPL_{open} = 20*\log_{10}(|p(x,y,z)|/p_{ref}) \text{ with } p_{ref} = 2\text{e-}5 \text{ Pa}$$

$$SPL_{occluded} = 20*\log_{10}(|p(x,y,z)|/p_{ref}) \text{ with } p_{ref} = 2\text{e-}5 \text{ Pa}$$

Finally, OEs were calculated by subtracting open and occluded *SPL*s:

$$\text{OE} = SPL_{occluded} - SPL_{open}$$

## 3. PRELIMINARY RESULTS

Figure 1 and Figure 2 illustrate the OEs that were calculated using the 3D finite element model for shallow and deep occlusions respectively (solid lines). In addition to that, each figure illustrates two dash-dotted graphs that were taken from the literature (Stenfelt & Reinfeldt, 2007). These graphs represent envelopes of objective, forehead-bone conducted OEs of 20 subjects. Experimental occlusion depths equalled 7mm and 22mm. Literature results were adjusted to the present frequency range.

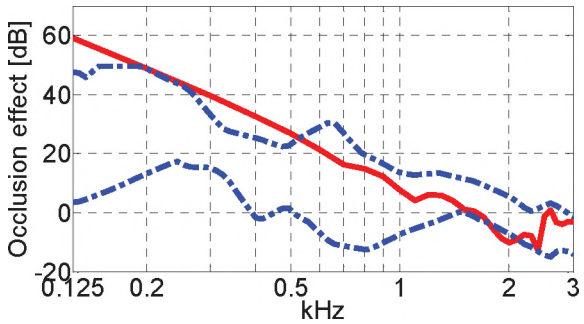


**Figure 1: Simulated OE (solid line) and experimental envelope curves (dash-dotted lines) for a shallow (7mm) occlusion. The experimental reference data can be found in Stenfelt & Reinfeldt, 2007.**

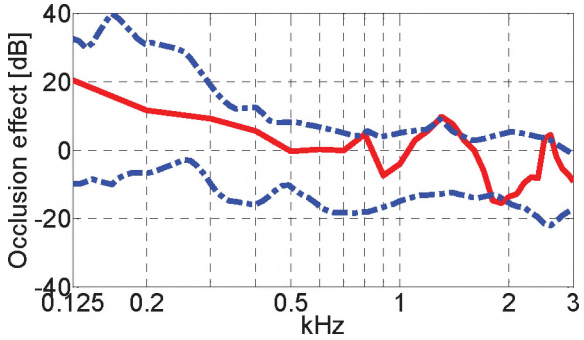


**Figure 2: Simulated OE (solid line) for a deep insertion (22mm). Dash-dotted lines represent the envelopes of 20 objective, forehead bone-conducted OE measurements. The original data can be found in Stenfelt & Reinfeldt, 2007.**

For a shallow insertion (7mm) the highest OE (60dB) occurs at 0.125 kHz. Afterwards, the modeled OE decreases by about 20dB/octave until 0.7 kHz is reached. At 1.7 kHz the simulated occlusion effect crosses the 0dB line. Afterwards it gets negative (1.7 kHz to 2.6 kHz). The OE vanishes a second time at 2.6 kHz and remains negative at the highest frequencies. Compared to the literature findings (dash-dotted lines) the model overestimates the OE by about 15dB at the frequencies below 0.2 kHz. At the frequencies between 0.2 kHz and 0.3 kHz the modeled OE and the upper limit of the experimental envelope curve are superimposed. Between 0.3 kHz and 0.5 kHz the model deviates by about 10dB from the upper bound of the experimental envelope curve. At the frequencies above 0.5 kHz the modeled OE stays within the boundaries that are set by the experimental data.

For a deep insertion (22mm) condition the OE is overall smaller in magnitude. At 0.125 kHz the simulated OE equals 20dB. Afterwards it decreases by about 10dB/octave. Between 0.5 kHz and 0.7 kHz the simulated OE disappears. Subsequently, the OE progresses in a zig-zag-like manner. Further 0dB crossings occur at 0.85, 1, 1.6, 2.5 and 2.7 kHz. The simulated OE stays within the experimentally determined bounds throughout the entire analyzed frequency range.

## 4. DISCUSSION AND CONCLUSIONS

The obtained results indicate that the implemented 3D finite element model can be employed to calculate the auditory OE. Obtained OEs vary as a function of insertion depth and are plausible when compared to literature findings. For a shallow insertion, the model overestimates the OE in two frequency bands below 0.5 kHz. This might be due to leakage or noise phenomena. In order to further validate the model, it is planned to conduct experimental work on an equivalent physical model to be able to compare the numerical model predictions to experimental results that are independent of the materials properties, tympanic membrane impedance and excitation location. Comprehensive tests regarding the influence of each of these factors have yet to be completed. Preliminary results suggest that the OE model is very promising. Nevertheless, further testing should be conducted.

## REFERENCES


Berger, E. H. (2000). Hearing Protection Device Utilization Around the World. *Spectrum*, *17*(Suppl. 1), 18.

Lusk, S. L., Kerr, M. J., & Kauffman, S. A. (1998). Use of hearing protection and perceptions of noise exposure and hearing loss among construction workers. *American Industrial Hygiene Association Journal*, *59*, 466-470.

Morata, T. C., Fiorini, A. C., Fischer, F. M., Krieg, E. F., Gozzoli, L., & Colacioppo, S. (2001). Factors affecting the use of hearing protectors in a population of printing workers. *Noise & Health*, *4*(13), 25-32.

Organisation mondiale de la santé (OMS). (2001). Le bruit au travail et le bruit ambiant. Organisation mondiale de la santé.

Shaw, E. A. G. (1977). Eardrum representation in middle-ear acoustical networks. *J. Acoust. Soc. Am.*, *62*(1), S 12.

Shaw, E. A. G., & Stinson, M. R. (1981). Network concepts and energy flow in the human middle ear. *J. Acoust. Soc. Am.*, *69*(1), 43.

Stenfelt, S., & Reinfeldt, S. (2007). A model of the occlusion effect with bone-conducted stimulation. *International Journal of Audiology*, *46*(10), 595 - 608.


## ACKNOWLEDGEMENTS


The authors gratefully acknowledge the financial support received from the IRSST.

# DEVELOPMENT OF AN EQUIVALENT SOLID MODEL TO PREDICT THE VIBROACOUSTIC BEHAVIOUR OF EARMUFF CUSHIONS

**Sylvain Boyer[1], Franck Sgard[2], and Frédéric Laville[1]**
[1]Dept. Génie Mécanique, École de technologie supérieure (ÉTS),
1100 rue Notre-Dame Ouest, Montréal (QC), Canada, H3C 1K3, sylvain.boyer.1@ens.etsmtl.ca
[2]Institut de recherche Robert-Sauvé en santé et sécurité au travail (IRSST),
505 Boul. de Maisonneuve Ouest, Montréal (QC), Canada, H3A 3C2

## 1. INTRODUCTION

Performances of earmuffs for hearing protection are largely affected by the seal between the earcup and the head [1]. The seal is done by a cushion, generally made of a foam piece in a polymeric sheath. In order to predict the sound transmission loss through earmuffs, it is necessary to model correctly both the mechanical and acoustical behaviour of the cushion. A lump model – which is generally used [2] – is sufficient at low frequency as it reproduces the whole body motion of the earcup with respect to the head. At higher frequency, this model is no longer appropriate as it does not account for sound transmission through the cushion material [3].

The aim of this work is to investigate the relevance of using an equivalent isotropic viscoelastic solid model to capture the sound transmission law of an annular cushion from a commercial earmuff.

In a first step, vibration analysis is done on a batch of ten cushions to (1) determine effects of a reproduced static force of the headband, (2) determine the roles of the holes drilled in the sheath, and (3) calculate the mechanical parameters (density, Young's modulus, Poisson's ratio and material damping) comparing vibration analysis results to a Finite Element model. Then these parameters are introduced in a combined Boundary Element – Finite Element (BEM-FEM) model to study the sound transmission loss through the lateral walls of the cushion.

## 2. VIBRATION ANALYSIS

Ten cushions from a hygienic spare set are studied. They are mounted on a shaker and submitted to the weight of three metal blocks with masses of 1.15kg, 1.65kg and 2.13 kg, representing the force applied by the head band when the earmuffs are positioned on the head. They are in the common range of tightening force [4]. A lighter fourth mass of 0.65kg is also used to test separately the foam and its protective sheath.

Transfer function $H_1$ between the acceleration of the mass and the acceleration delivered by the shaker is recorded for each experiment. As the first resonance peak is observed below 100 Hz, the frequency range of interest is from 10 to 100 Hz, with a frequency step of 125 mHz. The input signal chosen is a white noise, and 42 records are averaged per measurement. The transfer function is then compared to a 1-Degree of Freedom (1-DOF) system (mass-spring-damper). The comparison allows determining the frequency resonance (linked to the stiffness) and the material damping.

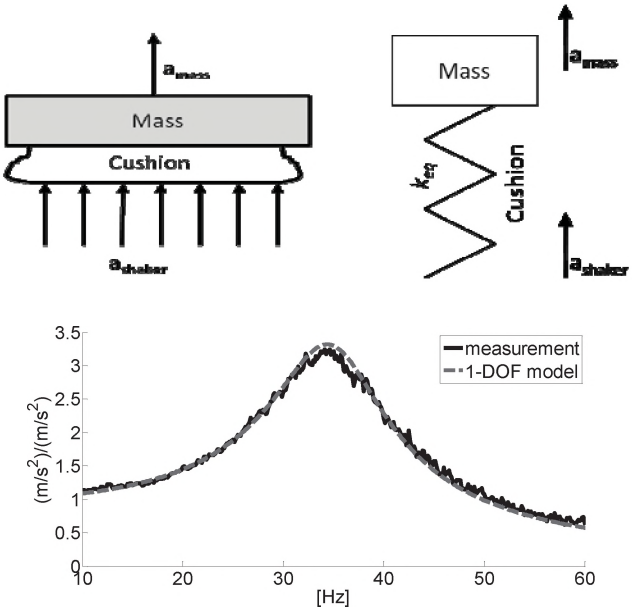


**Figure 1. Vibration experiment result and its associated 1-DOF lump model.**

### 2.1. Effect of mass and variation of the samples

For the three mass: 1.15 kg, 1.65 kg and 2.13 kg, the ten cushions are tested. Results presented Table 1 show that the frequency resonance decreases and the loss factor increases with the mass. The stiffness increases as the cushion is compressed. Equivalent stiffness of a 1-DOF system is obtained by the following formula: $k_{eq} = M \times 4\pi \times f_0^2$.

**Table 1. Frequency resonances and loss factor, determined by fitting a 1-DOF system on data from measurements.**

| Mass $M$ | 1.15 kg | 1.65 kg | 2.13 kg |
|---|---|---|---|
| $f_0$ (Hz) | 32 ± 0.9 | 31.8 ± 0.5 | 28 ± 0.5 |
| $\eta$ | 0.17 ± 0.004 | 0.18 ± 0.004 | 0.20 ± 0.005 |
| $k_{eq}$ (N/m) | 55,695 | 65,913 | 66,020 |

### 2.2. Effect of holes

The cushions have two perforations in the sheath. Effects of these holes are investigated in two ways:

1) Holes are glued with cyanoacrylate glue, when each cushion was under compression, to evacuate air from it. Vibration experiments were conducted and then cushions were immerged into water to make sure that apertures were completely occluded. Such verification has demonstrated that the sheath is a microporous material: micro air bubbles appear around the sheath when cushion are pressed. No bubble, hence no air, went out from the glued holes. Later, all glued cushion recovered their originally uncompressed form. It was then found that it is unnecessary to constrain the cushion before closing its holes, as after a time long enough, inner air will be evacuated by the microporous sheath. It was also found that the use of electrical tape provides a good occlusion of the holes, hence using glue is not necessary.

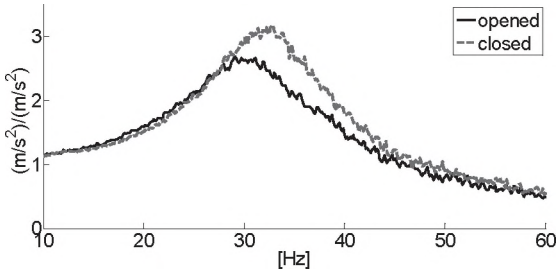


**Figure 2. Effect of occluding holes. Experiment performed with a mass of 1.65kg.**

Results presented Figure 2, for a mass of 1.65kg show that closing holes adds stiffness and decreases the loss factor, by introducing an air cavity. Similar results are obtained with a 1.15kg mass. Experiments were performed on three different cushions giving the same behaviour.

2) Holes are added around the cushion. A total of 14 holes of 1mm diameter were drilled progressively. Results can be observed on Figure 3. Resonance frequencies and amplitudes (as well as phases) of the transfer function are not changed when more than two holes are present. Consequently adding holes beyond the standard ones do not change significantly the dynamic behaviour of the cushion.

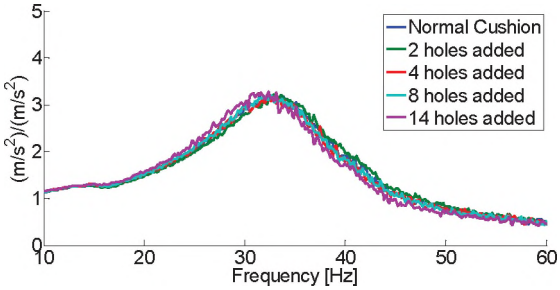


**Figure 3. Effect of adding holes. Experiment performed with a mass of 1.65kg.**

### 2.3. Foam and sheath stiffness separation

The foam and the sheath are tested separately under a mass of 0.65kg and compared to a cushion. This mass is chosen to avoid hysteretic compression of the foam. The sheath is obtained by cutting through the side of the cushion that is glued to the earcup. Loss factor and equivalent stiffness $k_{eq}$ calculated as previously are presented in Table 2. The sheath has a dominant stiffness over the foam but its value is surprisingly greater that the combination of the two, this is attributed to the fact that the foam gives an initial curved shape to the sheath, hence reducing its buckling strength.

**Table 2. Mechanical parameters of a cushion and its component, for a mass of 0.65kg**

| | Cushion | Sheath | Foam |
|---|---|---|---|
| $f_0$ (Hz) | 36.2 | 44.8 | 14.8 |
| $\eta$ | 0.165 | 0.214 | 0.105 |
| $k_{eq}$ (N/m) | 33,627 | 51,503 | 5,621 |

## 3. OUTLINE OF THE FOLLOWING STEPS OF THE DEVELOPMENT OF EQUIVALENT SOLID MODEL

Results from the vibration analysis will be used to determine the mechanical parameters of an equivalent solid modelled with a FEM method [3]. We expect to obtain a set of Young's modulus ($E$) and Poisson's ratio ($\nu$) pairs. Each ($E$, $\nu$) pair will be then introduced in a BEM-FEM acoustic model to determine sound transmission loss through the lateral walls of the cushion when it is compressed, compare it to experimental data and determine the optimal ($E$, $\nu$) pair. The results will be given during the oral presentation.

## REFERENCES


[1] P. Henrique Trombetta Zannin et S.N. Gerges, « Effects of cup, cushion, headband force, and foam lining on the attenuation of earmuffs », *The Journal of the Acoustical Society of America*, vol. 105, févr. 1999, p. 1132.

[2] E.A.G. Shaw et G.J. Thiessen, « Acoustics of circumaural earphones », *J. Acoust. Soc. Am.*, vol. 34, 1962, p. 1233-1246.

[3] F. Sgard, H. Nélisse, M.-A. Gaudreau, J. Boutin, J. Voix, et F. Laville, *Étude de la transmission sonore à travers les protecteurs auditifs et application d'une méthode pour évaluer leur efficacité effective en milieu de travail - Partie 2: Étude préliminaire d'une modélisation des protecteurs auditifs par éléments finis*, 2010.

[4] J.G. Casali et J.F. Grenell, « Noise-attenuating earmuff comfort: A brief review and investigation of band-force, cushion, and wearing-time effects », *Applied Acoustics*, vol. 29, 1990, p. 117—138

# INFLUENCE OF SOURCE LOCATION, SUBJECTS AND HPD SIZE ON THE SOUND FIELD AROUND EARMUFFS

**Cécile Le Cocq[1], Hugues Nélisse[2], Jérôme Boutin[2], Jérémie Voix[1], and Frédéric Laville[1]**
[1]Dépt. de Génie mécanique, École de technologie supérieure, Montréal, Québec, Canada
[2]Institut de recherche Robert-Sauvé en santé et en sécurité du travail, Montréal, Québec, Canada

## 1. INTRODUCTION

In most noisy workplaces, workers are exposed to complex sound fields ranging from diffuse field to more directional field conditions. Hearing protection devices (HPD) attenuations are generally measured in a laboratory either subjectively or objectively in a diffuse sound field (ANSI 2008). Other sound field conditions are usually not considered even though attenuation of HPDs is known to vary with the incident sound field direction (Gaudreau et al 2007). The Field-MIRE (F-MIRE) technique has been developed to objectively quantify the attenuation of earplugs using two microphones: one is located under the HPD while the other one is used to capture the exterior sound field (Voix and Laville 2009). Recently, this method has been employed on earmuffs in the workplace but the authors raised some concerns regarding the location of the exterior microphone (Nélisse et al 2011). Moreover, advanced hearing protectors (level-dependant, active noise control, etc.) make also use of an exterior microphone to control and adjust the attenuation as a function of the incident sound field (Giguère et al 2011). It is therefore important to assess the effect of the location of this exterior microphone located on an earmuff with respect to the incident sound field (type, location, frequency content) in order to better understand its impact on the evaluation of the attenuation of HPDs.

This paper presents a short laboratory study performed in semi-anechoic and diffuse-field conditions where various earmuffs, microphone positions, source locations and subjects were tested. The methodology is presented and examples of results are given and discussed.

## 2. METHODS

The objective of the experiment is to demonstrate the influence of the type and location of the source as well as the location of the microphone on the measurement of the incident sound pressure on earmuffs. The tests were conducted in a diffuse field in a reverberant room and in a free field in a semi-anechoic room on 4 subjects with 5 different earmuffs (EAR 1000, Peltor Optime 95, Peltor Optime 98, Peltor Optime 101, and Peltor Optime 105) and without earmuffs. In free field conditions, twelve sound directions from -150° to 180° with 30° steps were considered as depicted on the left part of figure 1. Six miniature microphones were fixed on each earmuff as illustrated on the right part of figure 1 for the right ear. In the experiments without earmuffs, only one microphone was used and positioned, close to the ear canal entrance for each ear. The sound pressure level (SPL) was measured in third octave bands. To take into account the individual frequency responses of the 12 microphones, the free-field SPL measurements were normalized by the microphone responses obtained in a diffuse field where all microphones were located at the same location in the reverberant room. The tests in the semi-anechoic room were realized with a pink noise of about 85 dB overall SPL.

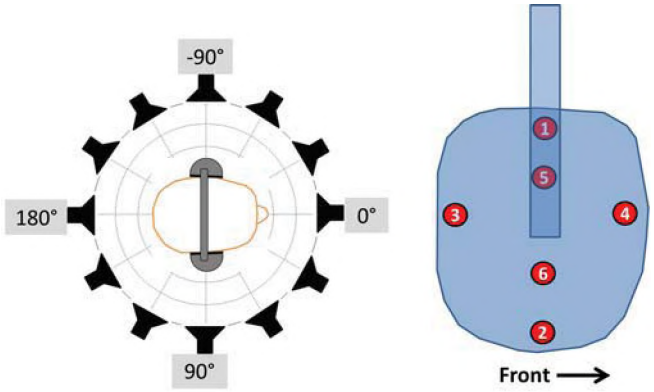


**Figure 1. Location of the speaker for the free field experiments (left). Position of the microphones for the right ear (right).**

In the next section, examples of results are presented. A more complete analysis is currently under way. .

## 3. RESULTS

In this section, two specific are presented. The first one is related to the effect of the sound source location while the second one is related to the effect of the microphone location on the earmuff.

### 3.1 Effect of sound source location

On figure 2, mean values of the normalized SPL for the microphones located on the right cup are depicted for three frequency bands as a function of the angle of the sound source. The mean value was taken over 4 subjects, 2 ears, 5 earmuffs, and 6 microphones (240 data sets). Vertical lines represent ± one standard deviation.

As expected, SPL variations are more important at high frequencies compared to low frequencies. At 5000 Hz, the normalized SPL varies from -5 ±3 dB at -90° to +8 ±2.5 dB at +90°; whereas at 500 Hz, the normalized SPL varies from -4 ±1.5 dB at -120° to +2.5 ±1 dB at +90°.

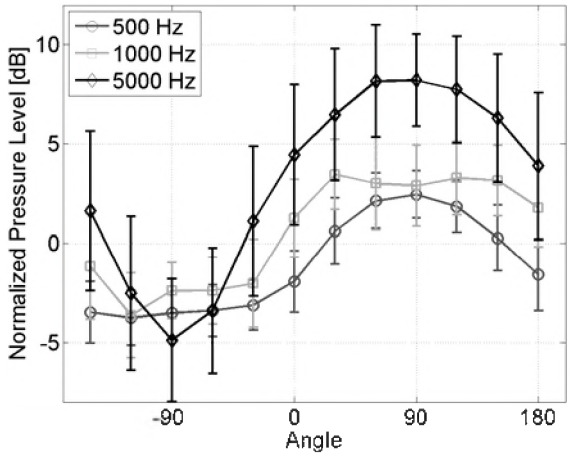


**Figure 2. Mean normalized SPL on 4 subjects, 2 ears, 5 earmuffs, and 6 microphones for three third octave frequency bands as a function of the sound source location.**

### 3.2 Effect of microphone location on the earmuff

On figure 3, mean and standard deviation values of the normalized SPL on the right earmuff are represented for the six microphones, when the sound source is directly facing the subject (0° angle). The mean value is taken over 4 subjects and 5 earmuffs (20 data sets). For this frontal incidence, it can be seen that for two of the microphones (positions 3 at the back and position 4 at the front of the earmuff) the normalized SPL is significantly different than for the other four. At the front of the earmuff, the mean and the standard deviation values of the normalized SPL are the highest for all frequencies, whereas at the back of the earmuff, the mean and the standard deviation values are the smallest for all frequencies.

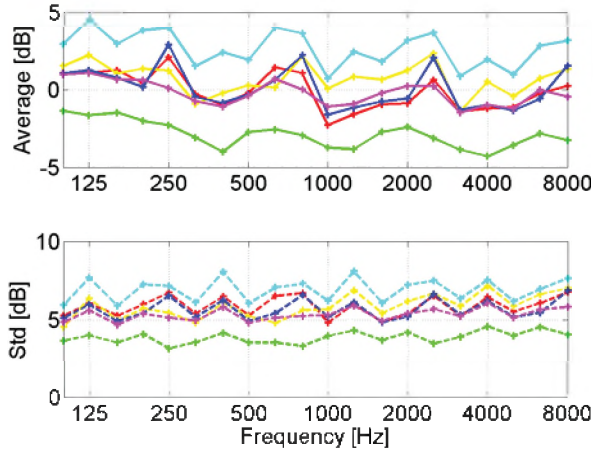


**Figure 3. Mean and standard deviation values of the normalized SPL on the right earmuff for the six microphones when the sound source is located directly in front of the subject (0° angle) (color online).**

On figure 4, the mean and the standard deviation values of the normalized SPL on the right earmuff is again represented for the six microphones but now when the sound source is on the right of the subject (90° angle). The mean value is calculated over 5 earmuffs and 4 subjects (20 data sets). For this lateral incidence, for every microphones position considered, the mean and the standard deviation of the normalized SPL are very similar from one microphone to the other.

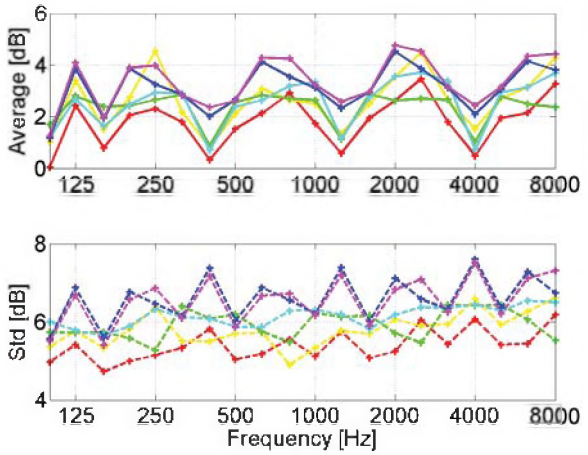


**Figure 4. Mean and standard deviation values of the normalized SPL on the right earmuff for the six microphones when the sound source is located at the right of the subject (90° angle) (color online).**

## 4. DISCUSSION AND CONCLUSIONS

Both the sound source location and the microphone location on the earmuff seem to have a significant effect on the measured sound pressure level. In order to adapt the F-MIRE technique from earplugs to earmuffs, the location of the exterior microphone is of first importance especially since one are interested to measure the attenuation of the HPD. Hopefully, the set of data obtained in this study will help to better quantify the deviations observed in the attenuation when using an external microphone in comparison with standardized tests (e.g. REAT or IL)

## REFERENCES

ANSI (2008) Methods for Measuring the Real-Ear Attenuation of Hearing Protectors. American National Standards Institute, S12.6-2008.

Gaudreau M-A, Laville F, Voix J, et al. (2007) Variabilité de l'atténuation des protecteurs auditifs mesurée par la méthode field-mire en fonction de la direction du son incident et des bruits du porteur. Proceedings of the annual conference of the Canadian Acoustical Association. Annual conference of the Canadian Acoustical Association, Montréal, Canada.

Voix J, Laville F. (2009) The objective measurement of individual earplug field performance. The Journal of the Acoustical Society of America 125(6): 3722.

Nélisse H, Gaudreau M-A, Boutin J, et al. (2011) Measurement of hearing protection devices performance in the workplace during full-shift working operations. Accepted for publication in The Annals of Occupational Hygiene.

Giguère C, Laroche C, Vaillancourt V, and Brammer A. (2011) Advanced hearing protection and communication: progress and challenges. Proceedings of the 10th International Congress on Noise as a Public Health Problem (ICBEN). The 10th International Congress on Noise as a Public Health Problem (ICBEN), London, UK.

# DEVELOPMENT OF A SIMPLIFIED AXI-SYMMETRIC FINITE ELEMENT MODEL OF THE AUDITORY CANAL OCCLUDED BY AN EARPLUG: VARIABILITY OF THE ATTENUATION AS A FUNCTION OF THE INPUT PARAMETERS

**Guilhem Viallet[1], Franck Sgard[2], and Frédéric Laville[1]**
[1]Dept.de génie mécanique, École de technologie supérieure (ETS),
1100, rue Notre-Dame Ouest, Montréal (Qc), Canada, H3C 1K3, guilhem.viallet.1@ens.etsmtl.ca
[2]Institut de recherche Robert-Sauvé en santé et en sécurité du travail (IRSST),
505, Boulevard De Maisonneuve Ouest, Montréal(Qc), Canada, H3A 3C2

## 1. INTRODUCTION AND OBJECTIVES

In Quebec, 500 000 workers are confronted to the problem of noisy work environment [1]. A common solution to prevent the problem of hearing loss due to noise exposure consists in using hearing protection devices (HPD's), like earplugs (EP) or earmuffs. In practice, EP are often uncomfortable and/or do not always perform as desired [2]. The present study deals with the development and the use of an axi-symmetric finite element model (FEM) of the ear canal (EC) occluded by a silicon EP. This model is used to determine how the input parameters influenced the attenuation, in order to improve it.

The first step of this study is to implement and to validate the simplified axi-symmetric model with the help of the paper [3] and to extend this model for a more realistic boundary condition for the EP. The second step consists in using indirectly the FEM model to perform a global sensitivity analysis and to determine Sobol indices. These indices give the information about how the variation of the output of a physical system is influenced by the variation of the input parameters. Unfortunately, applying directly these tests on the FEM model is cumbersome because they require a huge number of computations. The FEM EP/EC model is used here to determine a meta-model, as a combination of a polynomial regression of the response given by the FEM EP/EC model, obtained by a complete design of experiments and corrected by the most probable residual function. Two different meta-models are built. The first one is a function of the mechanical parameters of the EP (Young's modulus, Poisson ratio and density) and the second one is a function of the geometrical parameters of the EP (length and radius). Once the meta-models are validated with the EC/EP FEM for a new set of parameters (mechanical or geometrical), the statistical tests are applied to the meta-models that give instantaneously the predicted attenuation values.

## 2. METHODOLOGY

### 2.1 Modeling the EP/EC system

Based on the axi-symmetric assumption [4], a recent study [3] showed the feasibility of the FEM to predict the attenuation of a silicon cylindrical earplug, with fixed boundary conditions, inserted in a cylindrical EC. Here, the EP is also considered as a solid cylinder inserted into a cylindrical EC, modeled as an air cavity. This system is terminated by a tympanic membrane (TM) which is supposed to act as a locally reacting boundary impedance condition (impedance values of the IEC711 artificial ear). In real life, the EC is constituted by a complex assembly of skin, soft tissues and bone parts. An innovative alternative is used here to take into account the coupling between the EP and the EC. This coupling (calculated with the help of an axi-symmetric model including skin, soft tissues and bone parts) is applied as a mechanical impedance on the lateral walls of the EP. This fluid/structure problem is solved using the FEM to calculate the displacement field in the EP and the acoustic pressure in the remaining domain of the EC. The noise reduction ($NR_0$) indicator is used to characterize the attenuation of the EP, i.e. the transfer function between the acoustic pressure at the center of the tympanic membrane and the incident one:

$$NR_0 = 20LOG_{10}\left(\frac{|P_{TM}|}{|P_{incident}|}\right) \qquad (1)$$

### 2.2 Global sensitivity analysis

The meta-models (one for each set of parameters) are constructed to approximate the output $NR_0$ of the FEM model:

$$NR_0 \cong \widehat{NR}_0 = G(x_i) + Z(r_k) \qquad (2)$$

The $G(xi)$ term in (2) is a multi-linear regression of the output based on a complete design of experiments with three different levels for each parameters xi. All the values used for the design of experiments, are reported in table 1. In both cases, the aim is to determine the polynomial coefficients relative to each parameter and their interaction. The $Z(rk)$ term in (2) is a correction factor of the multi linear regression using the known residual values between and $NR_0$ and $\widehat{NR}_0$.

**Table 1: Values of the parameters of the EP used to compute the twice meta-model.**

| Code level | $E$ (Mpa) | $\rho$ (kg/m³) | $v$ | $L$ (mm) | $R$ (mm) |
|---|---|---|---|---|---|
| -1 | 7.5 | 850 | 0.44 | **12.5** | **3.75** |
| 0 | **8.5** | **1000** | 0.46 | 15 | 4.75 |
| 1 | 9.5 | 1150 | **0.48** | 17.5 | 5.75 |

The bold values correspond to the ones used in [3]. The approximate polynomial function allows to obtain the instantaneous calculation of the response for a new set of parameters inside the [-1;1] domain.

## 3. RESULTS AND DISCUSSION

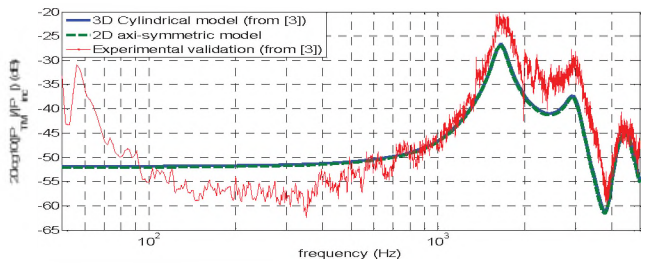


**Figure 1: Validation of the axi-symmetric model with the help of [4], for fixed boundary condition**

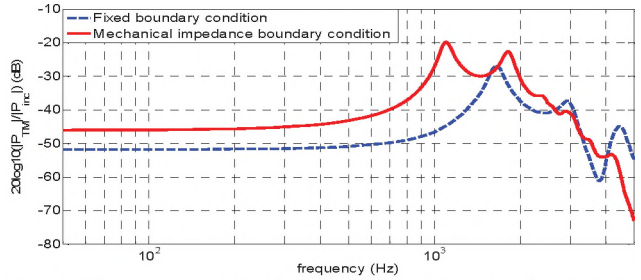


**Figure 2 : Influence of the boundary condition applied to the lateral walls of the EP**

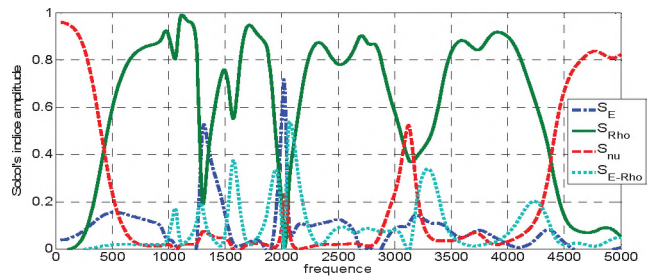


**Figure 3 : Sobol indices calculated with the first meta-model (mechanical parameters)**

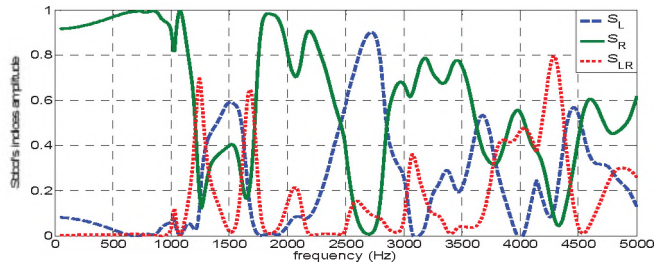


**Figure 4 : Sobol indices calculated with the second meta-model (geometrical parameters)**

Figure 1 indicates good agreement between the curve obtained by [3] (cylindrical 3D model) and those obtained here (2D axi-sym). The third curve corresponds to an experimental validation, realized in the study [3]. Between 400 Hz up to 5000 Hz, the axi-sym model matches the experiment data. The difference between the model and the experimental data is explained by the author [3] due to a small leakage on the coupler. The peaks observed in figure 1 correspond to particular vibration modes of the plug. A modal analysis on the «in vacuo» structure allows finding the frequency of these vibration modes together with their mode shapes.

Figure 2 shows the modification of the $NR_0$ indicator for a more realistic boundary condition. The vibration modes of the structure were influenced by the boundary conditions and by applying a mechanical impedance to the laterals walls of the EP are able to move. This result shows that it is not enough to take a fixed boundary condition to predict correctly the attenuation of an EP inserted in the EC. Even for a simplified numerical model, the coupling between the EC and the EP are to be taken into account.

Figure 3 indicates that the variation of the system rigidity (Young modulus and Poisson ratio) strongly influences the variation of the attenuation in low frequencies (up to 500 Hz). In the rest of the frequency domain, the variation of the density, the Young modulus and their interaction influence the attenuation on the whole frequency band (approximately 80% of the variation of the attenuation). In this frequency domain (500 Hz to 5000 Hz), it is important to control the density of the EP as it is the factor that mostly influences the variation of the attenuation.

Figure 4 indicates that the radius influenced the variation of the attenuation more than the length. Up to the first resonance of the system (1200 Hz), and between each resonance, the variation of the radius counts for more than 80% of the variation of the attenuation. For the first two resonances (1200 Hz and 2700 Hz), the variation of the length and the length/radius interactions act locally for 60% of the variation of the attenuation.

Finally, the obtained models could be used to determine the best set of parameters that will improve the attenuation of the EP. This method could be extended to other types of EP.

## REFERENCES


[1] J.P. Vigneault, "Pour un meilleur support de la recherche au plan d'action 2006-2008 du réseau de santé publique en santé au travail," *La recherche sur le bruit en milieu de travail*, IRSST, Éd., IRSST: 2007.

[2] E.H. Berger, L.H. Royster, et D.P. Driscoll, *The noise manual*, AIHA Press, 2003.

[3] F. Sgard, H. Nélisse, M. Gaudreau, J. Boutin, J. Voix, et F. Laville, *Étude de la transmission sonore à travers les protecteurs auditifs et application d'une méthode pour évaluer leur efficacité effective en milieu de travail - Partie 2 : Étude préliminaire d'une modélisation des protecteurs auditifs par éléments finis*, 2010.

[4] M.R. Stinson et B.W. Lawton, "Specification of the geometry of the human ear canal for the prediction of sound-pressure level distribution," *The Journal of the Acoustical Society of America*, vol. 85, Juin. 1989, p. 2492-2503.

# IMPULSE NOISE LEVELS GENERATED BY A .22 CALIBER STARTER PISTOL

**Jacob Sondergaard[1], Deanna K. Meinke[2], Michael Stewart[3], Donald S. Finan[2], James Lankford[4], and Greg A. Flamme[5]**

[1]GRAS Sound and Vibration, 2285 East Enterprise Parkway, Twinsburg, OH 44087
[2]University of Northern Colorado, Audiology and Speech-Language Sciences, Gunter 1400, Box 140, Greeley, CO 80639
[3]Central Michigan University, Communication Disorders Department, 2161 Health Professions Building, Mount Pleasant, Mich. 48859
[4]Northern Illinois University, Allied Health and Communication Disorders Department, 323 Wirtz Hall, DeKalb, IL 60115
[5]Western Michigan University, Department of Speech Pathology and Audiology, Kalamazoo MI 49008-5243

## 1. INTRODUCTION

A .22 or .32 caliber starter pistol is commonly used in athletic events to generate a loud impulse signaling participants that the event (i.e. race) has started. Studies have been undertaken investigating starter pistols and the advantages introduced to athletes closer to the source, and also the negative image of having guns around teenagers at high school track and field events. However, there have been no published studies evaluating the noise levels generated by starter pistols.

In this paper, impulses generated from a typical .22 caliber starter pistol firing blanks will be compared to impulses generated from a .22 revolver firing both black powder blanks and standard velocity projectiles. Also, results from a .32 caliber starter pistol will also be used for comparison.

Preliminary findings on this topic were presented at NHCA in Mesa, Arizona, February 25, 2011.

## 2. APPARATUS AND METHODS

### 2.1. Apparatus

Measuring sound levels from a firearm requires a few key components; primarily the firearms as a sound source. A .22 caliber starter pistol, Italian Model 413 firing blank ammunition, and a .22 caliber revolver, Smith & Wesson K-22 Masterpiece firing both blanks and two types of standard velocity cartridges, were used for the first two experiments. The final experiment includes a Harrington and Richardson (H&R) .32 caliber starter pistol firing a Winchester .32 Smith & Wesson blank and a H& R .32 caliber revolver firing both the same Winchester .32 blank cartridge and a Winchester .32 Smith & Wesson 85 gr. lead round nose cartridge.

Moreover, since the impulses generated contain high frequency content and very high amplitude sound pressure level (SPL), we need to consider a lower sensitivity microphone of small dimensions in order to capture this acoustic data accurately. For these experiments, 1/8" microphones with a sensitivity of 1mV/Pa were selected, thereby providing a useable frequency range up to 80 kHz and a dynamic range topping at 186dB peak sound pressure level (SPL). The microphones were equipped with ¼" preamplifiers capable of carrying the potentially large signals without overloading or experiencing slew rate limitations. The power to the front end equipment was supplied by two 2-channel power modules giving us a maximum signal carrying capacity of +-60V. The power modules also feature gain and attenuation controls to adjust accordingly during testing.

Finally, a National Instruments data acquisition system, PXI 6120, was used to capture the measurements. The pertinent features of this system were the high sample rate (800kS/s), the on-board buffer (64MSample), and the trigger function. The 16-bit resolution, providing 90dB dynamic range was deemed sufficient. The data acquisition process was controlled by a custom LabView program, and post processed in MATLAB.

### 2.2. Setup

Three experiments were conducted using the same equipment; yet slightly different methodology was employed for each. The three experiments were designed to 1) explore the directionality of the .22 caliber starter pistols shooting blanks; 2) compare the .22 starter pistol and a .22 revolver and 3) describe the peak levels when measured from selected positions for a simulated track event.

Directionality

This looked at the directionality of the noise emitted from a .22 caliber starter pistol by placing four microphones equidistant in a 50cm radius circle around the firearm. Five shots were fired when the firearm was placed horizontally, and five shots when placed vertically.

Comparison

This experiment looked at the differences in the SPL at various spatial locations for the .22 caliber starter pistol and the .22 caliber revolver. The primary location was at the shooters left ear. The remaining three locations were at 10cm adjacent to the chamber, 10cm adjacent to the muzzle, and 10cm adjacent but 1.5m downrange.

Track Setup

Microphones were placed at the shooter's right ear and the equivalent of lane 1, 4 and 8 of a regulation sized

running track. The shooter was placed at two National Federation of High School (NFHS) suggested locations for event starter positions.

### 2.3. Analysis

Data was analyzed and presented in the time domain with the peak SPL value illustrated for this discussion.

## 3. RESULTS

The results of the first experiment revealed that contrary to prevailing knowledge a .22 caliber starter pistol was shown to produce 165 dB $SPL_{peak}$ at 50cm distance from the shooter's ear. This exceeds many common revolvers and even rifles significantly.

The subsequent .22 comparison experiment was spawned by the findings in the first experiment. It was discovered that a blocked barrel .22 caliber started pistol produces significantly higher SPLs than a comparable .22 caliber revolver, regardless of ammunition. A sub-set of the results are shown in Table 1 below.

**Table 1. Microphone at shooters ear**

| Firearm | Level (Pa) | Level (dB) |
|---|---|---|
| .22 Starter Pistol w/blanks | **3692** | **165.3** |
| K-22 w/CCI | 1604 | 158.1 |
| K-22 w/blanks | 491 | 147.8 |
| K-22 w/shorts | 1143 | 155.1 |

Finally, the track setup experiment highlighted that with the shooter at NFHS appointed starting locations using the .32 caliber, the shooter was on average exposed to 163.2dB $SPL_{peak}$, whereas the runners in lanes 1, 4 and 8 were exposed to 136.6dB, 132.3dB and 127.8dB respectively. This exceeds impulse noise limits for children, as specified by the WHO (120dB).

## 4. DISCUSSION

The current track and field starting mechanism is almost exclusively the blocked barrel starter pistol. In fact, it is against regulations to operate open-barreled pistols, so as to avoid potentially loading projectiles and creating a dangerous situation. The problem is that the findings herein show that not only are blocked barrel starter pistols produce hazardous sound levels, they are also much louder than open barrel pistols of similar caliber at the shooter's ear position.

Clearly, the immediate conclusion from this is that, under all circumstances, the shooter should be using hearing protection in both ears. These peak levels are very hazardous for the unprotected ear, and will result in some permanent auditory loss.

Ironically there are many misconceptions regarding the SPLs generated by a starter pistol. Because of the relative small caliber (.22 or .32), many shooters and non-shooters alike jump to the conclusion that a starter pistol does not represent a significant aural danger. Moreover, because the ammunition does not contain projectiles, there is a further assumption that no physical hazard is involved. Finally, since this has been the preferred event starting mechanism for decades at youth, amateur and professional track and field events, the proliferation and ubiquity has diminished the notion of starter pistols and aural risk.

As it happens there are regulations and guidelines for what constitutes impulse noise hazards. These numbers are typically given as 140dB $SPL_{peak}$ for adults (NIOSH) and 120dB $SPL_{peak}$ for children (WHO). Drawing on the results from the track setup experiment, we can draw the conclusion that a majority of the athletes and potentially nearby spectators are also at risk of hearing damage. This is especially relevant for school organized events were rules and guidelines for shooter position, relative to athletes and/or spectators, may not be as clear, well-known or adhered to. There are countless examples of athletic officials firing starter pistols (without hearing protection) and being in close proximity to child-athletes. This is obviously something that should be prevented.

Finally, it is interesting to note that NCAA has an electronic starter guideline, which stipulates an impulse noise being generated by speakers from 15 feet (5m) behind the athletes at a level of 112dB. Curiously, there are no regulations for the SPL for a starter pistol. If we were to extrapolate using the inverse square law for the starter pistol, the athletic official generating a 165 dB peak SPL at 50cm should be located 256m(!) away from the athletes to adhere to the NCAA electronic starter guidelines.

## REFERENCES

NIOSH (1998). *Revised criteria for a recommended standard: occupational noise exposure* (No. NIOSH Publication 98-126). Cincinnati U.S. Department of Health and Human Services, Public Health Service, Centers for Disease Control and Prevention, National Institute for Occupational Safety and Health, DHHS

World Health Organization (1999). Guidelines for community Noise. Berglund, B., Lindvall, T., Schwela, D.H., eds. Geneva: World Health Organization.

## ACKNOWLEDGEMENTS

The authors wish to express their thanks to National Instruments for use of equipment throughout the years.

# TESTING AND RATING OF HEARING PROTECTOR DEVICES – A REAL HEADACHE

**Alberto Behar[1], and Willy Wong[1]**
[1]Institute of Biomaterials & Biomedical Engineering, University of Toronto, 164 College Street, Toronto, Ontario, Canada

## 1. INTRODUCTION

Noise is often identified as the most common occupational hazard. Since the use of hearing protection devices (HPDs) is the popular choice for hearing loss prevention, it is easy to understand the importance of the standard CAN/CSA Z94.2 – R2007 "Hearing Protection Devices - Performance, Selection, Care, and Use" (Z94.2 further in this presentation).

Z94.2 is up for review by the Subcommittee SC1 of the Occupational Hearing Conservation Technical Committee S304 of the Canadian Standards Association. The work involves editorial changes as well as updating of the text. However, there is one fundamental issue to be sorted out: How to deal with testing and rating of protectors.

Specifying the laboratory testing procedure for the subjective measurement of attenuation of HPDs is very important, since it has a strong influence on the results. Different procedures may yield significantly different attenuation results.

The rating of the HPDs, on the other hand, provides a simple way for the calculation of the noise level of the protected ear. It is the parameter used by the safety personnel to choose a protector for a given noisy environment. Another very important HPD property is the comfort experienced by the user. However, there is no standard, Canadian or otherwise for its measurement.

Since the 1994 issue of Z94.2, new kinds of protectors have appeared. Some even operate following different principles. Examples of the new devices are active protectors, communication headsets, etc. Also, there are now systems that test the fit experienced by the individual wearer. Updating for these new products is an integral part of the review of Z94.2.

In this paper, however, we will limit to only the testing of the protectors and their rating. A very important development is expected to appear in the near future. It is the EPA's pending document on labelling of protectors [1]. It will have a huge impact on the way testing and rating are performed, impact that will be felt across the USA borders, at every place HPDs are manufactured and sold.

## 2. THE EXISTING Z94.2 STANDARD (R2007)

### 2.1 Testing

As per the existing Z94.2, protectors must be tested following procedures in ANSI S12.6 [2] that specifies two attenuation testing procedures, known as Method A and Method B.

Method A, referred to as "trained-subject fit", requires that test subjects be familiar with the protectors and their use and testing procedures. During the training phase, the experimenter actively guides the subject in achieving a good and reproducible fit through explanations of the manufacturer's instructions, demonstrations and physical assistance. For the actual testing, however, the subject must fit the HPD without assistance.

Method B, referred to as "inexperienced-subject fit", uses naïve subjects that are not familiar with protectors and their use. They must fit the protector by themselves using the instructions printed on the protectors' package. In case of earplugs available in multiple sizes, they must also select the size that is best for them based on the manufacturer's instructions.

Results from Method A are supposed to represent an optimum fitting scenario that could be accomplished by a motivated and proficient user. Method B, on the other hand, is meant to approximate realistic results for workers in hearing conservation programs.

Z94.2 stipulates that testing must be done following the Method B. However, it also accepts results from measurement performed following the now withdrawn ANSI S3.19 [3], which is performed using a direct experimenter-fit procedure.

### 2.2 Ratings

Z94.2 provides two types of ratings. The first one is calculated using results from attenuation testing performed as per ANSI S3.19 [3]. Accordingly, protectors are classified as "A", "B" and "C". Class "A" protectors are offering the highest attenuation. The class required is specified in Z94.2 determined according to the noise level in the workplace in such a way that the noise level of the protected ear be safe.

The second rating is the Grade system, based on a Single Number Rating, subject-fit 84th percentile (SF84), going from Grade 0 (the lowest) to 4 (the highest). The SF84 is calculated from the attenuation and standard deviation resulting from the Method B measurement procedure. When SF84 is subtracted from the noise level measured in dBC the result is the noise level of the protected ear, expressed in dBA.

## 3. THE EPA PROPOSAL

EPA is proposing protectors to be tested as per ANSI S12.6-2008 Method A. The result of the measurement is then used for the calculation of Noise Level Reduction Statistic (NRS) according to ANSI S12.68-2007 [4] that is different from the by now infamous Noise Reduction Rating (NRR). The difference consists in:

a) Two ratings (instead of one) are calculated, corresponding to the protection obtained by 20% and 80% of users. The $NRS_{A20}$ corresponding to the 20% of users with the highest A-weighted noise reduction. as would be typical of highly motivated and proficient users. Most of the users (80%) will only achieve the lower value or $NRS_{A80}$. As an example if the two ratings are $NRS_{A80}$ of 18 dB and $NRS_{A20}$ of 32 dB, 20% of the users will have an A-weighted noise reduction of 32 dB or more, while 80% will have 18 dB or more.

   This, of course, creates a problem when trying to achieve an optimum selection.. Because of the large NRR spread (18 – 32 dB), there will be individuals that will be overprotected since their noise level of the protected ear will be way below the limit of 70 dBA (recommended as the lowest sound level limit to avoid overprotection). Another problem is how to make the decision of using the higher or the lower number in a given workplace.

b) The noise level of the protected ear is calculated as a difference between the ambient noise level measured in dBA and the NRS.

c) NRSs will be calculated using an ad hoc calculator, designed by EPA/NIOSH that uses a bank of 100+ workplace noises.

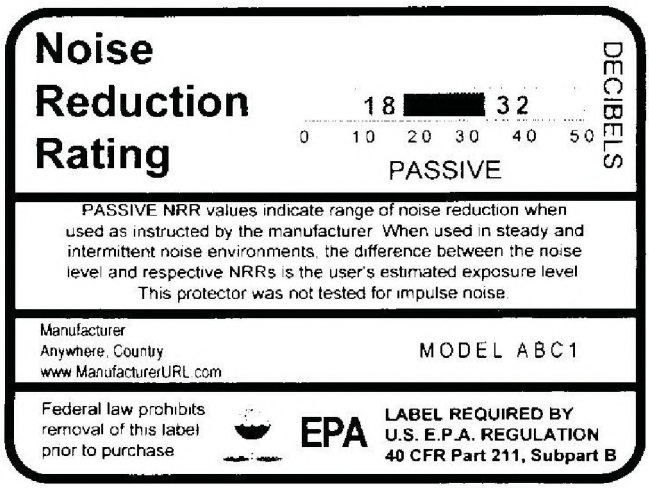


**Figure 1. Example EPA Label**

Manufacturers will have to label their products using a standardized, EPA designed label, as in the example shown in Figure 1. It is expected that the new EPA rule will be enacted some time in 2012.

## 4. THE TASK AT HAND

SC1 has now to make decisions regarding both issues: attenuation testing and protector rating.

One option is to eliminate the Class rating and to keep the Grade system. By doing so, there will be almost no changes for the Z94.2 users, since the Class rating is seldom used. However, if the EPA recommendation is approved, manufacturers will have to measure their products using the Method A. That will be the end of the Grade system, since it requires the use of $SF_{84}$ that can only be calculated from measurement results using Method B.

The second option will be to include the existing NRR as rating. NRR was never included in the Z94.2 because of the overly optimistic and unrealistic results. However, this is the most widely used and well known rating, although many users wrongly subtract NRR from the ambient noise level measured in dBA, instead of dBC. Eventually, NRR could be derated using the NIOSH procedure.

Finally, there is the option of doing nothing and keeping both Grade and Class until the EPA comes with the new rule. All the other sections of the Z94.2 will be reviewed, since they will not be affected by the new development.

## REFERENCES


[1] FR Part 211 Product Noise Labelling Hearing Protection Devices; Proposed Rule. Federal Register / Vol. 74, No. 149 / Wednesday, August 5, 2009 / Proposed Rules.

[2] ANSI/ASA S12.6–2008: American National Standard Methods for the Measuring the Real-Ear Attenuation of Hearing Protectors

[3] ANSI/ASA S12.68–2007: American National Standard Methods of Estimating Effective A-Weighted Sound Pressure Levels When Hearing Protectors are Worn

[4] ANSI/ASA S3.19–1974 (R1990): American National Standard Method for the Measurement of Real-Ear Protection of Hearing Protectors and Physical Attenuation of Earmuffs.


## ACKNOWLEDGEMENTS


The authors would like to acknowledge Dr. Christian Giguère for reviewing the manuscript and providing most useful suggestions.

# SENSORIAL SUBSTITUTION SYSTEM WITH ENCODING OF VISUAL OBJECTS INTO SOUNDS

**Damien Lescal[1], Jean Rouat[1], and Stéphane Molotchnikoff[2]**
[1]NECOTIS, Dept. GEGI, Université de Sherbrooke, Quebec QC, Canada, J1K 2R1
[2] Dept. de sciences biologiques, Université de Montréal, Quebec QC, Canada, H3C 3J7

## 1. INTRODUCTION

Visual and auditory prostheses involve surgeries that are complex, expensive and invasive. They are limited to a small number of electrodes and can only be used when the impairment is peripheral. Non invasive prostheses (sensorial substitution systems) have existed for more than 40 years but have not been well accepted in the disability sector. Severals systems have been developped since the emergence of this concept. Paul Bach-Y-Rita proposed a substitution system from vision to touch (1969) in which pictures captured by a camera were converted into electrical stimulation of the tongue. Other studies have shown that some simple tasks such as localization (Jansson, 1983), shape recognition (Sampaio et al., 2001; Kaczmarek and Haase, 2003) and reading (Bliss et al., 1970) can be achieved using vision-to-touch substitution devices.

More recently, substitution systems from vision to audition have been proposed: (Akinbiyi, 2007; Merabet, 2009; Hanneton 2010). The following systems are the most important to have been developed so far: the vOICe (Meijer, 1992), PSVA (Prosthesis for Substitution of Vision by Audition) (Capelle et al., 1998), the device developed by Cronly-Dillon (Cronly-Dillon, 1999) and the Vibe (Hanneton et al., 2010). These systems encode a full image with no prior analysis of the visual scene. Thus, they overload the ears of the patient with wasteful sounds that carry useless characteristics of the image. Usually these systems encode the luminosity of all pixels from the image in the amplitude of modulated sounds. The vOICe and the Cronly-Dillon device use left-to-right time scanning to encode horizontal position. The Vibe and PSVA encode the entire image in one complex sound. The PSVA uses frequencies that are associated with each pixel and increase from left to right and from bottom to top of the image. The Vibe splits the image into several regions that are equivalent to receptive fields. Each receptive field is associated with a single sound and the sum of all sounds forms a complex sound transmitted to the two ears. The receptive fields design is inspired by work on the retina.

The challenge in this project resides in the design of a suitable encoding of the visual scene into auditory stimuli such that the content of the sound carries the most important characteristics of the visual scene. These sounds should be shaped in a way that the subject can build mental representations of visual scenes even if the information carrier is the auditory pathway. A sensorial substitution system using an object-based approach is described. An image segmentation algorithm using a spiking neural network combined with a sound generation is proposed. That neural system has a good potential for object based image and visual scene analysis. Also, human auditory features such as interaural time difference (ITD) and interaural level difference (ILD) are used to synthesize sounds that better characterize the visual scene for real-life environments.

## 2. DESCRIPTION

The image analysis system has to be able to find and track objects in image sequences. For this purpose, a spiking neural network that offers a good potential is used for object-based image processing.

### 2.1 Mapping between image analysis and sound generation

An image is presented to a one layer self-organized spiking neural network (Figure 1).The positions of neurons from a given group are encoded into the same sound.

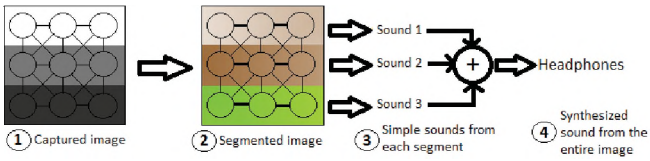


**Figure 1. Pixels are input to the neural network (1). After synchronization, segments appear (2) and are encoded into sounds (3). In (2) color encodes moments of spike times and thickness of lines between neurons encodes weight values.**

In the two following sections, the segmentation and the sound generation are described.

### 2.2 The spiking neural network

The neural network described by Molotchnikoff and Rouat (2011) is used. The neuron model is the conventional simplistic integrate and fire neuron. The sub-threshold potential of the neuron with a constant input is:

—— - - (1)

is the transmembrane potential, is the input current. When crosses, at time , a predetermined threshold θ, the neuron fires. Then is reset to (resting potential). C is the membrane capacitance; τ has the dimension of a time constant expressed in seconds. In this case – must be superior to θ for the neuron to be able to fire.

Each neuron characterizes a pixel of the image and is connected to eight neighbours. A synaptic weight between two neurons encodes the similarity between the respective features (here gray levels of pixels). The weight between neuron i and neuron j is computed according to:

$$w_{i,j} = 1 - \frac{1}{1+e^{-\alpha(|f_i - f_j| - \Delta)}} \qquad (2)$$

α=0.1, 0.05 or 0.015, Δ=100, 128 or 200 and $|f_i - f_j|$ is the absolute value of the gray level difference between neuron i and neuron j. A segment represents a group of neurons that spike at the same time (thus being synchronized). So, neurons associated to pixels with a small difference in gray level will spike at the same time and are identified as belonging to the same group (segment). Results of segmentation with this neural network are shown in Figure 1 and 2.

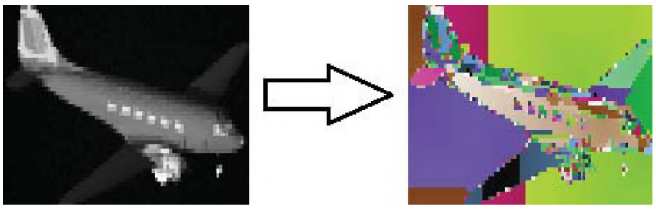

**Figure 2. Input (left) and time moments of spiking (right).**

### 2.3 Sound generation

The segmented image is then encoded into sounds. A single sound is generated for each segment using the averaged gray level, the size and the position of the segment in the image. $S_j^R(t)$ is the sound from the segment to be played in the right ear and $S_j^L(t)$ is the one in the left ear.

$$S_j^R(t) = A_j^R \sin(w_j t + \Phi_j^R) \qquad (3)$$
$$S_j^L(t) = A_j^L \sin(w_j t + \Phi_j^L) \qquad (4)$$

- $\boldsymbol{w_j = \overline{g_j}}$ with $\overline{g_j}$: average level of gray of the segment j
- $\boldsymbol{A_j^L = \alpha . S_j}$ with $S_j$ : size of the segment j and α : average distance of the segment j from the center of the image (ILD)
- $\boldsymbol{\Phi_j^L = \frac{\alpha}{\alpha_{max}} * \frac{\pi}{2}}$ with $\alpha_{max}$ the half of the width of the image (ITD)
- The expression of $\boldsymbol{\Phi_j^R}$ and $\boldsymbol{A_j^R}$ are the same than $\boldsymbol{\Phi_j^L}$ and $\boldsymbol{A_j^L}$ except that the reference locations in the image are different.

The complex sound is the sum of all single sounds from each segment. One complex sound is generated for the right ear and another one for the left. In short, the differences between the right and the left sound reside in the size of the objects and their positions in the image.

## 3. DISCUSSION AND CONCLUSIONS

The approach described in this paper is very promising. The next step of this project is to adapt and modify the neural network to identify highly textured regions of an image. In others words, highly textured portions of an image would be isolated and the most homogeneous segment would be identified. Using this neural network, it would be possible to identify textured objects (natural objects) and non-textured objects (objects man-made objects). The strength of this approach is the combination of an object-based image analysis with the sound generator so that mental visual representations can be carried via an auditory stimulation. Indeed, this system does not convert the entire image into sound but only parts corresponding to important features of the image. This is not the case in the literature. Furthermore, the sound generation is based on human auditory features like ITD, ILD and the size of the object for the depth in the image. Using this approach, it might be possible to help people with visual disabilities with tasks like localisation or shape recognition.

## REFERENCES


Akinbiyi, T. et al., (2006). "Dynamic augmented reality for sensory substitution in robot-assisted surgical system."*Proc.: Annual I. C. of the IEEE Eng. in Med. Bio. Society.*.

Bach-y Rita, P. et al., (1969). "Vision substitution by tactile image projection." *Nature,* vol. 221, p. 963-964.

Bliss, J. C. et al., (1970). "Optical-to-tactile image conversion for the blind" *IEEE Transactions on Man-Machine Systems*

Capelle, C. et al., (1998). "A real-time experimental prototype for enhancement of vision rehabilitation using auditory substitution." *Biomedical Engineering, IEEE Trans.*

Cronly-Dillon, J. et al., (1999). "The perception of visual images encoded in musical form: a study cross-modality information transfer." *Proc. Biological sciences / The Royal Society*

Hanneton, S. et al., (2010). "The vibe : a versatile vision-to-audition sensory substitution device." *Applied Bionics and Biomechanics,* vol. 7, num. 4, p. 269-276

Jansson, G. (1983). "Tactile guidance of movement" *International Journal of Neuroscience,* vol. 19, p. 37-46

Kaczmarek, K. A. and Haase, S. J. (2003). "Pattern identification and perceived stimulus quality as a function of stimulation current on a fingertip-scanned electrotactile display" *Transaction on Neural System Rehabilitation Engineering,* vol. 11, p. 9-16

Meijer, P. (1992). "An experimental system for auditory image representations" *Biomedical Engineering, IEEE Trans.*

Merabet, L. B. et al., (2009). "Functional recruitment of visual cortex for sound encoded object identification in the blind" *Neuroreport,* vol. 20, num. 20, p. 132-138

Molotchnikoff, S. and Rouat, J. (2011). "Brain at work: Time sparness and multiplexing/superposition principles", *Frontiers in Bioscience*, in press.

Sampaio, E. et al., (2001). "Brain plasticity: Visual acuity of blind persons via tongue" *Brain Research,* vol. 908, p. 204-207


## ACKNOWLEDGEMENTS


Sean Wood for English corrections, FQRNT of Québec and ACELP/CEGI of Univ. de Sherbrooke for funding this project.

# THE ROLE OF ATTENTION IN AUDIO-VISUAL INTEGRATION

**Michael Schutz[1] and Laura Silverman[2]**
[1] School of the Arts, McMaster University (Hamilton, Ontario) schutz@mcmaster.ca
[2] University of Rochester Medical Center (Rochester, New York) laura_silverman@urmc.rochester.edu

## 1. INTRODUCTION

When listening to a person speak, our perceptual system effortlessly integrates the sounds detected by our ears with the gestures and lip movements seen by our eyes, giving rise to the experience of a unified event. However, this *illusion of unity* is in fact the end-result of a complex process integrating disparate information. The dominant theory for explaining this process is known as optimal integration – predicting that sensory information is weighted in proportion to its quality (Ernst & Banks, 2004). Given the superior temporal acuity of the auditory system, audition generally dominates when resolving conflicts in timing - such as judging event duration (Alais et al., 2010).

### 1.1. An exceptional pattern of audio-visual integration

One exception to this otherwise consistent framework can be found in a musical illusion in which professional marimbists use visible gestures to control the perceived duration of musical notes (Schutz & Lipscomb, 2007). Because this effect is not the result of a response bias or cognitive correction (Schutz & Kubovy, 2009), it represents a curious exception to an otherwise lawful pattern of optimal integration. Subsequent research has demonstrated that this exception is not related to uni-modal information quality, but rather the cross-modal causal link between the striking gesture and the resultant impact sound. Manipulations breaking this link demonstrate no visual influence (Armontrout et al., 2009; Schutz & Kubovy, 2009), consistent with the theory of optimal integration.

### 1.2. Autism and audio-visual integration

The importance of sensory integration in our everyday experience becomes clear when considering special populations with sensory integration dysfunction. For instance, it is well documented that individuals with autism spectrum disorders (ASD) have difficulties with auditory-visual integration. For example, they struggle with using lip movements to improve speech perception (Smith & Bennetto, 2007), matching faces and voices (Loveland et al., 1995), and integrating communicative gestures with co-expressive speech (Silverman, Bennetto, Campana, & Tanenehaus, 2010). Despite these difficulties, the full extent of sensory integration dysfunction in ASD is unclear. For example, research examining low-level integration of auditory beeps with visual flashes suggests intact audio-visual integration abilities – at least in the context of simple non-social stimuli (Keane et al., 2010; van der Smagt et al., 2007). However, such work generally involves artificial synthesized sounds and stationary visual images, which are not necessarily indicative of real world perceiving (Gaver, 1993). Therefore, we would like to use the Schutz-Lipscomb task to explore audio-visual integration in ASD, as it allows for rigorous analysis of the effect of naturalist visual stimuli (i.e. biological motion) on the perception of ecologically common auditory events (i.e. impact sounds). Furthermore, given that it lacks social and communicative demands, it is well suited for use in ASD populations.

To date, all work in this illusion has used the same procedure and instructions, varying only the stimuli. Participants have always been asked to make judgments of (1) the duration of the heard sound independent of the seen gesture, and (2) the degree to which the duration of the seen gesture "agrees with" the duration of the heard sound.

In order to reliably use this task when working with ASD individuals, we must ask participants to rate the duration of both the musical note and the accompanying striking gesture separately. This differs from previous approaches, which asked participants to rate the duration of the note and the level of *agreement* between the gesture and the note. This modification is an important precursor to testing ASD individuals who often have trouble shifting cognitive set. Therefore when working with this population it is preferable to use a task involving consistent judgments of one dimension (duration), rather than shifting between multiple dimensions (i.e. duration and agreement).

This new procedure differs from previous work by using a task that explicitly calls attention to the gesture's length when judging tone duration. Although the illusion is robust in the face of manipulations preserving the causal link between auditory and visual stimuli, we felt it necessary to first determine whether this alteration in instructions changes the magnitude of the illusion. This is an important consideration, given that attention can diminish task-irrelevant information's influence (Schwarz & Clore, 1983).

### 1.3. Drawing attention to task-irrelevant information

In order to explore the effect of attentional focus in this paradigm, we conducted two experiments using (1) the original instructions asking about the degree of agreement between the observed gesture and the heard sound, (2) the new instructions calling attention to the length of the observed gesture. This serves as an important precursor to our subsequent investigations of audio-visual integration amongst children with autism. It also explores whether the illusion is robust to manipulations of attention, which will provide further insight into an illusion at odds with the otherwise widely-accepted theory of optimal integration.

## 2. METHODS

We recruited 42 undergraduate students and ran them in one of two experiments. Two participants who did not appear to be attentive to the task instructions were dropped from subsequent analysis, leaving 40 participants. Although both experiments asked participants to rate the duration of the heard tone, they differed in their instructions regarding a second question about the observed gesture. The first experiment used the original wording ("indicate how much the length of sound 'agrees' with the length of the gesture"), whereas the second experiment used new wording ("indicate how long each gesture looks"). In all other respects the two experiments were identical. The auditory component of the stimuli consisted of the sound produced by either the "long" striking gesture or the "damped" sound created by muffling the bar shortly after striking. The visual component consisted of long and short striking motions produced by a world-renowned marimbist (Schutz & Lipscomb, 2007).

## 3. RESULTS

Duration ratings were assessed with a 2 (gesture) x 6 (marimba tone) x 2 (question style) repeated-measures ANOVA with *gesture* and *marimba tone* as within-participants variables and *question style* as a between-participants variable. The most important finding (shown in Fig 1) was that question style did not have a significant influence on ratings of tone duration ($F_{1,38}$ =.6664, $p$ = 0.4194), nor was there a question-style x gesture interaction ($F_{1,38}$ =.6401, $p$ =.4286). As expected, there was a main effect of gesture ($F_{1,38}$ = 42.333, $p < 0.0001$).

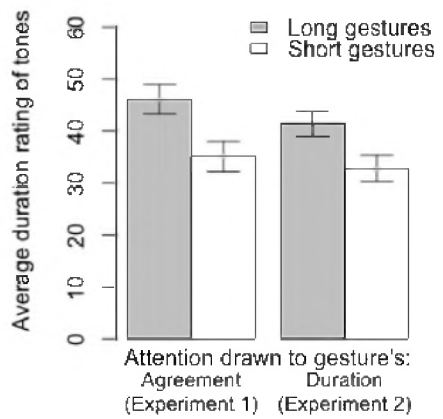


**Figure 1. Duration ratings as a function of attentional focus. Vision's influence on perceived tone duration did not differ between presentation conditions (i.e. experiments). Error bars represent 95% confidence intervals about the mean.**

## 4. DISCUSSION AND CONCLUSIONS

Previous research has shown that explicitly drawing attention to task-irrelevant information can reduce its influence (Schwarz & Clore, 1983). However, it appears that explicitly calling attention to the duration of the observed gesture does not compromise the magnitude of this particular illusion. This demonstrates that the illusion is robust with respect to the manipulation of instructions. Although not entirely unexpected, this outcome nonetheless provides an important step forward in our broader goal of adopting this paradigm for using in clinical settings – such as exploring sensory integration dysfunction in children with autism. Given the clear conflict between this illusion and current theoretical viewpoints (predicting minimal visual influence on a temporal duration task), the robust nature of this illusion is also informative with respect to theories of audio-visual integration.

Illuminating the extent of sensory integration abilities and impairments in ASD has the potential for helping us to better understand the underlying mechanisms that may contribute to social and communicative difficulties at the heart of the disorder. In addition, studies delineating aspects of high- and low-level integration and the processing of biological motion could help to clarify the neural basis of the disorder by providing the groundwork for future imaging studies.

In conclusion, the "marimba illusion" provides a rare opportunity to test audio-visual integration that involves biological motion but lacks social and communicative demands. Therefore, this adapted methodology demonstrates an important first step towards using this paradigm as a new tool for novel explorations that assess sensory integration disorder in ASD. Furthermore, the modified procedure described in this abstract makes the task more accessible to a wider range of individuals with varied cognitive skills and social/communicative abilities, opening up many possibilities for future use in studying sensory integration dysfunction amongst a wide range of clinical populations.

## REFERENCES


Alais, D. et al. (2010). *Seeing and Perceiving.*

Armontrout, J., et al. (2009). *Attention, Perception, & Psychophysics.*

Gaver, W. (1993). *Ecological Psychology.*

Keane, B. et al. (2010). *Research in Autism Spectrum Disorders.*

Loveland, K. et al. (1995). *Development and Psychopathology.*

Schutz, M. & Kubovy, M. (2009). *JEP:HPP.*

Schutz, M. & Lipscomb, S. (2007). *Perception.*

Schwarz, N., & Clore, G. L. (1983) *J Personality and Social Psychology.*

Silverman, L et al. (2010). *Cognition.*

Smith, E. G., & Bennetto, L. (2007). *J Child Psychology and Psychiatry.*

van der Smagt, M. (2007). *J Autism and Developmental Disorders.*


## ACKNOWLEDGEMENTS


Support for this project was provided in part by the NSERC (RGPIN/386603-2010), the Ministry of Research and Innovation's Early Research Award (ER10-07-195), and the NIH (1R03 PAR-07-287). The authors would also like to acknowledge Allison Canfield's helpful contributions to this study.

# FILLED DURATION LENGTHENING TAKES PLACE IN A SOUND PRECEDED BY A MORE INTENSE SOUND

**Tsuyoshi Kuroda and Simon Grondin**
École de psychologie, Université Laval, Québec (QC), G1V 0A6, Canada

## 1. INTRODUCTION

The *time-stretching illusion* is an auditory illusion where a sine tone is perceived as longer when it is preceded by a more intense noise (Figure 1). This illusion was reported by Carlyon et al. (2009) and Sasaki et al. (2010), and the latter authors assumed that the illusion is caused by the fact that the onset of the sine tone is masked by the preceding noise. This onset is restored in perception, but it is interpreted to be buried in the noise. Thus, the sine tone's duration is overestimated.

Sasaki et al. (2010) demonstrated the occurrence of the time-stretching illusion, however, with only one condition where the sine tone was preceded by the noise. The present experiment employing the method of constant stimuli examined whether or not the sine tone would be overestimated when it was *followed* by the noise.

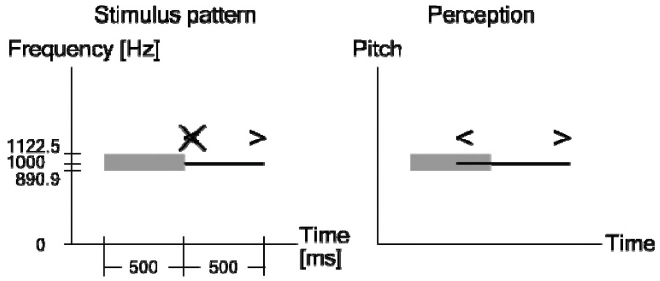


**Figure 1. The time-stretching illusion: "<" represents the tone's onset and ">" the tone's offset.**

## 2. METHOD

### 2.1. Participants

Eight Laval University students and employees volunteered to participate. The participants all reported they had normal hearing. They received $60 CAN for their participation.

### 2.2. Apparatus and stimuli

Digital signals of stimuli were sampled at 44100 Hz and quantized to 16 bits. The stimuli were delivered from headphones (Sennheiser HD 477) connected to a computer (IBM Netvista).

The *standard* tone and the *comparison* tone were presented successively in each trial. They were sinusoidal tones of 1000 Hz at 58 dBA. The standard tone was fixed at 500 ms, and the comparison tone was varied from 360 to 640 ms in steps of 40 ms.

The standard tone was adjoined temporally by a 500-ms 1/3-octave band noise with a center frequency of 1000 Hz in four ways (Figure 2). (1) In the noise-preceding condition, which is the typical pattern causing the time-stretching illusion, the noise was placed just before the standard tone. (2) In the noise-following condition, the noise was placed just after the standard tone. (3) In the noise-on-both-side condition, the noise was placed on both sides of the standard tone. (4) In the control condition, no noise adjoined the standard tone. The noise was 6 dB higher than the standard tone. The comparison tone was always without any noises.

The amplitude of each sound rose and decayed during 10 ms at the beginning and the end, and a half part of a cosine window was applied to the envelope of these transitions.

The standard pattern and the comparison tone were presented in two types of order: The standard pattern preceded the comparison tone in the standard-comparison type, and vice versa in the comparison-standard type. A silent interval, which was varied from 2000 to 3000 ms randomly, was placed before the beginning of stimulus presentation and was inserted between the standard pattern and the comparison tone.

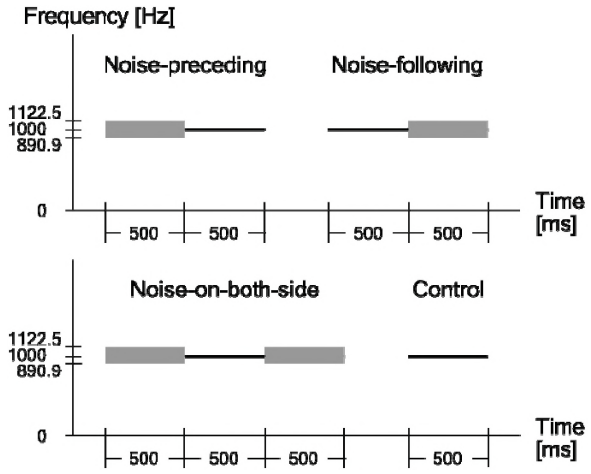


**Figure 2. Standard patterns**

### 2.3 Procedure

The task was performed by clicking on panes on a computer display. The participants listened to the stimulus pair by clicking on the "play" pane. The participants were allowed to listen to the stimulus pair only once in each trial except when listening was disturbed for some specific reason (e.g., a sleep or a cough)—in such a case, the participants listened to the pair again by clicking on the "replay" pane.

The participants judged whether the second sine tone was "shorter" or "longer" than the first sine tone. The participants could answer that the two tones were "equal" in duration, and they could also answer that they perceived the two tones as different but were "unsure" whether the second tone was shorter or longer. The participants were instructed not to use the last two alternatives except when definitely necessary.

There were six sessions: three sessions for the standard-comparison order and three sessions for the comparison-standard order. These two sets of sessions were carried out in counterbalanced order. Each session consisted of four blocks corresponding to four standard configurations, which were carried out in counterbalanced order. Each block consisted of 80 trials for ten repetitions of 8 steps of comparison duration, which were arranged in random order. Breaks of a few minutes were inserted between the blocks. A warm up of two trials was carried out at the beginning of each block, for which the stimulus pairs were selected randomly. The participants finished each session in about an hour.

## 3. RESULTS

The probability that the comparison was perceived as longer was calculated for each comparison duration to make 8-point psychometric functions for each configuration and for each order. Each point was based on 30 responses, and the alternative responses of "equal" and "unsure" were split between the "shorter" and the "longer" responses. A cumulative normal distribution was fitted to the resulting curves. Because two participants showed poor goodness of fit ($R^2$ values of less than .30) in some conditions, they were replaced with new participants. As a result, the $R^2$ value was above .90 in 59 cases out of 64 (8 participants × 2 orders × 4 configurations), and was between .90 and .70 in 5 cases.

From each curve, the point of subjective equality (PSE) was calculated for determining the perceived duration of the standard tone (Figure 3). A repeated-measure ANOVA according to a 2 order × 4 configuration design revealed that the configuration effect was significant, $F(3, 21) = 4.659$, $p = .012$, $\eta_p^2 = .400$, the interaction was marginally significant, $F(3, 21) = 2.856$, $p = .062$, $\eta_p^2 = .290$, and the order effect was not significant, $F(1, 7) = .286$, $p = .610$, $\eta_p^2 = .039$.

## 4. DISCUSSION

It turned out that a sine tone was perceived as longer when it was adjoined by a more intense noise. This overestimation was the largest when the sine tone was preceded by the noise, which is the typical case of the time-stretching illusion. Less overestimation was observed when the sine tone was followed by the noise. In this case, the offset of the sine tone is supposed to be masked by the noise. The classical studies of auditory masking have indicated, however, that there is limited evidence supporting the backward masking (i.e., the peripheral masking of the preceding sound by the following sound; see Moore, 2003). If the masking of the tone's offset is similar to the classical backward masking in their mechanism, it is not difficult to assume that the masking of the tone's offset has weaker effect on the tone's perceived duration than the masking of the tone's onset.

It is interesting to note that the overestimation was not so high when the noise was placed on both sides of the sine tone. In this case, the preceding noise should have caused the same overestimation as in the time-stretching illusion. Rather, the observed overestimation was similar to that in the situation where the noise was placed only after the sine tone. In order to explain this effect, it may be required to assume another mechanism, which is not related to the masking of tone's onset and offset. When the noise is placed on both sides of the sine tone, this configuration may shrink the perceived duration of the sine tone, and cancel the overestimation by the masking of the tone's onset. If so, it should be valuable to conduct an experiment where the noises on both sides are weaker than the sine tone. In this situation, the onset and the offset of the sine tone should not be masked, and only the effect of configuration can be examined.

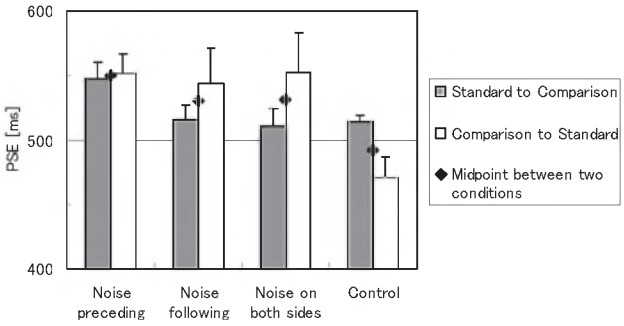


**Figure 3. The estimated point of subjective equality**

## REFERENCES

Carlyon, R. P., Deeks, J. M., Shtyrov, Y., Grahn, J., Gockel, H. E. Hauk, O, and Pulvermüller, F. (2009). "Changes in the perceived duration of a narrowband sound induced by a preceding stimulus," Journal of Experimental Psychology: Human Perception and Performance, **35**, 1898-1912.

Sasaki, T., Nakajima, Y., ten Hoopen, G., van Buuringen, E., Massier, B., Kojo, T., Kuroda, T., and Ueda, K. (2010). "Time stretching: Illusory lengthening of filled auditory durations," Attention, Perception, & Psychophysics, **72**, 1404-1421.

Moore, B. C. J. (2003). *An introduction to the psychology of hearing* (5th ed., Academic Press, San Diego, CA).

## ACKNOWLEDGEMENTS

This research was made possible by a research grant awarded to SG by the Natural Sciences and Engineering Council of Canada.

# RHYTHMIC GROUPING AND TEMPORAL GAP DISCRIMINATION

**Tsuyoshi Kuroda, Emi Hasuo, and Simon Grondin**
École de psychologie, Université Laval, Québec (QC), G1V 0A6, Canada

## 1. INTRODUCTION

The temporal sensitivity for discriminating a gap marked by two tones is affected by the structure of markers. The sensitivity is impaired when the markers are lengthened (Rammsayer & Leutner, 1996), and the sensitivity is improved when the markers are repeated (Schulze, 1989). The purpose of the present experiment was to examine how temporal sensitivity, expressed with the probability of responding correctly, would be changed by repeating a short and a long marker alternately (Figure 1A).

It is known that successive tones are segmented to construct rhythm in perception, and the temporal sensitivity for repeated gaps is changed depending on what rhythmic grouping takes place (Trainor & Adams, 2000). To examine whether similar effects would be caused for the present discrimination tasks, an additional phase was conducted for measuring what rhythmic grouping would be caused for the repetition of a short and a long marker.

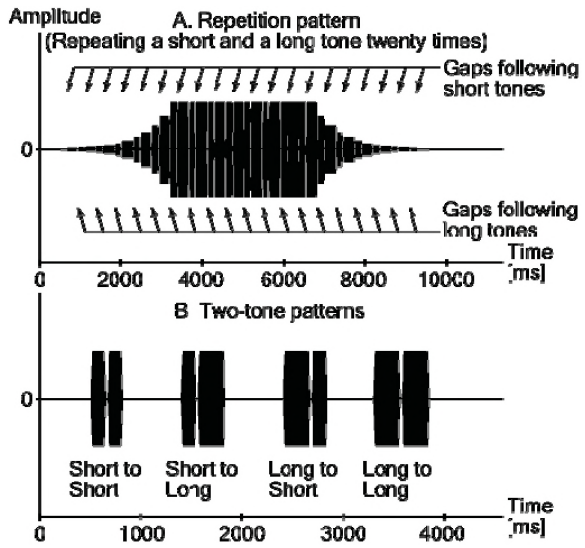


**Figure 1. Stimulus patterns**

## 2. METHOD

### 2.1. Participants

Sixteen Laval University students and employees volunteered to participate. They were all native French speakers between 19 and 30 years-old, and reported they had normal hearing. They received $50 CAN for their participation.

### 2.2. Apparatus and stimuli

Digital signals of stimuli were sampled at 44100 Hz and quantized to 16 bits. The stimuli were delivered from headphones (Sennheiser HD 477) connected to a computer (IBM Netvista). Each stimulus pattern was made of a 150-ms tone called the *short* tone (S) and/or a 262.5-ms tone called the *long* tone (L). Each tone was square-like wave generated by mixing the fundamental and the first three odd sinusoidal components. The amplitude of each tone rose and decayed during 20 ms at the beginning and the end with raised-cosine ramps. The markers were presented at a level that was 30 dB higher than the threshold level measured before each session.

### 2.3. Grouping measurement

Due to the lack of space, the details of this measurement are omitted here. The purpose of this measurement was to estimate the participants' preferred rhythmic grouping for the repetition patterns (Figure 1A). The results indicate that the current French-speaking participants were likely to perceive the repetition patterns as successive chunks consisting of a short and a long marker in this order, not as chunks consisting of a long and a short marker.

### 2.4. Discrimination measurement

This measurement was conducted after the grouping measurement, and estimated participants' gap discrimination level for the repetition patterns (R) and for the two-tone patterns. It was divided into two phases carried out in counterbalanced order.

The repetition-pattern phase consisted of two sub-phases for two types of tasks, which were carried out in counterbalanced order. In the gap-following-short-tone task (RS), two repetition patterns were presented successively in each trial, and the second pattern was compared with the first pattern in terms of the gap duration following the short tones. In the gap-following-long-tone task (RL), the second pattern was compared with the first pattern in terms of the gap duration following the long tones.

There were 11 gap-duration pairs to be compared for each task. In the gap-following-short-tone task, the gaps following the short tones in the first pattern were varied from 10 to 30 ms and those in the second pattern were varied from 30 to 10 ms both in steps of 2 ms. The gaps following the long tones were fixed at 20 ms. In the gap-following-long-tone task, the gaps following the long tones in the first pattern were varied from 10 to 30 ms and those in the second pattern were varied from 30 to 10 ms both in steps of 2 ms. The gaps following the short tones were fixed at 20 ms.

In the two-tone-pattern phase, two two-tone patterns were presented successively, and the second pattern was compared with the first pattern in terms of the gap duration between two tones. This phase consisted of four sub-phases for four arrangements of a short and a long marker: SS, SL, LS, and LL. These sub-phases were carried out in counterbalanced order. There were 11 gap-duration pairs to be compared; the gap in the first pattern was varied from 10 to 30 ms and the gap in the second pattern was varied from 30 to 10 ms both in steps of 2 ms.

Both in the repetition-pattern phase and in the two-tone-pattern phase, a silent interval of 2500, 2750, or 3000 ms was inserted between the first pattern and the second pattern. The participants judged whether the gap in the second pattern was "shorter" or "longer" than the gap in the first pattern. The participants could answer that the second gap was "equal" to the first gap, and they could also answer that they perceived the two gaps as different but were "unsure" whether the second gap was shorter or longer. The participants were instructed not to use the last two alternatives except when definitely necessary.

The participants went thorough ten blocks in each sub-phase for the repetition and the two-tone patterns. Each block consisted of 11 trials for 11 duration pairs, which were arranged in random order. Two warming-up trials were carried out, and, for these trials, the stimulus pairs that were to be presented at the last two trials of the block were presented.

## 3. RESULTS and DISCUSSION

The gap discrimination level for each pattern was determined by two types of probability to respond correctly: one type called *correct-shorter* is the probability that the participant selected "shorter" when the second gap was physically shorter than the first gap, and the other type called *correct-longer* is the probability that the participant selected "longer" when the second gap was physically longer. Conditions where the two gaps were physically equal were omitted from these probabilities, and thus, each probability was based on 50 responses (5 steps × 10 responses) for each condition and for each participant. The average probabilities of correct responses are shown in Figure 2. A repeated-measure analysis of variance (ANOVA) according to a 2 probability-type × 6 pattern design adjusted with the arcsine square root transformation and the Greenhouse-Geisser criterion showed that the pattern effect was significant, $F(5, 75) = 10.417$, $p < .001$, $\eta_p^2 = .410$, the probability-type effect was significant, $F(1, 15) = 15.417$, $p = .001$, $\eta_p^2 = .507$, and the interaction was significant, $F(5, 75) = 3.674$, $p = .020$, $\eta_p^2 = .197$.

It turned out that the gap discrimination level was changed systematically according to the arrangements of a short and a long marker. In the two-tone patterns, the correct-probability decreased when the markers were lengthened. This decrease was larger when the preceding marker was lengthened than when the following marker was lengthened. Lengthening both markers, however, didn't cause larger decrease than lengthening only the preceding marker. The correct-probability was increased by repeating a short and a long marker, but the discrimination for the gaps following short tones and for the gaps following long tones caused almost the same correct-probability. Finally, analyses with Pearson's correlation coefficient revealed that the gap discrimination results didn't depend on the participants' preferred rhythmic grouping.

It should be noted that, whereas lengthening the preceding marker decreased the correct-probability more largely than lengthening the following marker in the two-tone patterns, the discrimination for the gaps following short tones and for the gaps following long tones caused almost the same correct-probability in the repetition patterns. If a *linear* improvement of the temporal sensitivity had been caused by repeating the gaps, the discrimination performance should have been better for the gaps following short tones than for the gaps following long tones. This indicates that discriminating repeated gaps is based on a different mechanism from discriminating single gaps.

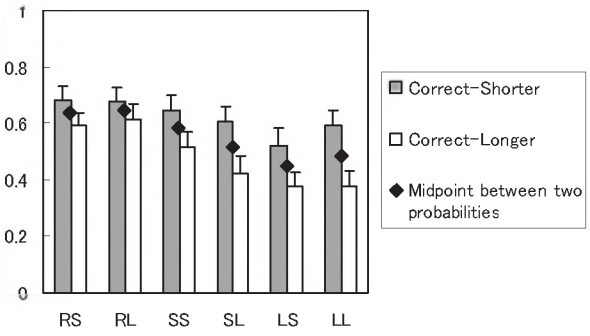


**Figure 2. Correct-probability: RS represents the repetition pattern where the gaps following short tones were discriminated. RL represents the repetition pattern where the gaps following long tones were discriminated.**

## REFERENCES

Rammsayer, T. H., & Leutner, D. (1996)."Temporal discrimination as a function of marker duration," Perception & Psychophysics, **58**, 1213-1223.

Schulze, H. H. (1989). "The perception of temporal deviations in isochronic patterns," Perception & Psychophysics, **45**, 291-296.

Trainor, L. J., & Adams, B. (2000). "Infants' and adults' use of duration and intensity cues in the segmentation of tone patterns," Perception & Psychophysics, **62**, 333-340.

## ACKNOWLEDGEMENTS

This research was made possible by a research grant awarded to SG by the Natural Sciences and Engineering Council of Canada.

# PROPAGATION OF SOUND BEHIND VEHICLES EQUIPPED WITH DIFFERENT BACKUP ALARMS

**Hugues Nélisse[1], Chantal Laroche[2], Jérôme Boutin[1], Christian Giguère[2], and Véronique Vaillancourt[2]**

[1] Institut de Recherche Robert Sauvé en Santé et Sécurité du Travail, Montréal Québec, Canada
[2] Audiology & SLP Program, University of Ottawa, Ottawa, Ontario K1H 8M5, Canada

## 1. INTRODUCTION

In the last few years, a new type of acoustic signal has been introduced for vehicle backup-alarms and has drawn increasingly more interest from many industrial sectors. This signal, based on the use of broadband noise, sounds rather different from the typical tonal ("beep") signal and is deemed to reduce annoyance for residents living in close proximity to industrial settings and construction sites. From a safety perspective, the broadband signal is believed to be more efficient in terms of spatial localization and uniform sound propagation behind vehicles, thus reducing the risk for workers. While conceptually appealing, few published and peer-reviewed scientific studies have demonstrated the advantages and disadvantages of such an alarm signal to ensure worker safety, particularly in comparison to existing technologies (Burgess and McCarty 2009; Homer 2008; Withington 2004). This study focused on sound propagation behind vehicles by examining the distribution of sound pressure levels for three types of backup alarms: the standard tonal "beep" signal, a multi-tone signal and the broadband noise technology. Sound pressure levels were measured at various fixed locations behind heavy vehicles by using a test method inspired from the ISO 9533 standard (1989). Sound propagation contour maps were also obtained for various vehicles and terrain configurations.

## 2. METHODS

Three backup alarms were tested in this study: i) a standard tonal alarm; ii) a broadband alarm and; iii) a custom-made multi-tone alarm. The multi-tone was proposed by Laroche (1995) as an improvement over the conventional tonal alarm and was included in this study for comparison with the two other signals. The frequency content of the alarms is illustrated in Figure 1. The multi-tone alarm consists of three major tones between 1000 and 1300 Hz, in contrast to the standard tonal alarm with its acoustic energy concentrated around 1250 Hz. For the broadband alarm, energy is distributed over a larger frequency span, most of the energy being found in the 700-4000 Hz range.

Field tests were performed at three different locations: a sawmill site, a limestone, and a quicklime plant, all with various terrain configurations (hard soil or gravel & dirt) and vehicles. The tested vehicle was stationary and two mounting scenarios of the alarm were considered: i) a "realistic" one, which consisted of using the alarm as installed on the vehicle (the alarm was off-centered in all three cases tested) and; ii) an "ideal" one where the alarm was centered, unobstructed and facing outward.

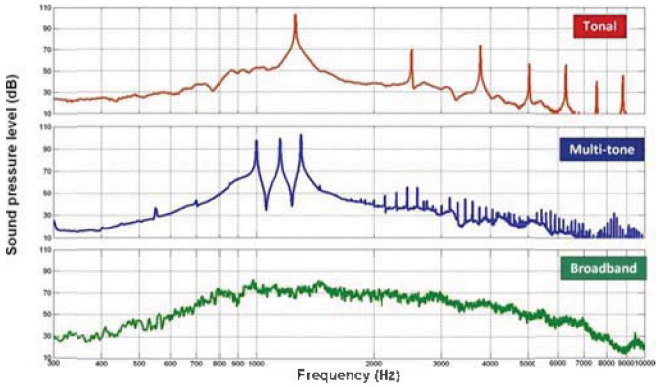


**Figure 1: Frequency content of the three alarms tested**

Two sets of measurements were performed for each alarm. In the first set, alarm level adjustments were performed by measuring sound pressure levels at the seven fixed microphone positions specified in the ISO 9533 standard (see Figure 2(a)). The alarm level was manually adjusted so that a difference equal to or greater than 0 dB (signal-to-noise ratio S/N≥0dB) was obtained at all measurement points between the noise levels generated when the vehicle was operating at high idle without the alarm and those prevailing when the reverse alarm was activated and the vehicle operated at low idle. The procedure was repeated for each alarm to determine if one alarm type would require higher levels than the others to maintain the desired S/N≥0 dB at all microphone positions. In a second set of measurements, a microphone was mounted to a pole and digital audio time recordings were performed while the alarm was activated by moving the microphone slowly along 9 axes and 2 curvilinear arches behind the vehicle (see Figure 2(b)). The alarm levels were set at the values found during the first set of measurements and the vehicle engine was stopped. A post-processing scheme was developed to extract the alarms' sound pressure levels along the various lines. Afterwards, an interpolation algorithm was used to produce sound pressure level contour maps behind the vehicle when the alarm is activated. Such procedures were used to investigate the uniformity of the sound field generated by each alarm.

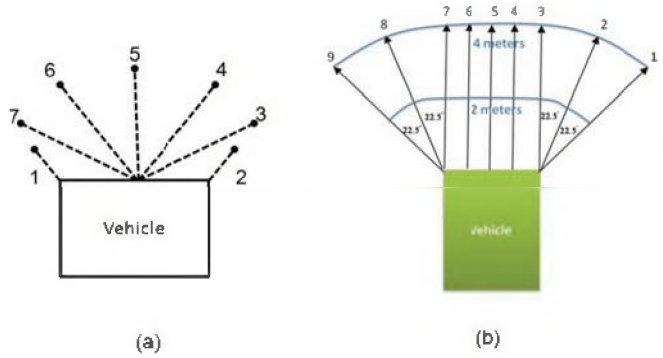


**Figure 2: (a) Position of the microphones during alarm level adjustments; (b) Illustration of the scanning lines for sound mapping measurements**

## 3. RESULTS

### 3.1. Alarm level adjustments as per ISO 9533

Results obtained for the "S/N≥0 dB" procedure are summarized in Table 1. For each alarm and site, the mean and standard deviation of the S/N ratio is presented, as well as the sound pressure levels at a reference microphone located 1 m directly in front of the alarm device. It should be noted that higher levels were required for the tonal alarm compared to the multi-tone and broadband signals. Also, higher mean S/N ratios and standard deviations were obtained for the tonal alarm, suggesting more sound level variations for this signal.

**Table 1: Mean (standard deviation) values of the S/N ratio (expressed in dB) & sound pressure levels (in dBA) at the 1m reference microphone (alarm position: "ideal" mounting).**

| | Site 1 | | Site 2 | | Site 3 | |
|---|---|---|---|---|---|---|
| | Mean (std) | Level @ 1m | Mean (std) | Level @ 1m | Mean (std) | Level @ 1m |
| Tonal | 6.9 (4,2) | 107.2 | 8.0 (5.9) | 112.0 | 3.2 (2.3) | 106.0 |
| Multi-tone | 3.9 (2,3) | 99.4 | 5.4 (4.0) | 105.2 | 4.9 (3.1) | 102.8 |
| Broadband | 1.9 (1.2) | 99.3 | 3.1 (2.9) | 104.9 | 1.0 (0.7) | 102.1 |

### 3.2. Noise levels behind vehicles

Contour maps of the sound pressure levels behind a vehicle are presented in Figure 3 for one of the sites, with the alarms positioned in the "ideal" mounting condition. Variations in sound pressure levels on the order of 10 dB within a short range of ~1 meter can be observed for the tonal alarm due to acoustic interference effects. Such interference effects appear to be quite prominent for signals characterized by a single tonal component. However, they tend to be smoothed out considerably with the addition of tonal components, as is the case for the multi-tone alarm. Finally, an even more uniform sound field was obtained for the broadband alarm.

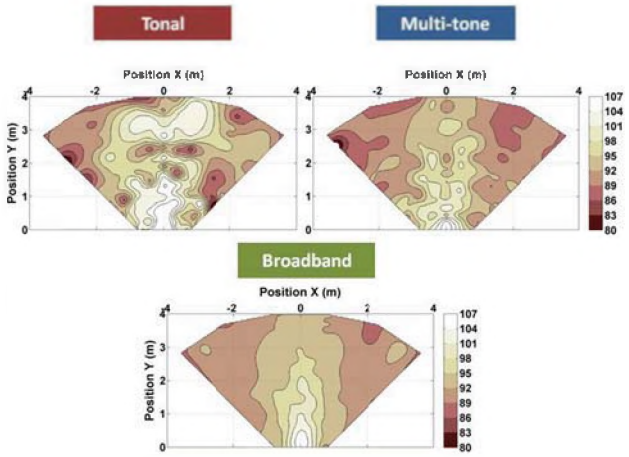


**Figure 3: Sound pressure levels behind the vehicle (expressed in dBA) at one site, for the "ideal" alarm mounting position**

## 4. CONCLUSIONS

The uniformity of the sound field behind vehicles produced by backup alarms was investigated by comparing three types of alarm signals: tonal, multi-tone and broadband. The results suggest that alarms with broader frequency content present some advantages over conventional single-tone alarms, including: 1) a more uniform sound propagation pattern behind heavy vehicles; and 2) lower sound pressure levels to meet the requirements set forth in ISO 9533. However, it remains to be seen if such a broadband signal would be recognized as a valid alarm signal from a subjective standpoint (detection, urgency, localization, etc.).

## REFERENCES

Burgess M, McCarty M. (**2009**) Review of alternatives to "beeper" alarms for construction equipment Report AVU 0129, Acoustics & Vibration Unit, School of Aerospace, Civil & Mechanical Engineering, UNSW, Canberra, Australia.

Homer JP. (**2008**) Audible warning devices used in the mining industry. Proceedings of the Noise-Con 2008. Noise-Con 2008, Dearborn, MI, USA.

ISO 9533 (**1989**). Earth-moving machinery -- Machine-mounted forward and reverse audible warning alarm -- Sound test method. International Standards Organization, Geneva.

Laroche C. (**1995**). Détermination des caractéristiques acoustiques optimales des alarmes de recul. Montréal, Canada: Études et recherches / Rapport R-177 / IRSST.

Withington DJ. (**2004**) Reversing goes broadband. Quarry Manage 31: 27–34.

## ACKNOWLEDGEMENTS

The authors would like to thank the Institut de Recherche Robert Sauvé en Santé et Sécurité du Travail (IRSST) for its financal support.

# RELEARNING SOUND LOCALIZATION WITH DIGITAL EARPLUGS

**Régis Trapeau[1] and Marc Schönwiesner[1]**
[1]Dept. of Psychology, Université de Montréal, BRAMS (International Laboratory for Brain, Music and Sound), Pavillon 1420 boul. Mont Royal, Outremont, QC, Canada, H2V 4P3

## 1. INTRODUCTION

The auditory system infers the location of sound sources from the processing of different acoustic cues. As the size of the head and the shape of the ears change over development, the association between acoustic cues and our expectation of external spatial position can not be fixed at birth, but has to be plastic. Recent studies on humans have shown that the auditory system is still capable of such plasticity during adulthood (Javer and Schwartz, 1995; Hofman et al., 1998; Van Wanrooij and Van Opstal, 2005). We aim to explore the principles that govern an adaptation to shifted Interaural Time Differences (ITDs), one of the two binaural cues for azimuthal perception with the Interaural Level Differences (ILDs).

We equipped six participants with binaural digital earplugs that allow us to delay the input to one ear, and thus disrupt the ITDs. Participants were asked to wear the plugs during all waking hours for 10 days and their ability to localize sounds on the horizontal plane was tested everyday in free field conditions.

## 2. METHODS

*Participants.* Two female and four male students aged 26-32 years, with no history of hearing disorder or neurological disease, participated as paid volunteers, after having given informed consent. The experimental procedures were approved by the local ethics committee.

*Plugs.* Each plug contains a programmable signal processor, microphone and transducer and was fitted to the ears of each participant to create an acoustic seal (attenuation around 25 dB). The gain of the plugs was adjusted to achieve normal loudness levels. The plugs could be programmed to delay the incoming sound by a desired duration.

*Design and stimuli.* Sound localization tests were controlled by a custom-designed Matlab script (r.2009a; MathWorks) and stimuli were generated using TDT System 3 (Tucker-Davis-Technology). The listener was seated in a hemi-anechoïc room, in front of an array of 25 speakers (Orb Audio) mounted on a 180° arc placed at 90 cm of the listener's head on the horizontal plane, giving an azimuthal resolution of 7,5°. In a first sound localization task, the stimulus consisted of 250 ms pulsed-train (5 bursts of 25 ms) of low-pass filtered pink noise (cf = 2 kHz). This type of stimulus ensures that the ITDs contribute largely to the azimuthal perception (Middlebrooks and Green, 1991). In a second sound localization task, the stimulus was identical to the first one, except that its spectrum was randomized from trial to trial by roving the intensity in 1/6 octave bands by up to 40 dB. The spectral uncertainty of this stimulus was used to reduce the effectiveness of spectral cues (Wightman and Kistler, 1997 ; Kumpik et al., 2010). The overall level of both stimuli was 60 dB(A) at the position of the listener's head.

To allow a listener to indicate the perceived location a of stimulus, a laser pointer and a head-tracker (Polhemus Fastrak) were attached on his head, both pointing toward a 0° in azimuth and elevation direction for a centred head position.

*Procedure.* During a sound localization run, each location was pseudorandomly presented five times, for a total of 125 trials per run. No feedback was given. At the beginning of a run, the listener was asked to seat and lean his neck on a neck rest, so that his head was centred and that the laser pointed the central speaker (0° in azimuth and elevation). This initial head position was recorded and the listener had to place his head back in this position (at less than 2 cm and 2°) before starting each trial. To start a new trial, the listener had to press the button of a stylus. If his head was correctly placed when the button was pressed, a stimulus was played from one of the 25 speakers. If the head was misplaced no sound was played and the listener was asked to place his head back to the initial position. After a stimulus was played, the listener had to direct his head (and the laser pointer) toward the speaker from which he perceived the sound originating and to press the stylus button to validate his answer. The azimuth of the pointed speaker was computed from the data given by the head-tracker.

Both sound localization measurements (fixed spectrum and random spectrum tasks) were first taken without plugs. Secondly, they were repeated with the plugs inserted and no delay added. Participants were then asked to continue wearing the plugs while engaging in daily activities, during all waking hours. The sound localization measurements were repeated the next day and repeated with a delay of 625 µs added in the left plug. At this point of the experiment, no further modification were made to the plug's sound processing. These measurements were then repeated each day during a 10 to 12 days period. At the end of the experiment, measurements were taken with the plugs still inserted, and repeated immediately after removal of the plugs.

*Analysis.* The metric used to measure the localization accuracy of each listener was the mean signed error (MSE), a measure of the average discrepancy between listener's responses and targets locations. Permutation tests were used

to compare the MSEs between different tests of a given listener.

## 3. RESULTS

Insertion of the earplugs without delay affected the localization accuracy of three participants (results significantly different from those without plugs), even after 24 hours of wearing the plugs. Additionally, the delay added in the left earplug introduced a much smaller shift in the auditory space representation of these participants than the others. For these reasons, only the results of the remaining three participants (P2, P3 and P5) are presented here. For those participants, no significant difference has been found between the results obtained during the task using a fixed spectrum stimulus and the task using a random spectrum stimulus. Therefore, only the results of the fixed spectrum stimulus task are detailed.

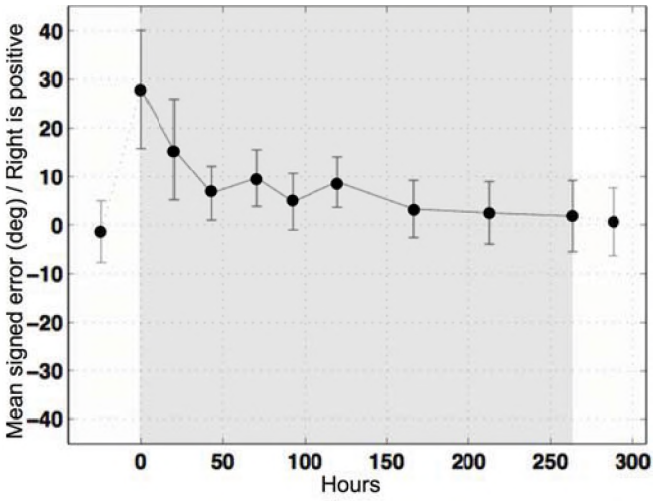


**Figure 1. Evolution of P3's MSE. Hour zero corresponds to the measurement immediately after insertion of the plugs. First measurement was taken without plugs, last one, immediately after removal of the plugs.**

The delay added in the left earplug shifted importantly the responses of P2, P3 and P5 in the right direction: MSE differences between the measurement without plugs and the first measurement with plugs and delay = 24.2° (P2), 29.3° (P3) and 21.4° (P5). After 48 hours, MSE differences between without and with plugs decreased to: -0.95° (P2), 7.8° (P3) and 5.4° (P5). At the end of the experiment (10 to 12 days of wearing the plugs), the MSEs of P2, P3 and P5 were not significantly different to those measured before the experiment, without plugs. When measured immediately after removal of the plugs, the MSEs of those participants were still not significantly different to those measured before the experiment, therefore no aftereffect has been observed. Figure 1 shows the MSE evolution of P3 during the experiment. Figure 2 shows the raw data of the sound localization tests of P3 before, during and after wearing of the plugs.

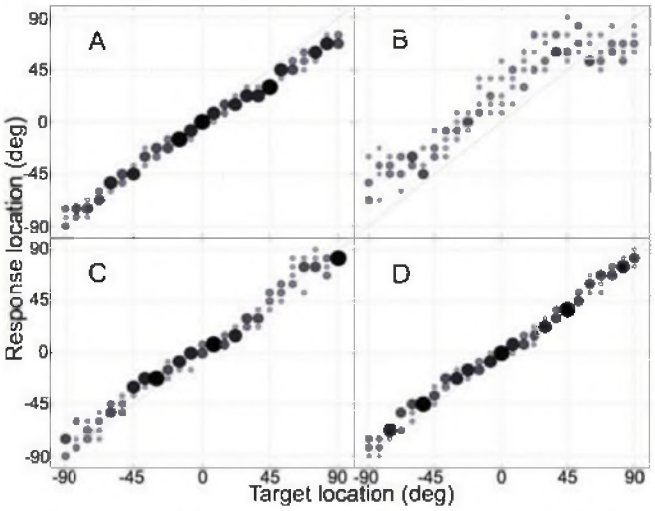


**Figure 2. Raw results of P3: without plugs (A), immediately after addition of a 625 µs delay in the left plug (B), on the last day of wearing the plugs (C) and immediately after removal of the plugs (D). Grey value and radius of the dots increase with the number of similar responses for a specific target.**

## 4. DISCUSSION AND CONCLUSIONS

The results show that the human auditory system is capable of a fast adaptation to shifted ITDs. The finding that the three participants showed no aftereffect in the opposite direction indicates that the adaptation could be attributed to a reweighting in the processing of the different spatial cues, more than to a recalibration of the ITDs. When wearing the plugs, the shifted ITDs are in contradiction with the other spatial cues and with visual feedback. A potential strategy of the auditory system could be to progressively put this biased information aside and to start relying exclusively on the other cues. As comparable results have been measured when testing with fixed or random spectrum stimuli, the spectral cues do not seem to play a key role in the adaptation to altered ITDs. Thus, a reweighting in favour of ILDs may have been the optimal strategy for sound localization with shifted ITDs. Future experiments will aim to deepen our understanding of this adaptive process and to determine the cortical sites that are involved.

## REFERENCES


Hofman, P. M., Van Riswick, J. G. and Van Opstal, A. J. (1998). Relearning sound localization with new ears. *Nature Neuroscience*. 1, 417-421.

Javer, A. R. and Schwarz, D. W. (1995). Plasticity in human directional hearing. *Journal of Otolaryngology*. 24, 111-117.

Middlebrooks J. C. and Green D. M., (1991). Sound localization by human listeners. *Annual Review of Psychology*. 42, 135-159.

Kumpik, D. P., Kacelnik, O. and King, A. J. (2010). Adaptive Reweighting of Auditory Localization Cues in Response to Chronic Unilateral Earplugging in Humans. *The Journal of Neuroscience*. 30(14), 4883-4894.

Van Wanrooij, M. M. and Van Opstal, A. J. (2005). Relearning sound localization with a new ear. *The Journal of Neuroscience*. 25, 5413-5424.

Wightman F. L. and Kistler D. J. (1997). Monaural sound localization revisited. *J Acoust Soc Am*. 101, 1050-1063.

# A NEW IPAD APPLICATION FOR HEARING SCREENING IN CHILDREN

**Nicolas Ellaham[1], Yirgu Yilma[2], Guy-Vincent Jourdan[1], and Matthew Bromwich[3]**
[1] School of Electrical Engineering and Computer Science, University of Ottawa, 800 King Edward av, ON, Canada, K1N6N5
[2] Epsidon Inc., 36 David dr, Ottawa, ON, Canada, K2G2N1
[3] Div. of Pediatric Otol. Head & Neck Surgery, Children's Hospital of Eastern Ontario, 401 Smyth rd, ON, Canada, K1H8L1
Email: nellaham@uottawa.ca, yyilma@gmail.com, gvj@site.uottawa.ca, mbromwich@cheo.on.ca

## 1. INTRODUCTION

Hearing plays a critical role in the development of speech and communication skills in children **Error! Reference source not found.**. Undiagnosed hearing impairment in childhood interferes with normal social, emotional and cognitive development.**Error! Reference source not found.**. A battery of physiological and behavioural tests has been designed specifically for testing children for hearing loss. Physiological tests that measure auditory function include: tympanometry, acoustic reflexes, otoacoustic emissions, and auditory brainstem response. Behavioural tests achieve threshold measurements by observing the child's behaviour in response to sound stimuli. Such tests have been developed for different age groups and include: behavioural observation audiometry (BOA, zero to five months), visual reinforcement audiometry (VRA, six months to two years), conditioned play audiometry (CPA, two to five years) as well as conventional audiometry (five years and over) **Error! Reference source not found.**.

Conditioned play audiometry is a standard way to test the hearing of children who are still too young for a convention audiometry test. During CPA testing, instead of simply raising one's hand in response to a sound, the child is engaged in a listening game: for example, hold a toy and wait for the sound, then drop the toy in a bucket when the sound is heard. The game is intended to keep the child interested in the listening task for the duration of the test. A CPA test consists of a familiarization phase followed by the actual hearing test. During the first phase, the audiologist or operator running the test establishes the child's interest in the game by teaching them how to play, and offering praise and rewards to reinforce correct responses. CPA tests are ideally conducted with the child (and possibly the parent) seated in a sound booth. However, screening tests using CPA are often performed in pre-schools, in a relatively quiet room, in order to identify children at risk of hearing loss.

Apple's iPad, and other tablet platforms in general, present a valuable medium to perform interactive tasks such as CPA. The iPad has quickly become a popular toy among children. The intuitive nature of the interaction with the iPad enables children as young as 2 years old to tap, swipe, draw, play and learn using an array of apps. In addition, there are now several apps that perform hearing tests using standard pure-tone audiometry.

In this work, we present a new app developed for the iPad to perform CPA as a hearing loss screening tool for pre-school children, ages 3 to 5. To the best of our knowledge, no app exists at the time of this writing, which is dedicated to the target age-group for CPA. The remainder of this article will give an overview of the system and discuss important considerations relevant to the design and use of the app.

## 2. APPLICATION OVERVIEW

### 2.1. Design and usage specifications

The app aims to engage children in game play where calibrated audio cues are essential to the interaction. As such, the app creates a virtual CPA test. In the familiarization phase, the child is taught to play an interactive listening game that involves touching items on the iPad screen that make sound. This phase can continue until the child understands the task and develops an interest in the game. During the testing phase the child plays the same game, while carefully-chosen sound stimuli are used to determine the hearing thresholds at four audiometric frequencies: 500, 1000, 2000, and 4000 Hz. For each frequency, the stimulus is presented at decreasing sound levels, until the child is no longer able to detect sound when touching the iPad screen, indicating that the hearing threshold at that specific frequency was reached.

In its first iteration, the app has been developed to conduct CPA screening in free-field environments. Audiometric tests are usually conducted with sound stimuli presented through earphones to obtain ear-specific information. For infants and young children who may not tolerate earphones, it is often more suitable to conduct tests using loudspeakers (free-field audiometry). However, aside from lacking ear-specificity, free-field audiometry presents other limitations imposed by room acoustics, background noise, listener head movement, and the type of sound stimulus used. Therefore, using the app for screening purposes requires an awareness of these limitations as outlined by the American Speech-Language Hearing Association (ASHA) [4]. For example, when access to a sound booth is not available, care must be taken in choosing the room where the screening is conducted; setting up the loudspeakers and listener locations. The app has been designed with these considerations in mind (cf. Section 3).

### 2.2. Screening results

The goal is to use the app as a screening tool, and not as a complete hearing assessment tool. Therefore, the final aim

is not a precise audiogram but a pass-refer decision. Once all four audiometric frequencies have been tested, the thresholds measured at each frequency in free field represent the child's binaural hearing thresholds. Along with the thresholds, the app also indicates the level of the ambient noise during the test. The app, therefore, assists the operator in determining the validity of the test. Children with elevated thresholds can then be referred to a specialist.

## 3. DESIGN CONSIDERATIONS

### 3.1. Free-field considerations

Under earphone listening conditions, audiometric tests are performed using pure tone signals. In free field, these signals create standing waves which result in a non-uniform sound intensity across the sound field. This, coupled with unpredictable listener movements, makes pure tone signals not suitable for use in this app. The ASHA guidelines [4] recommend using frequency-modulated (FM) tones with carrier frequency, modulation rate and bandwidth detailed by Walker (1984) [5]. Particularly, specifications for wide bandwidth were chosen for the stimuli used in this app, thus favouring sound-field uniformity over audiometric accuracy.

The app also provides a means to monitor the background noise in the room using an external microphone (the use of the iPad's internal microphone was avoided since it is more susceptible to disturbance from the child's body movement and touching the iPad screen). Monitoring the background noise during the screening test is important in free-field measurements, especially when dealing with (potentially noisy) young children.

### 3.2. Technical limitations of the iPad

The iPad houses a built-in speaker and microphone. A headset, including an earphone and microphone, is available as an accessory (and is also included with the iPhone). The popular headset connects to the audio port through a TRRS connector, and the microphone's flat frequency response makes it suitable for high-quality sound recordings. For this app, using the external microphone to monitor background noise and the built-in speakers to play sounds would be an appropriate scenario. In the Cocoa framework, the Audio Toolbox application programming interface (API), used to read and write audio, provides a means for redirecting audio routes to select either the built-in microphone and speaker, or the external headset. The API, however, does not permit using the built-in route for output and the external route for input. One solution consists of using third-party accessories, like TouchMic's Handsfree Lapel Microphone & Adapter, to connect an external microphone and loudspeakers to the audio port. An added benefit of this solution is the ability to move the loudspeakers around to make optimal use of the room acoustics. It is however possible to use an external USB microphone with the built-in speaker using an iPad USB adaptor.

### 3.3. Device calibration

Calibrating an audio system is essential before it is used to perform any scientific measurement and is recommended to be done periodically. The calibration of an audiometric system requires the use of expensive sound level meters and octave band analyzers and should be performed under the same acoustic conditions in which the device is used during measurements [6]. Since the aim of this work, is precisely to produce a portable system (iPad with the loudspeakers and microphone) for use where such equipment is not available, the app provides a means to carry out a two-step calibration. First, a standard "absolute calibration" is performed in which the system is calibrated in a controlled acoustical environment to conduct free-field measurements at each of the four audiometric frequencies used. The next step is an "on-site calibration" performed at the site where screening will take place, with the loudspeakers set up in position and the microphone placed where the subject's head would be. In this step the app auto-calibrates for each frequency at different presentation levels: for each level, the app plays the FM tones and adjusts the output signal level such that the microphone reading corresponds to the intended level.

## 4. SUMMARY

This paper presented a new app developed for the iPad platform to perform CPA tests for screening pre-school children for potential hearing loss. The app is intended for use in free-field environments where access to sound booths and elaborate equipment is not available. Equipment and environment limitations were discussed along with elegant solutions. A means of calibrating the system in two stages is also provided. A prototype of the app has been developed and is presently being tested in trials at the Division of Pediatric Otolaryngology, Head and Neck Surgery at the Children's Hospital of Eastern Ontario.

## REFERENCES


[1] Canadian Association of Speech-Language Pathologists and Audiologists (2000), "Hearing health for children: Fact sheet", available from: http://www.speechandhearing.ca/files/children_hearing_fact_sheet.pdf. Accessed: July, 21, 2011.

[2] American Speech-Language-Hearing Association (1997), "Guidelines for Audiologic Screening" [Guidelines], available from: www.asha.org/policy. Accessed: July, 21, 2011

[3] Buttross, S.L., Gearhart, J.G., and Peck, J.E. (1995), "Early identification and management of hearing impairment", American Family Physician, 51(6), 1437–1447.

[4] American Speech-Language-Hearing Association (1991), "Sound Field Measurement Tutorial" [Relevant Paper], available from: www.asha.org/policy. Accessed: July, 21, 2011

[5] Walker G., Dillon H. and Byrne D. (1984), "Sound field audiometry: Recommended stimuli and procedures", Ear and Hearing, 5, 13–21.

[6] American National Standards Institute (1996), *Specification for audiometers* (ANSI S3.6-1996 (R2004)), New York: Acoustical Society of America.

# VERY-LOW-FREQUENCY EVANESCENT LIQUID PRESSURE WAVES

**Reinhart Frosch**
Sommerhaldenstrasse 5B, CH-5200 Brugg, Switzerland; reinifrosch@bluewin.ch
PSI (Paul Scherrer Institute), Villigen and ETH (Eidgenoessische Technische Hochschule), Zurich (retired)

## 1. INTRODUCTION

Evanescent liquid sound-pressure waves are standing waves of limited spatial extension. These waves involve variable pressure and liquid-particle velocity but negligible liquid-density variation; they are predicted to occur also in strictly ideal (incompressible, non-viscous) liquids. The free-oscillation frequency reduction observed if resonators (e.g., tuning forks or drinking glasses tapped with spoons) are submerged in water has been shown to be predominantly due to the kinetic energy of the evanescent liquid sound-pressure waves generated by the resonators [e.g., Frosch (2010a, 2010b)]. Such waves are conjectured to occur also, in the cochlear liquid, during spontaneous oto-acoustic emissions [Frosch (2011a, 2011b)]. These spring-driven waves are similar to certain low-frequency evanescent liquid pressure waves, namely to standing water surface waves in cubic vessels. Such gravity-driven waves are discussed, e.g., in Sinick and Lynch (2010) and in Chapter IX of Lamb (1895). The present note is intended to show that classroom demonstrations of these latter waves can provide a plausible introduction to the subject of spring-driven evanescent liquid sound-pressure waves.

## 2. THEORY OF STANDING LIQUID SURFACE WAVES

### 2.1. Gravity-driven waves

A possible gravity-driven *travelling* liquid surface wave in an infinitely long wave channel of $x$-independent width and height is defined by the following equations [e.g., Frosch (2010a)]:

$$\xi(x,z,t) = \zeta_m \cdot \frac{\cosh(kz)}{\sinh(kH)} \cdot \sin(\omega t - kx); \qquad (1)$$

$$\zeta(x,z,t) = \zeta_m \cdot \frac{\sinh(kz)}{\sinh(kH)} \cdot \cos(\omega t - kx). \qquad (2)$$

In Eqs. (1,2), $\xi$ and $\zeta$ are the $x$- and $z$-components of the displacement of the considered liquid particle from its no-wave place $(x,z)$. A liquid particle can be defined to consist of the water molecules that occupy, at time $t = 0$, a given cubic millimetre. Since thermal motion and diffusion of the molecules are neglected, in the no-wave state the liquid particle is concluded to keep its initial place and shape. The quantity $k$ in Eqs. (1,2) is the wave number [$k = 2\pi/\lambda$; $\lambda$ = wavelength]; $H$ is the water depth; at the channel floor, the vertical coordinate $z$ equals zero; $\omega = 2\pi f$ is the angular wave frequency. Eqs. (1,2) are based on the small-displacement approximation, i.e., $\zeta_m$ is assumed to be small compared to $\lambda$. As shown, e.g., in Frosch (2010a) and in the references quoted there, $\omega$ and $k$ are related as follows:

$$\omega^2 = g \cdot k \cdot \tanh(kH). \qquad (3)$$

The quantity $g = 9.81\ \mathrm{m/s^2}$ is the free-fall acceleration. Eqs. (1,2) imply that the involved water particles move on closed elliptical trajectories. At the channel floor ($z = 0$), the width of these ellipses vanishes.

A *standing* liquid surface wave results if a wave according to Eqs. (1,2) and a similar wave, obtained by the replacement of $\omega t$ by $(\pi - \omega t)$, are superimposed:

$$\xi(x,z,t) = 2\zeta_m \cdot \frac{\cosh(kz)}{\sinh(kH)} \cdot \cos(kx) \cdot \sin(\omega t); \qquad (4)$$

$$\zeta(x,z,t) = 2\zeta_m \cdot \frac{\sinh(kz)}{\sinh(kH)} \cdot \sin(kx) \cdot \sin(\omega t). \qquad (5)$$

The liquid particles involved in the standing wave defined by Eqs. (4,5) move back and forth on linear trajectories. The corresponding "sound pressure" $p$, i.e., the deviation of the liquid pressure from its no-wave value, can be derived from Eqs. (4,5) via the small-displacement version of Newton's second law,

$$\rho \cdot (\partial \vec{v} / \partial t) = -\vec{\nabla} p. \qquad (6)$$

Here, $\rho = 1000\ \mathrm{kg/m^3}$ is the water density, and $\vec{v}$ is the liquid particle velocity, having the components $\partial\xi/\partial t$ and $\partial\zeta/\partial t$. Resulting sound-pressure formula:

$$p = a_p \cdot \sin(\omega t); \quad a_p = a_{p0} \cdot \frac{\cosh(kz)}{\cosh(kH)} \cdot \sin(kx) \cdot \qquad (7)$$

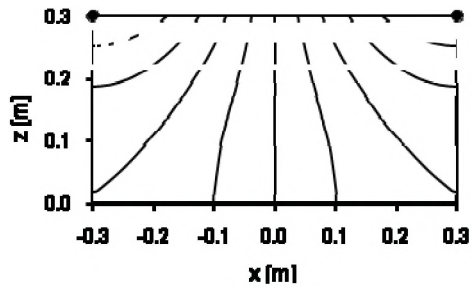


**Figure 1. Constant-$a_p$ lines, $a_p/a_{p0} = \pm 0.8, \pm 0.6, \pm 0.4, \pm 0.2, 0.0$, according to Eq. (7); $a_{p0}$ is defined in Eq. (8); at the two filled circles, $a_p$ equals $\pm\, a_{p0}$; $H = 0.3$ m; $\lambda = 2\pi/k = 1.2$ m.**

In Eq. (7), the quantity

$$a_{p0} = 2\zeta_m \cdot \rho \cdot \omega^2 / [k \cdot \tanh(kH)] = 2\zeta_m \cdot \rho \cdot g \qquad (8)$$

is a pressure constant. Eqs. (4,5) are consistent with time-independent *streamlines* [along which the liquid particles oscillate linearly; e.g., Frosch (2010a)]:

$$\frac{n}{N} = \frac{\sinh(kz)}{\sinh(kH)} \cdot \cos(kx). \qquad (9)$$

In Eq. (9), $n$ = 1, 2, … , $N$ is the running number of the streamlines; see Fig. 2.

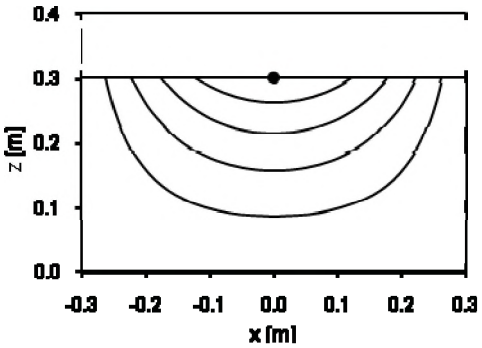


**Figure 2. Streamlines according to Eqs. (4,5,9), for $N$ = 5, at time $t$ = 0.**

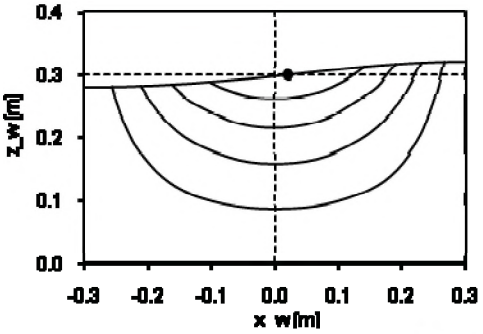


**Figure 3. Same as Fig. 2, at time $t = \pi/(2\omega)$; $\zeta_m$ = 1 cm.**

In Fig. 2 (valid at time $t$ = 0), the no-wave places $x,z$ of certain liquid particles are shown, namely of those at the surface and on the streamlines defined by Eq. (9). In Fig. 3 the with-wave places $x_w = x + \xi$, $z_w = z + \zeta$ of the same liquid particles at time $t = T/4$ (where $T=2\pi/\omega$) are shown.

The water cross section in Fig. 3 is slightly smaller than that in Fig. 2, in contradiction to the assumed incompressibility of the liquid. That inaccuracy occurs because the small-displacement approximation has been used.

### 2.2. Spring-driven waves

Eqs. (1,2,4,5,6,7,9) are valid also for surface waves in a box model of the cochlear channel with $x$-independent properties [Frosch (2010a)]. In that case, gravity is negligible; the waves are spring-driven by the basilar-membrane (BM) elements. Eqs, (3,8) must be replaced as follows:

$$\omega^2 = S/\{M + 2\rho/[k \cdot \tanh(kH)]\}; \qquad (10)$$

$$a_{p0} = \zeta_m \cdot S/\{1 + [Mk/(2\rho)] \cdot \tanh(kH)\}; \qquad (11)$$

$S$ is the BM stiffness (spring constant per surface unit, N/m$^3$), and $M$ is the BM surface mass density (kg/m$^2$).

Eqs. (10,11) hold for a box model of the cochlear channel with liquid both below and above the basilar membrane.

## 3. EXPERIMENTS

For a standing wave in a water-filled vessel as shown in Figs. 1-3, the wave length is $\lambda$ = 1.2 m, and the corresponding wave number is $k \approx 5.236$ m$^{-1}$. Eq. (3) yields a frequency of $f \approx 1.09$ s$^{-1}$, so that this oscillation has indeed a very low frequency and is therefore easy to observe. If one throws visible particles having a density about equal to that of water into a vessel equal or similar to that shown in Figs. 1-3, then one can observe, e.g., that the oscillation amplitude at the floor is much smaller than that at the surface. For $\zeta_m$ = 1.0 cm, Eqs. (4,5) yield the following amplitudes:

$\zeta$(0.3m,0.3m,$T$/4) = 2.0 cm;

$\xi$(0.0m,0.3m, $T$/4) ≈ 2.18 cm;

$\xi$(0.0m,0.0m, $T$/4) ≈ 0.87 cm;

$\xi$(0.3m,0.0m, $T$/4) = $\zeta$(0.3m,0.0m,$T$/4) = 0.

Sinick and Lynch (2010) have described how, with Styrofoam strips, one can excite not only the fundamental oscillation mode (having one node, as shown in our Fig. 3), but also three higher modes (with two, three, or four nodes).

## 4. CONCLUDING REMARKS

It is justifiable to designate the waves described in Section 2.1 as "evanescent" because of the just mentioned smallness of the oscillation amplitude at the floor, and also because of their similarity to the evanescent waves near submerged resonators. In both cases, standing waves with linear oscillations of liquid particles along time-independent streamlines are generated.

## REFERENCES


Frosch, R. (2010a). Introduction to Cochlear Waves. vdf, Zurich, pp. 257-279, 301-302, 423-426.

Frosch, R. (2010b). Evanescent Liquid Sound-Pressure Waves Near Underwater Resonators, Canadian Acoustics Vol. 38 No. 3 (2010) 62-63.

Frosch, R. (2011a). Cochlear evanescent liquid sound-pressure waves near localized oscillations of the basilar membrane. In: Proceedings of Forum Acusticum 2011, Aalborg, Denmark, pp. 1241-1246.

Frosch, R. (2011b). Cochlear Evanescent Liquid Sound-Pressure Waves During Spontaneous Oto-Acoustic Emissions. Contribution to this conference.

Lamb, H. (1895). Hydrodynamics. Cambridge University Press.

Sinick, S.J., Lynch, J.J. Surface Gravity Waves: Resonance in a Fish Tank. The Physics Teacher 48 (2010) 330-332.

# COCHLEAR EVANESCENT LIQUID SOUND-PRESSURE WAVES DURING SPONTANEOUS OTO-ACOUSTIC EMISSIONS

**Reinhart Frosch**
Sommerhaldenstrasse 5B, CH-5200 Brugg, Switzerland; reinifrosch@bluewin.ch
PSI (Paul Scherrer Institute), Villigen and ETH (Eidgenoessische Technische Hochschule), Zurich (retired)

## 1. INTRODUCTION

In the diagram on the left in Fig. 1, the streamlines of an evanescent (standing) liquid sound-pressure wave generated by a miniaturized and idealized underwater tuning-fork prong are shown [Frosch (2010a, 2010b)]. The prong is assumed to oscillate in the $z_r$-direction. Liquid particles having a no-wave location on one of these streamlines stay on that line during their oscillation. In the diagram on the right in Fig. 1, the corresponding lines of constant liquid sound-pressure amplitude are displayed; see Section 2.1.

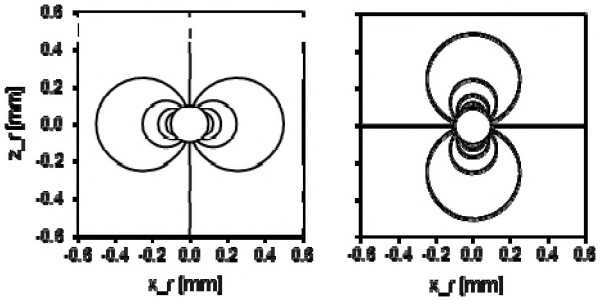


**Figure 1. Underwater mini-tuning-fork prong oscillating in the $z_r$-direction. Left: streamlines. Right: lines of constant liquid sound-pressure amplitude.**

In this study it is assumed that spontaneous oto-acoustic emissions (SOAEs) from the human inner ear [e.g., Frosch (2010a)] are generated, in a feedback process, by outer-hair-cell-driven localized oscillations of the basilar membrane (BM), and it is shown that a corresponding liquid motion above and below the BM of an idealized cochlear box model [cubic channel, $x$-independent properties] can be found by a superposition of three standing waves similar to that shown in Fig. 1, generated by a prong centred at $x_r = 0$ and by two prongs at $x_r = \pm a$, where typically $a = 0.01$ mm. It is assumed that at time $t = T/4$ (where $T$ = oscillation period) the central prong is at $z_r = +2\delta$ and the two lateral prongs are at $z_r = -\delta$; typically, $\delta = 0.1$ µm.

## 2. METHODS AND RESULTS

The liquid-particle oscillation amplitudes are small compared to the half-pressure distance of ~0.1 mm visible in Fig. 1. In the corresponding small-displacement approximation [see e.g. Frosch (2010a)] the sound-pressure $p$ and the liquid-particle velocity $v$ in a liquid of density $\rho$ and of negligible compressibility and viscosity obey Newton's second law in the form

$$\rho \cdot (\partial \vec{v} / \partial t) = -\vec{\nabla} p \,, \tag{1}$$

and, in the present two-dimensional case, the Laplace equation,

$$\partial^2 p / \partial x^2 + \partial^2 p / \partial y^2 = 0 \,. \tag{2}$$

A possible (standing-wave) solution for $p$ is:

$$p(x, y, t) = a_p(x, y) \cdot \sin(\omega \cdot t) \,, \tag{3}$$

where the angular frequency $\omega = 2\pi \cdot f$ is assumed to be constant. The real function $a_p(x, y)$ in Eq. (3) must fulfil the Laplace equation (2).

### 2.1. Oscillation of a "miniprong" according to Fig. 1

As explained e.g. in Frosch (2010b), the real and imaginary parts of the function $F(n_c) = n_c^{-1}$ (where $n_c = x_r + i \cdot z_r$) yield the circular streamlines and lines of constant sound-pressure amplitude shown in Fig. 1. Streamlines:

$$r = R \cdot (N / n) \cdot \cos(\varphi) \;; \tag{4}$$

$n = 0, \pm 1, \pm 2, \ldots, \pm N$ is the running number of the streamlines; in Fig. 1 $N = 5$ was chosen; $R = 0.1$ mm is the prong radius; $r$ and $\varphi$ are plane polar coordinates:

$$r = \sqrt{x_r^{\,2} + z_r^{\,2}} \,; \; \tan(\varphi) = z_r / x_r \,. \tag{5}$$

Lines of constant sound-pressure amplitude:

$$r = R \cdot (a_{p0} / a_p) \cdot \sin(\varphi) \;. \tag{6}$$

In Eq. (6), $a_{p0}$ is a pressure constant, and $a_p$ is defined by Eq. (3). The lines of constant liquid sound-pressure amplitude in Fig. 1 are for $a_p / a_{p0} = 0.0, \pm 0.2, \pm 0.4, \ldots, \pm 1.0$.

### 2.2. Localized oscillation of the basilar membrane

The superposition described in Section 1 yields the following liquid sound-pressure amplitude [Frosch (2011)]:

$$\frac{a_p}{a_{p0}} = \frac{-R \cdot z_r}{x_r^{\,2} + z_r^{\,2}} + \frac{0.5R \cdot z_r}{(x_r - a)^2 + z_r^{\,2}} + \frac{0.5R \cdot z_r}{(x_r + a)^2 + z_r^{\,2}} \,; \tag{7}$$

The corresponding streamlines are defined as follows:

$$\frac{q \cdot n}{N} = \frac{R \cdot x_r}{x_r^{\,2} + z_r^{\,2}} - \frac{0.5R \cdot (x_r - a)}{(x_r - a)^2 + z_r^{\,2}} - \frac{0.5R \cdot (x_r + a)}{(x_r + a)^2 + z_r^{\,2}} \,; \tag{8}$$

the number $q$ in Eq. (8) is the maximum of the expression on the right-hand side for $z_r = R$; for $R = 0.1$ mm and $a = 0.01$ mm one finds $q = 0.007224$; that maximum is located at $x_r = 41.7\,\mu$m; see Fig. 3.

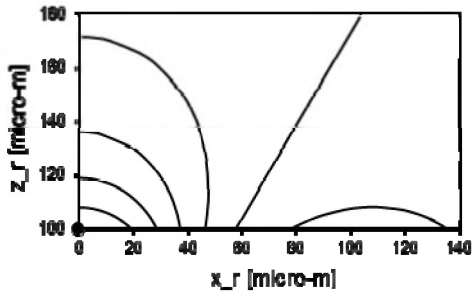


**Figure 2. Constant-pressure lines, $a_p/a_{pmin}$ = 0.8, 0.6, 0.4, 0.2, 0.0, –0.2, according to Eq. (7); $a_{pmin}$ is the value of $a_p$ at $x_r = 0$, $z_r = R = 0.1$ mm; the BM is at $z_r = R$.**

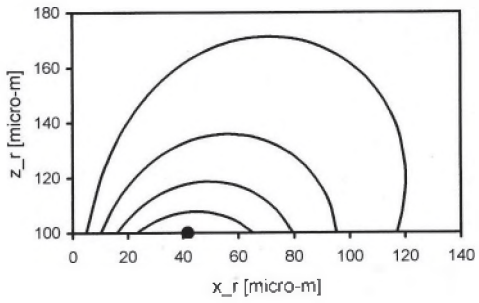


**Figure 3. Streamlines according to Eq. (8), for $N = 5$.**

The BM is assumed to have a negligible thickness and to be located at $z_r = R = 0.1$ mm In the case of both Fig. 2 and Fig. 3, the patterns at $z_r < R$ (below the BM) and at $x_r < 0$ are mirror images of those shown.

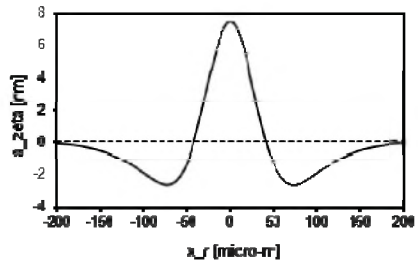


**Figure 4. Shape of the basilar membrane at time $t = T/4$, according to Eqs. (1,3,7); $z_r = R = 100$ µm; $a_{p0} = 1$ Pa; oscillation frequency $f = 1$ kHz; liquid density 1 g/cm$^3$.**

The amplitudes of the $z$-components $\zeta = a_\zeta \cdot \sin(\omega t)$ of the displacements of the liquid particles in Figs. 2 and 3 from their no-wave locations $x_r$, $z_r$, according to Eqs. (1), (3), and (7), are given by Eq. (25) of Frosch (2011). The corresponding shape of the BM at time $t = T/4$ is shown in Fig. 4.

## 3. DISCUSSION AND CONCLUSIONS

The evanescent (standing) liquid sound-pressure wave described in Section 2.2 fulfils the Laplace equation. It is however incompatible with Newton's second law (force = mass × acceleration) applied to the friction-less passive basilar-membrane (BM) elements of a cochlear box model [Frosch (2010a)] with $x$-independent BM stiffness $S$ and BM surface mass density $M$, and with negligible direct mechanical coupling of the BM elements. That disagreement can be corrected by introduction of a periodic force exerted on the BM by active outer hair cells (OHCs). In the present frictionless case, the OHC force must be proportional to $\sin(\omega t)$. In Fig. 5, the amplitude of the required force on a BM element of $5 \times 300\,\mu\text{m}^2$, centred at $x_r$, is shown versus $x_r$ for three different values of the assumed BM stiffness.

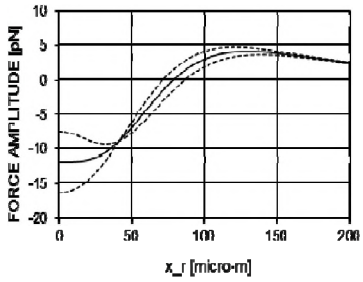


**Figure 5. Active-outer-hair-cell force amplitude required by Newton's law (see text). Curves starting at –16.4, –12.0, and –7.6 pN are for $S / S_{res} = 1.3$, 1.4, and 1.5.**

The quantity $S_{res}$ in the caption of Fig. 5 is the without-liquid BM resonance stiffness, $S_{res} = \omega^2 \cdot M$; e.g., if $S = 1.4 S_{res}$ (solid curve in Fig. 5), then for the parameters in the caption of Fig. 4 and for $M = 0.1\,\text{kg/m}^2$, $t = T/4$, $x_r = 0$, the forces due to the BM stiffness, the liquid-pressure difference across the BM, and the active OHCs amount to –62.0, +29.7, and –12.0 pN. The resultant force, –44.3 pN, agrees with the downwards acceleration of the considered BM element. If both the liquid and the OHC force were removed, then the BM free-oscillation frequency in that box model with stiffness $S = 1.4 S_{res}$ would be $\sqrt{1.4} \cdot 1\,\text{kHz} = 1.18$ kHz, higher than 1 kHz by about 0.24 octave.

In the real cochlea, "slow" travelling surface waves of given frequency [Frosch (2010a)] are impossible at the without-liquid BM resonance place for that frequency, but are possible at the corresponding with-liquid resonance place, which is more basal by typically 0.24 octave distance, i.e., by about 1.1 mm. From that place, the with-liquid BM oscillations conjectured to occur during spontaneous oto-acoustic emissions could be efficiently carried, by such slow cochlear travelling waves, to the cochlear base (oval window, stapes) and then propagate to the ear canal.

## REFERENCES

Frosch, R. (2010a). Introduction to Cochlear Waves. vdf, Zurich, pp. 257-279, 301-302, 423-426.

Frosch, R. (2010b). Evanescent Liquid Sound-Pressure Waves Near Underwater Resonators, Canadian Acoustics Vol. 38 No. 3 (2010) 62-63.

Frosch, R. (2011). Cochlear evanescent liquid sound-pressure waves near localized oscillations of the basilar membrane. In: Proceedings of Forum Acusticum 2011, Aalborg, Denmark, pp. 1241-1246.

# MOVING TO THE BEAT IMPROVES TIMEKEEPING IN A RHYTHM PERCEPTION TASK

**Fiona C. Manning, and Michael Schutz**
McMaster Institute for Music and the Mind, McMaster University, Hamilton, ON Canada

## 1. INTRODUCTION

The relationship between perception and action is of recent interest in psychological research (Hommel, Musseler, Aschersleben, & Prinz, 2001), and particularly in music perception (Phillips-Silver & Trainor, 2005; Repp & Knoblich, 2007; Zatorre, Chen, & Penhune, 2007). We explored this issue through a novel paradigm designed to measure the effect of "moving to the beat" when listening to an auditory rhythm. Specifically, we investigated the effect of tapping on participants' sensitivity to changes in the temporal location of a probe tone. In doing so, we have documented a novel perception-action link by showing the importance of moving when timekeeping while performing an objective task, using participants selected without regard for musical training.

## 2. EXPERIMENT 1

### 2.1 Method

The experiment was conducted using a customized program design by the MAPLE lab at McMaster University. Tones were presented to participants through headphones and participants tapped on an electronic drum pad. Each trial consisted of fourteen tones divided into groups of four, occurring in a repeating pattern (Figure 1). The first tone of each grouped pattern was "accented" using a higher relative pitch (C5; ~523Hz) than the unaccented tones (G4; ~392Hz). In the last group, the 2nd, 3rd and 4th tones were silent. The four groups were followed by a final probe tone. In half of the trials the probe tone was consistent with the pattern (offset = 0ms), and in the other half of the trials the probe tone was inconsistent with the pattern at one of four offset positions; 30% of the inter-onset interval (IOI) early or late, or 15% of the IOI early or late. The pattern of tones was presented at two different IOIs; 400ms and 600ms.

During the experiment, participants were presented with a total of 64 trials; eight blocks each containing eight trials. Half of the blocks employed an IOI of 400ms and the other half employed an IOI of 600ms. Within the four blocks of each IOI, participants were asked to tap along to two of the blocks ("tapping" condition) and asked to not tap during the other half of the blocks ("non-tapping" condition). Within each block, four of the trials included a final probe tone that occurred at the "correct" time (i.e., an offset of 0ms), and four of the trials the probe tone occurred at the "incorrect" time; 15% or 30% of the IOI early, or 15% or 30% of the IOI late. Participants were presented with each of the four IOI (400ms, 600ms) X Tap condition ("tapping" or "non-tapping") combinations twice to make a total of eight experimental blocks. The order of the experimental blocks and the order of the trials within each block of the experiment were also randomized for each participant.

During "tapping" blocks, participants tapped on a drum pad using a drumstick for all beats including the probe tone. During the "non-tapping" blocks, participants were instructed to remain as still as possible. For each block, participants were asked to judge whether the final probe tone was "on-time" (i.e., positioned on a down-beat).

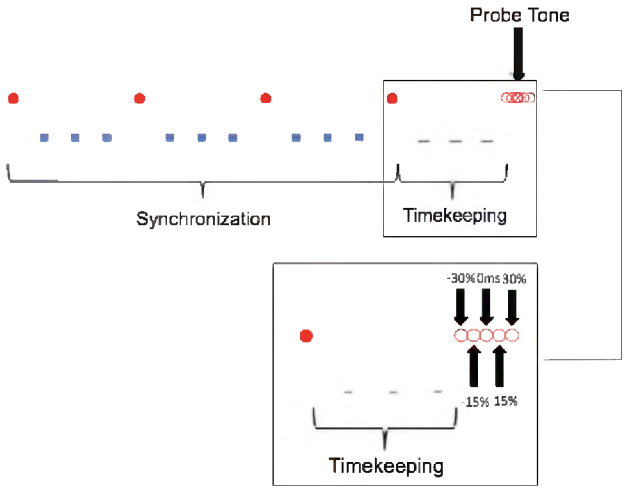


**Figure 1. One trial with synchronization and timekeeping periods labeled.**

Participants included 48 undergraduate students (32 females), ranging in age from 17 to 35 years ($M$ = 18.6 years, $SD$ = 2.65), from the undergraduate psychology participant pool. Participants reported normal hearing and normal or corrected-to-normal vision. All participants gave informed consent and were remunerated with course credit for their participation.

### 2.2 Results

The proportion of correct responses on perceptual timing judgments was generated by taking an average of the percentage of responses that were correct. These scores were assessed using a 2(IOI) X 5(offset) X 2(tap-instruction) repeated-measures ANOVA.

As expected, there was a main effect of offset ($F_{4,188}$ = 48.656, $p$ < 0.0001), indicating that participants were sensitive to the timing of the probe-tone. However, the most important finding was a main effect of tapping ($F_{1,47}$ =

25.178, $p < 0.0001$), reflecting a difference in task performance between the with-tap and without-tap conditions. Additionally, a two-way interaction was observed between tap-instruction and offset ($F_{4,156} = 13.882$, $p < 0.0001$), indicating that tapping affected responses differently at different probe-tone locations (Figure 2).

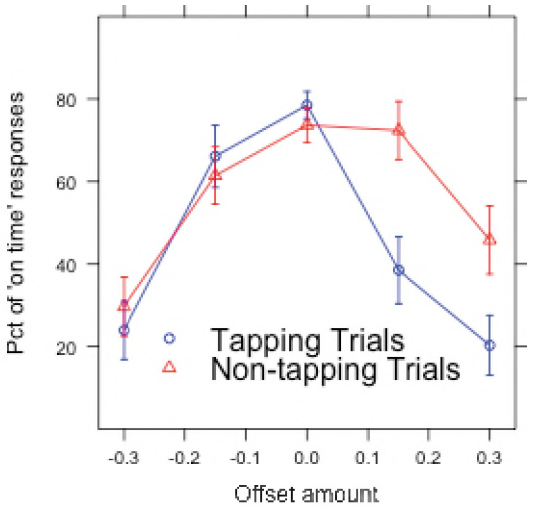


**Figure 2. The proportion of responses indicating an "on-time" probe tone in experiment 1. Error bars indicate a 95% CI.**

## 3. EXPERIMENT 2

Experiment 1 demonstrated a clear effect of tapping on task performance. Experiment 2 extended that work by exploring the segment of the tapping (i.e., synchronization vs. timekeeping) driving this effect.

### 3.1 Method

Experiment 2 differed from Experiment 1 only with respect to the instructions during the "tapping" blocks. Here, participants were instructed to tap for only the sounded beats (i.e., the synchronization measures and the probe tone) and to remain still for the "silent" beats – a.k.a. the timekeeping measure (see Figure 1 for details).

Participants included 49 undergraduate students (36 females), ranging in age from 17 to 24 years ($M$ = 18.7 years, $SD$ = 1.15), from the undergraduate psychology participant pool. Participants reported normal hearing and normal or corrected-to-normal vision.

### 3.2 Results

Once again, there was a main effect of offset ($F_{4,192}$ = 14.014, $p < 0.0001$), participants were sensitive to the location of the probe tone. However, the most important finding was the lack of a main effect of tapping ($F_{1,48}$ = 1.799, $p$ = 0.186), indicating no significant difference between performance during the tapping and non-tapping trials. Therefore, movement appears to affect responses only when it occurs during the timekeeping phase.

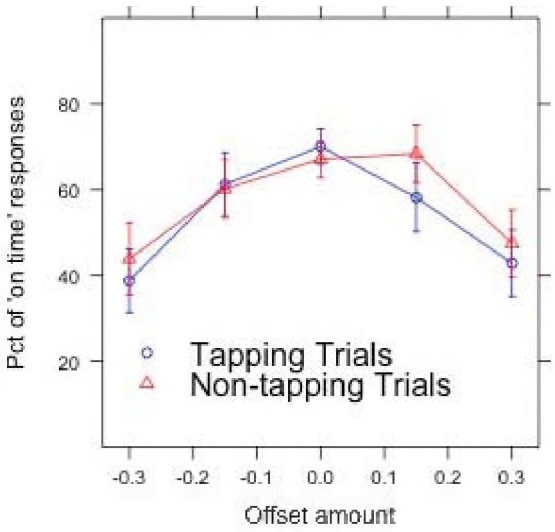


**Figure 3. The proportion of responses indicating an "on-time" probe tone in experiment 2. Error bars indicate a 95% CI.**

## 4. DISCUSSION

Experiment 1 demonstrates that tapping affects participants' ability to detect timing variations in the location of a final probe tone. This effect was eliminated when movement during the timekeeping (silent) measure was omitted in Experiment 2. Together, these experiments show that moving along to a perceived beat improves timekeeping in the absence of an external signal.

The effect of movement on rhythm perception is consistent with previous work showing that movement can affect the perception of metrically ambiguous stimuli (Phillips-Silver & Trainor, 2005). Therefore these results also add to the growing literature on the role of timing in perception (Repp, 2002), as well sensorimotor interactions in music perception and performance (Zatorre et al., 2007). Our data suggest that rhythmic movement may act as a surrogate for timekeeping in rhythmic music, an issue of great practical importance for music performers and listeners alike.

## REFERENCES


Aschersleben, G. (2002). *Brain and Cognition*

Hommel, B., Musseler, J., Aschersleben, G., & Prinz, W. (2001). *Behavioral and Brain Sciences*

Phillips-Silver, J., & Trainor, L. J. (2005). *Science*

Repp, B. H., & Knoblich, G. (2007). *Psychological Science*

Zatorre, R. J., Chen, J. L., & Penhume, V. B. (2007). *Nature Reviews Neuroscience*


## ACKNOWLEDGMENTS


This work was supported in part through grants from the Natural Sciences and Engineering Research Council - RGPIN/386603-2010, and the Early Researcher Award - ER10-07-195 (Michael Schutz, PI), as well as the National Institutes of Health - 1R03 PAR-07-287 (Laura Silverman, PI).

# ON THE EXTRACTION OF EXCITATION FROM A PLUCKED STRING SOUND IN TIME DOMAIN

**Jung Suk Lee, Philippe Depalle, and Gary P. Scavone**
Music Technology Area, Centre for Interdisciplinary Research in Music Media and Technology (CIRMMT),
Schulich of School of Music of McGill University, 555 Sherbrooke Street West, Montreal, Quebec H3A 1E3, Canada
jungsuk.lee@mail.mcgill.ca, depalle@music.mcgill.ca, gary.scavone@mcgill.ca

## 1. INTRODUCTION

Since the emergence of the concept of physical modeling synthesis, plucked strings have been one of the major applications. The sound quality of plucked-string physical models is often highly dependent on the excitation model, or the way that energy is input into the system. The first quasi-physical model of plucked strings was presented by Karplus and Strong (Karplus and Strong, 1983) and used a noise signal as a pluck excitation. A series of works (Välimäki *et al.*, 1996, Erkut *et al.*, 2000) addressed the extraction of the pluck excitation using more advanced physical models, such as digital waveguides (DW) (Smith, 1992) and a single delay loop (SDL) model (Karjalinen *et al.*, 1998). In this paper, we propose a simple but physically intuitive method to extract the excitation signal from a plucked string signal in the time domain. By observing the behavior of the traveling wave components in the given plucked string sound signal and comparing that to a DW simulation, the pluck excitation is 'visually' identified and extracted simply by time windowing.

## 2. TIME DOMAIN PROFILE OF A PLUCKED STRING SOUND

### 2.1 Plucked string signal

In order to observe the motion of a string when plucked, a string of an electric guitar is plucked and the output signal from an electromagnetic pickup is recorded using a high impedance port of an audio interface. As both terminations of an electric guitar string are almost ideally rigid, especially compared to an acoustic guitar, a signal captured by the electromagnetic pickup mounted on the electric guitar is preferred to a signal of acoustic guitar string recorded by a microphone. Figure 1 shows an example of the recorded signal, $y(n)$. To obtain $y(n)$, the middle (approximately 32.4cm away from the bridge, at the 12th fret) of the lowest E string of length 64.8cm is plucked by a plectrum and the front pickup (the one closest to the nut) is chosen to capture the signal. The distance between the bridge and the front pickup is 16cm and the sampling frequency $f_s$ is 44100 Hz. The fundamental frequency $f_0$ of $y(n)$ is 83Hz, estimated simply by referring to the spectrum and the autocorrelation of $y(n)$.

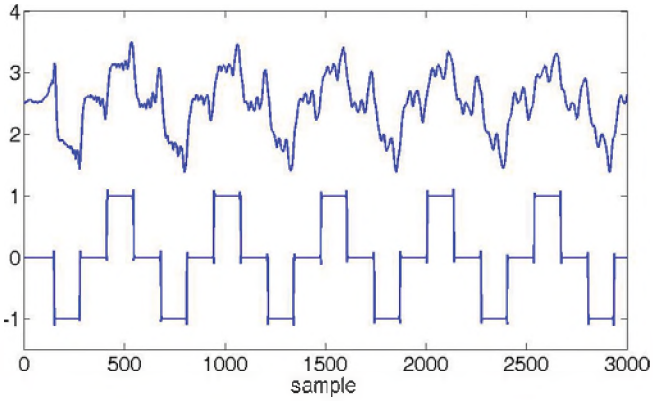


**Figure 1. Top : A plucked string sound signal of an electric guitar $y(n)$; Bottom : DW simulation of the plucked string sound, $v_{Lp}$.**

### 2.2 DW simulation of a plucked string

A DW simulation of $y(n)$ is carried out for comparison to the recorded $y(n)$. Figure 2 illustrates the DW model used for this simulation (Karjalinen *et al.*, 1998). The length of a delay line $L$ is $f_s/2f_0$ = 265.6 samples. The pickup position $L_P$ can be calculated by subtracting the number of delays representing the distance between the bridge and the pickup from $L$. Thus $L_P$ becomes $L$-16×266/64.8= 200.3210. Fifth-order Lagrange interpolation is employed to deal with fractional delays. For simplicity, $R_b(z)$ and $R_f(z)$ are assumed to be -1, only functioning as phase inverters. Acceleration wave variables are simulated in the DW system because an ideal pluck corresponds to an acceleration impulse. $I(z)$, the first-order integrator defined as $1/(1-z^{-1})$, accounts for the characteristic of an electromagnetic pickup which detects the velocity wave (actually, change in the magnetic flux). Thus, to obtain the impulse response of the model, $a(n)$, the input acceleration, is set to -1, assuming a downward pick direction. $a(n)$ is then equally split to $a_1(n)$ and $a_2(n)$ ($a(n) = 0.5a_1(n) + 0.5a_2(n)$, $a_1(n) = a_2(n)$) and fed into each delay line as shown in Figure 2. Then, $a_{Lp}(n)$ in Figure 2 is a sum of $a_{1,Lp}(n)$ and $a_{2,Lp}(n)$ that goes into the pickup.

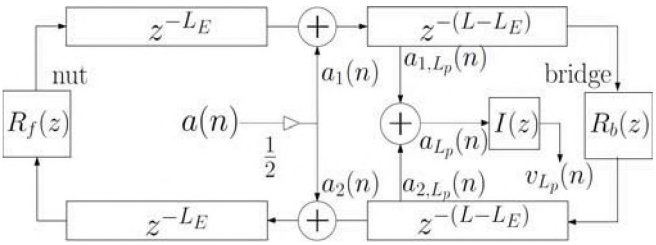


**Figure 2. DW pluck string model**

## 3. EXCITATION EXTRACTION IN TIME DOMAIN

In Figure 1, the impulse response of the DW model $v_{Lp}(n)$ and the recorded signal $y(n)$ are depicted together for comparison. We are able to note the similarity in the time evolution of the 'bump' patterns in both $y(n)$ and $v_{Lp}(n)$. The phases of bumps in $y(n)$ and $v_{Lp}(n)$ vary in the same manner. However, the signal we actually see in $y(n)$ is in the velocity dimension as the pickup functions as an integrator. Thus considering that the excitation we wish to extract from $y(n)$ is in the acceleration dimension, we need to differentiate $y(n)$ to $y'(n)$ for comparison to $a_{Lp}(n)$. Figure 3 shows $y'(n)$ and $a_{Lp}(n)$ together. The signal phase, or reflection, characteristics of $y'(n)$ and $a_{Lp}(n)$ vary in a similar manner over time. This suggests that the excitation signal actually travels on the string in the same way that the impulse does in the DW simulation. Therefore, by carefully taking a look at both signals, we notice that the portion under the arrow in $y'(n)$ in Figure 3 corresponds to the first impulse in $a_{Lp}(n)$. If we assume that the duration of the pluck excitation used to generate $y(n)$ is shorter than the time interval between the first impulse and the second impulse in $a_{Lp}(n)$, the indicated portion in $y'(n)$ that we refer to as $a_{exc}(n)$ hereafter, the initial plucking excitation is not distorted by reflected wave components during this time period. Therefore, we can simply extract $a_{exc}(n)$ by windowing it out from $y'(n)$ as shown in Figure 4.

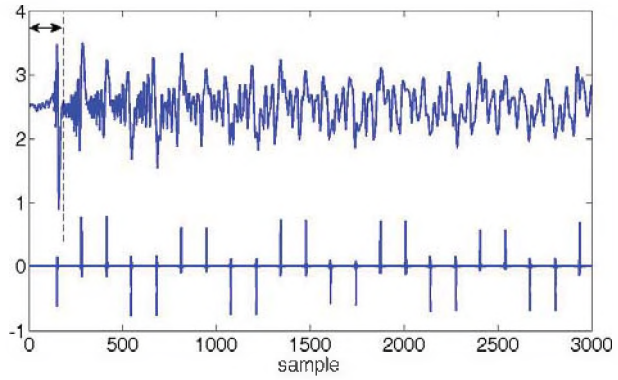


**Figure 3. Top : $y'(n)$, the time derivative of $y(n)$ . Bottom : $a_{Lp}(n)$**

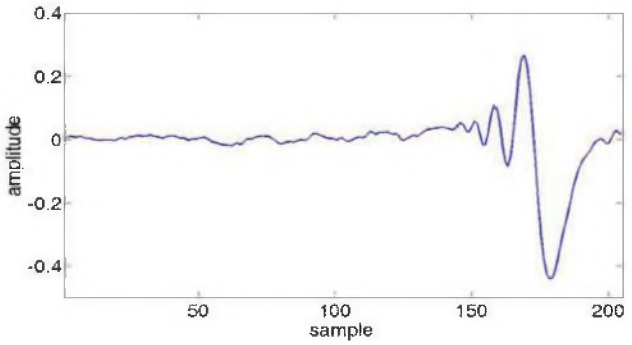


**Figure 4. Enlarged portion indicated by the arrow in $y'(n)$ in Figure 3, defined as $a_{exc}(n)$.**

Because the plucked string DW model is linear, this extracted excitation signal ($-a_{exc}(L_{exc}-n)$, where $L_{exc}$ is the length of $a_{exc}(n)$) can be used as input to the synthesis model. To validate the proposed method, we synthesized a pluck sound by convolving $-a_{exc}(L_{exc}-n)$ with $v_{Lp}(n)$ and compared that to $y(n)$. As shown in Figure 5 where $v_{Lp}(n)$, $y(n)$ and the convolution of $y(n)$ and $-a_{exc}(L_{exc}-n)$ are depicted together, we can see that the synthesis result reproduces the signal pattern of $y(n)$ to a reasonable degree.

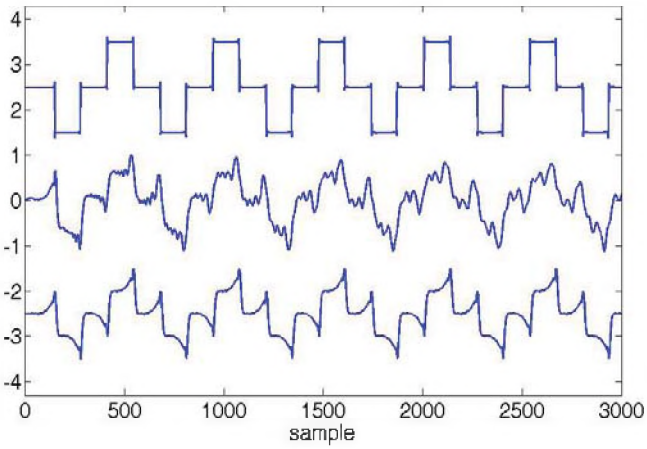


**Figure 5. Top : $v_{Lp}(n)$, Middle : $y(n)$, Bottom : convolution of $-a_{exc}(L_{exc}-n)$ and $v_{Lp}(n)$**

## 4. CONCLUSIONS

We have presented a novel method to extract the pluck excitation from a plucked string signal in the time domain. Our method is inspired by the observation of the way traveling wave components behave in the plucked string sound signal and by comparison with a DW simulation. The excitation extracted by the proposed method is compact and physically more meaningful, facilitating the use of the excitation for synthesis in conjunction with physical models such as DW. Future work will entail more systematic validation of the extracted excitation via inverse filtering approaches.

## REFERENCES


Karplus, K. and Strong. A. (**1983**). "Digital synthesis of plucked-string and drum timbres," Computer Music Journal. **7**(2), 43-55.

Smith. J. O. (**1992**). "Physical modeling using digital waveguides," Computer Music Journal. **16**(4), 74-91.

Välimäki. V., Huopaniemi J., Karjalainen M. and Jánosy Z. (**1996**). "Physical modeling of plucked-string instruments with application to real-time sound synthesis," J. Audio Engineering. **44**(5), 331-353.

Erkut. C., Välimäki. V., Karjalinen K. and Laruson, M. (**2000**). "Extraction of physical and expressive parameters for model-based sound synthesis of the classical guitar," in 108th AES Int. Convention, (AES, Paris).

Karjalainen K. and Välimäki V. (**1998**) "Plucked-string models: From the Karplus-Strong algorithm to digital waveguides and beyond," Computer Music Journal. **22**(3). 17-32.

# ON THE BORE SHAPE OF CONICAL INSTRUMENTS

**Antoine Lefebvre and Gary Scavone**
Computational Acoustic Modeling Laboratory (CAML), Centre for Interdisciplinary Research in Music Media and Technology (CIRMMT), Schulich School of Music of McGill University, 555 Sherbrooke Street West, Montreal, Quebec H3A 1E3, Canada

## 1. INTRODUCTION

Woodwind music instruments are either based on a cylindrical or a conical air-column. To behave properly, any woodwind instrument must be so designed that the lowest resonances of each note of the first register are well aligned, i.e. that they are harmonic (Fletcher, 1998). This is necessary for two reasons. First, this ensures a proper collaboration of each resonance in creating a rich, stable tone in the first register. Second, this ensures that the second register is well tuned with the first.

Conical-bored instruments such as the saxophone deviate in geometry from a perfect cone at both extremities. At the large end, the flare angle increases and forms the bell, enhancing the radiation of sound. The small end of the air column is normally cylindrical to allow a mouthpiece to be inserted into or over it. For saxophones, the larger end of the neck is also cylindrical so that it can be inserted into the main body of the instrument. Do these deviations hinder or improve the harmonicity of the instrument?

In this paper, we study the impact of the bore shape on the harmonicity of the resonances for each note of simplified saxophone-like instruments. A number of bore shapes were investigated including cones of varying taper angle and upper bore deviations in order to gather insight into what deviations might be necessary for the proper functioning of saxophones. The idea involves calculating the positions of the toneholes on a given bore shape for the fundamental resonance to correspond with the notes of the musical scale and then to calculate the deviation of the second resonance from perfect harmonicity. This is done with an optimization algorithm (Keefe, 1989; Lefebvre, 2010). For a well-designed instrument, the second resonance should be within about 10 cents of two times the fundamental resonance frequency, where the interval in cents is calculated as $1200\log(f_2/f_1)$. One semitone equals 100 cents.

The transmission matrix method (TMM) provides an efficient means for calculating the input impedance of a hypothetical air column (Caussé et al., 1984; Keefe, 1990). With the TMM, a geometrical structure is approximated by a sequence of one-dimensional segments, such as cylinders, cones, and closed or open toneholes, and each segment is represented by a matrix (TM) that relates its input to output quantities of pressure (P) and volume velocity (U). The multiplication of these matrices yields a single matrix, which must then be multiplied by an appropriate radiation impedance at its output. That is:

$$\begin{bmatrix} P_{in} \\ Z_0 U_{in} \end{bmatrix} = \left( \prod_{i=1}^{n} T_i \right) \begin{bmatrix} \overline{Z}_{rad} \\ 1 \end{bmatrix}. \quad (1)$$

The normalized input impedance is then calculated as $\overline{Z}_{in} = P_{in} / Z_0 U_{in}$.

## 2. RESULTS

Many bore shapes were simulated. Four of them were selected for this paper. All geometries are made of a cylindrical mouthpiece of 15.8 mm diameter and 50 mm length followed by the air-columns. Approximating the mouthpiece as a cylinder may not be the most appropriate model but this is standard practice in the literature and no better geometry appears obvious. For the sake of simplicity, the cylindrical model was adopted. All four air-columns start with a diameter of 12.5 mm, as is typical for an alto saxophone (there is a diameter jump). The first air-column (A) is a straight conical bore with an angle of 3 degrees. The second air-column (B) is also a straight conical bore but with an angle of 3.5 degrees. The third air column (C) starts with a segment of cylindrical pipe of 25 mm length followed by a conical bore with an angle of 3 degrees. Finally, the last air-column (D) starts with a segment of conical bore of 50 mm length with an angle of 3.5 degrees followed by a conical bore with an angle of 3 degrees. The first 200 mm of these geometries are displayed in Fig. 1. The first register of the instruments is in tune within 1 cent.

An instrument with a larger angle has a smaller truncation ratio (Nederveen, 1998) and is expected to display better harmonicity. Similarly, according to Dalmont et al. (1995), an instrument with an increased taper in the upper part of the bore should also have a better harmonicity. The geometries were selected to verify these hypotheses.

Figure 2 displays the deviation in cents of the second resonance for each note of the first register of the instruments. None of these instruments have sufficiently good harmonicity for all notes. For all geometries, the harmonicity is increasingly problematic for higher notes. Geometry A gives a decent harmonicity for the first 9 notes, after which the second resonance becomes increasingly too high. Geometry B, which differs from A only in the angle of conicity results in lower second resonance for all notes, which improves the harmonicity for many notes of the instruments but worsens other notes. For geometry C and D, the harmonicity is worse than for the straight cones.

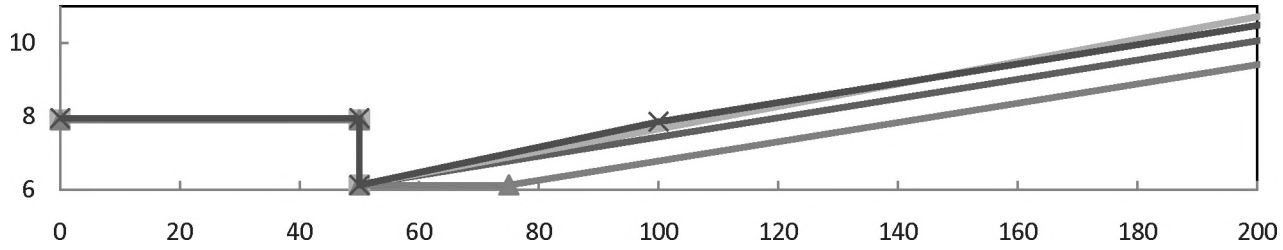


**Figure 1 Radius (in mm) of bore of the top part of the four instruments: A (diamonds), B (squares), C (triangles) and D (crosses)**

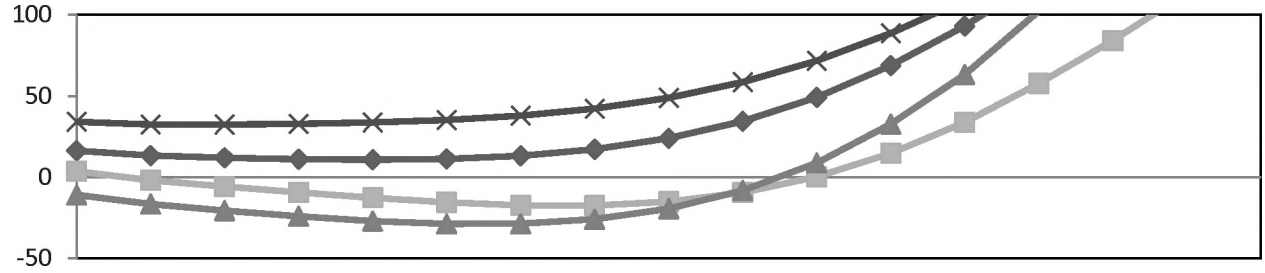


**Figure 2 Frequency deviation in cents of the second resonance relative to twice the fundamental resonance for the four conical air-columns: A (diamonds), B (squares), C (triangles) and D (crosses).**

In a recent paper (Lefebvre and Scavone, 2011), the input impedance of three complete saxophones was measured from which the resonance frequencies were estimated. These measurements correlated well with the calculated values based on their measured geometries and the harmonicity was very good compared to values of the current paper. This suggests that the deviations from a cone found on these instruments play a role in the proper harmonicity of the instrument and that simple modifications such as those studied in this paper are not sufficient. The question remains what bore shape might achieve the best harmonicity for each note.

## 3. CONCLUSIONS

It is generally admitted that the air-column shape of a saxophone is a cone, but this is only an idealized description. This brief study confirms that a straight conical tube is not an appropriate geometry for a saxophone, that deviations are necessary to bring the second resonance in harmonic relation with the first and that simple modifications in the upper part such as an increased angle or a segment of cylinder are not sufficient.

The application of an optimization algorithm that allows simultaneous variation of tonehole positions and bore shape could potentially lead to an improved design and a better understanding of the relation between the geometry of the bore and the quality of the instruments. Ongoing efforts on this topic are providing promising results.

## REFERENCES

Caussé, R., Kergomard, J., & Lurton, X. (**1984**). Input impedance of brass musical instruments - Comparaison between experimental and numerical models. *J. Acoust. Soc. Am.*, *75*, 241-254.

Dalmont, J. P., Gazengel, B., Gilbert, J., & Kergomard, J. (**1995**). Some aspects of tuning and clean intonation in reed instruments. *Applied Acoustics*, *46*, 19-60.

Fletcher, N. H., & Rossing, T. D. (**1998**). *The Physics of Musical Instruments* (2nd ed.). Springer.

Keefe, D. H. (**1990**). Woodwind air column models. *J. Acoust. Soc. Am.*, *88*, 35-51.

Keefe, D. H. (**1989**). Woodwind design algorithms to achieve desired tuning. *The Galpin Society Journal*, *1*, 14-22.

Lefebvre, A. (**2010**). "Computational Acoustic Methods for the Design of Woodwind Instruments." Ph.D. thesis. McGill University.

Lefebvre, A. and Scavone, G. (**2011**). A Comparison of Saxophone Impedances and their Playing Behavior. In Proceedings of the 2011 Forum Acusticum Conference, Aalborg, Denmark.

Nederveen, C. J. (**1998**). *Acoustical Aspects of Woodwind Instruments* (Revised Edition). Northern Illinois University Press.

## ACKNOWLEDGEMENTS

The authors wish to thank CIRMMT, NSERC, and the FQRNT for partial support of this research.

# DEVELOPMENT OF AN ELECTROLABIOGRAPH EMBEDDED IN A TROMBONE MOUTHPIECE FOR THE STUDY OF LIP OSCILLATION MECHANISMS IN BRASS INSTRUMENT PERFORMANCE

**Vincent Freour and Gary Scavone**
Computational Acoustic Modeling Laboratory, Centre for Interdisciplinary Research in Music Media and Technology, Schulich School of Music, McGill University, Montréal, Québec, Canada.

## 1. INTRODUCTION

The lips of a brass instrument player constitute a complex pressure-controlled valve from which the vibration of the air column originates. Due to their anatomical properties and the significant ability from the player to control their geometry and mechanical properties, lip valve systems display different vibratory behaviours across the traditional range of playing. In order to investigate lip mechanics on real performers, different *in-vivo* methods have been proposed. Lip opening area and frequency response have been evaluated on real players using high speed imaging [1]. This technique requires the use of a special transparent mouthpiece with cylindrical cup that allows the capture of undistorted images but may significantly affect the behavior of the lips. Lip vibratory mechanisms have been investigated using strain gauges placed between the lips and the mouthpiece rim [2]. This solution remains however quite invasive since the strain gauge is usually attached to the upper lip of the subject. Experiments have also been conducted on artificial lip systems which allow the use of highly intrusive measurement devices such as laser velocimetry or light transmission and video methods [1,3]. However, although artificial lips are becoming more accurate at reproducing the lip behaviour of human performers, they are still approximations of human lips and have not proven yet their ability to reproduce human players' behaviour over all registers of a trumpet or a trombone.

In this paper, we present a method for the investigation of lip motion in trombone players based on the measurement of lip conductivity. In the scope of this study, experimental data is evaluated regarding the phase relationship between the lip displacement and the acoustic pressure in the mouthpiece. This phase information provides knowledge about the predominant "outward" or "upward" striking characteristic of the valve as discussed in [4]. In order to evaluate the validity of our measurement device, results are compared to previous recordings obtained using different measurement techniques, as well as numerical simulations.

## 2. METHODS

### 2.1 Development of an electrolabiograph

For the purpose of *in-vivo* investigations on brass players' lips we developed an electrolabiograph (ELG) based on the principle electroglottography (EGG) as first presented by Fabre in 1956 [5]. Analogously to the EGG for the study of vocal folds contact, the ELG records the variations of electrical admittance between two electrodes by mean of a high frequency modulated current sent through the lips. The two electrodes are located across the lips (one electrode on the upper lip and one on the lower lip). Therefore, the ELG signal is assumed to be proportional to the degree of contact of the lips.

In order to reduce the intrusiveness of the system, the contact electrodes are made of tin-plated copper foil shielding tape glued on the mouthpiece rim. The resistance of the electrode pair is raised to 40Ω by a resistor and the electrodes connected to a commercial Voce Vista EGG signal conditioner. The analog output is sent then to a National Instrument converter. This system is therefore totally non-invasive, the main requirement being the use of a non conductive material for the mouthpiece; in this study, a plastic mouthpiece designed by CFMI Université Lille 3 (France) was used.

### 2.2 Determination of the valve mechanism

Since ELG amplitude is proportional to the degree of contact between the lips, when the ELG amplitude decreases, the contact area at the lip interface decreases and the lips tend to open. Therefore, we can reasonably assume that the ELG signal $\boldsymbol{E}$ and lip motion $\boldsymbol{\xi}$ are $\boldsymbol{\pi}$ out of phase, lip motion being defined as the distance between the center of mass of the two lips. Consequently, the inverse of the ELG signal is assumed to be in phase with the lip motion and thus in phase with the lip opening area $\boldsymbol{S_{lip}}$: $\varphi(-\boldsymbol{E}) = \varphi(\boldsymbol{\xi}) = \varphi(\boldsymbol{S_{lip}})$.

The predominant "outward" or "upward" striking mechanism of the lips is given by the sign of the phase difference between $\boldsymbol{S_{lip}}$ and the acoustic pressure measured in the mouthpiece cup $\boldsymbol{P_m}$. In the case of a positive phase difference ($\varphi(\boldsymbol{S_{lip}}) - \varphi(\boldsymbol{P_m}) > 0$), lip opening anticipates the drop of mouthpiece pressure so the lips behave as an "outward" striking valve. If the phase difference is negative, the pressure drop occurs before the lips tend to open so the lips behave as an "upward" striking valve.

## 3. EXPERIMENTS AND RESULTS

Experiments were conducted on one subject on a King 2102 tenor trombone. Figure 1 shows the results obtained for an overtone series from F3 to D5 and back to D5 in the closed position of the slide. The top graphic represents the waveform of the downstream (or "mouthpiece") pressure

and ELG signal. The bottom graphic represents the phase difference between the inverse of the ELG signal and the downstream pressure, calculated on a 512 samples sliding window with 448 samples overlap.

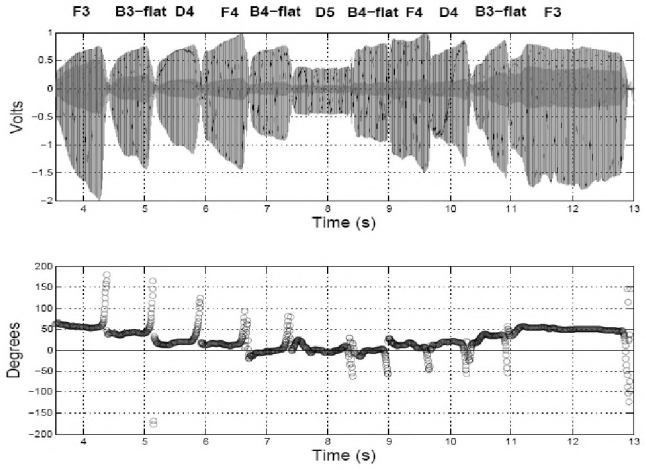


**Figure 1. Top: downstream pressure (lighter line), inverse of the ELG signal (darker line). Bottom: phase difference between lip motion and downstream pressure.**

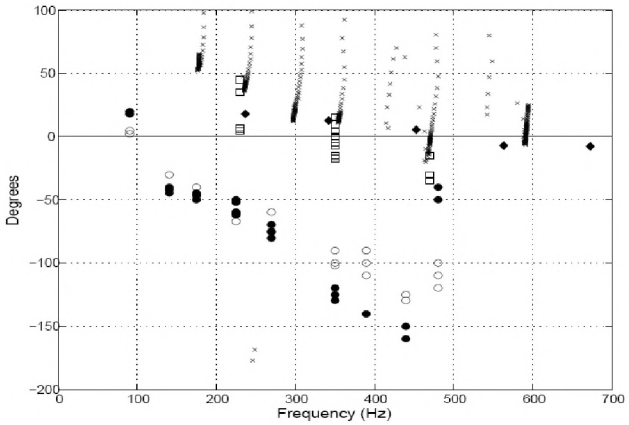


**Figure 2. Phase difference between lip motion and downstream pressure in French horn (filled and empty circles), trumpet (empty squares), numerical simulation of trumpet (diamonds) and trombone (crosses).**

The maximum phase difference is observed for the lower tone (F3) around 50 degrees and reveals a clear "outward" striking behaviour of the reed. The minimum value occurs for B4-flat and D5 for which the phase difference is near 0. Therefore, the tendency of a transition from an "outward" to an "upward" striking regime of oscillation is confirmed on this acquisition.

The phase data presented on Figure 1 is now plotted against the playing frequency on Figure 2. On the same graphic, the phase difference between lip motion and downstream pressure is plotted for a French horn and a trumpet as measured by Yoshikawa using strain gauges and human players [2]. The phase difference between lip opening area and downstream pressure in trumpet obtained from numerical simulations by Adachi and Sato [6] is also plotted on the same figure. Results from simulations and *in-vivo* measurements in trumpets are quite consistent, which suggests the two-dimensional lip model proposed by Adachi and Sato provides good results. Phase values obtained for the French horn are clearly lower than those obtained for the trombone and trumpet, possibility because of the specific geometry of the French horn bore and mouthpiece (conical bore). Results obtained for the trombone in this study are consistent with the tendency observed in previous studies with an order of magnitude close to values observed in trumpet.

## 4. DISCUSSION AND CONCLUSIONS

We have presented a new sensor for the measurement of lip electrical admittance in trombone performance. This method is non-invasive and provides a signal which is assumed to be proportional to the degree of contact of the lips. Moreover, the phase of this signal is robust to the phase of the lip motion and opening surface, which allows evaluation of lip vibratory mechanisms of real players, across all playing ranges. The results, which reveal a transition from an "outward" striking towards an "upward" striking regime of oscillation, corroborate previous work and support the validity of ELG in carrying information on lip motion. Although the scope of this paper is restricted to considerations on the phase of the ELG signal, the waveform displays some common features with EGG of vocal folds. Therefore, some techniques for the extraction of vocal folds parameters, such as the open quotient, may potentially be used for further investigation. Correlations between lip mechanisms, mouthpiece mechanical constraints and the acoustical influence of the vocal-tract are also part of future works.

## REFERENCES

[1] M. J. Newton, M. Campbell, J. Gilbert: Mechanical response measurements of real and artificial brass players lips. *J. Acoust. Soc. Am.* **123**(1) (2008).

[2] S, Yoshikawa: Acoustical behaviour of brass player's lips. *J. Acoust. Soc. Am.* **97**(3) (1995), 1929-1939.

[3] J. Gilbert, S. Ponthus, J-F Petiot: Artificial buzzing lips and brass instruments: Experimental results. *J. Acoust. Soc. Am.* **104**(3) (1998), 1627-1632.

[4] N. H. Fletcher: Autonomous vibration of simple pressure-controlled valves in gas flows. *J. Acoust. Soc. Am.* **93**(4) (1993), 2172-2180.

[5] P. Fabre: Un procédé électrique percutané d'inscription de l'accolement glottique au cours de la phonation : Glottographie de haute fréquence. Bulletin de l'Académie Nationale de Médecine (1957), 66-69.

[6] S. Adachi, M. Sato: Trumpet sound simulation using a two-dimensional lip vibration model. *J. Acoust. Soc. Am.* **99**(2) (1996), 1200-1209.

# A PHYSICALLY-INFORMED AUDIO ANALYSIS FRAMEWORK FOR THE IDENTIFICATION OF PLUCKING GESTURES ON THE CLASSICAL GUITAR

**Bertrand Scherrer, and Philippe Depalle**
Sound Processing and Control Laboratory (SPCL), Center for Interdisciplinary Research in Music Media and Technology,
McGill University, 555 Sherbrooke Street West, Montréal, QC, Canada H3A 1E3
bertrand.scherrer@mcgill.ca

## 1. INTRODUCTION

This paper presents one part of a larger system whose ultimate purpose is to identify how a classical guitar was played from the analysis of audio recordings. Such a system could be used in a variety of musical tasks ranging from guitar pedagogy to audio effects. In this paper, the emphasis is put on one parameter guitarists can modify when plucking the string: the angle with which the string is released at the end of the finger-string interaction. While most guitarists may not be familiar with the *angle of release* (AOR) per se, they change it when choosing between a *rest stroke* (where the plucking finger rests on the next string) and a *free stroke* (where the plucking finger clears the next string).

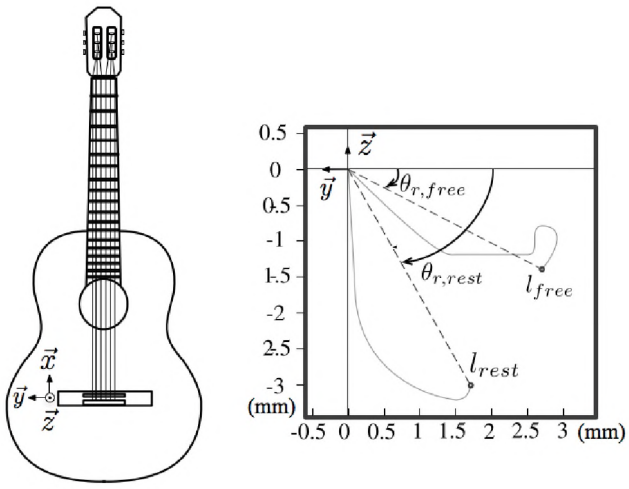


**Figure 1: Coordinate system used in this paper (left), and measured trajectories of the string, near the plucking point, for rest and free strokes [1] (right).**

The plot on the right of Figure 1, shows the difference in AOR between a free stroke and a rest stroke, respectively, as measured by [1]. The circled dots marked $l_{free}$ and $l_{rest}$ represent the points at which the string is released from the finger for the free and rest stroke.

## 2. MODELLING PLUCKING GESTURES

The Digital Waveguide (DW) paradigm [2] is used to devise a model for the vibration of one guitar string that takes into account the AOR. More specifically, a given string is represented by two bi-directional delay lines: the "*normal*" (z in Figure 1) and "*parallel*" (y in Figure 1) directions[1]. The coupling occurring between the two directions at the bridge is modelled using reflectance functions [2] as shown in Figure 2.

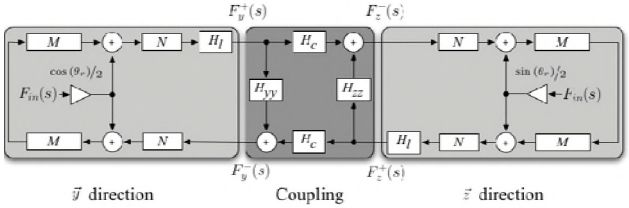


**Figure 2: Diagram of the DW network simulating a string observed along the y and z directions, including the coupling at the bridge.**

Force waves are used to study the mechanical behaviour of the coupled system. The AOR, $\theta_r$, distributes the excitation, represented by its Laplace transform: $F_{in}(s)$, over the two transverse directions. The filter, $H_l$, accounts for the losses as well as potential phase delay during a round trip of the waves in the string. The terms of the 2x2 admittance matrix of the body at the bridge, as well as the characteristic impedance of the string are included in $H_{yy}$, $H_{zz}$, and $H_c$. The propagation of the waves from the plucking point to the bridge, and from the plucking point to the nut (or fret), are modelled using pure delay lines of lengths $M$ and $N$, respectively.

Based on guitar radiation pattern measurements (e.g. [3]), it is assumed that the sound radiated by a guitar, and captured by a microphone positioned directly in front of it, only depends on the displacement of the bridge along z. The transfer function $T_z = F_z / F_{in}$ relating the input force to $F_z$, the force applied to the bridge along z, is given by:

$$T_z = \frac{e^{-Ns}(1 + e^{-2Ms})(\alpha_z + \beta_z e^{-Ds})}{2\left(1 - \left[H_{yy} + H_{zz}\right]e^{-Ds} + \left[H_{yy}H_{zz} - H_c^2\right]e^{-2Ds}\right)}$$

where $\alpha_z = [1 + H_{zz}]\sin\theta_r + H_c\cos\theta_r$ and $\beta_z = \left[H_c^2 - H_{yy} - H_{zz}H_{zz}\right]\sin\theta_r + H_c\cos\theta_r$. Due to the coupling at the bridge, $T_z$ exhibits pairs of poles with slightly different frequencies [4]. Each pair of poles (and their conjugate counterparts) give rise to one string "partial"

1 With respect to the guitar's top plate.

when observed with standard Fourier analysis. The factor $1 + e^{-2Ms}$ at the numerator of $T_z$ is a feedforward comb filter that represents the effect of the plucking position on the sound. A method to estimate the value of M from audio signals can be found in [5]. The effect of the AOR on $F_z$ is included in the terms $\alpha_z$ and $\beta_z$. This means that a change in the AOR will lead to a change in the amplitudes and phases of the 2D poles of $T_z$.

The analysis framework presented in the following section aims at extracting the amplitude, phase, frequency and damping factor of the poles of $T_z$ from a recording. The ratio of the complex amplitudes of the modes forming a string partial allows for the retrieval of the AOR.

## 3. ANALYSIS FRAMEWORK

The first step in the analysis chain is to pre-process the sound (high-pass filtering, DC-removal). Then, the signal is segmented to isolate plucks, and select the portion of the sound to analyze. In a global analysis step, the fundamental frequency is estimated on the audio segment. Then, a standard additive analysis is carried out (e.g. [6]) to identify the string partials. The frequency resolution is not sufficient, however, for the task of determining the frequency, damping factor, amplitude, and phase of the closely coupled modes in a given string partial.

Hence, the next step of the analysis chain consists of a focused analysis around each string partial. The frequencies and damping factors of the modes are estimated using the ESPRIT method [7]. The amplitudes and initial phases of the poles are estimated via the least squares method. To avoid numerical issues, a multi-band approach is adopted along with decimation. In other words, ESPRIT looks for $K$ modes (modelled as exponentially decaying sinusoids) around each partial. The partials are isolated using a linear phase FIR band pass filter, and the resulting signal is then decimated.

Based on the model in Section 2, $K=2$ should suffice since we assume a string partial is the result of the coupling of two transverse directions only. With ESPRIT, as with such parametric methods however, an overestimated $K$ is often advisable (K=5 in practice). Therefore, a pruning scheme is implemented in order to successfully identify the two modes of interest. Simple physical considerations are used in this process: a) the damping factor for the vibration along y will be lower than that of the vibration along z; b) the vibration along z will tend to have a slightly smaller effective vibrating length than the vibration along y, due to different terminations at the fret or nut [8]: we can expect $f_y > f_z$.

Also, for a given partial of frequency $f_n$, the components that are "too weak" in amplitude, "too far" from $f_n$, that are over-damped, or diverging, are discarded. The final choice of the coupled mode pairs is done based on "how well" each pair of components models the partial (using the Reconstruction Signal to Noise Ratio, a.k.a. RSNR.

## 4. RESULTS AND DISCUSSION

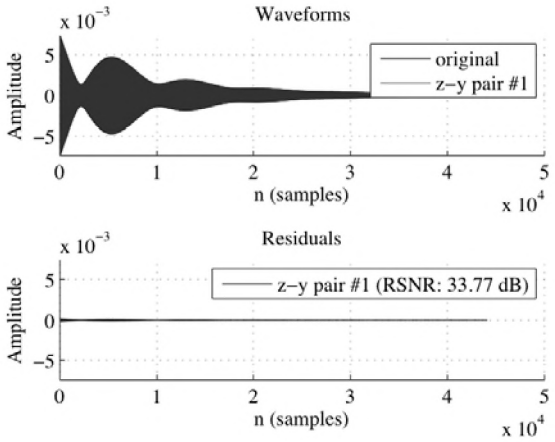


**Figure 3: Waveforms of the 8th partial of a synthetic sound (top-black), of the 8th partial modelled by the identified z-y pair (top-grey) , and of the residual (original – zy_pair) (bottom).**

An overview of an analysis framework of guitar sound has been presented. The physical model of Section 2 lead to the structure of the analysis chain presented in Section 3. The quality of the analysis of the framework is illustrated in Figure 3: the waveform of the 8th partial of a synthetic sound, and the waveform re-synthesized based on the estimated the z-y pair components are indistinguishable (RSNR of over 30dB). Future work includes the analysis of a database of plucks recordings with various AORs to evaluate the actual AOR estimation procedure.

## REFERENCES

[1] Pavlidou, M., (1997). A physical model of the string-finger interaction on the classical guitar. Ph.D. Thesis, University of Cardiff.

[2] Smith, J. O., (2011). Physical audio signal processing. https://ccrma.stanford.edu/~jos/pasp/, accessed July 26th 2011.

[3] Hill, T. J. W., Richardson, and B. E., Richardson, S. J., (2004). Acoustical parameters for the characterisation of the classical guitar. Acustica - Acta Acustica, vol. 90(2), pp. 335–338.

[4] Gough, C. E. The theory of string resonances on musical instruments. Acustica, vol. 49, pp. 124–41.

[5] Traube, C., and Depalle, P., (2003). Deriving the plucking point along a guitar string from a least-square estimation of a comb filter delay, Proc. of IEEE CCECE.

[6] Smith, J. O., and Serra, X. (1987). PARSHL: An analysis/synthesis program for nonharmonic sounds based on sinusoidal representation, in Proc. ICMC.

[7] Roy, R., Paulraj, A. and Kailath, T. (1986). ESPRIT – a subspace rotation approach to estimation of parameters of cisoids in noise. IEEE Trans. on Acoustics, Speech, Signal Processing, vol. 34, pp. 1340–1342.

[8] Woodhouse, J. (2004). Plucked guitar transients: Comparison of measurements and synthesis. Acustica – Acta Acustica, vol. 90, pp. 945–65.

# ASPECTS OF EXPERIMENTAL DESIGN FOR THE PERCEPTUAL EVALUATION OF VIOLIN QUALITIES

**Charalampos Saitis[1], Bruno L. Giordano[2], Claudia Fritz[3], and Gary P. Scavone[1]**
[1]Computational Acoustic Modeling Laboratory, Centre for Interdisciplinary Research in Music Media and Technology, Schulich School of Music, McGill University, Montreal QC, Canada, H3A 1E3
[2]Music Perception and Cognition Laboratory, Centre for Interdisciplinary Research in Music Media and Technology, Schulich School of Music, McGill University, Montreal QC, Canada, H3A 1E3
[3]Lutheries-Acoustique-Musique, Institute Jean le Rond d'Alembert, Universite Pierre et Marie Curie, UMR CNRS 7190, 4 place Jussieu, 75005 Paris, France

## 1. INTRODUCTION

In this paper, we present a method for the perceptual evaluation of violin qualities. In particular, we discuss the different experimental, musical and logistical issues concerning the design of reliable playing tests to explore the perceptual processes involved when the violinist interacts with the instrument in a musical context – for example, when comparing different violins in order to purchase a new one. Preliminary results are provided.

## 2. METHOD

### 2.1. Playing vs. listening tests

Psychoacoustic experiments based on listening tests using recordings, synthesized sounds or live performance have several disadvantages. Recorded sounds often lack the "naturalness" of live performance. Similarly, synthesized tones often sound rather unmusical [1]. And when using live players, listeners tend to focus more on the performer than the instrument: A "good" player is likely to make a "bad" violin sound "good" and vice versa. Most importantly, vibro-mechanical and tactile properties, such as "responsiveness," cannot be completely assessed without direct interaction with the instruments [2]. Playing tests are therefore more ecologically valid than listening tests.

A potential problem with playing tests is how to evaluate sound radiation from the violin and timbre-related qualities such as "richness." Radiation depends on the distance from the sound-producing source as well as the acoustics of the space in which the experiment is conducted. In the first case, the same individual might possibly assess the sound quality of the same instrument differently when in the role of player versus listener at a different location. In the second case, using a reverberant or acoustically dry room may affect how the sound is perceived. For our experiments, we used a rather dry room with a surface of $27m^2$ and reverberation time of approximately $0.18s$ in order to help players focus more on the vibrational response of the violins than on their sound,

### 2.2. Visual information

Anecdotal evidence strongly suggests that some visual information, such as the color of the varnish, the grain of the wood, or identifying marks on the violin, may influence judgement. To help minimize the effects of such visual cues as much as possible in listening tests involving live performance, the listeners or the performers or both are usually blindfolded. Another approach is to have the instruments played behind a physical divider [3]. However, blindfolding does not appear to be a viable solution for playing tests. To circumvent the potential impact of visual information on judgment while ensuring a certain level of comfortability for the musicians, as well as safety for the instruments, we used low light conditions and asked participants to wear a pair of extra tinted sunglasses. In this way, violinists can provide objective assessments while still retaining some visual contact with the instruments.

### 2.3. Choice of bow

A critical issue when conducting violin playing tests is the choice of bow. In this study, two alternatives were considered: asking players to use their own bow (or the one they are most familiar with) or choosing a common bow across all participants (the option of instead using a common set of different bows across all players was discarded due to logistical constraints concerning the duration of the experimental session). Although neither option is ideal, using a common bow is likely to raise the very same quality question as with the violin [4]. Moreover, participants may feel uncomfortable with a bow they are not familiar with. We therefore preferred the first option. This was also felt to be more typical of how violinists assess instruments while in the process of purchasing one.

### 2.4. Violins

Two pilot studies with five and nine violins respectively were run to help optimize the number and type of instruments to evaluate so as to increase the generality of the results. Accordingly, eight violins of different make (Europe, Québec, China) and age (ranging from 1840 to 2010) were selected in coordination with local luthiers. The strings, bridge, and chinrest were optimally setup for each violin by the luthiers prior to the experiment. All violins had identical shoulder rests (Kun Original model).

To avoid potential biases caused by the "mere exposure" effect by which familiarity with a stimulus object amplifies

preference toward it [5], the player's own violin was not included in the evaluation set. Instead, participants were permitted to use their own violin as a reference point during the experiments.

### 2.5. Data quality

To obtain reliable results from quality assessments, it is important to consider the statistical validity of the experimental procedure. The number of players can be maximized to better estimate the extent of inter-subject differences. For the purposes of our experiment, twenty violinists with at least fifteen years of performance experience were selected. To increase accuracy of intra-subject consistency and individual-specific preference data, players were asked to repeat the evaluation task five times. To obtain a stronger testing of intra-subject consistency, violinists were asked to return for a second, identical session within a period of three to seven days later.

Maximizing task repetitions as much as possible is desirable, but there are logistical constraints such as the total duration of the experimental session or physical limitations such as fatigue that must also be considered. Although having many repetitions can help reduce the experimental noise in the data, fatigue may have the opposite effect.

## 3. RESULTS

Participants were asked to play the different violins and order them by preference. For ecological validity reasons, no constraints were imposed on the evaluation process (e.g. specific repertoire). Preference judgments were collected as a measure of subjective evaluation of the quality of a violin based on choice behavior [6]. The Spearman's rank correlation coefficient across rankings from different trials was used as a measure of intra- and inter-subject consistency. A Wilcoxon signed-rank test was then adopted to test (a) whether inter-individual agreement was significantly different from intra-individual consistency, and (b) whether intra-subject consistency between the two sessions was significantly different from intra-subject consistency within one session.

Figure 1 depicts the results for inter-individual agreement and intra-individual consistency across the two sessions, and intra-individual consistency between the two sessions and within one session in the form of box plots (from left to right respectively). Results indicate that violin players are relatively self-consistent when evaluating different instruments in terms of preference. However, a significant amount of disagreement between violinists is observed ($p < 0.001$). Furthermore, participants appear more self-consistent in the same session than across the two sessions ($p = 0.0045$).

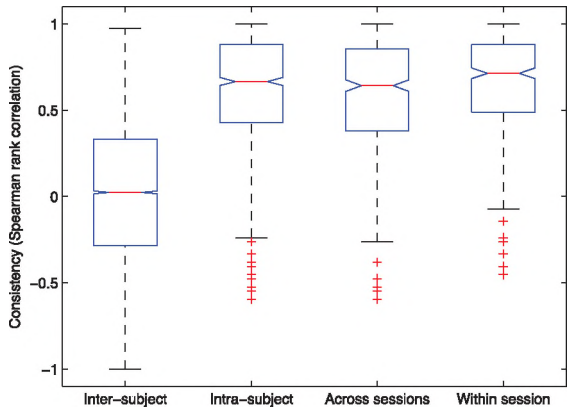


**Figure 1. Box plots of intra- and inter-subject variation: 1 corresponds to perfect consistency and -1 corresponds to perfect inconsistency (exactly opposite ranking between different trials); The red line is the median; Box brackets show the interquartile range; Red crosses depict outliers.**

## 4. CONCLUSIONS

We have presented a method for evaluating violins that is well-controlled by scientific standards. The musical and logistical difficulties related to the experimental design have been discussed. We applied the method to examine intra- and inter-subject variability in violin players across a certain set of violins using preference rankings. Experimental control is necessary to obtain reliable quantitative data, but a certain amount of musical context is required for such information to be meaningful. No single preference ranking can satisfactorily capture inter-individual differences. Preference rankings are still an important area of study in the perceptual evaluation of string instruments. Results suggest the need for further work to explain the large inter-individual variability in the preference for violins.

## REFERENCES

[1] Wright, H. (1996). *The Acoustics and Psychoacoustics of the Guitar*, Ph.D. thesis, Departmet of Physics and Astronomy, University of Wales, Cardiff, UK

[2] Fritz, C., Muslewski, A. and Dubois, D. (2010). "A situated and cognitive approach of violin quality," in Proc. International Symp. Musical Acoust., Sydney and Katoomba, Australia.

[3] Petiot, J.-F. and Caussé, R. (2007). "Perceptual differences between cellos: A subjective/objective study," in Proc. International Symp. Musical Acoust., Barcelona, Spain.

[4] Caussé, R., Maignet, J. P., Dichtel, C. and Bensoam, J. (2001). "Study of violin bow quality," in Proc. International Symp. Musical Acoust., Perugia, Italy.

[5] Zajonc, R. B. (1968). "Attitudinal effects of mere exposure." J. Pers. Social Psych., **9**, 1-27.

[6] Giordano, B. L., Susini, P. and Bresin, R. (2011). "Experimental methods for the perceptual evaluation of sound-producing objects and interfaces," in *Sonic Interaction Design*, edited by K. Franinovic and S. Serafin, MIT Press, Boston, MA.

# NUMERICAL AND EXPERIMENTAL MODAL ANALYSIS OF THE SETAR

**Hossein Mansour**[1]
[1]Computational Acoustic Modeling Laboratory, Centre for Interdisciplinary Research in Music Media and Technology, Music Technology, Schulich School of Music of McGill University, Montreal, Québec, Canada H3A 1E3

## 1. INTRODUCTION

Stringed musical instruments are complex vibrating systems from both the structural and the fluid-structure coupling perspective. The direct sound of the strings is a minor component of the sound output, with most of the radiated sound generated by the body and cavity of the instrument [1]. In fact, the whole instrument acts as a filter, which converts the excitation force of the strings to sound, and radiates it [2]. In this regard, the modal properties of the body and cavity are the key feature that defines the physical properties of the instrument [3].

In this study, the Persian setar is chosen as the test case, and its numerical and experimental modal analyses are described. After a brief introduction to the setar, the creation of its finite element model is described. The results of the finite element model are then compared with the experimental findings. The excellent agreement between the numerical and experimental results verifies the validity and accuracy of the numerical model. This verified numerical model serves as a platform for future studies on the setar, such as its virtual modification.

A detailed report of this work has been submitted for publication elsewhere (Mansour, 2011).

## 2. SETAR, A LONG-NECKED LUTE

The origin of the setar can be traced to the ancient Tanbour of pre-Islamic Persia. The Setar has four strings normally tuned at C4 (262 Hz), G3 (196 Hz), C4 (262 Hz), and C3 (131 Hz), respectively. The setar is used mainly to play Persian classical music, called Dastgah. This instrument is played with the tip of the index fingernail, by strumming up and down. Its fingerboard usually has twenty-five adjustable gut frets, which provide the fundamental frequency range of 131 Hz to 831 Hz (two and a half octaves). Although each string can be played individually, melodies are usually played on the first two strings while the other strings provide drones.

## 3. APPARATUS AND METHOD

An impact hammer (LDS® model 5200-B2 with metal tip) is used to excite the body, and the resultant velocity is measured by Laser Doppler Vibrometer (Bruel & Kjaer® LDV Type 8337). The recommended operating ranges of the impulse hammer and LDV are 2.5 KHz and 22 KHz, respectively. The experimental set up, including contactless LDV and impulse hammer, guarantees there will be no disturbance on the structure. The setar was clamped by its neck in a stiff vise.

The excitation is imposed on a fixed point on the apex of the bridge, beside the notch where the first C4 string is passing, and the response is measured at 60 points all over the soundboard. The choice of the excitation point ensured that all prominent modes in the working condition of setar are properly excited. The strings were damped by three rubber bands to eliminate their sound/vibration and to keep their preload on the structure.

The PHOTON II® data acquisition unit gathered the data, and RT Photon® V.6.33 software was used to calculate the Frequency Response Functions (FRFs). Later, the FRFs were fed to ME'scope® commercial software to extract the modal properties, including the natural frequencies, dampings, and mode shapes.

A finite element model of a setar was developed in MSC/NASTRAN taking into account structural details such as orthotropic properties, direction of the grains, non-ideal joints, and the effect of strings preload. The geometry has been precisely measured by a Coordinate-Measuring Machine (CMM), imported into CATIA, and meshed in Altair Hypermesh® environment. The orthotropic material properties and thicknesses have been defined separately for different components of the instrument. For consistency, the same fixed boundary condition of our experiments is applied to the finite element model.

## 4. RESULTS

The finite element model is solved, and the results are compared with the experimental data up to 2.5 KHz, as illustrated in Figure 1. The criteria in comparing the results are natural frequencies and mode shapes. The SB($m$,$n$) system is used to name different modes, where $m$ represents the number of longitudinal half-waves on the soundboard, and $n$ stands for the number of transverse half-waves. The two last HF modes are named differently as they are more complicated and do not follow the SB($m$,$n$) form. R(2) is also a radial mode and can be considered as the high frequency version of the SB(1,1).

Damping is not considered in the numerical model; therefore, the calculated modes are all normal and real. It is noteworthy that the mode shapes are not necessarily symmetric, because the soundboard does not have the exact same thicknesses on both sides.)

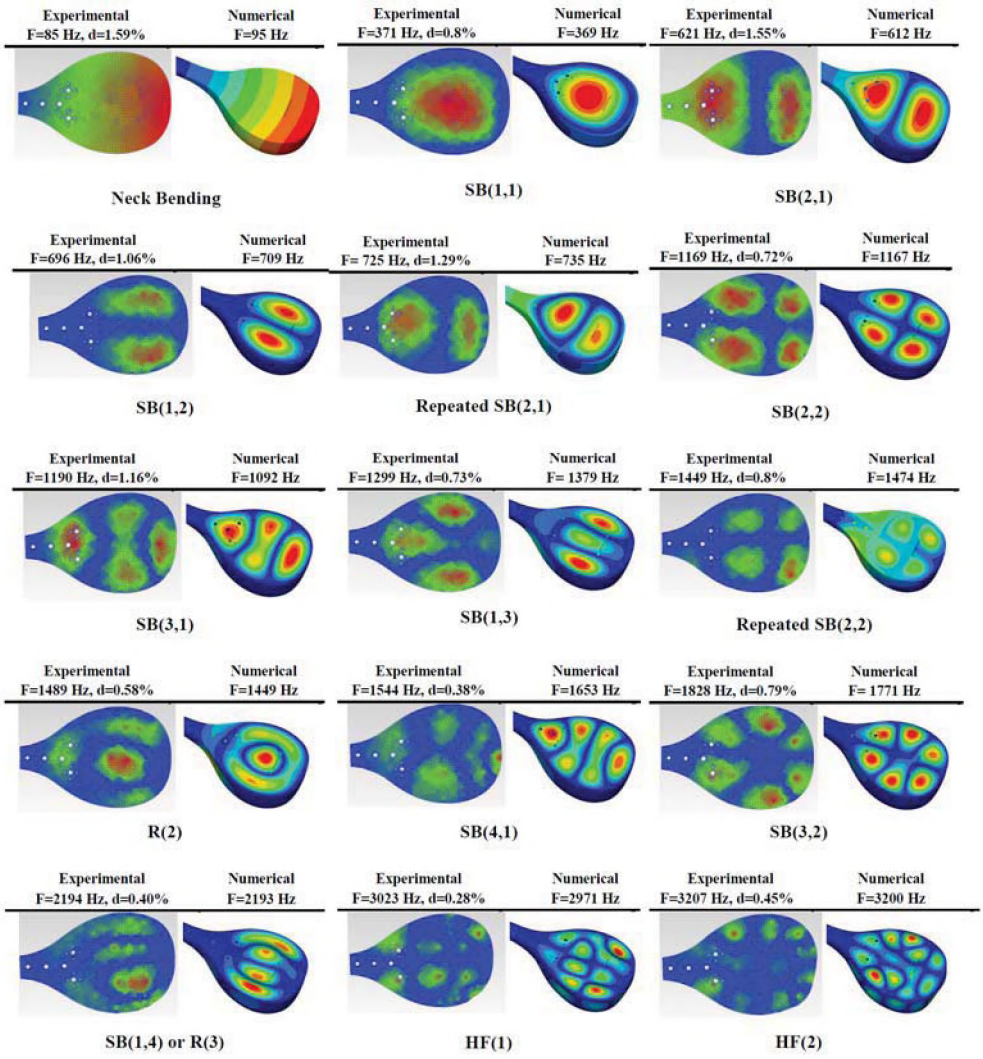


**Figure 1: Modes shapes and natural frequencies of the soundboard obtained from the experimental and numerical results, compared together. The setar was clamped by its neck**

## 5. DISCUSSION

A comparison of the first thirteen structural modes shows a good match between the numerical and experimental results. The frequency range of study is shown to be expandable to higher modes according to the results of two higher-frequency modes. The broad range of agreement between the numerical and experimental results is noticeable. The soundboard is found to be the sole resonator in all modes below 2.5 Hz, with the exception of SB(2,2) and R(2) where the bowl throat makes a minor contribution. The numerical model can be used to find the key structural parameters making the most significant effect on each mode. The results of this study can lead to more insightful structural modifications of the setar and yield better-quality instruments. In addition, the validated numerical model serves as a platform for future studies of the setar. Finally, most of the techniques used in this study can be applied to other stringed musical instruments, as well.

## REFERENCES

[1] Jansson, E., "Acoustics for violin and Guitar Makers", Kungl Tekniska Högskolan, Stockholm, Chapter IV, 4.1–4.26, (2002)
[2] Benade, A., "Fundamentals of musical acoustics" New York: Oxford University Press, 527–554, (1976)
[3] Fletcher, N.H., "The nonlinear physics of musical instruments", Reports on Progress in Physics, 62, 723–764, (1999)

## ACKNOWLEDGEMENTS

I would like to acknowledge the support of Dr. Mohamed Ferahi from MSC softwares in providing the research license of MD-NASTRAN. I'm grateful to Mr. Alireza Kasaiezadeh for his assistance in the finite element modeling, also to Dr Siamak Arzanpour from Mechatronics SFU for providing the experimental facilities. Lastly, I would like to acknowledge the support of master setar makers: Ramin Jazayeri, Yousef Pouria, Qioumars Bozorgi, and Mahmoud Mohammadi for their useful advices and preparing test samples for this study.

# ANALYSIS AND CONTROL OF BRIDGE EXPANSION JOINT CROAKING NOISE

**Clair W. Wakefield[1] and Duane E. Marriner[1]**
[1]Wakefield Acoustics Ltd., 301 - 2250 Oak Bay Avenue, Victoria, B.C., Canada, V8R 1G5

## 1. INTRODUCTION

Large bridges require expansion joints to accommodate thermal expansion and contraction as well as movements induced by seismic events. Virtually all expansion joints create additional noise over and above that due to normal tire-pavement interaction. Many joints create "slapping", "banging" or "booming" sounds from the impact of tires on the leading edges of the joints. Another type of expansion joint noise arises from the sequential impact of rolling tires on series of transverse joint elements (bars, tubes) – the familiar "cattle guard" effect. This noise is tonal and its pitch varies directly with vehicle speed.

In response to community concerns, Wakefield Acoustics Ltd. has investigated expansion joint noise at two new bridges in B.C. While of very different constructions, these two expansion joints produced similar sounds, variously described as a "croaking frog" or a giant "zipper". The first bridge utilizes Mageba "modular expansion joints" (Figure 1), which feature a series of transverse "lamella" beams (I-beams) with v-shaped rubber seals between them to keep water and debris out the sliding joint mechanism below. The second joint (Figure 2) is produced by Alba and features a "saw-toothed" rolling surface constructed from rubber-encased steel strips which expand and contract like accordion bellows.

## 2. INITIAL FIELD MEASUREMENTS

Initial measurements conducted close to one of the Mageba Modular Expansion Joints using a Larson-Davis 2800 Real Time Analyzer revealed that the characteristic frequency of the "croaking sound", while not constant, fell within a limited range centred on the 630 Hz. one-third octave band (Marriner & Wakefield, 2011). The frequency did not vary directly with vehicle speed so that this was not the cattle guard effect. While the intensity of the croaking noise varied with vehicle type and speed, virtually all light vehicles made the noise, while heavy trucks, tended not to.

## 3. JAPANESE RESEARCH

Researchers in Japan (K. A. Ravshanovich et al) investigated modular expansion joint noise and created a full-size replica of a modular expansion joint in a test compound. They postulated that the croaking noise was created when pulses of air are injected into the joint cavities by tires rolling over the gaps between lamella beams. While not identifying the precise source mechanism behind the croaking noise they found that the sound (again centred around 630 Hz.) was substantially suppressed when "rubber fillings" were inserted into the cavities bounded by the joint seals and the lamella beams. The specific nature of the "rubber fillings" was not described nor was such information subsequently obtainable. An experimental investigation was therefore required to identify an optimal noise suppression material.

## 4. JOINT INSERT EXPERIMENTS

An initial experiment involved filling the cavities of one modular expansion joint with 2 mm diameter crumb rubber from recycled tires. Crumbs of this size have been shown (Asdrubali et al, 2008) to have optimal sound absorption capabilities at 630 Hz. One third-octave and narrow band spectra of croaking noise were obtained on the bridge deck directly adjacent to the expansion joints, both before and after, the crumb rubber was inserted. By averaging spectra from many vehicle pass-bys, the crumb rubber was found to have reduced the maximum band-limited (400 to 900 Hz.) noise levels created during these very brief noise events by approximately 3.2 dB. The crumb rubber had then dissipated just over 50% of the joint noise energy. While a significant noise reduction, it was not sufficient to resolve the community noise issue.

A similar 3 dB noise reduction effect was attained when closed-cell foam rubber strips were glued between the lamella beams flanges leaving the v-shaped cavities below empty. Here part of the observed noise reduction may have resulted from the closed-cell foam strips acting to reduce the intensity of pressure pulses entering the joint cavities.

## 5. SOUND ABSORPTION TESTS

To find a more effective joint insert material, eight different open and closed-cell foam rubbers as well as other porous materials were tested to determine their sound absorption coefficients. The tests were conducted at UBC's Department of Mechanical Engineering using the impedance tube method under the direction of Dr. Murray Hodgson. The best combination of high sound absorption capacity and good physical properties was found to be provided by a fibrous "geotextile" material developed for use in soil/slope stabilization. At 50 mm thick, the geotextile had a sound absorption coefficient of 0.85 at 630 Hz. and, because of its intended use, was suitable for prolonged exposure to the elements.

## 6. ADDITIONAL FIELD EXPERIMENTS

To provide a long-term solution to the joint noise issue, the joint cavities were first filled with geotextile material and then "capped" with strips of 6 mm thick solid neoprene rubber, The caps, which were bonded to the flanges of the lamella beams keep the geotextile material in place and exclude water and debris from the joint.

When measured on the bridge deck, these geotextile and neoprene inserts were found to reduce the maximum band-limited noise levels by an average of 10.3 dB compared to the levels from the untreated joint - corresponding to roughly a halving of the subjective loudness of the croaking noise. Since this noise reduction was achieved at the source, similar reductions were anticipated at the quite distant (700 m) residences most bothered by the noise. Digital sound recordings made before and after the geotextile joint treatment using a B&K Type 2250 portable analyzer confirmed this expected outcome.

**Figure 1. Mageba Modular Expansion Joint**

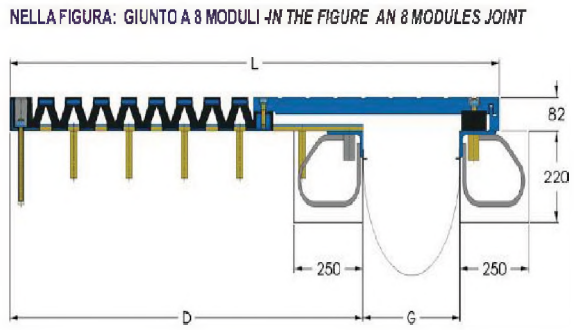


**Figure 2. Alba Expansion Joint (cross section)**

## 7. CROAKING NOISE MECHANISM

### 7.1 Helmholtz Resonator Theory

Initially it was suspected that the croaking noise was due to an acoustic resonance involving the compliance of both the volume of air in the joint cavities and the compliance of the rubber joints seals. However, when the Alba expansion joint, which has no lamella beams or rubber seals, was seen to produce a very similar noise, it became apparent that the compliance of mechanical joint components themselves had little influence on the observed resonant frequency. The standard equation for the frequency of a Helmholtz resonator could then be used in an attempt to confirm the source mechanism.

The classic Helmholtz resonator is a spherical volume connected to the outside air by an opening with or without a "neck". Such resonators can be used to absorb sound at frequencies close to resonance. However. if excited by a pulse of air pressure, as when one slaps the top of a empty bottle, sound energy at the resonant frequency is radiated to the outside world. In the classic Helmholtz resonator, the air volume in the sphere, or bottle, provides the compliance element while the "slug" of air in the resonator's neck provides the mass or inertance. If no physical neck is present, a short air column on either side of the opening (i.e., end correction) will provide the acoustical inertance. end correction length is related to the radius of opening.

Figure 3 shows a vehicle tire rolling over the gap between two adjacent lamella beams within a modular expansion joint. As the tire rolls over each successive gap, a semi-enclosed volume of air is temporarily created between the tire tread above and the v-shaped rubber surface, lamella beam edges and the joint seals, then act as "necks" on either side of the resonator volume.

Type equation here.

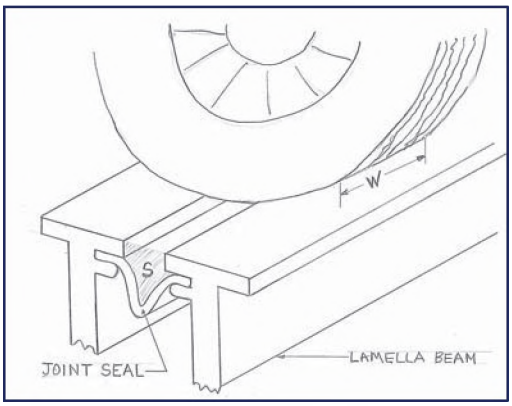


**Figure 3. Modular Expansion Joint with Tire**

The natural frequency of a Helmholtz resonator (Kinsler and Frey, 1950) is given by:

$$f = \frac{c}{2\pi}\left(\frac{S}{lV}\right)^{1/2} \text{ Hz.} \qquad \text{Equation 1}$$

If the area of the resonator's openings, or necks, is "S" and the typical width of a light vehicle tire is "W", then the resonator cavity volume "V" is:

$$V = SW \qquad \text{Equation 2}$$

The effective length of the neck "l" is equal to the actual neck length, (here zero), plus two end corrections, "Δl", assumed (Kinsler and Frey, 1950) to be approximately 0.85a, where "a" is the equivalent radius of the neck opening. In this case, "a" is roughly 24 mm. Substituting for V from Equation 2 into Equation 1, we obtain:

$$f = \frac{c}{2\pi}\left(\frac{1}{lW}\right)^{1/2} \text{ Hz.} \qquad \text{Equation 3}$$

Solving Equation 3 with c = 345 m/sec, l = 41 mm and W = 180 mm, we obtain a Helmholtz frequency of 635 Hz.

## 8. CONCLUSIONS

While the Helmholtz frequency varies with assumed tire width and effective resonator neck length, the excellent agreement between the predicted resonance frequency and the central value obtained from many croaking noise events, confirms the mechanism behind this unusual noise. The two joint types, while very different in design, create similar croaking frequencies because this frequency is primarily a function of tire width. The effectiveness of the geotextile inserts is attributed to a combination of sound absorption in the cavity and vibration damping of the rubber seals.

## REFERENCES

1., D. Marriner and C. Wakefield. "Modular Expansion Joint Noise in BC", Inter-noise 2011, Osaka Japan.

2., K.A.Ravshanovich, H. Yamaguchi, Y. Matsumoto, and S. Uno, "Mechanism of Noise Generation from Modular Expansion Joint under Vehicle Passage", Dept. of Civil and Environmental Eng., Saitama University, Sakura-Ku, Saitama, Japan.

2., F. Asdrubali, F.D. Alessandro and S. Schiavoni, "Sound Absorbing Properties of Materials made of Rubber Crumbs", Acoustics 08 Paris, www.acoustics08-paris.org.

3., Lawrence E. Kinsler and Austin R. Frey, "Fundamentals of Acoustics", John Wiley & Sons Inc., 1950.

# INFRASOUND NOISE RADIATED FROM VIBRATING SCREENS AT AN ORE REFINERY: PART 1 – PROBLEM ANALYSIS AND SMALL SCALE MODEL DESIGN

**Louis-Alexis Boudreault, Michel Pearson and André L'Espérance**
Soft dB inc., Quebec, QC, Canada, G1S 3G3, www.softdb.com

## 1. INTRODUCTION

An infrasound problem has been identified at an ore refining factory. Despite being inaudible, the infrasound levels are high enough to generate discomfort among workers and to generate vibration in the building structure.

Measurements were taken on site and led to identify the vibrating screens as the dominant source. The 10 m by 3 m screen area vibrating in a vertical motion produces an average pressure level of 115 dB at 14 Hz at 2 m from the source.

In order to evaluate potential solutions allowing to reduce the screens' acoustical emission, a 1:15 scale model was built to be tested in laboratory. This approach proved to be appropriate considering the acoustical complexity, the cost and difficulty related to the evaluation of solutions on site.

Noise mapping techniques were used to highlight the radiating patterns and measure the performance of tested solutions. (Part 2)

## 2. NOISE SOURCE DESCRIPTION

The vibrating screen consists of a concave shaped vibrating plate. The ore inflow comes at the top of the screen and the coarse particles go out at the bottom. The screened particles are collected using a pyramidal shaped hopper.

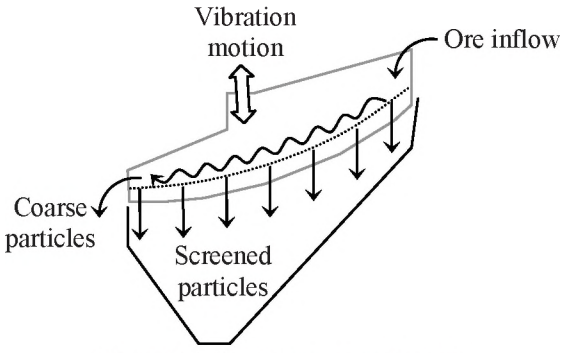


**Figure 1. Vibrating screen schematic**

The vibrating plate associated to the pyramidal hopper acts like a giant baffled loudspeaker:

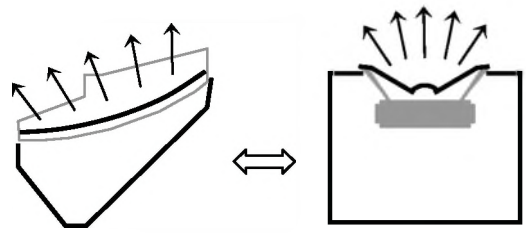

**Figure 2. Loudspeaker analogy**

## 3. MODEL DESCRIPTION

The 1:15 scale model is built from wood and has basically four parts: the screen plate, the hopper, the inertial base and the structure. Each of these elements is mechanically isolated from the others using neoprene pads.

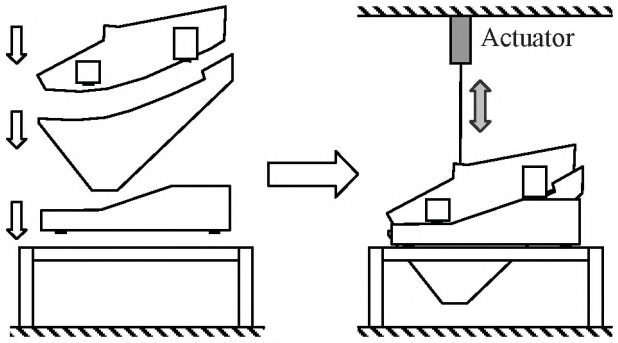


**Figure 3. Small scale model elements**

A vibration actuator is fixed to the ceiling and attached to the screen to generate the vibration motion.

## 4. ACOUSTICAL TREATMENTS

### 4.1. Acoustical short-circuits

Acoustical short-circuits, or holes in the screen plate were made in order to equilibrate the acoustical pressure on each side of the screen plate. The holes also reduce the radiating area of the screen plate reducing even more the generated sound pressure.

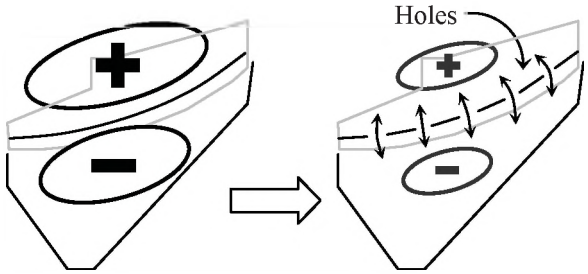


**Figure 4. Acoustical short-circuits concept**

The final solution took the shape of a slot in the center of the screen plate running from the top to the bottom. This solution allowed maximizing the holes' area without comprising the industrial process.

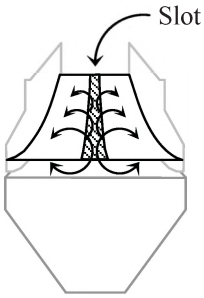


**Figure 5. Acoustical short-circuits implementation**

### 4.2. Enclosure volume

A closed-box acoustical system acts as a first order high-pass filter where its cut-off frequency is linked to the enclosure volume. The cut-off frequency increases as the enclosure volume is reduced. If the operating frequency is located on the rolloff, increasing the cut-off frequency will cause attenuation. To validate this concept, several hopper volumes where tested on the model.

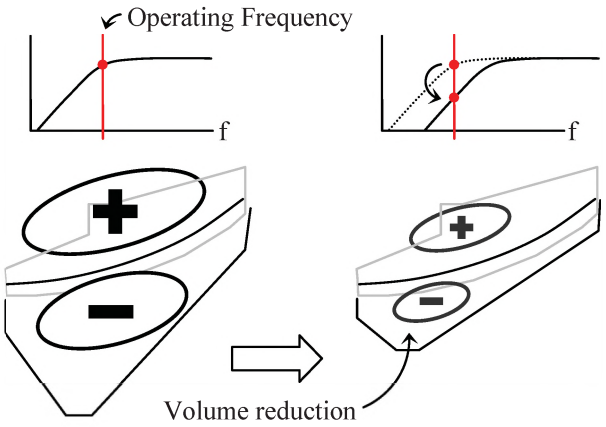


**Figure 6. Enclosure volume reduction concept**

Tests performed on the small scale model indicated that a smaller enclosure volume led to greater attenuation. A new hopper was designed with this phenomenon in mind:

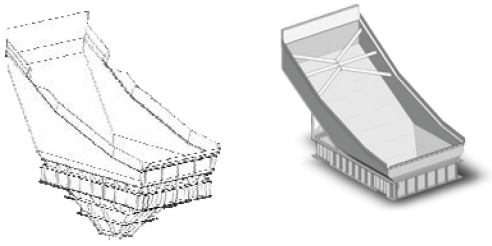


**Figure 7. Hopper comparison**

## 5. FINAL CONCEPT AND RESULTS

The final concept includes the two basic phenomena described above: acoustical short-circuits and enclosure volume reduction.

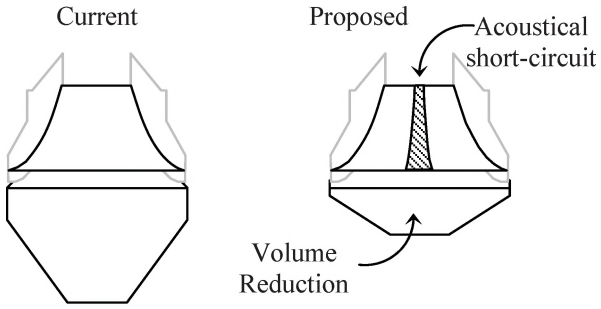


**Figure 8. Final Concept**

The first implementation stage is to implement the slot on the screen plate. The second stage is to implement the reduced volume hopper. The graph below presents the attenuation provided by each implementation stage on the small scale model.

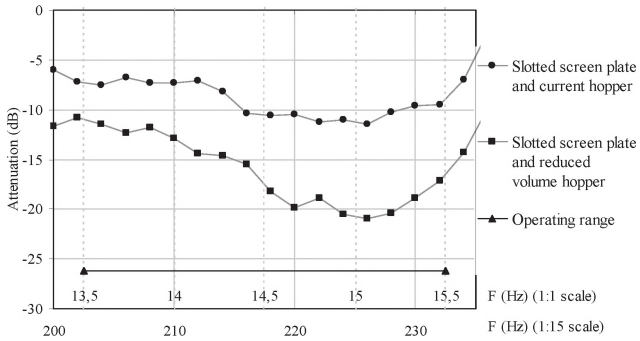


**Figure 9. Attenuation results on small scale model**

Tests performed on the small scale model led to 5 to 12 dB attenuation for the first stage of implementation. The second stage adds additional 5 to 10 dB attenuation for a total of 10 to 20 dB attenuation over the operating range. On-site implementation is currently ongoing.

## 6. CONCLUSION

In conclusion, it has been shown that the small scale model approach proved to be an appropriate way to analyze the problem and identify solutions for this particular case.

Part 2 of current article covers noise mapping techniques used on the small scale model to identify radiating patterns and measure the performance of tested solutions.

# INFRASOUND NOISE RADIATED FROM VIBRATING SCREENS AT AN ORE REFINERY: PART 2 – NOISE REDUCTION TREATMENTS AND NOISE MAPPING TECHNIQUE

**Louis-Alexis Boudreault, Michel Pearson and André L'Espérance**
Soft dB inc., Quebec, QC, Canada, G1S 3G3, www.softdb.com

## 1. INTRODUCTION

An infrasound problem has been identified at an ore refining factory and large vibrating screens were identified as the dominant source.

In order to evaluate potential solutions allowing to reduce the screens' acoustical emission, a 1:15 scale model was built to be tested in laboratory.

Noise mapping techniques were used to highlight the radiating patterns and measure the performance of tested solutions.

Read part 1 of the current article for exhaustive noise source description and methodology.

## 2. NOISE MAPS

Noise maps were performed on the side and the top of the small scale model (Figure 1 and 2).

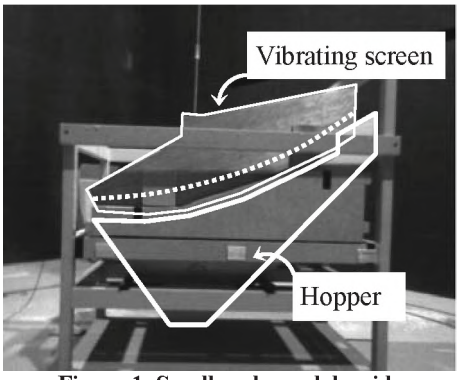


**Figure 1. Small scale model – side noise maps' background picture**

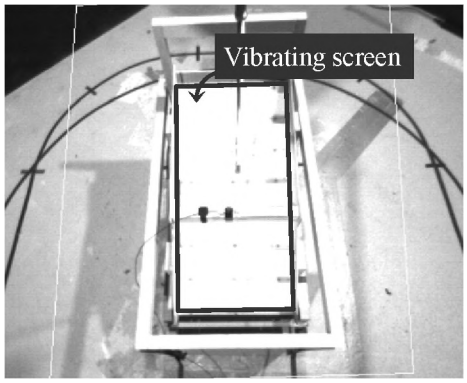


**Figure 2. Small scale model – top noise maps' background picture**

The displayed value is the sound intensity global level ranging from 205 to 235 Hz which represents the 13.5 to 15.5 Hz operating range for the full scale vibrating screen and the color scale ranges from 65 to 85 dB. The noise maps were performed at a 15 cm distance from the sound source.

## 3. RESULTS

The noise maps were performed for the key configurations:

1. Complete screen plate and current hopper (reference case)
2. Slotted screen plate and current hopper (first implementation stage)
3. Slotted screen plate and reduced volume hopper (second implementation stage)

These configurations are explained in part 1 of the current article

Figure 4 and 7 show the current configuration (prior to treatments implementation). The strongest sound source is identified at the gap between the screen plate and the hopper. The lack of acoustical short-circuit generates a high pressure level in the hopper and the leak at the hopper's perimeter radiates the energy to the outside. When seen from the top (Figure 7) the energy is evenly distributed on the screen plate with a slight increase at the center region.

Figure 5 and 8 show the first stage of implementation with the slotted screen plate. The acoustical short-circuit generated by this opening in the screen plate reduces the radiated energy by 8 to 9 dB. It also reduces the sound pressure in the hopper subsequently reducing energy radiated from the leaks located at the hopper's perimeter.

Figure 6 and 9 show the second stage of implementation with a reduced volume hopper and the slotted screen plate. This proposed hopper gives an additional 5 to 8 dB. The hopper replacement reduces globally the radiated energy but doe not modify significantly the radiating pattern.

## 4. CONCLUSION

The noise mapping technique proved to be useful in the process of acoustical phenomena identification on the small scale model. It also helped to improve the treatments performance by providing a visual representation of the radiated energy.

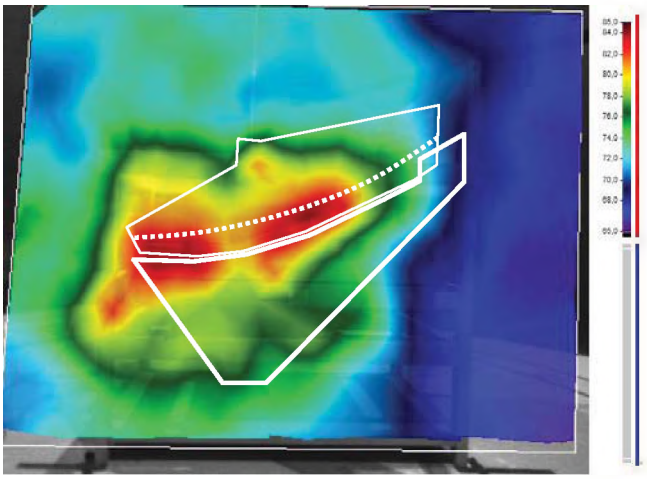

**Figure 3. Complete screen plate and current hopper – side**
**205 to 235 Hz global level**
**$L_I$ = 81 dB**

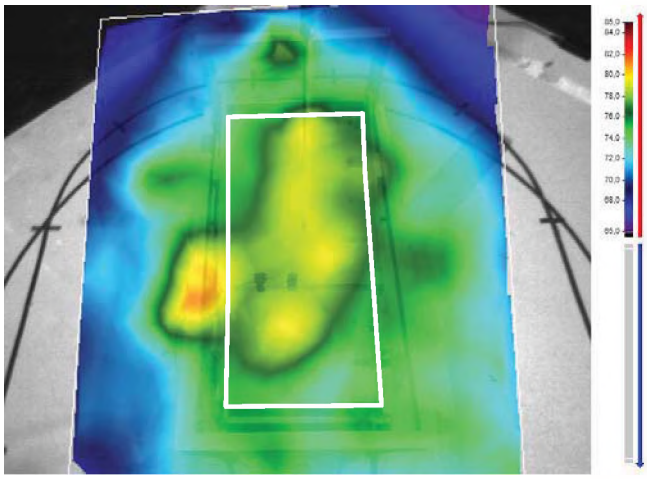

**Figure 6. Complete screen plate and current hopper – top**
**205 to 235 Hz global level**
**$L_I$ = 81 dB**

**Figure 4. Slotted screen plate and current hopper - side**
**205 to 235 Hz global level**
**$L_I$ = 72 dB**

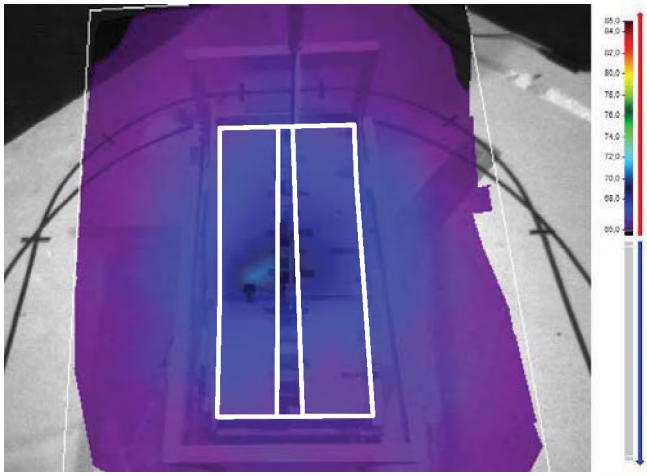

**Figure 7. Slotted screen plate and current hopper - top**
**205 to 235 Hz global level**
**$L_I$ = 73 dB**

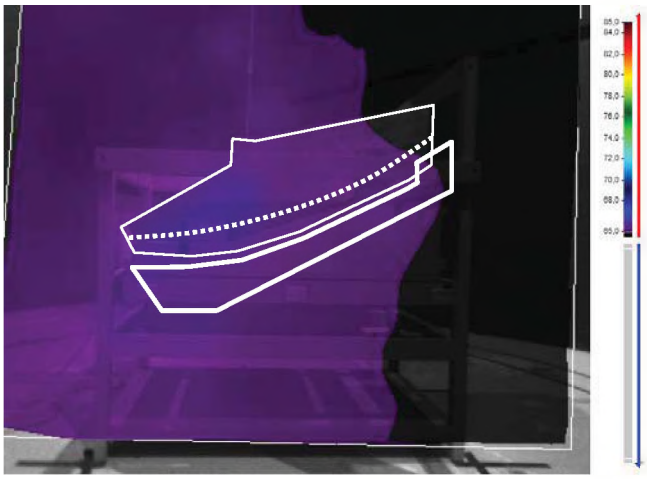

**Figure 5. Slotted screen plate and proposed hopper – side**
**205 to 235 Hz global level**
**$L_I$ = 67 dB**

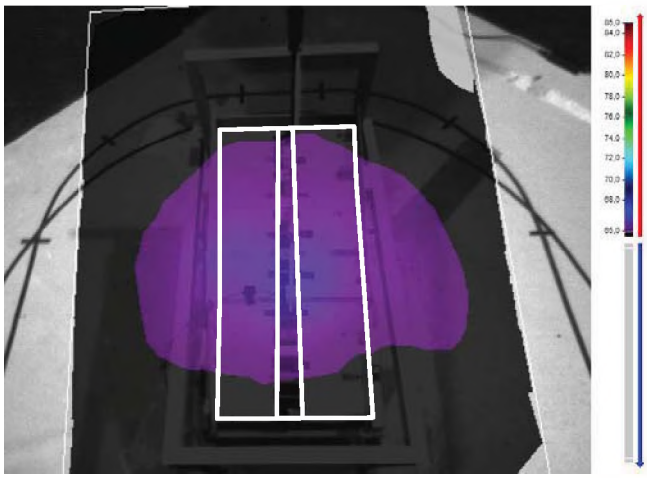

**Figure 8. Slotted screen plate and proposed hopper – top**
**205 to 235 Hz global level**
**$L_I$ = 65 dB**

# PERFORMANCE EVALUATION OF DUCT BENDS

**Ramani Ramakrishnan[1] and Romain Dumoulin[2]**
[1]Department of Architectural Science, Ryerson University, Toronto, ON, rramakri@ryerson.ca
[2]3126 Blvd. Rosemont, Montreal, Quebec, dumoulin.acoustics@gmail.com

## 1. INTRODUCTION

Acoustical performances of simple elbow (round and rectangular) fittings, used in building HVAC systems, have been conventionally evaluated using empirical relations based on laboratory and/or field measurements as seen in the results of Ver[1]. Basic tabular results can also be obtained from ASHRAE handbooks[2]. One dimensional modelling techniques were unable to provide reliable results. And hence a-multi-dimensional commercially available software, COMSOL, was used to provide simple design curves for rectangular elbows lined on all four sides[3]. The software applies finite element techniques to solve for the acoustical performances. The model is also capable of using the material properties of the liner materials. The liner is considered to be bulk reacting. Preliminary results of the multi-dimensional model will be presented in this paper.

## 2. ATTENUATION OF DUCT FITTINGS

The American Society of Heating, Refrigerating and Air-Conditioning Engineers (ASHRAE) have developed simple steps to evaluate the attenuation of duct fittings such as elbows, lined and unlined, based on the results of Ver[1]. Examples of these results are shown in Figures 1 and 2. However, these results couldn't be represented easily in a tabular form and in addition are based on simple empirical relationships. With the availability of powerful numerical tools, the simple results can be updated to provide a larger set of attenuation results.

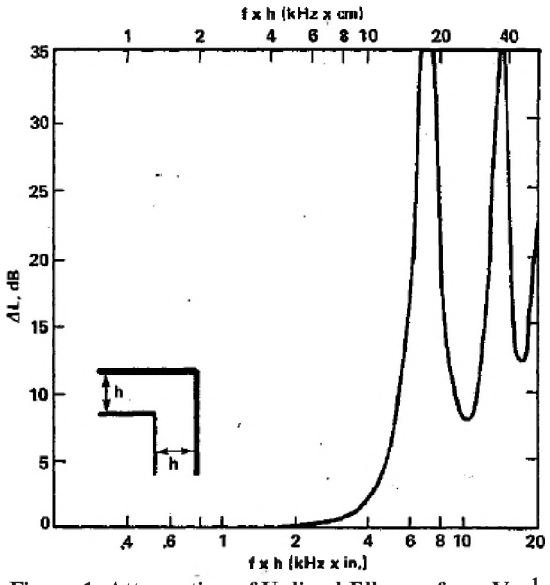


**Figure 1. Attenuation of Unlined Elbows, from Ver[1].**

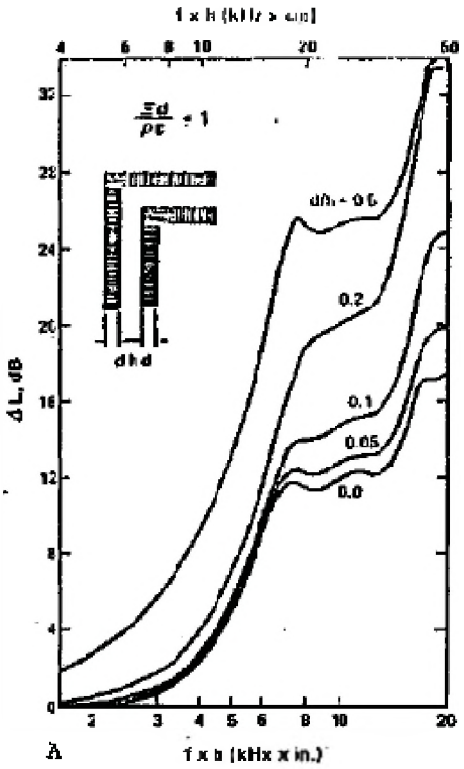


**Figure 2. Attenuation of Lined Elbows, from Ver[1].**

[Ξ is the flow resistivity of the liner per unit thickness and ρc is the characteristic impedance of air in Figure 2.]

The current investigation has made use of COMSOL, a powerful multiphysics numerical analysis tool and has attempted to provide results based on multi-dimensional analysis.

## 3. BACKGROUND

The schematic details of a lined elbow fitting are shown in Figure 3. The liners are symmetric in Figure 3. The liner details are: liner depth is 'd'; the open air-way width is 'h'; and the liners are used for a minimum of two-duct width on either side.

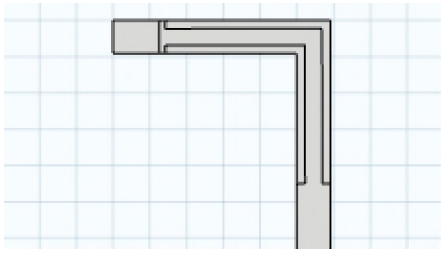

**Figure 3. Details of a Lined Elbow.**

The sound propagates along the centre axis from left to right. The baffle materials are bulk reacting and hence appropriate complex wave speed and material density (complex in this case) can be obtained from Bies and Hanson[4]. The mathematical modelling details were presented in Ramakrishnan and Watson[5].

## 4. COMSOL MODEL

The elbow geometry can be easily modelled as 3-D. In this investigation, however, the elbow is modelled in a 2-D configuration as shown in Figure 3. The liner material is assumed to be isotropic and homogeneous fibrous material of given flow resistivity, 'Ξ'. The acoustic propagation in the liner material uses the complex propagation constant and complex density of bulk reacting material. A given acoustic field was assumed at the inlet of the elbow and the outlet is connected to a long anechoic termination. To accommodate high frequency calculation, COMSOL suggests using a length of pipe in front of the elbow within which scattered acoustic field is calculated to provide the required acoustic field at the inlet of the lined (or unlined) elbow. The application of COMSOL for simple rectangular ducts with baffles was validated in Ramakrishnan[6].

The elbow attenuation is given in Equation (1) below.

$$IL = \frac{W_{in}}{W_{out}}, dB \qquad (1)$$

where, $W_{in}$ is the sound power at elbow inlet and $W_{out}$ is the sound power at the elbow outlet. The results of the acoustic propagation from COMSOL model are presented in the next section.

## 5. RESULTS AND DISCUSSION

The main focus of the current investigation is to provide an extensive tabular set of results for lined elbows similar to the tables given in Reference 2. The first step is to compare the COMSOL results to those of Ver[1]. Two sets of results are shown in Figures 4 and 5.

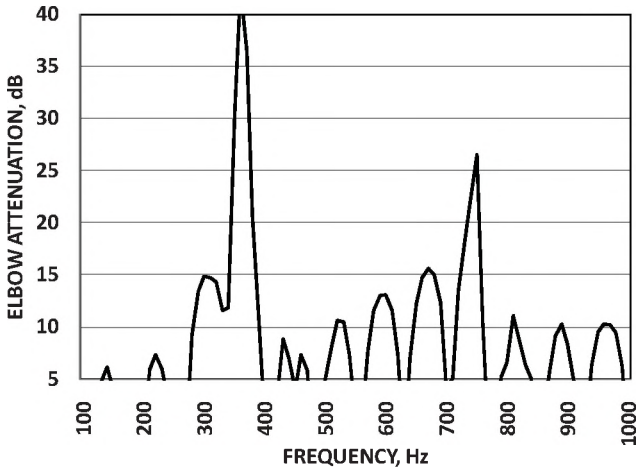


**Figure 4. Attenuation of Unlined Elbows, h = 0.56 m.**

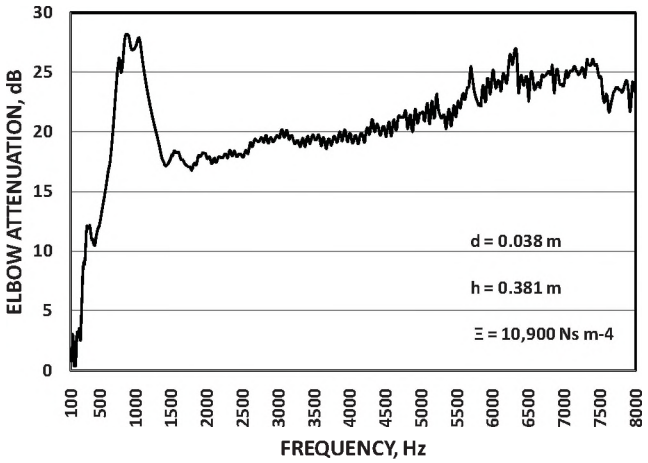


**Figure 5. Attenuation of Lined Elbows.**

The COMSOL results from 2-D modelling are seen to produce results similar in trend to the results of Ver[1]. It must be pointed out that the scales are different between the results of Figures 1 and 4 and Figures 2 and 5. Further, sample results of three elbows (unlined, lined- d/h of 0.1 and 0.5) are given in Table 1 below.

**Table 1. Attenuation of Elbow Fittings, dB.**

| | 125 | 250 | 500 | 1000 | 2000 | 4000 |
|---|---|---|---|---|---|---|
| Type 1 | 1.5 | 4.4 | 5.4 | 5.3 | 6.2 | 8.7 |
| Type 2 | 1.3 | 5.8 | 13.2 | 22.7 | 18 | 20.2 |
| Type 3 | 4.4 | 12.2 | 22.9 | 23.4 | 16.4 | 14.4 |

## 6. CONCLUSIONS

Attenuation results for duct elbow fittings were evaluated using two-D representation in commercial application software, COMSOL Multiphysiscs[3]. COMSOL model results were seen to be closer to the test data similar to the results of Istvan Ver[1]. The intent of producing a large set of tabular results has also been initiated.

## REFERENCES


1. Istvan Ver, "A Study to Determine the Noise Generation and Noise Attenuation of Lined and Unlined Duct Fittings," Report #5092, ASHRAE RP-265, June 1983.
2. "Sound and Vibration Control, Chapter 47" ASHRAE Handbook – HVAC Applications, 2007.
3. COMSOL Multi-Physics Application Software, Boston, MASS, Version 4.2. (2011).
4. D. A. Bies and C. H. Hansen, *Engineering Noise Control-Theory and Practice*, 3rd Edition, Spon Press, London. (2003).
5. R. Ramakrishnan and W. R. Watson, "Design Curves for Rectangular Splitter Silencers," *Applied Acoustics*, Vol 35, No.1, pp. 1-24 (1992).
6. Ramani Ramakrishnan, "Validation of COMSOL Multiphysics and Acoustical Performance of Splitter-Silencers," Proceedings of Acoustics Week in Canada, *Canadian Acoustics*, Vol. 38, No.3 pp 178-179 (2010).

# REDUCTION OF NOISE USING MULTIPLE EXPANSION CHAMBERS

**Muhammad A. Hawwa and Ma'mon M. Horoub**
Department of Mechanical Engineering, King Fahd University of Petroleum and Minerals, Dhahran 31261, Saudi Arabia

## ABSTRACT

Expansion chambers are often used to reduce the noise in different systems like air conditioning systems, exhaust systems, and car muffler systems. This study focuses on the effectiveness of multiple expansion chambers in reducing noise in such systems. Optimized designs are realized by utilizing changes in cross sectional areas, changes in the lengths of the expansion chambers, or combined changes of both. It is found beneficial to apply taper functions to the expansion chambers' geometry, resulting in similar effects of the window functions utilized in the field of digital signal processing.

## 1. INTRODUTION

Expansion chambers are effective tools for reducing noise in several applications. The most familiar example is probably the automotive muffler, where a single tuned expansion chamber is utilized.

Double expansion chambers were considered by Lamancusa,[5] who calculated the transmission loss coefficients for various cases with different geometric parameters. Kim and Ih[6] studied the sound attenuation due to an expansion chamber with curved duct bends. Gerges et al.[12] studied the transmission loss caused by expansion chambers with and without inlet/outlet extend tubes. Suwandi et al.[13] considered the acoustic performance of simple expansion chamber mufflers using a plane wave transmission line theory. Wu et al.[3] presented transmission loss predictions for a single-inlet-double-outlet cylindrical expansion-chamber muffler by using the modal meshing approach. Chiu and Chang[7] performed a shape optimization analysis on multi-chamber cross-flow mufflers using SA optimization. Venkatesham et al.[11] analyzed transmission loss of rectangular expansion chamber with arbitrary location of inlet-outlet by means of Green's functions. Chiu[2] optimized the shape of multi-chamber mufflers with plug-inlet tube on a venting process using genetic algorithms (GA). Chiu and Chang[9] made a numerical assessment of a space constrained venting system with multi chamber plug mufflers by GA method. Chaitanya and Munjal[10] studied the effect of wall thickness on the end corrections of the extended inlet and outlet of a double-tuned expansion chamber.

In this study, a duct with multiple expansion chambers is analyzed. The chambers are considered with different sectional areas. The choice of the areas is determined by analytical formulae inspired by the theory of windowing often used in the field of digital signal processing. Comparison of acoustic performance is made using the calculated transmission loss spectra.

## 2. ANALYSIS

Although the analysis presented in this paper is made general to account for an arbitrary number of expansion chambers, focus is placed on three expansion chambers illustrated in Figure 1.

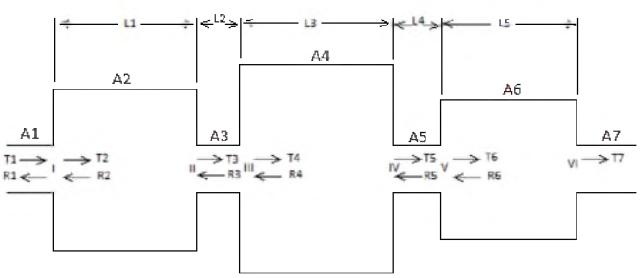


**Figure 1. Geometry of three expansion chambers with unequally area chamber [ Aj: Area, Lj: Length].**

The theoretical transmission loss is defined as the logarithmic ratio of incident to transmitted acoustic powers as

$$TL = 20Log_{10}(T_1 / T_7) \quad \text{.....(1)}$$

where $T_1$ Is the pressure amplitude of the acoustic wave incident into the first expansion chamber, and $T_7$ is the pressure amplitude of the transmitted acoustic wave exiting the third expansion chamber.

Transmission phenomenon in a duct with expansion chambers can be considered by several methods, one of them is the transfer matrix method which is easy to program on computer to obtain theoretical values for transmission loss. Adopting acoustic pressure P and mass velocity V as the two state variables,[1] every junction in the duct system can be related to the previous junction by a matrix. Then, a global transfer matrix can relate variables at the seventh junction to those at the first junction by applying continuity conditions of pressure and volume velocity as

$$\begin{bmatrix} P(r) \\ U(r) \end{bmatrix} = \begin{bmatrix} T & 2X2 & transfer & matrix \\ for & the & rth & junction \end{bmatrix} \begin{bmatrix} P(r-1) \\ U(r-1) \end{bmatrix} \quad \text{.....(2)}$$

illustrated below

where $\begin{bmatrix} P(r) & U(r) \end{bmatrix}$ is called the state vector at the upstream point r, $\begin{bmatrix} P(r-1) & U(r-1) \end{bmatrix}$ and is called the state vector at the

downstream point $r-1$.The transfer matrix for the rth element can be denoted by $[T_r]$.[1],[4]

Choice of the cross sectional areas of expansion chambers are based on tapering function (window function), illustrated in Table 1.

**Table 1. Taper Functions[8]**

| Taper Functions | DSP Window |
|---|---|
| $w(n) = 0.54 - 0.46\cos(\frac{2\pi n}{N-1})$ | Hamming Window |
| $w(n) = \cos(\frac{\pi n}{N-1} - \frac{\pi}{2})$ | Cosine Window |
| $w(n) = n$ | Linear Window |
| $w(n) = 1$ | Rectangular Window |

In figure (1) let $A_1=A_3=A_5=A_7$ , so in Hamming and linear window $A_2 < A_4 < A_6$ depend on table (1) and for Cosine window $A_2 < A_4 > A_6$, also in Decrease then Increase window $A_2 > A_4 < A_6$ Increase then Decrease window $A_2 < A_4 > A_6$, and in Rectangular window $A_2 = A_4 = A_6$.

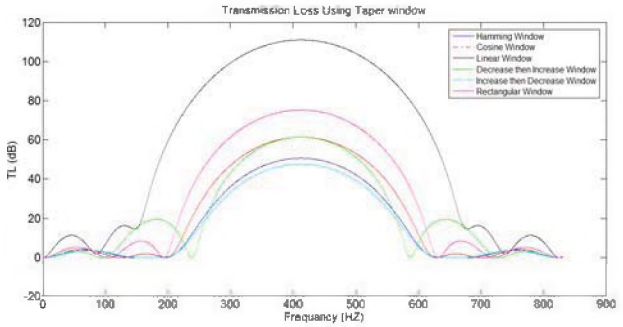


**Figure 2. Transmission Loss due to three expansion chambers with various geometry.**

## 3. RESULTS

The transmission loss due to multiple duct expansion chambers is calculated using the transfer matrix method and. The basic geometry of the expansion chambers is selected to have the following properties: $L_1 = L_2 = L_3 = L_4 = L_5 =$ 0.2m, the radius of the tube = 0.1m. The areas of the expansion chambers are decided upon imposing taper functions listed in Table (1) with a mean radius of the expansion chamber = 0.21m. Thus, the areas of the chambers ($A_2$ , $A_4$ , $A_6$) depend on the taper function and $A_1=A_3=A_5=A_7$.

As seen in Figure 2, the transmission loss is affected by the taper function. The best result is the linear taper function according to which the areas of chamber increase or decrease linearly, it attenuate high value of transmission loss and wide range.

## REFERENCES


1- M. L. Munjal, "Acoustics Of Ducts And Mufflers", John wiley and sons (1987).

2- B. Venkatesham, M. Tiwari and M.L. Munjal, "Transmission loss analysis of rectangular expansion chamber with arbitrary location of inlet-outlet by means of Green's functions", Journal of Sound and Vibration 323 (2009) 1032–1044.

3- C.J. Wu, X.J. Wang, and H.B. Tang, "Transmission loss prediction on a single-inlet-double-outlet cylindrical expansion-chamber muffler by using the modal meshing approach", Applied Acoustics 69 (2008) 173–178.

4- F. Masson, P. Kogan, and G. Herrera, " Optimization of muffler transmission loss by using microperforated panels", FIA 2008 –A168.

5- J.S. Lamancusa, "the transmission loss of double expansion chamber muffler with unequal size chambers", Applied Acoustics 24 (1988) 15-32.

6- J-T. Kim and J-G. Ih, "Transfer matrix of curved duct bends and sound attenuation in curved expansion chambers", Applied Acoustics 56 (1999) 297-309.

7- K.S. Andersen, "Analyzing Muffler Performance Using the Transfer Matrix Method", Excerpt from the Proceedings of the COMSOL Conference 2008 Hannover.

8- M.A. Hawwa, "Waveguides with periodic undulations inspired by DSP windowing", Journal of Sound and Vibration 209 (1998) 699-706.

9- M-C. Chiu, "Shape optimization of multi-chamber mufflers with plug-inlet tube on a venting process by genetic algorithms", Applied Acoustics 71 (2010) 495–505.

10- M-C. Chiu and Y-C. Chang, "Numarical assessment of a space constrained venting system with multi chamber plug mufflers by GA method", Journal of Marine Science and Technology, Vol. 18, No. 3, pp. 317-332 (2010).

11- M-C. Chiu and Y-C. Chang, "Shape optimization of multi-chamber cross-flow mufflers by SA optimization", Journal of Sound and Vibration 312 (2008) 526–550.

12- S. N.Y. Gerges, S. N.Y. Gerges, J.L.B. Coelho, and J. P. Arenas, " Muffler Modeling by Transfer Matrix Method and Experimental Verification", 132 / Vol. XXVII, No. 2, April-June 2005.

13- D. Suwandi, J. Middelberg, K.P. Byrne, and N.J. Kessissoglou, "Predicting the acoustic performance of mufflers using transmission line theory", Proccding of acoustics 2005, Western Australia.

# PHONETIC AND PHONOLOGICAL INFLUENCE OF A SPEECH-IMPAIRED SPEAKER ON RHYTHM

**Gurnikaita Chhina[1], Tae-Jin Yoon[2], and Karin Humphreys[3]**
[1]Dept. of Life Science, McMaster University, 1280 Main St. W., Hamilton, Canada, L8S 4M2
[2]Dept. of Linguistics, McMaster University, 1280 Main St. W., Hamilton, Canada, L8S 4M2
[3]Dept. of Psychology, Neuroscience, and Behaviour, McMaster University, 1280 Main St. W., Hamilton, Canada, L8S 4M2

## 1. INTRODUCTION

We present detailed phonetic analyses of a 61 year-old monolingual female English speaker. The speaker from Halifax, Nova Scotia, acquired a speech disorder from a motor vehicle accident. The disordered speech was detected three years after the brain injury she suffered from the accident, and perceived by her family and friends as being similar to Southern U.S. dialect or Scottish English. It is reported that her disordered speech is a rare but possible case of Foreign Accent Syndrome (FAS; Louch 2009). FAS may lead to long-term muscular adjustments of the vocal apparatus that lead to changes in articulatory, phonatory, prosodic settings (Moen, 2000). There is considerable variability among reported cases of FAS in terms of phonetic characteristics and impairments (Varley, Whiteside, Hammill & Cooper, 2006). We hypothesize that one of the factors that make the accent change in her speech is due to a change in her rhythmic characteristics. In order to test the hypothesis, we calculated %V (proportion of vocalic duration over the total duration of an utterance) as a measure of rhythm. In order to find out factors that may affect the %V value, we further conducted detailed phonetic analyses to understand the impact of the speaker's speech characteristics on the %V that deviates from that of Canadian English. The results indicate that both phonetic and phonological factors contribute to her non-canonical rhythmic pattern.

## 2. DATA

The speaker, LA, is a monolingual English-speaking Canadian Woman and she was 61-year old when the data were collected. She was born in St. Catherines, Ontario, moved out east around age 6, and has resided in Nova Scotia since the fifth grade. She has lived in Eastern Atlantic Canada for most of her life. She was a retired special education teacher. The speaker acquired a speech disorder three years after suffering from a brain injury from a motor vehicle accident. One day three years after the accident, her family member observed noticeable changes in her speech such as word searching, stuttering, and a robotic style of speech. These changes were salient when the speaker was extremely tired or anxious. According to the family members, she woke up one morning speaking with slow and broken speech sounding like a foreign accent. Her speech is regarded as often shifting from her Atlantic Canadian English to what was perceived as Scottish English at times or as Southern United States English at times (Louch 2010).

Upon request by the family members, the third author visited the speaker and collected the speech recordings through sessions with the patient. The collected recordings range from simple read sentences to passages, and to spontaneous description of pictures. In this study, we report our preliminary analysis of a subset of the recordings of simple sentences.

In the subset of the collected data, the speaker pronounced 11 monophthongal vowels that are inserted in a /hVd/ context: *heed*, *hid*, *hade*, *head*, *had*, *who'd*, *hood*, *hoed*, *hud*, *hawed*, and *hod*. Each target was embedded in one of two carrier phrases, "the next word is /hVd/." and "I said /hVd/ again." In order to conduct phonetic analyses including %V, we segmented the utterances phonetically and then collapsed the segments into consonant intervals and vocalic intervals, using a custom-made script in Praat (Boersma & Weenink, 2010).

## 3. RESULTS

Typical stress-timed languages such as English have complex syllable structure and tend to have reduced vowels in unstressed positions. Therefore, the average vocalic duration is expected to be relatively shorter than the average consonantal duration. Indeed, Ramus *et al.* (1999) reports that the %V is about 40.1 in English. Given the complex syllable structure and reduced vowels in unstressed positions, relatively lower value of %V is expected. But measurement can be affected by different phonetic characteristics even within the same language group, or even between different dialects of the same language. For example, Grenon (2010) reports that the %V value is 47 in Canadian English, and she attributes the higher %V than the one reported in Ramus *et al.* (1999) to the relatively longer aspiration in Canadian stops. We found the %V of the speaker is 52, even higher than the average for Canadian English. At least two possibilities can be entertained: (1) disordered speech characteristics of our subject prolonged vocalic duration more than consonantal duration, or (2) the rhythmic characteristic of her speech may resemble syllable-timed languages (with simpler syllable structure).

## 4. DISCUSSIONS AND CONCLUSION

We conducted detailed phonetic analyses to understand the impact of the speaker's speech characteristics on the relatively higher %V than that of Canadian English. Speech characteristics of the speaker include slow, enunciated, and prolonged realization of segments, frequent insertion of pauses, and release of word-final stop consonants, as well as the following non-canonical characteristics: (1) Occasional modification of syllable structure via a schwa-like vowel insertion, as in Figure 1, (2) fully aspirated stop in the intervocalic context, as in Figure 2, and (3) a variant realization of [aj] to [a] (monophthongization), as in Figure 4 compared to Figure 3. The perception of her speech sounding as though Southern US English can be attributed to the occasional monophthongization of a diphthong [aj] to [a].

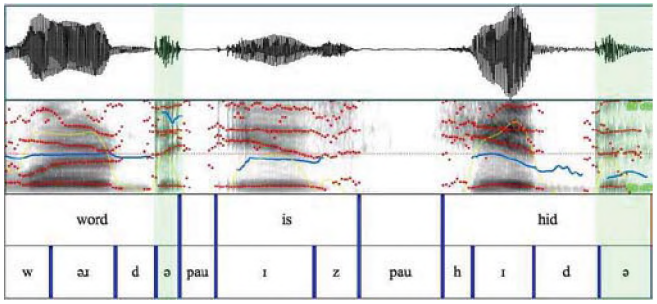


**Figure. 1. Insertion of two schwa vowels in words of the CVC structure. The words 'word' and 'hid' have modified syllable structure (i.e., CVCV) due to the vowel insertion.**

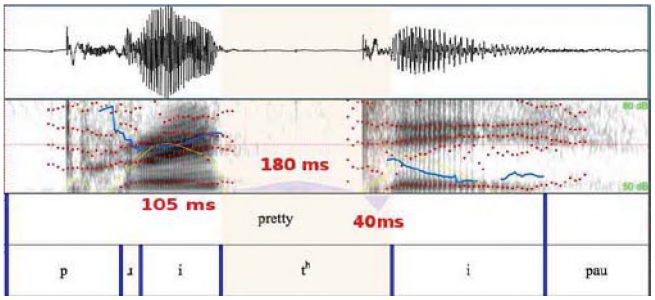


**Figure. 2. Fully aspirated stop in the intervocalic context. The intervocalic 't' is realized with long closure duration (180ms) and aspiration (40ms).**

Some of these non-canonical phonetic properties work toward reducing the %V value. The vocalic duration is asymmetrically longer than the consonantal duration. In addition, the perception of her speech sounding as though Southern U.S. English can be attributed to the occasional monophthongization of a diphthong [aj] to [a]. These phonetic differences make the speaker's post-stroke speech so distinctively different from her pre-stroke speech that her family and friend think she speaks a foreign accent. These characteristics of disordered speech that deviates from canonical speech properties of mainstream English poses a challenge on models of speech production that does not take into account possible modifications of phonetic properties and phonological structure. Further analyses and tests are needed to see whether these %V has indeed perceptual consequences.

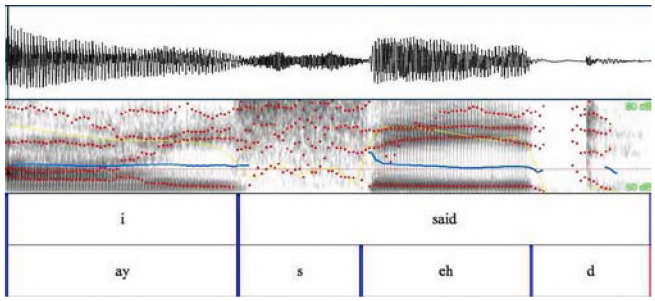


**Figure. 3. The canonical realization of the word 'I' as a diphthong is shown by two diverging F1 and F2. The release of final consonant is indicated by the stop burst on the final consonant in the word 'said.' The release of final consonant is optional in English, but the speaker tends to release most of the word final consonants.**

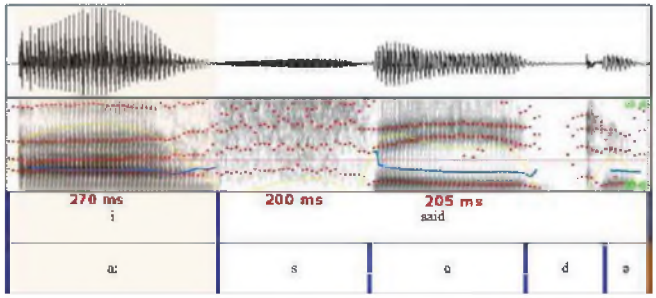


**Figure. 4. The non-canonical realization of the word 'I' as diphthong is shown by low two stable formants (F1 and F2). The final consonant is released and then followed by non-canonical schwa-like vowels as shown by voiced waveform and spectrogram at the end of the word 'said.' The figure is in contrast to Figure 3.**

## REFERENCES


Boersma, P. & Weenink D. (2010). *Praat: doing Phonetics by Computer (version 5.2)* [downloadable from http://praat.org].

Grenon, I. (2010). *An acoustic analysis of speech rhythm in Canadian English and Japanese*. (ms.) University of Victoria.

Louch, M. (2009). *A Case of Foreign Accent Syndrome*. B.Sc. Thesis. McMaster University.

Moen, I. (2000). "Foreign accent syndrome: A review of contemporary explanations." *Asphasiology*, 14, 5-15.

Ramus, F., M. Nespor & J. Mehler (1999) Correlates of linguistic rhythm in the speech signal. *Cognition* 73, 265-292.

Varley, R., Whiteside, S., Hammill, C., & Cooper, K. (2006). Phases in speech encoding and foreign accent syndrome. *Journal of Neurolinguistics, 19*, 356-369.


## AUTHOR NOTES


The work was conducted while the first author, Gurnikaita Chhina, was a student at McMaster University.

# SPEECH COMPENSATION IN PERSONS WHO STUTTER: ACOUSTIC AND PERCEPTUAL DATA

**Aravind K. Namasivayam[1,2] and Pascal van Lieshout[2,3,4,5,6]**

[1]The Speech and Stuttering Institute, Toronto, ON, Canada, M3B 3M4, e-mail:a.namasivayam@utoronto.ca
[2]Oral Dynamics Lab, Dept. of Speech-Language Pathology, University of Toronto, Toronto, ON, Canada, M5G1V7
[3]Dept. of Psychology, Human Communications Lab, University of Toronto. 3359 Mississauga Road, L5L1C6
[4]Institute for Biomaterials & Biomedical Engineering, 164 College Street, University of Toronto, ON, Canada M5S 3G9
[5]Toronto Rehabilitation Institute, 550 University Ave. Toronto, Ontario M5G 2A2
[6]Graduate Department of Rehabilitation Science, 500 University Ave. Toronto, Ontario M5G 1V7

## 1. INTRODUCTION

According to the Speech Motor Skills (SMS) approach stuttering dysfluencies are viewed as audible manifestations of errors in motor control arising from limitations in speech motor skill (Van Lieshout, Hulstijn, & Peters, 2004). Within this framework persons who stutter (PWS) fall on the lower end of a presumed normal speech motor skill continuum, while persons who do not stutter (PNS) are distributed across the higher end of the continuum. The underlying assumption is that if PWS are at the lower end of a speech motor skill continuum one should be able to find differences between PWS and PNS in tasks which tax their abilities to control their speech motor system. Specifically, these differences should be reflected in factors that typically characterize motor skill, such as the ability to compensate and adapt to changing and/or increasing task demands (Van Lieshout et al., 2004).

A method to increase demands on the speech motor system is through the use of oral-articulatory (bite-block) perturbations (McFarland & Baum, 1995). The presence of a bite-block decreases vocal tract constriction and increases the front cavity cross sectional area resulting in frequency increase in the first formant (F1) and decrease in the second formant (F2) with effects averaging approximately 20 to 100 Hz (McFarland & Baum, 1995). Although, much of the compensatory changes in format frequencies occur early (i.e. immediate compensation), studies on PNS indicate that compensation to bite-block perturbation may develop over time (adaptation) reaching normal acoustic pre-perturbation frequency ranges for vowels after about 10-15 minutes of speaking practice with the bite-block in place and even longer for consonants like fricatives (Baum, McFarland, & Diab, 1996; McFarland & Baum, 1995).

If delayed compensation is found in PNS with perfectly intact sensory-motor systems, then one would expect that if PWS have speech motor skill limitations, they would compensate to a lesser degree (i.e., with higher F1 and lower F2 values and lower perceptual speech quality ratings) and/or may take longer time to adapt to oral articulatory perturbations relative to PNS. For this study, we also included measures of fundamental frequency (F0) of vowels, word and vowel duration. F0 of vowels (especially for high vowel /i/) is related to neural and/or mechanical coupling between oral-articulatory and laryngeal subsystems. Raising the tongue body for high vowels in the presence of a bite-block may result in tensing of the vocal folds and subsequent changes in the F0 of vowels (Whalen & Levitt, 1995). We expect this effect to be stronger for PWS, especially with increasing speech rate, given their presumed limited ability in controlling and coordinating oral and laryngeal subsystems to mitigate the impact of the bite-block. Word and vowel duration measures provide an index of how task requirements relating to speech rate are implemented by PWS and PNS.

## 2. METHODS

### 2.1 Subjects

Five male adult PWS (M = 26.1, S.D. = 9.1) and five male adult PNS (M = 25.3, S.D. = 4.2) participated in this study. Based on stuttering severity instrument, two PWS were rated moderate and the remaining three were rated to be very mild, mild and severe. For the perceptual part of the study, listeners included 30 speakers of Canadian English (M= 25.9 yrs., S.D. = 4.7). Subjects reported no problems in vision, hearing and language (other than stuttering for the PWS) prior to participating in this study. The Human Ethics Review Committee at the University of Toronto approved the study.

### 2.2 Stimuli and Procedures

Subjects reiterated a bi-syllabic nonword /bapi/ for approximately 12 seconds at a pre-determined self-paced speech rate (habitual rate or fast but intelligible). Subjects started with a jaw-free condition (JF), immediately followed by the insertion of the bite-block between the 1st premolars (immediate bite-block [BB] condition) which was then followed by a 10-minute practice period (reading aloud with the bite-block in place), subsequent to which a post-practice (PBB) recording was carried out. For the bite-block conditions the inter-incisor distance was fixed at about 12 mm. Immediate compensatory changes relate to differences between the JF and BB sessions, while delayed adaptation changes are defined as the differences between BB and PBB sessions.

All audio signals were tape recorded and then digitized (16-bit / 16 kHz sampling), using PRAAT (Boersma & Weenink, 2006). For the perceptual part of the study, an AX paradigm was used, where the medial iteration of /bapi/ in the jaw free condition was chosen as the exemplar stimulus (A) and the test stimuli (X) were initial, medial or final iterations of the target word /bapi/ from each session

(JF/BB/PBB). 30 listeners then rated the speech quality of the test stimulus (X) on how closely it resembles the exemplar (A), by moving an indicator on a 10-cm computerized visual analog scale. A rating of 10 implies that the test stimulus is a perfect reproduction of the exemplar and a rating of 0 would mean that the test stimulus is a very poor reproduction of the exemplar. All stimuli in the AX paradigm were blocked by speech rate and speaker.

## 3. RESULTS AND DISCUSSION

For speech acoustics, first and second (F1 and F2) formants, duration, pitch and intensity values relating to vowels /a/ and /i/ from the bisyllabic nonword (/bapi/) were analyzed. The results of the acoustic evaluation revealed immediate, but partial, vocal tract compensation in the presence of a bite-block. In general, these changes were related to significant increases in F1 for /i/ [$F(2,14) = 13.94$, $p = 0.000$] and decreases in F1 and F2 for /a/ in the immediate BB condition. Some of these effects disappeared as speakers adapted to the presence of a bite-block with practice (e.g. F1 for /i/ returned to pre-perturbed JF baseline values following practice). Other spectral effects failed to return to pre-perturbation JF values even after practice (e.g. F2 for /a/) for both groups.

In terms of interactions, for F1 values of /a/ there was a significant two-way group x session interaction [$F(2,14) = 5.09$, $p = 0.021$] that was characterized by a significant decrease in F1 values for PWS from JF to BB and PBB conditions, while PNS showed minimal changes across conditions, indicating limited compensation and adaptation abilities in PWS. Furthermore, only for PWS, changes in F1 for /i/ across conditions were mirrored by pitch changes for the vowel as evidenced by a trend for a group x session interaction [$F(2,12) = 3.58$, $p = 0.060$]. This suggests a lack of fine-tuning in the control of compensatory responses.

The data also revealed that PWS may require additional time compared to PNS to adapt to perturbations. For example, pitch for /i/ returned to pre-perturbation baseline values for PWS after 10-minutes of practice with the bite-block, but this amount of practice was not sufficient to show a similar change in F1 for /a/. On the other hand, PNS immediately adjusted their vocal tract responses for these variables and these values remained more or less constant across all conditions. PWS also had longer word and vowel durations and spoke louder than PNS, but these factors did not interact with condition (JF/BB/PBB). Moreover, with increases in speech rate the predicted increase in difficulties in compensating and adapting to the bite-block perturbation for PWS was not found.

For the perceptual part of the study, the JF condition had significantly higher speech quality ratings than BB or PBB conditions at both normal [$F(2,58) = 178.12$, Greenhouse-Geisser adjusted, $p = 0.000$] and fast rates of speech [$F(2,58) = 191.92$, Greenhouse-Geisser adjusted, $p = 0.000$]. The fact that the JF session resulted in the highest quality ratings and did not result in any group effects indicates the reliability of the testing methodology. Importantly, a significant three-way group x condition x rate interaction [$F(2,58) = 11.48$, $p = 0.000$] was found. A two-way repeated measures ANOVA was carried out separately for each speech rate, with group (PWS/PNS) and condition (JF/BB/PBB) as within-subject factors. The analysis indicated a group effect only at fast rates of speech [$F(1,29) = 48.57$, $p = 0.000$], with significantly higher ratings for PNS in comparison to PWS (see Figure 1).

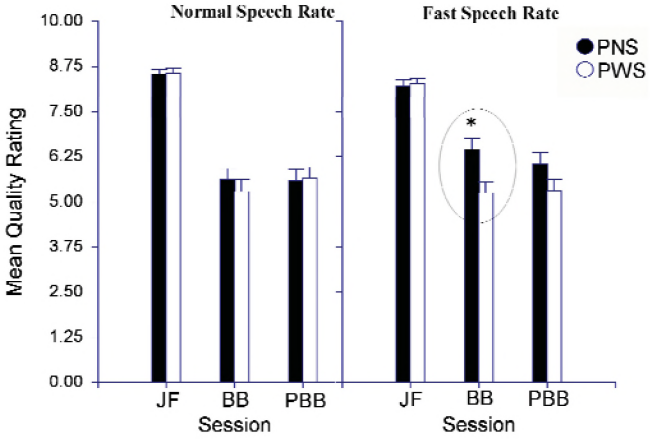


**Figure 1. Mean quality rating for normal and fast speech rate.**

## 4. CONCLUSIONS

The findings indicate that PWS have subtle difficulties in compensating and adapting to the presence of a bite-block perturbation not found in PNS. These differences support the claim that PWS may have speech motor skill limitations (Van Lieshout et al., 2004). These findings also highlight the need to assess multiple levels in speech production when looking at compensation and adaptation.

## REFERENCES


Baum, S. R., McFarland, D. H., & Diab, M. (1996). Compensation to articulatory perturbation: Perceptual data. *Journal of the Acoustical Society of America, 99,* 3791-3794.

Boersma, P., & Weenink, D. (2006). *Praat: doing phonetics by computer* (Version 4.4.12) URL http://www.praat.org. Viewed 2/26/2008.

McFarland, D. H., & Baum, S. R. (1995). Incomplete compensation to articulatory perturbation, *Journal of the Acoustical Society of America, 97,* 1865-1873.

Van Lieshout, P. H. H. M., Hulstijn, W., & Peters H. F. M (2004). Searching for the weak link in the speech production chain of people who stutter: A motor skill approach. In: B. Maassen, R. Kent, H.F.M. Peters, P. Van Lieshout, & W. Hulstijn (eds.). *Speech Motor Control In Normal And Disordered Speech* (pp. 313-355). Oxford, UK: Oxford University Press.

Whalen, D. H., & Levitt, A. G. (1995). The universality of intrinsic F0 of vowels. Journal of Phonetics, 23, 349-366.

# VOT AND F0 IN KOREAN INFANT-DIRECTED SPEECH

**Chandan Narayan[1], and Tae-Jin Yoon[2]**
[1]Dept. of Linguistics, University of Toronto, 100 St.George St., Toronto, Ontario, Canada, M5S 3G3
chandan.narayan@utoronto.ca
[2]Dept. of Linguistics and Languages, McMaster University, Hamilton, Ontario, Canada

## 1. INTRODUCTION

Korean oral stops are unique in their three-way laryngeal contrast for oral stops, called plain, fortis, and aspirated (/p,t,k/, /p*,t*,k*/, /$p^h$,$t^h$,$k^h$/). The primary acoustic correlates of the contrast have been shown to be voice onset time (VOT) (Lisker and Abramson 1964, Hirose et al. 1974, Cho et al. 2002), fundamental frequency (f0) of vowel onset (Kim & Duanmu 2004), and voice quality of vowel onset (Ahn & Iverson 2004).

Early research into the implementation of the acoustic correlates of the laryngeal contrasts suggest that aspirated stops have the longest VOT, followed by plain stops with an intermediate VOT, and tense stops with the shortest VOT. Plain stops have been shown to have the lowest f0, followed by similar, higher f0 measures in tense and aspirated stops. More recent research, however, suggests that in the speech of younger adult Korean speakers, the acoustic correlates are undergoing a shift, whereby VOT no longer reliably separates plain from aspirated stops, with the weight of distinction being shifted to the f0 of the following vowel, resulting in a high tone following aspirated stops (Wright 2007).

Our current research asks how the covariation between VOT and f0 is implemented during the earliest stages of the infant-directed register in Korean? As there is increasing evidence that laryngeal timing gestures like VOT are inaccurately produced in IDS (Sundberg & Lacerda 1991, Narayan 2011), do mothers exaggerate the f0 differences?

The current research has implications for phonological development in Korean infants in light of recent findings suggesting a change in the Korean laryngeal contrast. Silva (2006) shows that contemporary Korean is developing a tonal system reflecting a change in speakers' implementation of VOT and f0 cues to the three-way laryngeal contrast. Silva shows that the phonological difference between plain and aspirated stops, which is usually signaled by a VOT difference, is now manifested in f0 patterns. The plain/aspirated distinction in Silva's study showed insignificant VOT differences, with categorization occurring according to tone. Plain stops are associated with low tone and aspirated stops with high tone.

## 2. METHOD

Three native Korean-speaking mothers were recorded at their homes for one hour as they interacted with their 5-month-old infants. Mothers were told to interact with their young infants in an *everyday* manner, while the researcher was in an adjacent room. The same mothers were then recorded for 10 minutes speaking with an adult, Korean-speaking researcher. All recordings were made using a high-quality lapel microphone directly to a digital recording device. The resulting .wav files were transcribed by a native Korean speaker. CVs were tagged at consonant and vowel onset and offset. Measurements were collected automatically using specially written Praat (Boersma 2011) script, which logged VOT and f0 characteristics. VOT was taken as the difference (in ms) between the aspiration offset time and onset. Vowel onset was indicated by the first zero-crossing of periodicity after the aperiodic noise of aspiration. In order to account for overall speech rate differences between IDS and ADS registers, raw VOTs were divided by the following vowel duration. Maximum f0s (Hz) were first converted to the perceptually relevant Mel scale and normalized using the standard z-transformation. Data from approximately 2000 CVs were extracted from the audio. Analyses focused on only word-initial CVs, resulting in a total of 950 tokens.

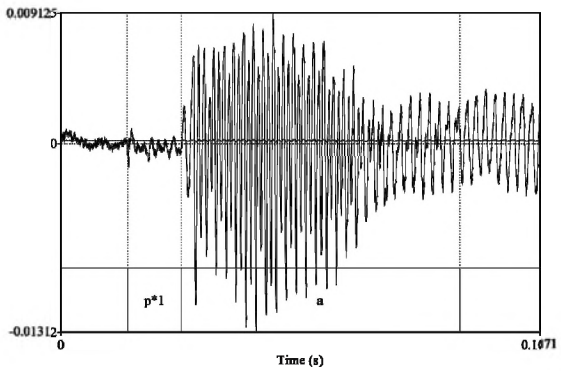


**Figure 1. Sample CV with aspiration and vowel onset/offset.**

## 3. RESULTS

Results suggest that plain and tense stops are not reliably different along the VOT dimension in IDS (figs.2,3), with aspirated stops having the longest VOTs ($p < 0.05$). VOT in tense stops was shortest in the ADS sample, with more similar VOTs observed in plain and aspirated stops ($p < 0.01$).

Fundamental frequency is significantly higher in tense and aspirated stops when compared to plain stops in IDS ($p < 0.05$). Fundamental frequency was low in plain stops relative to tense and aspirated stops ($p < 0.05$) in ADS.

VOT and f0 were used as predictors in a multinomial regression model of laryngeal state in both registers. The pattern of VOT according to consonant type was similar in both registers. While both VOT and f0 were predictive of laryngeal state, the interaction between the two was more significant in the IDS model, suggesting that the lack of distinction along VOT renders f0 more useful in the IDS model.

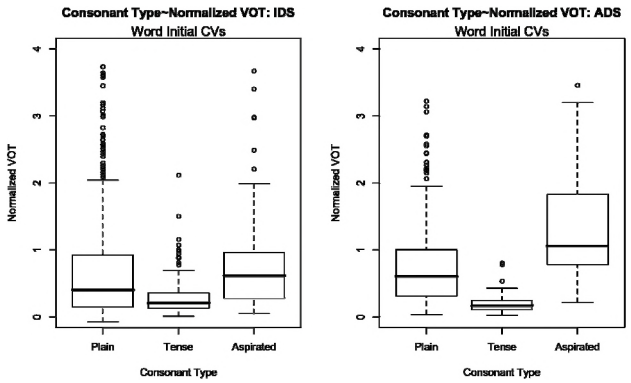


**Figure 2: VOT ratio according to laryngeal type in IDS and ADS registers**

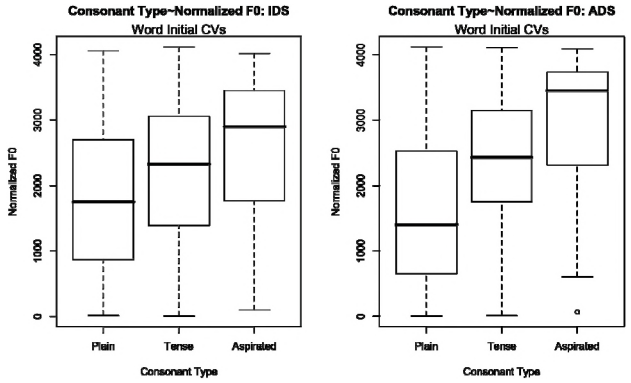


**Figure 3: Normalized f0 (mels) according to laryngeal type in IDS and ADS registers**

## 4. DISCUSSION

While fundamental frequency operates similarly in both registers, it is more predictive of laryngeal state in the IDS model than in ADS because VOT shows more ambiguity in speech to infants. These results are generally consistent with the tonogenesis results of Silva (2006).

The three-way laryngeal contrast of Korean is rendered binary along the very salient VOT dimension. For the 5 month olds in the current study to accurately segregate three consonant types, they must factor in to their perceptual categorization the f0 cue.

We must consider the possibility that the current results, showing ambiguous VOT cues to laryngeal state, arise as a result of the demands of IDS rather than an overall change in the implementation of the contrast in adult Korean speakers, as VOT remains predictive of the three consonant types in ADS. The current research is part of a larger, longitudinal study assessing the acoustics of laryngeals in Korean. If the VOT/f0 acoustic dynamics remain consistent in the speech to older infants, we might conclude that the seeds the qualitative change in the nature of the Korean laryngeal contrast (Silva 2006) are indeed to be found in the earliest input to infants.

## REFERENCES


Ahn, S.-C., and G. K. Iverson. (2004). Dimensions in Korean laryngeal phonology. Journal of East Asian Linguistics 13:345–379.

Cho, T., S. Jun, and P. Ladefoged. (2002). Acoustic and aerodynamic correlates of Korean stops and fricatives. Journal of Phonetics 30:193–228.

Hirose, H., C. Y. Lee, and T. Ushijima. (1974). Laryngeal control in Korean stop production. Journal of Phonetics 2:145–152.

Kim, M.-R., and S. Duanmu. (2004). 'Tense' and 'lax' stops in Korean. Journal of East Asian Linguistics 13:59–104.

Lisker, L., and A. S. Abramson. (1964). A cross-language study of voicing in initial stops; acoustic measurements. Word 20: 384–422.

Silva, D.J. (2006). Acoustic evidence for the emergence of a tonal contrast in contemporary Korean. Phonology 23: 287-308.

Sundberg, U. and Lacerda, F. (1999). Voice onset time in speech to infants and adults. Phonetica, 56:186–199.


## ACKNOWLEDGEMENTS


This work was made possible by a Standard Research Grant to the first author by the SSHRC (#487010).

# AN ULTRASOUND PILOT STUDY OF NORTH AMERICAN ENGLISH /ɹ/ PRODUCTION IN ONE TYPICALLY DEVELOPING ENGLISH-SPEAKING MONOLINGUAL CHILD

**Lyra Magloughlin**
Dept. of Linguistics, University of Ottawa, 70 Laurier Ave. E., Room 401, Ottawa, ON, Canada, K1N 6N5, lyra@uottawa.ca

## 1. INTRODUCTION

This paper presents an articulatory study of North American English /ɹ/ productions of one typically developing child. North American English /ɹ/ is of interest because it exhibits acoustic stability despite considerable articulatory variability. It is also often one of the last sounds to be acquired by children. While there is a growing body of research on articulatory variability in adult production of /ɹ/ (e.g. Campbell et al., 2010; Mielke et al., 2010), there remains virtually no articulatory data on children's /ɹ/ production during acquisition.

### 1.2. Child /ɹ/

North American English /ɹ/ is an articulatorily complex sound that has been described as "notoriously difficult for American children to learn to produce" (McGowan et al., 2004, p. 871). Findings on child production of /ɹ/ are often contradictory; Templin (1957) reported that 75% of children were able to produce /ɹ/ in word initial, medial, and final position by age 4, whereas Sander (1972) observed that while over 50% of children began articulating /ɹ/ by age 3, they were not "customarily producing the sound" until age 6 (p. 62), and Smit et al. (1990) listed age 8 as the 'recommended age of acquisition' for /ɹ/. Despite this apparent lack of consensus on developmental trajectories, there is consistent evidence to suggest that children demonstrate the greatest degree of difficulty producing /ɹ/ in prevocalic position. McGowan et al. (2004) reported that children attained adult-like postvocalic and syllabic /ɹ/ by 31 months of age, but showed no evidence of producing prevocalic /ɹ/ at this age. Smit et al. (1990) found that children had more difficulty producing /ɹ/ in word-initial position, and were more likely to use [w] in these contexts.

### 1.1. Adult /ɹ/

Research on adult production of North American English /ɹ/ suggests a great deal of inter- and intra-speaker variability in articulation. In a cineradiographic study of British and American English speakers' production of /ɹ/, Delattre and Freeman (1968) proposed eight different tongue shapes to describe this variability, frequently observing both 'bunched' (types 3 and 4) and 'retroflexed' (type 7) postures (Fig. 1) within and between speakers of American English. Zawadski and Kuehn (1980) also reported bunched and retroflexed tongue shapes and noted that speakers exhibited a greater degree of lip rounding in prevocalic /ɹ/ contexts. Mielke et al. (2010) observed bunched/retroflexed variability within and between speakers and found that retroflexion rates were highest in prevocalic contexts (and before /l/), and lowest next to coronals, most likely due to demands placed on the tongue that were antagonistic to retroflexion.

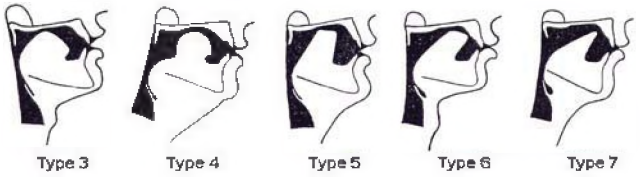


**Figure 1. Delattre and Freeman (1968) /ɹ/ shapes reported for rhotic varieties of North American English**

## 2. METHODS

The current study uses ultrasound imaging to investigate the articulations of one typically-developing North American English-speaking monolingual child, aged 4;3, during production of 35 lexical items containing /ɹ/ in prevocalic (e.g. *rocks*, *frog*), postvocalic (e.g. *car*, *pear*), and syllabic (e.g. *earth*, *flower*) contexts. Ultrasound is a safe, non-invasive way of obtaining images of the tongue in real time, making it ideally suited to an investigation of this sort. The experiment was conducted in a soundproof booth and consisted of one 45-minute session that included four short recordings, each approximately five minutes in length. The participant was seated on her mother's lap during recording and a hand-held transducer was placed gently under her chin to capture mid-sagittal views of the tongue during speech. An effort was made to ensure the transducer remained in a constant and stable position relative to the head during recording, despite considerable head movement (an inevitability in research with young children). The participant was asked to identify photographs of familiar objects presented to her one at a time on a computer screen positioned in front of her, and prompted with 'this is a ___' or 'we call these ___'. Audio was recorded in mono at a sampling rate of 44.1 kHz. A condenser microphone positioned near the speaker's mouth was connected to a USBPre preamp and A/D converter outside the booth, which was connected to a computer running Audacity software. Ultrasound was recorded using a Terason T3000 portable ultrasound machine. Video was recorded with a USB video camera, and UltraSpeech software was used to capture ultrasound and video images, at a rate of 30 fps. Audio tokens were coded impressionistically as adult-like, *non*-adult-like, or *near*-adult-like by the researcher and one other coder. Only tokens where consensus was reached were included in the analysis. Praat was used to determine formant values. Video and ultrasound images were inspected visually in order to code for tongue shape and lip rounding at the peak (most /ɹ/-like point) of each /ɹ/ gesture.

## 3. RESULTS

The participant accurately named all target items with the exception of 'crow', which was identified as 'bird' and included as a syllabic token. In total, at least two repetitions of each target were recorded. Preliminary coding of 63 audio tokens showed adult-like productions in 38 of 40 postvocalic and syllabic targets, and *non*-adult-like productions (generally [w]-like) in 15 of 23 prevocalic targets. The remaining 8 prevocalic targets consisted of *near*-adult-like productions and only included targets that were adjacent to coronal segments (*mu**sh**rooms, **t**ree, **t**ruck, **st**ripes, **Sh**rek*). Analysis of video and ultrasound images showed type 4 tongue shapes consistently in postvocalic and syllabic positions, with characteristic concavity at the tongue dorsum and a bunched, tip down posture (e.g. Fig. 2, *pear* and *sunflower*). There was an absence of /ɹ/-like tongue shapes in prevocalic targets coded as *non*-adult-like (e.g. Fig. 3, *road* and *zebra*), however, a pattern emerged in prevocalic, coronal-adjacent targets, where tongue shape at the peak of the *near*-adult-like gesture closely resembled the shape of the preceding coronal (e.g. Fig. 4, *mushrooms*). Lip rounding was generally observed in all prevocalic contexts, as expected.

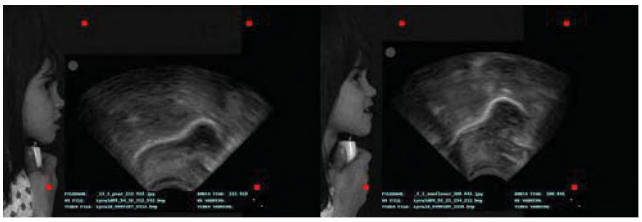

**Figure 2. Type 4 /ɹ/ gestures - *pear* (L), *sunflower* (R).**

**Figure 3. *Non*-adult-like gestures - *road* (L) and *zebra* (R).**

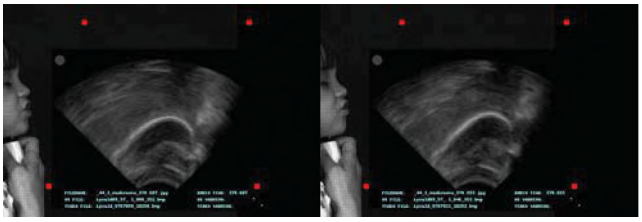

**Figure 4. Coronal /ʃ/ gesture (L) with adjacent *near*-adult-like gesture (R) - *mushrooms*.**

## 4. DISCUSSION AND CONCLUSIONS

Preliminary results indicate an established bunched /ɹ/ production strategy for this participant in postvocalic and syllabic, but not prevocalic, contexts. These findings are consistent with child /ɹ/ production literature on the developmental lag in prevocalic contexts during acquisition. While the participant's prevocalic productions demonstrated no overt /ɹ/ gestures, she may be exhibiting an early-stage production strategy in prevocalic contexts next to coronals. These targets, coded during the audio stage as *near*-adult-like, were produced with tongue shapes similar to those found in the preceding coronal segments and not unlike bunched /ɹ/s, suggesting that coronals may play a facilitative role during acquisition of prevocalic /ɹ/. Mielke et al. (2010) reported that adult's retroflexed tongue postures were most likely to occur in prevocalic position and least likely to occur next to coronals. Tiede et al. (2011) have argued that children might attempt different vocal tract configurations during acquisition, particularly in contexts where the articulatory demands are greater. It is conceivable that the participant could develop a retroflex strategy for non-coronal adjacent prevocalic /ɹ/, which would be consistent with a common adult pattern. If there is a relationship between articulatory variability during /ɹ/ production in childhood and covert variability observed in adulthood, children's acquisitional trajectories will prove informative. While reported findings are preliminary and based on the productions of one child, they provide strong motivation for longitudinal research with more than one participant.

## REFERENCES


Campbell, F., Gick, B., Wilson, I., Vatikiotis-Bateson, E. (2010). Spatial and temporal properties of gestures in North American English /r/. *Language and Speech*, 53:49-69.

Delattre, P., Freeman, D. (1968). A dialect study of American r's by x-ray motion picture. *Linguistics*, 44:29–68.

Mcgowan, R.S., Nittrouer, S., & Manning, C.J. (2004). Development of [r] in young, Midwestern, American children. *Journal of the Acoustical Society of America*, 115(2), 871-884.

Mielke, J., Baker, A., Archangeli, D. (2010). Variability and homogeneity in American English /ɹ/ allophony and /s/ retraction. In *Variation, Detail, & Representation*. Berlin: Mouton de Gruyter.

Smit, A.B., Hand, L., Freilinger, J.J., Bernthal, J.E., and Bird, A. (1990). The Iowa articulation norms and its Nebraska replication, *Journal of Speech and Hearing Disorders*, 55, 779–798.

Sander, E. K. (1972.) When are speech sounds learned? *Journal of Speech and Hearing Disorders*, 37, 55-63.

Templin, M. (1957). *Certain Language Skills in Children*. Minneapolis: University of Minnesota.

Tiede, M.K., Boyce, S.E., Espy-Wilson, C.Y., Gracco. V.L. (2011). *Variability of North American English /r/ production in response to palatal perturbation*. In Speech motor control: New developments in basic and applied research, ed. Ben Maassen and Pascal van Lieshout, 53–67. Oxford: Oxford University Press.

Zawadski, P.A., Kuehn, D.P. (1980). A cineradiographic study of static and dynamic aspects of American English /r/. *Phonetica*, 37: 253-266.


## ACKNOWLEDGEMENTS


This paper is based on Masters-level work completed in the Department of Linguistics at the University of Ottawa, and supported in part by a SSHRC Joseph-Armand Bombardier Master's Scholarship. Thanks to Jeff Mielke for his encouragement and valuable feedback, Tania Zamuner for her guidance, and my Sound Patterns Laboratory peers for their supportive exchange of ideas. Thanks also to my participant and her grandmother for their keen interest and willingness to take part.

# USING TWO-DIMENSIONAL BOX PLOTS TO VISUALIZE THE VOWEL SPACE: A STUDY OF ROUNDED VOWEL ALLOPHONES IN TIGRINYA

**Radu Craioveanu**[1]
[1]Dept. of Linguistics, University of Toronto, Toronto ON, Canada M5S3G3

## 1. INTRODUCTION

The depiction of vowels in phonetic figures is traditionally with points plotted in a stylized 'vowel space' quadrilateral; these points represent the mean F1 and F2 for each vowel. While reversing the axes allows an intuitive representation of the height and backness of each vowel, the use of just the average values makes it difficult to assess the distribution of the data.

A conventional box plot displays the median, interquartile range, and total distribution of the data along one axis. For bivariate data like formant plots, two box plots could be superimposed at right angles, but as these are computed for F1 and F2 separately, this is not entirely accurate. Instead, a *bivariate highest density regions box plot* displays the same properties of the data set, but is calculated based on the density of the data points (Hyndman et al., 2010).

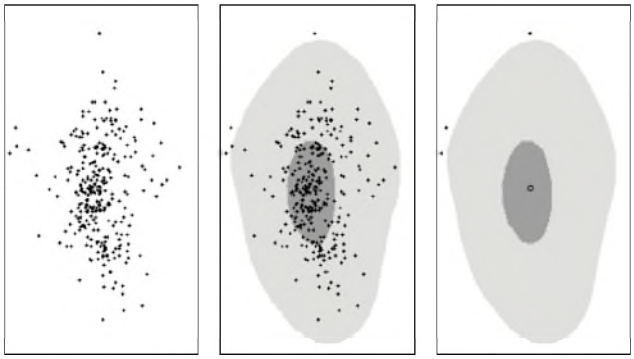

**Figure 1. F1 vs. F2, as scatterplot and 2D box plot.**

In the bivariate HDR box plot (henceforth 2D box plot) in Figure 1, the circle represents the median, and the darker area corresponds to the box of the conventional box plot. This visualization allows the distribution of the data to be seen clearly, and highlights any anomalies, as seen below. The use of these 2D box plots will be demonstrated through an investigation of rounded allophones in Tigrinya.

### 1.1. Rounding in Tigrinya

Tigrinya is an Ethio-Semitic language spoken in Eritrea and northern Ethiopia. It has received very little attention from a phonetic standpoint; as such, descriptions of two rounding processes in the language have only received an impressionistic description to date. In both of these processes, the vowels /ə/ and /i/ are described as becoming *o* and *u* respectively (Ullendorff, 1955). I use vowels in italics here because it is not clear what the rounded vowels' identities actually are.

One process, Labiovelar Rounding (LVR), causes these changes when /ə/ or /ɨ/ is found after a labialized dorsal—/kʷ, gʷ, k'ʷ/ in Tigrinya. This change is deeply-ingrained in the language, and the orthographic characters for e.g. /kʷə/ and /ko/ are considered equivalent; many orthographic alternations occur between plain and labialized velars. LVR may also regressively affect a preceding /ə/ or /ɨ/ although orthographic substitution of *o* and *u* for these is less common (Kane, 2000).

The second process is Vowel Harmony (VH), which also rounds /ə/ and /ɨ/ when these segments are followed by an /o/ or /u/ respectively in the next syllable. Harmony usually occurs between central and back vowels of the same height, but its application is less consistent, seeming to vary sometimes between utterances, and appearing more saliently in some words than others; isolated reports also find occasional cross-height harmony (Ullendorff, 1955).

These two processes leave us with two questions about vowel rounding in Tigrinya. First, do /i/ and /ə/ change to [u] and [o], or to other allophones (e.g. [u, ʊ]; [ɵ, ɔ])? Second, do both processes round these vowels in the same way (i.e. to the same allophones)?

## 2. METHODS

A word list was prepared based on dictionary searches, comprising target words which would display VH or LVR. Sentences were devised to carry the target words, some composed by the author, others by the experimental participant. A decision was made not to use a consistent carrier phrase, so as to make the reading task more natural for the participant, and also obtain a wider range of vowels. Data were collected from a middle-aged male native Tigrinya speaker of the Akkele Guzay dialect; following discussion of the words, the participant was asked to read through the list of sentences twice, repeating each sentence twice (total of four utterances each). Any words that the participant was unfamiliar with were excluded. The vowels' phonological environments were kept as consistent as possible.

The vowels in the recordings were annotated in Praat (Boersma & Weenink, 2011), and average FFT formant values for all vowels were extracted using a custom script. While values for F1, F2, and F3 were collected, no significant patterns were found in F3, so this data is excluded from the results below.

The formant values were then analysed using R and the *hdrcde* package to generate the 2D boxplots seen below (R Development Core Team, 2011; Hyndman et al., 2010).

## 3. RESULTS

Rounded allophones in VH environments were found to have F2 values between the plain phonemic vowel and the trigger. Figure 2 summarizes these findings; means are also indicated by the vowel labels.

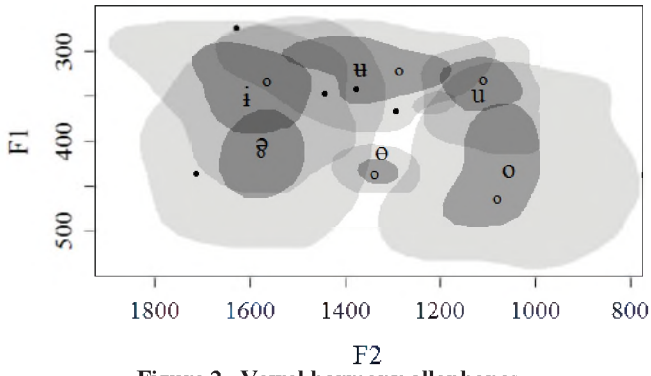


**Figure 2. Vowel harmony allophones.**

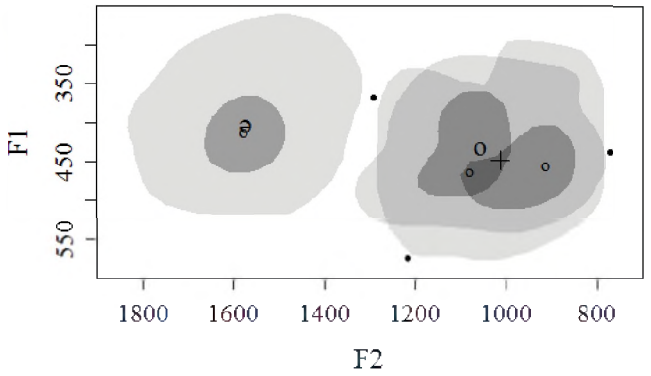


**Figure 3. Mid progressive LVR (P-LVR) allophone.**

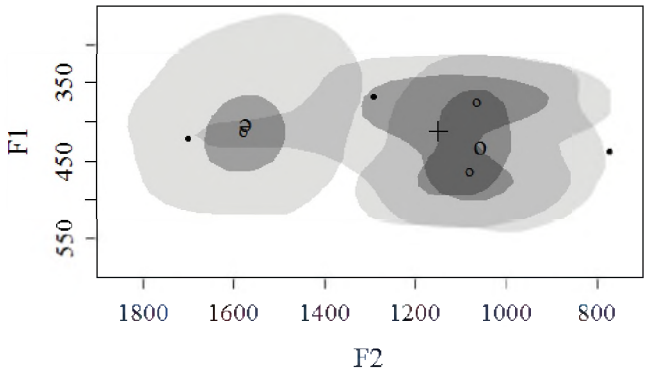


**Figure 4. Mid regressive LVR (R-LVR) allophone.**

Rounded allophones in LVR environments were found largely to overlap with /o/. Figures 3 and 4 summarize these findings for progressive and regressive LVR; '+' indicates the mean of the rounded allophone. F2 values for the P-LVR allophone were lower because of an over-representation of labial codas in the data; the odd "tail" of the R-LVR allophone is due to one word where none of the tokens displayed rounding.

## 4. DISCUSSION AND CONCLUSIONS

Although traditional descriptions of Tigrinya describe both VH and LVR as involving changes from /ə/ → *o* and from /ɨ/ → *u*, these are in fact clearly different processes with different outcomes.

VH operates solely in a regressive direction, between central and back vowels in adjacent syllables, whereby /ə/ and /i/ are rounded to intermediate allophones [ɵ] and [u] when followed by /o/, /u/, or other rounded allophones. Harmony is height-restricted, and seemingly variable in strength.

LVR rounds vowels adjacent to labiovelars, primarily in the progressive direction, but also potentially affecting preceding vowels or both preceding and following vowels. LVR causes a full shift from /ə/ → [o] and /i/ → [u].

The use of 2D box plots for this kind of research highlights anomalies in the data that would not be visible from just the mean values. One such anomaly is seen in Figure 4, where one of the words elicitated failed to exhibit R-LVR.

This could also be used to demonstrate that vowels in a particular language are only contrastive along one dimension: for instance, in Eastern Arrernte, only the vowels /a/ and /ə/ are phonemic, meaning the only distinction between the vowels is that of height. Consequently, the vowels vary a great deal in backness, even though their mean F2 is still central (Ladefoged & Maddieson, 1996). By displaying only the mean value, important information about the distribution of the vowels is lost. Ladefoged & Maddieson avoid this by providing a scatterplot, but 2D box plots can display the full range of the data, the centre two quartiles, the median, and the mean if desired, while remaining easier to read than a scatterplot.

## REFERENCES


Boersma, P., & Weenink, D. (2011). Praat: Doing phonetics by computer [Computer program]. Version 5.2.11. Available from http://www.praat.org.

Hyndman, R. J., Einbeck, J., & Wand, M. (2010). hdrcde: Highest density regions and conditional density estimation [Computer software manual]. Available from http://CRAN.R-project.org/package=hdrcde (R package version 2.15).

Kane, T. L. (2000). *Tigrinya-English dictionary*. Springfield, VA: Dunwoody Press.

Ladefoged, P., & Maddieson, I. (1996). *Sounds of the world's languages*. Oxford, UK: Blackwell Publishers.

R Development Core Team. (2011). R: A language and environment for statistical computing [Computer software manual]. Vienna, Austria. Available from http://www.R-project.org.

Ullendorff, E. (1955). *The Semitic languages of Ethiopia: A comparative phonology*. London, UK: Taylor's Foreign Press.

# VOICING IN PERSIAN WORD-FINAL OBSTRUENTS

**Mercedeh Mohaghegh**[1]
[1]Dept. of Linguistics, University of Toronto, 100 St. George St., Toronto, Canada, M5S 3G3
mercedeh.mohaghegh@utoronto.ca

## 1. INTRODUCTION

Analysis of voiced-voiceless contrast in final position in various languages has been the topic of numerous studies (see e.g. Charles-Luce, 1985, for German; Dmitrieva et al., 2010, for Russian). Some studies show that word final voiced obstruents get fully devoiced, resulting in complete, phonological neutralization (e.g. Jassem & Richter, 1989). Others provide evidence that final devoicing is phonetically incomplete with resulting obstruents being different from their voiceless counterparts (e.g. Burton & Robblee, 1997).

Persian obstruents exhibit a two-way voicing contrast, (voiced vs. voiceless), which is also maintained in word-final position. These obstruents can appear both as single (e.g. /xiz/ "jump" vs. /xis/ "wet".) as well as in clusters (e.g. /Gæbz/ "receipt" vs. /habs/ "imprison"). Previous studies have noted that voiced obstruents may be partially devoiced when occurring word-finally (e.g. Mahootian, 1997:288). However, there haven't been any phonetic studies of this process in Persian.

The goal of the present study was to investigate the acoustic properties of voicing of Persian obstruents in both word-final single consonants and clusters, and to find whether any instances of devoicing (or voicing), if present, is partial or complete. For this purpose an acoustic analysis of voicing in Persian word-final obstruents is conducted based on the data gathered from 6 Persian native speakers.

## 2. METHODS

### 2.1 Participants

Six Persian native speakers, three females and three males, were recorded. All of them were native speakers of the Tehrani dialect of Persian, ranging in age from 22-29 years old, except for one participant who was 51 years old. None of them had ever lived outside of Iran for more than 5 years or had any history of hearing or speaking disorders.

### 2.2 Materials

Speech materials consisted of 22 words presented within the carrier sentence, "hala bɛgin ___." ("now say ___."). Among these words, 10 ended in a cluster (C1C2: stop+fricative or vice versa) as in /dʒæzb/ "attract", and 6 ended in a single consonant (C#) as in /ʃæb/ "night". The target consonants were fricatives [s] and [z] and stops [p] and [b] in the context of the vowel [æ] (or [a] in 6 words). Six words with the same consonants in intervocalic position (VCV) were recorded as controls as in /Gæzæb/ "anger". All items were real Persian words with high frequency of usage, except four nonsense words. Each sentence was repeated six times throughout the recording session.

### 2.3 Acoustic Measurements

Three temporal measurements were applied to the target fricatives and stops: 1- duration of the consonant: longer stop closure or frication duration is associated with voicelessness (e.g. Dinnsen & Charles-Luce, 1984), 2- duration of the preceding vowel: duration of the vowels followed by a voiced consonant is often longer compared to the vowels preceding voiceless consonants (e.g. Burton & Robblee, 1997), and 3- duration of the voice bar: voiced consonants often have a visible voice bar at lower frequencies; on the other hand, voiceless or partially devoiced consonants have no or very short voice bars (e.g. Warner et al., 2004).

## 3. ANALYSIS AND RESULTS

Separate sets of two and three-way repeated measure ANOVAs were run for fricatives and stops for each of the three measurements. Three independent factors were: 1- Position (C1: the first consonant in a cluster, C2: the second consonant in a cluster, VC, and VCV). Only the results related to the first three levels are discussed in the current paper. 2- Context voice (voiced and voiceless): underlying voicing of the neighbouring obstruent within a cluster. 3- Voice (voiced and voiceless): underlying voicing of the obstruent.

As indicated in Table 1 the interaction between the factors Position and Voice was in most cases significant except for consonant duration and vowel duration for stops. The interaction between the factors Voice and Context voice was also significant except for duration of voice bar. On the other hand no significant interaction between Position and Context voice was indicated for any of the measurements.

**Table 1. Summary results of 2-way and 3-way repeated measure ANOVAs for all measurements.**

| Measure-ments | Factor / Sound | Position-Voice | | Position-Context | | Voice-Context | |
|---|---|---|---|---|---|---|---|
| | | F3(3,15) | *p* | F(1,5) | *P* | F(1,5) | *p* |
| C-Dur | Fric | 15.61 | **<.001** | 1.11 | 0.3 | 22.99 | **0.004** |
| | Stop | 1.02 | 0.4 | 0.56 | 0.4 | 10.89 | **0.02** |
| V-Dur | Fric | (2,10) 5.16 | **0.02** | N/A | N/A | 9.07 | **0.02** |
| | Stop | (2,10) 1.12 | 0.3 | N/A | N/A | 88.83 | **<.001** |
| Vbar-Dur | Fric | 7.39 | **0.002** | 0.43 | 0.5 | 0.47 | 0.5 |
| | Stop | 4.3 | **0.02** | 0.9 | 0.3 | 0.11 | 0.7 |

For consonant duration and vowel duration (Figure 1a,b), the results of t-test and Tukey HSD post hoc analysis indicated that final voiced and voiceless stops or fricatives in clusters (C2) were not significantly different when preceded by a voiceless consonant. The same results were observed when the target sounds were followed by a voiceless consonant. However, overall in all cases where there was an interaction between Position and Voice, voiceless consonants were significantly longer compared to their voiced counterparts regardless of their position. For duration of voice bar (Figure 1c), no significant difference was indicated between voiced and voiceless fricatives in C2 and voiced and voiceless stops in C2 and VC (also C1) positions ($\mu \approx 1.2$ ms).

a.

b.

c.

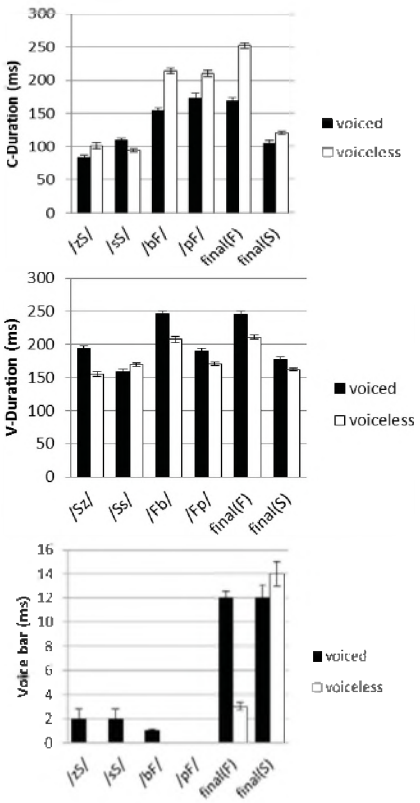


**Figure 1. Means and standard errors (error bars) of consonant duration, vowel duration and duration of the voice bar for voiced and voiceless fricatives (F) and stops (S) in cluster and as single.**

## 4. DISCUSSION AND CONCLUSION

The results of the acoustic analyses suggest that, contrary to the previous literature (e.g. Majidi & Ternes, 1999), in Persian word-final voiced obstruents are not always devoiced. The only indication of devoicing of word-final single obstruents was observed in the results from duration of the voice bar for stops but not for fricatives. Within final obstruent clusters, however, evidence from duration of voice bar indicated final devoicing for both fricatives and stops. Since none of the instances of final devoicing was supported by all measurements, they are not considered to be complete. This was consistent with what has been indicated in Persian literature (e.g. Mahootian, 1997:288). The results are also in line with the findings of some previous studies on final devoicing in other languages, which does not support the traditional view that processes such as voicing neutralization are phonological and thus categorical (e.g. Dinnsen, 1985; Dmitrieva et al., 2010). However, as it has been noted (e.g. Jassem & Richter, 1989), some possible limitations of the current investigation could be the effect of using orthography in presenting the stimuli, participants' careful reading style as well as knowledge of other languages which are suggested to be potentially influential on the results of the acoustic analyses.

In addition to final devoicing, the results also indicate that voicing assimilation in favour of the voiceless sound affects obstruents within word-final clusters in Persian. Since there were cases of both regressive and progressive voicing assimilation, no particular preference for direction of assimilation was observed.

Whether the current results can be generalized to other types of Persian word-final single consonants and consonant clusters is a question which needs to be investigated further in future studies. In addition it will be of interest to include results of other known measures such as spectral information and amplitude differences, among others.

## REFERENCES


Burton, M & Robblee, K. (1997). A phonetic analysis of voicing assimilation in Russian. *J. of Phonetics*, 25, 97-114.

Charles-Luce, J. (1985). Word-final devoicing in German: Effects of phonetic and sentential contexts. *J. of Phonetics*, 13, 309–324.

Dinnsen, D. A. (1985). A re-examination of phonological neutralization. *J. of Linguistics*. 21:265–279.

Dinnsen, D., & Charles-Luce, J. (1984). Phonological neutralization, phonetic implementation and individual differences. *J. of Phonetics*, 12, 49–60.

Dmitrieva, O., Jongman, A., & Sereno, J. (2010). Phonological neutralization by native and non-native speakers: the case of Russian final devoicing. *J. of Phonetics*, 38(3), 483-492.

Jassem, W., & Richter, L. (1989). Neutralization of voicing in Polish obstruents. *J. of Phonetics*, 17, 317–325.

Mahootian, Sh. (1997). *Persian.* Routledge, London.

Majidi, M., & Ternes, E. (1999). Persian. In International Phonetic Association (ed.), *Handbook of the International Phonetic Association*, 124–125. Cambridge: Cambridge University Press.

Warner, N., Jongman, A., Sereno, J., & Kemps, R. (2004). Incomplete neutralization and other sub-phonemic durational differences in production and perception: Evidence from Dutch. *J. of Phonetics,* 32, 251–276.


## ACKNOWLEDGEMENTS


I am most grateful to Dr. Alexei Kochetov, Dr. Daphna Heller and Prof. Elan Dresher for providing much help with their useful insights on this topic. This work was supported by a SSHRC Institutional Grant (SIG) award.

# PRODUCTION PLANNING CONSTRAINTS ON ALLOMORPHY

**Michael Wagner**
Dep. of Linguistics, McGill University, 1085 Avenue Dr. Penfield, Montréal, Québec, Canada, H3A 1A7, chael@mcgill.ca

## 1. INTRODUCTION

The realization of the English suffix *-ing* varies between (at least) two distinct pronunciations: [iŋ] vs. [in]. Across different varieties of English this variation has been shown to be influenced by gender, speaking style, and socio-economic factors (Fischer, 1958; Labov, 1972; Trudgill, 1972). The segmental phonological context has also been shown to matter (Houston, 1986, and references therein). Crucial for the present paper, the allomorph [in] is more likely when there is a coronal segment immediately following (as in 1a vs. 1b).

(1) a. While the man was read**in the** book, the glass feel off the table.
b. While the man was read**iŋ a** book, the glass feel off the table.

The effect of phonology is arguably not simply a case of co-articulation or assimilation, since it interacts with morphology. For example, *ing* is much less likely to be pronounced as [in] when it is part of an arguably mono-morphemic word like *ceiling* than when it is an affix (cf. Houston 1986). So the alternation between [in] and [iŋ] is sensitive to the identity of the morpheme the segmental string is part of. Whether the alternation involves the choice between two listed allormorphs [in] and [iŋ] or whether it is derived by morpho-phonological rule is a question that we can remain agnostic about since allomorph choice and morpho-phonological processes obey the same locality constraints (at least according to Kiparsky 1996). We can thus investigate *ing* to test claims about locality in morpho-phonology.

Cyclic theories of morphology assume that complex words are built up from inside out, and predict that the phonology of material that is compositionally added later cannot influence earlier morphological choices. This claim has been argued for in various cyclic theories, including Lexical Phonology (Kiparsky 1996) and Distributed Morphology (Bobaljik 2000, Embick 2010). It should then be impossible for the choice between *the* and *a* to influence *ing* across a syntactic boundary as in (2a) but not in (2b)—at least if the affix combines with the verb after the complement (as is assumed in Distributed Morphology):

(2) a. While the man was reading, || the/a book fell off the table.
b. While the man was reading the book, || the/a glass feel off the table.

In global theories of phonology/morphology like standard Optimality theory (see discussion in Embick 2010), there is no reason why such locality generalizations should hold. While one can add constraints to such theories that would force locality, a ranking without such locality effects in which a global phonological markedness constraints drives the choice of a particular affix without regard to syntactic or phonological boundaries should always be possible. In other words, this kind of theory cannot explain why locality should *necessarily* hold. The present paper reports on an experiment in which we crossed syntactic and phonological factors to test the locality of the [in]/[iŋ] alternation. The evidence suggests that neither type of theory can account for the full data pattern, and points to an explanation in terms of the locality of production planning.

## 2. METHODS

A production experiment was conducted using 42 items similar to those in (1), using a set of matlab scripts developed in our lab. The experiment was run in a 2x2 latin square design, such that each participant saw only one condition from each item in pseudo-random order, and saw an equal number of trails from each condition across the experiment. There were 42 participants, all native speakers of North American English having grown up in Canada or the US. The recorded data was forced aligned by segment and by word using the prosodylab forced-aligner (Gorman et al. 2011). We used a praat script to extract acoustic measures of pitch, duration and intensity for each word. Furthermore, the data were annotated perceptually by 2 RAs for whether or not [in] or [iŋ] was used. The annotation was using a Praat script that made the annotation blind to condition, and the annotators were only able to listen to the affix to make the choice.

## 3. RESULTS

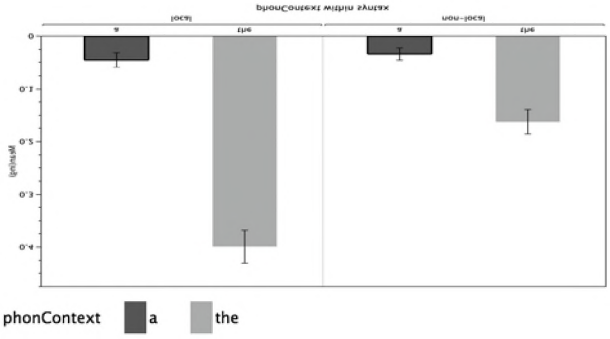


**Figure 1. Proportion of [in] by syntactic and phonological context. Error bars show 1 standard error from the mean.**

Figure 1 illustrates the proportion of [in] choice by syntax (non-local vs local) and phonology (*a* vs. *the*). A mixed model logistic regression with *syntax* and *phonology* as factors and *item* and *participant* as random effects (using the lme4 package in R) showed significant main effects and a significant interaction. In other words, using [in] is more likely when *the* follows than when *a* follows, and when a direct object follows than when no direct object follows. The significant interaction shows that the phonological influence of the following word is stronger in the local environment. The interaction is predicted by cyclic theories but not by the global theory. However, unexpectedly for the cyclic approach, the effect of phonology was also significant in the subset of data only consisting of the non-local cases.

Let's consider a third possibility: Maybe the effect of phonology on allomorph choice is restricted by the locality of production planning. To test this hypothesis, we quantified the strength of the boundary separating the affix and the following article by extracting a number of acoustic measures. The syntactic break in the examples in (2) correlates with a difference in prosodic boundary strength (Itzhak et al. 2010). One measure of boundary strength is the strength of the following word, so we measured the length of the article. Within the subset of data that included only the article *the,* the length of the article was a significant predictor of [in] pronunciation, and once that was added to the mixed model, *syntax* became irrelevant (the two factors are highly correlated). Furthermore, the length of the article was a significant predictor *even within the non-local and within the local syntactic environment*. This means that the effect of phonology on allomorph choice depends gradiently on the prosodic strength of the boundary separating the affix from the phonological trigger (which in turn is affected by syntax). Another test with similar results was conducted using the normalized duration of the verb plus affix (raw length minus the expected length based on phonemes), a measure which reflects pre-boundary lengthening.

## 4. DISCUSSION AND CONCLUSIONS

The results can be accounted for by the hypothesis that *phonological effects are constrained by the locality of production planning*—at least if we make the plausible assumption that the prosodic strength of the boundary between two words correlates with the likelihood that the beginning of the second word will already by phonologically encoded at the time when the first word is planned (see Levelt 1989 et seq., Wheeldon & Lahiri 1997, and Miozzo & Caramazza 1999 for discussions of the locality of production planning). *ing* is encoded as [in] with higher probability when a coronal sound follows—but whether the identity of the following segment is known at the time of encoding determines whether this phonological can take hold. Syntax and prosody influence how likely it is that segmental conditioning environment is present at the time of allomorph choice (or at the time of morpho-phonological alternation processes). The phonological environment can thus be stated in purely segmental terms.

The hypothesis that across-word-boundary phonological processes (sandhi phenomena) are constrained by the locality of production planning can explain why they tend to be variable (speakers don't consistently encode the next phonological word so the conditioning environments may not be present), and makes new predictions for what types of processes should obey what type of locality pattern (regressive processes should tend to be more variable than progressive ones; processes should be more local when sensitive to low-level segmental information than higher level information since it is encoded later). The hypothesis is supported by length effects on auxiliary contraction (Mackenzie 2011) that also point to production planning constraints, and it fits well with recent psycho-linguistic models of phonological processing (cf. Goldrick, in press).

## REFERENCES


Bobaljik, J.D. (2000). The Ins and Outs of Contextual Allomorphy. *University of Maryland Working Papers in Linguistics* **10**: 35-71

Embick, D. (2010). *Localism versus globalism in morphology and phonology*. Cambridge, MA: MIT Press.

Fischer, J.L. (1958). Social influences on the choices of a linguistic variant. *Word* **14**: 47-56

Goldrick, Matt (in press). Utilizing psychological realism to advance phonological theory. In J. Goldsmith, J. Riggle, & A. Yu (Eds.) Handbook of phonological theory (2nd edition).

Gorman, K., Howell J. and Wagner M. (2011). Prosodylab-Aligner: A tool for forced alignment of laboratory speech. Proceedings of the Annual Meeting of the CAA.

Houston, A.C. (1986). *Continuity and change in English morphology: the variable (ing)*. Doctoral Dissertation. U. Pennsylvania.

Itzhak, I., E. Pauker, J. E. Drury, S. R. Baum &K. Steinhauer (2010): Event-related potentials show online influence of lexical biases on prosodic processing. *NeuroReport* **21**: 8–13

Kiparsky, P. (1996). Allomorphy of Morphophonology? In: R. Singh: *Trubetzkoy's orphans: Proceedings of the Montreal roundtable Morphonology*. Amsterdam: Benjamins: 48-68.

Levelt, W. (1989). Speaking: From Intention to Articulation. Cambridge, MA: MIT Press.

Labov, W. (1972). *Sociolinguistic Patterns*. Philadelphia: University of Pennsylvania Press.

Mackenzie, L. (2011). English auxiliary contraction as a two-stage process: Evidence from corpus data. Paper presented at WCCFL, University of Arizona.

Miozzo & Caramazza (1999). *The selection of determiners in noun phrase production*. Journal of Experimental Psychology. Learning, Memory, Cognition **25.4**: 907-922.

Trudgill, P. (1972). *The social differentiation of English in Norwich*. Cambridge: Cambridge University Press.

Wheeldon, L. & A. Lahiri (1997). Prosodic Units in Speech Production. *Journal of Memory and Language* **37**: 356-381.


## ACKNOWLEDGEMENTS


Thanks to Itzhak et al. (2010) for letting me adapt their stimuli for this experiment. Thanks to Charles Boberg, Matt Goldrick, Dave Embick, Tobias Scheer, and the audience at talks at McGill and Stanford for helpful comments. This research was funded by FQRSC grant NP-132516 and a SSHRC Canada Research chair and CFI grant 212482.

# EGG Study of Czech Phoneme /ř/

**Phil Howson[1], Ekaterina Komova[2], and Bryan Gick[3]**
[1]Dept. of Linguistics, Univ. of BC, E270-1866 Main Mall, BC, Canada, V6T 1Z1, philhowson@live.ca
[2]Dept. of Linguistics, Univ. of BC, E270-1866 Main Mall, BC, Canada, V6T 1Z1, katekomova@gmail.com
[3]Dept. of Linguistics, Univ. of BC, E270-1866 Main Mall, BC, Canada, V6T 1Z1, gick@mail.ubc.ca

## 1. INTRODUCTION

### 1.1. Background

In a previous study investigating the conflicting descriptions of the distinction between the two Czech trills /r̝/ and /r/ in the literature, Howson, Komova & Gick (2011) concluded that tongue height is not the distinguishing factor between the two sounds, despite it being the most commonly-cited feature (Hála 1923, Dankovičová 1999). Tongue height was shown to be subject to systematic variation by individual and word position, and to be unaffected by region and age differences. Previous work has not provided an alternative feature by which to phonetically distinguish /r̝/ and /r/.

### 1.2. Present Study

The current study utilizes electroglottography (EGG) to test for a difference in laryngeal setting as the potential source of acoustic distinction inexplicable by tongue height, such as the higher airflow and prolonged trilling that has been reported for /r̝/ (Dankovičová 1999). Acoustic analysis is also utilized to obtain the difference between H1 and H2 which has been shown to correspond to the open quotient of the vocal folds (Holmberg, Hillman, Perkell, Guiod and Goldman 1995).

Due to the spectrographic evidence which shows that /r̝/ becomes more fricated towards the end of the sound, particularly in word-initial and word-final positions, we give special attention to monitoring this time-course variation in laryngeal setting over the duration of the sound.

### 1.3. Predictions

In terms of the laryngeal setting, we predict to see regular modal voicing for contrasting /r/. For /r̝/, however, previous descriptions lead us to expect a more open glottis, possibly with indications of breathiness. Moreover, to reflect the temporal transition in /r̝/ seen in spectrograms, we expect to find evidence of a spread glottis during the latter portion of the sound, as well as higher H1-H2 values in the vowels preceding and following /r̝/, consistent with a longer open quotient. We expect this to hold for all word-initial, word-medial and word-final positions.

## 2. METHODS

Six native speakers of Czech, two male and four female, participated in the study. Their mean age was 42 years (SD: 21 years, range 20-75 years) at the time of the study. As the speakers originated from a variety of regions within the territory of the Czech Republic, the data presented is representative of a wide range of dialects.

Stimuli words were selected in order to place /r̝/ and /r/ in contrasting environments, #rv, vrv, and vr#, covering word-initial, intervocalic and word-final positions. The words used were *rád*, *řád*, *paráda*, *pařát*, *tvar*, and *tvář*, which were delivered using PowerPoint.

The primary tool of investigation was a Kay Model 6103 electroglottograph. Audio was recorded with a Sennheiser MK66 short shotgun microphone. EGG and audio were recorded using Praat. EGG waveforms were inverted and smoothed using EGGWorks. Wavesurfer was used to produce a 512-point FFT spectrum from which H1 and H2 were measured at 5% and 50% into the vowel preceding and following /r/ and /r̝/. Results were compared statistically using ANOVA, with average values from each subject for each condition being treated as a single data point.

## 3. RESULTS

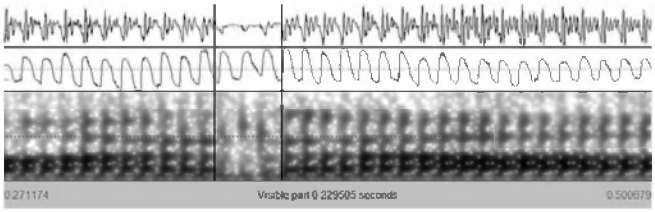


**Figure 1: Waveform, EGG and Spectrogram for the token *paráda*, respectively. Image shows only [ará].**

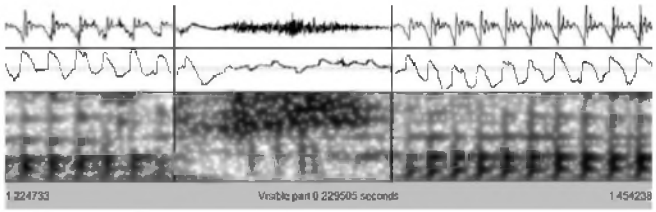


**Figure 2: Waveform, EGG and Spectrogram for the token *pařát*, respectively. Image shows only [ařá].**

The figures above show the canonical EGG patterns for /r/ and /r̝/. The EGG for /r/ exhibits the typical modal voicing pattern with a slightly larger open period, as compared to the rest of the token. However, the EGG pattern for /r̝/ differs substantially from typical modal voicing. The EGG demonstrates a wide open glottis with little to no glottal closure during the duration of articulation. We also note a substantially longer duration for /r̝/ as compared to /r/, which holds across all word positions.

The EGG results further indicate that the EGG patterns for /r/ and /r̝/ exhibit variation. While the EGG patterns for /r/ do exhibit a more open glottis in some tokens, the EGG pattern for /r̝/ always exhibits a more open glottis. The patterns for /r̝/ vary from a wide open glottis to more typical patterns for breathy voice.

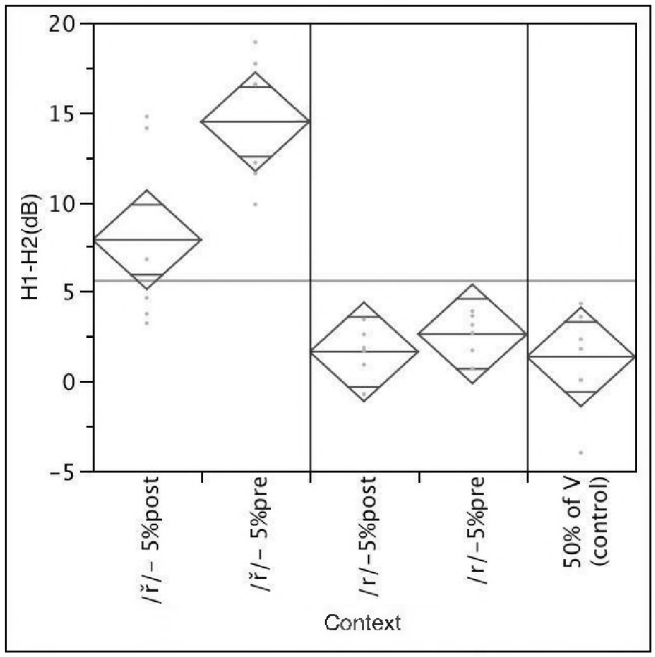


**Figure 3: Student's T-test comparing H1-H2 /r̝/, /r/ and 50% of participants vowel (control).**

In the acoustic test for glottal open quotient, overall ANOVA results show significant variation in the data [$F(4,25)=17.64$; $p < .0001$]. Post-hoc comparisons (Student's t-test) indicate significant differences in spectral tilt (H1-H2) between the control measure (at 50% of vowel) and 5% before and after /r̝/ ($p < .0001$ and $p = .0020$, respectively). No difference was observed between /r/ and control ($p > .05$).

## 4. DISCUSSION AND CONCLUSION

In line with our predictions, the EGG for /r̝/ reveals a more open glottis than the EGG for /r/. It also maintains a distinction in duration, with /r̝/ being substantially longer in duration than the contrasting phoneme /r/. In the tokens where /r̝/ demonstrated a temporal transition, the glottis was the most open for the later portion of the sound. This suggests that the first portion of this sound is simply the glottis transitioning from modal voice to a more open glottis, setting up the conditions necessary for trilling and breathiness to co-occur; the fact that the trilling happens during the second portion, as well as the high H1-H2 of the portion before frication, supports this claim.

The canonical EGG pattern seen during /r̝/ closely mimics the EGG pattern seen during speakers' regular breathing and breathy speech, which additionally provides evidence for a degree of breathiness in /r̝/. This is most evident in the word-initial and word-final positions but also obtains intervocalically for many speakers. This is different from the vocal fold action of the voiceless allophone because intervocalic position ensures that the tokens are voiced so that the pattern seen in /r̝/ could not be simply explained as a result of voicelessness.

The acoustic analysis further confirms an increase in breathiness associated with /r̝/ compared to /r/, indicated by higher H1-H2 values. The considerable spike in H1-H2 for /r̝/ in contrast to the values found at 50% of the vowel and /r/ suggests that a more widely open glottis is necessary for producing a trill-fricative. The notable difference in glottal openness and distinction in duration constitutes the most prominent contrast between /r/ and /r̝/.

The distinction in glottal opening suggests that there should be the addition of the feature [+spread glottis] to the feature set which describes this sound.

At present, the Czech trill /r̝/ is represented in the IPA as [r̝], stressing the tongue height as the distinctive feature between /r̝/ and /r/. However, in view of the findings refuting this in Howson, Komova & Gick (2011), as well as the strong evidence for a difference in the laryngeal setting presented here, we propose that a breathy [r̥] would constitute a more accurate transcription for this sound.

## REFERENCES


Boersma, Paul & David Weenink. 2010. Praat v. 5.2.3.3. http://www.fon.hum.uva.nl/praat/

Dankovičová, Jana. 1997. Czech. *Journal of the International Phonetic Association* 27: 77-80.

Hála, Bohuslav. 1923. *K popisu pražské výslovnosti: studie z experimentální fonetiky*. V Praze Nákl.

Howson, Phil, Ekaterina Komova & Bryan Gick. 2011. Ultrasound Analysis of the Czech Phoneme /r̝/. *Journal of the Acoustical Society of America* 129, 4:2453.

Holmberg, E. B., R. E. Hillman, J. S. Perkell, P. Guiod, & S. L. Goldman. 1995. Comparisons among aerodynamic electroglottographic, and acoustic spectral measures of female voice. *JSHR* 38: 1212-1223.

Sjölander Kåre & Jonas Beskow. 2005. Wavesurfer v.1.8.5. http://www.speech.kth.se/wavesurfer/download.html

Tehrani, Henry. 2010. EGG Works v. 2010.07.07. http://www.linguistics.ucla.edu/faciliti/facilities/physiology/EggWorksSetup.exe


## ACKNOWLEDGEMENTS


We would like to thank Jan Černy for helping us organize all of the participants, as well as Denise Tom and Donald Derrick for their technical support. Research was funded through an NSERC Discovery Grant to the third author.

# AN ARTICULATORY STUDY OF RHOTIC VOWELS IN CANADIAN FRENCH

**Jeff Mielke**
Dept. of Linguistics, University of Ottawa, Arts 401, 70 Laurier Ave E, Ottawa, ON, Canada, K1N6N5, jmielke@uottawa.ca

## 1. INTRODUCTION

Some speakers of Canadian French produce the vowels /ø/, /œ/, and /œ̃/ with an r-like quality, leading *pneu*, *docteur*, and *brun* to sound like [pnɻ], [dɔktʌɹʁ], and [bʁɻ]. These rhotic vowels are perceptually similar to English /ɹ/, which can be produced with a variety of tongue shapes, including bunched and retroflex variants shown in Figure 1 (Delattre and Freeman, 1968, etc.).

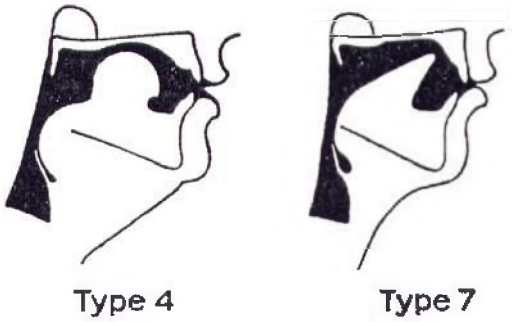


**Figure 1. Two tongue shapes for English /ɹ/: type 4 bunched (left) and type 7 retroflex (right). Images adapted from Delattre and Freeman (1968).**

Variability in English /ɹ/ raises the question of whether French rhotic vowels are also produced with more than one categorically different tongue posture. To investigate this, ultrasound was used to image the tongues of three Canadian French speakers during production of these vowels.

## 2. METHODS

Subjects produced words containing /ø/, /œʁ/, and /œ̃/ in a carrier phrase, as well as a comparable number of filler words. Each word was produced twice in the frame "Je dis X" and once in the frame "Je dis X encore." Mid-sagittal ultrasound video was recorded using a Terason T3000 portable ultrasound machine. The Palatron system (Mielke et al., 2005) was used to collect data for head movement correction, but no correction was necessary for the qualitative analysis on tongue shapes in this paper. Video of the subject's head in profile and ultrasound video were collected using Ultraspeech (Hueber et al., 2008) on the T3000, and audio was recorded using a condenser microphone, a USB preamplifier, and Audacity on a separate computer. The word list was randomized and presented on a monitor and the subjects advanced through the prompts at their own pace with a remote control. The subjects were three native speakers of Canadian French, aged 22-24, two female and one male. The female subjects (S1 and S2) were raised in Gatineau, QC, and report moderate English proficiency. The male subject (S3) was raised in Ottawa, ON and is fluent in English.

Target tokens were analyzed in three ways: (1) they were categorized impressionistically according to whether the target vowels sound rhotic to an English speaker, (2) F3 was measured for each target segment, and (3) the peak of each vowel gesture was visually categorized according to whether it matched an English /ɹ/ tongue shape such as those on Figure 1, or it looked more like a tongue shape expected for a front vowel.

## 3. RESULTS

Acoustic analysis of vowels categorized as rhotic- and non-rhotic-sounding reveals that sounding rhotic is associated with low F3, which is an important acoustic cue for English /ɹ/. Inspection of ultrasound images reveals that S1 and S2 produced rhotic vowels with a tip-down bunched tongue shape closely resembling Delattre and Freeman's type 4, and S3 produced rhotic vowels predominantly with a retroflex tongue shape, with the exception of *heureux* ([ɻʁɻ]), which he produced with two bunched rhotic vowels.

Table 1 shows the results of categorizing tokens by auditory impression. All tokens produced by S3 were categorized as sounding rhotic. S1 and S2 were variable for /ø/ and /œ̃#/ (e.g., *pneu* and *brun*), S2 was consistently rhotic for /œʁ#/ (e.g., *coeur*), and S1 was variable.

**Table 1. Auditory impression of vowel tokens.**

| | S1 | S2 | S3 |
|---|---|---|---|
| /ø/ | variable | variable | rhotic |
| /œʁ#/ | variable | rhotic | rhotic |
| /œ̃#/ | variable | variable | rhotic |

Figure 2 shows a representative spectrogram of S2's *majeure*, categorized auditorily and articulatorily as rhotic. Note the low F3 (~2000Hz) during the interval labeled as [ɹ], and that the expected uvular rhotic consonant [ʁ] is still present following the rhotic vowel.

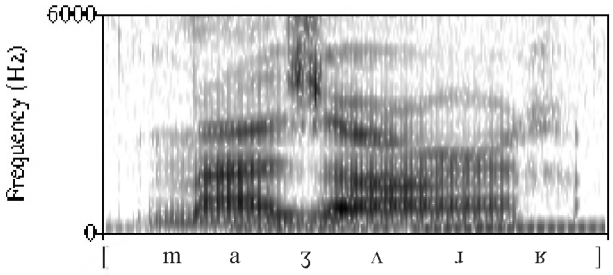


**Figure 2. Representative spectrogram : *majeure* (S2)**

Figure 3 shows representative ultrasound images. The top two images show bunched tongue shapes produced by S2 and S1, the bottom left image shows a retroflex tongue shape produced by S3, and the bottom right image shows a non-rhotic tongue shape produced by S2.

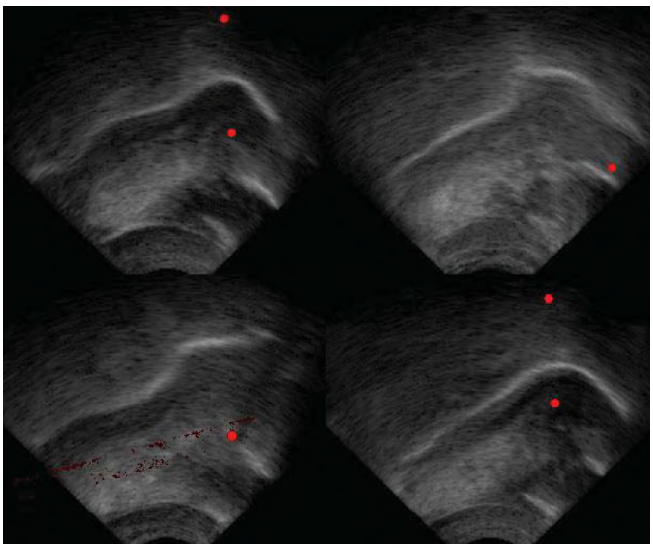

**Figure 3. Representative tongue images: (clockwise from top left) bunched in *cœur* (S2); bunched in *pneu* (S1); non-rhotic *pneu* (S2); retroflex in *pneu* (S3).**

Figure 4 shows F3 values for tokens produced by the two variable subjects (S1 and S2). The plot on the left shows tokens impressionistically coded as rhotic and non-rhotic. The plot on the right shows F3 for the same vowels, grouped by whether the tongue shapes appear [ɹ]-like. In both cases, vowels categorized as rhotic are lower in F3, which is consistent with F3 being an important cue for /ɹ/.

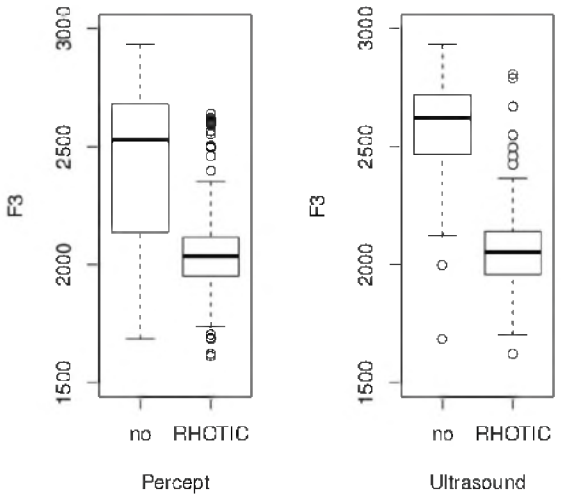


**Figure 4. F3 for vowels categorized as rhotic or non-rhotic auditorily (left) and by tongue shape (right)**

## 4. DISCUSSION AND CONCLUSIONS

The rhotic variants of Canadian French /ø/, /œ/, and /œ̃/ share phonetic properties with English /ɹ/. Like English /ɹ/, the vowels categorized as rhotic-sounding have low F3 compared to non-rhotic vowels. Further, the rhotic variants are produced with bunched and retroflex tongue postures closely resembling those observed in studies of English /ɹ/. Three speakers exhibit two categorically different tongue postures, much like English /ɹ/, with one exhibiting variation between bunched and retroflex. While the similarities with the English sound are striking, and while Canadian French is obviously in contact with English, it is not clear that the rhotic variant is borrowed from English

Previous descriptions of Montreal speech have associated variants of /ø/ and /ʁ/ described as retroflex with men and with English contact (Dumas, 1972; Sankoff and Blondeau, 2007). However, the present study has found rhotic vowels in the core French vocabulary of females with only moderate English proficiency. Rhotic vowels are also found in a wider range of segmental contexts than had previously been reported. While previous descriptions have used the term "retroflex" to describe related sounds, articulatory imaging indicates that a bunched tongue shape is used as well, and may be the most frequent tongue posture for the rhotic variants of these vowels. Some descriptions of retroflex /ʁ/ may reflect rhotic vowels in the presence of a uvular [ʁ], as seen above in Figure 2.

It remains to be seen how bilinguals' French rhotic vowels compare to their English /ɹ/. Allophonic variation between bunched and rhotic variants is common among English speakers (Mielke et al., 2010), and if the variation is articulatorily motivated, similar allophonic patterns are expected in both languages. These parallel cases of articulatory variability raise opportunities for investigating articulatory-acoustic mapping in bilinguals.

## REFERENCES


Delattre, P. and D. Freeman (1968) A dialect study of American r's by x-ray motion picture. *Linguistics* 44: 29-68.

Dumas, D. (1972) Le français populaire de Montréal: description phonologique. University of Montreal MA thesis.

Hueber, T., G. Aversano, G. Chollet, B. Denby, G. Dreyfus, Y. Oussar, P. Roussel, and M. Stone (2007) EigenTongue Feature Extraction For An Ultrasound-based Silent Speech Interface. IEEE International Conference on Acoustics, Speech and Signal Processing. Honolulu, HI: Cascadilla Press. 1245-1248.

Mielke, J., A. Baker, and D. Archangeli (2010) Variability and homogeneity in American English /ɹ/ allophony and /s/ retraction. In C. Fougeron, B. Kühnert, M. d'Imperio, and N. Vallée, ed., Variation, Detail, and Representation. Berlin: Mouton de Gruyter.

Mielke, J., A. Baker, D. Archangeli, and S. Racy (2005) Palatron: a technique for aligning ultrasound images of the tongue and palate. In S. Jackson and D. Siddiqi, ed., Coyote Papers vol. 14.

Sankoff, G. and H. Blondeau (2007) Language Change across the Lifespan: /r/ in Montreal French. *Language* 83.3: 560-88.


## ACKNOWLEDGEMENTS


This research was supported by a CFI grant to Jeff Mielke and Marc Brunelle and SSHRC grant to Jeff Mielke. Thanks to members of the Sound Patterns Laboratory and the Ottawa-Carleton Phonology group and Robin Dodsworth for their help.

# VOT DRIFT IN 3 GENERATIONS OF HERITAGE LANGUAGE SPEAKERS IN TORONTO

**Melania Hrycyna, Natalia Lapinskaya, Alexei Kochetov and Naomi Nagy**
Dept. of Linguistics, University of Toronto, 100 St. George St., Toronto, ON, CANADA, M5S 3G3
al.kochetov@utoronto.ca, naomi.nagy@utoronto.ca

## 1. INTRODUCTION

Voice onset time (VOT) – an interval between the stop burst and the onset of vocal fold vibration – is an important acoustic correlate of the voiceless/voiced contrast, and is known to vary considerably across languages (Lisker & Abramson, 1964). In languages like English, voiceless stops /p, t, k/ are realized with long-lag VOT (>30 ms). In other languages, including Italian, Russian and Ukrainian, these consonants exhibit short-lag VOT (0-30 ms). Recent studies show that speakers' native short-lag VOT can be affected by their exposure to non-native long-lag VOT, and vice versa (Flege, 1987; Fowler *et al.*, 2008). In contrast to previous studies of VOT based on experimental elicitations, we investigated VOT in conversation, from recordings of Torontonians speaking their Heritage Language (HL). Data, from the Heritage Language Variation and Change Project (HLVC), consists of sociolinguistic interviews with speakers in three generations of six HLs, stratified by age and sex (Nagy, 2009). In this paper we present results for onset /p, t, k/ produced by 34 individuals representing three generations of Russian, Ukrainian, and Italian. Comparing our data to published reports on monolingual patterns shows that HL speakers' VOT tends to drift from the homeland standard toward that of English in successive generations.

## 2. METHODS

HLVC defines generations as follows. G1: lived in the country of origin until age 18+ and in Toronto for 20+ years. G2: born in Toronto or arriving before age 6, with at least one G1 parent. G3: born in Canada, with at least one G2 parent.

VOT was examined in conversational speech of 3-4 speakers in each generation in each language, plus one fluent G5 Ukrainian. Time-aligned transcripts of the interviews were searched for the first 25 instances of word-initial /p/, /t/, and /k/ preceding stressed /a/ or /o/, beginning 15 minutes into the interview. A total of 2,515 words were selected and manually annotated in *Praat* (Boersma & Weenink, 2011). VOT was defined as the duration from the onset of the stop burst to the first zero-crossing of the first periodic wave of the following vowel. The following vowel duration was measured and used as a control for speech rate (it was expected that later generations may speak more slowly). Duration measurements were extracted by script.

Mean VOT values for each speaker were submitted to repeated measures ANOVAs, separately for each language. Within-subjects factors were Consonant (/p/, /t/, /k/) and Vowel (stressed /a/, /o/), while the between-subjects factor was Generation (1-3; and 5 for Ukrainian). Additionally, we orally administered an Ethnic Orientation Questionnaire (EOQ, Keefe & Padilla, 1987) in the interview. Open-ended responses were quantified into scores to represent a speaker's self-identified ties to Canadian society vs. their country of origin, as well as past and current exposure and attitudes to English and their HL. EOQ influence was examined through correlations between individual speakers' deviation from the VOT mean for their language and their EOQ score. The expected trend is to see more English-like VOT from speakers with a more Canadian orientation.

## 3. RESULTS

### 3.1. Overall VOT Trends

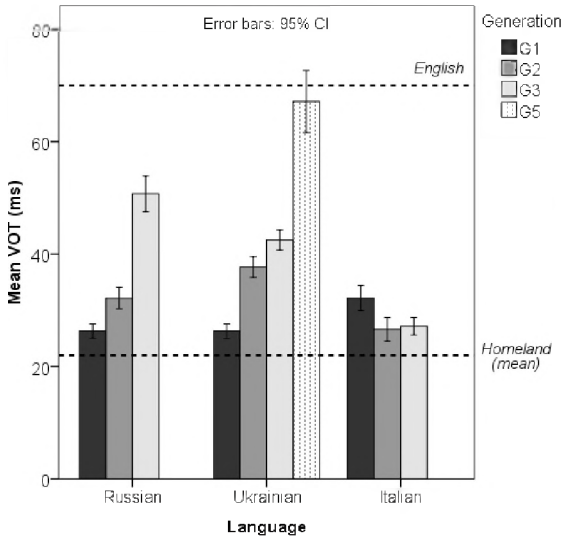


**Figure 1. Mean VOT(in ms) for all languages, with English and mean homeland comparison values**

Fig. 1 shows the mean VOT (all contexts) for each generation of HL speakers. Horizontal lines indicate the comparator English (Fowler, *et al.* 2008) and homeland varieties' average duration (Ringen & Kulikov, 2010, Sorianello, 1996). Note that homeland and English values are from sentence reading data, while HL data is from conversation. Mean VOT for Russian and Ukrainian increases as generations progress, as predicted. However, Italian exhibits stability across generations. (Speech rate, estimated by vowel duration, does not account for this surprising outcome.) The largest increase in VOT occurs between G2 and G3 for Russian, and between G3 and G5 for Ukrainian. Note that the VOT of the latter speaker is very close to English. The observed differences were confirmed statistically, with results showing a main effect of Generation for Russian ($F(2,7)=6.10$, $p<.05$) and Ukrainian

(F(2,7)=12.01, p<.01), but not Italian (F(2,7)=1.299, p=.33). Bonferroni post-hoc tests revealed that VOT was significantly higher for G3 compared to G1 in Russian (p<.05; adjusted for multiple comparisons), and higher for G5 compared to the other generations in Ukrainian (p<.01-.05). For the latter group, there was also a non-significant tendency towards higher VOT for G3 than G1 (p=.094). All languages showed a significant effect of Consonant. Based on Bonferroni post-hoc tests, VOT was significantly longer for /k/ than for /p/ and /t/ (p<.001-.05). VOT was significantly longer before /o/ than before /a/ for Russian and Ukrainian (Vowel: F(2,15)=11.52, p<.01; F(2,15) =34.73, p<.001)

### 3.2. Ethnic Orientation Influence on VOT

EOQ measures speakers' self-identified ethnicity and exposure to their HL, and attitudes toward the heritage language and culture. Higher EOQ score indicates closer association with the country of origin (on the y-axis in Fig. 2). Mean value refers to VOT mean of the speaker sample for a particular language. Positive deviation from the mean indicates longer, more English-like VOT (on the x-axis). Russian and Ukrainian show the predicted shorter VOT correlating with higher EOQ, while Italian has the opposite trend. However, in all cases the correlations are weak ($r^2$ = 0.06 for Italian, 0.15 for Russian and 0.41 for Ukrainian).

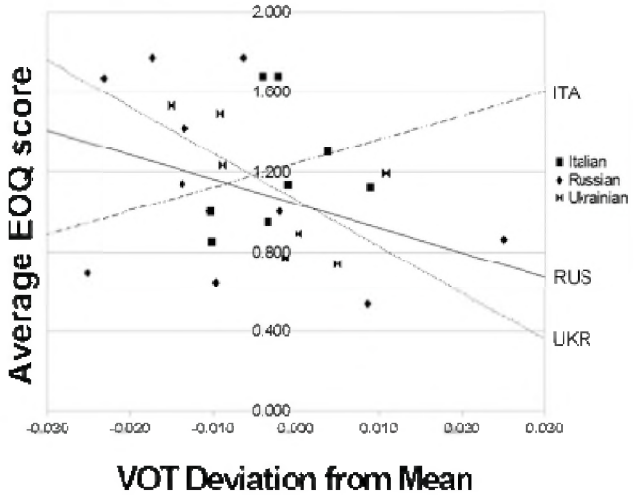


**Figure 2. Individuals' deviation from language's VOT mean (ms) *vs.* Overall Ethnic Orientation score**

One more outcome illustrates that Russian and Ukrainian speakers are more influenced by English than Italians are. /t/ in all three HLs is dental, but alveolar in English. G2 and G3 Russian and Ukrainian speakers show less drift toward English values for /t/ than for /p/ and /k/, sounds which are more similar across the languages. This illustrates Flege's (1987) claim that bilinguals undergo more influence on segments that are more similar in both languages: Russian and Ukrainian /t/ is not drawn toward the English long-lag value as much as /p/ and /k/ because dental and alveolar are different categories. Again, Italian is an anomaly.

## 4. DISCUSSION AND CONCLUSIONS

Russian VOT exhibited the expected pattern of drift from short-lag to long-lag VOT, with the biggest increase occurring between G2 and G3. This is likely because G3 speakers in Toronto do not form a cohesive Russian community and therefore have little opportunity to talk casually in Russian outside the home. In contrast, an active Ukrainian community creates ample opportunity for casual speech with other generations. Thus the VOT of G2 speakers is more rapidly pulled towards the community norms. Italian, a considerably larger community in Toronto, shows no such drift. Possibly, negative attitudes toward Calabrese Italian in Italy cause G1 to place more value on integrating into English-speaking society. However G2 and G3 Italians continue to value their language and heritage more than the Russians and Ukrainians, illustrated by the Italian's small cross-generational drop in EOQ scores: Average EOQ of G1 – G3 is 0.3 for Italian *vs*. 0.7 for each of the other two groups.

The lack of significant differences between consecutive generations can be attributed to inter-speaker variability. Some Russian G2 and G3 speakers had VOT values considerably lower than typical for their groups. The VOT of one G2 Ukrainian was similar to the average for G1, while the VOT of another was higher than the average for G3. These differences, reflecting individual and family lifestyle differences, might be eliminated by increasing the sample size. Future work will accomplish this, examine VOT in the other languages in the corpus, and compare VOT to other linguistic variables, in the hopes of better understanding contact-induced language change.

## REFERENCES


Boersma, P. & Weenink, D. (2011). Praat: doing phonetics by computer [Computer program]. http://www.praat.org/.

Flege, J.E. (1987). The Production of "new" and "similar" phones in a foreign language: Evidence for the effect of equivalence classification. *J. Phonetics, 15*:47-65.

Fowler, C. Sramko, V., Ostry, D.J., Rowland, S.A., & Hallé, P. (2008). Cross language phonetic influences on the speech of French-English bilinguals. *J. Phonetics, 36*:649-663.

Keefe, S. & A. Padilla. (1987). *Chicano Ethnicity*. Albuquerque, NM: UNM Press.

Lisker, L. & Abramson, A. (1964). Cross-language study of voicing in initial stops: Acoustical measurements. *Word, 20:* 384-422.

Nagy, N. (2009). *Heritage Language Variation and Chan*ge. http://individual.utoronto.ca/ngn/research/heritage_lgs.htm.

Ringen, C. & Kulikov, V. (2010). Voice onset in Russian. 16th Annual Mid-Continental Workshop on Phonology. Chicago.

Sorianello, P. (1996). Indici fonetici delle occlusive sorde nel cosentino. *Rivista Italiana di Dialettologia, 20*:123-159.


## ACKNOWLEDGEMENTS


We thank SSHRC (SRG 410-2009-2330) and the RAs listed at http://individual.utoronto.ca/ngn/research/HLVC_personnel.htm for recruiting, intervewing, and analysis.

# AN ULTRASOUND IMAGING STUDY OF THE TENSE-LAX DISTINCTION IN CANADIAN FRENCH VOWELS

**Will Dalton**
Dept. of Linguistics, University of Ottawa, 70 Laurier Ave. East, ON, Canada, K1N6N5, wdalt017@uottawa.ca

## 1. INTRODUCTION

Advanced tongue root (ATR) vowels are produced with significant tongue root advancement, creating a large pharyngeal resonant cavity that is not present during production of non-advanced vowels. Acoustically, this results in a lowered first formant (F1) for ATR vowels as compared to non-ATR vowels. This difference is most prominent among high vowels (Ladefoged and Maddieson, 1996). In terms of phonological features, advanced and non-advanced tongue root correspond to [+ATR] and [-ATR], respectively. These features are correlated with traditionally labelled 'tense' and 'lax' vowels in Germanic languages. Cross-linguistically, a number of gestural strategies are employed to create a distinction among so-called tense and lax vowels. In Igbo, these vowels differ only in tongue root position, while in Akan and Germanic languages such as English, they differ in both tongue root position and tongue body height (Ladefoged and Maddieson, 1996). A third possible method of contrasting tense and lax vowels is by varying tongue body height alone.

With respect to Canadian French (CF), there has been no articulatory evidence to support the hypothesis that tense and lax vowels are distinguished in a way similar to Igbo on the one hand, or Akan, English and German on the other. Acoustic evidence (Séguin, 2010) shows that tense high vowels in CF have a lower F1 than their lax counterparts. However, as mentioned above, a decrease in F1 could be caused by a number of lingual gestures, of which tongue root advancement is one possibility. Nonetheless, a prevalent assumption in literature that treats with the phonetic and phonological properties of tense and lax high vowels in Canadian French, especially with respect to harmony (Poliquin, 2006), is that these vowels are distinguished by tongue root position. More specifically, tense high vowels (/i y u/) are assumed to be articulated with an advanced tongue root while lax vowels ([ɪ ʏ ʊ]; allophonic variants of the tense vowel phonemes) are not. This assumption appears to be based on analogy with Germanic and West African languages and is not motivated by any experimental (articulatory) evidence. The purpose of this experiment is to determine which articulatory gestures are used to distinguish between tense and lax vowels using ultrasound imaging to directly measure tongue position during speech production of native speakers of CF. Findings from this study, based on data from one speaker, indicate that tense and lax high vowels are not produced with an advanced tongue root, but rather that tongue body height alone is used to distinguish between these vowels, which suggests that CF does not distinguish tense and lax vowels in the same way as Germanic or West African languages.

## 2. METHODS

Thirteen native speakers of various dialects of Canadian French (Québec French, Ontario French and Acadian) participated in this study, recruited in the Ottawa-Gatineau region through university classes and word of mouth. Due to the lack of normalization procedures for ultrasound data, the results of one participant (a female Québec French speaker from Gatineau) are discussed below.

Stimuli for this experiment consisted of mono- and disyllabic words containing tense and lax vowels elicited in final open syllables and final closed syllables, respectively. Words were produced in carrier sentences "Je dis…" and "Je dis … encore". Participants were seated in an optometry chair in a sound-proof booth in front of a computer display. Stimuli sentences were displayed on screen and participants advanced to the next sentence using a remote control. The ultrasound transducer was placed under the participant's chin to obtain a mid-sagittal tongue image, with a headrest and transducer placement used for head stabilization. Attached to the transducer and a pair of goggles worn by the participant were two wooden sticks, each painted with two white dots. These dots were later used to correct for head movement and place all ultrasound images on the same coordinate system using the Palatron algorithm (Mielke et al., 2005). Ultrasound and video were recorded at 30 frames per second using the Ultraspeech software (Hueber et al., 2008) on a Terason T3000 portable ultrasound machine. Audio was recorded throughout using a gooseneck microphone connected to a USBPre amplifier. Recordings were made using Audacity at a sampling rate of 44.1 kHz. Praat (Boersma, 2001) TextGrids for the resulting WAV files were created using the Penn Phonetics Forced Aligner (Yuan and Liberman, 2008). Acoustic measurements of high vowel formants were made at the midpoint of each vowel using a Praat script. Ultrasound and video images were superposed using a Python script. Tongue surface contours were subsequently traced in Palatoglossatron (Baker, 2005). Statistical differences in tongue position were examined using a smoothing spline ANOVA (Davidson, 2006; Gu, 2002) for pairwise comparisons in R.

## 3. RESULTS

Acoustic analysis results echo those of Séguin (2010); tense high vowels are produced with a significantly ($p<.001$) lower F1 than their lax counterparts (see Table 1). No significant difference in F2 was found between any tense-lax vowel pair. The results of the articulatory analysis are shown in Figure 1, in the form of tongue surface contour comparisons for each tense-lax pair. The dotted lines represent the 95% Bayesian confidence intervals.

Significant differences in tongue position occur where these intervals do not overlap.

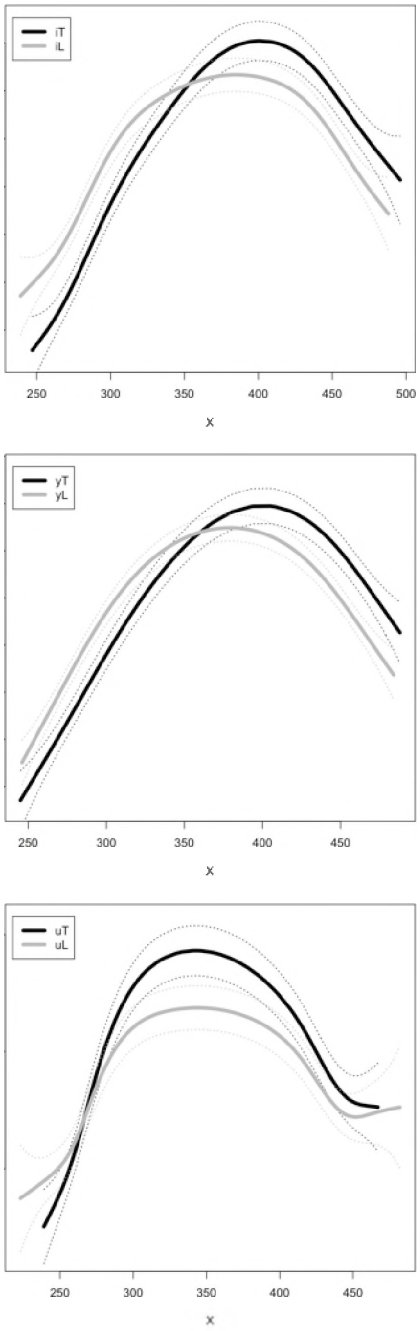


**Figure 1. Tongue surface comparison plots for tense vs. lax high vowels (tense: black, lax: grey). From top: [i]-[ɪ], [y]-[Y], [u]-[U]**

The comparisons of [i]-[ɪ] and [y]-[ʏ] reveal significant differences at the back of the tongue and at the anterior portion of the tongue body. The comparison of [u]-[ʊ] shows a significant difference in tongue position only in the tongue body. In all three comparisons, the tense vowel is produced with a higher tongue body. None of the comparisons shows evidence of a concavity at the tongue root that is typical of ATR vowels.

**Table 1. Mean F1 values for tense and lax high vowels (Hz)**

| Phoneme | /i/ | /y/ | /u/ |
|---|---|---|---|
| Tense | 322.7 | 344.4 | 353.4 |
| Lax | 443.6 | 449.3 | 439.1 |

## 4. DISCUSSION AND CONCLUSIONS

This paper presented evidence that contradicts the assumption that tense vowels in CF are articulated with an advanced tongue root. The results indicated instead that tense and lax high vowels are distinguished by tongue body height alone. These findings contribute to our knowledge of the typology of gestures used to distinguish between tense and lax vowels. Igbo makes this distinction using tongue root position, while Akan, German and English employ tongue root position and tongue body height. CF resorts to a third strategy; using tongue body height alone to create a perceptible acoustic difference between two classes of high vowels. These results also have implications for phonological analyses of high vowels in CF, in particular motivating a reanalysis of laxing harmony that does not crucially rely on the existence of a ±ATR contrast among high vowels.

## REFERENCES

Baker, A. (2005). Palatoglossatron 1.0. University of Arizona. http://dingo.sbs.arizona.edu/~apilab/pdfs/pgman.pdf

Boersma, P. (2001). "Praat, a system for doing phonetics by computer," Glot International **5**, 341-345.

Davidson, L. (2006). "Comparing tongue shapes from ultrasound imaging using smoothing spline analysis of variance," J. Acoust. Soc. Am. **120**, 407-415.

Gu, C. (2002). *Smoothing Spline ANOVA Models* (Springer, New York).

Hueber, T., Chollet, G., Denby, B. and Stone, M. (2008). "Acquisition of ultrasound, video and acoustic speech data for a silent-speech interface application," in the Proceedings of the International Seminar on Speech Production 2008.

Ladefoged, P. and Maddieson, I. (1996). *The Sounds of the Worlds Languages* (Blackwell, Cambridge, Mass.).

Mielke, J., Baker, A., Archangeli, D. and Racy, S. (2005). "Palatron: A technique for aligning ultrasound images of the tongue and palate," in *Coyote Papers, Vol. 14*, edited by S. Jackson and D. Siddiqi.

Séguin, M.-C. (2010). Catégorisation acoustique des voyelles moyennes antérieures arrondies en français laurentien. PhD dissertation, University of Ottawa, Ottawa.

Poliquin, G. (2006). Canadian French Vowel Harmony. PhD dissertation, Harvard University, Cambridge, Mass.

Walker, D. (1984). *The Pronunciation of Canadian French* (University of Ottawa Press, Ottawa).

Yuan, J. and Liberman, M. (2008). "Speaker identification on the SCOTUS corpus" in the Proceedings of Acoustics '08.

# REGIONAL VARIATION IN THE ALLOPHONES OF CANADIAN ENGLISH /æ/

**Charles Boberg**
Department of Linguistics, McGill University, Montreal, QC, H3A 1A7; charles.boberg@mcgill.ca

## 1. INTRODUCTION

This paper reports on regional variation in the phonetic realization of /æ/, or "short-a", the vowel of *bat*, *bad*, *band* and *bag*, in Canadian English (CE). Labov (1991) called /æ/ one of two "pivot points" that determine the larger patterns of vowel shifting that serve to differentiate regional varieties of North American English at the phonetic level. These are variables of phonemic contrast in the front and back corners of the lower vowel space: in the back, the potential contrast is between /ɑ/ (LOT) and /ɔ/ (THOUGHT); in the front, it is between lax /æ/ (TRAP), the main development of Middle English short /a/, and what Labov labels /æh/, a tensed variant that occurs before voiceless fricatives, like its British "broad-a" counterpart (BATH), as well as before variable sets of voiced obstruents and nasals. CE has only one phoneme in each corner, so that TRAP and BATH both have /æ/ and LOT and THOUGHT both have /ɑ/. The latter lack of contrast is referred to as the low-back merger, and has been suggested as the structural impetus for what Labov, Ash and Boberg (2006) found to be the main distinguishing phonetic characteristic of CE in comparison with adjacent American varieties, the Canadian Vowel Shift (Clarke, Elms and Youssef 1995). The Canadian Shift involves the lowering and retraction of the short front vowels /ɪ, ɛ, æ/ (KIT, DRESS and TRAP), led by the retraction of /æ/, first noted by Esling and Warkentyne (1993), into the low-central space made vacant by the low-back merger (American dialects without this merger tend to have /ɑ/ in this position, blocking any retraction of /æ/).

Labov *et al*. (2006) find that among the dialects with a single low-front phoneme there are three main allophonic systems. In the U.S. Inland North, the whole /æ/ class is tensed, rising to mid-front position. Much of the Midland and West exhibit a "nasal system", in which /æ/ is regularly tensed and raised before nasals (/æN/, e.g. *band*, *ram*), so that pre-nasal tokens form a distinct set from the rest of the distribution (e.g. *bat*, *bad*), which remains in low-front position. CE is characterized by a "continuous short-a system", in which allophones of /æ/ form a phonetic continuum along the low-front margin of the vowel space, from low-front *bat* to raised and fronted *band*. Crucial in this classification is the behavior of /æ/ before /g/ (*bag*). In "nasal" systems, /æg/ is lax, remaining with the rest of the /æ/ distribution; in Canada, by contrast, /æg/ shows an intermediate degree of tensing, distinct from both the more advanced tensing of /æN/ and the absence of tensing in *bat* or *bad*. Further research with a Canadian focus, reported here and in Boberg (2008, 2010), finds that this is a simplification, obscuring important regional differences. While this "continuous" system does apply across the country, it is realized slightly differently in each region.

## 2. METHODS

This paper presents data from the *Phonetics of Canadian English* project carried out by the author at McGill University between 1999 and 2005 and first reported in Boberg (2008, 2010); these earlier sources contain full methodological details. The data below are from word list productions elicited during recorded sociolinguistic interviews with 86 undergraduate students from every region of Canada. The word lists, which contained 145 words representing all of the vowels of English in a range of allophonic contexts, were analyzed acoustically using Kay Elemetrics' CSL 4400 system, with single-point nuclear measurements of F1 and F2 taken at the F1 maximum or at a point of inflection in F2 representing the central tendency of the formant trajectories. The formant data were then normalized using the additive point system of Nearey (1978). This paper focuses on the 16 tokens of /æ/, including 4 pre-nasal tokens (*band*, *ham*, *stamp*, *tan*), 3 before /g/ (*bag*, *gag*, *tag*), 3 before /r/ (*barrel*, *carry*, *charity*) and 6 others (*bad*, *sack*, *sad*, *sat*, *tap*, *tally*).

## 3. RESULTS

The results of the acoustic analysis are presented in Fig. 1 and Table 1.

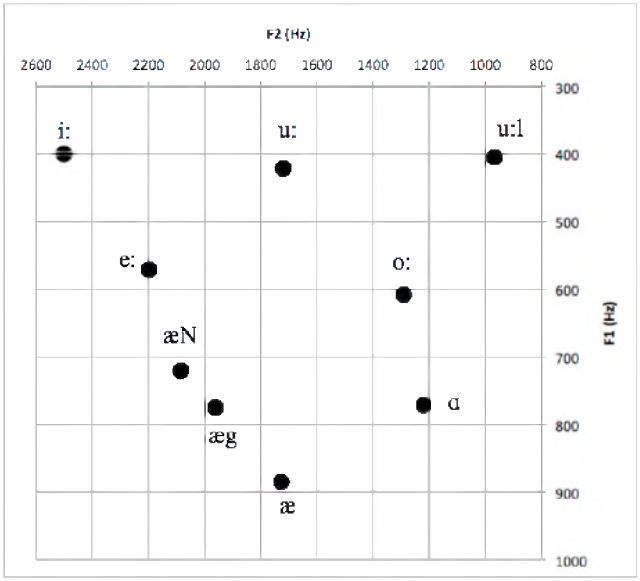


**Figure 1. Mean formant values for CE vowels (n=86)**

**Table 1. Regional means and standard deviations for position of raised /æ/ allophones relative to main distribution (Cartesian distances in Hz).**

| | /æ/ - /æg/ | | /æ/ - /æN/ | |
|---|---|---|---|---|
| *Region (n)* | *Mean* | *S.D.* | *Mean* | *S.D.* |
| BC (12) | 335 | 129 | 382 | 147 |
| Prairies (15) | 358 | 161 | 356 | 143 |
| S. Ontario (7) | 318 | 115 | 522 | 143 |
| Gr. Toronto (8) | 244 | 92 | 458 | 73 |
| E. Ontario (9) | 316 | 95 | 535 | 148 |
| QC (Mtl, 13) | 157 | 78 | 328 | 175 |
| Maritimes (16) | 244 | 75 | 410 | 128 |
| Nfld (6) | 139 | 88 | 310 | 81 |
| CANADA (86) | 270 | 130 | 404 | 151 |

## 4. DISCUSSION AND CONCLUSIONS

Figure 1 shows the mean positions of /æ/ and its two raised allophones in F1/F2 space, together with a selection of other vowels (FLEECE, GOOSE, *pool*, FACE, GOAT and LOT), included here to establish the general outline of the space. It can be seen that, as a result of the Canadian Shift, modern CE is developing a triangular vowel system, with a single low-central vowel, /æ/, now considerably lower than /ɑ/ and aligned in F2 space directly below the main distribution of /u:/, which has been strongly centralized; only the pre-lateral allophones of /u:/ remain in high-back position. In the lower-front quadrant, the raised allophones of /æ/ are positioned along the frontal periphery, halfway between the main /æ/ distribution and that of /e:/ (FACE); the distinct position of /æg/ confirms the classification of Labov *et al.*

A multivariate statistical analysis (in SPSS) of the effect of speakers' home regions on vowel production, found a significant effect on the position of both /æg/ and /æN/, measured in terms of either absolute values of F1 and F2, or Cartesian distance between each allophone and the main distribution of /æ/ (Boberg 2010: 203). Regional means and standard deviations of the distance measures are shown in Table 1, which reveals three distinct patterns. In Western Canada, including BC and the Prairies, /æ/ is raised equally before nasals and /g/, the two distance measures being roughly equivalent. In comparison, the three Ontario regions have more advanced raising before nasals but less before /g/, a pattern they share with the Maritimes. This similarity may have historical roots, arising from initial settlement of these regions by former American colonists (the "United Empire Loyalists") fleeing the American Revolution. By contrast, Quebec (mostly greater Montreal) and Newfoundland, areas with more British and less Loyalist influence, show comparatively little raising, falling below the Canadian mean given in the last row of the table. In Montreal, this has a striking auditory effect, particularly in the speech of the city's large Italian and Jewish ethnic minorities, who show even less raising than speakers of British ethnic origin (Boberg 2010: 222), producing *band* and *bag* with more or less the same vowel as *bat*.

Another distinguishing feature of Quebec and Newfoundland English, not shown in Figure 1, is resistance to the neutralization of the contrast between /æ/ and /ɛ/ before intervocalic /r/, as in *marry* and *merry*, or *barrel* and *beryl*, which prevails across the rest of Canada and much of the middle and western U.S. In Montreal and in much of Newfoundland /ær/ retains its low-front quality, whereas from Ottawa to Victoria it is merged with /ɛr/.

A further regional peculiarity, first identified by Labov *et al.* (2006: 223), was found in the Maritime region, where several speakers produced raised tokens of /æ/ before /d/; Boberg (2010: 238) illustrates this in the speech of an older man from Nova Scotia. This phonetic pattern is normally associated with the two-phoneme systems of the U.S. Mid-Atlantic coast, particularly New York City and Philadelphia, where /æd/ is among the environments that feature the tense phoneme, /æh/ (with some lexical exceptions). While there is no evidence of an analogous phonemic split in the Maritimes, raised vowels in *bad* and *sad* do resemble the American pattern at the phonetic level, and may be a relic of an older, colonial /æ/ pattern brought to the region by the Loyalists, who were the most important element in the initial English-speaking settlement of Nova Scotia and New Brunswick. Among younger Maritime speakers, this pattern appears to be recessive.

Thus, what at first seems to be a homogeneous, trans-national feature of CE, its "continuous short-a system" with less raising of /æg/ than of /æN/, turns out to be subtly differentiated among Canada's regions. Pre-velar raising is maximal in the West; pre-nasal raising is strongest in the old Loyalist areas of Ontario and the Maritimes; and Quebec and Newfoundland, exceptions to general Canadian cultural and linguistic patterns in so many ways, are distinct in this respect too, with little raising in either environment. CE is perhaps less uniform than it is often imagined to be.

## REFERENCES


Boberg, C. (**2008**). "Regional phonetic differentiation in Standard Canadian English", J. Engl. Ling. **36**, 129–154.

Boberg, C. (**2010**). *The English Language in Canada: Status, History and Comparative Analysis* (Cambridge U.P., Cambridge).

Clarke, S., F. Elms and A. Youssef (**1995**). "The third dialect of English: Some Canadian evidence", Lang. Var. & Change **7**, 209–228.

Esling, J. and H. Warkentyne (**1993**). "Retracting of /æ/ in Vancouver English," in *Focus on Canada*, ed. S. Clarke (J. Benjamins, Amsterdam), pp. 229–246.

Labov, W. (**1991**). "The three dialects of English," in *New Ways of Analyzing Sound Change*, ed. P. Eckert (Academic Press, New York), pp. 1–44.

Labov, W., S. Ash and C. Boberg (**2006**). *The Atlas of North American English: Phonetics, Phonology and Sound Change* (Mouton de Gruyter, Berlin).

Nearey, T. (**1978**). *Phonetic Feature Systems for Vowels* (Indiana University Linguistics Club, Bloomington, IN).


## ACKNOWLEDGEMENTS


This research was supported by the Social Sciences and Humanities Research Council of Canada, Standard Research Grants # 410-2005-1924 and 410-02-1391.

# AN ULTRASOUND STUDY OF CORONAL STOP DELETION IN PERSIAN

**Reza Falahati and Jeff Mielke**
Department of Linguistics, University of Ottawa, 70 Laurier Avenue East, Ontario, Canada, K1N 6N5, rfala042@uottawa.ca

## 1. INTRODUCTION

This study examines the production of word-final consonant clusters in Persian in order to provide an account of their optional acoustic simplification. Persian optionally allows the simplification of word-final coronal stops when preceded by obstruents or the homorganic nasal /n/. The words /ræft/ 'went', /duχt/ 'sew' and /qæsd/ 'intention', for example, are optionally simplified to [ræf], [duχ], and [qæs] in fast or casual speech. What is unclear is whether there is any coronal gesture left after simplification occurs. This type of issue was first discussed in the Articulatory Phonology literature. For example, Browman and Goldstein (1990) hypothesized that the alveolar closure gesture for the apparently deleted /t/ in *must be* [mʌsbi] in fluent/casual speech is still present but completely overlapped or hidden by the labial closure gesture. This means that the gesture for the alveolar /t/ (raising the tongue tip towards the alveolar ridge) is masked during the time that lips are closed or narrowed for labial /b/ and that is why the closure for /t/ is not audible. The current study aims to investigate this issue in Persian.

## 2. METHODS

Audio and real time ultrasound video recordings were made while subjects had a guided conversation with a native speaker of Persian. The subjects of the study were 10 Persian-speaking graduate students from Carleton University and the University of Ottawa, five male and five female. Three of these were excluded from the analysis due to poor imaging and some other technical issues. Subjects were seated in an optometry chair located in a sound booth in the Sound Patterns Laboratory. After subjects held water in their mouth (for palate imaging) and produced three clicks (for audio-video synchronization), they engaged in a casual conversation with the first author. Each conversation lasted 30-35 minutes. At the end of the conversation, the subjects were asked to read a short passage in a casual style.

Real time images of the tongue were collected using a Terason T3000 ultrasound system. Mid-sagittal ultrasound images of the tongue were recorded at a scan rate of 60 frames per second and a focal depth of 10 cm. The transducer probe was fixed under each participant's chin using a headset made for this purpose by Articulate Instruments. Audio was recorded in Audacity, using a Shure condenser microphone mounted close to the subject's mouth and a USB preamplifier.

All coronal stops and their preceding segments were marked in TextGrids, resulting in a total of 662 word-final coronal clusters for the conversational speech of the seven subjects.

Tokens of singleton /t/ in coda position (referred to here as real V[t]) were selected as a reference point for unreduced /t/, and control tokens with singleton /f q χ/ in coda position were selected as a reference point for the complete absence of /t/, because the complete deletion of /t/ in word-final consonant clusters involving non-coronals would result in singleton [f q χ] as the only remaining segment in the clusters. The underlying assumption here is that if gestural simplification is complete, then the gestures of the final segment of the resulting word should be similar to those of singletons. The non-simplified tokens are expected to have gestures similar to real V[t]. Finally, several palate images showing the alveolar ridge clearly were selected for each subject.

A python script was used to extract the ultrasound images corresponding to the speech intervals marked in the TextGrids. Due to the challenge of separating the coronal gestures belonging to two adjacent coronals from each other, only final coronal stops in a non-coronal environment were selected for further analysis. This resulted in the exclusion of about 20% of the captured cluster tokens. For each token, the frame which showed the highest position of the tongue tip was analyzed. Palatoglossatron (Baker, 2005) was used to trace the tongue tip and blade in each tongue image and alveolar ridge in each palate image.

## 3. RESULTS

Table 1 shows the rate of acoustically simplified C[t] for each subject (i.e., whether /t/ was inaudible in each recorded token). The seven subjects in the study showed different rates of [t]-simplification. On the two extremes, S1 simplified almost 87% of the C[t]-clusters whereas S7 simplified only 2%.

**Table 1. Number of C[t] tokens and C[t] simplification rate, for each subject.**

| | | | | | | | |
|---|---|---|---|---|---|---|---|
| **Subject** | S1 | S2 | S3 | S4 | S5 | S6 | S7 |
| **Number of tokens** | 46 | 56 | 52 | 45 | 53 | 44 | 55 |
| **Simplified C[t] rate** | .87 | .70 | .79 | .38 | .70 | .86 | .02 |

Table 2 shows the mean distance between the tongue and alveolar ridge for the two reference points (i.e., control and real V[t]). The control condition shows a range of 4.20-9.30 mm distance between the tongue and alveolar ridge whereas this comes to 0.40-1.80 for real V[t] condition. As the data related to real V[t] shows, small distances like 2mm in this table still show closure. The simplified C[t] and non-simplified C[t] can be compared with these two reference points, respectively. There is a clear difference for the tongue-alveolar ridge distance between non-simplified C[t] and simplified C[t] conditions. All the subjects show much less distance in the non-simplified C[t] condition than in the simplified C[t] condition. This could be expected if we assume that the coronal gesture is partially or fully deleted in the simplified C[t] condition. Except for S6, all the subjects show a positive correlation for the mean of tongue-alveolar ridge distance in control and simplified C[t] conditions. For example, the subjects who show the largest tongue-alveolar ridge distance in the control condition (i.e., S1, S4, and S7) also show the largest distance in the simplified C[t] condition. A similar correlation is apparent between non-simplified C[t] and real V[t] conditions. The distribution of different types of [t] shows that the simplified C[t] has the widest range of articulation.

**Table 2. Mean and SD for tongue-alveolar ridge distance (mm) across different conditions.**

| | Subjects | | | | | | |
|---|---|---|---|---|---|---|---|
| Conditions | S1 | S2 | S3 | S4 | S5 | S6 | S7 |
| **Control** | | | | | | | |
| Mean | 8.4 | 4.2 | 4.5 | 9.3 | 6.6 | 4.8 | 7.3 |
| SD | 3.4 | 2.6 | 1.7 | 3.8 | 3.7 | 1.8 | 2.7 |
| **Simplified C[t]** | | | | | | | |
| Mean | 6.1 | 5.4 | 5.2 | 10.8 | 5.4 | 7.9 | 7.7 |
| SD | 4.1 | 2.3 | 3.2 | 4.7 | 3.8 | 3.0 | 7.7 |
| **Non-simplified C[t]** | | | | | | | |
| Mean | 0.7 | 0.8 | 0.7 | 1.2 | 2.4 | 1.5 | 0.3 |
| SD | 0.2 | 0.4 | 0.4 | 0.9 | 1.3 | 1.3 | 0.2 |
| **Real V[t]** | | | | | | | |
| Mean | 0.4 | 0.6 | 0.9 | 1.6 | 1.8 | 1.1 | 0.7 |
| SD | 0.1 | 0.3 | 0.8 | 1.7 | 0.6 | 0.2 | 0.5 |

## 4. DISCUSSION AND CONCLUSIONS

In addition to variation for C[t]-simplification rate across subjects, the distance between the tongue and alveolar ridge is shown to have a wide range within and across subjects for this condition. This distance for most of the subjects started from 2 mm and extended to 17 mm as the maximum point for tongue tip raise in simplified [t] condition. This means that the tokens which are perceived as simplified clusters can be realized either with full coronal gesture or without it. This is in line with the predictions made by both Articulatory Phonology and perceptual accounts; however, perceptual accounts make further prediction regarding the simplified clusters. It is predicted that among C[t]-simplified clusters with 2-17 mm tongue tip-alveolar ridge distance, there are some tokens which are perceived as more [t]-like or less [t]-like than the others. This needs to be explored.

Despite the fact that there is substantial variation in the tongue-alveolar ridge distance, the general patterns of the simplified [t] look to be very similar across subjects. This suggests that variation and optional processes are not necessarily related to performance and that they behave in a systematic and predicable way (For more discussion see Kochetov and Pouplier 2008).

Additionally, the tongue-alveolar ridge distance shared between the simplified and non-simplified /t/ suggests that the cut-off point between categorical (i.e., non-simplified [t]) and gradient (i.e., simplified [t]) aspects of phonology is obscure. The fact that the border line between simplified and non-simplified [t] is very narrow could trigger the likelihood of their misperception. This also applies to the tokens within [t]-simplification category standing on either ends of a wide spectrum of tongue-alveolar ridge distance.

Zsiga (2000) stated that with the shortening of the gesture the chance of having that sound overlapped also gets increased. Perceived deletion of this type can lead to actual deletion. Ohala (1981) has emphasized that analyzing phonological processes in terms of articulatory gestures does not rule out a perceptual/acoustic component to these processes. Any change in gestures or their magnitude or timing can result in perceptual/acoustic changes.

## REFERENCES


Baker, A. (2005). *Palatoglossatron 1.0*. University of Arizona, Tucson, Arizona. http://dingo.sbs.arizona.edu/~apilab/pdfs/pgman.pdf.

Browman, C. P., & Goldstein, L. (1990b). Tiers in articulatory phonology, with some implications for casual speech. In J. Kingston & M. E. Beckman (Eds.), *Papers in laboratory phonology I: Between the grammar and physic* Press.

Kochetov, A. & Pouplier, M. (2008). Phonetic availability and grammatical knowledge: an articulatory study of Korean place assimilation. *Phonology,* 25, 399-431.

Ohala, J. (1981). The listener as a source of sound change. In Masek, C.S., R.A. Hendrik, M.F. Miller, eds., *CLS 17-2,* 178-203. Chicago: CLS.

Zsiga, E. C. (2000). Phonetic alignment constraints: Conso-nant overlap and palatalization in English and Russian. *Journal of Phonetics* 28 (1): 69–102.


## ACKNOWLEDGEMENTS


The authors wish to express their thanks to Marc Brunelle and Marie Hélène Côté for their valuable comments on the earlier versions of this paper. We also wish to thank the participants of BWTL 14 for their comments and feedback. We also thank all Persian speaking students at Carleton University and the University of Ottawa who participated in this study.

# PHARYNGEAL /h/ IN JAPANESE

**Noriko Yamane[1], Bryan Gick[1, 2], and Douglas Pulleyblank[1]**
[1] Dept. of Linguistics, University of British Columbia, 2613 West Mall, Vancouver, BC, Canada, V6T 1Z4
[2] Haskins Laboratories, 300 George Street, Suite 900, New Haven, Connecticut, USA, 06511

## 1. INTRODUCTION

Glottal fricatives are generally assumed to be "placeless" (Steriade (1987), Keating (1988), Stemberger (1993)). The widely-held view about Japanese is that /h/ is placeless, based on the observation that, synchronically, /h/ becomes a palatal fricative before /i/, and a bilabial fricative before /u/, suggesting that /h/ has no independent constriction location. We interpret this as an argument for the idea that Japanese /h/ is pharyngeal rather than placeless.

In our view, Japanese /h/ assimilates in these high vowel environments due to articulatory conflict (Meechan (1992), Archangeli & Pulleyblank (1994), Gick & Wilson (2006)) at the tongue root. Gick & Wilson argue that conflicting tongue root targets beget crosslinguistically diverse repair strategies. Furthermore, in many languages that have a pharyngeal /h/, a sequence of /h/ and a high vowel (*hi, *hu) is banned. In languages with sequences of this kind, vowel lowering or laxing may occur (e.g., /hilt/ > [helt] 'many' in Gitksan (Rigsby (1986: 205)), see Shahin & Blake (2004) for a vowel lowering effect in Salish, and Shaw (1991) for both pharyngeal and placeless glottals within Nisgha).

A lingual ultrasound study was conducted to test whether Japanese /h/ shows evidence of an independent pharyngeal place of articulation.

## 2. METHODS

### 2.1 Participants

Seven native speakers of standard Japanese (5 females and 2 males, ranging from early 20s to early 40s) participated in the experiment. The purpose of this experiment was not told. One participant's data was omitted, as her speech was affected by previous temporomandibular joint surgery.

### 2.2 Materials

All stimuli were pseudo words, phonologically and morphologically controlled. Target word was *ahha*, and dummy words were *ihhi, ihha, ahhi, ahhe, ihhe, uhhe, ahho, ihho, uhho*. Geminated *hh* rather than a singleton *h* was selected so that the lingual movement would be slower and more visible to us. The word list consists of 14 blocks. Each block contains target and dummy words that were randomized in ordering. The first and the last token of each block and all words in the first and last blocks were not used for the measurements. The list was printed and presented in katakana orthography as in アッハ, with HGP Mincho E Font of 12 point, in white letter size papers.

### 2.3 Procedure

Recording was conducted in the Interdisciplinary Speech Research Laboratory at the University of British Columbia. Participants were trained to read all tokens with initial-accent at a natural rate.

An Aloka SSD-5000 ultrasound machine was used with a UST-9118 and 180° electronic convex EV probe. Movie clips were recorded into iMovie, and converted to DV files. Still images were extracted at midpoints of consonants and vowels, using Final Cut Express ver. 1.01. Midsagittal tongue contours were produced and measured using EdgeTrak software (Stone (2005), among others).

### 2.4 Design

/h/ and flanking /a/ vowels were compared, and presented in the form of i) SSANOVAs (cf. Davidson (2006)) to **show overall tongue configuration**, and ii) boxplots of y-axis (constriction degree) to show **peak tongue height**, and x-axis (constriction location) to show **peak tongue backness**). It is predicted that pharyngeal /h/ should be significantly different from flanking /a/ vowels.

## 3. RESULTS

Results show that some speakers have a distinct pharyngeal constriction for /h/, but there seems to be inter-speaker variation in the details.

### 3.1 TT: Pharyngeal Constriction

Figure 1 gives sample graphics of SSANOVA, from one subject (TT), who has significant tongue root retraction.

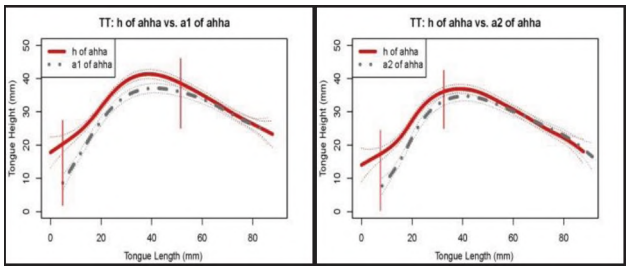


**Figure 1. Tongue root retraction in SSANOVA**

In each graph, the left hand side is tongue root, and the right hand side is tongue tip. A pair of vertical lines over tongue

surfaces indicate the area that has a significant difference (>.05) in tongue configurations between /h/ and /a/.

Figure 2 shows the distributions of the height (on the left hand side) and backness (on the right hand side) of the highest point of the tongue. Table 1 presents t-test results.

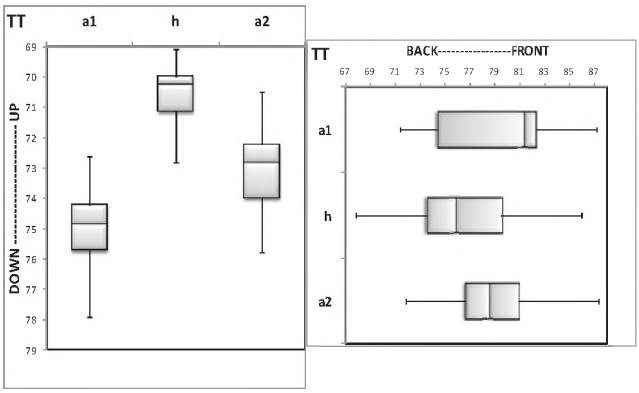


**Figure 2. Peak tongue: Height and Backness**

**Table 1. Dorsum peak comparison of TT**

| t-test | a1 vs. h | h vs. a2 | a1 vs. a2 |
|---|---|---|---|
| Tongue Height | ***<.0001 | ***<.001 | **<.01 |
| Tongue Backness | 0.25 | 0.32 | 0.8 |

The results for /h/ vs. a1 or a2 indicate that the highest tongue point for /h/ is significantly raised, but not significantly backed or fronted.

### 3.2 All: Inter-speakers Variation

The results of six subjects are given in Table 2.

**Table 2. Combined Results of R and Boxplots**

| | SSANOVAs | y-axis (height) | x-axis (backness) |
|---|---|---|---|
| AM | ≠a1 only | | |
| HS | ***≠a1&a2*** | ***≠a1&a2*** | ≠a2 only |
| TT | ***≠a1&a2*** | ***≠a1&a2*** | |
| YS | ≠a1 only | ≠a2 only | ≠a1 only |
| KK | | ≠a1 only | |
| MK | ***≠a1&a2*** | ≠a1 only | ≠a2 only |

(Shadowed boxes show no significant difference between /h/ and a1, and /h/ and a2. '≠' indicates significant difference from /h/.)

The overall results consist of three groups: (i) HS, TT and MK have a significantly different retraction and/or raising around uvular/pharyngeal area for /h/, relative to /a/ on both sides, (ii) KK has no significant difference, and (iii) AM and YS show a significant difference between /h/ and a1 only.

## 4. DISCUSSION AND CONCLUSIONS

Based on the hypothesis of Generative Phonetics (Pierrehumbert (1980), Keating (1988), Cohn (1990)) that phonetic implementations reflect phonological feature specifications at the output of phonology, features should be specified differently for each of those three ways of implementations: (i) **α-β-α**, where the intervocalic /h/ is different from vowels, or (ii) **α-0-α**, where /h/ is unspecified for place so that it can be interpolated, and (iii) **α-β**, where β is linked to both /h/ and a2. Since β shows retraction or raising around uvular/pharyngeal area, the feature could be [pharyngeal] (McCarthy (1991)) or Tongue Root (Cole (1987)), which should be distinguished from vowel place α.

The possibility of multiple possible feature specifications as above may come from the phonetic ambiguity of /h/: it is classically dubbed as 'fricative', implying it behaves like **consonants**, but could be 'glide' (Chomsky & Halle (1968)) or 'approximant' (Keating (1988)) implying it behaves more like **vowels** or expects interpolation. Such highly variable characteristics of /h/ may allow speakers to access different resolutions to the potential ambiguity. Interestingly, although the multiple resolutions are available, the individual choice is found to be discrete and categorical.

Based on this observation, the audibly unclear covert contrast between [pharyngeal] and placelessness may be suggested as being active in Japanese phonology, and speaks in favor of the emergentist position of distinctive features (Pulleyblank (2003), Mielke (2008), Kim & Pulleyblank (2009), Mielke, Baker & Archangeli (2010)).

## SELECTED REFERENCES


Archangeli, D. & Pulleyblank, D. (1994). *Grounded Phonology*. Cambridge, MA: The MIT Press.

Gick, B., & Wilson, I. (2006). Excrescent schwa and vowel laxing: Cross-linguistic responses to conflicting articulatory targets. *In L. Goldstein, D. H. Whalen & C. T. Best (eds.) Papers in Laboratory Phonology VIII: Varieties of Phonological Competence*, 635-660.

Kim, E., & Pulleyblank, D. (2009). Glottalization and Lenition in Nuu-chah-nulth. *Linguistic Inquiry*, *40*(4), 567-617.

McCarthy, J. (1991). Semitic gutturals and distinctive feature theory, in B. Comrie and M. Eid (eds.). In *Perspectives on Arabic Linguistics III: Papers from the third annual symposium on Arabic Linguistics* (pp. 63-91). Amsterdam: John Benjamins.

Meechan, M. (1992). Register in Khmer: The laryngeal specification of pharyngeal expansion. MA thesis, U. of Ottawa.

Mielke, J., Baker, A., & Archangeli, D. (2010). Variability and homogeneity in American English /r/ allophony and /s/ retraction. *Laboratory Phonology*,*10*(Phonology and Phonetics), 4-4, Berlin, New York: de Gruyter Mouton, 699-730.

Pulleyblank, D. (2003). Covert feature effects. *WCCFL 22: Proceedings of the 22nd West Coast Conference on Formal Linguistics*, *22*, 398-422.

Steriade, D. (1987). Locality conditions and feature geometry. *NELS*, *17*, 595-617.


## ACKNOWLEDGEMENTS


This work has been supported by an NSERC Discovery Grant to the second author and a SSHRC Standard Research Grant to the third author. The authors thank Denise Tom for technical assistance.

# THE ACOUSTICS AND ARTICULATION OF MANDARIN SIBILANTS: IMPROVING OUR DATA BY MODELING THE PALATE WITH EMA

**Chris Neufeld[1] and Andrei Anghelescu[2]**
[1]Dept. of Speech and Language Pathology, University of Toronto, christopher.neufeld@utoronto.ca
[2]Dept. of Linguistics, University of Toronto, aanghelescu@gmail.com

## 1. INTRODUCTION

Electromagnetic articulography (EMA) is a tool for tracking the motion of the articulators during speech (1, 2). One drawback of fleshpoint measurements is the absence of clear anatomical boundaries. Although we may know the location of EMA coils in 3D space (here *x* is horizontal displacement, *y* lateral, *z* vertical), we have only a rough idea of the tongue coils' location relative to the palate. Here we outline a procedure for creating a 3D model of the hard palate, and offer a small exploratory dataset examining Mandarin sibilants (3), finding that our articulatory measurements are improved if they are redefined relative to the palate.

## 2. METHODS

Mandarin has a three-way place contrast for sibilants: alveolar, palatal and retroflex. For each place there are three possible manners of articulation: fricatives, unaspirated affricates and aspirated affricates. Phonotactically licit monosyllables were created by pairing target consonants with vowels [a] and [ɤ̯] with high level tone. Target words were put in the frame *'tā shuō __ ma?'* "Does he say__?" Stimuli were presented in a random order on a screen in Pinyin for 20 seconds each. One male participant repeated each phrase continuously while it was displayed, and the set was repeated twice, yielding roughly 25 tokens per condition.

Speech was recorded at 64 kHz with a head-mounted mic. Consonants were manually annotated in Praat, and the centre of gravity (COG) was extracted with a 25 ms Hanning window every 5 ms for the duration of each consonant. For each consonant, we found the peak COG and the relative time of peak COG (consonant = 0, offset = 1).

Data was collected using the AG-500 system, with a sampling rate of 200 Hz. All trials were normalized to the occlusal bite plane, filtered and smoothed according to standard procedures (4). We constructed a 3D model of the participant's palate by tracing its surface with an EMA coil attached to a stick. A 3D surface was fit to the palate data using the lowess algorithm with a span of 5%. The constriction location (*cl*) and constriction degree (*cd*) of the tongue tip (TT) and tongue body (TB) coils were calculated using this model. At each sample, the shortest line in the sagittal plane between the tongue coil and the palate model was found. The line's length is *cl*, and its point of intersection with the palate model is *cd* (5). For EMA data in both absolute and palate-relative space, we found the point of maximum closure within the span of the consonant (highest *z*-value for absolute space, lowest *cd* for palate-space). At this point, we extracted (*x*, *z*)/(*cl*, *cd*) and the relative time of maximum closure. All articulatory measurements discussed below are extracted at the point of maximum stricture.

## 3. RESULTS

Place of articulation (PoA) of Mandarin Sibilants is readily distinguished by peak COG. For all manners of articulation, alveolar sibilants had the highest COG, retroflex the lowest, and palatal in the middle. Manner of articulation is distinguished by the relative time of the COG peak, with fricatives' COG peak occurring roughly in the middle of the consonant, aspirated affricates' peak COG occurring quite early, and unaspirated affricates' coming late.

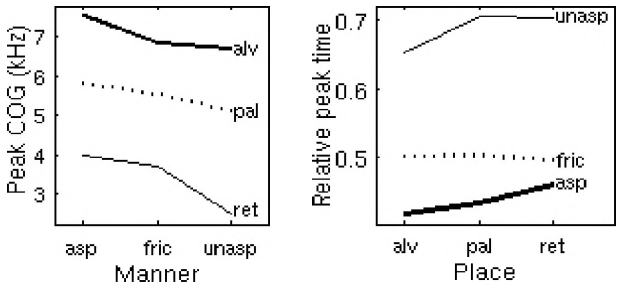


**Figure 1. Mean peak COG & relative time by consonant**

In figure 2, we show *x*/*cl* at the point of maximum constriction for TT and TB. While there is some overlap in all four boxplots, it can be seen that TB*cl* in palate space gives the most categorical picture of PoA for Mandarin Sibilants, and conforms to descriptive accounts of these speech segments (3), with alveolar being the most front, retroflex the most back, and palatal in the middle. In figure 3, we show a series of scatterplots, with peak COG on the abscissa, and spatial variables on the ordinates. A line of best fit is shown, and the corresponding Pearson's *r* is written in each panel. Examining these scatterplots we should hope to see either a clear linear relationship between acoustics and articulation, or three clusters which correspond to PoA. Here we can have our cake and eat it too: for TB in palate-relative space, *cl* exhibits a fairly linear relationship with peak COG. When peak COG is plotted as a function of TB*cd*, we see three fairly obvious clusters. In figure 4 we present this scatterplot sorted by PoA, and see a highly categorical grouping. For all other articulatory variables, we do not see as high a linear correlation, nor

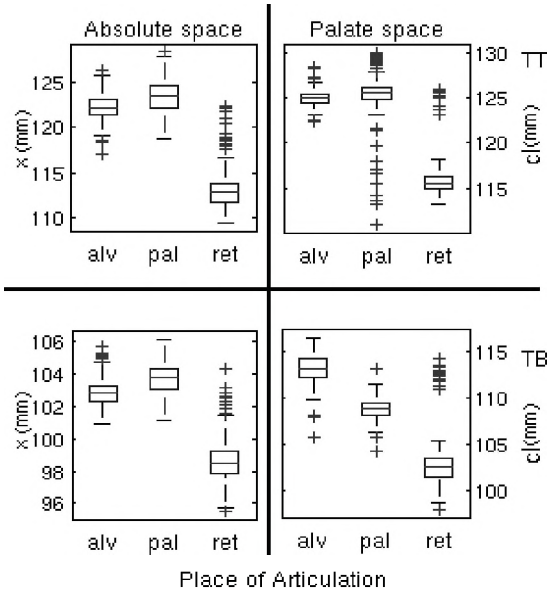


**Figure 2: x/CL by PoA and coil in different co-ordinate spaces**

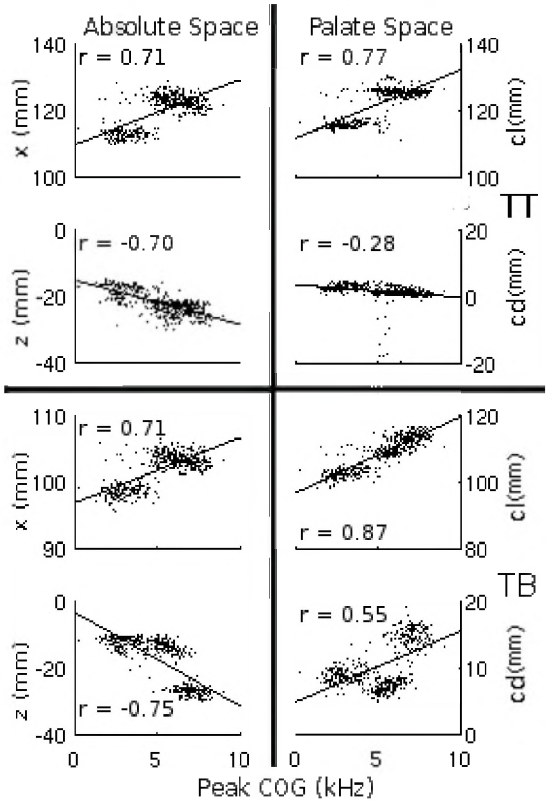


**Figure 3: COG and articulatory variables**

do we observe such a clear 3-way grouping. These findings suggest that what may *appear* to be a quantal effect (6) such as the relationship between COG and TB*x* in absolute space, may actually be a simple linear relationship if translated into palate-space. Furthermore, true quantal effects may also be *more* quantal in palate-space, as in the relationship between COG and TB*cd*. Or, to put it another way, since palate-relative space more accurately captures the shape of the oral cavity, acoustic-articulatory correspondences are more accurately revealed, and true non-linearities are amplified and false non-linearities may be 'linearized.'

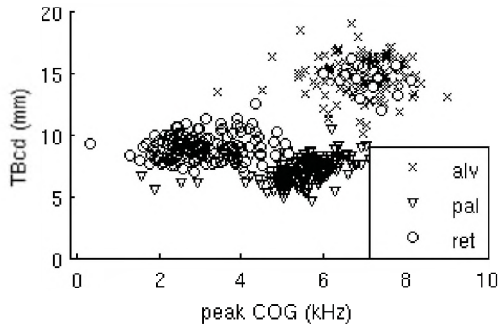


**Figure 4: Correlation between COG and TBcd by PoA**

## 4. DISCUSSION AND CONCLUSIONS

In addition to providing some descriptive data on Mandarin sibilants, we believe we have also demonstrated several benefits of redefining the location of EMA tongue coils relative to the palate. Describing EMA data in this fashion both gives a clearer picture of the physical state of the vocal tract, and has a closer affinity with several theoretical approaches to phonology or speech motor control (i.e. Articulatory Phonology (7), Task Dynamics (8)) which are couched in terms of variables or goals of the vocal tract, rather than purely spatial parameters. We conclude that this may be a useful method for deriving vocal tract variables from EMA data, and hope this continues to be found to be a productive research tool.

## REFERENCES

**[1]** Yunusova Y, Green J.R. & Mefferd A. (2009). Accuracy Assessment for AG500, Electromagnetic Articulograph. *Journal of Speech, Language and Hearing Research*. 52, 547-555.

**[2]** Hoole, P. & Zierdt, A. (2010). Five-dimensional articulography. In P.H.H.M van Lieshout & B. Maassen (Eds.), *Speech Motor Control: New developments in basic and applied research* (pp. 331-349). Oxford University Press.

**[3]** Ladefoged, P. & Wu, Z. (1984) Places of articulation: an investigation of Pekingese fricatives and affricates. *Journal of Phonetics* 12: 267-278, 1984.

**[4]** Van Lieshout, P. H. H. M., & Moussa, W. (2000). The assessment of speech motor behaviors using electromagnetic articulography. T*he Phonetician*, 81(1), 9-22.

**[5]** Neufeld, C. & van Lieshout, P.H.H.M. (2011). Alternative co-ordinate spaces for EMA. Submitted to JASA.

**[6]** Stevens, K. N. (1972) The quantal nature of speech: evidence from articulatory-acoustic data. In E.E. David & P.D. Denes (Eds.), *Human communication: a unified view*. (pp. 51-66)

**[7]** Browman, C.P. & Goldstein, L. (1986). Towards an articulatory phonology. In C. Ewan & J. Anderson (Eds.), *Phonology Yearbook 3*. Cambridge: Cambridge University Press, pp. 219-252.

**[8]** Saltzman, E.L. & Munhall, K.G. (1989). A dynamic approach to gestural patterning in speech production. *Ecological Psychology*, 1(4), 333-382.

# CATEGORICAL VARIATION IN LIP POSTURE IS DETERMINED BY QUANTAL BIOMECHANICAL-ARTICULATORY RELATIONS

**Bryan Gick[1, 2], Ian Stavness[3], Chenhao Chiu[1], and Sidney Fels[3]**

[1] Dept. of Linguistics, University of British Columbia, 2613 West Mall, Vancouver, BC, Canada, V6T1Z4, gick@mail.ubc.ca

[2] Haskins Laboratories, 300 George St., New Haven, CT, USA 06511

[3] Dept. of Electrical and Computer Eng., University of British Columbia, 2356 Main Mall, Vancouver, BC, Canada, V6T1Z4

## 1. INTRODUCTION

The labial place of articulation exhibits categorical variation in lip postures corresponding with different manners or degrees of constriction. Specifically, across many languages, stops (complete closures) are most often produced using a flat bilabial constriction; fricatives (critical closures) are produced using labiodental constrictions; and vowels or semivowels (approximant constrictions) are produced using rounded and protruded constrictions (Ladefoged & Maddieson 1996).

The present paper investigates why the lips should adopt such different postures in an attempt simply to modulate degree of constriction. We propose that this categorical variation in lip posture is the result of the speech production system taking advantage of quantal properties (after Stevens 1972) in lip biomechanics. Specifically, we expect to find that assuming different initial settings will allow the lips to achieve the desired speech outcomes with highly variable activation levels and minimal active control.

We test this proposal by simulating lip constrictions using a three-dimensional biomechanical face model in ArtiSynth (www.artisynth.org). The model accounts for passive tissue mechanics as well as active muscle stress and stiffness and can be used to analyze the effect of muscle activation on lip shaping, protrusion, and contact. It will be shown that this hypothesis is supported for stops via ballistic overshoot and for approximants via sphincteric saturation (Nazari et al., 2011). Labiodental fricatives will be treated as stop constrictions against an irregular dental surface.

## 2. METHODS

We used a model of lip-face dynamics to analyze the effect of muscle activations on lip shaping and opening in different lip configurations. Simulations were made with the ArtiSynth simulation toolkit, which is described in detail by Stavness et al. (2011). The 3D finite-element method (FEM) face model is based on a reference model reported by Nazari et al. (2011) and uses a hyper-elastic, incompressible Mooney-Rivlin material. The face model was adapted and registered to a specific speaker (Bucki et al., 2010) for which we also have jaw, skull, and tongue models (Stavness et al., 2011). Contact between the lips, and between the lips and teeth, is detected and handled as a constraint on the FEM dynamics, allowing for lip compression, as is known to occur in labial stops and fricatives.

The lip musculature is modeled using a transversely anisotropic FEM material (Weiss et al., 1996). The muscle fiber paths for the face muscles are consistent with Nazari et al. (2011), who used simplified line-based muscles with functional isotropic stiffening during muscle activation. Our FEM-based muscles provide a better distribution of muscle stress within the face model and more realistic transverse-anisotropic stiffening during muscle activation. Mesh elements are associated with fibers by finding those elements that are near the muscle fiber paths for each muscle group. The transverse direction of each element is interpolated from the muscle fiber path and represents the muscle's line-of-action. Stress is added in the transverse direction to represent passive muscle stress (varying non-linearly with strain along the preferred direction) and active muscle stress (varying linearly with muscle activation).

Muscle activations were manually set to achieve canonical lip postures for bilabial (stop) and protruded (approximant) constrictions. Lip shapes were achieved by activating muscles up to a maximum stress as indicated in Table 1. The maximum stress values correspond to an average of about 50% of maximum voluntary muscle contraction. Postures for rest position, bilabial constriction and approximant constriction are shown in Figures 1, 2 and 3.

**Table 1. Maximum muscle stress (kPa) used for simulated bilabial and approximant constrictions, including the peripheral/marginal fibers of orbicularis oris (OOP/M), risorius (RIS), and mentalis (MEN) muscles.**

| | Bilabial constriction | Approximant constriction |
|---|---|---|
| OOP | – | 50 |
| OOM | 60 | – |
| RIS | 40 | – |
| MEN | 40 | – |

## 3. RESULTS

The plot in Figure 4 shows that a large range of possible muscle activation levels will produce equivalent degrees of constriction. Closure/protrusion was achieved at relatively low activation (0.2, or ~10% of max. voluntary contraction). Increased activation yielded more compression for stops and more protrusion for approximants, but did not materially affect constriction area or posture.

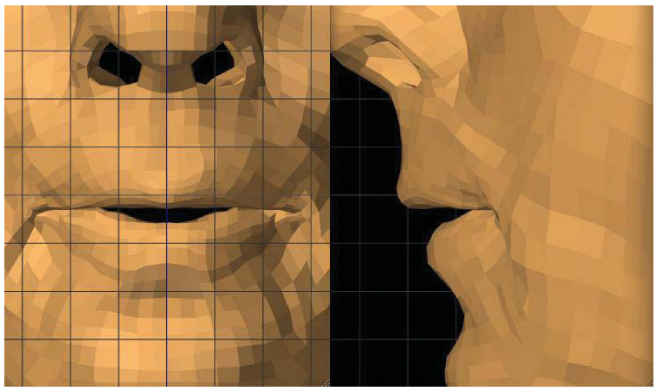

**Figure 1. Rest position.**

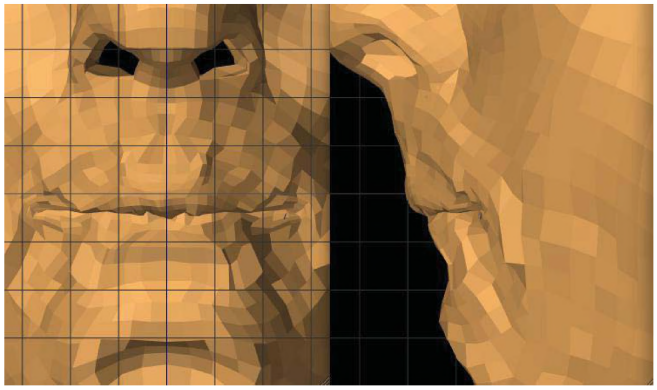

**Figure 2. Maximum bilabial constriction.**

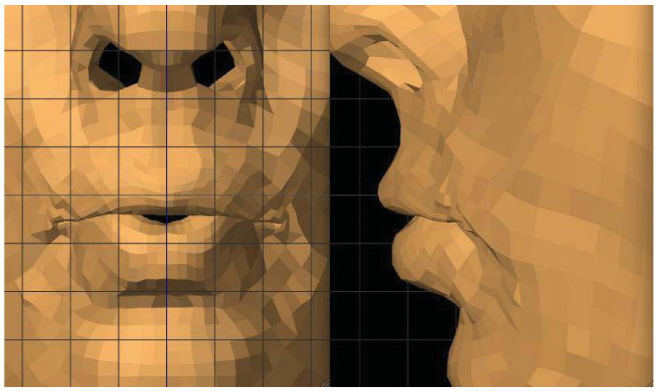

**Figure 3. Maximum approximant constriction.**

## 4. DISCUSSION AND CONCLUSIONS

Our results show that different initial muscle settings produce regions in which large variations in input activation yield stably different degrees of constriction, all corresponding to the feature of labial. We consider a labiodental fricative similar in principle to a bilabial stop, except that the teeth constitute an imperfect closure surface.

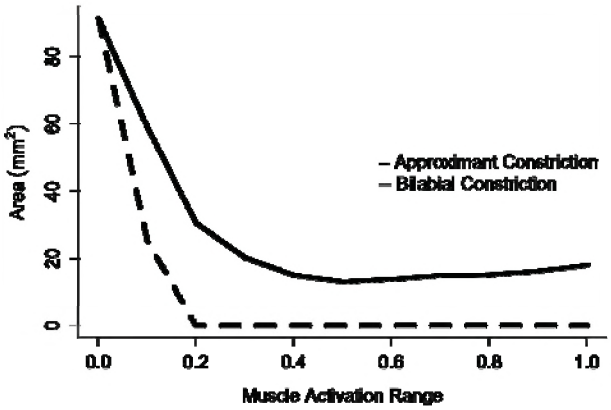


**Figure 4. Area of opening as muscle stress increases from 0–1, where 1 is the maximum stress level indicated in Table 1.**

We conclude that language speakers use these quantal regions in biomechanical-articulatory space to control constriction degree at the lips. It is important to note that we do not view the lips in this analysis as exceptional. Future work will treat this as a general mechanism driving speech production.

## REFERENCES


Bucki, M., Nazari, M.A., and Payan, Y. (2010), Finite element speaker-specific face model generation for the study of speech production. *Computer Methods in Biomechanics and Biomedical Engineering*, 13(4):459–467.

Ladefoged, P. and Maddieson, I. (1996). *The Sounds of the World's Languages*. (Blackwell, Oxford).

Nazari, M.A., Perrier, P., Chabanas, M. and Payan, Y. (2011), "Shaping by Stiffening: A Modeling Study for Lips," *Motor Control*, 15(1):141–168.

Stevens, K.N. (1972). "The Quantal Nature of Speech: Evidence from Articulatory-Acoustic Data," In *Human Communication: A Unified View*, edited by E.E. David, Jr. and P.B. Denes (McGraw-Hill, New York), pp. 51–66.

Stavness, I., Lloyd, J., Payan, Y., and Fels, S. (2011). "Coupled hard-soft tissue simulation with contact and constraints applied to jaw-tongue-hyoid dynamics," *International Journal of Numerical Methods in Biomedical Engineering*, 27(3):367–390.

Weiss, J. A., Maker, B. N., and Govindjee, S. (1996), "Finite element implementation of incompressible, transversely isotropic hyperelasticity," *Computer Methods in Applied Mechanics and Engineering*, 135(1-2):107–128.


## ACKNOWLEDGEMENTS


We acknowledge Yohan Payan from TIMC-IMAG lab, Grenoble for his assistance in creating the face-jaw model and Pascal Perrier and Mohammad Ali Nazari from Gipsa-lab, Grenoble for providing the face model geometry. Research funded by an NSERC Discovery Grant (B. Gick) and an NSERC Strategic Project Grant (S. Fels).

# EVALUATING THE VOWEL SPACE EFFECTS OF LARYNX HEIGHT USING LARYNGEAL ULTRASOUND

**Scott R. Moisik and John H. Esling**
Dept. of Linguistics, PO Box 3045, University of Victoria, BC, V8W 3P4, Canada
srmoisik@uvic.ca, esling@uvic.ca

## 1. INTRODUCTION

In this paper we apply laryngeal ultrasound to the task of evaluating the effect of larynx height on vowel formant frequencies. Our technique accurately quantifies change in larynx height, and from this basis we will demonstrate that, while larynx lowering generally yields expected lowering effects on formants, larynx raising has a lowering effect on F2 and F3 more characteristic of what has been labeled *pharyngealization*. There are two principal articulatory axes in the larynx, in addition to pitch control, associated with laryngeal acoustics: the axis of constriction and the axis of height. Therefore we attribute the formant effects observed in larynx raising to co-occurring laryngeal constriction.

Larynx height is generally assumed to correlate positively with the resonant frequencies of the vocal tract. In the simple uniform tube model of the vocal tract, lengthening or shortening the tube to represent change to larynx height yields this effect, since resonant frequencies are inversely proportional to vocal tract length (Stevens 1998: 139). Sundberg and Nordström (1976; 'SN76') studied resonance effects of larynx height. They provide simulated results using an acoustic model with 1.5 cm changes to pharynx length and canonical results from phonetic productions made by two participants with "informal estimations" that laryngeal displacements were about 1.5 cm from the normal position with "normal speaking voice pitch". It is noteworthy that SN76 do not manipulate the cross-sectional area of the epilaryngeal tube in their acoustic model. Overall their results indicate that formant frequency has a positive correlation with larynx height, but the strength of the effect differs by vowel: open vowels show the greatest effect for F1, and close (front) vowels show the greatest effect for F2. F3 and F4 are claimed to positively correlate for all vowels. Their claim is that pharynx length drives the first order effect of larynx height on vowel formant frequencies.

## 2. METHODS

Our objective was to repeat the basic protocol of the SN76 study testing subject's articulations but also to provide more robust observations for larynx height change. To accomplish this goal we collected laryngeal ultrasound data and processed it using optical flow analysis to calculate vertical change in larynx position.

Two phonetician participants (A and B) produced careful productions of [i æ *a* u] in normal (N), raised (R), and lowered (L) larynx states while attempting to maintain constant F0. Productions followed two different larynx height manipulation regimes: NRN and NLN, and NRNL and NLNR. Elicitations lasted ~6 seconds on average. Laryngeal ultrasound was manually administered using a 12L-RS probe with a 3.84 cm FOV connected to a LOGIQe portable ultrasound machine set to 8 MHz with a 2.0 cm depth. The probe is applied to the participant's neck, 1 cm posterior to the thyroid notch. Audio and video data were routed through a Canopus TwinPact100 AD video converter and captured using Sony Vegas 8.0.

Change in larynx height was observed using laryngeal ultrasound and quantified by means of an optical flow algorithm (Moisik et al. 2011), a block-wise, absolute differences method. Gradient methods for optical flow were avoided since ultrasound data do not meet assumptions of smoothness in the brightness pattern of images (Horn and Schunck 1981). To obtain larynx height change, the vertical components of the resulting velocity field vectors were averaged using a weighting based on estimated accuracy. This velocity function is then numerically integrated to yield position change.

The first three formants were obtained by sliding-Gaussian-window LPC analysis ($8^{th}$ order) of the audio signal. Formant measurements are averages taken from ROIs defined for stable larynx height targets. F0 was measured to evaluate consistency. All computation was performed in MATLAB R2009a.

## 3. RESULTS

Change in formant frequency by vowel and larynx height condition is shown in "Figure 1" for Participants A and B. "Figure 2" shows box plots for change in larynx height by vowel and by larynx height condition. Larynx height targets are consistently achieved, but there is a tendency for elevated neutral position. The tendency was for the $N_2$ in $N_1RN_2L$ and $N_1LN_2R$ targets to be higher in elevation than $N_1$, indicating undershoot in return to neutral height, which ultimately skews the mean value. For both raised and lowered, the change in height is usually on the order of 1 cm above or below neutral.

Relative formant changes expressed as percentages are presented in "Table 1". F1 uniformly raises with larynx height regardless of the neutral F1 value. This runs entirely contrary to SN76 where close vowels, particularly the front ones were claimed not to be sensitive to larynx height. The larynx lowering condition is less impactful on F1, with a tendency towards lower frequency, except for [u] where F1 actually rises for participant B despite larynx lowering.

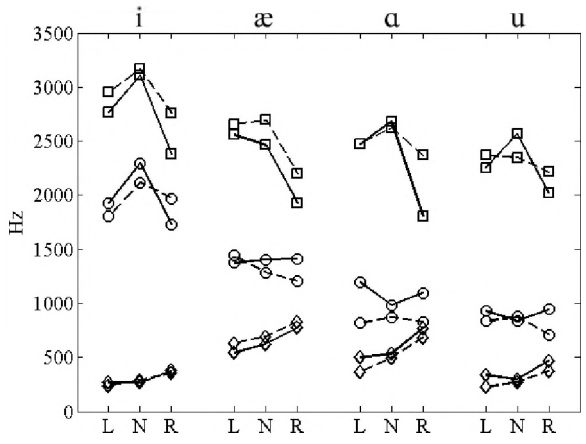


**Figure 1. Formant change by larynx height (Participant A = dashed line; Participant B = solid line).**

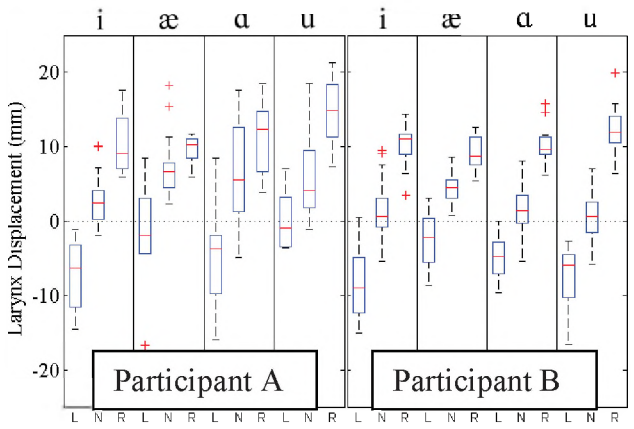


**Figure 2. Average larynx height change by vowel, larynx height condition, and participant.**

**Table 1. Relative formant change averages (%).**

| | | i | æ | *a* | u |
|---|---|---|---|---|---|
| F1 | R | +36 | +22 | +43 | +53 |
| | L | −4 | −12 | −13 | +5 |
| F2 | R | −20 | −2 | +8 | +3 |
| | L | −15 | +2 | +12 | +6 |
| F3 | R | −20 | −20 | −25 | −16 |
| | L | −10 | +1 | −7 | −8 |

F2 diverges from the expected pattern in a few cases: larynx lowering actually yields raised frequency for [æ *a* u], although [i] shows the anticipated lowering. Larynx raising also presents unexpected results; this time for [i æ] there is a drop in frequency. Finally, F3 is exhibits the familiar frequency drop for all vowels examined with respect to larynx lowering, but larynx raising once again surprises with an average F3 drop of −20.25% of frequency across the board. The production of neutral larynx height was judged auditorily in several cases to be closer to raised-constricted than to the lowered posture.

## 4. DISCUSSION AND CONCLUSIONS

Our data represent an altogether different picture from what was reported on by SN76. It is quantifiably clear from the laryngeal ultrasound that in terms of performance the target conditions for larynx height were achieved by both participants. While we cannot rule out the possibility that our results partially reflect simultaneous change in lingual configuration, we believe that any lingual co-adjustment reflects what is entailed articulatorily in raising the larynx, i.e. *pharyngealization*. The occurrence of pharyngealization may be a consequence of our strict control of F0: the pitch raising mechanism (CT muscles) counteracts constriction. Since we prevented pitch change from occurring, larynx raising associated with airway closure (as in swallowing) was induced. In phonetic terms, larynx raising entails epilaryngeal stricture. The uniform tube model does not account for the role of larynx height in epilaryngeal constriction (Esling 2005). Part of the mechanism involves retraction of the tongue in conjunction with larynx raising, and this might account for the more elevated than normal laryngeal height and undershoot of larynx raising during open vowels (evident in "Figure 2", particularly for Participant B). Pharyngealization in Tsez (Maddieson et al. 1997) shows parallels with our raised larynx data, with elevated F1 (for all vowels and particularly [i]) and lowered F3. For Tsez, F2 rises for back vowels, indicating fronting; this only occurred mildly for Participant B, but its absence is taken to reflect that tongue positions were as consistent as possible. Ladefoged and Maddieson (1996: 312-313) state that F2 and F3 show a tendency for convergence in the strident vowels in !Xóõ, which also feature strong epilaryngeal stricture. We leave the question of how this acoustic effect should be modeled for future research.

## REFERENCES


Esling, J.H. (**2005**). There are no back vowels: the laryngeal articulator model. *Can. J. Ling.* **50**. 13-44.

Horn, B.K.P. and Schunck, B.G. (**1981**). Determining optical flow. *Artificial Intelligence* **17**. 185-203.

Ladefoged, P. and Maddieson, I. (**1996**). The Sounds of the World's Languages. Cambridge, MA: Blackwell.

Moisik, S.R., Esling, J.H., Bird, S., and Lin, H. (**2011**). Evaluating laryngeal ultrasound to study larynx state & height. In *Proc. 17th ICPhS*. Hong Kong, China.

Maddieson, I., Rajabov, R. and Sonnenschein, A. (**1996**). The main features of Tsez phonetics. *UCLA Working Papers in Phonetics* **93**. 94-110.

Stevens, K.N. (**1998**). Acoustic Phonetics. Cambridge, MA: The MIT Press.

Sundberg, J. and Nordström, P.E. (**1976**). Raised and lowered larynx–the effect on vowel formant frequencies. *QPSR* **2-3**. 35-39. Speech Transmission Laboratory, KTH, Stockholm.


## ACKNOWLEDGEMENTS


This research was funded by the Social Sciences and Humanities Research Council of Canada, research grant #410-2007-2375.

# RECOGNITION OF EMOTIONAL SPEECH FOR YOUNGER AND OLDER TALKERS: BEHAVIOURAL FINDINGS FROM THE TORONTO EMOTIONAL SPEECH SET

**Kate Dupuis[1] and M. Kathleen Pichora-Fuller[1, 2]**
[1]Dept. of Psychology, University of Toronto, 3359 Mississauga Rd North, Mississauga, Ontario, Canada
[2]Toronto Rehabilitation Institute, 550 University Ave, Ontario, Canada

## 1. INTRODUCTION

Spoken communication involves integrating what is said (lexical information) and how it is said (prosodic information). Emotion can be conveyed through both lexical and prosodic cues, and the ability to understand emotion in speech is important for effective communication. Researchers have examined how both healthy and clinical populations understand affective prosody using speech stimuli ranging from monosyllables to full sentences. Unlike in the visual domain, where a select number of well-validated sets of stimuli (e.g., Ekman faces [1], IAPS photos [2]) are used across many studies, in the auditory domain researchers have typically created their own sets of stimuli. As a result, numerous inconsistencies that are likely related to the semantic and lexical properties of the stimuli exist across experiments. One goal of the current programme of research was to create a set of stimuli with well-controlled lexical and semantic properties based on an existing test of speech intelligibility, the Northwestern University Auditory Test- Number 6 (NU-6 [3]), so that the lists of stimuli in the set are balanced for properties such as word frequency as well as word and syllable length.

Experiment 1 provides a description of the actors, recording process, and stimulus selection process used for the creation of the novel set of stimuli, the Toronto Emotional Speech Set (TESS). In Experiment 2 recognition rates for the emotions portrayed in these stimuli were determined for a group of healthy younger listeners.

## 2. EXPERIMENTS

### 2.1 Experiment 1

Recording methodology

Two female actors, one younger and one older, were recruited from the community. Respectively, they were 26 and 64 years of age. The actors consented to create voice recordings which would be used as stimuli for research purposes, in educational presentations at scientific or professional conferences or in public education or community presentations. Both actors spoke English as a first language and had clinically normal hearing thresholds in the speech range (see Table 1 for demographic characteristics of the actors). The recording stimuli were the 200 items from the NU-6 test. Each item begins with the same carrier phrase and terminates in a monosyllabic noun (e.g., "Say the word *bean*"). The actors recorded each item to portray seven different emotions (anger, disgust, fear, happiness, pleasant surprise, sadness, and neutral). These seven emotions were chosen because they were recently used by two groups of researchers to create sets of German and Portuguese sentences [4, 5]. In this way we could extend work on affective prosody understanding for these seven emotions to the English language.

Each actor recorded the stimuli individually in a sound-attenuating booth for approximately 20 hours. During the recording sessions, which typically lasted three to four hours, the majority of the time was spent creating the voice recordings, while approximately 10% of the time was devoted to practicing and fine-tuning each actor's portrayal of each of the emotions. Emotion was blocked such that the actor would finish recording all stimuli in one emotion before moving on to the next. At each session the actor recorded at least one emotion. For each emotion, the experimenter (KD) would request repetitions of specific items until that emotion was judged by the experimenter to have been appropriately conveyed. In total, 2607 stimuli were recorded by the younger actor while 3004 stimuli were recorded by the older actor. Three female undergraduate students (all aged 18 years) with normal hearing listened to the stimuli and identified, for each actor, which token of each NU-6 item they considered to be the most representative for each of the seven emotions. The experimenter used the same procedure to listen to each of the sound files. The sets of ratings were then compared. Rater agreement between the experimenter and at least one of the students as to which token was the best was 80% and 92% for sentences spoken by the younger and the older actor, respectively. In this way, a final set of 2800 TESS stimuli (200 NU-6 items x 7 emotions x 2 actors) was created. In order to facilitate the use of these stimuli in future experiments, they were made available online through the University of Toronto library [6].

**Table 1. Demographic information for the two actors in Experiment 1**

| | Younger actor | Older actor |
|---|---|---|
| Age | 26 years | 64 years |
| Education (years) | 19 | 18 |
| Vocabulary (out of 20) | 12 | 15 |
| Health (1-4) | 4 | 2 |
| Right ear (PTA dB) | 0 | 6.7 |
| Left ear (PTA dB) | 3.3 | 6.7 |

### 2.2 Experiment 2

Methods

Fifty-six undergraduate students at the University of Toronto were tested in this experiment. All participants spoke English as a first language and had clinically normal hearing thresholds from 250 to 8000 Hz (see Table 2 for participant characteristics). Participants listened to stimuli spoken either by the younger or by the older talker. Each participant listened to an equal number of stimuli spoken in each of the seven emotions. The stimuli were presented through a loudspeaker in a sound-attenuating booth at an average presentation level of 70 dBA. In response to each stimulus they used a touch computer screen to indicate which emotion the talker was portraying.

| | **Younger adults (N=56)** |
|---|---|
| Age (years) | 19.7 (.38) |
| Education (years) | 13.5 (.28) |
| Vocabulary (out of 20) | 12.4 (.36) |
| Health (1-4) | 3.5 (.08) |
| Right ear (PTA dB) | -.3 (.46) |
| Left ear (PTA dB) | 1.0 (.45) |

**Table 2. Demographic information (Means and SEs) for the participants in Experiment 2**

Results

The primary measure of interest was the percentage of correctly recognized emotions. The overall accuracy was 82% (*SD* = 11.08). Stimuli spoken to portray anger and sadness had the highest accuracy while stimuli spoken to portray disgust and pleasant surprise had the lowest accuracy. Results from an ANOVA indicated a significant main effect of emotion, $F(6, 360) = 13.22$, $p < .01$, but no significant main effect of talker, $F(1, 30) = 2.33$, $p = .14$, and no significant emotion by talker interaction, $F(6, 360) = 2.07$, $p = .08$. These null results suggest that both talkers portrayed the different emotions in a similarly effective manner, as can be seen in Figure 1.

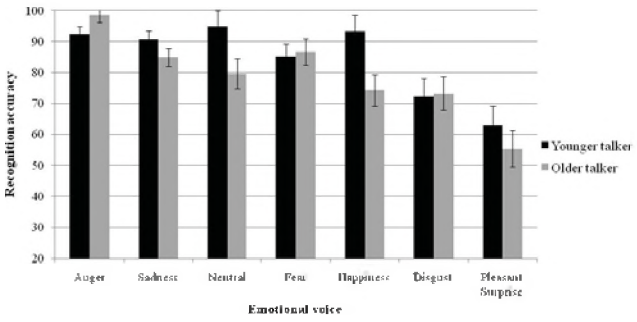


**Figure 1. Mean recognition accuracy for participants in Experiment 2 plotted by talker and by the emotion portrayed**

Discussion

The results from this experiment indicate that participants were able to recognize the emotions portrayed in the TESS stimuli with very good accuracy. The accuracy rate of 82% was almost six times greater than chance and higher than the 55-65% level described in recent reviews of studies in this field that used sentences with similar emotions [7, 8]. Furthermore, the lack of a main effect of talker indicates that the two actors created highly recognizable portrayals of the seven different emotions.

Although overall recognition of the emotions was high, there were significant differences in the accuracy with which some emotions were recognized. Consistent with previous findings [9, 10], angry and sad emotions had the highest recognition rates overall.

This is the first experiment to examine how well listeners can recognize the emotions portrayed in the Toronto Emotional Speech Set. Future studies should attempt to replicate these findings by using the TESS with healthy good-hearing younger listeners and extend this work to include older adults, participants with poor hearing, and those who suffer from cognitive difficulties.

## REFERENCES


[1] Ekman, P., & Friesen, W. V. (1976). *Pictures of Facial Affect.* Palo Alto, CA: Consulting Psychologists Press.

[2] Lang, P. J., Bradley, M. M., & Cuthbert, B. N. (1999). *International affective picture system (IAPS): Instruction manual and affective ratings.* Technical Report A-4, The Centre for Research in Physiology. Gainesville, FL: University of Florida.

[3] Tillman, T. W., & Carhart, R. (1966). An expanded test for speech discrimination utilizing CNC monosyllabic words: Northwestern University Auditory Test No. 6. Technical report no. SAM-TR-66-135. San Antonio, TX: USAF School of Aerospace Medicine, Brooks Air Force Base.

[4] Paulmann, S., Pell, M. D., & Kotz, S. A. (2008). How aging affects the recognition of emotional speech. *Brain and Language, 104,* 262-269.

[5] Castro, S. L., & Lima, C. F. (2010). Recognizing emotions in spoken language: A validated set of Portuguese sentences and pseudosentences for research on emotional prosody. *Behavior Research Methods, 42,* 74-81.

[6] Dupuis, K., & Pichora-Fuller, M. K. (2010). Toronto Emotional Speech Set (TESS). Available from https://tspace.library.utoronto.ca/handle/1807/24487

[7] Scherer, K. R. (2003). Vocal communication of emotion: A review of research paradigms. *Speech Communication, 40,* 227-256

[8] Scherer, K. R., Johnstone, T., & Klasmeyer, G. (2003). Vocal expression of emotion. In R. J. Davidson, K. R., Scherer, & H. H. Goldsmith (Eds.), *Handbook of affective sciences* (pp. 433-456). Oxford: Oxford University Press.

[9] Pell, M. D., Monetta, L., Paulmann, S., & Kotz, S. A. (2009). Recognizing emotions in a foreign language. *Journal of Nonverbal Behavior, 33,* 107-120.

[10] Scherer, K. R., Banse, R., Wallbott, H. G., & Goldbeck, T. (1991). Vocal cues in emotion encoding and decoding. *Motivation and Emotion, 15,* 123-148.

# THE EFFECT OF AN EMOTIONAL CARRIER PHRASE ON WORD RECOGNITION

**Dario Coletta[1], Kate Dupuis[1], and M. Kathleen Pichora-Fuller[1, 2]**
[1]Dept. of Psychology, University of Toronto, 3359 Mississauga Rd North, Mississauga, Ontario, Canada
[2]Toronto Rehabilitation Institute, 550 University Ave, Ontario, Canada

## 1. INTRODUCTION

The ability to understand emotion in speech is crucial for successful communication. Emotional information can be transmitted both through the words a talker uses and through affective prosody (i.e., the acoustic cues in speech used to express a talker's emotional state). Although numerous studies have examined how well listeners can recognize affective prosody, and have identified the acoustical parameters which are modified when different emotions are expressed, little is known about how emotion affects a listener's ability to understand speech in noise.

### 1.1 Intelligibility of emotional speech

Traditional speech intelligibility tasks have used stimuli which were recorded in neutral voices; however, these are not representative of real-world communication. This may explain, at least in part, the poor correspondence between performance on speech tests and listeners' subjective reports of their everyday communication difficulties [1]. Emotion has yet to be examined in the context of speech intelligibility. Emotion could potentially exert an influence on intelligibility through a form of cognitive processing, such as an attentional mechanism and/or by modifying acoustical cues produced when a target word is spoken.

### 1.2 Current experiments

These experiments were designed to test the cognitive hypothesis by examining if emotion could influence word recognition when the acoustical properties of the target word were unaltered. In order to determine whether emotion could potentially improve word recognition in noise, the presence of emotional prosody was manipulated such that it was only present in the carrier phrase, with a neutral target word either following (Experiment 1) or preceding (Experiment 2) the carrier. A final set of analyses compared results from these two experiments.

## 2. EXPERIMENTS

### 2.1 Experiment 1

Method

Twenty-eight participants were tested in each of the two experiments. All participants were University of Toronto undergraduates in good health who had clinically normal hearing thresholds in the speech range (see Table 1 for participant characteristics). The stimuli used were taken from the Toronto Emotional Speech Set (TESS, [2]). In this set, 200 items from the NU-6 test [3] were recorded by two female actors, one 26 years old and the other 64 years old, to portray seven different emotions (anger, disgust, fear, happiness, pleasant surprise, sadness, and neutral), for a total of 2800 stimuli. Each NU-6 item consists of the carrier phrase "Say the word" followed by a target word, which is a unique monosyllabic noun (e.g., "Say the word *dog*"). In the current experiments, the stimuli spoken by the younger actor were modified such that the carrier phrase spoken by her with emotion preceded each neutral target word which was spoken by a male in a commercially available recording of the NU-6 test (Auditec, St. Louis). The stimuli were equated for RMS and presented in the multi-talker babble background from the Speech Perception in Noise Test [4]. In order to determine the presentation level, a pilot study was conducted using only stimuli spoken in a neutral voice (similar to the neutral stimuli used in typical intelligibility tasks). A 75% identification rate was achieved with an SNR of -5 dB. It is common for the NU-6 test items to be divided into 4 half-lists of 25 items. Seven half-lists were used in this experiment while the eighth was used for practice. Participants were instructed to repeat the target word.

**Table 1. Demographic information (Means and SDs) for participants in each of the two experiments.**

| | Exp 1 (N=28) | Exp 2 (N=28) |
|---|---|---|
| Age (years) | 18.50 (1.17) | 20.80 (2.14) |
| Education (years) | 13.18 (1.59) | 15.00 (1.74) |
| Vocabulary (out of 20) | 12.39 (2.93) | 12.30 (2.53) |
| Health (1-4) | 3.32 (0.55) | 3.30 (.60) |

Results

The measure of interest for all the analyses reported in this paper was the number of target words correctly repeated by each participant. Results from an ANOVA indicated that emotion had a significant influence on performance, $F(6,126) = 2.55$, $p = .02$. Specifically, sad (67%) and pleasant surprise (66%) were the emotions that yielded the best intelligibility while fear (61%) was the emotion that yielded the worst intelligibility.

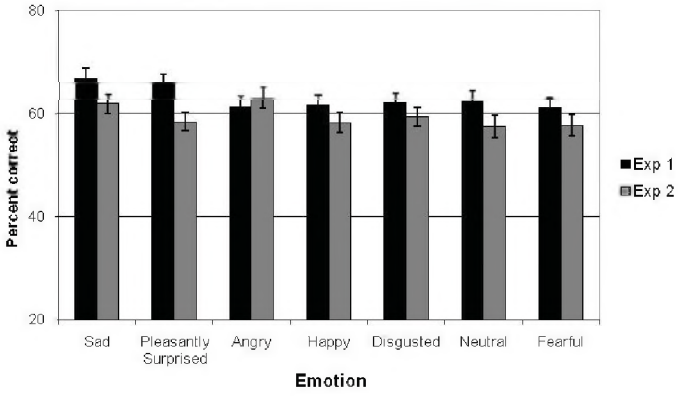


**Figure 1. Mean percent accuracy for word recognition with each of the seven emotions in each of the two experiments.**

Discussion

Results indicate that emotion did have a significant influence on how well listeners were able to understand the target word in a sentence. However, it is not known whether simply having part of the sentence portrayed in an emotional voice would improve performance, or whether the emotion must precede the neutral target. This question was examined in the following experiment.

### 2.2 Experiment 2

Methods

The stimuli used were identical to those used in the previous experiment; however, Praat software [5] was used to move the neutral target word from the end of the sentence (e.g., "Say the word dog") to the beginning of the sentence (e.g., "Dog, say the word"). Testing procedures were identical to those used in the preceding experiment.

Results

Results from an ANOVA indicated that emotion did not have an effect on participants' ability to correctly identify the target word, $F(6, 126) = 1.58$, $p = .16$.

Discussion

In this experiment, having the emotional carrier phrase follow the neutral target word eliminated the effect of emotion. This suggests that the presence of emotion at any point in the sentence is not sufficient to improve intelligibility; the emotion must precede the target word.

### 2.3 Comparison between Experiments 1 and 2

Methods

In order to compare results from the two experiments, an ANOVA was run with emotion as the within-subjects factor and experiment as the between-subjects factor.

Results

Overall, the emotional carrier phrase presented prior to the neutral target word (Experiment 1) resulted in more accurate recognition of the target word. This description was confirmed by the ANOVA which revealed that the mean accuracy rates for participants in Experiment 1 were significantly higher ($M = 63.02\%$, $SD = 1.26$) than for participants in Experiment 2 ($M = 59.37\%$, $SD = 1.26$), $F(1,42) = 4.20$, $p = .047$. Although there was a main effect of emotion, $F(6, 252) = 2.44$, $p < .01$, the analysis failed to reveal an emotion by experiment interaction, $F(6, 252) = 1.54$, $p < .01$. This suggests that participants responded to emotions in the two experiments in a similar manner.

Discussion

The comparison of results from the two experiments indicates that, overall, participants identified a larger number of target words when the emotion preceded the target word. The influence of emotion on performance was similar across experiments.

## 3. GENERAL DISCUSSION

In these experiments, the effect of emotion on performance was only present when the participants heard the carrier phrase spoken with emotion before hearing the target word. Thus, the emotion in the carrier phrase had a prospective effect on subsequent word recognition. In contrast, when participants were presented with the neutral target word initially, the subsequent emotion depicted in the carrier phrase had no retrospective effect on performance. Participants may have simply focused on remembering the target word throughout the presentation of the emotional carrier phrase, rendering the emotion moot. Accuracy was highest to the portrayals of sadness, which may be the most acoustically similar to neutral, causing the sad carrier to serve as a prime for the neutral target word. The high accuracy for portrayals of pleasant surprise may be due to the positive and rewarding nature of this emotion, which may have caused listeners to orient to this emotion. In contrast, the low accuracy for portrayals of fear may reflect the fact that participants chose to orient away from this negative emotion

It is important to note that there was a discontinuity between the male-spoken neutral word and the female-spoken carrier phrase which may have influenced the participant's ability to correctly identify the target word. Future studies should use target words spoken in a neutral voice by the TESS talkers to control for this discontinuity.

The results from these experiments relate to the ways in which individuals communicate in the real world; it is very rare to hear speech devoid of some sort of affective prosody. It may be that individuals are much more responsive to the identity of a target utterance based on the emotion that was present prior to and/or during pronunciation.

## REFERENCES


[1] Taylor, B. (2007). Predicting real world hearing aid benefit with speech audiometry: An evidence-based review. *Audiology Online, 1802.* Retrieved from http://www.audiologyonline.com/articles/article_detail.asp?article_id=1802

[2] Dupuis, K., & Pichora-Fuller, M. K. (2010). Toronto Emotional Speech Set (TESS). Available from https://tspace.library.utoronto.ca/handle/1807/24487

[3] Tillman, T. W., & Carhart, R. (1966). An expanded test for speech discrimination utilizing CNC monosyllabic words: Northwestern University Auditory Test No. 6. Technical report no. SAM-TR-66-135. San Antonio, TX: USAF School of Aerospace Medicine, Brooks Air Force Base.

[4] Bilger, R. C., Nuetzel, M. J., Rabinowitz, W. M., & Rzeczkowski, C. (1984). Standardization of a test of speech perception in noise. *Journal of Speech and Hearing Research,* 27, 32-48.

[5] Boersma, P., & Weenink, D. (2005). Praat: Doing phonetics by computer (Version 4.5.08) [Computer program]. Retrieved from http://www.praat.org/

# CAN I [F$^{W}$]*EED* YOU SOME [F$^{J}$]*OOD*?
## THE ROLE OF SUBPHONEMIC CUES IN WORD RECOGNITION

**Tae-Jin Yoon[1], Anna Moro[1], John Connolly[1], Jessica Arbour[1], and Janice Lam[2]**
[1]Dept. of Linguistics and Languages, McMaster University, 1280 Main Street W., Hamilton, Canada, L8S4M2
[2]Dept. of Psychology, Neuroscience, and Behaviour, McMaster University, 1280 Main St. W. Hamilton, Canada, L8S4M2

## 1. INTRODUCTION

It is well known that a phonological segment often varies to "become more like an adjacent or nearby segment" (Hardcastle & Hewlett 2000) due to overlapping articulatory gestures Coarticulation accounts for the realization of the same phonological segment – for example, the initial /k/ of *key* and *car* – in different areas of the vocal tract. Reserachers agree that coarticulation is the result of the vocal tract producing gestures in 'real time' by transitioning instantaneously from one target configuration to the next. When it comes to the degree, role and function of coarticulation, however, conflicting theories and findings abound. The goal of this study is to find out if and to what extent coarticulatory properties have an impact on spoken word recognition. We designed two experiments: a speech perception experiment, and an ERP (Event Related Potentials) experiment. Both experiments used the same auditory stimuli made with a splicing technique. For example, the initial consonant of *feed* was replaced with the initial consonant of *food*. The spliced stimuli, which contain incorrect sub-phonemic (coarticulatory) properties, were used to investigate the processing of coarticulatory information in word recognition (see Archibald and Joanisse 2011). Thirty-six monolingual English-speaking adults participated in the experiments. We report here preliminary results from both experiments. Results obtained thus far indicate that sub-phonemic cues are indeed utilized by many speakers in spoken word recognition, but the extent to which coarticulatory cues are used depends both on the nature of the initial consonant and on the type of vowel.

## 2. METHOD

### 2.1 Stimuli

We used 30 real words of a CVC shape to examine the processing of anticipatory coarticulatory effects on different types of initial consonants. The stimuli contained either an initial stop /p, t, k/ or a fricative /f, s, ʃ, h/. Each monosyllable contained one of the four corner vowels /i, u, æ, ɑ/ for maximal contrast. One of the following consonants filled the coda position: /p, t, d, k, l/. To reduce any possible effects of regressive coarticulation stemming from the final consonant, only minimal sets were used: stimuli sharing an initial consonant also had to contain the same final consonant. Table 1 shows two sets of stimuli used in the experiments, one set displaying an initial stop, and the other an initial fricative. In each set the onset consonant is followed by one of the four contrasting vowels, and the same coda consonant.

**Table 1. Examples of stimuli used for splicing**

| | Stops | | Fricatives | |
|---|---|---|---|---|
| | **Front** | **Back** | **Front** | **Back** |
| **High** | peal | pool | Heat | hoot |
| **Low** | pal | Paul | Hat | hot |

A female adult speaker of Canadian English produced each word three times. One of the tokens was chosen to prepare the spliced stimulus items. The complete set of stimulus items contained both onsets with congruent coarticulatory acoustic cues (e.g., [f$^{j}$] as the onset of *feed*) and onsets with incongruent coarticulatory information (e.g., [f$^{w}$] as the onset of *feed*).

### 2.2 Behavioural Speech Discrimination Task

For the behavioural tasks, 20 native speakers of Canadian English were recruited through poster advertisements. Participants were asked to match an auditory stimulus to a pair of stimuli (ABX paradigm).

### 2.3 ERP Task

For the ERP task, 12 native speakers of Canadian English were recruited through poster advertisements. Electrical activity from the scalp was recorded while the participant listened to auditory stimuli. The written form of the word appeared on a computer monitor as a visual stimulus. Participants were asked to indicate whether the written word and the auditory stimulus matched or not by pressing one of two keys on a handheld keypad.

## 3. RESULTS

### 3.1 Behavioural Speech Discrimination Task

Measures of $d'$, $\beta$, $A'$, and $B''_d$ were made to analyze the discriminability and bias of the experiment. In this paper, we present the values obtained from $A'$ and $B''_d$, as in Figure 1. The same interpretation can be made in terms of $d'$ and $\beta$, which have correlation values of 0.96 and 0.91, respectively with $A'$, and $B''_d$. In Figure 1, the mean value of $A'$ is 0.92 and the standard deviation is 0.02. An $A'$ value near 1.0 indicates good discriminability, while a value near 0.5 means chance performance. Participants were able to detect subtle coarticulatory cues. $B''_d$ is a measure of bias, and ranges from -1 to 1 in value. A $B''_d$ value of 0.0 indicates no bias; a number close either to -1 or 1 reflects the degree of bias of a participant (the value calculates how many times

the participant clicks either 'yes' alone or 'no' alone without discriminating the correct stimulus). In Figure 1, the mean of $B''_d$ is 0.006, and the standard deviation is 0.372. In general, it appears that most participants can detect coarticulatory cues.

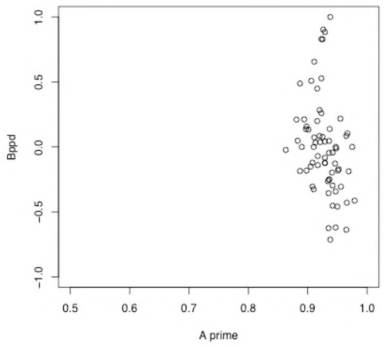


**Figure. 1. Scatterplot between the values of $A'$ and the values of $B''_d$.**

The behavioural experiment alone cannot tell us is if participants are merely responding to the presence of deviant acoustic properties or if their behaviour is related to phonological processing.

### 3.2 ERP studies: the PMN

The most important finding for our purposes is that of the phonological mapping negativity, or PMN (Steinhauer & Connolly 2008). The PMN, a negative-going component (N280) that peaks around the 200-300 ms range, is elicited by a phonological mismatch between the expected and heard onset of a target. The PMN has been understood to be sensitive to phonological processing. More recently, Archibald and Joanisse (2011) investigated whether the N280 is sensitive to a mismatch "between expected [and] perceived phonetic information." Their study provides strong evidence that the PMN is as sensitive to subphonemic information as it is to phonemic information, a finding that argues in favour of the view that subphonemic information is integrated in real time as it unfolds, and aids in word recognition (Gow and McMurray 2007). We designed our stimuli in minimal sets to reduce the effects of coda consonants on the rime, and with a view to controlling for sensitivity to coarticulatory effects based on the onset consonant and the height or backness of the vowel.

As can be seen in Figure 2, which is taken from the central front site in the scalp for the condition of stop consonants, the difference between forms of congruent coarticulatory cues and those of incongruent cues is at its maximum near 300 ms. This confirms that the coarticulatory information is related to phonological expectancy. A further analysis of other conditions indicates that the detection of coarticulatory cues is largely dependent both on the nature of the onset consonant (stop vs. fricative), and on the type of vowel that follows the initial consonant.


**Figure. 2. Average waveform comparing the coarticulatory match and coarticualtory mismatch conditions at the site Fz under the condition of stop consonants**

## 4. DISCUSSION

We have presented two experiments that investigate the processing of coarticulatory information. The speech discrimination experiment showed that speakers are sensitive to coarticulatory cues: many participants detected the coarticulatory mismatch between onset and rime. The neurophysiological study indicates that the detection is not due to pure acoustic deviants, but is done due to its phonological effects. By correlating the behavioral findings with findings from the ERP study, we are aiming to better understand the cognitive and neural processes associated with coarticulatory properties, and the role they play in spoken word recognition.

## REFERENCES

Archibald, L. & M. Joanisse. (2011). Electrophysiological Responses to Coarticulatory and Word Level Miscues. *Journal of Experimental Psychology: Human Perception and Performance*, Advance online publication. doi: 10.1037/a0023506.

Steinhauer, K. & J. Connolly (2008) Event-Related Potentials in the study of language. In Stemmer, B. and H. A. Whitaker (eds.) *Handbook of the neuroscience of language*, Academic Press.

Connolly, J. & N. Phillips. (1994). Event-related potential components reflect phonological and semantic processing of the terminal word of spoken sentences. *Journal of Cognitive Neuroscience*, 6: 256-266.

Hardcastle, W. & N. Hewlett (eds.) (1999) *Coarticulation: theory, data, and techniques*. Cambridge: Cambrige University Press.

Gow, J. and B. McMurray (2007). Word recognition and phonology: The case of English coronal place assimilation. In (eds.) J. Cole and J. Hualde, *Papers in Laboratory Phonology 9*. Berlin: Walter De Gruyter: 173-200.

## ACKNOWLEDGEMENTS

This work is supported by Arts Research Board (ARB) at McMaster University and NSERC. Statements in this paper reflect the opinions and conclusions of the authors, and are not endorsed by the granting agencies.

# AN AUDIO-VISUAL PERCEPTION STUDY OF BULGARIAN AND RUSSIAN PALATALIZED CONSONANTS

**Sonia Pritchard**
Dept. of Linguistics, University of Ottawa, 70 Laurier Ave. East, Ontario, Canada, sprit001@uottawa.ca

## 1. INTRODUCTION

The existence of palatalized consonants in Standard Bulgarian has been a source of debate in Bulgarian linguistics. Horàlek (1950) hypothesized that the secondary palatal gesture /ʲ/ had decomposed into the palatal glide /j/. This argument has gained strength since Scatton (1984) and Maddieson & Ladefoged (1996) observed articulatory data from x-ray studies in Stojkov (1942, 1961) and noted that the height of the tongue body of the palatalized consonants /tʲ dʲ sʲ zʲ, lʲ rʲ nʲ/ was virtually indistinguishable from their plain counterparts. Furthermore, Tilkov (1983) conducted an experiment which tested the perception of Bulgarian palatalized and plain consonants. His results indicated that hard consonants could be identified from the duration and spectral shape of the burst alone. With the exception of the velars /kʲ gʲ xʲ/, the Bulgarian listeners needed the formant transitions to identify the remainder of the consonants as palatalized. The implication is that the secondary palatal gesture is not enough to cue the perception of these consonants.

Pritchard's (2009) recent acoustic study indicated that the acoustic attributes for Bulgarian and Russian palatalized consonants are very similar. This is important as the Russian subjects of Richey's (2000) experiment did not need the formant transitions to identify the secondary palatal gesture. The goal of the current study is to try to reconcile these potentially conflicting results. To this end, two variations of the gating task (Grosjean, 1980) were employed. In a gating task, a subject hears a stimulus over a number of gates, and at each gate an increased amount of information is available. Auditory-only and audio-visual gating tasks were performed in order to establish how much auditory and visual information a listener needs in order to identify a consonant as palatalized.

## 2. METHODS

The participants were 20 native Bulgarian and 22 native Russian speakers. They were all educated in their native countries and immigrated to Canada as adults.

The stimuli for both conditions (auditory and audio-visual), and for both languages, consisted of minimal or near-minimal pairs of the plain and palatalized consonants from Stojkov's (1942; 1961) x-ray studies (except for /v/) in which the tongue body gesture was identical for both types. The consonants occur word-initially in syllables with a primary stress. They precede the vowels /a/ and /u/ which, together with the vowel /ɔ/, are the only environments where palatalized consonants occur in Standard Bulgarian. The stimuli were produced by 2 male speakers of Russian and Bulgarian. They were recorded in a sound-proof booth. Noise was introduced to the sound file of the audio-visual condition to encourage the subjects to attend to the visual information. The stimuli for both conditions were gated at an interval of 30ms. They were presented randomly in a within-subject design, with a break between conditions.

The experimental procedure was as follows. A minimal pair appeared on a computer screen. Then, subjects heard a gated sound. Afterwards, in a forced-choice task, they selected one of the words which they associated with that sound. Next, they rated how confident they were in their choice, on a scale from 1 to 4 (1-very sure, 2-fairly sure, 3-fairly unsure, 4-very unsure). This cycle continued until they heard all gates of each stimulus.

## 3. RESULTS

At this stage of the project, only descriptive statistics have been performed. For each language, and for all stimuli, subjects' confidence ratings were graphed with boxplots. Figure 1, below, illustrates an increase of confidence ratings at the gate (5) where the secondary palatal gesture occurred, with a median of 1. As no information about the vowel is available, some subjects tend to be more conservative and select a rating of 2 (fairly sure). At gate 6, the confidence level increases to 1 (very sure) as a part of the vowel, including the transitions, is heard.

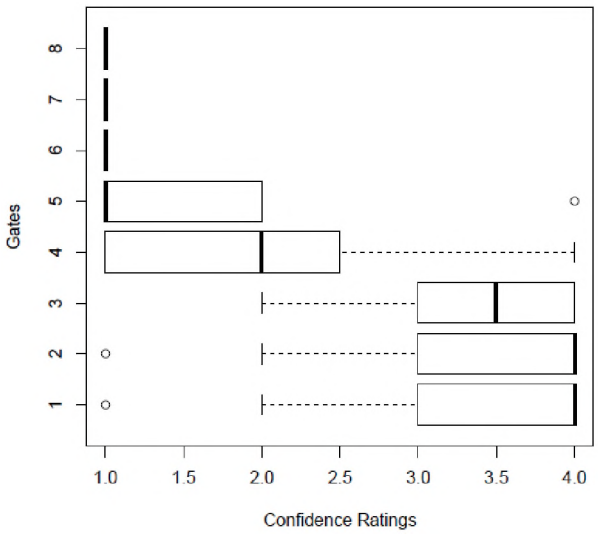


**Figure 1. Boxplots of all gates of Bulgarian /dʲuna/, audio condition.**

The frequency of confidence rankings of 1 and 2 is shown in

the histogram below, Figure 2. The 1 and 2 confidence rankings are associated with correct responses only. From a sample of 20 subjects, 65% selected a correct response, with a confidence of 1; 35% of them also selected the right answer with a confidence of 2.

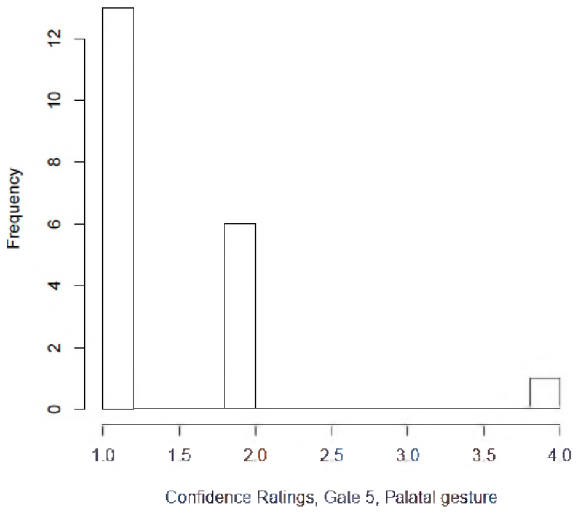


**Figure 2. Histogram of Bulgarian /dʲuna/.**

Tables 1 and 2, below, contain the combined percentage of the confidence rankings of 1 and 2 at the gate of the palatal gesture for each palatalized consonant in the environments of the vowels /a/ (Cʲa) and /u/ (Cʲu). Again, only the correct answers associated with those rankings were included. Overall, the palatal gesture is perceived better in the auditory condition (Aud) compared to the audio-visual condition (AV), for both languages and vowel environments. The palatal gesture of the sonorant consonants (rʲ lʲ nʲ) seems to be perceived better than that of the others in both conditions.

**Table 1. Confidence Ratings (%) – Cʲa .**

| Language and Condition | Palatalized Consonants | | | | | | | |
|---|---|---|---|---|---|---|---|---|
| | tʲ | dʲ | vʲ | sʲ | zʲ | rʲ | lʲ | nʲ |
| Bul – Aud | 75 | 75 | 90 | 85 | 95 | 85 | 95 | 100 |
| Bul – AV | 50 | 50 | 45 | 50 | 75 | 60 | 65 | 100 |
| Rus – Aud | 67 | 69 | 86 | 100 | 91 | 96 | 81 | 96 |
| Rus – AV | 32 | 77 | 0 | 47 | 0 | 91 | 56 | 35 |

In terms of the Bulgarian audio-visual data, the palatal gesture of the consonants /tʲ dʲ vʲ sʲ/ is perceived at chance, or worse. Only the gesture of /zʲ/ in the context of /a/ appears to be perceived better by the subjects. In some instances, the percentages for the Russian audio-visual data are higher than the Bulgarian ones(/dʲ/ next to /a/, / tʲ/ & /dʲ/ next to /u/), although half, or fewer, of the Russians chose the wrong answer in some instances (shown as 0 in Table 2).

**Table 2. Confidence Ratings (%) – Cʲu .**

| Language and Condition | Palatalized Consonants | | | | | | | |
|---|---|---|---|---|---|---|---|---|
| | tʲ | dʲ | vʲ | sʲ | zʲ | rʲ | lʲ | nʲ |
| Bul – Aud | 60 | 95 | NA | 80 | NA | 95 | 85 | 80 |
| Bul – AV | 35 | 60 | NA | 30 | NA | 72 | 60 | 80 |
| Rus – Aud | 91 | 91 | NA | 86 | NA | 67 | 87 | 86 |
| Rus – AV | 74 | 94 | NA | 0 | NA | 74 | 90 | 61 |

## 4. DISCUSSION AND CONCLUSIONS

This study aims to compare the perception of palatalized consonants in Standard Bulgarian and Standard Russian. According to the current results, in the auditory gating task subjects from both language samples are able to perceive a consonant as palatalized at the gate at which the palatal gesture becomes available. The transitions with the following vowel are not essential. These findings are not in line with those of the Tilkov's (1983) study of the perception of Bulgarian palatalized consonants. The results from the audio-visual task indicate that visual cues by themselves may not be sufficient for the identification of the secondary palatal gesture, particularly in noisy environments.

## REFERENCES


Grosjean, R. (1980). Spoken word recognition processes & the gating paradigm. *Perception & Psychophysics*, 38, 299-310.

Horàlek, K. (1950). K otàzce palatàlnich souhlàsek v Bulharštině. *Slavia, 20*, 57-60.

Ladefoged, P & Maddieson, I. (1996). *The Sounds of the World's Languages.* Blackwell Publishing: Massachusetts, US.

Pritchard, S. (2009*). Cross-language comparison of CV/CjV sequences.* Annual Conference of CLA, Carleton University.

Richey, C. (2000). Cues for place and palatalization in Russian stops. The Journal of the Acoustical Association of America, 108(5), 2507.

Scatton, E. (1984). A Reference Grammar of Modern Bulgarian. Slavica, Cambridge, MA.

Stojkov, S. (1942). Bulgarian literary pronunciation: preliminary investigations. *Sbornick na Bulgarskata Akademija na Naukite I Izkustvata, 37(3)*. Durzhavna Pechatnitsa, Sofia.

Stojkov, S. (1961). *Uvod v Bulgarskata Fonetika.* (2nd revised edition.) Nauka i Izkustvo, Sofia.

Tilkov, D. 1983. Akustichen systav i distribucija na palatalnite syglasni v knizhovnija bylgarski ezik. In Bojadzhiev, T. and M. Mladenov (eds.), *Izsledvanija vyrhu bylgarskija ezik,* pp. 79-139. Sofia: Nauka i izkustvo.


## ACKNOWLEDGEMENTS


I would like to thank Jeff Mielke for his assistance with this project. I also wish to thank all Bulgarian and Russian people who participated in this project.

# FINDING SCHWA: COMPARING THE RESULTS OF AN AUTOMATIC ALIGNER WITH HUMAN JUDGMENTS WHEN IDENTIFYING SCHWA IN A CORPUS OF SPOKEN FRENCH

**Peter M Milne**
Dept. of Linguistics, University of Ottawa, 70 Laurier Ave East., ON, Canada, K1N 6N5, pmiln099@uottawa.ca

## 1 INTRODUCTION

The value in working with natural language corpora is the ability to collect large volumes of emprical data with which to test research hypotheses. The challenge is to generate these data quickly and accurately. Accumulating the linguistic data required to test and evaluate hypotheses can be a time consuming and labour intensive job. The availability of an accurate automatic aligner, which can aid in the analysis of larger volumes of natural language data than is possible when working manually, would greatly assist in this task. This paper addresses the question of how the results of an automatic aligner compare with human judgments when identifying the presence or absence of schwa in a word-final, post-consonantal context.

All word-final, postconsonantal possible schwa insertion sites were identified in the standardized read text portion of investigations conducted in both Québec and France. All data was systematically coded for presence or absence of schwa by trained researchers. The data was also time aligned at both the word and phone level by a forced aligner. The results of the two methods of coding were statistically compared to determine their level of agreement. Results show a significant correlation between the two methods and a high likelihood of overall agreement. Possible effects of dialect or phonetic context were investigated using a two-way, between subjects analysis of variance. Initial results have found no significant effect of dialect or context. An examination of the confusion matrix indicated that the majority of errors were the result of the aligner finding schwa where none existed. This suggests that the results of automatic alignment are comparable with human judgments in both dialects of French, regardless of phonetic context, but that improvements to the acoustic model for French schwa are needed.

### 1.1 The forced aligner

The forced aligner used is the Penn Phonetics Lab Forced Aligner (Yuan and Liberman, 2008), modified for use with French (described in Milne, 2010). The Penn Phonetics Lab Forced Aligner is an automatic phonetic alignment toolkit based on HTK, the Hidden Markov Model toolkit maintained by the Cambridge University Engineering department. Both are distributed for use free of charge. It takes as input an audio .wav file along with a corresponding .txt orthographic text file and, using the HTK toolkit, produces a Praat TextGrid with interval boundaries for segments and words on two tiers. The pronunciation dictionary used in conjunction with the modified aligner is an expanded version of Lexique, version 3 (New et al., 2001, 2004). Lexique is a database that provides > 135,000 words of French including orthographic and phonemic representations, syllabification, parts of speech, gender and number, frequency, and associated lemmas, etc. This information is stored in tables that can be downloaded or searched online. Lexique is an open database to which everyone is encouraged to participate. Using a word list generated from the transcription files, the pronunciation dictionary was expanded to include alternate pronunciations for all words containing possible schwa insertion sites, as well as liason consonants and consonant cluster reduction possibilities. The current expanded dictionary used for this project contains entries for each word in the transcription containing a possible schwa insertion site having pronunciation candidates both with and without schwa.

In addition to expanding the pronunciation dictionary, the aligner was modified by mapping all French phones that do not occur in English onto the acoustic models that best matched their phonetic qualities. These mappings included the nasalized vowels [œ̃,ɛ̃,ɑ̃,ɔ̃ ], the rounded vowels [ø, œ, y], and the consonant [ɥ].

### 1.2 The corpus

The corpus used was obtained through the Projet Français Contemporain (Durand et al., 2002, 2005). This is an ongoing research project aimed at providing researchers interested in the French language with a database of oral data. One of the main goals is to gather data from as many varieties of French as possible, in all parts of the world, in order to investigate dialectal variation. It is the largest collection of spoken French, and one of the largest collections of spoken language data for any language.

The data obtained was from the standardized read text portion of 9 investigations conducted in both France and Québec. This data set is appropriate for several reasons. First, the text was systematically constructed to maximize both the frequency of possible schwa sites as well as the variety of contexts under which schwa patterns can be tested. Second, there exists a comparable volume of data for both dialects under consideration.

## 2 METHODS

The corpus contains data from 38 speakers (19 each from Québec and France) and includes 6458 possible schwa insertion sites. Each site was individually coded (manually by researchers trained in the PFC protocol and automatically via the forced aligner) for presence or absence of schwa, position in the word, and both left- and right-hand contexts.

From this, 3160 word-final, post-consonantal possible schwa insertion sites were extracted. The results of automatic alignment were compared with human judgment with respect to the presence or absence of schwa. An agreement value was calculated with values of 1, indicating agreement between the two methods of coding on the presence or absence of schwa, or 2, indicating disagreement.

876 sites were randomly sampled from the dataset. These were evenly balanced for Dialect (n=438) and RHContext ($n_{vowel}$=149, $n_{consonant}$=145, $n_{pause}$=144). An overall accuracy rate was calculated by dividing the number of items that agreed on the presence or absence of schwa by the total number of items. This accuracy rate was compared with both chance and a baseline scenario in which schwa was never inserted. In order to determine whether the values for agreement differed according to either dialect or right-hand context, this sample was subjected to a two-way, between subjects analysis of variance with the dependent variable as Agree, and two independent variables of Dialect (2 levels, "QF", "FR") and RHContext (3 levels, "V", "C", "pause"). Finally, the conditions under which the two methods of coding disagreed were examined.

## 3 RESULTS

In our sample, 651 of 876 items agreed between the two methods of coding for an overall accuracy rate of 74.3%. This is significantly better than chance ($\chi^2(1)=110$, $p<.05$), but not better than the baseline scenario in which no schwa was ever inserted. In fact, the results indicate that the baseline scenario would agree with the PFC coding significantly more often than the forced aligner ($\chi^2(1)=119$, $p<.05$).

The results of the ANOVA indicate no significant differences in agreement either between dialects ($F(1,872)=0.15$, $p=0.67$), or among contexts ($F(2,872)=0.41$, $p=0.66$). This suggests that the forced aligner produces judgments similar to the manual results of the PFC on the presence or absence of schwa in both dialects and in all three of the right-hand contexts.

In examining the conditions under which the two methods of coding disagree, there were 225 instances of disagreement between the two methods of coding. 218 of those instances, or 96.9%, were of the kind where the forced aligner judged a schwa segment to be present, while the human PFC coder perceived no schwa segment. This is shown below in Table 1. In Table 1, **FA** indicates the values obtained for items by the forced aligner and **PFC** indicates the values obtained for items by manual coding.

*Table 1: Confusion Matrix*

| | **PFC schwa** | **PFC no schwa** |
|---|---|---|
| **FA schwa** | 50 | 218 |
| **FA no schwa** | 7 | 601 |

## 4 DISCUSSION AND CONCLUSIONS

This study was conducted to determine whether the Penn Phonetics Lab Forced Aligner, modified for use with French, could aid in automating the task of determining the presence of absence of schwa in a large corpus of spoken French. The results suggest that the modified aligner works equally well in both dialects, and is unaffected by right-hand context. However, the disagreements between the two methods of coding indicate that the modified aligner frequently finds schwa where no schwa exists. It is suspected that this confusion may be due to the differences in acoustic cues between the French and English schwa. The Penn Phonetics Lab Forced Aligner is built on English monophone acoustic models and the French schwa is more front and rounded than the English schwa (closer to [ø] or [œ]). Perhaps in this context (word-final, post-consonantal), the aligner is interpreting some elements of consonantal release as an inserted schwa. A possible way to improve this aligner is to update the acoustic model of schwa to better approximate the different phonetic qualities of French schwa as compared with English schwa.

## REFERENCES


Durand, J., Laks, B., and Lyche, C. (**2002**). La phonologie du français contemporain: usages, variétés et structure. In Pusch, C. and Raible, W., editors, Romanistische Korpuslingquistik - Korpora und gesprochene Sprache/Romance Corpus Linguistics Corpora and Spoken Language, pages 93–106. Gunter Narr, Tubingen.

Durand, J., Laks, B., and Lyche, C. (**2005**). Un corpus numérisé pour la phonoloegie du français. In Williams, G., editor, La linguistique de corpus, pages 205–217. Presses Universitaires de Rennes, Rennes.

Milne, P. (**2010**). The effects of syllable position on allophonic variation in québec french /ʁ/: A corpus analysis using a modified version of the penn phonetics lab forced aligner. http://aix2.uottawa.ca/~pmiln099.

New, B., Pallier, C., Brysbaert, M., and Ferrand, L. (**2004**). Lexique 2 : A new french lexical database. Behavior Research Methods, Instruments, and Computers, **36(3)**:515–524.

New, B., Pallier, C., Ferrand, L., and Matos, R. (**2001**). Une base de données lexicales du français contemporain sur internet: Lexique. L'Année Psychologique, **101**:447–462. http://www.lexique.org.

Yuan, J. and Liberman, M. (**2008**). Speaker identification on the scotus corpus. In Proceedings of Acoustics '08.

# PROSODYLAB-ALIGNER: A TOOL FOR FORCED ALIGNMENT OF LABORATORY SPEECH

**Kyle Gorman,[1] Jonathan Howell,[2] and Michael Wagner[2]**

[1]Department of Linguistics and Institute for Research in Cognitive Science, University of Pennsylvania, 619 Williams Hall, 255 S. 36th St., Philadelphia, PA, U.S.A., 19104-6305

[2]Department of Linguistics, McGill University, 1085 Dr. Penfield, Montreal, QC, Canada, H3A 1A7

## 1. INTRODUCTION

Recordings of speech, whether spontaneously generated or elicited in the lab, are an important data source for linguists, but the time required to produce by hand the time indices necessary to perform acoustic feature extraction is often prohibitive. The Penn Forced Aligner (Yuan & Liberman 2008) automates the alignment process using the Hidden Markov Model Toolkit (HTK),[1] a speech recognition software package. However, it is limited to certain sample rates, and can only perform alignments according to an included North American English acoustic model; it does not support training of new acoustic models for different languages or domains.

## 2. A NEW TOOL

We have constructed a new software package, Prosodylab-Aligner, which, like the Penn Forced Aligner, uses HTK for forced alignment. However, it also permits the experimenter to use transcribed (but not necessarily aligned) audio to train new acoustic models. Prosodylab-Aligner is open-source and available for free online.[2]

The core of Prosodylab-Aligner is `align.py`, a script which performs acoustic model training and alignment. This script automates calls to HTK and SoX,[3] an open-source command-line tool which is capable of resampling audio. The included `README` file provides instructions for installing HTK and SoX on Linux and Mac OS X, and can also be run on Windows.

### 2.1 Preprocessing

The `align.py` script checks for missing data files, and terminates if an audio or transcript file (indicated by the extensions `.wav` and `.lab`, respectively) is lacking its companion label or audio file, after printing a list of "orphan" data files. It also checks for words in the transcripts which are not found in the pronunciation dictionary, if any out-of-dictionary words are found, terminates after printing this list. Both of these steps permit the experimenter to correct for missing data before proceeding with alignment or training.

### 2.2 Acoustic Model

The Prosodylab-Aligner acoustic models are monophone Gaussian mixtures consisting of 39 Mel frequency cepstral coefficients (Mermelstein 1976).

### 2.3 Training Routine

By default, the input data is aligned using a precomputed acoustic model trained from North American English laboratory speech (see Section 4), but with the `-t` flag, the experimenter can provide training data for estimating a new acoustic model. In many cases, it is desirable for the training set will be the same as the test set.

During training, the model is initialized with flat-start monophones, which are then submitted to a single round (by default, four iterations) of model estimation. Then, a tied-state "small pause" model is inserted and used in a second round of estimation. The data is then aligned once to choose the most likely pronunciation of all homonyms (i.e., dictionary entries with the same orthographic form), and a final round of estimation is performed. The optimal alignments are computed and the resulting word and phone alignments are written to Praat[4] TextGrid files.

A separate flag (`-T`) can be used to trigger a final round of speaker-dependent training and speaker-dependent alignment.

### 2.4 Helper Scripts

Several other scripts are included for related tasks: aligning a single audio/label pair (`align_ex.sh`), fixing errors in label files (`fix_lab.py`), or downloading the CMU English pronunciation dictionary (`get_dict.sh`).

## 3. EXPERIMENTAL PIPELINE

Prosodylab-Aligner plays an integral part in an experimental pipeline for speech data, both elicited in the laboratory with controlled experiments, and harvested from the web (Howell & Rooth 2009; Rooth et al. 2011).

### 3.1 Laboratory Data elicited

Laboratory data is using a suite of MATLAB scripts designed for production experiments. The experimenter enters the stimuli into a spreadsheet, indicating "words of interest" found in target stimuli, and organizes stimuli into items and conditions. These are them randomized and

1 http://htk.eng.cam.ac.uk/

2 http://prosodylab.org/tools/aligner/

3 http://sox.sourceforge.net/

4 http://www.fon.hum.uva.nl/praat/

presented as the elicitation "script" for the subject. The experimenter then verifies that the resulting utterance produced matches the text presented to the subject.

### 3.2 Web Data

Web audio (in MP3 format) is downloaded from Ramp,[5] a company which indexes radio and television programming, including NBC, PBS, Fox and CBS Radio, and processed using standard UNIX tools. The transcriptions produced by Ramp are sufficient for identifying a targeted linguistic construction (with approximately 50% accuracy), but the experimenter must still listen to the audio files to eliminate false positives.

### 3.3 Data Comparison

It is desirable to be able to compare lab and web data, and thus to use the acoustic model for alignment. While WAV files and a uniform sample rate is used in the laboratory, web audio recording quality is inconsistent (bit rate between 32-256 kbit/s and sample rate between 11025-44100Hz). For this reason, when training is performed by `align.py`, the experimenter may also specify sample rate (with the `-s` flag): any training or test audio data that does not conform to this sample rate is automatically resampled using SoX.

### 3.4 Post-alignment Processing

A script marks "words of interest" in the aligned TextGrids, and a Praat script extracts acoustic measurements from each word of interest for later statistical analysis.

## 4. EVALUATION

The North American English acoustic models provided with Prosodylab-Aligner produce alignments of impressionistically high quality. To quantify alignment quality, we use a single annotator's hand alignment from a prior study as a gold standard: Howell & Rooth (2009) and Howell (2011) gathered tokens of the phrase "than I did" embedded in longer utterances harvested from the web, and 127 tokens of this phrase hand-aligned at the phone level.

For each file and for each phone boundary in this phrase, we compute the magnitude of the distance from the gold standard for Prosodylab-Aligner, as well as for the Penn Forced Aligner. The results in Table 1 suggest that the two aligners produce alignments of comparable quality. Figure 1 shows that both aligners have comparable magnitude difference compared to the gold standard.

## 5. CONCLUSIONS

The Penn Forced Aligner is a useful tool for linguists interested in acoustic properties of speech. Prosodylab-Aligner further empowers the experimenter by automating the difficult task of constructing domain-appropriate acoustic models to use for forced alignment.

5 `http://www.ramp.com/`

**Table 1. Magnitude difference compared to hand-aligned gold standard**

| | Mean \|Δ\| (s) | Median \|Δ\| (s) |
|---|---|---|
| Prosodylab-Aligner | 0.3060 | 0.0119 |
| Penn Forced Aligner | 0.2061 | 0.0124 |

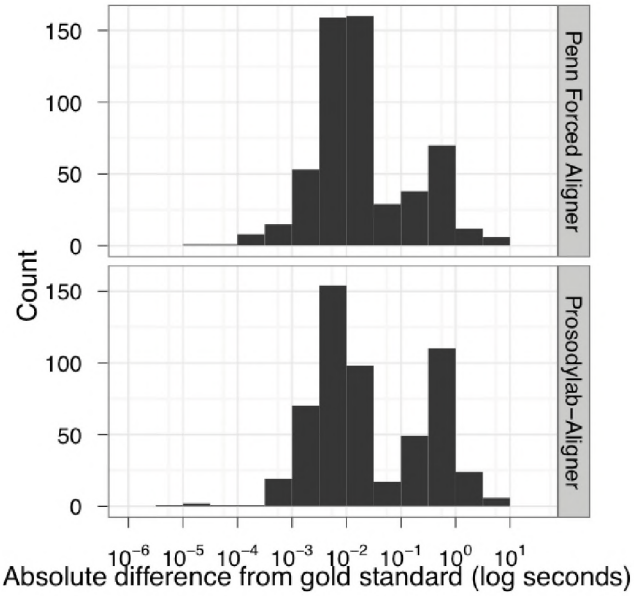


**Figure 1. Magnitude difference compared to hand-aligned gold standard**

## REFERENCES


Howell, J. And Rooth, M. (2009). Web harvest of minimal intonational pairs. In I. Alegria, I. Leturia, and S. Sharoff (ed.), *Proceedings of the 5th Web as Corpus Workshop,* 45-52. San Sebastian: Elhuyar Fundazioa.

Howell, Jonathan. (2011). Meaning and prosody: On the web, in the lab and from the theorist's armchair. Doctoral dissertation, Cornell University.

Mermelstein, P. (1976). Distance measures for speech recognition, psychological and instrumental. In C-H Chen (ed.), *Pattern recognition and artificial intelligence*, 374-388. New York: Academic Press.

Rooth, M., Howell, J., and Wagner, M. (2011). Harvesting speech datasets for linguistic research on the web. Paper presented at Digging into Data Challenge Conference.

Yuan, J. And Liberman, M. (2008). Speaker identification on the SCOTUS corpus. In *Proceedings of Acoustics 2008,* 5687-5690.


## ACKNOWLEDGEMENTS


This research was supported by grants to the third author from FQRSC (Nouvelle NP-132516) and SSHRC (Digging into Data Challenge Grant 869-2009-0004; Canada Research Chair 218503).

# AUTOMATIC ANALYSIS OF SIBILANT ASSIMILATION IN ENGLISH

**Clayards, Meghan[12], and Doty, Eric[2]**
[1]School of Communication Sciences and Disorder, McGill University, 1266 Pine Ave. West, Montreal, Quebec, Canada
[2]Dept. of Linguistics, McGill University, 1085 Ave Dr. Penfield. Montreal, Quebec, Canada

## 1. INTRODUCTION

Assimilation across word boundaries is a common phenomenon in language. For example, the English coronal sibilant /s/ is pronounced more like a post alveolar sibilant /ʃ/ when followed by the post-alveolar sibilant (e.g. “glass shoe” pronounced as “glash shoe”).

Of theoretical interest in the extent to which these assimilation processes are complete versus partial and the extent to which they are under the cognitive control of the speaker. Holst and Nolan (1995) investigated sibilant assimilation in British English speakers and found a range of assimilation strengths from partial to complete. Niebuhr et al (in press 2011) found mostly cases of complete assimilation. In both studies the assimilation was directionally asymmetric in that /s/ assimilated to /ʃ/ when the /ʃ/ followed (e.g. “glass shoe”) but not when it preceded (e.g. “fish soup”). In contrast Neibuhr et al (in press 2011) found less directional asymmetry and less complete assimilations in the productions of French speakers. The differences between the French and English speakers and the (nearly) complete nature of the assimilations suggest that these processes are language specific and under the control of the speaker. Others have argued that even co-articulation (which may be equivalent to partial assimilation) may be under the control of the speaker. Whalen (1990) asked talkers to begin speaking before they knew the full VCV sequence He found co-articulatory effects of the consonant or second vowel on the first vowel *only* when their identity was known before hand. The lack of these co-articulatory effects in the absence of pre-planning strongly suggest that they are the result of pre-planning.

The purpose of the current study was to 1) test new automated methods for doing phonetic analysis by replicating previous work, 2) to compare sequences of identical sibilants as well as single sibilants (which was not done in Niebuhr et al) and 3) to investigate issues of planning of assimilation across word boundaries.

## 2. METHODS

Nineteen North American English speakers were recorded reading a set of sentences from a computer screen in a casual speaking. Recordings were made into a headset microphone and recording and stimulus presentation were controlled by Matlab.

### 2.1. Stimuli

All sentences were of the form, "Say X Y please/now," where words of type X and Y were nonsense words. In type X words one of the test phonemes /s/ or /ʃ/, or the control /p/ was at the right edge of the word and in type Y words at the left edge, resulting in sibilant sequences at the word boundary (e.g. /ʃ/-/s/ sequence in "Say caveesh sival please"). Each of the 3 consonants was used in two different nonsense words (e.g. /ʃ/ in "tamash" and "caveesh") resulting in 6 words for each of type X and Y. All 12 Words are listed in Table 1. These words were stimuli in a related perception experiment (Clayards, Gaskell, & Niebuhr, 2011). Participants were presented with all 36 X/Y combinations in a random order.

**Table 1. Nonsense words used in production.**

| | |
|---|---|
| Word 1 (X) | tamash, caveesh, pidas, cavees, nalip, remope |
| Word 2 (Y) | shinnow, shamal, sival, samal, pentuf, pagoon |

### 2.2. Analysis

Segmentation of the recordings was done automatically through forced alignment using HTK and the Prosody Lab aligner (Gorman, Howell, & Wagner, this volume). Figure 1 shows an example alignment with the accompanying spectrogram and waveform.

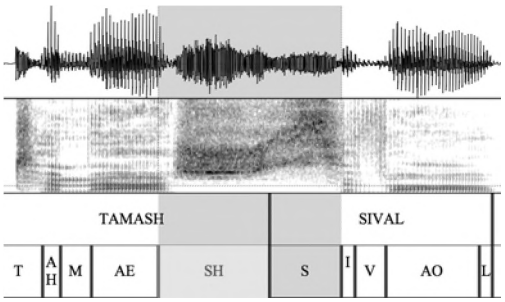


**Figure 1. Example alignment displayed in Praat.**

In many cases the segmentation of the sibilants included part of an adjacent vowel as in Figure 1. For this reason the first and last 20% of each sibilant (or sequence) was excluded from analysis. Segmentation of the sibilants within the sequence was not reliable, since in many cases there was no clear boundary between sibilants. For this reason, all analyses were done on the entire sibilant sequence.

A total of 603 productions were collected. Of these, 224 (37%) had a short silence between the two critical words. Productions without silence were analyzed separately. All analyses were conducted in Praat (Boersma & Weenik, 2010). Sibilant sequences were extracted and band-pass filtered between 1500 and 15000 Hz. Spectral slices were extracted every 7 ms using a 30ms Gaussian window and 50 Hz bins. Spectral centre of gravity (CoG) was calculated on each slice and the mean and range of the CoG measurements was calculated for each sibilant sequence.

## 3. RESULTS

Figure 2 shows the distribution of mean CoGs for each of the single sibilants and mixed sibilant sequences investigated by Niebuhr et al. (in press, 2011).

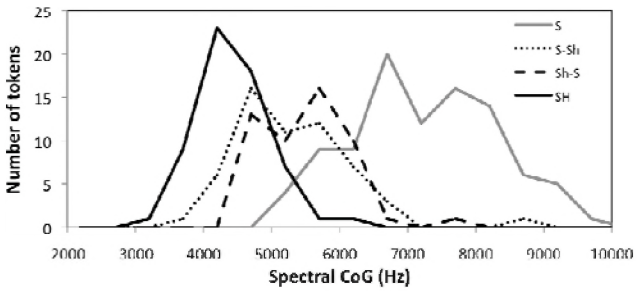


**Figure 2. Distribution of mean CoG for single sibilants and sibilant sequences.**

The CoG of both of the mixed sibilants are on average closer to /ʃ/ than to /s/ indicating some assimilation and the /s ʃ/ sibilants are most like /ʃ/. This pattern is much more like Holst and Nolan (1992) than Niebuhr et al. (in press, 2011) in that the /s ʃ/ sequences show a range of assimilation strengths and most are not complete.

The second goal was to make comparisons between the single sibilants (in the context of /p/) and /s s/ and /ʃ ʃ/ sequences. Table 2 lists the means and ranges (as well as standard deviations) of each of the sibilant conditions.

**Table 2. Mean and range of CoG (SD) for each sibilant.**

| Sibilant(s) | Mean CoG (Hz) | CoG range (Hz) |
|---|---|---|
| /s s/ | 7333 (1041) | 3224 (1827) |
| /s ʃ/ | 5040 (849) | 3000 (1663) |
| /ʃ s/ | 5245 (609) | 4203 (1569) |
| /ʃ ʃ/ | 4083 (523) | 1524 (731) |
| /s/ | 6999 (1049) | 2504 (1435) |
| /ʃ/ | 4189 (537) | 1048 (747) |

The mean CoG of the /s s/ sequence is 334 Hz higher than the singleton /s/ and this difference is marginally significant ($t$ = 1.94, $df$ = 126.1, $p$ = 0.054). The /ʃ ʃ/ sequence is 106 Hz lower than the /ʃ/ singleton but this difference is not significant ($t$ = -1.07, $df$ = 112.6, $p$ = 0.286).

Finally, we examined the relationship between planning and assimilation by analysing the 224 productions in which a short pause had been inserted between the sibilants. Here we found very little assimilation. The /s/ sibilants produced before /ʃ/ were nearly identical to those in other contexts. We did however, find that there was a significant correlation between the length of the silence (log ms) and the CoG of /s/ produced before /ʃ/ ($R^2$ = 0.21, $t$ = 2.13, $df$ = 17, $p$(two tailed) = .048). This is illustrated in Figure 3. No such relationships existed between any of the other segments and pause duration.

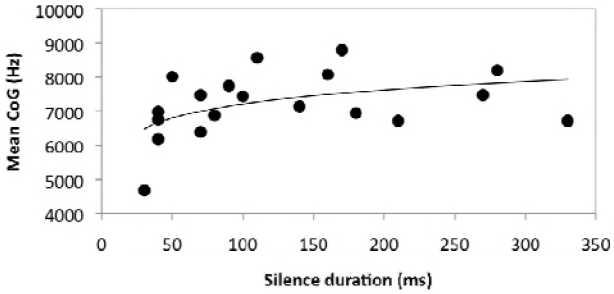


**Figure 3. Relationship between duration of the silence and mean CoG of /s/ before /ʃ/.**

## 4. DISCUSSION AND CONCLUSIONS

Our results are in line with previous studies, using much less labour intensive methods. However, discrepancies will need to be investigated further to determine if they are due to analysis techniques or dialect differences. Single /s/ in the context of a labial consonant had a significantly lower mean CoG than /s s/ sequences. Finally, assimilation is restricted to cases where there is no pause between words, but traces of co-articulation are visible for short pauses suggesting they could be due to the degree of articulatory planning.

## REFERENCES


Boersma, P., & Weenik, D. (2010). Praat: doing phonetics by computer (Version 5.1.31). 2010

Clayards, M., Gaskell, G., & Niebuhr, O. (2011). *Comparing French and English listeners' on-line perception of assimilated speech.* Paper presented at the BCBL 10th International Symposium on Psycholinguistics, Donostia-San Sebastian.

Gorman, K., Howell, J., & Wagner, M. (this volume). Prosodylab-Aligner: A tool for forced alignment of laboratory speech. . *Proceedings of Acoustics Week, the annual conference of the Canadian Acoustical Association.*

Holst, T., & Nolan, F. (1995). The influence of syntactic structure on [s] to [ʃ] assimilation. In B. Connell & A. Arvaniti (Eds.), *Papers in Laboratory Phonology IV: Phonology and Phonetic Evidence* (pp. 315-333). Cambridge: CUP.

Niebuhr, O., Clayards, M., Lancia, L., & Meunier, C. (in press 2011). On place assimilation in sibilant sequences - comparing French and English. *Journal of Phonetics*.

Whalen, D. H. (1990). Coarticulation is largely planned. *Journal of Phonetics, 18*, 3-35.

# SOUND INSULATION STANDARDS IN THE UK: A DECADE OF CHANGE.

**Roderick Mackenzie[1], R. Sean Smith[1], Chris Steel[1] and Richard Mackenzie[1]**
[1]Building Performance Centre, Institute for Sustainable Construction, Edinburgh Napier University, 42 Colinton Road, Edinburgh, United Kingdom, EH10 5BT, ro.mackenzie@napier.ac.uk

## 1. INTRODUCTION

The last decade has seen a great deal of change in residential sound insulation standards across the UK. Diversification in the measurement criteria and intensification of testing requirements have coincided with changes to the design of separating and internal wall and floor partitions and increasing standardization in design. This paper outlines the causes and consequences of these changes.

## 2. Regulation changes in England and Wales

### 2.1 Approved Document Part E (ADE, 2003)

Prior to the release of ADE 2003 of the building regulations in England and Wales, an airborne $D_{nTw}$ and impact $L'_{nTw}$ criteria was used across the UK. Minimum airborne mean partition performance levels for a new-build site were 52 dB for floors and 53 dB for walls (with individual minimums 48 dB and 49 dB respectively), and mean impact level of 61 dB (65 dB individually). The requirement to test generally lay at the discretion of the local authority, and acoustic test compliance rates were generally poor. The new ADE 2003 document opted for a change in criteria to $D_{nT,w} + C_{tr}$, primarily to account for low-frequencies given a primary cause of complaint in attached dwellings was bass music. At this time, 11 European countries used $D_{nT,w}$ or $R_w$, whilst 2 countries (Sweden and France) used C correction and no country used $C_{tr}$ for party walls or floors (this is still the case today). The $C_{tr}$ correction weights heavily against poor performances in the 100 Hz to 315 Hz range, and particularly against lightweight frame partitions. Its introduction was subject to much debate within the UK acoustics community.

It was also put forward in the draft document, and later confirmed in the full ADE, that 10% of attached dwellings of any partition type on a site should be subject to Pre-completion Testing (PCT) for sound insulation. Whilst initial government estimates put the cost to the house building industry of this increased site test regime at £3m per annum, independent estimates put the cost at closer to £15m, with the government figure revised in late 2003 to £17.3m. There were also serious concerns over the supply of qualified acoustic testers and equipment. As such the industry lobbied hard to be allowed to use standardized partition designs, repeatably and reproducibly achieving results in excess of ADE targets. The government agreed providing the industry could set-up a robustly designed system of approval, certification and monitoring of such partitions within 9 months.

### 2.2 Robust Details (RD, 2003)

This would require a complete review of current methods of partition design with new constructions to be researched, developed and tested to achieve significantly higher levels of sound insulation. The project was called the "Robust Standard Details" (RSD) project and this contract was awarded to Edinburgh Napier University.

It was decided that any RD partition must be capable of consistently exceeding ADE performance standards by a mean 5 dB and minimum 3 dB. They must also be deemed to be practical to construct on site and reasonably tolerant to workmanship. To use the RD option to avoid PCT, the 'Person carrying out the work' must register each plot, build in accordance with the relevant RD specification, and give registration document to the building control body before work starts.

The RSD project commenced in September 2002 and was to be completed 9 months later for submission by the house building industry to the government. The scale of the *design and test* element to the project was a world first. As each new wall and floor design would require at least 30 tests, spread over 4 different construction sites, using at least 2 different developers and 3 different testing companies. Over 60 house builders took part in the project covering 175 testing sites. Successful RD partition designs were entered into the new RD handbook along with tables outlining which wall could be used with which floor. This booklet is produced by RDL, an independent body overseeing the approval and monitoring of the RD scheme. 2% of RD registrations are subject to random inspection per year.

The process of gaining RD status remains the same today, with over 30 RD wall designs and over 20 RD floor designs incorporating masonry block work, concrete, timber frame and steel designs. Typical performance levels are 7 dB better than ADE 2003. Since 2003, the RD project scheme is used by 410 local authority building control departments, all major warranty providers and 70% of all new attached homes per annum (over 500,000 new homes since 2004). The government had initially estimated in 2001 that it would take 10 years to bring compliance levels to 95% under the original proposed Part E process. The RD scheme produced a system resulting in compliance levels of 97% within one year of the new RD scheme's operation. In successive years (2006-2009) compliance levels have continued between 97% and 98%. There has been a 4-fold decrease in noise complaints as a direct result of the RD scheme. In 2010, Edinburgh Napier University work on the RD project was awarded the Queen's Anniversary Prize for services to improving quality of life in the UK.

### 2.3 Code for Sustainable Homes (CSH, 2006)

The Code for Sustainable Homes (CSH) was introduced to promote low-carbon and sustainable new building design. In Section 7: Health and Well-being, aspirational targets were set for sound insulation where 1, 3, and 4 credits would be awarded to attached homes whose partitions repeatedly exceeded the requirements of ADE 2003 by 3, 5, and 8 dB respectively. The CSH's overall target points are due to increase every few years throughout the next decade, making acoustic points more valuable.

## 3. Regulation changes in Scotland

### 3.1 Section 5 Noise (2010)

Historically Scotland had had amongst the highest sound insulation standards in Europe. However by 2010, they had fallen behind the progress made in England and other countries in Europe. The required levels for residential sound insulation had not changed since 1987 (with guidance on construction only being partially amended in 2001). Thus in the 2010 edition of the Scottish Building Standards Authorities' (SBSA) Technical Handbook 2010, Section 5: Noise was completely rewritten.

Firstly the scope of the standard was widened to include all residential buildings, including hotels and halls of residence. Secondly, the 2010 edition set forth a significant increase in the sound insulation performance of separating walls and separating floors in attached housing. Whilst maintaining the $D_{nT,w}$ criteria, rather than adopting $D_{nT,w} + C_{tr}$, minimum airborne sound levels were increased from a mean result of 53 dB and / 52 dB walls and floors respectively, to a minimum of 56 dB. Similarly impact was set at a maximum 56dB and not a mean of 61 dB ($L'_{nTw}$). This has resulted in an effective increase of 8 dB in on-site design specification criteria to achieve such targets when compared with previous standards. Thirdly, a robust post-completion testing regime was implemented and is effective from May 2011 (apartments) and October 2011 (attached houses). One of the most striking illustrations of the change in required performance levels can been seen from how these example constructions have changed in Figure 1.

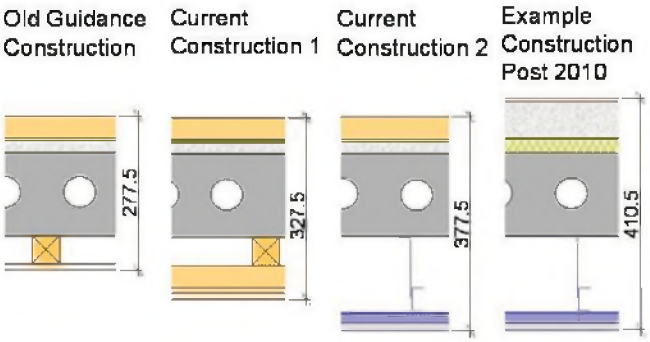


**Figure 1 Changes in Precast concrete floor design**

This represents a 48% increase in pre-cast concrete floor depths, whilst solid block work walls increase in thickness by 30% and unsheathed timber frame walls by 15%.

### 3.2 Section 7 Sustainability (Scotland 2011)

Comparable to the CSH in England and Wales, the new Section 7: Sustainability of the SBSA Technical Handbook set out further aspirational targets for sound insulation. As a result Silver and Gold standards are awarded to homes which improve by 2 dB and 4 dB respectively on Section 5's airborne and impact performances for separating and internal partitions (Bronze level).

## 4. CONCLUSIONS

The change in UK sound insulation standards in the past decade has been like no other before it. However, a net result of all these changes has been a 4-fold reduction in noise complaints in England and may also likely occur in Scotland. The standardization of residential partition design under the RD scheme and new Scottish example constructions means home builders who were just barely achieving the previous standards (which were intended as a minimum) or indeed failing compliance testing, now regularly exceed the targets as has been seen in RD compliance rates. Standards now set for separating floors and walls are relatively high compared with the rest of the UK and much of Europe (The median sound insulation levels achieved, as a result of the project, which are designed and tested, have placed England and Wales 2nd top in the international league table of airborne sound insulation).

Perhaps the most contentious issue involving UK sound regulations in the last decade has been the $+C_{tr}$ question. Scotland never adopted the $+C_{tr}$ adaptation term being used in England and Wales. This presents a problem for designers and house builders who operate UK wide.

It has been found that to develop a widespread increase in sound insulation standards in a short time across the entire house building industry requires the development of robust details, site checklists and random site testing monitoring collectively.

Looking to the future the work of COST Action TU0901 reviewing the potential for harmonized criteria across Europe has the potential to assist designers, product manufacturers and developers and reduce potential barriers to trade.

# CHANGES TO ISO STANDARDS AND THEIR EFFECTS ON MACHINERY NOISE DECLARATIONS

**Stephen E. Keith[1] and Stephen H.P. Bly[1]**

[1] Healthy Environments and Consumer Safety Branch, Environmental and Radiation Health Sciences Directorate, Consumer and Clinical Radiation Protection Bureau, 775 Brookfield Rd. 6301B, Ottawa, Ontario, Canada, K1A 1C1

skeith@hc-sc.gc.ca

## 1. INTRODUCTION

This paper describes recent improvements in the basic ISO standards for measurement of machinery noise and how they can affect the ease of determination, or the reliability, of machinery noise declarations. These standards include the 3740 series [1-5] for measurement of sound power and the 11200 series [6-8] for measurement of emission sound pressure level. There have been a number of changes, particularly in the estimation of uncertainty. Their primary impetus was to facilitate compliance with the European Union's Machinery and Outdoor Equipment Directives [9,10]. Both require machinery noise declarations of emission sound pressure level and sound power level. Furthermore, the latter Directive prescribes limits to the sound power levels for certain machines.

Improvements to the ISO standards could be incorporated into potential revisions of the Canadian voluntary standard [11] for machinery noise declarations. These should aid conformance to the Health Canada recommendation [12] that machinery sold in Canada includes standardized noise emission declarations in sales literature and instructions for use. Health Canada's recommendation was made to strengthen efforts to reduce the number of workers who suffer hearing impairments (currently about 9000 per year). Noise declarations enable purchasers to select quieter machinery and plan noise controls to reduce risks caused by excessive occupational noise.

## 2. SUMMARY OF CHANGES

### 2.1. Uncertainty

Uncertainty must be included in noise emission declarations [13] and is an important consideration in meeting noise limits. Therefore the most significant change to the ISO machinery noise measurement standards was to incorporate uncertainty budgets [14]. Each standard now has an annex with a detailed listing of typical uncertainty components. These components can be quantified by measurements (statistically), experience, general knowledge, or manufacturers specifications [14]. Previous standards had only addressed one aspect of uncertainty; i.e., the reproducibility of the method, $\sigma_{R0}$, (as estimated for measurements at different times in different labs and by different users). In the past, the means to account for the remaining uncertainty components was implicitly left to the users.

In the new standards, the ability to explicitly account for each component of uncertainty allows the total uncertainty to be smaller than previously possible. In specific measurement situations, contributions to uncertainty can be systematically identified and reduced. This was not possible previously when uncertainty was based on generic estimates.

In addition to the detailed uncertainty budget, the standards also include a simplified uncertainty budget. This assumes that the dominant source of uncertainty is due to operating and mounting conditions, $\sigma_{omc}$. This component is combined with the reproducibility of the method, $\sigma_{R0}$, to obtain an estimate of the total uncertainty. Tabulated values for $\sigma_{R0}$ values are similar to those given in the previous versions of the standards. Tabulated values for operating and mounting conditions can be as high as 4 dB when noise generated by the material processed varies strongly.

Uncertainties due to the reproducibility of the method, $\sigma_{R0}$, have been significantly reduced in some standards. In the standards for emission sound pressure level [6-8] uncertainties used to be on the order of 4 dB, comparable to survey grade estimates. Now these standards have been improved to include precision grade (0.5 dB uncertainty) and engineering grade uncertainty (1.5 dB). Also, precision grade uncertainty for sound power measurements in reverberation rooms [1] has been improved from 1 dB to 0.5 dB

### 2.2. Mounting and Operational modes

In the past there was some ambiguity about the conditions under which a noise emission value should be determined. Recommendations for mounting and operational modes are now included in all standards [1-8]. It is required that the source is tested, under conditions that are reproducible and representative of the noisiest operation in typical usage. This can have an important effect on the noise emission declaration.

### 2.3. Reference Meteorological conditions

To achieve repeatable results in different locations, measurements according to the new ISO machinery noise standards are normalized to reference meteorological conditions. This correction accounts for the different sound levels produced by machinery when the temperature and pressure change. The correction is usually small enough to ignore for survey grade standards. It is also unnecessary for

engineering grade measurements at elevations less than 500 m above sea level when the temperature range is −20 °C to 40 °C.. This change will have most effect on measurements related to noise emission declarations in Western Canada, (particularly Alberta where most cities or towns are above 500 m elevation).

### 2.4. Frequency Range

In the current standards, the frequency range is explicitly extended to include all frequencies that have a significant effect on the A-weighted levels. Previous standards indicated the measurement range was from 100 Hz to 10 kHz. Some sources primarily emit sound at frequencies outside of this range, and omission of these frequencies could have led to under reporting of A-weighted levels in declarations.

### 2.5. Single Event Sound levels

All standards now include instructions to calculate sound levels for single events such as impulsive noise or noise from characteristic individual work cycles. The measured quantities are numerically the same as the familiar "sound exposure level" used in environmental noise. Use of sound energy levels can help to calculate declared values.

### 2.6. Calibration

All standards have a similar section on calibration of the required instrumentation. It is recommended that the calibrator is calibrated every year, and other equipment is to be calibrated every 2 years. Conformance with these requirements gives greater confidence in the declaration.

### 2.7. Changes Specific to ISO 3744

Requirements for the environmental correction K2 in the most common engineering grade sound power measurement standard [3] have been relaxed to allow free field measurements in more reverberant environments. As a result, adequate absorption is obtained in a room with a volume that is one quarter of the volume previously required. This significantly increases the number of facilities that can be used for noise declaration measurements.

The positions of measurement points have been changed. This may require changes in some facilities making machinery noise declarations. However, the new arrays are not mandatory, and alternative arrays can be used if they do not adversely affect uncertainty (see 2.1). The simplified measurement arrays of the now withdrawn ISO4872 [15] for outdoor construction equipment have also been added.

## 3. CONCLUSIONS

Changes to these standards as described above make noise emission declarations easier to obtain and more reliable. This facilitates implementation of noise emission declarations both in Canada and internationally.

## REFERENCES


[1] ISO 3741 Acoustics - Determination of sound power levels and sound energy levels of noise sources using sound pressure -- Precision methods for reverberation test rooms, (2010)

[2] ISO 3743-1 Acoustics - Determination of sound power levels and sound energy levels of noise sources using sound pressure -- Engineering methods for small movable sources in reverberant fields -- Part 1: Comparison method for a hard-walled test room (2010)

[3] ISO 3744 Acoustics - Determination of sound power levels and sound energy levels of noise sources using sound pressure -- Engineering methods for an essentially free field over a reflecting plane (2010)

[4] ISO 3746 Acoustics - Determination of sound power levels and sound energy levels of noise sources using sound pressure -- Survey method using an enveloping measurement surface over a reflecting plane (2010)

[5] ISO 3747 Acoustics - Determination of sound power levels and sound energy levels of noise sources using sound pressure -- Engineering/survey methods for use in situ in a reverberant environment (2010)

[6] ISO 11201 Acoustics - Noise emitted by machinery and equipment -- Determination of emission sound pressure levels at a work station and at other specified positions in an essentially free field over a reflecting plane with negligible environmental corrections (2010)

[7] ISO 11202 Acoustics - Noise emitted by machinery and equipment -- Determination of emission sound pressure levels at a work station and at other specified positions applying approximate environmental corrections (2010)

[8] ISO 11204 Acoustics - Noise emitted by machinery and equipment -- Determination of emission sound pressure levels at a work station and at other specified positions applying accurate environmental corrections (2010)

[9] Directive 2000/14/EC of the European Parliament and the Council of 8 May 2000 on the approximation of the laws of the Member States relating to the noise emission in the environment by equipment for use outdoors, OJ L 162, 3.7.2000, (2000)

[10] Directive 2006/42/EC of the European Parliament and the Council of 17 May 2006 on machinery, and amending Directive 95/16/EC (recast), . OJ L 157, 9.6.2006, (2006)

[11] CSA Z107.58-02 Noise Emission Declarations for Machinery. Canadian Standards Association: Mississauga, Ontario

[12] Health Canada Notice to Stakeholders Noise from Machinery Intended for the Workplace, (2010), http://www.hc-sc.gc.ca/ewh-semt/noise-bruit/machinery-machines-eng.php Accessed 2011 July 27

[13] ISO 4871 Acoustics - Declaration and verification of noise emission values of machinery and equipment, (1996)

[14] ISO/IEC Guide 98-3 Uncertainty in measurement - Part 3: Guide to the expression of uncertainty in measurement,(2008)

[15] ISO 4872 Acoustics - Measurement of airborne noise emitted by construction equipment intended for outdoor use -- Method for determining compliance with noise limits, (1978)

# DEVELOPMENT OF LOW-COST UNDERWATER ACOUSTIC ARRAY SYSTEMS FOR THE NORTHERN WATCH TECHNOLOGY DEMONSTRATION PROJECT

**G.J. Heard, N. Pelavas, C.E. Lucas, Isaias Peraza, Derek Clark, Colin Cameron, and Val Shepeta**
Defence Research & Development Canada Atlantic, PO Box 1012 Dartmouth, NS, CANADA B2Y 3Z7

## 1. INTRODUCTION

### 1.1 RDS Array Technology

In the recent past Defence Research and Development Canada (DRDC) undertook a project to develop low-cost underwater array systems for research and other applications that were complete with on-board processing, acoustic messaging, and battery-powered operations. The project was a major effort requiring over $7.5m in research funding that was known as the Rapidly Deployable Systems (RDS) Technology Demonstration Project (TDP). MacDonald Dettwiler & Assoc. was the lead contractor [1]. The RDS project led to the development of a flexible digital array technology, which is often just called RDS today.

Developments since the end of the TDP project include upgraded quantization from 16 to 24-bits, an increased sampling rate range from a few Hertz to 240 kHz, reduction in power requirements for each node (typically 20 mW) and the array controller (1.5W), improved digital bus structures with extra data and power pairs, and modernized interfaces including Ethernet and universal serial bus. Other changes relate to the packaging of the various sensors and the production of larger and smaller arrays (typically 64 nodes/array), as well up to 5000-m depth capability [2,3].

The RDS technology has been licensed by Omnitech Electronics Inc. [4] and eleven arrays have been sold to defence science organizations and contractors to date. RDS technology has also been applied to produce long-range acoustic homing systems for the autonomous underwater vehicles that have been used by Canada in the mapping of the seafloor under Arctic ice cover [5]. It has been used in the development of DRDC Starfish systems for underwater research that incorporate both electromagnetic and acoustic sensors [2]. And RDS technology is being applied to provide underwater acoustic sensing for Northern Watch.

### 1.2 The Northern Watch TDP

The Northern Watch TDP is multi-million-dollar, multi-laboratory project to demonstrate integrated surveillance over a portion of Barrow Strait near the southwest corner of Devon Island for an extended period of up to 1-year duration. The original project concept is described in reference [6]. The biggest difference between the original project and the current plan is the requirement for up to a 1-year period of unmanned operation. This change in the project goal has required a steady series of improvements to the base camp on Devon Island and an expanded role in system integration and autonomy. As a result of the changes, the project timeline has been extended through to 2015.

The underwater sensing portion of the Northern Watch TDP is being provided by ruggedized RDS array systems. Two nested-aperture 160-m long linear arrays will be deployed on the seafloor near the southwest corner of Devon Island in summer of 2013 or 2014.

The arrays must operate continuously for up to 1 year and may have to remain operational for a period of at least two years during which they may be turned on or off depending on requirements of the TDP. These arrays must be cost effective and employ a low-cost set of cables and telemetry repeaters to supply power to the arrays, provide a command and control path, and return the array data to the shore where it will be processed and integrated with data from other systems. Further details are provided in an initial array sensor design concept document [7].

## 2. Northern Watch RDS Arrays

The arrays for the Northern Watch project have been developed by Omnitech Electronics Inc. as prime under contract to DRDC. The arrays have undergone two prototype developments. The original array design was based on an absolute minimum cost and made extensive use of standard plastic piping and resin materials for the mechanical structure.

Although the mechanical design was sufficient for pressure and stresses of deployment, the arrays began to allow water to leak into the hydrophone nodes after they were deployed. The arrays operated for approximately 2 weeks before they were permanently shut down. While the arrays functioned, valuable supporting data were collected by the operating hydrophone nodes [8].

Even as one or more nodes began to short the main digital bus, data from other nodes was still received. The system was able to maintain partial array operation. As the water found additional leak paths and seeped along the interior of the cable we were able to watch a slow degradation occur.

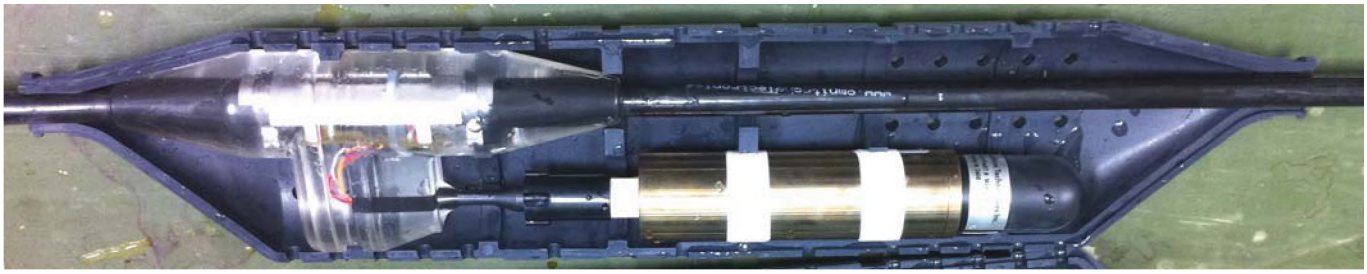

**Figure 1. Second generation cantilevered hydrophone node mechanical design.**

A forensic analysis of array failure was conducted [9]. Careful inspection and dye penetrant testing revealed that material chemical incompatibilities had provided unexpected leakage paths. The compatibility of the many plastics and resins along with some resin contamination, off-gas bubbling, and construction practices led to the array failures.

A second generation array design was undertaken that limited the role of plastics and resins. The new mechanical design employs Nickel-Aluminium-Bronze canisters for the electronics, commercially constructed hydrophones with screw mountings and O-ring seals, new transparent resin materials for cable breakouts with an internal metal support skeleton, a tough clam-shell protective casing, and a cantilevered hydrophone arrangement as shown in Fig. 1.

The new array design also makes use of connectors to allow for hydrophone replacement. The use of connectors, commercially manufactured hydrophones, and pressure canisters has roughly tripled the cost of the original minimal cost array design; however, every part of the array is now serviceable and is much more robust. The electronic components remain largely similar, except that additional data buses are added to provide for an isolation capability in the event of bus shorts. The mechanical and electrical changes have resulted in a very robust, and still relatively low-cost, array design.

To ensure that the arrays are long-lived, short prototype array segments and component assemblies have been produced and subjected to extensive pressure, strain, and temperature tests. The array segments have been repeatedly acoustically calibrated at intervals during the stress testing to ascertain not only mechanical survivability, but also electronic and acoustic reliability.

The new array segments have been pressure tested to ten times their operational depth requirement of 200 m over 24 cycles. Interspersed among the pressure tests have been a sequence of freezing and heating of wet soaked components. The intent was to try to open cracks and create leakage paths. The arrays were operated continuously during testing to ensure stable data telemetry and acoustic sampling.

In addition, the array segments have been operated while being mechanically strained to more than four times the stress loads expected during deployment. All tests were successfully passed by the prototype units. Finally, the segments were mechanically strained to destruction while still operating to determine the failure mode, symptoms, and ultimate cable strength.

## 3. CONCLUSIONS

Throughout the production and operation of over 1800 hydrophones based on RDS technology there has never been an electronic failure except for damage due to water leakage or crush damage. The new mechanical array design for Northern Watch appears to bring the system packaging development in line with the electronic development. Extremely robust, low-cost arrays are now possible.

## REFERENCES


[1] Heard, G.J., Kennedy, T., and McInnis, J., Rapid Deployable Systems (RDS) for Underwater Surveillance: Final Report. DRDC Contractor Report CR2006-223, 121 pages, 18 December 2006.

[2] Ebbeson, G.R., Heard, G.J., Desharnais, F., Lucas, C.E., and Matthews, M-N,R. Hardware and Software Progress in Deployable Systems. Proc. of the 36th TTCP MAR TP-9, DSTO Edinburgh, South Australia, 12-16 Nov 2007.

[3] Rapidly Deployable Systems Array Technology. DRDC Atlantic Fact Sheet NetALS0108, 2008.

[4] http://www.omnitechelectronics.ca/products/under-water-systems/custom-sensor-arrays.html

[5] Kamninski, C., Crees, T., Ferguson, J., Williams, J., Hopkin, D., Heard, G., 12 days under ice - an historic AUV deployment in the Canadian High Arctic. Proc. of Autonomous Underwater Vehicles (AUV), 2010 IEEE/OES, 1-3 Sept 2010.

[6] Forand, J.L., Larochelle, V., Brookes, D., Lee, J.P.Y., MacLeod, M., Dao, R., Heard, G.J., McCoy, N., Kollenberg, K., Surveillance of Canada's High Arctic. Proc. OCEANS 2008, 15-18 Sept 2008.

[7] Heard, G.J., Pelavas, N., Northern Watch Underwater Sensor System Design Concept. DRDC Atlantic TM 2010-248, Sept. 2010.

[8] Heard, G.J., Pelavas, N., Ebbeson, G.R., Hutt, D.L., Peraza, I., Schattschneider, G., Underwater Sensor System 2009 Field Trial Report: Northern Watch Technology Demonstration Project. DRDC Atlantic TM2010-241, July 2011.

[9] Cameron, C.G., Northern Watch: Summary of the Material Investigations. Jan-Nov 2010. DRDC Atlantic TN2010-343, 2010.

# ACOUSTIC RESPONSE OF MULTI-FLUID SHELL SYSTEMS WITH STRUCTURAL ENHANCEMENT

**Serguei Iakovlev [1], Kyle Williston[1], and Martin Mitchell[1]**
[1] Dept. of Engineering Mathematics and Internetworking, Dalhousie University, Halifax, Nova Scotia, Canada

## 1. INTRODUCTION

The present study is a further development of our earlier work on a shell with a co-axial core but identical internal and external fluids [1,2], and a shell filled with and submerged into two different fluids [3], both subjected to an external shock wave. Specifically, it was shown that when the internal and external fluids are different, there are up to four different scenarios of the interaction possible, depending on the properties of the fluids. It was also shown that placing a rigid core inside a shell filled with and submerged into identical fluids dramatically changes both internal and external acoustic patterns. Thus, investigating the result of combining these two enhancements of the system's complexity is of definite interest.

## 2. MATHEMATICAL FORMULATION AND SOLUTION METHODOLOGY

We consider a thin elastic circular cylindrical shell of radius $r_0$ filled with and submerged into different fluids, and containing a rigid co-axial core of radius a. We assume that the shell is thin, and that its deflections are small in comparison to its thickness, so that the linear theory of shells can be employed; we further assume that the Love-Kirchhoff hypothesis holds true (using the Reissner-Mindlin model was shown to provide more accurate results in the present context [4], but the accuracy provided by the Love-Kirchhoff model is adequate for our purposes). The fluids are assumed to be irrotational, inviscid, and linearly compressible.

The methodology developed in our earlier work [5-8] is used, i.e. we apply the Laplace transform time-wise and use the separation of variables for the spatial coordinates to obtain the pressure in terms of the series with time-dependent coefficients. The approach has been extensively validated and the results it produces have shown excellent agreement with experiments.

## 3. RESULTS AND CONCLUSIONS

A steel shell is considered with the thickness of 0.01 m and radius of 1 m, submerged into and filled with fluids of the same density but with varying acoustic speeds, and containing a rigid co-axial core, also of varying radius. The interaction with a cylindrical acoustic pulse is analyzed, and it is assumed that the rate of the exponential decay behind the front is 0.0001314 s and the peak pressure in the front is 250 kPa.

The "classical" case of the identical fluids inside and outside the shell was addressed in detail in [1], and the profound effect that the core, especially of the large radius, has on the hydrodynamic fields was discussed (the respective images are not reproduced here). We focus on determining what is the effect of the core on the hydrodynamic fields when the fluids are different.

Fig. 1 and 2 show the hydrodynamic field induced by the pulse on a shell with three different cores, a small-, medium-, and large-radius ones for the scenario where the internal acoustic speed is higher than external (or $\zeta>1$; in this case, $\zeta\sim1.43$ where $\zeta$ is defined as the ratio of the internal and external acoustic speeds [3]). The instant at which the fields were simulated was chosen to represent one of the most important stages of the interaction when the post-reflection focusing is developing in the internal fluid [3]. We can see that the focusing pattern characteristic of this stage is present for the small and, largely, medium core but is absent for the large core. Furthermore, the entire sequence of the internal pressure wave propagation, reflection, and focusing is "shifted" in time which results in the "head" waves seen in front of the incident wavefront.

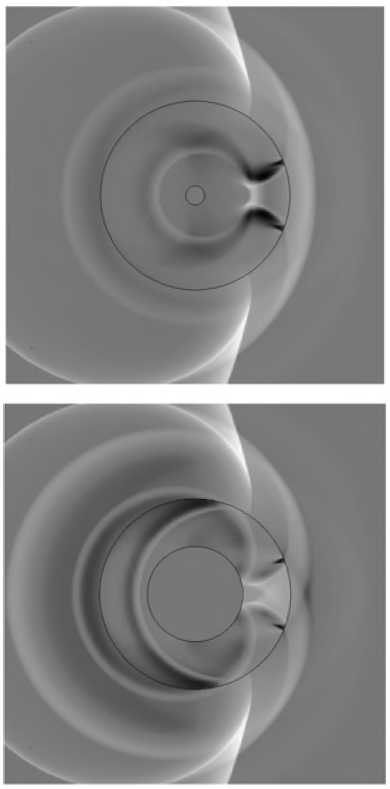

**Figure 1. The hydrodynamic pattern for $\zeta\sim1.43$ and two different cores, $a/r_0=0.10$ (top image) and $a/r_0=0.50$ (bottom image); $t=1.70$.**

Fig. 3 shows the hydrodynamic fields for the same shell and two cores, a small-radius one and a medium-radius one, but for a different value of $\zeta$, that is, for the case where the internal acoustic speed is lower than the external one ($\zeta\sim0.57$), the scenario that was found to be most interesting in our earlier work[3]. We can see that, even for a small-radius core, the overall hydrodynamic field has a much

more complex structure than in the absence of the core [3]; the same is definitely true for the medium-size core. This complexity requires a more in-depth study and is the subject of our current investigation.

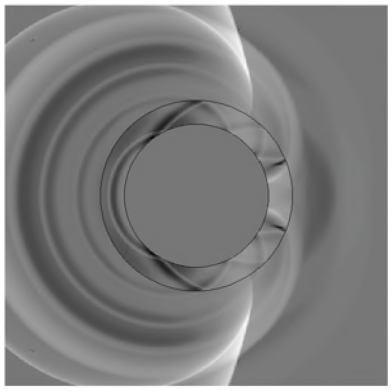

**Figure 2. The hydrodynamic pattern for $\zeta$~1.43 and $a/r_0$=0.75; t=1.70.**

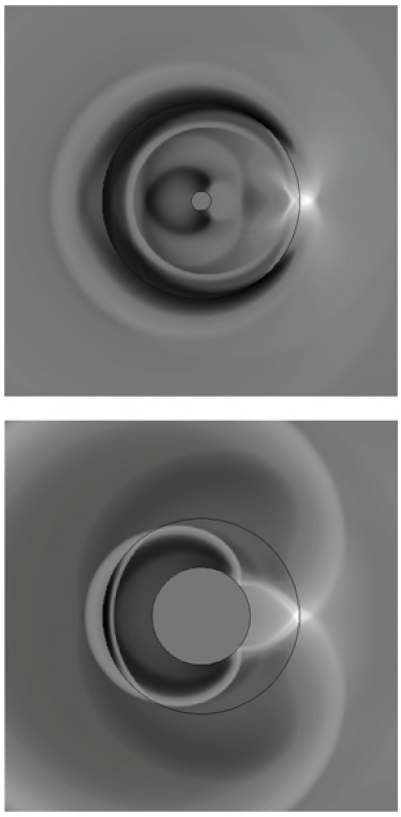

**Figure 3. The hydrodynamic pattern for $\zeta$~0.57 and two different cores, $a/r_0$=0.10 (top image) and $a/r_0$=0.50 (bottom image); t=3.70.**

We conclude that, very much like in the case of the identical fluids [3], the presence of the core dramatically changes the phenomenology of the interaction, and leads to a complete disappearance of some of the phenomena that are observed in the absence of the core. However, unlike in the case of the identical fluids, the diversity of the interaction is now incomparably greater for the hydrodynamic patterns observed change not only with the radius of the core but also with the acoustic properties of the fluids.

The scenario of $\zeta$<1, very much like in the case when no core is present, appears to be most interesting, and definitely deserves a more in-depth investigation. It is expected that the study of the diversity of the wave propagation, reflection, and focusing it that case will reveal some very interesting and, possibly, practically consequential effects that are not observed when the core is present but the fluids are identical or when the fluids are different but the core is not present.

## REFERENCES


[1] Iakovlev, S., Gaudet, J., Dooley, G., MacDonald, B. (2010) Hydrodynamic fields induced by the shock response of a fluid-filled submerged cylindrical shell containing a rigid co-axial core, *Journal of Sound and Vibration* 329 (16), 3359-3381.

[2] Iakovlev, S. (2004) Influence of a rigid coaxial core on the stress-strain state of a submerged fluid-filled cylindrical shell subjected to a shock wave, *Journal of Fluids and Structures* 19 (7), 957-984.

[3] Iakovlev, S. (2009) Interaction between an external shock wave and a cylindrical shell filled with and submerged into different fluids, *Journal of Sound and Vibration* 322 (1-2), 401-437.

[4] Iakovlev, S., Santos, H. A. F. A., Williston, K., Murray, R., Mitchell, M. (2011) Non-stationary radiation by a cylindrical shell: numerical modeling using the Reissner-Mindlin theory, submitted to *Journal of Fluids and Structures.*

[5] Iakovlev, S. (2006) External shock loading on a submerged fluid-filled cylindrical shell, *Journal of Fluids and Structures* 22, 997-1028.

[6] Iakovlev, S. (2007) Submerged fluid-filled cylindrical shell subjected to a shock wave: Fluid-structure interaction effects, *Journal of Fluids and Structures* 23 (1), 117-142.

[7] Iakovlev, S. (2008) Interaction between a submerged evacuated cylindrical shell and a shock wave. Part I: Diffraction-radiation analysis, *Journal of Fluids and Structures* 24, 1077-1097.

[8] Iakovlev, S. (2008) Interaction between a submerged evacuated cylindrical shell and a shock wave. Part II: Numerical aspects of the solution, *Journal of Fluids and Structures* 24 (7), 1098-1119.


## ACKNOWLEDGEMENTS


Authors acknowledge the financial support of the Natural Sciences and Engineering Research Council (NSERC) of Canada. S.I. also acknowledges the financial support of the Killam Trusts and Dalhousie University.

# ANALYSIS OF THE EXTREME ACOUSTIC PRESSURE IN MULTI-FLUID SHELL SYSTEMS SUBJECTED TO AN EXTERNAL PULSE

**Serguei Iakovlev [1], Kyle Williston[1], Garrett Dooley[2], and Jonathan Gaudet [3]**
[1] Dept. of Engineering Mathematics and Internetworking, Dalhousie University, Halifax, Nova Scotia, Canada
[2] Lunenburg Industrial Foundry & Engineering, Lunenburg, Nova Scotia, Canada
[3] O'Neil Scriven and Associates Ltd, Halifax, Nova Scotia, Canada

## 1. INTRODUCTION

As was recently established, the interaction between an external shock wave or acoustic pulse and a cylindrical shell filled with and submerged into different fluids is very complex, with up to four different scenarios possible [1]. This complexity was analyzed in some detail in that paper, but not all its aspects were covered.

Specifically, two important issues were not addressed. The first is the actual evolution of the hydrodynamic fields as the transition between different interaction scenarios happens – it is of definite interest to see exactly how the structure of the fields changes. The second, more practically important, issue is the analysis of the peak pressure that is observed as a result of the many shock wave reflection, propagation and focusing phenomena that take place during the evolution in question.

Our goal, therefore, is to present a summary of the most important aspects of the evolution of the hydrodynamic fields, and to complement that with an assessment of the maximum pressure observed in the system.

## 2. MATHEMATICAL FORMULATION AND SOLUTION METHODOLOGY

We consider a thin elastic circular cylindrical shell filled with and submerged into different fluids. We assume that the shell is thin enough, and that its deflections are small in comparison to its thickness, so that the linear shell theory can be employed; we further assume that the Love-Kirchhoff hypothesis holds true. We note that although using the Reissner-Mindlin model was shown to provide more accurate results [2], employing the Love-Kirchhoff model is still more than acceptable for the purposes of the present study.

The fluids are assumed to be irrotational, inviscid, and linearly compressible, thus the wave equations are used to model the fluid dynamics. The fluids and the shell are coupled through the dynamic boundary condition on the interface.

As it was established [1], a single most important parameter determines the appearance of the hydrodynamic fields observed in the system, namely $\zeta$ which is defined as the ratio of the sound speed in the internal fluid to that in the external one. Changing $\zeta$ implies varying the acoustic properties of the fluids.

The problem is approached with the methodology developed in our earlier work [3-6], i.e. we apply the Laplace transform time-wise to the wave equations and then separate the spatial variables in order to arrive at the expressions for the transforms of the internal and external pressure in a form of a series of modified Bessel functions of the first (internal fluid) and second (external fluid) kind. The pressure is then obtained as a Fourier series with time-dependant coefficients which, for the radiation pressure, depend on the unknown normal displacements of the shell.

Then, the same series form is used for the shell displacements and, substituting them into the shell equations, we arrive at the systems of the ordinary differential equations for each of the displacement harmonics. The systems are then approached numerically (finite differences) and the resulting normal displacement is used to compute the radiation pressure.

We note that although the present approach is used, in this case, to model structurally simple system (a single shell), it can also be successfully employed to address more complex structures [7].

## 3. RESULTS AND CONCLUSIONS

A steel shell is considered with the thickness of 0.01 m and radius of 1 m, submerged into and filled with fluids of the same density but the acoustic speeds varying according to the changes of $\zeta$. The interaction with a cylindrical pulse is analyzed, and the rate of the exponential decay is assumed to be 0.0001314 s while the initial pressure in the front is 250 kPa.

Fig. 1 shows three numerically simulated images of the internal field for the chosen pulse for various $\zeta$ during the reflection of the internal pressure wave off the surface of the shell which is one of the most important stages of the process. The evolution of the respective hydrodynamic pattern is clearly visible, and different values of $\zeta$ yield very different fields. Of particular interest to us here is the point-like high-pressure region observed right at the shell surface at $\zeta$=0.50 as it is expected to yield a peak of internal hydrodynamic pressure.

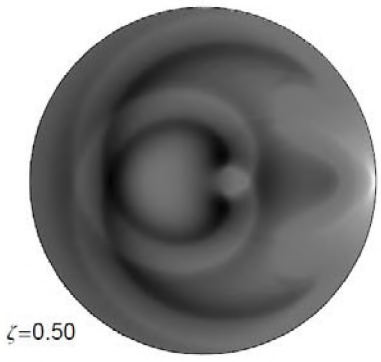

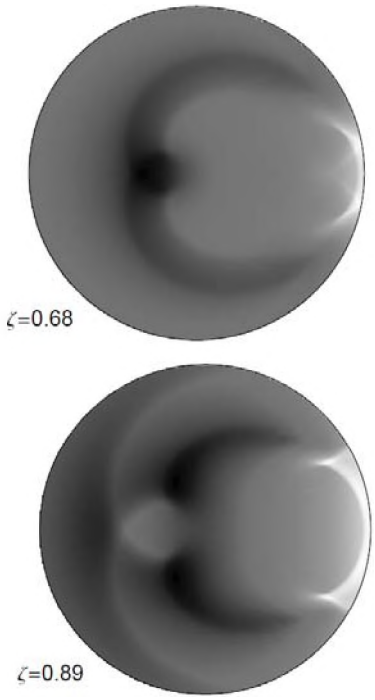


**Figure 1. The internal hydrodynamic pattern for three different values of ζ.**

For the other two values of ζ, the reflection pattern is less localized, and is expected to yield lower pressure than the ζ=0.50 case.

In order to assess the extremities of the hydrodynamic field, we analyze the highest pressure induced by the four phenomena: the two focusings (the pre- and post-reflection) and the reflection [1], and the peak pressure associated with the Mach stems [3], and plot it versus ζ for its practically meaningful values, Fig. 2.

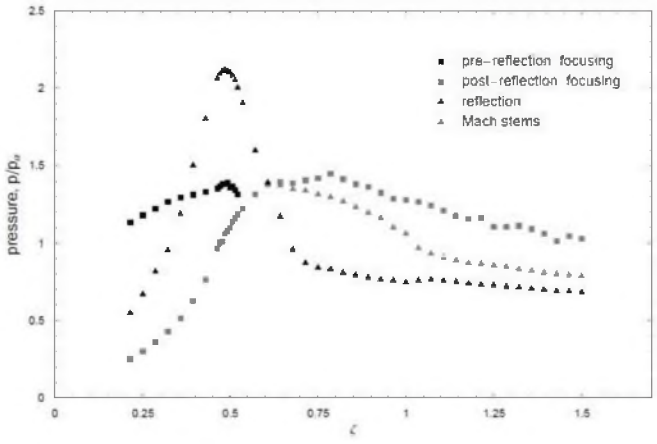


**Figure 2. The maximum pressure inside the shell for various ζ.**

As one can see, the overall highest pressure is associated with the reflection and is achieved at ζ~0.48. This corresponds to the transition between the scenario where both pre- and post-reflection focusing are observed to the scenario where only one, post-reflection focusing takes place (the latter being characteristic of the "classical" scenario of identical internal and external fluids). This peak pressure exceeds the peak incident pressure by 110%, a result that has obvious and far-reaching practical consequences. From the phenomenological point of view, the peak pressure in question is originated as a result of the near-simultaneous occurrence of the pre-reflection focusing and reflection at or very near the shell surface (note the termination of the pre-reflection focusing shortly after that).

For higher values of ζ, the peak pressure is due to the post-reflection focusing, a phenomena that was discussed in the present context in [3]. We also note that any value of ζ in the interval [0.38,0.58] yields very high pressure that exceeds the peak incident one by at least 50%. The highest pre- and post-reflection focusing pressure and the highest pressure associated with the Mach stems exceed the peak incident pressure by 40%, 45%, and 40%, respectively.

The observations made underscore the necessity for a careful pre-design analysis of multi-fluid shell systems in the context of impulse loading, especially when there is at least some freedom in varying the properties of the fluids. Even when the properties cannot be changed, the analysis in question is still valuable as to ensure that the extreme pressure observed during the interaction is accounted for.

## REFERENCES

[1] Iakovlev, S. (2009) Interaction between an external shock wave and a cylindrical shell filled with and submerged into different fluids, *Journal of Sound and Vibration* 322 (1-2), 401-437.

[2] Iakovlev, S., Santos, H. A. F. A., Williston, K., Murray, R., Mitchell, M. (2011) Non-stationary radiation by a cylindrical shell: numerical modeling using the Reissner-Mindlin theory, submitted to *Journal of Fluids and Structures*.

[3] Iakovlev, S. (2006) External shock loading on a submerged fluid-filled cylindrical shell, *Journal of Fluids and Structures* 22, 997-1028.

[4] Iakovlev, S. (2007) Submerged fluid-filled cylindrical shell subjected to a shock wave: Fluid-structure interaction effects, *Journal of Fluids and Structures* 23 (1), 117-142.

[5] Iakovlev, S. (2008) Interaction between a submerged evacuated cylindrical shell and a shock wave. Part I: Diffraction-radiation analysis, *Journal of Fluids and Structures* 24, 1077-1097.

[6] Iakovlev, S. (2008) Interaction between a submerged evacuated cylindrical shell and a shock wave. Part II: Numerical aspects of the solution, *Journal of Fluids and Structures* 24 (7), 1098-1119.

[7] Iakovlev, S. (2004) Influence of a rigid coaxial core on the stress-strain state of a submerged fluid-filled cylindrical shell subjected to a shock wave, *Journal of Fluids and Structures* 19 (7), 957-984.

## ACKNOWLEDGEMENTS

Authors acknowledge the financial support of the Natural Sciences and Engineering Research Council (NSERC) of Canada. S.I. also acknowledges the financial support of the Killam Trusts and Dalhousie University.

# BAYESIAN LOCALIZATION OF MULTIPLE OCEAN ACOUSTIC SOURCES WITH ENVIRONMENTAL UNCERTAINTIES

**Stan E. Dosso and Michael J. Wilmut**
School of Earth and Ocean Sciences, University of Victoria, Victoria BC Canada V8W 3P6, sdosso@uvic.ca

## 1. INTRODUCTION

This paper considers simultaneous localization of multiple acoustic sources when properties of the ocean environment (water column and seabed) are poorly known [1, 2]. A Bayesian formulation is applied in which the environmental parameters, noise statistics, and locations and complex strengths (amplitudes and phases) of multiple sources are considered unknown random variables constrained by acoustic data and prior information. The posterior probability density (PPD) over all parameters is defined and integrated using efficient Markov-chain Monte Carlo methods to produce joint marginal probability densities for source ranges and depth. This approach also provides quantitative uncertainty analysis for all parameters, which can aid in understanding the inverse problem and may be of practical interest (e.g., source-strength probability distributions). Closed-form maximum-likelihood expressions for source strengths and noise variance at each frequency (developed in the following section) allow these parameters to be sampled implicitly, substantially reducing the dimensionality and difficulty of the inversion. An example is presented of multiple-source localization in an uncertain shallow-water environment.

## 2. THEORY

Consider measured data $\mathbf{d} = \{\mathbf{d}_f; f = 1, N_F\}$ consisting of complex acoustic fields at $N_F$ frequencies recorded at an array of $N_H$ hydrophones. The acoustic field at each frequency is assumed to be due to $N_S$ sources at locations $\mathbf{x} = \{\mathbf{x}_s = (r_s, z_s); s = 1, N_S\}$, where $r_s$ and $z_s$ are the range and depth of the $s$th source. The complex source strengths (amplitude and phase) are denoted $\mathbf{a} = \{[\mathbf{a}_f]_s\}$. The data errors are considered complex Gaussian-distributed random variables with unknown standard deviation at each frequency denoted $\boldsymbol{\sigma} = \{\sigma_f\}$. The unknown environmental parameters are denoted by $\mathbf{e}$. Under these assumptions, the likelihood function is given by [2]

$$L(\mathbf{x},\mathbf{e},\mathbf{a},\boldsymbol{\sigma};\mathbf{d}) = \prod_{f=1}^{N_F} \frac{1}{(\pi\sigma_f^2)^{N_H}} \times \exp\left\{-\left|\mathbf{d}_f - \sum_{s=1}^{Ns} [\mathbf{a}_f]_s \mathbf{d}_f(\mathbf{x}_s,\mathbf{e})\right|^2 / \sigma_f^2\right\}, \quad (1)$$

where $\mathbf{d}_f(\mathbf{x}_s,\mathbf{e})$ represent the modelled acoustic field for a unit-amplitude, zero-phase source at location $\mathbf{x}_s$ in an environment $\mathbf{e}$. Rearranging, the data misfit (negative log-likelihood) function is given by

$$E(\mathbf{x},\mathbf{e},\mathbf{a},\boldsymbol{\sigma};\mathbf{d}) = \sum_{f=1}^{N_F} \left|\mathbf{d}_f - \mathbf{D}_f \mathbf{a}_f\right|^2 / \sigma_f^2 + 2N_H \log_e \sigma_f, \quad (2)$$

where the complex matrix $\mathbf{D}_f$ is given by

$$[\mathbf{D}_f]_{hs} = [\mathbf{d}_f]_h(\mathbf{x}_s,\mathbf{e}). \quad (3)$$

To estimate ML source strengths, setting $\partial E/\partial \mathbf{a}_f = 0$ for Eq. (2) leads to

$$\hat{\mathbf{a}}_f = (\mathbf{D}_f^H \mathbf{D}_f)^{-1} \mathbf{D}_f^H \mathbf{d}_f, \quad (4)$$

where $H$ indicates Hermitian (conjugate) transpose. Substituting this estimate back into the original misfit function (2) leads to a new misfit

$$E(\mathbf{x},\mathbf{e},\boldsymbol{\sigma};\mathbf{d}) = \sum_{f=1}^{N_F} \left|\left[\mathbf{I} - \mathbf{D}_f(\mathbf{D}_f^H \mathbf{D}_f)^{-1}\mathbf{D}_f^H\right]\mathbf{d}_f\right|^2 / \sigma_f^2 + 2N_H \log_e \sigma_f. \quad (5)$$

To estimate ML standard deviations, $\partial E/\partial \sigma_f = 0$ leads to

$$\hat{\sigma}_f^2 = \frac{1}{N_H}\left[\mathbf{I} - \mathbf{D}_f(\mathbf{D}_f^H \mathbf{D}_f)^{-1}\mathbf{D}_f^H\right]\mathbf{d}_f. \quad (6)$$

Substituting this estimate back into misfit function (5) and neglecting additive constants (representing fixed normalization factors for the likelihood) leads to new misfit

$$E(\mathbf{x},\mathbf{e};\mathbf{d}) = N_H \sum_{f=1}^{N_F} \log_e \left|\left[\mathbf{I} - \mathbf{D}_f(\mathbf{D}_f^H \mathbf{D}_f)^{-1}\mathbf{D}_f^H\right]\mathbf{d}_f\right|^2. \quad (7)$$

Evaluating misfit function (7) for a specific source location and environment ($\mathbf{x}$ and $\mathbf{e}$) implicitly applies the ML estimates for complex source strengths and standard deviations ($\mathbf{a}$ and $\boldsymbol{\sigma}$). This implicit sampling can replace explicit sampling in optimization and integration algorithms reducing the dimensionality of the inversion from $2N_SN_F + N_F + 2N_S + N_E$ to $2N_S + N_E$, where $N_E$ is the number of unknown environmental parameters. For instance, in the example presented in the following section the dimensionality is reduced from 35 to 14. Finally, it is interesting to note that in the special case of a single source ($N_S = 1$), the magnitude-squared term of Eq. (7) reduces to

$$\left|\left[\mathbf{I} - \mathbf{D}_f(\mathbf{D}_f^H \mathbf{D}_f)^{-1}\mathbf{D}_f^H\right]\mathbf{d}_f\right|^2 = \left|\mathbf{d}_f\right|^2 - \frac{\left|\mathbf{d}_f^H(\mathbf{x},\mathbf{e})\,\mathbf{d}_f\right|^2}{\left|\mathbf{d}_f(\mathbf{x},\mathbf{e})\right|^2}, \quad (8)$$

which is equivalent to the Bartlett misfit commonly used in matched-field localization and geoacoustic inversion.

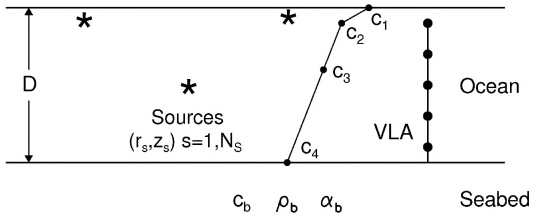


**Figure 1.** Schematic diagram of the geometry of the three-source localization indicating unknown environmental parameters.

## 3. EXAMPLE

The multiple-source localization procedure outlined above is demonstrated here with a synthetic example [2], as illustrated in Fig. 1. The geoacoustic parameters include the sound speed $c_b$, density $\rho_b$, and attenuation $\alpha_b$ of a uniform seabed. The water-column sound speed profile is represented by four unknown sound speeds $c_1$-$c_4$ at depths of 0, 10, 50, and $D$ m, where $D$ is the water depth. All environmental parameters are considered unknown with prior information consisting of uniform distributions over wide bounds. The three acoustic sources are located at ($r$, $z$) = (7 km, 4 m), (3 km, 2 m) and (5.4 km, 50 m) with relative amplitudes of 1, 0.5 and 0.13, phases of 45°, 90° and −90°, and signal-to-noise ratios of 10, 4 and −4 dB, respectively, at three frequencies of 300, 400 and 500 Hz. Simulated acoustic data were computed for a 24-sensor vertical line array using a normal mode propagation model. Fig. 2 shows joint marginal probability densities over source range and depth: All sources are successfully localized, with the greatest uncertainty for the weak submerged source for which the marginal density is strongly multi-modal.

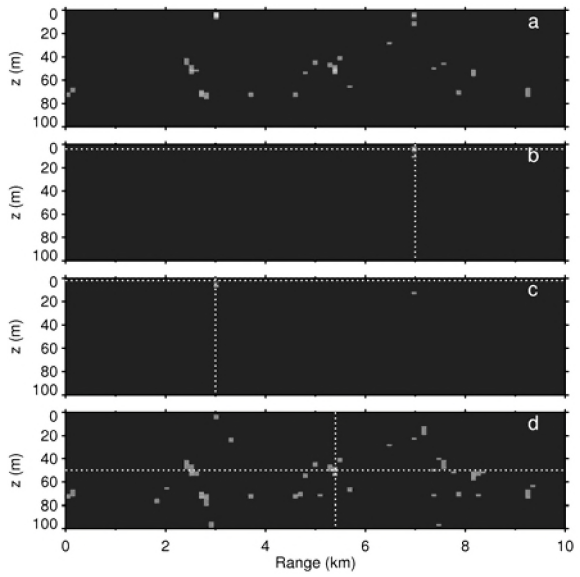


**Figure 2.** Joint marginal probability densities over source range and depth for all 3 sources (a), and individual sources (b-d). Dotted lines indicate true ranges and depths.

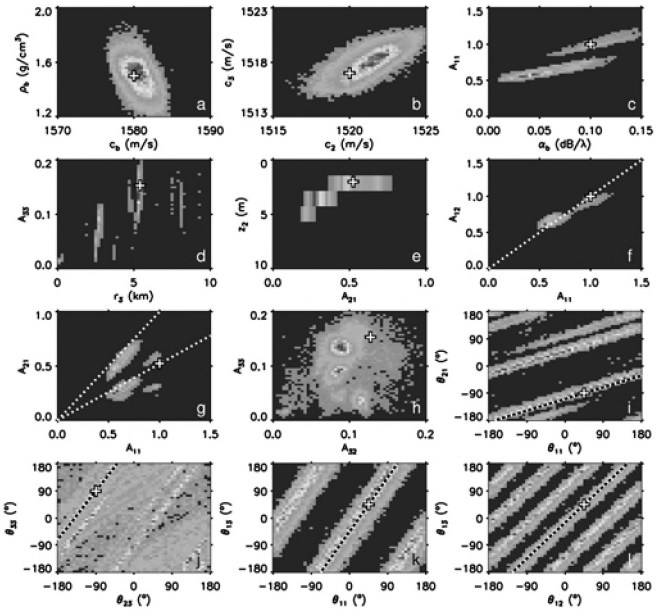

**Figure 3.** Joint marginal densities for selected geoacoustic parameters and source amplitudes and phases. Crosses indicate true values.

Fig. 3 illustrates joint marginal densities over selected environmental parameters and source amplitudes, $A_{ij}$, and phases, $\theta_{ij}$, (where $i$ indicates the source number and $j$ the frequency number). Several interesting features can be observed. For instance, Fig. 3(f) shows that the probability for the amplitude of source 1 at frequencies 1 and 2 is concentrated along the (dotted) line $A_{11} = A_{12}$, which represents the correct inter-frequency scaling. Fig. 3(g) shows that the highest probability for the amplitude of sources 1 and 2 at frequency 1 follows the correct scaling $A_{21} = 0.5A_{11}$ (lower dotted line), and virtually all probability satisfies $A_{21} < A_{11}$ (i.e., is below the upper dotted line). Amplitude relationships for the weak source 3 are less clearly defined (Fig. 3h). Fig. 3(i) and 3(j) show that the joint marginal probability for the phase of different sources at the same frequency follow a (dotted) line with slope equal to the ratio of the source ranges (with phase wraps), as can be derived from modal considerations [2]. Finally, Fig. 3(k) and 3(l) show that the joint marginal probability for the phase of the same sources at different frequencies follow a (dotted) line with slope equal to the ratio of the frequencies, which can also be derived from modal considerations [2].

## REFERENCES

[1] Dosso, S.E. and M. J. Wilmut, 2009. Comparison of focalization and marginalization for Bayesian tracking in an uncertain ocean environment, J. Acoust. Soc. Am., **125**, 717-722.

[2] Dosso, S.E. and M. J. Wilmut, 2011. Bayesian multiple-source localization in an uncertain environment, J. Acoust. Soc. Am., **129**, 3577-3589.

# BAYESIAN TRACKING OF MULTIPLE OCEAN ACOUSTIC SOURCES WITH ENVIRONMENTAL UNCERTAINTIES

**Michael J. Wilmut and Stan E. Dosso**
School of Earth and Ocean Sciences, University of Victoria, Victoria BC Canada V8W 3P6, mjwilmut@uvic.ca

## 1. OVERVIEW

This paper describes a Bayesian approach to the problem of simultaneous tracking of multiple acoustic sources in a shallow-water environment in which water-column and seabed properties are not well known [1, 2]. The Bayesian formulation is based on treating the environmental parameters, noise statistics, and locations and complex strengths (amplitudes and phases) of multiple sources as unknown random variables constrained by acoustic data formulated in terms of a likelihood function and be prior information (bounds on source speed and environmental parameters). Markov-chain Monte Carlo methods are applied to numerically sample the posterior probability density (PPD) to integrate over unknown environmental parameters in a principal-component space. Closed form maximum-likelihood expressions for source strengths and noise variance at each frequency allow these parameters to be sampled implicitly, substantially reducing the dimensionality of the inversion [3]. The result is a set of time-ordered joint marginal probability distributions for the range and depth of each source, which quantify the information content for multiple-source tracking. Optimal track estimates (with uncertainties) can be extracted from the marginal densities using the Viterbi algorithm [4].

## 2. EXAMPLE

The multiple-source tracking procedure outlined in the previous section is demonstrated here with a two-source synthetic example involving shallow and deep sources moving along similar tracks. The parameters of the ocean environment are illustrated in Fig. 1. The geoacoustic parameters include the thickness $h$ of an upper sediment layer with sound speed $c_s$, density $\rho_s$, and attenuation $\alpha_s$, overlying a semi-infinite basement with sound speed $c_b$, density $\rho_b$ and attenuation $\alpha_b$. The water-column sound speed profile is represented by four unknown sound speeds $c_1$-$c_4$ at depths of 0, 10, 50, and $D$ m, where $D$ is the water depth. All of these environmental parameters are considered to be unknown random variables with prior information consisting of uniform distributions over wide bounds representing physically reasonable limits (true parameter values and prior bounds are given in Table 1).

In the simulation, 300-Hz acoustic fields from the two moving sources are recorded at 120-s intervals for 16 minutes (i.e., 9 recordings) at a 24-sensor vertical line array (VLA) which spans the 100-m water column. (The acoustic fields are computed using a normal-mode propagation model with additive Gaussian noise.) The shallow source moves with an inward radial velocity of 7 m/s (14 kts) from 14- to 7.7-km range over the 16-minute time interval and remains at a constant depth of 4 m. The deep source moves at 8.5 m/s (17 kts) from 15- to 7.4-km range and decreases depth at a uniform rate from 80 to 64 m (a vertical velocity of 0.017 m/s). The signal-to-noise ratio (SNR) for the incoming deep source varies from 15-21 dB along the track; for the shallow source the SNR varies from 6-13 dB. In the

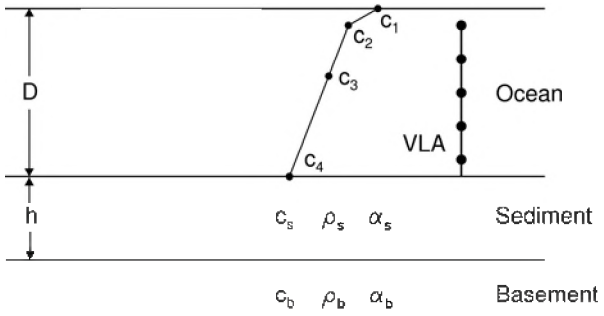


**Figure 1. Schematic diagram of the geometry of the two-source tracking problem, indicating unknown environmental parameters.**

**Table 1. True values and uniform prior bound limits for environmental parameters of the synthetic test case.**

| Parameter & Units | Value | Prior Bounds |
|---|---|---|
| *SSP:* | | |
| $D$ (m) | 100 | [98, 102] |
| $c_1$ (m/s) @ 0 m | 1520 | [1516, 1524] |
| $c_2$ (m/s) @ 10 m | 1514 | [1510, 1518] |
| $c_3$ (m/s) @ 50 m | 1509 | [1505, 1513] |
| $c_4$ (m/s) @ 130 m | 1507 | [1505, 1513] |
| *Seabed:* | | |
| $h$ (m) | 10 | [0, 30] |
| $c_s$ (m/s) | 1500 | [1450, 1600] |
| $c_b$ (m/s) | 1560 | [1500, 1650] |
| $\rho_s$ (g/cm$^3$) | 1.45 | [1.4, 2.2] |
| $\rho_b$ (g/cm$^3$) | 1.8- | [1.4, 2.2] |
| $\alpha_s$ (dB/$\lambda$) | 0.05 | [0, 1] |
| $\alpha_b$ (dB/$\lambda$) | 0.10 | [0, 1] |

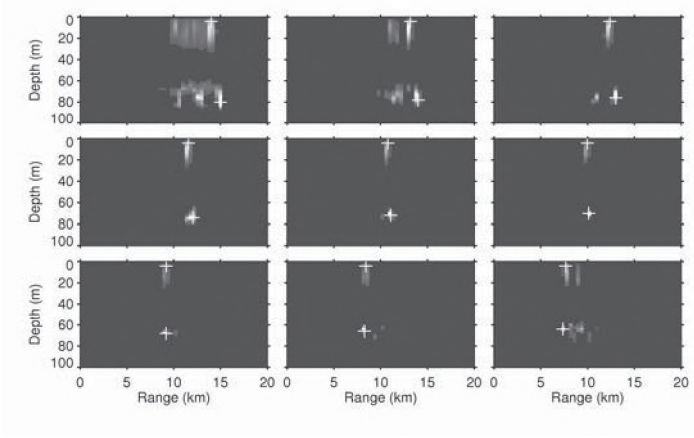


**Figure 2. Joint marginal probability densities for the two-source tracking problem (time increases from left to right, top to bottom). Crosses indicate the true track position.**

tracking inversion, the radial and vertical velocities are constrained to be less than 10 m/s and 0.0333 m/s, respectively.

Figure 2 shows the time-ordered sequence of marginal probability densities for range and depth for the two sources along the track. The two sources are generally well tracked, with range and depth uncertainties that decrease with source range (increasing SNR). At the longest ranges the marginal densities for both sources are multi-modal in range; however, the modes coalesce with decreasing range.

Figure 3 shows the optimal source location estimates along the tracks extracted from the marginal densities via the Viterbi algorithm (applying the source velocity constraints noted above). One-standard deviation uncertainties in range and depth are included as error bars. The estimated track is close to the true track for both deep and shallow sources. The largest uncertainties occur at the longest ranges, and at the track endpoints due to the fact that only one-sided velocity constraints are applied here. The mean absolute range and depth errors are 41 m and 8 m respectively for the shallow source and 18 m and 1.1 m for the deep source.

## 3. SUMMARY

This paper presented a Bayesian approach to simultaneous tracking of multiple sources in an uncertain environment. Markov-chain Monte Carlo methods are applied to integrate the PPD over environmental nuisance parameters, yielding joint marginal probability densities for source ranges and depths, from which optimal source location estimates and uncertainties can be extracted. The approach was illustrated with a synthetic example of tracking a deep submerged source in the presence of a loud interfering surface source.

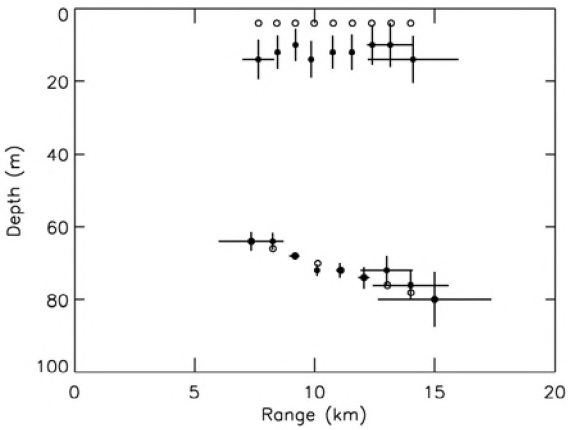


**Figure 3. Optimal source locations for the two sources computed using the Viterbi algorithm (filled circles), with one-standard deviation error bars in range and depth. True source locations are indicated by open circles.**

## REFERENCES

[1] Dosso, S. E. and M. J. Wilmut (2011). Bayesian multiple-source localization in an uncertain ocean environment, J. Acoust. Soc. Am., vol 129, 3577-3589.

[2] Dosso, S. E. and M. J. Wilmut (2007). Uncertainty estimation in simulaneous Bayesian tracking and envirnomental inversion, J. Acoust. Soc. Am., vol 124, 82-97.

[3] Dosso, S. E. and M. J. Wilmut (2011). Bayesian localization of multiple ocean acoustic sources with environmental uncertainties, Canadian Acoustics (this issue).

[4] Viterbi, A. J. (1973). Error bounds on convolutional codes and an asymptotically optimal decoding algorithm, Proc. IEEE vol. 61, 268–278.

# DEPENDENCE OF AIRBORNE SURF NOISE ON WAVE HEIGHT

**Cristina Tollefsen[1] and Brendan Byrne**
Defence Research and Development Canada – Atlantic, P. O. Box 1012, Dartmouth, NS B2Y 3Z7
[1]cristina.tollefsen@drdc-rddc.gc.ca

## 1. INTRODUCTION

Airborne noise from breaking waves is an important component of the ambient noise in coastal areas. The surf noise may mask unwanted noise arising from sources such as offshore wind turbines or naval gunfire exercises. Work is being undertaken on behalf of the Department of National Defence (DND) to determine whether naval gunfire exercises may have an impact on bird colonies, nesting areas, or other sensitive sites on land in close proximity to naval operational areas. In order to determine whether the received sound pressure level from naval gunfire is above the ambient sound level at these sites, the ambient sound level in coastal areas as a function of sea state and weather conditions needs to be understood.

Underwater noise originating from breaking waves has been well-studied (e.g., [1]); however, there are fewer published papers on the corresponding airborne noise. Bolin and Åbom [2] measured airborne surf noise in third-octave bands as a function of significant wave height in ten locations along the Baltic Sea coast. They proposed several mechanisms for sound generation, including impact noise, single oscillating bubbles, collective bubble oscillation, and bursting bubbles; they also proposed a semi-empirical sound generation-propagation model. This paper describes a similar experiment and compares the results to those of Bolin and Åbom.

## 2. METHODS

A field trial was undertaken to study the relationship among ambient noise, surf conditions, and weather. Ambient noise levels were measured beginning on 1 June 2011 at Osborne Head, Nova Scotia (44° 36.70' N, 063° 25.20' W), on a grassy cliff 6 m above a rocky beach that experiences significant wave activity, 20 m from the high water mark. (The measurements are planned to extend into late August 2011; the data presented in this paper cover the period 1 to 21 June 2011.) The instrument used was a Brüel & Kjær (B&K) 2260 Observer fitted with an outdoor measurement kit and mounted at 73 cm height, set to record linear-weighted third-octave and broadband sound pressure levels with a 125-ms ("fast") time constant over 5-minute averaging periods. The calibrated measurements recorded by the B&K sound level meter included equivalent continuous sound level ($L_{eq}$), maximum and minimum levels ($L_{max}$ and $L_{min}$), and percentiles such as the $L_{95}$ (the sound pressure level exceeded 95% of the time). In addition to the calibrated measurements, five minutes' worth of uncompressed audio data were recorded every 30 minutes by sending the calibrated output from the B&K microphone through a National Instruments NI 9234 analog-to-digital converter using a 25600-Hz sampling rate. The resulting 24-bit *.wav* files were acquired using LabView software and saved to a laptop computer.

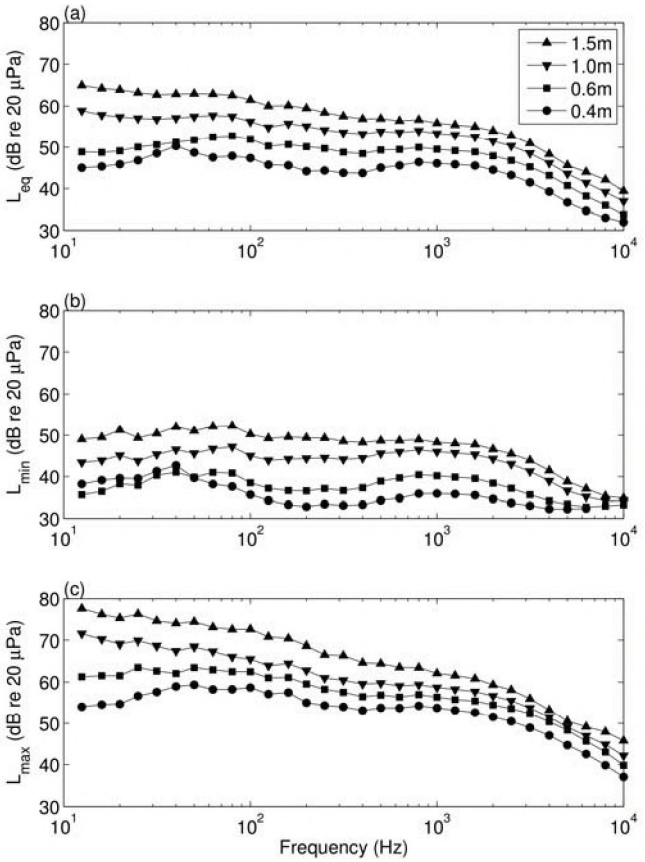


**Figure 1 (a) $L_{eq}$, (b) $L_{min}$, (c) $L_{max}$, in third-octave bands for values of significant wave height indicated in the legend.**

A self-contained Vaisala WXT 520 weather station was mounted on a pole at 10 m height to record environmental data at the site. A Teledyne RDI Acoustic Doppler Current Profiler (ADCP) was deployed 780 m SE of the measurement site, bottom-mounted in 11 m of water, in order to measure directional wave spectra. A qualitative record of breaking wave types was recorded with a camera mounted on top of a nearby building at the rate of 1 still photo every 5 minutes.

## 3. RESULTS

Figure 1(a) is a third-octave band spectrum of $L_{eq}$ for significant wave heights between 0.4 m and 1.5 m. Not surprisingly, $L_{eq}$ increases with increasing wave height at all

frequencies. The spectrum above 100 Hz for $L_{eq}$ has the same general shape for most wave heights: it remains reasonably flat (±3 dB) between 100 Hz and 1600 Hz, and it then drops off more steeply (between 5-6 dB/octave) for frequencies above 2000 Hz. Below 100 Hz, the spectral levels decrease for the 0.4-m and 0.6-m wave heights, and increase for the 1.0-m and 1.5-m wave heights.

Figure 1(b) is a plot of the third-octave band spectrum for $L_{min}$ as a function of significant wave height, and Figure 1(c) is the corresponding plot for $L_{max}$. $L_{min}$ is essentially flat below 1000 Hz for 1.5-m wave heights, and a broad peak near 1000 Hz for lower wave heights. For the 0.4-m and 0.6-m wave height, $L_{min}$ also has a second peak at 400 Hz. $L_{max}$ increases with decreasing frequency above 100 Hz for all wave heights, and shows a similar pattern to $L_{eq}$ below 100 Hz (decreasing at low frequencies for 0.4-m and 0.6-m wave height, and increasing at low frequencies for 1.0-m and 1.5-m wave height).

## 4. DISCUSSION AND CONCLUSIONS

Interestingly, the third-octave spectra in Figure 1 are rather different than the results presented in Fig. 3 of Bolin and Åbom [2]: for significant wave heights less than 1.0 m, their spectra show a distinct broad peak near 1000 Hz, with a shifting of the peak to 250-400 Hz for significant wave heights greater than 1.0 m. However, direct comparisons are difficult because it is not clear from Bolin and Åbom's paper what exactly was plotted for the third-octave spectrum. It is assumed that they were measuring the peak sound pressure level in each third-octave band because the *y*-axis in Figure 3 of their paper is labelled $L_p$ (dB). Aside from possibly measuring different quantities, the differences between the datasets likely arise because the experiment described here differed from Bolin and Åbom's experiment in two key ways. First, in this experiment, the ADCP is deployed within 1 km of the measurement site; in contrast, Bolin and Åbom used a combination of wave height data from wave buoys (30-200 km away) and a wave prediction model. Local bathymetry modifies the wave field and has a significant impact on the character of the breaking waves [3]. Second, the Osborne Head measurement site consisted of a grass-covered cliff where the microphone was placed that dropped sharply to a gravel and rock seabed and beach; in contrast, all the sites described by Bolin and Abom were gravel, rock, or sand. The noise of wind through the grass was clearly audible in the Osborne Head recordings, therefore, it is not surprising that the spectra differ, especially at lower frequencies, where grass noise can be significant [4].

In choosing the Osborne Head measurement site, the difficulties posed by the grassy cliff were not appreciated until the experiment was well underway. The 1-m tall grass had the effect of shielding the microphone from the substantial wind noise and turbulence present at the edge of the cliff, which varied significantly with height above the cliff. The choice of microphone location was guided by the desire to have measurements that are representative of the environment experienced by nesting birds, weighed against the likelihood of losing the equipment during a storm.

Considering the environment near the microphones, the spectra in Figure 1 are likely a superposition of sound originating from three sources: (a) breaking waves [1], (b) wind interacting with the grass [4], and (c) inherent turbulence in the flow [5]. The nature of breaking waves, which consist of louder "crashes" followed by "lulls" between breaking wave events, suggests that the noise spectrum observed for $L_{min}$ may be a superposition of the noise from more distant waves and the wind through the grass, whereas the observed spectrum for $L_{max}$ is likely dominated by nearby wave breaking events. Assuming 7-s period waves, the 5-minute averaging period for $L_{eq}$ would include 43 breaking wave events averaged into one quantity. The fact that the spectral levels increase at low frequencies and higher wave heights (which are associated with higher wind speeds) for $L_{eq}$ and $L_{max}$ suggests that the low-frequency component is caused by the inherent turbulence in the airflow that is observed at higher wind speeds outdoors [5].

## REFERENCES


[1] Deane, G. B. (1997) "Sound generation and air entrainment by breaking waves in the surf zone," *J. Acoust. Soc. Am.* **102** 2671-2689.

[2] Bolin, K., and Abom M. (2010) "Air-borne sound generated by sea waves," *J. Acoust. Soc. Am.* **127**, 2771-2779.

[3] Battjes, J. A. (1974) "Surf Similarity", in *Proc. of the 14th Coastal Eng. Conf.* (American Society of Civil Engineers, Copenhagen, Denmark), 466-480.

[4] Boersma, H. F. (1997) "Characterization of the natural ambient sound environment: Measurement in open agricultural grassland," *J. Acoust. Soc. Am.* **101** 2104-2110.

[5] Morgan, S., and Raspet, R. (1992) "Investigation of the mechanisms of low-frequency wind noise generation outdoors," *J. Acoust. Soc. Am.* **92** 1180-1183.


## ACKNOWLEDGEMENTS


Thanks to M. Fotheringham and D. Wile for their technical support; the Bedford Institute of Oceanography and the DND staff at Naval Electronics Systems Test Range (Atlantic) for use of their facilities. Work was funded by Formation Safety and Environment, Maritime Forces Atlantic.

# VIBRATION D'UN TRAIN LORSQUE LE SOL EST GELÉ

**Claude Chamberland et Franck Duchassin**
SNC-LAVALIN INC., Division Environnement

## 1. INTRODUCTION

La vibration causée par le passage des trains est une source potentielle de nuisance pour les résidants le long des voies ferrées. Elle peut avoir des effets sur l'intégrité de la structure des bâtiments, sur la santé à long terme des individus exposés et sur le confort au cours des activités quotidiennes. La vibration est causée par les locomotives et par la rotation des roues sur les rails. Elle est transmise aux supports des rails et se propage dans le sol vers les fondations. La prévision des niveaux de vibration se fait généralement pour un sol non gelé en considérant la distance et des ajustements pour la source, le sol et le récepteur (1). Toutefois, pour les régions nordiques, le sol gelé en hiver peut avoir un effet sur la propagation des vibrations. Selon une étude de la vibration induite par la circulation des camions et des autobus à Montréal (2), les nivaux de vibration mesurés en hiver sont environ la moitié de ceux mesurés en automne.

## 2. RELEVÉS

### 2.1 Site

Le site est situé le long d'une portion rectiligne de la voie ferrée, dans un champ non construit. La voie ferrée est légèrement surélevée et bordée par des fossés de chaque côté. Le sol est plat et constitué d'un schiste argileux recouvert de till, d'une couche d'argile de 5 à 20 m et de sable. Les relevés ont été effectués en novembre, avant que le sol soit gelé, et en février, alors que le sol était gelé. La profondeur du gel (3) peut atteindre 2,2 m dans la région.

### 2.2 Source

Les trains de marchandises étaient composés de trois locomotives et d'une centaine de wagons. Les trains circulaient dans la même direction et à des vitesses de l'ordre de 30 km/h.

### 2.3 Procédure et acquisition

La vibration dans l'axe transversal, vertical et longitudinal (T, V, L) a été mesurée simultanément à deux distances de la voie ferrée, 15 m et 45 m. Le capteur a été déposé sur le sol et maintenu en place avec une tige métallique et un sac de sable. L'axe longitudinal est perpendiculaire à la voie ferrée. La vibration a été mesurée avec des géophones triaxiaux (Instantel 714A) ayant une sensibilité de 0,006 V/mm/s de 2 à 250 Hz. Le signal a été enregistré avec des moniteurs Intantel Minimate Plus. L'onde vibratoire a été enregistrée pendant le passage qui a duré environ trois minutes. L'analyse a été effectuée avec le logiciel Blastware v10.20 d'Instantel afin de déterminer la vitesse crête de particule (PPV), la somme vectorielle des vitesses crête (PVS) et la fréquence de l'onde à la crête la plus élevée (ZCF). Le signal de vitesse de vibration a été dérivé pour obtenir l'accélération et filtré à travers un filtre passe-bas avant de faire la transformée de Fourrier (FFT) de l'onde. À partir du spectre en fréquence, le niveau de vibration par bandes de 1/3 d'octave a été calculé et l'effet de la vibration sur les humains a été évalué selon la norme ISO-2631-1 :1997 en appliquant la pondération Wk pour la perception et la pondération Wd pour les effets sur la santé.

## 3. RÉSULTATS ET ANALYSE

Les ondes de vibration mesurées à 15 m, sont présentées à la figure 1 et les niveaux de vitesse de particules sont présentés au tableau 1. Les vitesses de particules PPV et PVS sont inférieures aux valeurs guide de la norme DIN4150-3 : 1999 pour des résidences (vertical 10 mm/s, horizontal 5 mm/s). Lorsque ces valeurs sont observées, les vibrations ne devraient pas avoir d'effets défavorables sur la fonctionnalité de la structure.

Le ratio de vitesse de particule, sol gelé vs non gelé, est présenté au tableau 1. Les vibrations sont plus faibles lorsque le sol est gelé et l'atténuation est plus marquée à 15 m qu'à 45 m. Les vibrations du sol gelé sont plus atténuées dans le plan horizontal (T et L) que dans l'axe vertical (V). On note également que la fréquence de l'onde (ZFC) a diminué dans le plan horizontal, mais qu'elle a augmenté dans l'axe vertical. Ce comportement en fréquence peut possiblement expliquer que la vibration ait diminué plus fortement dans le plan horizontal. Lorsque le sol est gelé, il est plus rigide, ce qui change la réponse du sol lorsqu'il est soumis à une excitation. Si la fréquence d'excitation dans l'axe vertical s'est rapprochée d'une fréquence où la réponse est élevée, alors le niveau de vibration sera plus élevé. Par contre, si la fréquence d'excitation s'en éloigne, le niveau de vibration sera alors plus faible.

Les accélérations pondérées mesurées sont présentées au tableau 2. Les accélérations AWk sont supérieures au seuil de perception de la norme ISO-2631-1 :1997 (axe dominant 15 mm/s$^2$). Si des logements sont construits au site de mesure, il est possible que les occupants se plaignent, que le sol soit gelé ou non. Toutefois, les accélérations AWd sont inférieures à la zone de précaution santé de la norme ISO-2631-1 :1997 (3200 mm/s$^2$ pour une durée d'exposition inférieure à 10 minutes) et ne devrait pas avoir d'effets sur la santé. Le ratio d'accélération mesuré, sol gelé vs non gelé, est présenté au tableau 2. Comme pour les vitesses de particules, les vibrations sont plus faibles lorsque le sol est

gelé et l'atténuation est plus marquée à 15 m qu'à 45 m. Les vibrations du sol gelé sont plus atténuées dans le plan horizontal (T et L) que dans l'axe vertical (V). On note aussi que les atténuations sont plus grandes en accélération en pondérée ( Wd et Wk) qu'en vitesse de particule.

## 4. CONCLUSION

Les relevés effectués supportent le fait que la vibration est atténuée lorsque le sol est gelé. Les atténuations observées sont plus faibles dans l'axe vertical que dans le plan horizontal et l'atténuation est plus prononcée près de la voie ferrée. Donc, pour la prévision des vibrations du passage d'un train, lorsque le sol est gelé, il est possible de considérer que la vibration sera égale ou inférieure au niveau de vibrations lorsque le sol n'est pas gelé, sans toutefois préciser le facteur d'atténuation. Les vibrations mesurées à 15 m et 45 m, sol gelé et non gelé, sont perceptibles, mais ne devraient pas avoir d'effets défavorables sur la fonctionnalité de la structure des bâtiments, ni sur la santé des occupants.

Ces observations ont été établies à partir de relevés à un seul site et pour un seul passage de train avec le sol gelé et non gelé. Il serait pertinent de procéder à des relevés additionnels pour confirmer les tendances.

**Tableau 1 : Vitesse de particule**

| Sol | Distance (m) | PPV (mm/s) | | | ZCF (Hz) | | | PVS (mm/s) |
|---|---|---|---|---|---|---|---|---|
| | | T | V | L | T | V | L | |
| Non gelé | 15 | 4,9 | 3,8 | 3,5 | 28,0 | 9,0 | 24,0 | 5,0 |
| | 45 | 2,0 | 2,0 | 1,8 | 15,0 | 8,8 | 6,8 | 2,3 |
| Gelé | 15 | 1,0 | 2,7 | 0,8 | 6,7 | 24,0 | 6,4 | 2,7 |
| | 45 | 0,7 | 1,8 | 0,6 | 8,3 | 13,0 | 6,4 | 1,8 |
| Ratio (%) gelé vs non gelé | 15 | 20 % | 72 % | 24 % | 24 % | 267 % | 27 % | 54 % |
| | 45 | 33 % | 89 % | 33 % | 55 % | 148 % | 94 % | 80 % |

**Figure 1 : Ondes de vibration mesurées à 15 m. a) sol non gelé et b) sol gelé**

**a)**

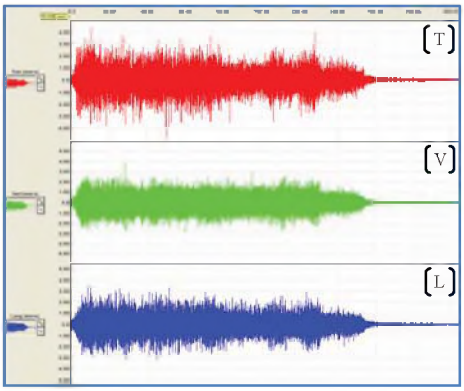


**b)**

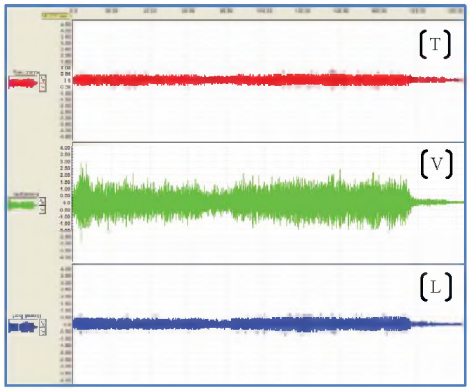


**Tableau 2 : Accélération**

| Sol | Distance (m) | A (mm/s² rms) | | | A Wk (mm/s² rms) | | | A Wd (mm/s² rms) | | |
|---|---|---|---|---|---|---|---|---|---|---|
| | | T | V | L | T | V | L | T | V | L |
| Non gelé | 15 | 132 | 99 | 114 | 53 | 47 | 46 | 10 | 9 | 9 |
| | 45 | 45 | 41 | 40 | 24 | 29 | 25 | 5 | 6 | 5 |
| Gelé | 15 | 28 | 88 | 28 | 10 | 35 | 11 | 2 | 6 | 2 |
| | 45 | 20 | 43 | 18 | 7 | 23 | 8 | 2 | 4 | 2 |
| Ratio (%) gelé vs non gelé | 15 | 22 % | 89 % | 24 % | 19 % | 76 % | 23 % | 24 % | 74 % | 26 % |
| | 45 | 44 % | 104 % | 44 % | 30 % | 79 % | 31 % | 32 % | 74 % | 33 % |

## RÉFÉRENCES


1. Federal Transit Administration (2006). *Transit Noise and Vibration Impact Assessment*
2. O. Hunaidi, M. Tremblay, NRC (1997). *Traffic-induced building vibration in Montréal*, Can. J. Civ. Eng. 24: 736-753 (1997)
3. *BNQ 1809-300/2004 (R2007), Travaux de construction – Clauses techniques générales –Conduites d,eau potable et d'égout* (Bureau de normalisation du Québec)
4. ISO-2631-1 (1997). *Vibrations et chocs mécaniques – Évaluation de l'exposition des individus à des vibrations globales du corps – Partie 1 : Spécifications générales* (Organisation internationale de normalisation)
5. DIN4150-3 (1999). *Structural vibration – Part 3 : Effects of vibrations on stuctures* (Deutsches Institut für Normung)

# A LOW COST WIRELESS ACQUISITION SYSTEM FOR MULTI-CHANNEL VIBRATION MEASUREMENT

**Pierre Marcotte[1], Sylvain Ouellette[2], Jérôme Boutin[1], and Gilles LeBlanc[2]**
[1] IRSST, 505 boul. de Maisonneuve West, Montréal, QC, Canada, H3A 3C2, marcotte.pierre@irsst.qc.ca
[2] CANMET Mining and Mineral Sciences Laboratories, 1 Peter Ferderber, P.O. Box 1300, Val-d'Or, QC, Canada, J9P 4P8

## 1. INTRODUCTION

In order to perform multi-channel time signal acquisition in harsh environments like underground mines, where there is a high risk of having the equipment damaged or destroyed, it is convenient to use a robust low cost system that allows remote control and monitoring. Such a system, with at least 6 input channels, was not available on the market at the time it was needed to perform a study on human vibration in underground mines. Thus, an acquisition system based on *National Instrument* NI-9234 boards and *LabVIEW*™ has been developed and successfully tested in underground mines for human vibration assessment, and will be presented in this paper.

## 2. METHODS

The acquisition system was built using two *National Instrument* NI-9234 USB boards (IEPE, 24 bits), giving a total of 8 channels, an external LI-ION battery, one minicomputer with solid-state hard disk for added robustness, and a small waterproof *Pelican*™ case. Pictures of the acquisition system are shown in Figure 1. The system had to be very compact in order to be installed on certain equipment where the space is very limited (see Fig. 1b). The acquisition process was implemented under *LabVIEW*™, with two different sampling rates for hand-arm (5120 Hz) and whole-body vibration (512 Hz). Using the "*Remote desktop*" function of *Windows XP*®, a second laptop computer was used to wirelessly control and monitor (time signals and spectra) the acquisition process.

The IEPE mode of the NI-9234 boards was used to supply electrical power to the accelerometers, requiring the use of AC coupling. Since the NI-9234 board has, in AC coupling, a roll-off of 3 dB at 0.5 Hz, a digital FIR filter was added to correct the low frequency response in whole-body vibration (WBV) measurement mode, in order to satisfy the newer standard ISO 8041 (2005). In addition, Notini et al. (2006) have shown that low frequency components can have a significant effect on WBV metrics. The digital FIR filter coefficients for the sampling rate of 512 Hz were calculated using the FIR2 function of *MATLAB*®. The target frequency response of the filter was the measured compensation needed to achieve a flat response in the entire frequency range. In practice, compensation was only needed between 0 and 6.3 Hz. A total of 2000 coefficients were used for the FIR filter. Having a linear phase, the FIR filter resulted in a time delay of 2 seconds, and thus it was possible to implement the filter in real time during the acquisition of the vibration signals.

**(a)**

**(b)**

**Figure 1. Acquisition system: (a) without the mini Laptop to show the components; (b) with a triaxial accelerometer installed on a "muck machine".**

## 3. RESULTS

### 3.1 System validation

The acquisition system was validated using a function generator to generate a swept sine of 4.5 V peak amplitude, using a logarithmic sweep between 0.1 and 5000 Hz over a period of 180 seconds. Figure 2 shows the differences, in dB, between the reference signal magnitude and the signal as measured by the acquisition system for the first 6 channels in "hand-arm" and "whole-body" acquisition modes. The results are presented in one-third octave bands between 0.8 and 2000 Hz for hand-arm vibration (HAV) and between 0.1 and 200 Hz for WBV. The allowed

tolerances of ISO 8041 (2005) standard for HAV and WBV are also presented in these figures. For the WBV mode, the low frequencies are compensated by a FIR filter, as described previously. It is noted that the acquisition system completely satisfies the ISO 8041 standard tolerances.

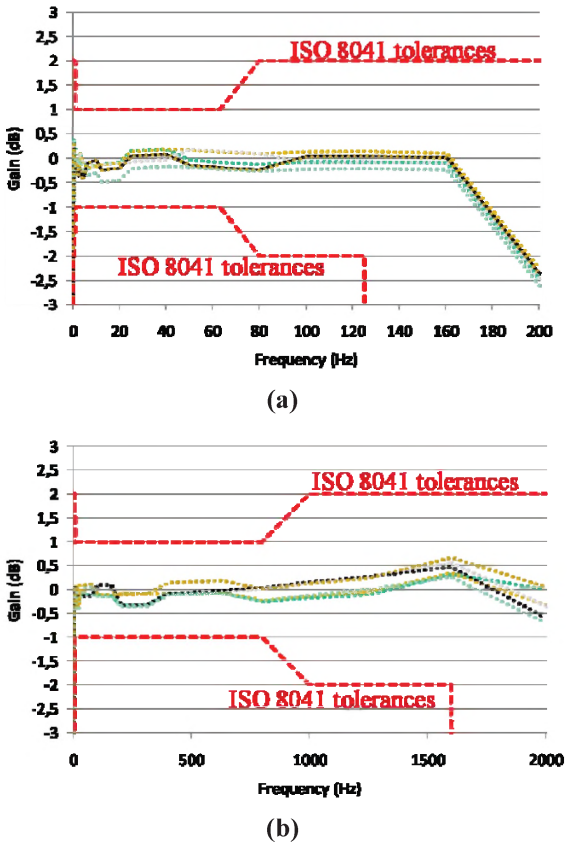


**Figure 2. Differences between reference signal and acquisition system for first 6 channels: (a) WBV; (b) HAV.**

Frequency weightings ISO 5349-1 (2001) for HAV and ISO 2631-1 (1997) for WBV were applied in postprocessing on the recorded accelerations time signals. The weightings were applied using the *LabVIEW*™ "*Sound and Vibration*" module. It is also possible to implement these weightings directly using digital FIR or IIR filters (Rimell and Mansfield, 2007). Then, from the weighted accelerations, vibration exposure values such as the weighted rms acceleration ($a_w$) and the vibration dose value (VDV) for WBV were calculated.

### 3.2 Application example and artefacts detection

The acquisition system was used to measure vibration levels of 28 different mining equipments operating in 8 underground mines located in Quebec. Figure 3 shows an example of measured acceleration on a "CAVO" (similar to the "muck machine" shown in figure 1b). The measurement was performed on the "CAVO" floor (where the operator is standing) in the $x_h$-axis direction, as defined in ISO 2631-1 (1997). The signal clearly shows some DC shift, even if the measurement was carried out with an accelerometer of relatively high capacity (500 g or 5000 m/s$^2$) for WBV. Usually, DC shift occurs with impact hand-held power tools while assessing HAV. Since DC shift does not necessarily produce saturation of the signal, it can be difficult to detect it without having the time signal. As recommended by the ISO 5349-2 (2001) standard for HAV, measurements containing DC shift were not considered for WBV assessment.

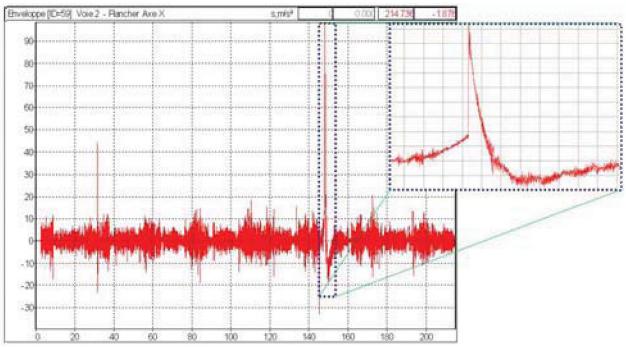

**Figure 3. Time signal showing an example of DC shift.**

## 4. CONCLUSION

A low cost acquisition system has been developed, validated and successfully used to assess human vibration in different underground mines. Acquisition of the time signal allowed the detection of DC shift artefacts.

## REFERENCES


ISO 2631-1 (1997), *Mechanical vibration and shocks – Evaluation of human exposure to whole-body vibration – Part 1: General requirements* (International Organization for Standardization, Geneva, Switzerland).

ISO 5349-1 (2001), *Mechanical vibration and shocks – Measurement and evaluation of human exposure to hand-arm vibration – Part 1: General requirements* (International Organization for Standardization, Geneva, Switzerland).

ISO 5349-2 (2001), *Mechanical vibration and shocks – Measurement and evaluation of human exposure to hand-arm vibration – Part 1: Practical guidance for measurement at the workplace* (International Organization for Standardization, Geneva, Switzerland).

ISO 8041 (2005), *Human response to vibration – Measuring instrumentation* (International Organization for Standardization, Geneva, Switzerland).

Notini, L., Mansfield, N.J., and Newell G.S. (2006), An assessment of the contribution of earth moving machine WBV components below 1 Hz to ISO 2631-1 and ISO 2631-5 metrics, in *Proceedings of the 41st UK group meeting on human response to vibration* (Farnborough, Hampshire, England, 20-22 September 2006).

Rimell A.N., Mansfield N.J. (2007), Design of digital filters for frequency weightings required for risk assessments of workers exposed to vibration. Industrial Health, 45: 512-519.

# APPLICATION OF MODAL ASSURANCE CRITERION ON METALLIC AND COMPOSITE STRUCTURES

**Raef Cherif[1], C.K. Amedin[1], and N. Atalla[1]**
[1]Dept. of Mechanical Engineering, Université de Sherbrooke, Sherbrooke, QC, Canada, J1K2R1, raef.cherif@usherbrooke.ca

## 1. INTRODUCTION

This paper presents the use of the Modal Assurance Criterion (MAC) for the purpose of spatially comparing mode shapes to identify differences in the degrees of freedom between test and analysis modes. In modal analysis, direct use of experimental results may include errors due to measurements limitations, for example modes duplications. Before using experimental data for analytical operations, it is essential to validate first experimental test results through correlation with FEM models [1]. The MAC methodology can be used to check this correlation. This article begins with an overview of methods used in test and analysis for correlation Next, MAC is evaluated using simple metallic beams and plates in various mounting (boundary) conditions. Finally, further experimental investigations using composite sandwich-composite panels are presented to demonstrate the practicality of this algorithm for real life applications.

### 1.1. Test and analysis using correlation [1]

Most popular applications of modal testing provide direct comparisons of deformed modal shapes between analytical and experimental findings. The responses of modal testing are measured at a number of sensors, which allow visualization of the measured motion. Visualization is key for a proper quality assessment of an experimental result. To do this effectively, several steps must be followed.

A. Topology correlation [2]:

Analysis performed using the Finite Element method gives predictions at DOFs {q} of the FEM model. FEM predictions and measurements {y} are not directly comparable. Thus the first step of correlation, called topology correlation, consists in building a function allowing prediction of FEM responses at sensors. In most applications, DOFs and responses are linearly related with an observation matrix [c], so that an observation equation can be written in the form [2]:

$$\{y(t)\} = [c]\ \{q(t)\}$$

B. Correlating shapes known at sensors

Before performing any operation to assess the quality of the analytical model, it is paramount that a correspondence be established between the analytical and experimental methods. The approximation of modal frequencies is sufficient evidence to do this, but a comparison of deformed modal shapes is recommended for further validation between analytical and experimental findings. The Modal Assurance Criterion can be used in this goal.

Modal Assurance Criterion (MAC):

A quantifiable correlation between experimental and analytical mode shapes can be determined based on the Modal Assurance Criteria (MAC) [3]. For two shapes U, V defined on the same sensors, the MAC is the correlation coefficient between the two vectors.

$$\mathrm{MAC}(U,V) = \frac{\left|\{U\}^T\{V\}\right|^2}{\left|\left(\{U\}^T\{U\}\right)\left(\{V\}^T\{V\}\right)\right|}$$

A perfect correlation between two modes gives a MAC result equal to 100%. An example definition of MAC correlations is provided in Table.1 below:

**Table 1: MAC correlations**

| | |
|---|---|
| 100 %≤ MAC≤ 90% | Correlated modes |
| 90 %≤ MAC≤ 70% | Doubtful correlation |
| 10 %≤ MAC≤ 70% | Uncorrelated modes |
| MAC=10% | Modes are nearly orthogonal |

## 2. MEASUREMENT SETUP

In Figure 1, the measurement setup to measure mode shapes and frequency response functions (FRFs) of simple metallic beams, plates and sandwich-composite panels in various mounting (boundary) conditions using a Laser Doppler Vibrometer (LDV - Polytec PDV-100) is shown. A shaker (B&K type 4810) was used for vibration excitation. In the experiment an initial "FFT" acquisition was performed to obtain FRFs using a periodic white noise excitation. This provided natural frequency determination by finding local maxima in an averaged FRF graph. Responses were measured at a number of sensors, which had a spatial distribution allowing a visualization of the measured motion

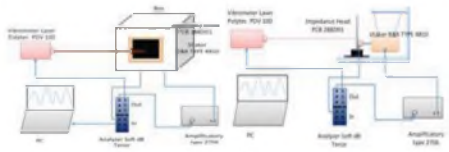

**Figure 1: Measurement Setup for measuring mode shapes and frequency response functions (FRFs) of simple metallic beams, plates, and sandwich-composite panel in various boundary conditions.**

## 3. RESULTS

An aluminum beam has been tested in clamped free condition by the setup mentioned above. Figure 2 presents the device for testing the aluminum beam.

**Figure 2: bench tests**

The MAC was applied. Figure 3 presents the Modal assurance criterion of the aluminum beam.

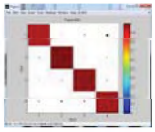

**Figure 3: Modal assurance criterion of the aluminum beam**

Table 3 presents a comparison between the modal shapes of the first four flexible modes, calculated and measured by SDtools.

**Table. 2: modal shapes**

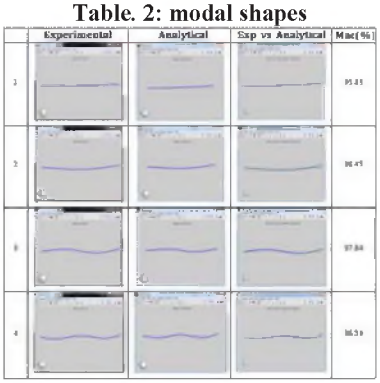


A steel plate was also tested in both free-free and clamped conditions using the setup mentioned above.
Figure 4 presents the device for measuring the steel plate

**Figure 4: Bench tests**

Table 4 presents the MAC value between the modal shapes of the first four flexible modes, calculated and measured by SDtools

**Table 4: MAC Value**

| MAC (%) Free Free | MAC (%) Clamped |
|---|---|
| 92.05 | 99.22 |
| 92.97 | 86.61 |
| 88.84 | 85.68 |
| 85.54 | 91.81 |

Finally a composite-sandwich panel was tested with clamped boundary conditions using the same experimental setup as mentioned above. Figure 4 presents the device for measuring the composite sandwich panel. Figure 5 shows the frequency response functions (FRFs) of the sandwich-composite panel identified by SDtools.

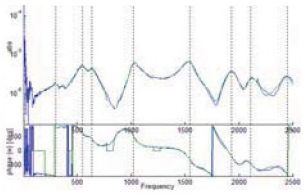

**Figure 5: Frequency response functions (FRFs) of the sandwich-composite panel**

Figure 5 shows a parasite frequency at 350Hz and 500Hz. These frequencies can be caused by the effect of the interaction between the cabin and the plate. To ensure the identified modes, MAC was used as a verification technique. Table 5 presents a comparison between the modal shapes of the first four flexible modes of the plate reference EDEC using analytical (Artec) and experimental (SDTools) techniques.

**Table 5: modal shapes**

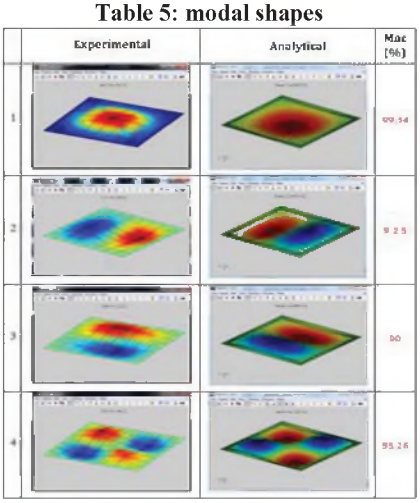


## 4. DISCUSSION AND CONCLUSIONS

The MAC methodology was evaluated on simple metallic beams, plates and sandwich-composite panels. MAC was verified on real measured data, which lead to the necessity of this algorithm for real life applications especially for sandwich-composite structures. Finally MAC overcame some of the limitations of experimental measurement such as mode duplication.

## REFERENCES

[1] A. Chouaki, P. Ladeveze, and L. Proslier, "Updating Structural Dynamic Models with Emphasis on the Damping Properties," AIAA Journal, vol. 36, pp. 1094–1099, June 1998.

[2] E.Balmes."Orthogonal maximum sequence sensor placements algorithms for modal tests, expansion and visibility," IMAC, January 2005.

[3] R. Allemang and D. Brown, \A correlation coeffcient for modal vector analysis," International Modal Analysis Conference, 1982.

# Abstracts for Presentations without Proceedings Paper
# Résumés des communications sans article

## Acoustical Materials / Matériaux Acoustiques

**Thermo-acoustic Investigations of Molecular Interactions in Polymer Solutions of HTPB+Chlorobenzene**
D.P. Singh & Arun Upmanyu

Thermo-acoustic investigations of polymer solutions of Hydroxyl-terminated polybutadiene (HTPB) and Chlorobenzene, in the temperature range of 303 K to 323 K, have been done using ultrasonic velocity and density data taken from literature. Various acoustical parameters such as molar sound velocity, molar adiabatic compressibility, acoustic impedance, van der Waal's constants, free volume, internal pressure, and cohesive energy have been determined. A large number of thermo-dynamical parameters such as available volume, geometrical volume, space filling factor, intermolecular free length, relative association, surface tension, refractive index, molar refraction, pseudo-Gruneisen parameter and Debye temperature have been evaluated. Schaaff's Collision Factor Theory, Nomoto's relation, Vandeal-Vangeel relation, Impedance dependent relation and Ideal mixing relation have been used to predict the values of ultrasonic velocities in the systems under study, within the temperature range 303 K – 323 K. The obtained results have been compared with the experimental results as available in literature. Several Excess parameters e.g. Excess Adiabatic Compressibility (KSE), Excess Isothermal Compressibility (KTE), Excess Intermolecular Free Length (LfE), Excess free volume (VfE), Excess Internal Pressure (PiE), Excess Wada's Constant (WE), Excess Rao's Constant (RE) and Excess pseudo-Gruneisen parameter (ΓE), have also been evaluated at several compositions of the polymer solutions in the temperature range under investigation. The variations of thermo-acoustic parameters of the polymer solution provide a deep insight into the nature, type and strength of intermolecular interactions prevalent in it. The non-ideal behaviour of the solution has been explained in terms of the composition and temperature dependence of its acoustical and thermo-dynamical parameters.

## Aeroacoustics / Aéroacoustique

**Scaling of jet noise spectra measurement vs predictions**
Werner Richarz

It now widely accepted that subsonic jet noise has at least two distinct spectral components: one due to 'small scale turbulence' the other from 'large structures'. The former, sometimes called self noise, is prevalent at 90o to the jet axis while latter appears to dominate near the jet axis. Ribner's self and shear noise theory has similar features, although the source terms are more general. Recent work by Richarz (AIAA Paper 2011-2924) has revealed that Ribner's formalism must be revised, in order to bring it back in line with measured data. This paper describes the results of applying a more general methodology for separating the self noise and thereby determining the other spectrum component. The scaling of the extracted spectra is compared with scaling predicted by several jet noise theories.

**Numerical prediction of the vibroacoustics of sandwich panels with add-on damping**
Imen Rzig, Amedin Kafui Amedin & Noureddine Atalla

This paper discusses the numerical modeling of the vibroacoustics response of sandwich-composite panels with add-on damping under various excitations: Point load, Diffuse acoustics field and Turbulent Boundary layer excitation. The studied damping is of the form of a viscoelastic layer located within the panel. A modal synthesis approach is used for the calculation of the structural response and the Rayleigh's integral is used for the acoustic response (the panel is assumed flat and baffled). Since the panel has a viscoelastic core, a methodology is presented to handle efficiently the modeling of the frequency depended properties of the viscoelastic layer. A direct frequency response is used to validate the proposed approach. Next, a parameters study on the effect of the Viscoelastic layer location is presented, In particular, three locations are compared: within the Honeycomb core, within the skins and added to the skin with a constraining layer. The effects of the excitation type on the vibration and acoustic response are also discussed.

## Bioacoustics / Bioacoustique

**Insect sound generators: cuticular shapes and forms in katydids**
Glenn Morris

The cuticle of insects (exoskeleton) is often modified to generate sound by rubbing. Insects stridulate with diverse body parts, but commonly among crickets and katydids, left forewing upon right. The form of acoustically modified wing cuticle differs when it serves as a radiator, as a baffle or for elastic storage of energy (i.e., as a spring to enhance movement). Radiating cuticle is extremely thin, relatively stiff and transparent; costal regions serving to baffle doublet sources are thick, flaccid and opaque; elastomeric proteins such as resilin can aid highspeed contact of generator parts and resilin's location and shape within the exoskeleton can be detected via fluorescence. The comparative method gives insight into biological function. At a level of organization above cuticle one can compare the sound- generating organs of different insect species, revealing cuticular forms that suggest novel ways of making sound. A common generator form in katydids combines brachyptery (shortened wings used only for stridulation), a posterior-produced pronotal metazona acting as a sound deflector or source of secondary radiation, together with a return to bilateral symmetry of the tegmina. In some species pronotal trends result in a complete chamber enclosing the sound-radiating speculae of the wings from above. The air thus loaded above the radiating wing cells acts in a fashion not well understood: laser vibrometry of the pronotal chamber of one species reveals a spectral band in the high audio range; removing the chamber acts to broaden this band.

## Education in Acoustics / Enseignement de l'acoustique

**Intégration de l'acoustique dans l'apprentissage de l'architecture**
Jean-Philippe Migneron

La pratique de l'architecture correspond à la construction de bâtiments pour répondre adéquatement aux besoins de leurs occupants, ce qui inclut plusieurs aspects. Parmi les performances souhaitées, on compte les critères acoustiques. Ceux-ci influencent directement le confort des gens et les communications qu'ils peuvent échanger. Même si l'acoustique architecturale est omniprésente, son importance est très variable et elle demeure souvent un élément négligé par les concepteurs. À l'École d'architecture de l'Université Laval, l'étude de l'acoustique fait partie des apprentissages optionnels depuis de nombreuses années. Les étudiants peuvent suivre un cours théorique avec des travaux pratiques en laboratoire ou compléter un projet dans le cadre de l'atelier d'ambiances physiques. Cette présentation vise à décrire et comparer ces deux modes d'enseignements dans le contexte propre à la formation en architecture.

**La 'biodiversité' en acoustique**
Annie Ross

Le but de cet article est de considérer la qualité et l'efficacité des communications au sein de la communauté acousticienne. Il s'agit plutôt d'une réflexion que d'une recherche scientifique fondamentale. L'acoustique est un domaine de spécialisation à la fois pointu et transversal. Il existe une grande diversité d'individus qui s'y intéressent. D'une part, les forums spécialisés rassemblent des chercheurs et praticiens dont la provenance est extrêmement variée, de l'ingénieur mécanicien expert en réduction de bruit au luthier expert en qualité sonore des instruments, en passant par le psychoéducateur, l'audiologiste et autre bioacousticien. D'autre part, le domaine compte de nombreux amateurs en sonorisation et une multitude de passants tels le mélomane ou le citoyen ennuyé par un bruit environnemental. Dans un tel contexte, où les objectifs professionnels ou personnels des uns et des autres sont si variés, comment peut-on assurer, dans les formations collégiales et universitaires, le développement d'une saine communication entre les divers groupes intéressés ? Il y a certes un vocabulaire commun qui réunit les professionnels du domaine, mais ce vocabulaire est méconnu du public, ce qui peut nuire à la dissémination de la connaissance. De plus, les cultures professionnelle, les outils et les méthodes de travail de l'ingénieur, du musicien ou du psychologue peuvent être assez distinctes l'une de l'autre. Conséquemment, il y a lieu de transmettre dans les diverses formations une plateforme commune de connaissances et d'indicateurs qui puisse permettre aux gens de toutes disciplines de collaborer efficacement pour l'avancement de l'acoustique.

**Enseignement en ligne de l'acoustique pour les nouveaux étudiants en audiologie et orthophonie à l'Université d'Ottawa**
Christian Giguère, Elizabeth Campbell Brown & Daniel Dostie

La majorité des étudiants qui font demande d'admission à la maîtrise en audiologie ou en orthophonie à l'Université d'Ottawa possèdent une formation en linguistique, psychologie, éducation ou autre domaine d'études pour lequel l'acoustique ne fait pas

partie intégrante du curriculum. Or, ces futurs cliniciens feront face presque quotidiennement à des situations demandant une bonne connaissance du son et des systèmes électroacoustiques, par exemple lors de l'ajustement des prothèses auditives ou de l'évaluation instrumentale de la qualité de la voix. Tous les programmes canadiens de 2e cycle en audiologie ou orthophonie exigent un cours préalable en acoustique avant l'admission. Ces cours ne sont pas faciles accessibles, et lorsqu'offerts, ils s'adressent généralement à une clientèle en physique ou en génie. Pendant plusieurs années, l'Université d'Ottawa a offert une cours d'été en acoustique d'une durée de 6 semaines sous forme face-à-face en salle de classe pour permettre aux candidats de compléter ce préalable avant la rentrée de septembre. Toutefois, en raison de la distribution géographique pancanadienne des nouveaux étudiants en audiologie ou orthophonie, cette méthode d'apprentissage occasionnait des frais de déplacement et d'hébergement pour plusieurs étudiants ainsi qu'une perte potentielle de revenus en travail d'été. Depuis 2009, le cours est offert entièrement en ligne à l'aide d'outils généraux d'enseignement à distance (p. ex. Blackboard ™, Bridgit ™) et la mise au point de matériel spécialisé en acoustique (p. ex. vidéos de démonstration, animations, figures) produit en français dans le contexte de l'audiologie et de l'orthophonie. Cette présentation vise à partager l'expérience tirée par ce projet d'enseignement.

**L'enseignement de l'acoustique à l'intention des musiciens à la Faculté de musique de l'Université de Montréal**
Caroline Traube

C'est en 1953 que Jean Papineau-Couture met sur pied le premier cours d'acoustique musicale donné à la Faculté de musique de l'Université de Montréal. À l'époque, le compositeur faisait figure de pionnier, considérant l'acoustique comme matière essentielle dans le parcours académique de tout musicien. Par la suite, l'enseignement de l'acoustique musicale, pris en charge par Louise Gariépy dès 1970, est devenu le socle de la formation en composition électroacoustique, un programme novateur développé par la compositrice Marcelle Deschênes. Un ensemble de cours reliés au domaine de l'acoustique musicale (psychoacoustique, organologie, traitement du signal audionumérique, etc.) s'intègre maintenant à différents programmes de 1er cycle, autant en composition, interprétation qu'en musicologie, et plus récemment dans le cadre du nouveau programme de mineure/majeure « Musiques numériques ». Alors que le cours d'introduction à l'acoustique musicale constitue la porte d'entrée à tous les cours qui touchent aux sciences et technologies de la musique, les cours plus avancés (psychoacoustique, organologie et acoustique instrumentale, techniques d'enregistrement, etc.) sont pour les étudiants l'occasion de mener des projets de création et de recherche (projets individuels ou en équipe) en lien direct avec la pratique musicale et de répondre à des questions qu'ils se posent comme musiciens : les phénomènes acoustiques reliés aux différents modes de jeu d'un instrument, la perception du timbre instrumental, l'acoustique de la voix chantée, la synthèse et le traitement des sons, etc. Certains étudiants poursuivent d'ailleurs leurs recherches aux cycles supérieurs et aboutissent à des projets interdisciplinaires et originaux.

## Environmental Noise / Bruit environnemental

**Operative Tests of a Landing and Take-Off Time Marker as a Means of Improving Noise Measurements and Modeling**
R.D. Tommasi

When measuring noise from aircraft in the vicinity of airports, the major source of uncertainty is by far the unavailability of reliable time markers to assess the precise timing of the aircraft movement so that noises unrelated to airport activities could be eliminated. It is a fact that spectrum- and envelope-based filters alone cannot provide a complete matching, and a more precise time synchronization is needed. This can be provided for example by the radar tracks. These are however not available for the vast majority of smaller airports, therefore various methods have been developed in the last several years. In this paper we present a discussion and results of on-field tests of a device that is specifically designed as an aid for acoustical measurements. In fact the tested unit records take off, landing and taxiing movements of aircrafts, providing a real-time feedback to the acoustical consultant. The dataset is completed by metadata like direction, speed and height above ground as well as captured pictures of the event. This information can be used for automatic identification of noise signatures recorded by sound level meters (SLMs), thus eliminating extraneous sources and providing a much more accurate assessment of the noise levels due to airport's activities. Leveraging the metadata, especially the direction and speed information, it is possible to use a single apparatus to cover the whole SLM network, improving the accuracy in A-weighted level by more than 5 dB in comparison to the basic threshold method, as shown by the presented charts and tables. For larger facilities, a network of interconnected units can be deployed, and the output data can be also used by the airport management for improving the administrative flow.

## Hearing Sciences / Sciences de l'audition

**Comparison of tonal, multi-tonal and broadband backup alarms on psychoacoustic measures**
Chantal Laroche, Christian Giguère, Véronique Vaillancourt, Pascal Laferrière & Hugues Nélisse

Despite the use of audible backup alarms on heavy vehicles to alert nearby workers during reversing manoeuvres, serious and sometimes fatal accidents occur each year. To improve workplace safety and reduce annoyance in the vicinity of industrial and construction settings, a new alarm signal, the broadband (BBS) alarm was proposed in the United Kingdom. Theoretically, the advantages of the BBS over traditional alarms are convincing, although few studies have demonstrated them empirically. In the current study, twenty-four subjects with normal hearing took part in laboratory measures of psychoacoustic metrics (detection thresholds, equal loudness judgments and perceived urgency ratings) and spatial localization tasks, both with and without hearing protection devices (HPDs), in background noises measured in the field and played back in a noise simulation room, using the broadband alarm, a multi-tonal alarm and a more traditional tonal alarm. While the broadband signal seems to present some advantages over conventional single-tone alarms, such as lower sound pressure levels to meet the requirements of a signal to noise (S/N) ratio of at least 0 dB set forth in ISO 9533, higher urgency ratings at high S/N ratios without protection devices and better sound localization performance, some disadvantages are also noted. Higher S/N ratios are required to detect the broadband alarm, at least in noises rich in high-frequency content. Moreover, detection thresholds and urgency ratings appear to be more severely affected by the use of HPDs for the broadband alarm than the tonal alarm. Results are discussed from a work safety standpoint.

## Musical Acoustics / Acoustique musicale

**The physics and psychophysics of musical instruments ... from the performer's perspective**
Caroline Traube

## Speech Communication / Communication par la parole

**The perception of syntactic disambiguation in infant-directed speech**
Suzanne Curtin & Stephen Winters

It is known that infant-directed speech is more intelligible than adult-directed speech. But is it also less ambiguous? We recorded speakers reading a series of short, illustrated children's stories to both infants and adults. Each children's story ended in a syntactically ambiguous phrase that was depicted in a drawing. For example, a phrase like "the giant hands over the candy" was read either as a noun phrase or as a complete sentence, depending on its story context. These phrases were then excised from the recordings and presented to adult listeners, who were asked to identify (1) whether they had been read to infants or to adults, and (2) whether they were noun phrases or complete sentences. Results showed that listeners were able to reliably distinguish between infant-directed and adult-directed utterances. The listeners were also able to better distinguish between the two syntactic types of phrases when they heard infant-directed utterances, as opposed to adult-directed utterances. This finding suggests that there are prosodic cues in infant-directed speech which may assist infants in their syntactic interpretation of speech, and also guide them in the acquisition of the syntactic structures of their native language.

**Cross-dialectal analysis of vowel production in Cuban and Peninsular Spanish**
Irina Marinescu

This study provides acoustic descriptions of vowels in two understudied local varieties in Spain (PS) and Cuba (CS), by comparing normalized vowel locations in the F1xF2 space, distances from point vowels to centroids, variability patterns and durations. Cross-dialectal differences are predicted. H1 – vowel location: back vowels are more fronted in PS than in CS. H2 – vowel dispersion: different distances from point vowels to centroids signal more dispersion towards front in PS and towards back in CS. H3 – variability patterns: Cross-dialectal differences in standard deviations for F1 and F2 are predicted: less variability for PS front vowels and less variability for CS back vowels. H4 – duration: Vowels are shorter in PS than in CS. Speech samples were obtained from 40 participants (21 PS and 19 CS) through a reading task. 800+ vowels in bilabial context were extracted; vowel durations and F0-F3 were measured. Formants were normalized using Lobanov's (1971) transformation. Several ANOVAs revealed significant results as follows: Vowel locations: [i] is higher and more fronted and [o] is more fronted in PS. Vowel dispersion: /i/-C distance is greater in PS. Variability: Along F1, there is more variability for PS vowels, but along F2, there is less variability in PS for /i, e/ and more variability for /a, o/ in PS as compared to CS. Duration: [e, a, o] are shorter in PS. This study contributed data on Cuban Spanish and corroborated previous reports on Peninsular Spanish. Cross-dialectal

differences are discussed as a potential source of differences in L2 perception and production.

**The acoustic and articulatory qualities of Cape Breton 'slit-t'**
Matthew Gardner

This paper investigates acoustic and articulatory similarities and differences between the non-standard fricative realization of word-final /t/ and other voiceless coronal sounds in Cape Breton English. The 'slit-t' of other Irish/Irish-English influenced dialects has been described as a "voiceless alveolar slit fricative" (Wells, 1982: 429), a "voiceless apico-alveolar fricative" (Hickey, 1984: 234, 246) and an "apical alveolar fricative formed with a broad central channel" (Pendeli et al., 1997: 68). It has been reported using up to 15 different IPA transcriptions (Pendeli et al., 1996: 69). An acoustic analysis using static paleography and one local dialect speaker suggests that 'slit-t' in Cape Breton is similar to that of Liverpool, UK (Pendeli et al., 1996) in that it is also apical, aveolar – rather than dental like /θ/ – and formed with a broader central channel than /s/ or /ʃ/. An acoustic analysis using data from six speakers from the Cape Breton Regional Municipality Corpus (Gardner, 2010) found that 'slit-t' had a significantly shorter mean duration than /s/ but not a significantly different duration from /ʃ/ or /θ/ – contrary to findings presented by Pandeli et al (1996), Sangster (2001) and Jones & Llamas (2008). Jones & Llamas (2008) and Jones & McDougall (2010) find that, spectrally, 'slit-t' is generally more like /ʃ/ than /s/. Analysis of centre of gravity, deviation, skewness, kurtosis, and central peak frequency in this data suggests that in Cape Breton 'slit-t' is neither more like /s/ or /ʃ/, but firmly somewhere in between.

**Neutralization in Wakashan 'hardening' contexts**
Fiona Campbell

Certain affixes in Wakashan languages condition a change in the final consonant of a stem, causing an underlying 'plain' stop, affricate, nasal consonant, or glide to be perceived as ejective/glottalized. For example, in Haisla a regular suffix with the root bəkʷ- does not affect the final consonant (e.g. bəkʷ-ai 'body, self'; bəkʷ-əlusəmi 'character'), but a 'hardening' suffix generally does (e.g. bək'ʷ-əs 'sasquatch'; bək'ʷ-ala 'speak, talk') (examples from Bach, 1990). These languages have a full series of underlying glottalized consonants as well, and the present study investigates whether or not there are phonetic differences between glottalized consonants which arise through affixation and their underlyingly present counterparts. Temporal and spectral cues for 'hardened' consonants were compared with those of underlying ejectives and plain stop consonants for both oral and nasal stops in several Wakashan languages. Nasal consonants showed variable patterning across varieties and derived ejective oral stop consonants did not clearly belong to either class in terms of burst intensity, however their average VOT is close to that of the underlying ejectives, suggesting that neutralization is still a possibility.

**Acoustic Cues to Laryngeal Contrasts in Hindi**
Susan Jackson & Stephen Winters

Hindi uses both aspiration and differences in the timing of voicing to signal a four-way laryngeal stop contrast. This study investigates the importance of aspiration and closure voicing cues in the perception of these stops by native speakers of English and Hindi. Three cues were tested for their effect on perception: 1) the presence/absence of aspiration, 2) aspiration quality (voiced/voiceless), and 3) the length of voicing during stop closure. In an ABX task, native English and Hindi speaking students (n=30) at the University of Calgary were presented with monosyllabic, stop-initial nonce words created from recordings done with native Hindi speakers. Word onsets were manipulated to create nine different types of stimuli that varied in terms of aspiration and closure voicing, while controlling for all other potential cues. Higher scores for English listeners were expected for pairs that contrasted by the presence of aspiration, regardless of accompanying phonation, while lower scores were expected for those that contrasted by closure voicing alone. This was confirmed by preliminary results (80.6% vs. 60.8%). Differences in the quality of aspiration (i.e. +/- voicing during the aspirated phase) were also perceived less well (64.9%), pointing to aspiration as a more reliable cue than voice onset time for English speakers. Interestingly, the Hindi speakers performed with the same rate of accuracy on all contrasts as the English speakers, which suggests that the length of voicing during stop closure is not a reliable cue for distinguishing voiced stops in Hindi.

**Speech Quality Evaluation of Dereverberation Algorithms with Hearing Impaired Listeners**
Jonathan Pietrobon, Arvind Venkatasurbramanian, Paula Folkeard & Vjay Parsa.

Reverberation significantly impacts the quality and intelligibility of speech. In particular, background noise and reverberation synergistically degrade the speech understanding capabilities of hearing impaired listeners. Dereverberation algorithms have been developed to mitigate reverberation effects, but very few studies have investigated their performance with hearing impaired listeners. In this study, the performance of four dereverberation algorithms was evaluated in terms of perceived speech quality

by 14 hearing impaired listeners. These algorithms include: (1) the linear prediction residual enhancement method, (2) spectral subtraction, (3) a combination of spectral subtraction and Wiener filtering (SS+WF), and (4) a combination of minimum mean square error log-spectral amplitude (logMMSE) and harmonic speech enhancement (HSE). Male and female speech samples recorded in two different reverberant environments (RT60 = 0.9 s and 1.4 s respectively) were processed by the four dereverberation algorithms. Processed and unprocessed speech samples were then played back to hearing impaired participants, and their ratings of speech quality were collected using the MUSHRA protocol. Results showed that all dereverberation algorithms improved the speech quality scores. Statistical analysis using repeated measures ANOVA revealed the following: (a) there was a significant main effect of reverberation time, (b) there was no significant effect of talker gender nor were there any interactions between reverberation time, talker gender, and algorithm, and (c) the quality ratings for the logMMSE + HSE and the SS+WF algorithms were statistically not different, and were the best

**Mesure objective d'un gain de ratio signal/bruit dans la réponse du tronc cérébral à une voyelle synthétique**
François Prévost, Marilyn Laroche, Hilmi Dajani et André Marcoux

Ces travaux portent sur le traitement auditif de la parole chez l'auditeur normal, par la mesure de la réponse du tronc cérébral à la voyelle synthétique /a/. Cette voyelle est présentée dans le silence et dans un bruit blanc continu à différents ratios signal/bruit (S/B) de +5, 0, -5 et -10 dB. Les résultats montrent que la latence des ondes V et A de la réponse transitoire évoquée dans le bruit est augmentée lorsque comparée à la réponse évoquée dans le silence. L'amplitude de l'onde V est également réduite en présence de bruit, et la pente de la transition entre les ondes V et A est fortement réduite. La composante spectrale de la réponse soutenue qui correspond à la fréquence fondamentale (F0) de la voyelle présente une amplitude et un ratio S/B significativement supérieurs dans toutes les conditions de bruit, sauf dans la plus sévère, à -10 dB S/B. De telles augmentations de l'amplitude et du ratio S/B ne sont pas observées à l'endroit de la composante spectrale correspondant au premier formant de la voyelle. Ces résultats suggèrent que le tronc cérébral adopte différentes stratégies de traitement auditif de la parole. Dans le cas de la F0, le renforcement de la réponse du tronc cérébral dans le bruit peut refléter une stratégie auditive qui priorise la synchronie temporelle aux dépens d'une représentation spatiale.

## Standards and Regulations / Normalisation et Réglementation

**Community Noise Complaint Management in Airports - A discussion relating to N. American and European approaches**
R.D. Tommasi

Community noise awareness and sensibility around airport areas has grown during last decades, mainly due to the increased emphasis on the environment and quality of life standards. Countries both in the American and European continents require major noise sources, most notably airports, to give attention to community complaints by means of a traceable and comprehensive management system. This paper aims to present some general criteria that need to be addressed by such systems, and the applicability to international regulations. Ideally, the responsible manager should be able to distinguish plausible complaints from spam, for example by comparing the location of the complaining person and the four dimensional radar tracking of each aircraft movement, and follow the evolution of the thread, while maintaining full documentation of every step for potential future needs. On the other hand, the complainants expect to have a feedback for their actions and the assurance to receive an answer from the management in a short time, possibly responding to a published "Service Level Agreement" (SLA). We will discuss the SLA and its requirements. In order to give the public the maximum level of usability such system should work with multiple channels, like web interface, smartphone, email, toll-free number, fax, letter and so on. The status and capability of different tools is briefly assessed, also in terms of applicability to different countries' regulations.

# ICSV19
# PRESS RELEASE

**The 19th International Congress on Sound and Vibration (ICSV19), sponsored by the International Institute of Acoustics and Vibration (IIAV) and Vilnius University, will be held from 8 - 12 July 2012 at Vilnius University in Vilnius, Lithuania. Vilnius is the historical capital of Lithuania and dates back to the 14th century and has since been awarded the status of World Cultural Heritage by UNESCO. Vilnius University is one of the oldest universities in Eastern Europe and the friendly atmosphere of the modern city will mesmerize you and leave you with unforgettable memories.**

**Theoretical and experimental research papers in the fields of acoustics, noise, and vibration are invited for presentation. Participants are welcome to submit abstracts and companies are invited to take part in the ICSV19 exhibition and sponsorship. For more information, please visit < http://www.icsv19.org >.**

**For further details, please contact Malcolm J. Crocker at, crockmj@auburn.edu >.**

---

## A Symposium on

# VIBRATION AND STRUCTURAL ACOUSTICS MEASUREMENT AND ANALYSIS

Promoted by

**César M. A. Vasques**
INEGI–Instituto de Engenharia Mecânica e Gestão Industrial, Universidade do Porto
Campus da FEUP, R. Dr. Roberto Frias 400, 4200-465 Porto, Portugal
Tel: +351-22 957 87 10
E-mail: cmav@fe.up.pt

## In Conjunction with

# 15TH INTERNATIONAL CONFERENCE ON EXPERIMENTAL MECHANICS (ICEM15)

**Faculty of Engineering, University of Porto**
**PORTO, PORTUGAL**
**July 22-27, 2012**

**(http://paginas.fe.up.pt/clme/icem15)**

---

## POSITION OPEN - Assistant Editor, Canadian Acoustics Journal

The current Editor-in-Chief, Ramani Ramakrishnan, will be stepping down in 2012. A new Editor will be elected during the Annual General Meeting (AGM) in October 2012 and will become the new Editor-in-Chief from 2013 onwards. CAA is looking for an Assistant Editor who will work with Ramani Ramakrishnan and will be trained to be the next Editor. He or she will be nominated during the 2012 AGM and it is hoped that the membership will vote him/her to be the Editor-in-Chief.

The current proposal is to aid in the smooth transition from Ramani Ramakrishnan to the new Editor.

Interested person should contact either the president, Christian Giguère or Ramani Ramakrishnan.

For Digital Recorders

# Introducing

For USB A/D Systems

## PHANTOM POWER

## 7052PH

Measurement Mic System

**7052H Type 1.5™**

Titanium Diaphragm

3Hz to >20 kHz

<20 dBA > 140 dBSPL

**MK224** (<14 dBA to >134 dBSPL) Optional

**4048 Preamp**

Superior
IEC 1094 Type 1
Long-term Stability
Temperature and Humidity
Performance

**Now in Stock**

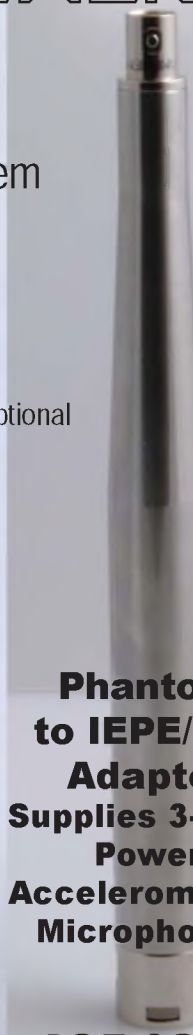

**Phantom to IEPE/ICP Adaptor**

**Supplies 3-4 mA Power**
**Accelerometers**
**Microphones**

**ICP1248**

**MATT™ Family**

## MATT™

**Mic Attenuator**

**Handle Higher Sound Pressure Levels**

**Acoustics Begins with ACO**


**ACO Pacific, Inc., 2604 Read Ave., Belmont, CA 94002**

**Tel:(650) 595-8588 FAX: (650) 591-2891 E-Mail: sales@acopacific.com**

**Web Site: www.acopacific.com**


**TM**

# Better testing... better products.

## The Blachford Acoustics Laboratory

**Bringing you superior acoustical products from the most advanced testing facilities available.**

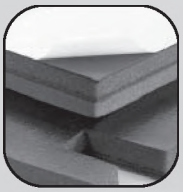

Our newest resource offers an unprecedented means of better understanding acoustical make-up and the impact of noise sources. The result? Better differentiation and value-added products for our customers.

### Blachford Acoustics Laboratory features

- Hemi-anechoic room and dynamometer for testing heavy trucks and large vehicles or machines.
- Reverberation room for the testing of acoustical materials and components in one place.
- Jury room for sound quality development.

### Blachford acoustical products

- Design and production of simple and complex laminates in various shapes, thicknesses and weights.
- Provide customers with everything from custom-engineered rolls and diecuts to molded and cast-in-place materials.

Blachford QS 9000 REGISTERED

www.blachford.com | Ontario 905.823.3200 | Illinois 630.231.8300

## INSTRUCTIONS TO AUTHORS FOR THE PREPARATION OF MANUSCRIPTS

**Submissions:** The original manuscript and two copies should be sent to the Editor-in-Chief. The manuscript can also be submitted electronically.

**General Presentation:** Papers should be submitted in camera-ready format. Paper size 8.5" x 11". If you have access to a word processor, copy as closely as possible the format of the articles in Canadian Acoustics 39(1) 2011. All text in Times-Roman 10 pt font, with single (12 pt) spacing. Main body of text in two columns separated by 0.25". One line space between paragraphs.

**Margins:** Top - 0.75"; bottom - 0.75" minimum; sides - 0.75".

**Title:** Bold, Times New Roman 14 pt with 14 pt spacing, upper case, centered.

**Authors/addresses:** Names and full mailing addresses, 10 pt with single (12 pt) spacing, upper and lower case, centered. Names in bold text.

**Abstracts:** English and French versions. Headings, 12 pt bold, upper case, centered. Indent text 0.5" on both sides.

**Headings:** Headings to be in 12 pt bold, Times-Roman font. Number at the left margin and indent text 0.5". Main headings, numbered as 1, 2, 3, ... to be in upper case. Sub-headings numbered as 1.1, 1.2, 1.3, ... in upper and lower case. Sub-sub-headings not numbered, in upper and lower case, underlined.

**Equations:** Minimize. Place in text if short. Numbered.

**Figures/Tables:** Keep small. Insert in text at top or bottom of page. Name as "Figure 1, 2, ..." Caption in 9 pt with single (12 pt) spacing. Leave 0.5" between text.

**Line Widths:** Line widths in technical drawings, figures and tables should be a minimum of 0.5 pt.

**Photographs:** Submit original glossy, black and white photograph.

**Scans:** Should be between 225 dpi and 300 dpi. Scan: Line art as bitmap tiffs; Black and white as grayscale tiffs and colour as CMYK tiffs;

**References:** Cite in text and list at end in any consistent format, 9 pt with single (12 pt) spacing.

**Page numbers:** In light pencil at the bottom of each page. For electronic submissions, do not number pages.

**Reprints:** Can be ordered at time of acceptance of paper.

## DIRECTIVES A L'INTENTION DES AUTEURS PREPARATION DES MANUSCRITS

**Soumissions:** Le manuscrit original ainsi que deux copies doivent être soumis au rédacteur-en-chef. Le manuscrit peut être aussi acheminé par voie électronique.

**Présentation générale:** Le manuscrit doit être soumis avec mise en page en format de publication. Dimension des pages, 8.5" x 11". Si vous avez accès à un système de traitement de texte, dans la mesure du possible, suivre le format des articles dans l'Acoustique canadienne 39(1) 2011. Tout le texte doit être en caractères Times-Roman, 10 pt et à simple (12 pt) interligne. Le texte principal doit être en deux colonnes séparées d'un espace de 0.25". Les paragraphes sont séparés d'un espace d'une ligne.

**Marges:** Haut - 0.75"; bas - minimum 0.75" ; côtés,- 0.75".

**Titre du manuscrit:** Caractères gras, Times New Roman 14 pt,avec espace interligne de 14 pt, lettres majuscules, texte centré.

**Auteurs/adresses:** Noms et adresses postales. Lettres majuscules et minuscules, 10 pt à simple (12 pt) interligne, texte centré. Les noms doivent être en caractères gras.

**Sommaire:** En versions anglaise et française. Titre en 12 pt, lettres majuscules, caractères gras, texte centré. Paragraphe 0.5" en alinéa de la marge, des 2 cotés.

**Titres des sections:** Tous en caractères gras, 12 pt, Times-Roman. Premiers titres: numéroter 1, 2, 3, ..., en lettres majuscules; sous-titres: numéroter 1.1, 1.2, 1.3, ..., en lettres majuscules et minuscules; sous-sous-titres: ne pas numéroter, en lettres majuscules et minuscules et soulignés.

**Équations:** Minimiser le nombre et les numéroter. Insérer directement dans le texte les équations très courtes.

**Figures/Tableaux:** De petites tailles. Les insérer dans le texte au haut ou au bas de la page. Les nommer "Figure 1, 2, 3,..." Légende en 9 pt à simple (12 pt) interligne. Laisser un espace de 0.5" entre le texte.

**Largeur des traits:** La largeur des traits sur les schémas techniques doivent être au minimum de 0.5 pt pour permettre une bonne reproduction.

**Photographies:** Soumettre la photographie originale sur papier glacé, noir et blanc.

**Figures numérisées:** Doivent être au minimum de 225 dpi et au maximum de 300 dpi. Les schémas doivent être en format bitmap tif. Les photos noir et blanc doivent en format tif sur une échelle de tons de gris et toutes les photos couleurs doivent être en format CMYK tif.

**Références:** Les citer dans le texte et en faire la liste à la fin du document, en format uniforme, 9 pt à simple (12 pt) interligne.

**Pagination:** Au crayon pâle, au bas de chaque page. Ne pas paginer si le manuscrit est envoyé par voie électronique.

**Tirés-à-part:** Ils peuvent être commandés au moment de l'acceptation du manuscrit.

# The Canadian Acoustical Association
# l'Association Canadienne d'Acoustique

## Application for Membership

CAA membership is open to all individuals who have an interest in acoustics. Annual dues total $80.00 for individual members and $35.00 for Student members. This includes a subscription to ***Canadian Acoustics***, the Association's journal, which is published 4 times/year. New membership applications received before August 31 will be applied to the current year and include that year's back issues of ***Canadian Acoustics***, if available. New membership applications received after August 31 will be applied to the next year.

## Subscriptions to *Canadian Acoustics* or Sustaining Subscriptions

Subscriptions to ***Canadian Acoustics*** are available to companies and institutions at the institutional subscription price of $80.00. Many companies and institutions prefer to be a Sustaining Subscriber, paying $350.00 per year, in order to assist CAA financially. A list of Sustaining Subscribers is published in each issue of ***Canadian Acoustics***. Subscriptions for the current calendar year are due by January 31. New subscriptions received before August 31 will be applied to the current year and include that year's back issues of ***Canadian Acoustics***, if available.

*Please note that electronic forms can be downloaded from the CAA Website at* **caa-aca.ca**

**Address for subscription / membership correspondence:**

Name / Organization _____

Address _____

City/Province _____ Postal Code _____ Country _____

Phone _____ Fax _____ E-mail _____

**Address for mailing Canadian Acoustics, if different from above:**

Name / Organization _____

Address _____

City/Province _____ Postal Code _____ Country _____

**Areas of Interest:** (Please mark 3 maximum)

1. Architectural Acoustics
2. Engineering Acoustics / Noise Control
3. Physical Acoustics / Ultrasound
4. Musical Acoustics / Electro-acoustics
5. Psychological / Physiological Acoustic
6. Shock and Vibration
7. Hearing Sciences
8. Speech Sciences
9. Underwater Acoustics
10. Signal Processing / Numerical Methods
11. Other

For student membership, please also provide:

_____ _____ _____ _____

*(University)* *(Faculty Member)* *(Signature of Faculty Member)* *(Date)*

I have enclosed the indicated payment for:
[ ] CAA Membership $ 80.00
[ ] CAA Student Membership $ 35.00

Corporate Subscriptions:
[ ] $80 including mailing in Canada
[ ] $88 including mailing to USA,
[ ] $95 including International mailing

[ ] Sustaining Subscriber $350.00 includes subscription (4 issues /year) to ***Canadian Acoustics.***

Payment by: [ ] Cheque
[ ] Money Order
[ ] Credit Card *(Indicate VISA or M/C)*

Credit card number _____

Name on card _____

Expiry date _____

_____

(Signature) (Date)

**Mail application and attached payment to:**

**Executive Secretary, Canadian Acoustical Association, PO Box 74068, Ottawa, Ontario, K1M 2H9, Canada**

# l'Association Canadienne d'Acoustique
# The Canadian Acoustical Association

## Formulaire d'adhésion

L'adhésion à l'ACA est ouverte à tous ceux qui s'intéressent à l'acoustique. La cotisation annuelle est de 80.00$ pour les membres individuels, et de 35.00$ pour les étudiants. Tous les membres reçoivent ***l'Acoustique Canadienne***, la revue de l'association. Les nouveaux abonnements reçus avant le 31 août s'appliquent à l'année courante et incluent les anciens numéros (non-épuisés) de ***l'Acoustique Canadienne*** de cette année. Les nouveaux abonnements reçus après le 31 août s'appliquent à l'année suivante.

## Abonnement pour la revue *Acoustique Canadienne* et abonnement de soutien

Les abonnements pour la revue ***Acoustique Canadienne*** sont disponibles pour les compagnies et autres établissements au coût annuel de 80.00$. Des compagnies et établissements préfèrent souvent la cotisation de membre bienfaiteur, de 350.00$ par année, pour assister financièrement l'ACA. La liste des membres bienfaiteurs est publiée dans chaque issue de la revue ***Acoustique Canadienne***. Les nouveaux abonnements reçus avant le 31 août s'appliquent à l'année courante et incluent les anciens numéros (non-épuisés) de ***l'Acoustique Canadienne*** de cette année. Les nouveaux abonnements reçus après le 31 août s'appliquent à l'année suivante.

*Pour obtenir des formulaires electroniques, visitez le site Web:* **caa-aca.ca**

***Pour correspondence administative et financière:***

Nom / Organisation _____

Adresse _____

Ville/Province _____ Code postal _____Pays _____

Téléphone _____ Téléc. _____ Courriel _____

***Adresse postale pour la revue Acoustique Canadienne***

Nom / Organisation _____

Adresse _____

Ville/Province _____ Code postal _____Pays _____

**Cocher vos champs d'intérêt**: (maximum 3)

1. Acoustique architecturale
2. Génie acoustique / Contrôle du bruit
3. Acoustique physique / Ultrasons
4. Acoustique musicale / Electro-acoustique
5. Physio / Psycho-acoustique
6. Chocs et vibrations
7. Audition
8. Parole
9. Acoustique sous-marine
10. Traitement des signaux /Méthodes numériques
11. Autre

Prière de remplir pour les étudiants et étudiantes:

_____ _____ _____ _____

*(Université) (Nom d'un membre du corps professoral) (Signature du membre du corps professoral) (Date)*

Cocher la case appropriée:

[ ] Membre individuel 80.00 $
[ ] Membre étudiant(e) 35.00 $

Abonnement institutionnel

[ ] 80 $ à l'intérieur du Canada
[ ] 88 $ vers les États-Unis
[ ] 95 $ tout autre envoi international
[ ] Abonnement de soutien 350.00 $ (comprend l'abonnement à *L'acoustique Canadienne*)

Méthode de paiement:

[ ] Chèque au nom de l'Association Canadienne d'Acoustique
[ ] Mandat postal
[ ] VISA ou M/C (Indiquez)

Numéro carte de crédit _____

Nom sur la carte _____

Date d'expiration _____

_____

(Signature) (Date)

**Prière d'attacher votre paiement au formulaire d'adhésion. Envoyer à :**
**Secrétaire exécutif, Association Canadienne d'Acoustique, CP 74068, Ottawa, K1M 2H9, Canada**

# The Canadian Acoustical Association
# l'Association Canadienne d'Acoustique

# SUSTAINING SUBSCRIBERS / ABONNES DE SOUTIEN

The Canadian Acoustical Association gratefully acknowledges the financial assistance of the Sustaining Subscribers listed below. Their annual donations (of $350.00 or more) enable the journal to be distributed to all at a reasonable cost.

L'Association Canadienne d'Acoustique tient à témoigner sa reconnaissance à l'égard de ses Abonnés de Soutien en publiant ci-dessous leur nom et leur adresse. En amortissant les coûts de publication et de distribution, les dons annuels (de $350.00 et plus) rendent le journal accessible à tous nos membres.

**ACI Acoustical Consultants Inc.**
Mr. Steven Bilawchuk - (780) 414-6373
stevenb@aciacoustical.com - Edmonton, AB

**ACO Pacific Inc.**
Mr. Noland Lewis - (650) 595-8588
acopac@acopacific.com - Belmont, CA

**Acoustec Inc.**
Dr. J.G. Migneron - (418) 834-1414
courrier@acoustec.qc.ca - St-Nicolas, QC

**ACOUSTIKALAB Inc.**
Jean Laporte - (514) 692-1147
jlaporte@acoustikalab.com - Montréal, QC

**AECOM**
Frank Babic - (905) 747-7411
frank.babic@aecom.com - Markham, ON

**Aercoustics Engineering Ltd.**
Mr. John O'Keefe - (416) 249-3361
johno@aercoustics.com - Toronto, ON

**Bruel & Kjaer North America Inc.**
Mr. Andrew Khoury - (514) 695-8225
andrew.khoury@bksv.com - Pointe-Claire, QC

**Conestoga-Rovers & Associates**
Tim Wiens - (519) 884-0510 x2352
twiens@craworld.com - Waterloo, ON

**Dalimar Instruments Inc.**
Mr. Daniel Larose - (514) 424-0033
daniel@dalimar.ca - Vaudreuil-Dorion, QC

**Dessau Inc.**
Jacques Boilard - (418) 839-6034
jacques.boilard@dessau.com - Lévis, QC

**DuraSystems Barriers Inc.**
Fred Woo - (905) 660-4455
fred.woo@durasystems.com - Vaughan, ON

**Eckel Industries of Canada Ltd.**
(613) 543-2967
eckel@eckel.ca - Morrisburg, ON

**ECORE International**
Mr. Paul Downey - (416) 440-1094
pcd@ecoreintl.com - Toronto, ON

**Golder Associates Ltd.**
(905) 567-4444
Mississauga, ON

**H.L. Blachford Ltd.**
Mr. Dalton Prince - (905) 823-3200
amsales@blachford.ca - Mississauga, ON

**Hatch Associates Ltd.**
Mr. Tim Kelsall - (905) 403-3932
tkelsall@hatch.ca - Mississauga, ON

**HGC Engineering Ltd.**
Mr. Bill Gastmeier - (905) 826-4044
bgastmeier@hgcengineering.com -
Mississauga, ON

**Hydro-Québec TransÉnergie**
M. Blaise Gosselin - (514) 879-4100 x5309
gosselin.blaise@hydro.qc.ca - Montréal, QC

**Integral DX Engineering Ltd.**
Mr. Greg Clunis - (613) 761-1565
greg@integraldxengineering.ca - Ottawa, ON

**J.E. Coulter Associates Ltd.**
Mr. John Coulter - (416) 502-8598
jcoulter@on.aibn.com - Toronto, ON

**J.L.Richards & Assoc. Ltd.**
Mr. Terry Vivyurka - (613) 728-3571
mail@jlrichards.ca - Ottawa, ON

**Jacobs & Thompson Inc.**
Chris Brand - (416) 749-0600
cmaida@jacobs-thompson.com - Toronto, ON

**Jade Acoustics Inc.**
Ms. Dalila Giusti - (905) 660-2444
dalila@jadeacoustics.com - Concord, ON

**JASCO Research Ltd.**
Mr. Scott Carr - (902) 405-3336
scott@jasco.com - Dartmouth, NS

**Mc SQUARED System Design Group**
Mr. Wade McGregor - (604) 986-8181
info@mcsquared.com - North Vancouver, BC

**MJM Conseillers en Acoustique Inc.**
M. Michel Morin - (514) 737-9811
mmorin@mjm.qc.ca - Montréal, Canada

**Novel Dynamics Inc.**
Stan Thompson - (613) 598-0026
stan@noveldynamics.com - Ottawa, ON

**Owens-Corning Canada Inc.**
Mr. Salvatore Ciarlo - (800) 988-5269
salvatore.ciarlo@owenscorning.com -
St. Leonard, QC

**OZA Inspections Ltd.**
Mr. David Williams - (800) 664-8263 x25
oza@ozagroup.com - Grimsby, ON

**Peutz & Associés**
M. Marc Asselineau, +33 1 45230500
m.asselineau@peutz.fr - Paris, France

**Pliteq Inc.**
Wil Byrick - (416) 449-0049
wbyrick@pliteq.com -Toronto, ON

**Pyrok Inc.**
Mr. Howard Podolsky - (914) 777-7770
info@pyrok.com -Mamaroneck, NY

**RWDI AIR Inc.**
Peter VanDelden - (519) 823-1311
peter.vandelden@rwdi.com - Guelph, ON

**Scantek Inc.**
Mr. Richard J. Peppin - (410) 290-7726
peppinr@scantekinc.com - Columbia, MD

**SNC-Lavalin inc., div. Environnement**
M. Jean-Luc Allard - (514) 393-1000
jeanluc.allard@snclavalin.com - Longueuil, QC

**Soft dB Inc.**
M. André L'Espérance - (418) 686-0993
contact@softdb.com - Sillery, QC

**Sound & Vibration Solutions Canada Inc.**
Mr. Andy Metelka - (519) 853-4495
ametelka@cogeco.ca - Acton, ON

**Soundtrap Inc.**
Roger Foulds - (705) 357-1067,
roger@soundtrap.ca - Sunderland, ON

**Spaarg Engineering Ltd.**
Dr. Robert Gaspar - (519) 972-0677
gasparr@kelcom.igs.net - Windsor, ON

**Stantec Consulting Ltd.**
Mrs. Zohreh Razavi - (604) 696-8472
zohreh.razavi@stantec.com - Vancouver, BC

**State of the Art Acoustik Inc.**
Dr. C. Fortier - (613) 745-2003
cfortier@sota.ca - Ottawa, ON

**Swallow Acoustic Consultants Ltd.**
Mr. John Swallow - (905) 271-7888
jswallow@jsal.ca - Mississauga, ON

**Tacet Engineering Ltd.**
Dr. M.P. Sacks - (416) 782-0298
mal.sacks@tacet.ca - Toronto, ON

**True Grit Consulting Ltd.**
Ina Chomyshyn - (807) 626-5640
ina@tgcl.ca - Thunder Bay, ON

**Valcoustics Canada Ltd.**
Dr. Al Lightstone - (905) 764-5223
solutions@valcoustics.com - Richmond Hill, ON

**Vibro-Acoustics**
Mr. Tim Charlton - (800) 565-8401
tcharlton@vibro-acoustics.com -
Scarborough, ON

**Wakefield Acoustics Ltd.**
Mr. Clair Wakefield - (250) 370-9302
clair@wakefieldacoustics.com - Victoria, BC

**West Caldwell Calibration Labs**
Mr. Stanley Christopher - (905) 595-1107
info@wccl.com - Brampton, ON

**Wilrep Ltd.**
Mr. Don Wilkinson - (905) 625-8944
info@wilrep.com - Mississauga, ON

**Xscala Sound & Vibration**
Jim Ulicki - (403) 274-7577
info@xscala.com - Calgary, AB